

Dissertation zur Erlangung des Doktorgrades der Fakultät für Chemie und
Pharmazie der Ludwig-Maximilians-Universität München

**Antibiotics inhibiting bacterial protein synthesis,
and novel resistance mechanisms**

Von Fabian Nguyen

Aus Augsburg, Deutschland

2018

Erklärung

Diese Dissertation wurde im Sinne von §7 der Promotionsordnung vom 28. November 2001 von Herrn Prof. Dr. Daniel N. Wilson betreut.

Eidesstattliche Versicherung

Diese Dissertation wurde eigenständig und ohne unerlaubte Hilfe erarbeitet.

München, den 04.04.2018

Fabian Nguyen

Dissertation eingereicht am 17.04.2018

1. Gutachter: Herr Prof. Dr. Daniel N. Wilson

2. Gutachter: Herr Prof. Dr. Roland Beckmann

Mündliche Prüfung am 20.06.2018

Acknowledgements

First, I want to express my sincere gratitude to Prof. Dr. Daniel N. Wilson for the interesting position, five years of good supervision with numerous ideas and talks and the opportunity to travel to national and international conferences to present my own results and to learn about the current state of our field of research.

Thanks to Dr. Daniel Sohmen and Dr. Agata Starosta who were my mentors teaching me the experimental techniques that I needed during my Master's- and my PhD thesis. Thanks also to all other active and former members of the Wilson group for scientific exchange and discussions and especially for creating such a nice working atmosphere.

I also want to thank Prof. Dr. Roland Beckmann, our closest collaborator, and his whole group for sharing their material, machines and experience with me. Special thanks to Heidemarie Sieber for all the help and equipment that I got from you and to Dr. Eli van der Sluis for the pdk-46 plasmid that enabled me to perform genomic mutations. I also want to thank all the other members of the Beckmann group for all their advice and help.

I further want to express my appreciation to all other national and international collaboration partners, thank you so much for our successful cooperations, all the materials that you provided, all the experiments that you performed and all the help that I got from you.

Summary

Antibiotic resistant pathogens are one of the most dangerous threats to public health of our time. Understanding of resistance mechanisms is the basis for the development of new drugs to counter resistant bacteria.

Tetracycline antibiotics belong to the most important classes of antimicrobial drugs, they have been in use for decades and therefore numerous resistances have developed. Ribosome protection proteins (RPPs), like TetM, represent one of the most widespread resistance mechanisms. A high resolution cryo-EM structure of TetM in complex with the *E. coli* ribosome and analysis of TetM mutants gained further insights into the principle of how these proteins protect ribosomes from tetracyclines and which residues of TetM remove the drug from its binding site. RPPs are GTPases highly homologue to elongation factor G, it was observed whether the G' domain, which has been studied in the elongation factor, plays the same role in the RPP that it does for EF-G. However TetM does not confer resistance to the latest generation of tetracyclines including tigecycline, omadacycline and eravacycline. It was therefore analyzed whether bacteria expressing TetM from a plasmid could develop mutants that are able to confer resistance against tigecycline when grown in the presence of raising concentrations of the drug. Although the bacteria became resistant, no mutant versions of TetM were observed, instead changes in the genome of the bacteria, that resulted in the over-expression of a multidrug efflux pump complex were identified as the main source for the resistance. Thermorubin is an antibiotic whose chemical structure shows some similarities to tetracycline even though the mechanism of action of the drug differs from the later. No resistance mechanism against thermorubin have been described in detail so far, therefore bacteria were grown in the presence of increasing concentrations of the drug until they gained high level resistance compared to their parental strain. Sequencing and analysis of their genome identified a loss-of-function mutation in a transcriptional repressor protein that regulates the expression of a multidrug efflux pump system.

Antimicrobial peptides (AMPs) are regarded as an alternative to traditional small-molecule antibiotics. Natural occurring thiopeptides represent one important class of AMPs and have been discovered decades ago as natural products of bacteria. Amythiamicin D and three semi-synthetic derivatives were produced via a *de novo* synthesis pathway. The natural occurring thiopeptide and derivative 3a showed antibacterial activity against numerous pathogens when tested *in vivo*. Further, it could be shown that the derivative 3a contains superior translation inhibition activity *in vitro*

compared to the natural occurring thiopeptide. Derivatives 3b and 3c were inactive. Molecular dynamics simulations found a conformation of amythiamicin D and derivative 3a similar to the conformation that was found for the chemically related elongation factor Tu inhibitor GE2270 A. Inhibition of translation by derivative 3a could be neutralised by the addition of external EF-Tu. A point mutation on EF-Tu conferring resistance to GE2270 A also conferred resistance to derivative 3a indicating that both antibiotics share the same binding site on the elongation factor.

In eukaryotes, numerous AMPs were isolated. Some of which belong to the class of proline-rich antimicrobial peptides. Unlike most AMPs, the proline-rich class (PrAMPs) does not primarily perforate the bacterial membrane but targets translation instead. Crystal structures of the PrAMPs Onc112, pyrrocoricin, metalnikowin I and Bac7 bound to the ribosome of *Thermus thermophilus* identified the binding site of the peptides to be located in the ribosomal exit tunnel. They bind in a reverse orientation compared to the nascent chain with the N-terminus reaching into the A-site of the ribosome. Onc112 and Bac7 binding allows the formation of the initiation complex but their binding sites overlap with the binding site of the A-site tRNA. Biochemical analysis of truncated versions of the PrAMPs showed that the N-terminus of the peptide Onc112 is the active part that binds to the ribosome whereas the C-terminus is required for the uptake of the drug into the bacterial cell. It could further be shown that the inner membrane transporter SbmA is the key protein for the import of Onc112 into the cytoplasm of Gram-negative bacteria. Other antibacterial peptides of various species were tested for their potential as translation inhibitors. Mammalian PrAMPs with high sequence similarity to Bac7 turned out to be potent inhibitors of protein synthesis whereas the tested arthropod and amphibian PrAMPs showed weak activity. To overcome one of the most critical drawbacks of AMPs, their susceptibility to proteases, a Bac7 derivative containing D-amino acids was created. However it inhibited translation with lower efficiency than the natural occurring PrAMP.

More research will be necessary before PrAMPs can be used to supplement traditional antibiotics but the understanding of their mechanism of action is an important step towards clinical application of PrAMPs.

The aims of this thesis were to get further insights into resistance mechanisms against tetracycline antibiotics and the structural related drug thermorubin. Further the mechanism of action of peptide antibiotics was to be determined.

List of publications

Stefan Gross, Fabian Nguyen, Matthias Bierschenk, Daniel Sohmen, Thomas Menzel, Iris Antes, Daniel N. Wilson, and Thorsten Bach. Amythiamicin D and Related Thiopeptides as Inhibitors of the Bacterial Elongation Factor EF-Tu: Modification of the Amino Acid at Carbon Atom C2 of Ring C Dramatically Influences Activity. *ChemMedChem* 2013; 8(12):1954-62

Fabian Nguyen, Agata L. Starosta, Stefan Arenz, Daniel Sohmen, Alexandra Dönhöfer and Daniel N. Wilson. Tetracycline antibiotics and resistance mechanisms. *Biol. Chem.* 2014; 395(5): 559-575

Stefan Arenz, Fabian Nguyen, Roland Beckmann, and Daniel N. Wilson. Cryo-EM structure of the tetracycline resistance protein TetM in complex with a translation ribosome at 3.9 Å resolution. *Proc Natl Acad Sci USA.* 2015; 112(17): 5401-6

A. Carolin Seefeldt, Fabian Nguyen, Stéphanie Antunes, Natacha Pérébasquine, Michael Graf, Stefan Arenz, K. Kishore Inampudi, Céline Douat, Gilles Guichard, Daniel N. Wilson & Axel Innis. The proline-rich antimicrobial peptide Onc112 inhibits translation by blocking and destabilizing the post-initiation complex. *Nat Struct Mol Biol.* 2015; 22(6):470-5

A. Carolin Seefeldt, Michael Graf, Natacha Pérébasquine, Fabian Nguyen, Stefan Arenz, Mario Mardirossian, Marco Scocchi, Daniel N. Wilson and C. Axel Innis. Structure of the mammalian antimicrobial peptide Bac7(1-16) bound within the exit tunnel of a bacterial ribosome. *Nucleic Acids Res.* 2016 44(5):2429-38

Michael Graf, Mario Mardirossian, Fabian Nguyen, A. Carolin Seefeldt, Gilles Guichard, Marco Scocchi, C. Axel Innis and Daniel N. Wilson. Proline-rich antimicrobial peptides targeting protein synthesis. *Nat Prod Rep.* 2017 34(7):702-711

Contribution report

Paper 1: This study describes the synthesis of amythiamicin D and three semi synthetic derivatives and their antimicrobial and biochemical characterization. I created an *in vitro* translation system on the basis of an S12 extract of *E. coli* BL21 DE3 cells. I used this extract to determine the concentrations of amythiamicin D and of three semi synthetic derivatives that is necessary to inhibit the translation reaction of the extract. I further tested the effect of an EF-Tu mutation on the activity of derivative 3a.

Paper 2: This review summarizes the mechanism of tetracycline antibiotics and gives a description of all known resistance mechanisms. I contributed to the review by summarizing and connecting current information on the topic, especially on the chapter about the TetX monooxygenase. Additionally, I performed site directed mutagenesis within loop III of domain IV of ribosomal protection proteins TetS and TetO to compare the role of the YY motif of the loop with its role in the ribosomal protection protein TetM.

Paper 3: This paper shows a cryo-EM structure of TetM bound to the *E. coli* ribosome and a biochemical characterization of TetM mutants to explain the mechanism of action of this ribosome protection protein. I performed site directed mutagenesis to create mutants of TetM and analyzed the consequences of the mutations on the ability of the ribosome protection protein to confer resistance to tetracycline.

Paper 4: This study shows a crystal structure of the insect-derived antimicrobial peptide Onc112 bound to the ribosome of *Thermus thermophilus*. The structure and biochemical experiments presented in this paper explain the mechanism of action of Onc112 and identify the residues of the peptide necessary for the cellular uptake of Onc112 and ribosome binding. I determined the concentrations of Onc112 and of four derivatives that are necessary to inhibit a coupled *in vitro* transcription/translation system on the basis of an *E. coli* cell extract and to inhibit the growth of different *E. coli* strains.

Paper 5: Crystal structures of the bovine derived antimicrobial peptide Bac7(1-16) and of the insect derived antimicrobial peptides metalnikowin I and pyrrocoricin bound to the ribosome of *Thermus thermophilus* are presented in this publication. Together with the biochemical experiments of this study the structures explain the mechanism of action of the antimicrobial peptides. I determined the concentrations of Bac7 fragments, metalnikowin I and pyrrocoricin that are necessary to inhibit a coupled *in vitro* transcription/translation system on the basis of an *E. coli* cell extract. I further determined the concentration of the Bac7 fragment 1-35 that is necessary to inhibit an *in vitro* translation system on the basis of a rabbit reticulocytes cell extract.

Paper 6: This review summarizes the discovery, genomic organization, antimicrobial activity and the mechanism of action of proline-rich antimicrobial peptides. I wrote chapters 2 (“Synthesis of PrAMPs”) and 5 (“Structure activity relationships of PrAMPs”) of this review and contributed to the other chapters.

Conferences

Parts of this thesis have been presented at international conferences

2nd International Symposium Membranes and Modules

March 26-29 2014 Berlin, Germany (Poster)

Ribosome Structure and function 2016

6-10 July 2016 Strasbourg, France (Poster)

List of Abbreviations

aa-tRNA	amino-acyl-tRNA
AlaR	Alanine racemase
AMP	antimicrobial peptide
ATP	adenosine triphosphate
D-Ala-L	D-alanine ligase
dHFA	dihydrofolic acid
DHFR	dihydrofolate reductase
dHPA	dihydroptericoic acid
DHPS	dihydropteroate synthase
DMSO	dimethylsulfoxid
DNA	deoxyribonucleic acid
EF-G	elongation factor G
EF-Tu	elongation factor Tu
EtOH	ethanol
FgBGT	$\beta(1,3)$ -glucanosyltransferase Gel1
Fluc	firefly luciferase
GDP	guanosine-5'-diphosphate
GMPPNP	5'-guanylyl imidodiphosphate
GTP	guanosine-5'-triphosphate
GTP γ S	guanosine 5'-O-[gamma-thio]triphosphate
gu	N,N,N',N'-tetramethylguanidino
IC	inhibitory concentration
IF	initiation factor
IM	inner membrane
IPTG	isopropyl β -D-1-thiogalactopyranoside
LD	lethal dose
MEGAWHOP	megaprimer PCR of whole plasmid
MIC	minimum inhibitory concentration
MK	menaquinone
mRNA	messenger RNA

MRSA	methicillin-resistant <i>Staphylococcus aureus</i>
MurA	UDP-N-acetylglucosamine enolpyruvyl transferase
NAG	N-acetylglucosamin
NAM	N-acetylmuramic acid
O	L-ornithine
OM	outer membrane
ORF	open reading frame
pABA	p-aminobenzoic acid
PBB	penicillin binding protein
PCR	polymerase chain reaction
Pi	inorganic phosphate
Ppase	pyrophosphatase
PrAMP	proline-rich antimicrobial peptide
PTC	peptidyl transferase centre
RF	release factor
RNA	ribonucleic acid
RPP	ribosome protection protein
RRF	ribosome recycling factor
SDS	sodium dodecylsulfate
TGL	transglycosylase
tRNA	transfer RNA
VRE	vancomycin-resistant <i>Enterococcus faecium</i>

List of Figures

Figure 1: Timeline of antibiotic discovery.

Figure 2: Peptidyl transferase reaction.

Figure 3: Schematic overview of antibiotics targeting intracellular processes.

Figure 4: Schematic overview of antibiotic targeting the synthesis of cell wall components and bacterial cell membranes.

Figure 5: Schematic overview over antibiotic resistance mechanisms.

Figure 6: Chemical structures of tetracycline antibiotics.

Figure 7: Chemical structure of thermorubin.

Figure 8: Chemical structures of amythiamicin D and thiostrepton.

Figure 9: Amino acid alignment of bovine cathelicidin Bac7 and human cathelicidin hCAP18.

Figure 10: Amino acid alignment of AMPs used in this thesis.

Figure 11: Effect of loop III mutations on TetM's ability to confer resistance against tetracycline.

Figure 12: Amino acid alignment of parts of the G' domains of TetM and EF-G

Figure 13: Effect of G' domain mutations on TetM's ability to confer resistance against tetracycline.

Figure 14: SDS PAGE analysis of TetM purification.

Figure 15: Absorption profiles at 254 nm of ribosome purifications after gradient centrifugation.

Figure 16: Effect of TetM G' domain mutations on the GTPase activity of the protein.

Figure 17: Serial dilution scheme of tigecycline resistance selection.

Figure 18: Quantification of tigecycline resistance of the RM60 and WT60 strains.

Figure 19: Overview of expression regulation of the AcrAB efflux pump.

Figure 20: Effect of the AcrB T329S mutation on TetM's ability to confer resistance to tigecycline.

Figure 21: Effect of *slyA* or *slyB* knockout on tigecycline susceptibility.

Figure 22: Inhibition of translation of the reporter protein Firefly luciferase (Fluc) by thermorubin.

Figure 23: Serial dilution scheme of thermorubin resistance selection using *E. coli* BW25113 $\Delta sbmA$.

Figure 24: Organization of the *emrRAB* operon.

Figure 25: Construction of genomic mutation Q150P in the gene coding EmrR.

Figure 26: Effect of the EmrR mutation Q150P on thermorubin resistance.

Figure 27: Effect of the EmrR mutation Q150P on nalidixic acid resistance.

Figure 28: Comparison of norfloxacin susceptibilities of T80 and BW25113 wild-type.

Figure 29: Inhibition of translation of the reporter protein Firefly luciferase (Fluc) by mammalian PrAMPs.

Figure 30: Chemical structures of the first six residues of the PrAMP Bac7.

Figure 31: Inhibition of translation of the reporter protein Firefly luciferase (Fluc) by mammalian L-bac7 and retro-D-bac7.

Figure 32: Inhibition of translation of the reporter protein Firefly luciferase (Fluc) by apidaecins.

Figure 33: Inhibition of translation of the reporter protein Firefly luciferase (Fluc) by insect PrAMPs.

Figure 34: Inhibition of translation of the reporter protein Firefly luciferase (Fluc) by amphibian AMPs.

Figure 35: Chemical structures of peptidomimetics.

Figure 36: Plasmid map of TetM in the plasmid pET-46 Ek/LIC.

Figure 37: Plasmid map of Firefly luciferase (Fluc) in the plasmid pIVEX 2.3.

Figure 38: Plasmid map of the λ -red plasmid pdk-46.

Figure 39: Plasmid map of *emrR* in the plasmid pQE-70.

List of Tables

Table 1: Concentrations of TetM G' domain mutants after Ni²⁺-affinity chromatography, gel filtration and concentration.

Table 2: Mutations found in tigecycline serial dilution strains WT60 and RM60.

Table 3: MIC₉₀ values of *E. coli* BL21 DE3; *E. coli* BL21 DE3+TetM WT and selection strain WT60 against tetracycline antibiotics.

Table 4: MIC₉₀ values of WT60 strain against antibiotics unrelated to tetracycline compared with *E. coli* BL21 DE3 wild type strain.

Table 5: List of all mutations identified by whole genome sequencing of the strain T80 compared to the parental *E. coli* BW25113 $\Delta sbmA$ strain.

Table 6: Amino acid sequences of mammalian PrAMPs tested for their translation inhibition potential.

Table 7. Amino acid sequences of apidaecin PrAMPs used in this thesis.

Table 8: Amino acid sequence of arthropod PrAMPs tested for their translation inhibition potential.

Table 9: Amino acid sequences of antimicrobial peptides of different *Xenopus* species.

Table of Contents

1. Introduction	1
1.1 Discovery of antibiotics	2
1.2.1 The synthesis of proteins is performed by a large complex of RNA and proteins: the ribosome	3
1.2.2 Initiation of bacterial translation	4
1.2.3 Elongation of bacterial translation	5
1.2.4 Termination of bacterial translation	8
1.2.5 Recycling of bacterial translation	9
1.3 Intracellular targets for antibiotics	9
1.3.1 Antibiotics targeting translation	10
1.3.2 Antibiotics targeting tetrahydrofolate synthesis	13
1.3.3 Antibiotics targeting transcription	13
1.3.4 Antibiotics targeting bacterial topoisomerases	13
1.4 The bacterial cell envelope as a target of antibiotics	13
1.4.1 Antibiotics targeting cell wall synthesis	14
1.4.2 Antibiotics targeting bacterial membranes	14
1.5 Antibiotic resistance mechanisms	16
1.5.1 Strategies to overcome antibiotic resistance	17
1.6 Tetracycline antibiotics represent an important class of translation inhibitors	18
1.7 The antibiotic thermorubin has a similar chemical structure than tetracyclines but uses a different mechanism	19
1.8 Peptide antibiotics could serve as an alternative for traditional antimicrobial drugs	20
1.8.1 Thiopeptides are antimicrobial peptides made of highly modified amino acids	21

1.8.2 Antimicrobial peptides are part of the innate immune system of animals.....	21
2. Cumulative thesis: summary of published results.....	25
3. Unpublished Results.....	32
3.1 Mutations within loop III of domain IV of TetM underline the importance of conserved tyrosines 506 and 507.....	32
3.2 The G' subdomain is crucial for the GTPase activity of elongation factor G.....	33
3.3 Effect of G' subdomain mutation of TetM on tetracycline resistance.....	33
3.4 Purification of TetM G' domain mutants.....	34
3.5 Purification of <i>E. coli</i> ribosomes.....	36
3.6 Effect of G' domain mutation on TetM's GTPase activity.....	36
3.7 Tigecycline resistance selection.....	37
3.8 Effect of thermorubin on bacterial and eukaryotic translation.....	45
3.9 Construction of a thermorubin resistant strain.....	46
3.10 Inhibition of <i>E. coli in vitro</i> translation by peptide antibiotics.....	50
3.10.1 Characterization of mammalian PrAMPs.....	50
3.10.2 Construction and testing of retro-D-Bac7.....	52
3.10.3 Characterization of arthropod PrAMPs.....	53
3.9.4 Characterization of antimicrobial peptides of amphibian origin.....	56
4. Discussion and Outlook.....	58
4.1.1 Proline 509 of TetM interacts with the tetracycline binding site.....	59
4.1.2 The G' domain of TetM is vital for its GTPase activity.....	60

4.1.3 Over-expression of the AcrAB efflux pump complex is the major source of tigecycline resistance in the RM60 and WT60 serial dilution strains	60
4.2 Thermorubin is an antibiotic with specificity to bacterial ribosomes and a substrate of the EmrAB efflux pump complex.....	63
4.3 Amythiamicin D derivative 3a possesses superior translation inhibiting properties compared to the the parental compound inhibiting elongation factor Tu.....	65
4.4.1 Proline-rich antimicrobial peptides inhibit translation by binding to the bacterial ribosome.....	66
4.4.2 Clinical use of antimicrobial peptides is limited by stability of the compounds and possible development of cross-resistance.....	70
4.4.3 Incorporation of peptidomimetics into the amino acid sequence of PrAMPs could generate protease stable derivatives.....	70
5. Materials and Methods	73
6. Buffers and Media	81
7. Plasmid Maps	83
8. List of Primers.....	85
9. List of Software.....	90
References.....	91
Appendix A: Amino acid alignment of OtrA isoforms.....	119
Appendix B: Amino acid alignment of OtrA and TetM.....	120
Appendix C: Amino acid alignment of TetO and TetM.....	121
Appendix D: Original publications.....	122

1. Introduction

Antibiotic resistant bacteria represent one of the most important threats to public health. The World Health Organization categorized carbapenem-resistant *Acinetobacter baumannii*, *Pseudomonas aeruginosa* and *Enterobacteriaceae* as the most critical bacteria with other pathogens like vancomycin-resistant *Enterococcus faecium* (VRE) or methicillin-resistant *Staphylococcus aureus* (MRSA) being next on the priority list for the development of new therapeutics¹. One of the main reasons for the proliferation of resistant pathogens is the overuse in human² and animal³ medicine. In Germany, the latest report estimated the total consumption of antibiotics in human medicine to be in the range of 700-800 tons for 2014⁴. In animal medicine a total of 1.238 t were applied, which was a significant decrease compared to 2011 (1.706 t). The most important classes were penicillins (450 t); tetracyclines (342 t); sulfonamides (121 t) and macrolides (109 t)⁵. Further, a recent study found high concentrations of antibiotics in the wastewater of pharmaceutical factories producing these drugs⁶. Numerous multi-resistant pathogens were found in the environment of these factories. However antibiotic resistance is not new. The first reports about sulfonamide-resistant bacteria appeared only few years after their discovery in the 1930's⁷⁻⁹. Whereas the first resistance against penicillin was reported in the same year its *in vivo* efficiency was published¹⁰ and even before the clinical application of the drug¹¹⁻¹³. Most antibiotics are natural products, produced by microorganisms or higher species to kill (other) microorganisms. The producing cell has to protect itself from the toxicity of its own antibiotic(s) whereas the target cell tries to become resistant as well as to develop its own antibiotic(s) to compete with the first. This arms-race did not start by human activity but what has changed in the decades since the clinical introduction of antibiotics is the dimension of antibiotics in the environment that lead to an unseen selective pressure on bacteria to develop resistance mechanisms. The latest study for Germany found that around 15% of analyzed strains of *Acinetobacter baumannii* showed resistance against carbapenems, whereas the portion of resistant *Pseudomonas aeruginosa* is in the range of 8%⁴. The share of MRSA dropped from 16.7% in 2010 to 13.5% in 2013 whereas VRE rate increased from 12.6% in 2010 to 16.6% in 2013. These high numbers of resistant pathogens highlight the need to discover and develop new and better antimicrobial drugs and strategies to overcome resistance mechanisms.

1.1 Discovery of antibiotics

Moulds were already used in medicine long before the discovery of microorganisms in the late 17th century¹⁴⁻¹⁶. In the 19th century, it was observed that liquid culture tubes exposed to the air are colonized by bacteria very fast but that tubes containing *Penicillium* could not be populated by them^{17,18}. In 1884 a *Penicillium glaucum* culture was used to heal a patient's gluteal abscess but the results were not published¹⁹. In 1897, the activity of *Penicillium* mould against *Salmonella typhi* was shown¹⁹.

Mycophenolic acid is considered to be the first antibacterial agents that has been isolated and systematically analyzed. It is produced by *Penicillium brevicompactum* and was shown inhibit the growth of *Bacillus anthracis* as early as 1893 but its discovery did not lead to its medical application²⁰⁻²². Today mycophenolic acid and its derivatives are used as immunosuppressives after organ transplantations²³ or to treat autoimmune diseases like systemic lupus erythematosus²⁴ but their side effects do not justify their use as antibiotics. The first commercially successful chemotherapeutic to treat bacterial infections was arsphenamine, marketed under its brand name Salvarsan^{®25}. It was an advancement of the earlier arsenic compound atoxyl which was effective in treating the African sleeping sickness caused by the protozoa *Trypanosoma brucei* in an animal model but turned out to be too toxic for use in human medicine. Arsphenamine was reported to be an effective drug to treat syphilis in 1910 and was successfully tested clinically soon after²⁶⁻²⁸. In spite of this success, arsphenamine has major drawbacks: it is still very toxic due to the arsenic content and oral application is impossible due to its low water solubility²⁹. The discovery of penicillin by Alexander Fleming in 1928 is widely regarded as the hour of birth of antibiotics³⁰. However it took 15 more years until penicillin was in large scale clinical use¹². Before the clinical introduction of penicillin, sulfamidochrysoidin was discovered as the first member of the class of sulfonamide antibiotics. The drug was patented as Prontosil[®] in 1932³¹. It was shown to be highly active against infections by *Streptococcus sp.* in animal models⁸. Prontosil is not effective *in vitro* but a pro-drug that has to be transformed into its biological active form inside of the bacterial cell³². The first translation inhibitor, streptomycin, was originally isolated from *Actinomyces griseus* in 1944³³. It was the first antibiotic that was able cure *Mycobacterium tuberculosis* infections. Its discoverer Selman Waksman also introduced the term "antibiotic"³⁴. In the next two decades most of the antibiotic classes used today were discovered³⁵ (see Figure 1). Semi-synthetic derivatives of natural occurring antibiotics were developed in the following years but the number of totally new classes of antibiotics has been steadily decreasing. Between January 2010 and December 2015 only eight new antibiotics were approved by the U.S. Food and Drug Administration: ceftaroline, fidaxomicin, bedaquiline, dalbavancin, tedizolid, oritavancin, ceftolozane-tazobactam and ceftazidime-avibactam³⁶. Seven of

these eight antibiotics are derivatives of established antibiotic classes or combinations of a β -lactam antibiotic and a β -lactamase inhibitor. Only bedaquiline, the first member of diarylquinolines, uses a novel mechanism of action: it targets subunit C of ATP synthase and is used against mycobacteria³⁷.

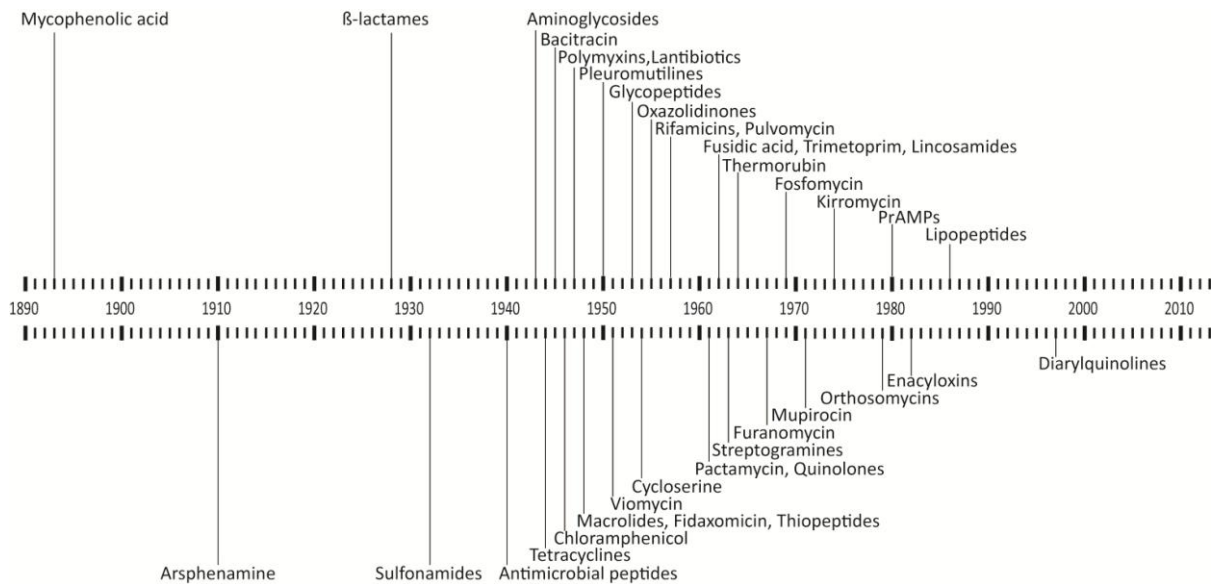


Figure 1: Timeline of antibiotic discovery. Most classes were found between the beginning of the 1940's and the end of the 1960's terming this period the "golden age" of antibiotic discovery³⁸⁻⁵⁷. PrAMPs: Proline-rich antimicrobial peptides.

Translation, the synthesis of new proteins, is one of the most important targets for antibiotics. Translation inhibitors like macrolides, tetracyclines and aminoglycosides belong to the most used classes of antibiotics⁵⁸. These drug families, together with numerous others, inhibit the synthesis of proteins via many different mechanisms of action. Some bind directly to the protein synthesis machinery whereas others act by inhibiting specific factors required for translation.

1.2.1 The synthesis of proteins is performed by a large complex of RNA and proteins: the ribosome

First isolations of ribosomes were already performed in 1948⁵⁹ and 1952⁶⁰ by ultracentrifugation of the cytoplasm of normal and leukemic mouse spleen. They were named "ultramicrosomes" or "macromolecules" respectively and were already identified as ribonucleic acid complexes. Ribosomes were first visualized in 1955 observing OsO_4 fixed rat and chicken tissues and organs under an electron microscope⁶¹. They were described as small, almost spherical particles with 100 to 150 Å in diameter. Furthermore it was already seen that some of the particles were associated with the membrane of the endoplasmic reticulum whereas others were freely distributed in the cytoplasm.

The ribosome is the key player in the production of novel proteins. In bacteria it is composed of a small subunit with a mass of 0.8 MDa and a sedimentation coefficient of 30 S and a large subunit

with a mass of 1.5 MDa and a sedimentation coefficient of 50 S⁶². Both subunits unite to form a complex with a sedimentation coefficient of 70 S. In *E. coli*, the small subunit contains of 21 proteins and a single RNA chain of 16 S. The decoding site is part of this subunit. Here, the interactions of the codons on the mRNA and the anticodons of the tRNAs decide over the amino acid sequence of the synthesized proteins. The large subunit of *E. coli* ribosomes contains 34 proteins and two RNA chains that sediment at 5 S and 23 S. The peptidyl transferase centre (PTC), which is the active site that catalyzes the formation of peptide bonds, represents the core of the large subunit. It is exclusively composed of rRNA residues of domain V of the 23S rRNA, the nearest protein side-chain lies about 18 Å away suggesting that the ribosome is a ribozyme⁶³. In the *E. coli* genome, 7 ORFs for rRNA genes have been found⁶⁴, each contains one sequence for 16S, 23S and 5S rRNA. A 30S precursor rRNA is transcribed that is cleaved by RNase III into fragments which are further processed by other RNases into the final 16S, 23S and 5S rRNA sequences⁶⁵. The subunits form by folding of the rRNA and the association of ribosomal proteins in a defined order^{66,67}. After assembly of the ribosome, the synthesis of proteins can start. The process of translation can be divided into four steps: Initiation, Elongation, Termination and Ribosome recycling.

1.2.2 Initiation of bacterial translation

The mature 70S bacterial ribosome consists of a 30S and a 50S subunit, before these subunits can associate, the mRNA and the initiator tRNA, fMet-tRNA^{Met}, have to be incorporated correctly⁶⁸. This process requires the help of three initiation factors (IFs). In a first step IF1 and IF3 bind to the 30S subunit. The binding site of IF1 overlaps with the A-site, directing the initiator tRNA to the P-site⁶⁹. IF3 binding permits premature joining of the 50S subunit⁷⁰. The mRNA and the GTPase IF2 (GTP) join the complex. IF2 binding promotes the binding of initiator fMet-tRNA^{Met} forming the 30S pre-initiation complex⁷¹. A highly conserved sequence was found on the 3'-terminal part of the 16S rRNA: ACCUCC⁷². It was shown that this sequence directly interacts with the ribosome binding site of coliphage mRNAs⁷³. The sequence on the mRNA has been named Shine-Dalgarno sequence and interacts with the complementary sequence located at the 3' end of the 16S rRNA which has been named Anti-Shine-Dalgarno sequence⁷². The Shine-Dalgarno sequence is positioned 5-13 nucleotides upstream of the initiator codon positioning the start codon into the P-site of the ribosome⁷⁴. Variations in the Shine-Dalgarno sequence, its length and its distance to the start codon lead to weaker interaction of the 16S rRNA with the mRNA generating a level of translation regulation. The fMet-tRNA^{Met} is first bound in a codon-independent way, the complex undergoes a conformational change that promotes codon-anticodon interaction between the fMet-tRNA^{Met} and the mRNA that

results in the 30S initiation complex⁷⁵⁻⁷⁷. IF1 and IF3 leave the complex enabling the 50S subunit to join. GTP hydrolysis of IF2 is stimulated by the joining of the 50S subunit and the factor dissociates from the complex. This last step forms the 70S initiation complex with empty E-, and A-sites and fMet-tRNA_f^{Met} in the P-site. The ribosome is now ready to start into the elongation cycle.

1.2.3 Elongation of bacterial translation

After formation of the 70S initiation complex the ribosome has an fMet-tRNA_f^{Met} in the P-site and an empty A-site, the second amino acid can associate. However, amino acids cannot directly bind to the ribosome, they have to be coupled to a tRNA molecule. This task is fulfilled by tRNA-synthetases which link every amino acid to a specific tRNA molecule. The error rate of this process is as little as 10⁻⁶^{78,79}. Elongation factor Tu (EF-Tu) binds GTP and an aminoacyl-tRNA (aa-tRNA) to form the ternary complex. This complex binds to the ribosome to deliver the aa-tRNA into the A-site of the ribosome. It is very important that the ribosome recognizes wrong amino acids to prevent the incorporation of mistakes. Therefore the codon on the mRNA, consisting of three nucleotides per codon, has to interact with the anticodon of the tRNA forming the Watson-Crick base pairs A-U and G-C in a process called decoding^{80,81}. The incoming tRNA-anticodon can either match perfectly (cognate) or with one (near-cognate) or 2-3 mismatches (non-cognate) to the codon on the mRNA. Initial association of the ternary complex is independent of the mRNA⁸² but the binding of a non-cognate tRNA is excluded through the lack of binding energy between the codon and the anticodon⁸³. However in the case of a near-cognate aa-tRNA this is not enough. Therefore, an additional discrimination mechanism is necessary. The original model proposed that interactions of mRNA and a cognate tRNA induces a conformational change in the bases A1492 and A1493 of the 16S rRNA flipping them out of helix 44 of the 30S subunit to interact with the first and the second base pair of the codon-anticodon helix⁸⁴. Together with universally conserved bases G530 of the 16S rRNA and A1913 of the 23S rRNA, these two bases monitor Watson-Crick base pairing to distinguish between cognate and near cognate codon-anticodon interaction^{83,85}. But another study found that a single mismatch at position one or two in the codon-anticodon helix is forced to form a Watson-Crick base pair-like geometry by 30S domain closure⁸⁶. In this model, the ribosome discriminates cognate from near-cognate aa-tRNAs by the energy that is needed to force a non-Watson-Crick base pair into a Watson-Crick conformation^{86,87}. The latest publication enabled a more detailed view on the nucleotides G530 and A1492 of the 16S rRNA and A1913 of the 23S rRNA⁸⁸. Formation of a codon-anticodon helix between a cognate aa-tRNA and the mRNA is stabilized by interactions of G530 and the backbone of the helix. Stacking of A1913 on A1492 is disturbed by the binding of the tRNA's

anticodon stem loop next to helices 44 and 69. A1492 therefore moves towards the minor groove of the codon-anticodon helix rearranging G530 to induce the closure of the 30S subunit. In case of a near-cognate aa-tRNA, the closure of the 30S subunit is not favored⁸⁸.

The third or wobble base pair of the codon-anticodon helix is not monitored so closely. In contrast, it could be shown that the interactions between the third position of a codon with the anticodon tolerates variations from Watson-Crick base pairing⁸⁹.

Before 30S closure, the aa-tRNA is simultaneously bound to the A-site and to EF-Tu (GTP), termed A/T conformation⁹⁰. The tRNA has to be distorted to bind in A/T conformation. Interactions of the tRNA with the shoulder domain of the 16S rRNA, ribosomal protein S12 and the L11 region of the 23S rRNA stabilize this distortion which is further strengthened by interactions of EF-Tu (GTP) with the sarcin-ricin loop of the 23S rRNA⁹⁰. The tRNA has to move from the A/T state to the full A/A state. 30S subunit closure after codon recognition rearranges the domains of EF-Tu (GTP) pulling it into the factor binding site inducing the hydrolysis of its GTP. GTP hydrolysis requires the attack of a water molecule on its γ -phosphate which is provided by catalytic His84 of EF-Tu⁹¹. It has been proposed originally, that the water is protected from the solvent by two of EF-Tu's amino acids, Val20 and Ile60 forming a hydrophobic gate that has to be opened to make the γ -phosphate of GTP accessible for the water⁹². However another study showed that there are only minor conformational changes of Val20 and Ile60 before and after GTP hydrolysis, instead His84 has to be positioned by interaction with A2662 of the sarcin-ricin loop to bring the water molecule in line for the attack on the γ -phosphate⁹³. After GTP hydrolysis, EF-Tu undergoes conformational changes interrupting the interactions of its G domain with the sarcin-ricin loop and between switch II of EF-Tu and the tRNA acceptor arm⁹². EF-Tu-GDP then leaves the ribosome. EF-Tu's stabilization of the aa-tRNA distortion is gone and the tRNA either relaxes into the accommodated state or dissociates from the ribosome if the codon-anticodon interaction of a near-cognate base pair is not strong enough to keep the aa-tRNA at the ribosome in the absence of EF-Tu⁸⁵. After that the tRNA has been completely accommodated into the A-site.

The 3'CCA-end of the tRNA now enters the peptidyl transferase centre forming a stacking interaction of its C74 and 23S rRNA base U2555 and a base pair between its C75 and 23S rRNA base G2553^{63,94}. A76 of the tRNA forms a class I A-minor interaction with G2583. The α -amine is within hydrogen bond distance of N3 and the 2'OH of 23S rRNA base A2451 as well as of the 2'OH of A76 of the peptidyl tRNA. C74 and C75 of the P-site tRNA form base pairs with P-loop nucleotides G2251 and G2252 whereas A76 forms a stacking interaction with A2451 and hydrogen bonds with A2450⁶³. The

α -amino group is now positioned to perform a nucleophilic attack on the aminoacyl ester of the peptidyl tRNA (see Figure 2).

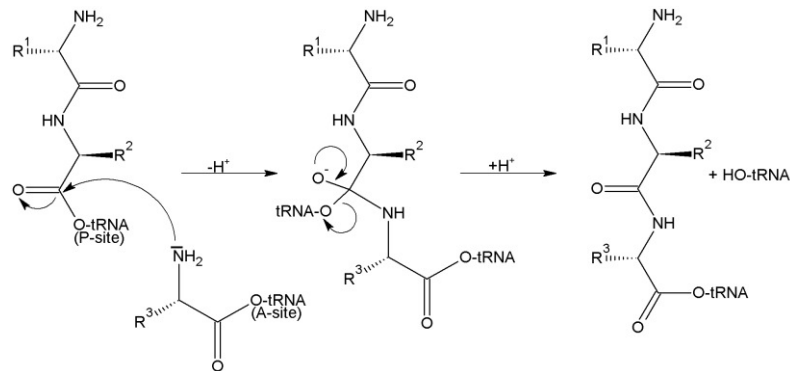


Figure 2: Peptidyl transferase reaction. The free electron pair of the N-terminal amino group of the A-site tRNA attacks the carbonyl atom of the C-terminal amino acid binding the A-site aa-tRNA to the nascent chain. In a second step, the bond between the P-site tRNA and the nascent chain is broken^{95,96}.

The exact mechanism of peptide bond formation remains an issue of debate. A recent model focuses on water molecules inside of the PTC⁹⁷. One water lies within a pit formed by 23S rRNA bases A2602 and A2451, the 3'CCA of the A-site tRNA and the N-terminus of protein L27. The water is positioned to deprotonate the α -amino group of the A-site tRNA which is thereby activated to perform the nucleophilic attack on the ester carbonyl carbon of the P-site tRNA forming a tetrahedral intermediate state before the bond to the P-site tRNA is broken.

After peptide bond formation, the ribosome has a deacylated tRNA in the P-site and a peptidyl tRNA in the A-site which represents the pre-translocation complex. To enable the next round of elongation, the P-site tRNA has to move to the E-site and the A-site tRNA has to move to the P-site in a process called translocation. Elongation factor G (EF-G) has to help the ribosome in this process⁹⁸, it accelerates the rate of the reaction by 4-5 orders of magnitude⁹⁹. The movement of the tRNAs takes place in two steps. First, the anticodon ends of both tRNAs stay bound to the small subunit, while the CCA-ends of the tRNAs move to the P- and E-sites of the large subunit forming an A/P and a P/E hybrid state^{87,100,101}. In a second step, EF-G moves the anticodon ends into the P- and E-site of the 30S subunit. EF-G cannot translocate ribosomes with a tRNA in the P-site but no tRNA in the A-site to prevent premature translocation¹⁰². EF-G interacts with the intersubunit space at the A-site of the ribosome^{103,104}. EF-G domain I binds the sarcin-ricin loop of the 23S rRNA and the L7/L12 stalk whereas domain V contacts the 1067 region of the 23S rRNA. Domain II interacts with the 360 region of the 16S rRNA. Domain III of EF-G interacts with ribosomal protein S12 whereas domain IV pushes into the decoding centre on the small subunit. After binding, EF-G immediately hydrolyses GTP and releases Pi phosphate undergoing a conformational change in EF-G that induces a rotation of the small with respect to large subunit without changing the positions of the tRNAs; the mRNA channel is

widened allowing the mRNA to advance by one codon^{105,106}. The ribosome now has the peptidyl-tRNA in the P-site and the deacylated tRNA in the E-site which represents the post-translocational complex. The A-site is left empty and ready to accept the next aa-tRNA-EF-Tu-GTP complex. The E-site is too small to bind an aa-tRNA ensuring that the P/E hybrid state can exclusively be formed after transpeptidation¹⁰⁷.

Depending on the growth conditions 12-20 codons per second are translated by the ribosome¹⁰⁸, thereby increasing the rate of peptide bond formation by the factor of 2×10^7 compared to the reaction in free solution¹⁰⁹. The rate of transcription has been measured to be 28-89 nucleotides per second in *E. coli*¹¹⁰. Given that one codon is made of three nucleotides one can say that both rates are similar, enabling the coupling of these processes. Ribosomes have been visualized that translate nascent mRNAs while they are synthesized by RNA polymerase¹¹¹. Besides its high speed, translation also occurs with a very high accuracy. Missense errors, the incorporation of a wrong amino acid, have been estimated to rates of 10^{-5} to 10^{-3} ¹¹²⁻¹¹⁵. That is again comparable with the situation during transcription which has an error rate of about 10^{-5} per nucleotide¹¹⁶.

1.2.4 Termination of bacterial translation

At the end of an open reading frame one of three universally conserved stop or termination codons (UAA, UAG and UGA) appears without a corresponding tRNA to bind it. Instead, a class I release factor binds to the mRNA. Two class I release factors have been identified and named RF1 and RF2 in bacteria¹¹⁷. RF1 recognizes the stop codons UAA and UAG whereas RF2 recognizes UAA and UGA¹¹⁸. A mutational analysis has identified the residues responsible for stop codon recognition¹¹⁹. The tripeptide Pro-Ala-Thr in RF1 enables UAA and UAG recognition whereas RF2 uses a Ser-Pro-Phe sequence to recognize UAA and UGA. Another important sequence is the strictly conserved GGQ motif found in class I release factors. Mutations of the glycines resulted in a complete loss of ability for the hydrolytic reaction, whereas the mutation of the glutamine resulted in partial defective factors¹²⁰. Furthermore, it has been shown that the glutamine side-chain of the GGQ motif is N5 methylated. Lack of methylation reduces the activity of RF1 and RF2 by 4-5 fold^{121,122}. The methylation is performed by the enzyme PrmC (former named HemK) in *E. coli*¹²³. The methylation of the GGQ motif packs the glutamine side chain against A2451 of the 23S rRNA stabilizing the GGQ motif and positioning the amide of the side chain away from the active site¹²⁴. This helps in orienting the carbonyl oxygen of the C-terminal amino acid into the active site to coordinate the catalytic water. The GGQ motif inserts into the PTC moving the 23S rRNA nucleotides U2506 and U2585 out of the A-site aminoacyl-binding pocket into a conformation they have when an aminoacyl-tRNA is

bound to the A-site. The glutamine side chain of the GGQ motif fills the space that is normally occupied by the aminoacyl group of an A-site bound aa-tRNA¹²⁵. A catalytic water molecule enters the PTC¹²⁶, the 2'OH group of A76 brings the water molecule in position for nucleophilic attack on the ester bond between the nascent chain and the tRNA¹²⁵. The backbone amide of the Gln253 is positioned to form a hydrogen bond with the 3'-OH group of the terminal nucleoside A76 of the P-site tRNA after deacylation. When the backbone amide of the GGQ glutamine is removed by mutation to proline, the ability of RF2 to catalyze splitting of the peptide chain of the P-site tRNA is reduced to zero¹²⁷. The class II release factor RF3 binds to the ribosome in its GDP form¹²⁸. The deacylation of P-site tRNA enables RF3 to exchange GDP to GTP^{128,129}. RF3-GTP induces conformational changes resulting in the dissociation of RF1 and RF2. RF3 hydrolyses GTP before it leaves the ribosome^{128,130}.

1.2.5 Recycling of bacterial translation

After dissociation of the nascent polypeptide chain and release factors, the ribosome is still bound to the deacylated P-site tRNA and the mRNA. Two factors are required to split the complex into its components to make them available for the next round of translation¹³¹. Ribosome recycling factor (RRF) binds to the large subunit of the ribosome¹³². Its three dimensional structure has been reported to strongly mimic the structure of tRNA in shape and size, suggesting that RRF binds the A-site like a tRNA. However subsequent structural studies showed that the conformation of RRF differs drastically from a bound A-site tRNA¹³²⁻¹³⁴. EF-G bound to GTP enters the complex. GTP hydrolysis of EF-G triggers a movement of domain II of RRF destabilizing inter-subunit bridges B2a and B3 resulting in the separation of the subunits^{132,135-137}. After splitting of the ribosome into subunits, IF3 associates to prevent rejoining of the subunits¹³⁸. The exact mechanism of how the deacylated tRNA and the mRNA dissociate remains unclear. According to one study, the tRNA and the mRNA are removed simultaneously to the splitting without the help of IF3¹³⁹. However another model says that IF3 is necessary to remove the tRNA whose dissociation allows the mRNA to slide along the 30S subunit and reinitiate translation or leave the subunit^{137,140}. The free subunits are now available to start with the next round of translation.

1.3 Intracellular targets for antibiotics

Many antimicrobial drugs that act inside of the bacterial cell inhibit the synthesis of new proteins described above but there are also compounds that target other intracellular targets like replication, transcription and tetrahydrofolate synthesis.

1.3.1 Antibiotics targeting translation

Every step of translation is targeted by numerous antibiotics. Many translation inhibitors bind to the ribosome directly whereas others target factors involved in translation.

Numerous translation inhibitors were found as natural products of bacteria, fungi and eukaryotes. In general, translation inhibitors do not lyse bacteria but prevent them from growing i.e. they employ a bacteriostatic rather than a bactericidal mechanism¹⁴¹. As a consequence, the bacteria stay intact and the content of the bacterial cell is not released into the environment. In some cases this is very favourable as some bacteria contain highly toxic molecules in their cells¹⁴². Their release can cause significant problems and should be avoided¹⁴³. Bactericidal drugs generally work better in growing than static cells, therefore a combination therapy with bactericidal and bacteriostatic antibiotics is usually not the method of choice¹⁴⁴. However when bacteriostatic antimicrobials are administered at very high concentrations they can also act bactericidal¹⁴⁵. But there are also exceptions among translation inhibitors like aminoglycosides or ketolides which exert a bactericidal mechanism at low concentrations^{146,147}.

The ideal antibiotic inhibits the growth of bacteria without effecting eukaryotic cells. The uptake of many antimicrobial drugs into eukaryotic cells is weak due to the differences of membrane composition between eukaryotic and prokaryotic cells¹⁴⁸. Some antibacterials are even substrates of eukaryotic efflux pumps removing the drugs from the inside of the cells¹⁴⁹. This protects the own ribosomes of the cell against the drugs but on the other hand limits the efficiency of these compounds against intracellular pathogens. Further, the differences of bacterial and cytoplasmic eukaryotic ribosomes are enough to make the later insensitive to some but not to all translation inhibitors^{150,151}. As mitochondrial (and in plants also chloroplast) ribosomes are evolutionarily related to bacterial ones they are also more vulnerable to translation inhibiting antibiotics¹⁵².

Almost every single step of translation is the target of antibiotics. Many translation inhibitors have more than one effect on translation, it is therefore not easy to categorize them into pure initiation or elongation inhibitors. But it is possible to say that some antibiotics are first and foremost initiation inhibitors as the concentration for secondary effects is far higher than for disturbing initiation. For example, kasugamycin is an aminoglycoside antibiotic but it utilizes a different mode of action than other antibiotics of this family. Kasugamycin binds within the mRNA channel inhibiting the correct codon-anticodon interaction that is necessary for the binding of fMet-tRNA_f^{Met 153,154}. Edeine binds to bases in helices 24, 28, 44 and 45 of the 16S rRNA blocking the binding site of P-site tRNA and therefore preventing the binding of fMet-tRNA_f^{Met} to the initiation complex¹⁵⁵⁻¹⁵⁷. The tetrapeptide GE81112 holds the small subunit in the 30S pre-initiation complex state, preventing the dissociation

of IF3 and the association of the 50S subunit^{158,159}. Orthosomycins interact with a binding site containing nucleotides of helices 89 and 91 of the 23S rRNA¹⁶⁰. The binding site of orthosomycins overlaps with the binding site of Initiation Factor 2 preventing the joining of the small with the large subunit. The binding site also overlaps with the binding site of A-site tRNA interfering with the accommodation of the tRNA into the A-site¹⁶¹. The synthetic nitrovinylfuran antibiotic G1 (MW297) binds to the P-site of the 30S subunit blocking the binding of fMet-tRNA_f^{Met}¹⁶².

Elongation is targeted by a higher number of antibiotics. The peptidyl transferase centre is the target of many of them. Chloramphenicol binds to domain V of the 23S rRNA and blocks the binding of A-site tRNA¹⁶³⁻¹⁶⁵. The binding site of Lincosamides partly overlaps with chloramphenicol's but they bind to the A- and P-site¹⁶⁶. They therefore disturb the correct positioning of the A- and P-site tRNA. They also block a part of the exit tunnel preventing the growth of the nascent chain¹⁶⁷. Macrolides bind at the entrance of the exit tunnel¹⁶⁶. The first proposed mechanism suggested that this class of antibiotics blocks the tunnel independently of the sequence of the nascent chain¹⁶⁷ but later studies identified discrete stalling and bypass sequences¹⁶⁸. Pactamycin interacts with the E-site of the 30S subunit. It displaces the mRNA preventing the interaction of E-site tRNA with the corresponding mRNA¹⁶⁹. Aminoglycosides bind to bases in the A-site that work together with A1492 and 1493 for precise codon-anticodon selection^{170,171}. As a consequence, wrong amino acids get incorporated into the nascent chain. Aminoglycosides are bactericidal, even at low concentrations, the incorporation of membrane proteins containing wrong amino acids is seen as the reason for the bactericidal action¹⁴⁶. Oxazolidinones bind to the A-site overlapping with the binding site with A-site tRNA¹⁷². Hygromycin A and A201A allow the binding of the ternary complex of aa-tRNA-EF-Tu-GTP but prevent complete accommodation of the tRNA into the A-site¹⁷³. Pleuromutilins interact with domain V of the 23S rRNA inhibiting the correct binding of the tRNA into the P-site^{174,175}. Streptogramins consist of mixtures of type A and type B compounds which act synergistically¹⁷⁶. Type A streptogramins block tRNA binding to the A-site¹⁷⁷. Their presence induces a conformational change of the ribosome increasing the affinity for type B streptogramins drastically. The binding of type B streptogramin causes incorrect positioning of the P-site tRNA stimulating its dissociation¹⁷⁸. Viomycin binds the ribosome only after a tRNA has been accommodated into the A-site, it binds between helix 69 of the 23S rRNA and helix 44 of the 16S rRNA¹⁷⁹ blocking the translocation process catalyzed by EF-G forcing the ribosome to stay in a pre-translocational state¹⁸⁰. Blasticidin S binds to the P-site of the ribosome inducing a conformation of the P-site tRNA that inhibits peptide release via release factor RF1 and peptidyl transfer during elongation¹⁸¹.

Other translation inhibitors do not bind directly to the ribosome but block protein synthesis by the inhibition of other translation factors. Fusidic acid binds to EF-G on the ribosome after GTP

hydrolysis¹⁸². Fusidic acid does not allow EF-G to dissociate from the ribosome inhibiting elongation and ribosome recycling¹⁸³. EF-Tu is targeted by structurally versatile drugs¹⁸⁴. Kirromycin binding reduces the affinity of EF-Tu-GTP to amino acyl tRNAs whereas kirromycin-EF-Tu-GDP can form a stable complex with aa-tRNAs. Instead of dissociating after GTP hydrolysis, kirromycin-EF-Tu-GDP stays on the ribosome blocking the arrival of the next EF-Tu-GTP-aa-tRNA complex¹⁸⁵. Enacyloxin IIa works in a similar way forcing EF-Tu-GDP into an EF-Tu-GTP-like conformation preventing the dissociation of the factor after GTP hydrolysis^{186,187}. Pulvomycin and the cyclic thiopeptides amythiamicin and GE2270 A do not allow the formation of the ternary complex of EF-Tu-GTP with a amino acyl tRNA¹⁸⁸.

An indirect way to inhibit translation is the prevention of aminoacylation of tRNAs. Purpuromycin binds unspecifically to all tRNAs blocking the addition of the amino acid¹⁸⁹. Mupirocin (also named pseudomonic acid) and furanomycin on the other hand specifically inhibit the activity of isoleucyl-tRNA synthetase^{190,191}. Furanomycin is loaded onto isoleucine tRNA with a similar efficiency than isoleucine and has been shown to be incorporated into the peptide chain¹⁹², whereas mupirocin has been proposed to block the binding of ATP to isoleucyl-tRNA synthetase¹⁹³.

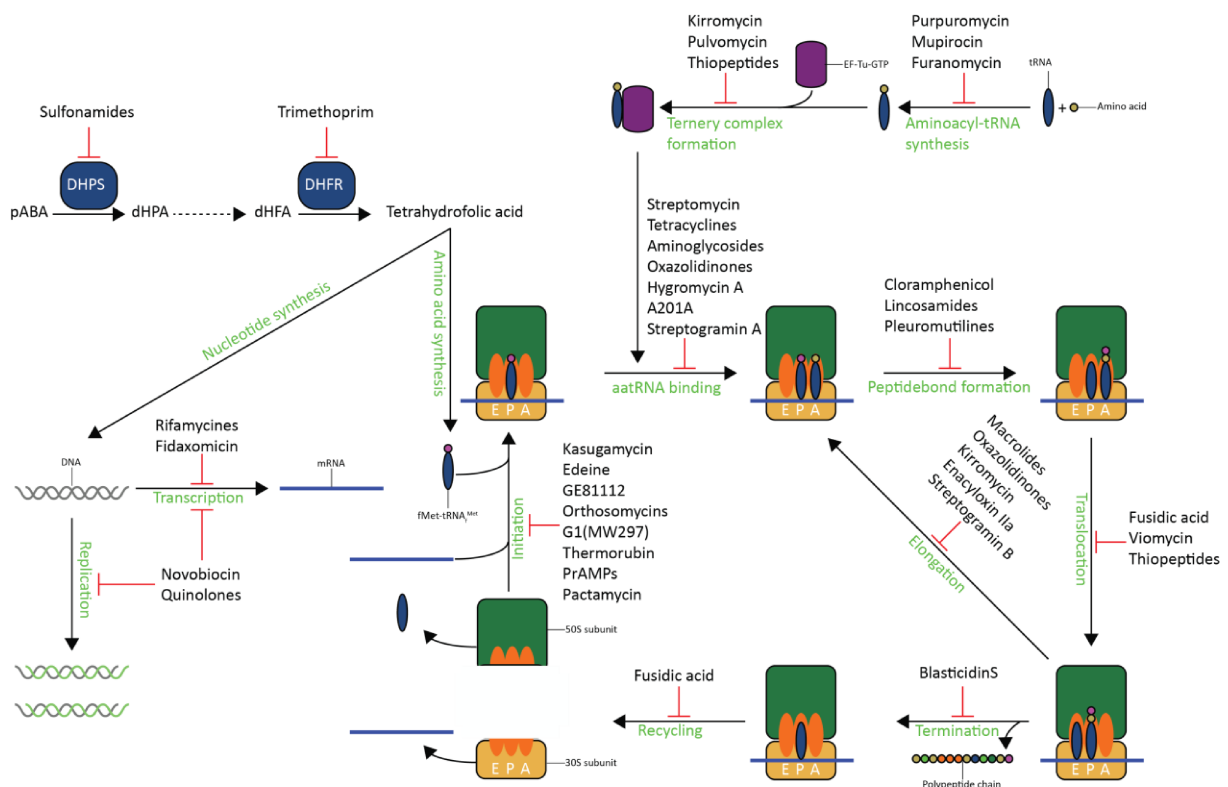


Figure 3: Schematic overview of antibiotics targeting intracellular processes. DHPS: dihydropteroate synthase; DHFR: dihydrofolate reductase; pABA: p-aminobenzoic acid; dHPA: dihydropteroic acid; dHFA: dihydrofolic acid.

1.3.2 Antibiotics targeting tetrahydrofolate synthesis

Tetrahydrofolate is an important cofactor for multiple biochemical pathways including the production of nucleotides and amino acids. Its synthesis is a multi-step process requiring multiple enzymes¹⁹⁴. Two classes of antibiotics target this reaction cascade¹⁹⁵. Sulfonamides inhibit the condensation of p-aminobenzoic acid (pABA) with 7,8-dihydropterin-pyrophosphate to form 7,8-dihydropteroate by acting as a substrate analog of the enzyme dihydropteroate synthetase^{196,197}. Trimethoprim on the other hand targets the reduction of dihydrofolate to tetrahydrofolate¹⁹⁸ catalyzed by the enzyme dihydrofolate reductase¹⁹⁸.

1.3.3 Antibiotics targeting transcription

Transcription of mRNA is targeted by various natural occurring antimicrobial compounds¹⁹⁹. But only two classes made it into clinical use so far. Rifamycines, like Rifampicin, bind to the β subunit of DNA-dependent RNA polymerase blocking the tunnel of the nascent RNA chain^{200,201}. Fidaxomicin (also named Lipiarmycin) binds to the sigma(70) subunit and the β subunit of DNA-dependent RNA polymerase disturbing the incorporation of the DNA into the polymerase^{202,203}.

1.3.4 Antibiotics targeting bacterial topoisomerases

Topoisomerases are enzymes that relax torsional tensions that appear during replication and transcription in the DNA double helix²⁰⁴. Two classes of antibiotics target this essential process. Coumarin drugs such as novobiocin target bacterial DNA gyrase. They block the ATPase activity of the enzyme by stabilizing the gyrase in a conformation with low affinity to ATP^{205,206}. Quinolones target bacteria gyrase or topoisomerase IV, depending on the applied quinolone and the target bacterium, either the first or the latter is targeted. Quinolone binding converts the enzymes into toxic enzymes that fragment the bacterial chromosome, therefore quinolones should be termed topoisomerase toxins rather than inhibitors which would block the reaction of the enzymes instead^{207,208}.

1.4 The bacterial cell envelope as a target of antibiotics

The bacterial cell envelope is the permeability barrier separating the inside of the cell from its environment²⁰⁹. However it is not only a physical border. Many important biochemical processes take place at or through the cell membrane. The synthesis of ATP is driven by a proton gradient between the cytosol and the periplasmic space²¹⁰. Import and export of nutrients and other substances is highly regulated through pores and active transporters. Therefore, the cell membrane(s) or the synthesis of cell-wall components are attractive targets for antibiotics. The composition of the cell enve-

lope of Gram-positive and Gram-negative bacteria differs drastically²¹¹. Gram-positive bacteria possess one cell membrane that is coated with a thick cell wall with teichoic acids spanning through its network. In contrast, Gram-negative bacteria possess two cell membranes with a thin cell wall between them. The outer membrane is further coated with a layer of lipopolysaccharides. The bacterial cell wall is composed of a network of peptidoglycan (murein) polymers to stabilize the shape of the cell against the intracellular pressure. In a peptidoglycan-monomer, one N-acetylglucosamin forms a $\beta(1\rightarrow4)$ glycosidic bond with one N-acetylmuramic acid. An amino acid chain is bound to the N-acetylmuramic acid which is used by transpeptidases (penicillin binding proteins) to crosslink single peptidoglycan chains to a three-dimensional network²¹². Depending on the bacteria, the amino acid chain is composed of four or five residues. In *E. coli*, its composition is L-alanine; D-glutamine; meso-diaminopimelic acid; D-alanine; D-alanine²¹³. The terminal D-alanine is removed in most chains of *E. coli* whereas other bacteria keep the fifth amino acid²¹⁴. In most species, D-Ala of position four covalently binds with its carboxyl group to the amino group of the opposing chain, either directly or using a small peptide as a bridge. However, variations in peptide composition, length and binding mode exist in some bacteria²¹³.

1.4.1 Antibiotics targeting cell wall synthesis

Cycloserine acts as a substrate analog of alanine and inhibits two enzymes: alanine racemase and D-alanine:D-alanine ligase^{215,216}. Fosfomycin blocks the enzyme MurA which is involved in the synthesis of N-acetylglucosamin²¹⁷. β -lactam antibiotics like penicillins, cephalosporines and carbapenemes prevent the cross-linking of peptidoglycan chains by acting as substrate analogs of acyl-D-alanyl-D-alanine blocking the binding site of acyl-D-alanyl-D-alanine on transpeptidases^{218–220}. Glycopeptides like Vancomycin or teicoplanin directly bind to the acyl-D-alanyl-D-alanine groups of peptidoglycan making them inaccessible for crosslinking^{221,222}. The cyclic polypeptide antibiotic bacitracin inhibits the dephosphorylation of bactoprenol pyrophosphate (C_{55} -isoprenyl pyrophosphate)^{223,224}. Bactoprenol pyrophosphate transports N-acetyl-glucosamine-N-acetylmuramic-acid monomers across the inner cell membrane of bacteria. Dephosphorylation is required for the reuse of the transporter²²⁵.

1.4.2 Antibiotics targeting bacterial membranes

Polymyxin B and E are cationic peptide antibiotics which integrate into both membranes of Gram-negative bacteria²²⁶, their main target is the lipid A component of the lipopolysaccharide permeabilizing the outer membrane^{227,228}, but polymyxins also form pores in the inner membrane at higher concentrations²²⁹. Lantibiotics are peptide antibiotics containing lanthionine- and methyllanthionine-

peptides. Nisin is the best-studied member of this family. It binds to lipid II blocking the transglycosylation reaction during the biogenesis of the cell wall and forms pores in the membrane resulting in lysis of the bacteria^{230,231}. The cyclic lipopeptide daptomycin interacts with the bacterial membrane with its lipid-tail requiring Ca^{2+} ions for its oligomerization in the membrane²³². It disturbs the correct conformation of the lipids resulting in pore formation and the loss of potassium which results in membrane depolarization²³³. Further, daptomycin has been reported to change the curvature of the

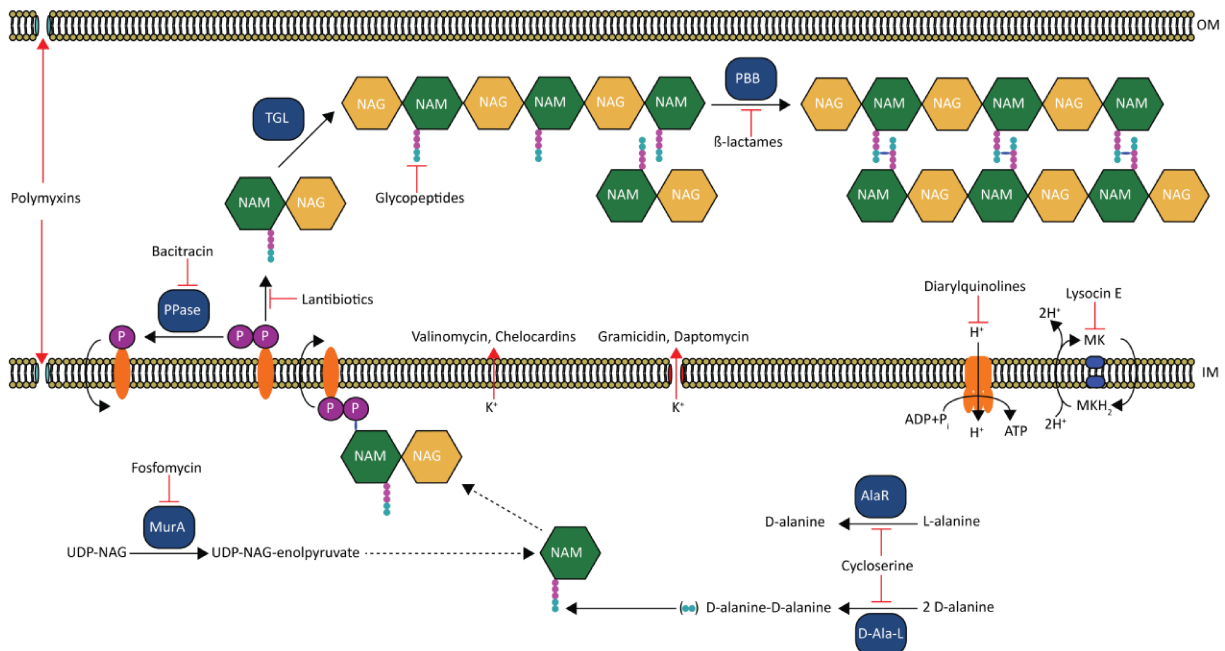


Figure 4: Schematic overview of antibiotics targeting the synthesis of cell wall components and bacterial cell membranes. OM: outer membrane; IM: inner membrane; Ppase: pyrophosphatase; NAG: N-acetylglucosamin; NAM: N-acetylmuramic acid; AlaR: alanine racemase; D-Ala-L: D-alanine ligase; MurA: UDP-N-acetylglucosamine enolpyruvyl transferase; PBB: penicillin binding protein; TGL: transglycosylase; MK: menaquinone.

membrane in a way that prevents the incorporation of important membrane proteins²³⁴. Gramicidins form membrane channels that allow the efflux of monovalent cations like potassium²³⁵. In contrast, carrier ionophores like the cyclic depsipeptide valinomycin destroy the membrane potential without the formation of pore shuttling the cations through the lipid bilayer^{236,237}. Lysocin E is another cyclic peptide antibiotic with a different mechanism of action. It specifically interacts with menaquinone (vitamin K2) which is involved in electron transport across bacterial membranes^{238,239}. However not all menaquinone-containing bacteria were reported to be susceptible to lysocin E²⁴⁰. The recently approved diarylquinoline bedaquiline (TMC207, R207910) is chemically similar to fluoroquinolones but does not target bacterial topoisomerases. Instead, it blocks the rotation of ATP synthase^{37,241}.

1.5 Antibiotic resistance mechanisms

Bacteria developed numerous resistance mechanisms against antibiotics as a response to the selection pressure created by antibiotic use (see Figure 5). Alexander Fleming already warned in his Noble Prize speech that the use of antibiotics can lead to the development of resistance mechanisms in 1945^{242,243}. Avoiding the contact with the drugs is an obvious way to escape their activity. Bacteria living inside of host cells are generally hard to reach for many drugs²⁴⁴. Other pathogens form biofilms which are impervious to many antibiotics^{245,246}. All antimicrobials targeting intracellular factors have to pass through the bacterial membrane. Hydrophobic antibiotics can diffuse directly through the membrane making it hard for the bacteria to counter but hydrophilic drugs must pass the membrane through a pore²⁴⁷ or use an active transporter^{248,249}. Mutations in membrane pores or the active transporters are common resistance mechanisms against such antibiotics²⁵⁰⁻²⁵².

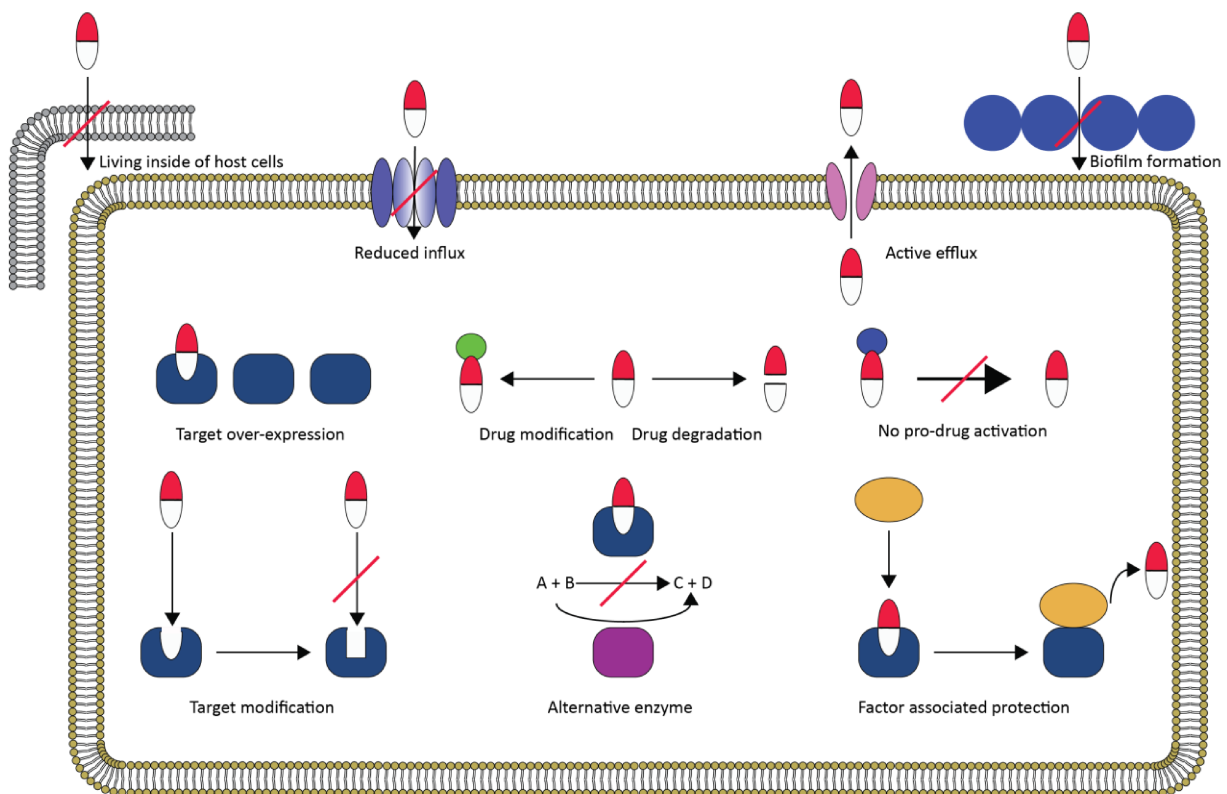


Figure 5: Schematic overview over antibiotic resistance mechanisms.

Once the antibiotic is within the cell, bacteria can try to extrude it again using efflux pumps. Several classes of pumps are known using ATP as energy source or act as symporters/antiporters²⁵³ to remove unwanted molecules like antibiotics from the inside of the cell²⁵⁴. Some of the efflux pumps are very specific for one class of antibiotics, others confer multidrug resistance by transporting several different classes of antibiotics which can be structurally and mechanistically very different²⁵⁵. Specialized factors can confer resistance to antibiotics either by removal of the drug from its binding

site^{256,257} or by conformational changes of the target protein that allows it to fulfil its purpose in the presence of the antibiotic²⁵⁸. If the antibiotic targets a specific molecule, bacteria can overcome its activity by overproduction of the target out-numbering the drug^{259,260}. If the antibiotic targets an enzyme, bacteria which are able to use an alternative enzyme for the same reaction can live in the presence of the drug^{261,262}. Another possibility for bacteria to escape antibiotic treatment lies in the modification of the drug target²⁶³. In case of protein binding antibiotics, changes in the amino acid sequence can confer resistance^{264,265}. To overcome antibiotics that bind to the ribosomal RNA, bacteria can change the rRNA sequence^{266,267} or modify the rRNA by methylation^{268,269} or other modifications²⁷⁰. At the same time, the lack of modifications which are present in wild-type ribosomes can also cause antibiotic resistance^{271,272}. Some antibiotics directly target essential elements of the bacterial membranes rather than the enzymes producing them. Chemical modifications of the components can confer resistance^{273,274}. Some antibiotics are administered as a pro-drug that has to be modified by cellular enzymes²⁷⁵, loss of function mutations in the enzyme can lead to resistant bacteria²⁷⁶. Some bacteria developed specialized enzymes that modify the chemical structure of the antibiotics instead of the antibiotic targets to prevent the correct interaction of the drug with its binding site^{202,277,278}. Other enzymes destroy antibiotics inside or outside of the bacterial cell before they can reach their targets^{10,279,280}.

1.5.1 Strategies to overcome antibiotic resistance

The most obvious way to treat an antibiotic resistant pathogen is the selection of alternative antibiotics that the pathogen cannot handle. If that is not possible, changes in the chemical structure of antibiotics can make them overcome resistance mechanisms²⁸¹⁻²⁸³, however the alterations must not decrease its efficiency or add side-effects. In case of intracellular pathogens which are hardly reachable for antibiotics, the addition of helper molecules can be used to shuttle the antibiotics into the infected cell²⁸⁴ or into bacterial cells which became resistant through a reduction of antibiotic uptake. Formation of biofilms can be overcome through the addition of anti-quorum sensing^{285,286}/biofilm dispersal agents²⁸⁷. If bacteria use an alternative enzyme to catalyze the reaction that is blocked by the antibiotic, another inhibitor for the alternative enzyme could restore the susceptibility of the pathogen. Resistance conferred by additional factors like efflux pumps, protection factors or drug- or target modifying enzymes can be countered by addition of inhibitors for these factors^{36,288,289}. Resistance through inactivation of pro-drug maturation might be countered by activation of an alternative maturation pathway²⁹⁰.

1.6 Tetracycline antibiotics represent an important class of translation inhibitors

The first tetracycline antibiotic was discovered as a natural product of *Streptomyces aureofaciens* and was named aureomycin but it is now designated as chlorotetracycline²⁹¹. Other isoforms including oxytetracycline and tetracycline were discovered soon after²⁸¹.

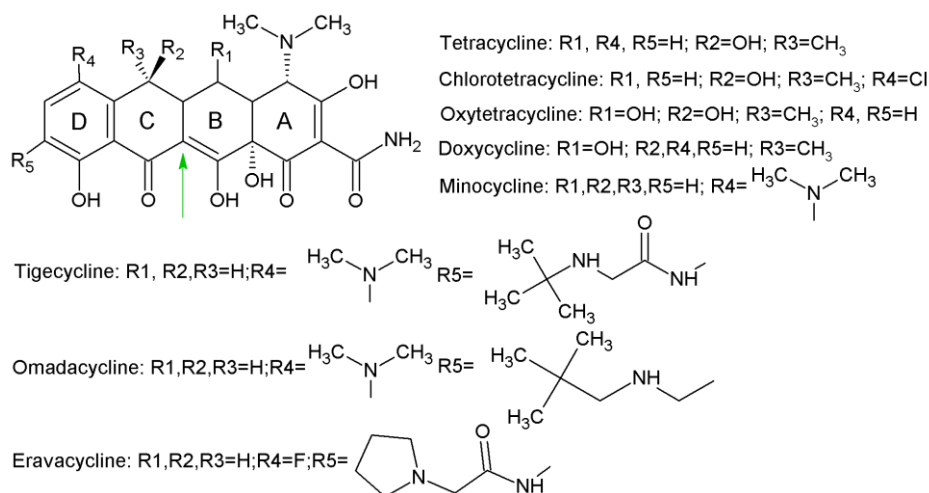


Figure 6: Chemical structures of tetracycline antibiotics^{281,292}. Position 11a, that is targeted by the TetX monooxygenase²⁸⁰ is marked with a green arrow.

The semi synthetic derivatives doxycycline and minocycline with improved antimicrobial activity were developed on the basis of the natural products²⁹³. The 9-t-butylglycylamido derivative of minocycline has been shown to overcome most resistance mechanisms against tetracyclines²⁹⁴ and is marketed as Tigacyl® as the first third generation tetracycline²⁹⁵. More third generation tetracyclines are in development at the moment. Omadacycline and eravacycline have already completed phase III clinical studies^{296–299}. From the beginning on, tetracyclines were used as broad spectrum antibiotics with activity against both Gram-positive and Gram-negative pathogens³⁰⁰. With a marked share of 1.6 billion dollars in 2009, tetracyclines belong to the most important classes of antimicrobial drug for human and animal medicine⁵⁸. Oral application is possible due to their good solubility in water³⁰¹. Tetracyclines exist in two forms: in a polar environment (i.e. water) the zwitterionic form dominates explaining its good solubility in water; in order to pass the unpolar cell membrane, tetracyclines adopt the non-ionized free base form³⁰². Tetracyclines are bacteriostatic antibiotics inhibiting the synthesis of proteins by binding to the small ribosomal subunit. The drugs D ring forms stacking interactions with base C1054 of helix 34 of the 16S rRNA. Hydrogen bonds are formed with A965 and G966 of helix 31; C1195 and U1196 of helix34. A magnesium ion is further complexed by G1197 and G1198 of helix 34 forming a salt bridge to rings C and B of tetracycline^{169,303}. Binding of tetracycline competes with binding of amino-acyl-tRNA to the ribosomal A-site preventing the accommodation of amino-acyl tRNAs into the A-site^{304,305}. Due to the long use of tetracyclines, numerous resistance

mechanisms have been developed. Specific efflux pumps like the proton antiporter TetA transport the drug from the cytosol to the periplasm³⁰⁶ but not through the outer membrane³⁰⁷. In a study analyzing avian *E. coli*, TetA was by far the most prevalent tetracycline resistance gene³⁰⁸. But unspecific multidrug resistance efflux pumps are also able to confer high level resistance against this class of antimicrobial²⁵⁵. Further, ribosome protection proteins have developed removing the drug from its ribosomal binding site³⁰⁹. Monooxygenases like TetX specifically attack carbon atom C11a (see Figure 6) of all known tetracyclines³¹⁰. Mutations in the ribosomal binding site of tetracyclines are rare but have been found to confer resistance in *Propionibacterium acnes*³¹¹ and *Helicobacter pylori*^{312,313}. Tetracyclines are also used for treatment³¹⁴ and prophylaxis³¹⁵ against the malaria germ *Plasmodium falciparum* where they target mitochondrial ribosomes³¹⁶ and *Plasmodium's* dihydroorotate dehydrogenase, an enzyme involved in the synthesis of pyrimidine³¹⁷. Atypical tetracyclines like chelocardin represent another branch of the tetracycline family³¹⁸. Chelocardin is produced by *Nocardia sulphurea* but its primary target is not the ribosome. It does interfere with protein synthesis but it mainly targets the bacterial membrane resulting in membrane depolarization but not in the formation of pores^{319,320}. Only the lipophilic but not the zwitterionic conformation of chelocardin has been reported, which offers an explanation for its accumulation in the cell membrane and its mode of action^{319,321}. Beside general side effects observed for most orally uptaken antibiotics, tetracyclines are phototoxic^{322,323}, under influence of visible light, the drugs are converted into toxic photoproducts.

1.7 The antibiotic thermorubin has a similar chemical structure than tetracyclines but uses a different mechanism

Thermorubin has been identified as a product of *Thermoactinomyces antibioticus*³²⁴. It is an orange-red product crystallizing in fine radiating needles soluble in dioxane, pyridine, tetrahydrofuran, dimethylformamide and dimethylsulfoxide but hardly in methanol, ethanol and acetone and insoluble in water. Thermorubin is highly active against Gram-positive bacteria, less active against Gram-negative bacteria and almost inactive against yeast and filamentous fungi³²⁴. It showed low toxicity with an LD₅₀ of 300 mg/kg in mice by intraperitoneal injection³²⁵. The chemical structure was determined using X-ray diffraction (see Figure 7)³²⁶. Thermorubin selectively inhibits translation with little effect on DNA replication and no effect on transcription^{327,328}. The drug has been shown to interact with both subunits of the ribosome³²⁹. With dissociation constants of 1.9×10^{-6} and 1.4×10^{-6} for the 30S and 50S subunit respectively. But it binds the mature 70S ribosome far more efficiently

1.8.1 Thiopeptides are antimicrobial peptides made of highly modified amino acids

Thiopeptides are natural products of various bacteria, the first member of this class of antibiotics, thiostrepton, has been isolated from *Streptomyces azureus*^{333–335}. It is highly active against Gram-positive bacteria including MRSA³³⁶. Besides their antimicrobial mode of action, thiopeptides have also been found to have signalling functions inducing biofilm formation³³⁷. Thiopeptides are characterized by a central six-folded ring containing a nitrogen which is part of a macrocycle of different sizes with numerous highly modified amino acids (see Figure 8)^{336,338}. Therefore, a precursor peptide has to be produced by the ribosome which is modified posttranslationally by enzymes^{339,340}.

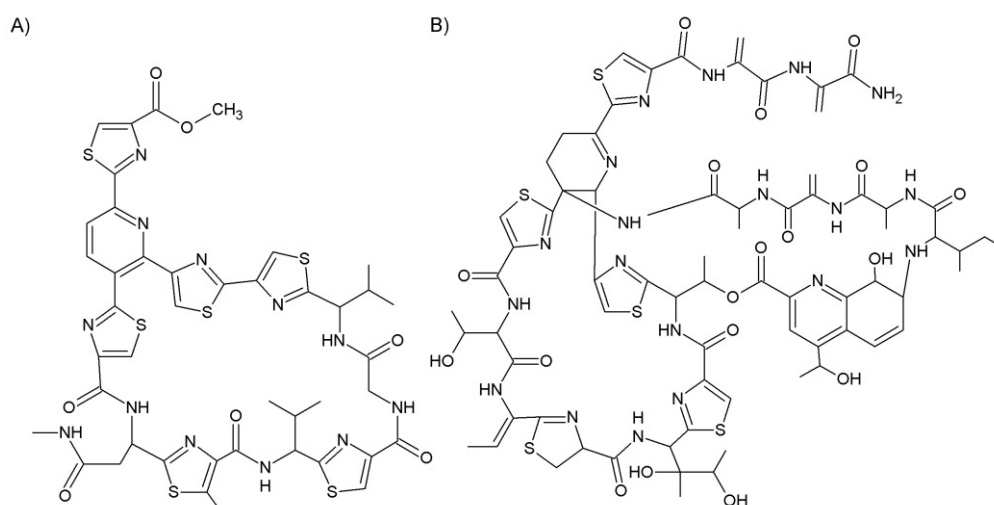


Figure 8: Chemical structures of A) amythiamicin D³⁴¹ and B) thiostrepton³³⁴.

Thiopeptides inhibit translation but two different modes of action have been found. Thiopeptides like amythiamicin or GE2270 A inhibit the formation of the ternary complex EF-Tu-GTP-aa-tRNA^{342,343}. The structure of GE2270 A bound to *E. coli* EF-Tu shows that the antibiotic binds to the second domain of EF-Tu-GDP contacting residues 215-230; 256-264 and 273-277. The binding site of the antibiotic overlaps with the binding sites of the guanine in the GTP but not in the GDP conformation and with the aminoacyl-tRNA binding site on EF-Tu³⁴⁴. On the other hand, other thiopeptides like thiostrepton inhibit translation by direct binding to the ribosomal large subunit. Thiostrepton interacts with helices 43 and 44 of the 23S rRNA and ribosomal protein L11³⁴⁵. Its presence prevent GTP hydrolysis of EF-G that is necessary for translocation³⁴⁶.

1.8.2 Antimicrobial peptides are part of the innate immune system of animals

The innate immune system is the first line of defense against pathogens that managed to invade a host after penetrating physical barriers like skin or bark. Antimicrobial peptides (AMPs) represent

an important part of the innate immune system in plants, vertebrate and invertebrate animals³⁴⁷. Several classes of AMPs have been identified including anionic peptides and cationic peptides, they can be linear or form α -helices, in many cases the active antimicrobial peptide is a fragment of a larger precursor protein³⁴⁸. Most AMPs kill bacteria by integrating into the membrane forming pores but some also possess intracellular targets.

Cathelicidins are an important class of small, cationic peptides found in many species³⁴⁹. They are constructed of an N-terminal cathelin domain of about 100 amino acids and the C-terminal active peptide³⁵⁰. The sequences of the active peptides are very variable including proline/arginine rich peptides, helical peptides and disulfide-linked peptides. Cathelicidins are expressed as pre-pro-peptides³⁵¹. The pre-region serves as signal sequence guiding the cathelicidin to a granule where the pre-region is cleaved of and the cathelicidin is stored as an inactive pro-peptide. After contact with a pathogen, the pro-region is cleaved by a protease to release the active mature peptide only when it is needed. In humans, one member of this class has been identified. The full length 19 kDa protein hCAP-18 was found in granules of neutrophil³⁵². It is encoded by a 1963 bp gene containing four exons. The first three coding for a signal sequence and the cathelin region and the fourth coding for the mature peptide of 37 amino acids in length³⁵³. As this peptide starts with two leucines, it was named LL-37³⁵⁴. Like most cathelicidins, LL-37 kills bacteria by permeabilizing the outer and inner cell membrane of bacteria³⁵⁵. But another group of cathelicidins, the family of proline-rich antimicrobial peptides (PrAMPs) must have a different mechanism of action since PrAMPs have been reported to inhibit the growth of bacteria at concentrations far lower than necessary for lysis³⁵⁶⁻³⁵⁸. Although PrAMPs share a similar cathelin domain with pore forming AMPs, their active C-terminal peptide is totally different containing a high percentage of proline and arginine residues (see Figure 9).



Figure 9: Amino acid alignment of bovine cathelicidin Bac7 and human cathelicidin hCAP18. The pre-signal sequence is marked in green, the pro-cathelin sequence is marked in blue, the active antimicrobial peptide sequence is marked in orange. Pre- and pro- sequences are very similar although the active antimicrobial peptide fragments are totally different in sequence and length.

PrAMPs were identified in numerous mammals including cow (Bac5, Bac7); pig (PR-39, prophenin, PRP-SP-B); sheep (Bac5, Bac6, Bac7, Bac11); goat (Bac3.4, Bac5, Bac7) and buffalo (Bac7)³⁵⁹. Insects also produce PrAMPs although non-vertebrate PrAMPs do not contain a cathelin-like domain at their N-terminus. Analysis of the genes for insect PrAMPs showed that the genes contain a single pre-pro region followed by multiple copies of the PrAMP which are separated by conserved linker regions³⁶⁰⁻³⁶². In some species multiple genes have been found coding for different isoforms of the PrAMP. The first insect PrAMPs has been identified in the European honey bee *Apis mellifera* and named apidaecin³⁶³. Similar peptides have been isolated from numerous other insects like the fire bug *Pyrrhocoris apterus* (pyrrhocoricin)³⁶⁴; the green shield bug *Palomena prasina* (metalnikowins)³⁶⁰; the milkweed bug *Oncopeltus fasciatus* (oncocin)³⁶⁵; the bean bug *Riptortus pedestris* (riptocin); and the fruit fly *Drosophila melanogaster* (drosocin)³⁶⁶.



Figure 10: Amino acid alignment of AMPs used in this thesis. A) Mammalian PrAMPs align well to each other but differ in length. B) The insect derived PrAMPs metalnikowin I; Onc112 and pyrrhocoricin are almost identical. C) Natural occurring apidaecins Api1A and Api1AL only differ by their C-terminal amino acid whereas semi-synthetic derivatives Api88 and Api137 contain a modified C- and a modified N-terminus; gu: N, N, N',N'tetramethylguanidino; O: L-ornithine D) The other arthropod AMPs have a different amino acid composition. Drosocin's O-glycosylated threonine 11 is marked in green.

In the genome of *Drosophila melanogaster*, the pro-region of pre-pro-drosocin lies behind the mature peptide, it has further to be O-glycosylated on threonine 11 to gain its activity³⁶⁶. Penaeidins found in the hemolymph of the shrimp *Penaeus vannamei* contain a proline-rich N-terminal region and a cysteine-rich C-terminal region³⁶⁷.

As PrAMPs target an intracellular process, they have to cross the bacterial membrane. The inner membrane protein SbmA has been identified to be the major transporter for the PrAMP Bac7 in

*E. coli*³⁶⁸. Mutations in *SbmA* or knock-out of this gene produced strains with strongly reduced susceptibility for PrAMPs³⁶⁹ but the uptake of the peptides was not fully stopped. The inner membrane protein MdtM was identified to be an alternative importer for PrAMPs²⁵². Once inside the cell, PrAMPs were first reported to inhibit the chaperone DnaK³⁷⁰. However the finding, that a *dnaK* knockout strain is as susceptible as wild type ones questions this mechanism of action³⁷¹. In parallel, the process of translation was found to be a target for PrAMPs.

Besides mammals and insects, amphibians have been shown to possess numerous antimicrobial peptides. Magainins belong to the best-studied members of amphibious AMPs. They have been shown to be active against bacteria and fungi³⁷² and protozoa by accumulating in the cell membrane creating pores^{373,374}. On the other hand magainin 2 hardly target eukaryotic cell membranes. Differences in the composition of the membranes like the presence of cholesterol, the lack of trans-membrane potential and the absence of acidic phospholipids in the eukaryotic membrane were reported to be the reason for magainins selectivity³⁷⁵. Numerous magainin derivatives were produced and tested for their antibacterial potential. Pexiganan (MSI-78) turned out to be one of the most promising candidate containing high activity against both Gram-positive and Gram-negative bacteria^{376,377}.

The use of antimicrobial peptides as an alternative to traditional antibiotics has been considered since many years but further research is required to characterize their mode of action and their clinical potential.

Cumulative thesis: summary of published results

Paper 1: Amythiamicin D and related thiopeptides as inhibitors of the bacterial elongation factor EF-Tu: Modification of the amino acid at carbon atom C2 of ring C dramatically influences activity

Stefan Gross, [Fabian Nguyen](#), Matthias Bierschenk, Daniel Sohmen, Thomas Menzel, Iris Antes, Daniel N. Wilson and Thorsten Bach

ChemMedChem 2013; 8(12):1954-1962

Amythiamicins belong to the class of thiopeptide antibiotics and have been isolated from *Amycolatopsis sp.* MI481-42F4³⁷⁸. They show significant structural similarities with GE2270 A, an antibiotic that has been shown to inhibit translation by binding to elongation factor Tu, preventing the formation of the ternary complex³⁴². Amythiamicin D and three semi-synthetic derivatives were synthesized and tested for their antimicrobial activity. *De novo* synthesis of amythiamicin D and the three derivatives 3a, 3b and 3c was based on the synthesis strategy for the structurally related thiopeptide GE2270 A³⁷⁹, with 2,6-dibromo-3-iodopyridine as basis. Derivative 3a contains a hydroxymethyl group in (S)-configuration similar to the α -hydroxybenzyl group of GE2270 A at carbon atom C2 of ring C; derivative 3b contains the same hydroxymethyl group of 3a in (R)-configuration. Derivative 3c carries a benzyloxymethyl group instead of the hydroxymethyl group in (S)-configuration at carbon atom C2 of ring C. Derivative 3a was able to inhibit the growth of Gram-positive but not of Gram-negative bacteria which has already been shown for parental amythiamicins³⁷⁸, whereas derivatives 3b and 3c were not able to inhibit bacterial growth. To determine whether the lack of activity against Gram-negative bacteria is caused by inefficient uptake of amythiamicin into the cells, an *in vitro* translation system was created on the basis of an S12 extract from *E. coli* BL21 DE3 cells³⁸⁰. Amythiamicin D and derivative 3a inhibited the expression of the reporter protein Firefly luciferase whereas derivatives 3b and 3c were completely inactive at all tested concentrations. The high similarity of the chemical structure of amythiamicin D to EF-Tu inhibitor GE2270 A suggests a similar mode of action. The *in vitro* translation system was partly blocked by 5 μ M of derivative 3a, addition of external EF-Tu completely re-established translation in a concentration dependent manner. Further, the EF-Tu mutation G257S has been shown to confer

resistance to GE2270 A³⁸¹. To test the effect of this mutation on amythiamicins, the *in vitro* translation system was completely blocked by 30 μ M of derivative 3a. Addition of up to 5.8 μ M EF-Tu G257S partly re-established translation in a concentration dependent manner. The crystal structure of GE2270 A bound to EF-Tu GDPNP identified its binding site to be at the interface of domains I and II where the 3'-end of the amino-acyl tRNA would bind¹⁸⁸. 1H-NMR spectra and molecular dynamics simulations of the amythiamicin derivatives showed a similar conformation in solution for the natural amythiamicin D and derivatives 3a and 3c but not for 3b that was found in the crystal structure for GE2270 A. Further simulation showed that binding of derivatives 3b and 3c to the GE2270 A binding site is not stable explaining the lack of activity of these derivatives *in vivo* and *in vitro*.

Taken together, this study proves the value of *de novo* synthesis to gain derivatives of naturally occurring thiopeptide antibiotics with improved antibacterial activity. The study further shows that amythiamicins target EF-Tu in the same way that was reported for GE2270 A.

Paper 2: Tetracycline antibiotics and resistance mechanisms

Fabian Nguyen, Agata L. Starosta, Stefan Arenz, Daniel Sohmen, Alexandra Dönhöfer and Daniel N. Wilson

Biol. Chem. 2014; 395(5): 559-575

The first members of the tetracycline family of antibiotics, chlorotetracycline and oxytetracycline, were discovered in the late 1940's and early 1950's as natural products of *Streptomyces spp.*²⁹¹, their chemical structure was identified a few years later³⁸²⁻³⁸⁴. Tetracyclines are composed of a naphthacene core with four rings termed DCBA, containing various side groups. Semi-synthetic derivatives have been developed with improved antimicrobial activity and reduced susceptibility for resistance mechanisms^{293,385}. Tetracyclines inhibit bacterial translation by binding to the ribosome, with the primary binding site being located at the base of the head of the small subunit³⁸⁶. The hydrophilic surface of tetracycline interacts with helix 34 of the 16S rRNA by forming hydrogen bonds to the phosphate backbone of nucleotides C1054, G1197 and G1198 of helix 34^{156,169,387,388}. A further Mg²⁺ mediated interaction between the phosphate backbone of G966 of helix 31 has been proposed. The primary binding site overlaps with the anticodon loop of A-site tRNA inhibiting the accommodation of aminoacyl-tRNA into the A-site³⁸⁸⁻³⁹⁰. Next to innate resistance through inefficient uptake or multidrug efflux pumps³⁹¹, bacteria developed four specific resistance mechanisms against tetracyclines. Tetracycline-specific efflux pumps are present in Gram-negative and Gram-positive bacteria³⁹², most of them belong to the class of proton antiporters like TetA^{306,307,393}. These efflux

pumps are very effective against naturally occurring tetracyclines but are less successful in conferring resistance against semi-synthetic derivatives^{394,395}. Another common resistance mechanism is factor-assisted protection. EF-G homologs, called ribosome protection proteins remove the drug from the ribosome using GTP hydrolysis as energy source^{256,309,396,397}. Loop III of domain IV of the ribosome protection protein directly overlaps with the drug-binding site removing the drug from the ribosome^{256,257}. Mutations in the tetracycline-binding site represent another way for bacteria to become resistant to this class of antibiotics. The resistance mutation G1058C inside of helix 34 of the 16S rRNA has been found in clinical isolates of *Propionibacterium acnes*³¹¹. In addition, the triple mutation A965U/G966U/A967C has been shown to confer resistance to tetracyclines in *Helicobacter pylori* isolates^{398,399}. The fourth mechanism to confer tetracycline resistance is the modification of the drug by the enzymes TetX or Tet37^{310,400}. These monooxygenases consume NADPH and O₂ to hydroxylate position C11a inside the naphthalene core resulting in further disintegration of the drug^{280,401}. Third generation tetracyclines overcome resistance conferred by most efflux pumps and all ribosome protection proteins but pathogens mutating their rRNA or expressing the TetX monooxygenase are still able to grow in the presence of the latest tetracyclines.

In perspective, tetracyclines will still be one of the most important classes of antibiotics in the future, with new derivatives in development and clinical trials.

Paper 3: Cryo-EM structure of the tetracycline resistance protein TetM in complex with a translating ribosome at 3.9 Å resolution

Stefan Arenz, [Fabian Nguyen](#), Roland Beckmann and Daniel N. Wilson

Proc Natl Acad Sci USA. 2015; 112(17): 5401-5406

Ribosome protection proteins (RPPs) are a common resistance determinant against tetracycline antibiotics. 12 different classes have been identified in different bacteria with TetO of *Campylobacter jejuni* and TetM of *Enterococcus faecalis* being the best characterized RPPs^{256,257,309,396,396}. They share a high sequence homology to each other (approximately 85% sequence similarity) and to elongation factor G (approximately 35% sequence similarity^{256,257}). A cryo-EM structure with an average resolution of 3.9 Å of TetM-GDPCP bound to the *E. coli* ribosome has been created on the basis of ErmCL-stalled ribosomes. Three loops protrude from the remote end of domain IV of TetM. Previous publications suggested that tyrosine 506 and tyrosine 507 are the key amino acids of loop III of domain IV as their mutation to alanine inactivate RPPs^{256,257,402}. But the higher resolution of the

structure of this publication shows that proline 509 at the tip of loop III of TetM stacks against C1054 of helix 34 of the 16S rRNA, which is part of the primary binding site of tetracycline antibiotics, pushing the drug from the ribosome. Instead of directly interacting with the drug, tyrosine 507 links loop III with loop I while tyrosine 506 hydrogen bonds with glycine 467 of loop II and with C1051 of helix 34 of the 16S rRNA stabilizing the correct conformation of loop III. Another conserved residue of all RPPs is phenylalanine 516. The structure shows F516 to be located in the hydrophobic core of loop III. *E. coli* BL21 DE3 cells were transformed with wild-type or mutant versions of TetM. The wild-type RPP raised the concentration necessary to inhibit the bacterial growth to 50% (MIC₅₀) to 10 µg/ml compared to 0.6 µg/ml for bacteria without TetM. Mutation F516A created an intermediate phenotype with a MIC₅₀ of 3 µg/ml. The mutation of F516 to negatively charged aspartate completely inactivated TetM underlining the importance of the hydrophobic character of F516 for the conformation of loop III. Tryptophan 442 within loop I further stabilized the conformation of loop III by interaction with valine 510. Its mutation to alanine in combination with S508A or P509A inactivated TetM while these mutations had little effect by themselves²⁵⁶.

Taken together, this study provides a more detailed view on the action of ribosome protection proteins identifying proline 509 as the residue pushing tetracyclines from their binding sites whereas tyrosines 506 and 507 are important to stabilize the conformation of loop III rather than to overlap with the drug binding site.

Paper 4: The proline-rich antimicrobial peptide Onc112 inhibits translation by blocking and destabilizing the initiation complex

A. Carolin Seefeldt, Fabian Nguyen, Stéphanie Antunes, Natacha Pérébaskine, Michael Graf, Stefan Arenz, K. Kishore Inampudi, Céline Douat, Gilles Guichard, Daniel N. Wilson and C. Axel Innis

Nat Struct Mol Biol. 2015; 22(6):470-5

Onc112 is a semi-synthetic derivative of naturally occurring proline-rich antimicrobial peptide (PrAMP) oncocin, which is part of the immune system of the milkweed bug *Oncopeltus fasciatus*^{365,403}. The crystal structure of the PrAMP bound to the ribosome of *Thermus thermophilus* has been solved at a resolution of 3.0 Å. Onc112 binds within the ribosomal exit tunnel in a reverse orientation compared to a nascent chain, positioning its N-terminal residues near the peptidyl transferase centre whereas its C-terminal amino acids extend into the ribosomal exit tunnel. The 10 N-terminal residues showed numerous interactions with nucleotides of the 23S rRNA. Asp2 of Onc112 interacts with G2553 blocking a base pairing that normally occurs between G2553 and C75 of

the A-site tRNA. Toe-print analysis showed that Onc112 allows the formation of the 70S initiation complex but does not allow the accommodation of the tRNA into the A-site. The structure further suggests that the formyl-methionine group of fMet-initiator tRNA would clash with Tyr6 and Leu7 of the PrAMP destabilizing the initiation complex. Ribosomes were incubated together with a dicistronic mRNA in the presence or absence of Onc112. An analytical sucrose gradient experiment showed a smaller increase in disome formation in the presence of Onc112 compared to a control experiment without antibiotic, than in the presence of erythromycin or thiostrepton, confirming that the formation of initiation complexes were destabilized by Onc112. Truncated versions of the PrAMP missing the last seven or nine C-terminal amino acids were produced and tested *in vivo* for their ability to inhibit bacterial growth and *in vitro* to test their ability to inhibit the translation of the reporter protein Firefly luciferase in a translation reaction based on a cell lysate of *E. coli*. *In vivo*, both derivatives lacking C-terminal residues were inactive at concentrations of up to 160 μM , whereas the full length (19mer) Onc112 already inhibited bacterial growth at 25 μM . In the *in vitro* system, 0.8 μM of full-length Onc112 were enough to reduce the translation activity to 50% (IC_{50}) whereas 5 μM of the derivative lacking the seven C-terminal amino acids were necessary. The derivative lacking the nine C-terminal amino acids showed an IC_{50} of almost 100 μM . Other proline-rich antimicrobial peptides have been shown to enter the bacterial cell using the transporter SbmA³⁶⁸. To determine whether that is also the case for Onc112, *E. coli* BW25113 wild-type cells and BW25113 cells lacking the gene for SbmA were grown in the presence of different concentrations of the PrAMP. The growth of BW25113 wild-type cells was reduced to 10% by 40 $\mu\text{g/ml}$ of Onc112 whereas the growth of the SbmA knockout strain showed almost no inhibition at 80 μM of Onc112.

In conclusion, this study identified the binding site of Onc112 and showed that the N-terminal residues are responsible for interaction with the ribosome whereas the C-terminal residues are important for cellular uptake of this peptide antibiotic.

Paper 5: Structure of the mammalian antimicrobial peptide Bac7(1-16) bound within the exit tunnel of a bacterial ribosome

A. Carolin Seefeldt, Michael Graf, Natacha Pérébasquine, [Fabian Nguyen](#), Stefan Arenz, Mario Mardirossian, Macro Scocchi, Daniel N. Wilson and C. Axel Innis

Nucleic Acids Res. 2016 44(5):2429-38

Bactenecin-7 (Bac7) is a proline-rich antimicrobial peptide which is part of the innate immune system of *Bos taurus*⁴⁰⁴. The crystal structure of a shortened Bac7 fragment containing its 16 N-terminal

residues, Bac7(1-16), bound to the ribosome of *Thermus thermophilus* was solved. Insect derived PrAMPs metalnikowin I and pyrrococin were also co-crystallized with *Thermus thermophilus* ribosomes. Bac7, metalnikowin I and pyrrococin bind in the ribosomal exit tunnel in an inverted orientation compared to nascent chains with the N-terminus pointing towards the peptidyl transferase centre and the C-terminus protruding into the tunnel. Bac7's N-terminal amino acids formed hydrogen bonds and stacking interactions with 23S rRNA nucleotides. Arg6 of Bac7 is clamped between Arg2 and Arg4 creating a positively charged block removing two Mg²⁺ ions from a groove formed by 23S rRNA bases anchoring the peptide to the ribosome. A competition assay in which ¹⁴C-labelled erythromycin was bound to ribosomes showed that the first five N-terminal amino acids of Bac7 are vital to push the macrolide away from the ribosome. To further characterize the effect of truncations of Bac7, Bac7 fragments containing residues 1-16; 1-35 and 5-35 were titrated into an *in vitro* translation system based on an *E. coli* cell extract. Production of the reporter protein Firefly luciferase was reduced to 50% by Bac7 (1-16) and Bac7 (1-35) at a concentration of 1 μM whereas Bac7 (5-35) showed an IC₅₀ of 10 μM. Bac7 (1-35) also inhibited translation in an eukaryotic *in vitro* system on the basis of a rabbit reticulocyte cell extract. But the IC₅₀ of 2.5 μM was about 2.5 fold higher than compared to the bacterial system. The mechanism of translation inhibition was further analyzed performing toe-print analysis. It showed, that Bac7 (1-16) and Bac7 (1-35) allow the formation of the 70S initiation complex but block elongation; partly at 1 μM and completely at 10 μM; Bac7 (5-35) on the other hand was only able to block the progression of translation at 100 μM.

Taken together, this study identified the binding mode of Bac7(1-16), it illustrated the importance of the N-terminal four residues, showed the higher susceptibility of bacterial compared to eukaryotic ribosomes to the drug and the mechanism of action of this peptide antibiotic.

Paper 6: Proline-rich antimicrobial peptides targeting protein synthesis

Michael Graf, Mario Mardirossian, Fabian Nguyen, A. Carolin Seefeldt, Gilles Guichard, Marco Scocchi, C. Axel Innis and Daniel N. Wilson

Nat Prod Rep. 2017 34(7):702-711

The first PrAMP, apidaecin, was discovered in the honey bee *Apis mellifera* in 1980³⁶³. Proline-rich antimicrobial peptides have since been found to be parts of the innate immune system of numerous insects and mammals^{364,365,405-409}. In insects, the genes for PrAMPs contain multiple copies of the peptides linked by inactivating spacer sequences^{361,362}. In some cases, different isoforms of the

mature PrAMPs are present in one species^{360,361}. In mammals, PrAMPs are synthesized as inactive pre-pro-peptide precursors by immature myeloid cells⁴¹⁰. *Bos Taurus* produces two PrAMPs, Bac5 and Bac7, both of which contain a 29 amino acids (aa) pre-signal sequence that target the peptide precursor into large granules of neutrophils where the pre-signal sequence is cleaved off. The 101 aa pro-sequence is not removed until pathogens are recognized. After recognition of a pathogen, the granules can then either release the pro-peptides to the outside of the cell or fuse with phagosomes that have internalized a pathogen⁴¹¹. The serine protease elastase cleaves the pro-sequence from the pro-peptide to mature it into the active PrAMP⁴¹². PrAMPs, unlike other antimicrobial peptides, do not primarily target the bacterial membrane but have to be internalized to reach their intracellular target^{356,356}. The inner membrane protein SbmA has been shown to be the most important factor for the uptake of PrAMPs³⁶⁸, its deletion results in a phenotype with high resistance against these peptides. However another inner membrane protein, MdtM, is also able to import PrAMPs²⁵². The Hsp70 family chaperone DnaK was originally proposed to be the binding partner for PrAMPs³⁷⁰. But further studies have shown that a DnaK knockout strain is as susceptible to the PrAMPs as the parental strain containing the chaperone. Instead, the ribosome has been identified to be the primary target for PrAMPs as ribosomal protein L10 was found to co-precipitate with biotin labelled apidaecin derivative Api88⁴¹³. Structures of PrAMPs bound to bacterial ribosomes show that the peptides bind in the ribosomal exit tunnel with reversed orientation compared to nascent chains⁴¹⁴⁻⁴¹⁶. Multiple hydrogen bonds and stacking interactions are formed by the backbone and by side-chains of the PrAMPs with the 23S rRNA. Further, PrAMPs reach into the binding site of the A-site tRNA. The binding of PrAMPs does not prevent the association of amino-acyl tRNA to the A-site but rather inhibit correct accommodation.

In perspective, proline-rich antimicrobial peptides offer a promising alternative to common antibiotics. The understanding of the mechanism of action of PrAMPs offers the opportunity to develop derivatives with increased stability and antimicrobial activity.

3. Unpublished results

3.1 Mutations within loop III of domain IV of TetM underline the importance of conserved tyrosines 506 and 507

Besides the mutations that were published in papers 2 and 3 of the cumulative report, further mutations of loop III of domain IV of TetM were created to analyze the role of the highly conserved tyrosines at positions 506 and 507. These tyrosines are conserved in 9 out of 12 known ribosome protection proteins³⁹⁹. However Tet of *Streptomyces lividans* contains FF and TetB(P) isolated in *Clostridium perfringens* contains FA instead of the two tyrosines. On the other hand OtrA of the oxytetracycline producer *Streptomyces rimosus* contains the amino acids VR in the corresponding positions⁴¹⁷. To determine the consequences of the different amino acid compositions on the ability to confer resistance, TetM mutants replacing the tyrosines with the other amino acids were introduced into TetM by site directed mutagenesis (see Materials and Methods 5.6). *E. coli* BL21 DE3 cells were transformed with TetM wild-type or one of the mutants to determine the ability of the RPPs to confer resistance (see Materials and Methods 5.7 and Figure 11).

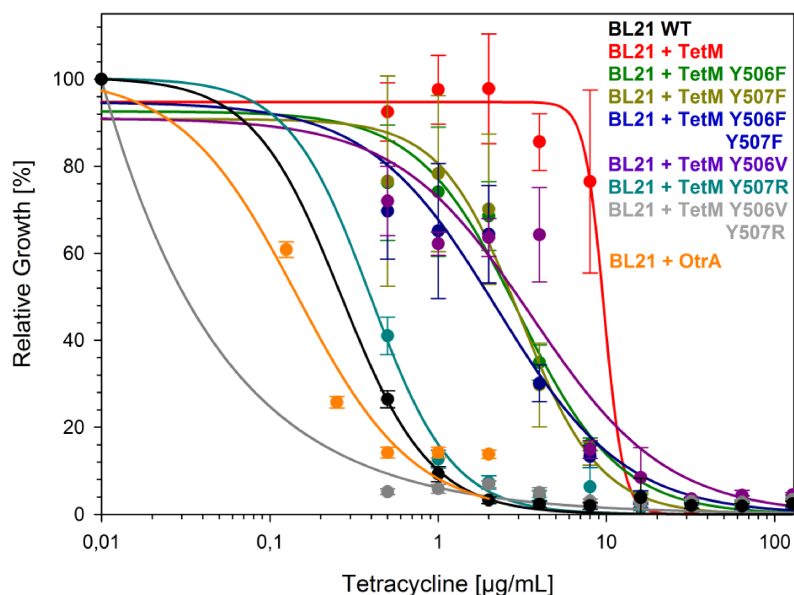


Figure 11: Effect of loop III mutations on TetM's ability to confer resistance against tetracycline. Relative growth of *E. coli* BL21 DE3 without TetM (black), expressing TetM wild-type (red) or expressing TetM Y506F (green), TetM Y507F (dark yellow), TetM Y506F Y507F (blue), TetM Y506V (violet), TetM Y507R (cyan) or TetM Y506V Y507R (gray) or OtrA (orange) in the presence of increasing concentrations of tetracycline. The growth of the cultures was determined by OD₆₀₀ measurement after 20 h of incubation. The growth of the strains in the absence of tetracycline was defined as 100%. The error bars represent the standard deviation of the mean for three independent experiments.

The mutants containing tyrosine to phenylalanine and the Y507R mutation were less efficient than wild-type TetM but still conferred significant resistance. On the other hand the TetM mutant containing the Y506V or the Y506V/Y507R mutations were not able to grow in higher concentrations of tetracycline than the negative control *E. coli* BL21 DE3 without TetM. Further, OtrA did not confer resistance when transformed into *E. coli*. However the gene coding for OtrA was cloned out of cDNA (see Materials and Methods 5.5), its amino acid sequence differed from the originally published version (see Appendix A). Its loop III composition is not VRSPV like in the original publication but FASPV.

3.2 The G' subdomain is crucial for the GTPase activity of elongation factor G

During translation elongation, EF-G helps the ribosome to translocate the mRNA by one codon, the A-site tRNA to move to the P-site and the P-site bound tRNA to move to the E-site. Release of inorganic phosphate after GTP hydrolysis leads to a conformational change that allows EF-G to leave the ribosome again^{99,418}. The binding of EF-G to the ribosome includes the interaction with EF-G's G' domain with ribosomal proteins L7/L12⁴¹⁹. It has been reported that the binding of negatively charged amino acids on EF-G with positively charged amino acids on L7/L12 is required for the release of inorganic phosphate after the hydrolysis of the GTP bound to EF-G^{153,183,420}. Ribosomal protection proteins like TetM are highly homologous to transcription factor EF-G^{256,421}. They also contain a G' domain, which has a similar amino acid composition like the G' domain of EF-G (see Figure 12).

```

EF-G  181  GVVDLVKMKAINWNDADQGVTFEYEDIPADMVELANEWHQNLIE SAAEASEELMEKYIIGG
TetM  163  -----NVCVTNFTSESEQW-----DVIIFGNDDLLEKYMSG

```

Figure 12: Amino acid alignment of parts of the G' domains of TetM and EF-G. Residues in red were reported to affect GTPase activity in EF-G and were mutated in TetM⁴¹⁹.

Mutation of the corresponding residues in TetM's G' domain were constructed to compare their effect on GTPase activity of TetM to the published effects on EF-G.

3.3 Effect of G' subdomain mutation of TetM on tetracycline resistance

All G' domain mutants were created using site directed mutagenesis (see Materials and Methods 5.6) of TetM wild-type on the plasmid pET-46 LIC. *E. coli* BL21 DE3 was transformed with plasmids

expressing TetM or TetM G' domain mutants (see Material and Methods 5.3) and MIC values were determined in the presence of tetracycline (see Materials and Methods 5.7 and Figure 13).

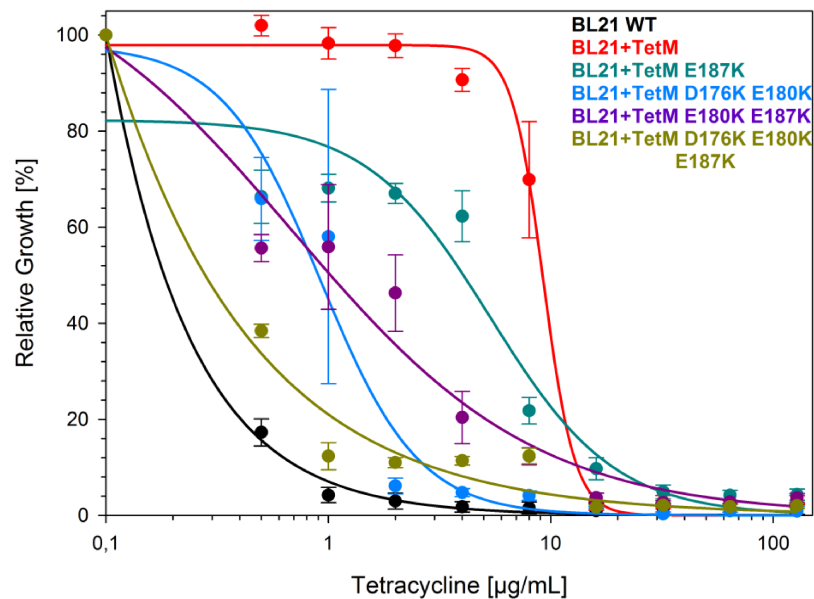


Figure 13: Effect of G' domain mutations on TetM's ability to confer resistance against tetracycline. Relative growth of *E. coli* BL21 DE3 without TetM (black), expressing TetM wild-type (red) or expressing TetM with one (green), two (blue and violet) or three (dark yellow) mutations within the G' domain of the RPP from the plasmid pET-46 Ek/LIC in the presence of increasing concentrations of tetracycline. The growth of the cultures was determined by OD₆₀₀ measurement after 20 h of incubation. The growth of the strains in the absence of tetracycline was defined as 100%. The error bars represent the standard deviation of the mean for three independent experiments.

Mutation of the G' domain showed a strong effect on the ability of TetM to confer resistance to tetracycline. Mutation of one or two of the negatively charged residues to positively charged lysine yielded an intermediate phenotype, whereas mutation of all three negatively charged amino acids resulted in a phenotype that was almost as susceptible to tetracycline as the BL21 DE3 strain lacking TetM.

3.4 Purification of TetM G' domain mutants

To verify the *in vivo* results, TetM G' domain mutants were purified to quantify their GTPase activity *in vitro*. TetM wild-type on the plasmid pET-46 LIC was transformed into BL21 DE3 and grown over night. 16 mL of the overnight culture were used to inoculate 1.6 L of fresh LB medium (see Buffers and Media 6.1). Cells were grown until an OD₆₀₀ of 0.3 was reached. The expression of the protein was started by the addition of IPTG. After 2 hours of expression time, the cells were harvested and lysed. The lysate was centrifuged and Ni²⁺-NTA beads were added to the supernatant to perform an affinity chromatography. After affinity chromatography the eluate was further purified over a gel

filtration column (see Materials and Methods 5.9). An SDS (see Materials and Methods 5.10) PAGE analysis displayed the purified protein with a calculated size of 72.4 kDa (see Figure 14).

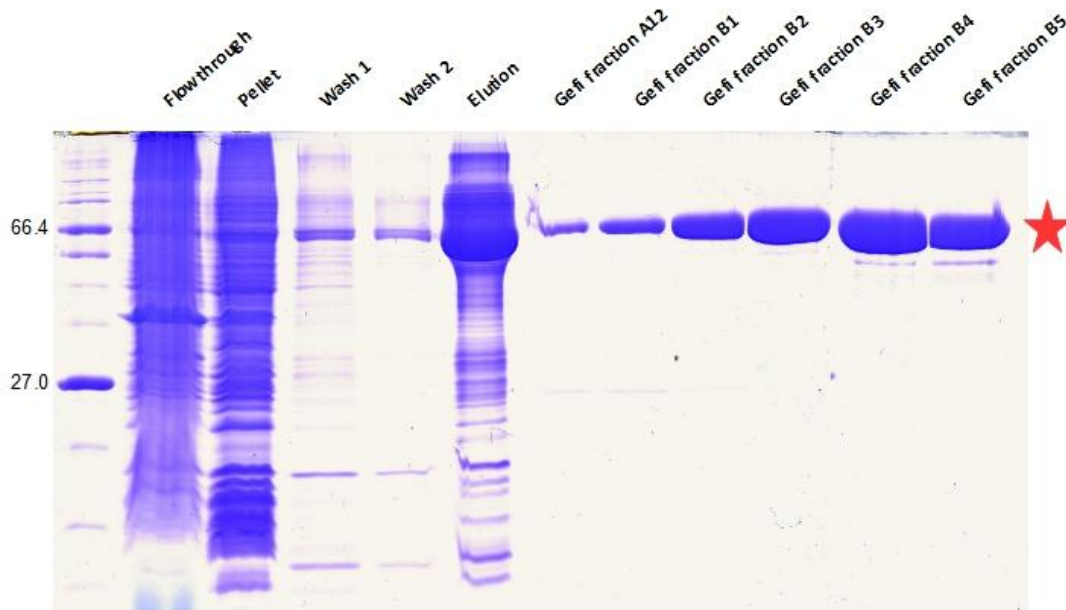


Figure 14: SDS-PAGE analysis of TetM purification stained with Coomassie blue. The protein of interest is marked with a red star. Gefi: gel filtration.

The purification procedure was repeated for all TetM G' domain mutants. The gel filtration fractions containing pure protein were pooled and concentrated by the use of a centrifugal filter. The concentration of the obtained proteins was determined via absorbance measurement (see Materials and Methods 5.9 and Table 1).

Table 1: Concentrations of TetM G' domain mutants after Ni²⁺-affinity chromatography, gel filtration and concentration.

	Concentration [mg/mL]	Concentration [μM]
TetM wild-type	1.423	19.18
TetM E187K	0.32	4.312
TetM D176KE180K	2.57	34.63
TetM E180KE187K	4.84	65.23
TetM D176KE180KE187K	3.45	46.49

The proteins were aliquoted and frozen in liquid nitrogen to be stored at -80°C in gel filtration buffer (see Buffers and Media 6.2).

3.5 Purification of *E. coli* ribosomes

E. coli ribosomes were purified from a 1.6 L culture of *E. coli* BL21 DE3. Cells were grown in LB medium to an OD₆₀₀ of 1.8, lysed and the ribosomes were isolated via multiple centrifugation steps (see Materials and Methods 5.11). The 70S peak was isolated after sucrose gradient centrifugation (see Figure 15).

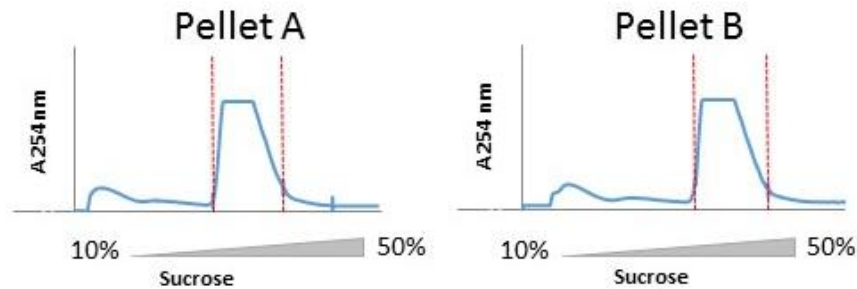


Figure 15: Absorption profiles at 254nm of ribosome purifications after gradient centrifugation. Fractions between dashed red lines were pelleted and solved in sucrose gradient buffer B (see Buffers and Media 6.3) to be stored at -80°C.

Pelleting of the 70S peak resulted in two pellets which were dissolved in 1000 μ L of sucrose gradient buffer B each (see Buffers and Media 6.3). Concentration determination measuring OD₂₆₀ (with 1 OD₂₆₀ = 24 pmol of 70S⁴²²) gave a concentration of 4.3 μ M for pellet A and 4.1 μ M for pellet B.

3.6 Effect of G' domain mutation on TetM's GTPase activity

To analyze the effect of mutations in the G' domain of TetM, phosphatase assays were performed quantifying the free phosphate that is released when GTP is hydrolyzed to GDP by TetM or TetM mutants (see Materials and Methods 5.12). A standard curve was created resulting in the following equation:

$$C(\text{PO}_4^{3-}) = 50.676 \times \text{OD}_{620} - 3.4355$$

The GTPase activity of 60 nM of TetM and TetM mutants, 30 nM of Ribosomes and 20 μ M of GTP was calculated as GTP molecules hydrolyzed per ribosome (see Figure 16).

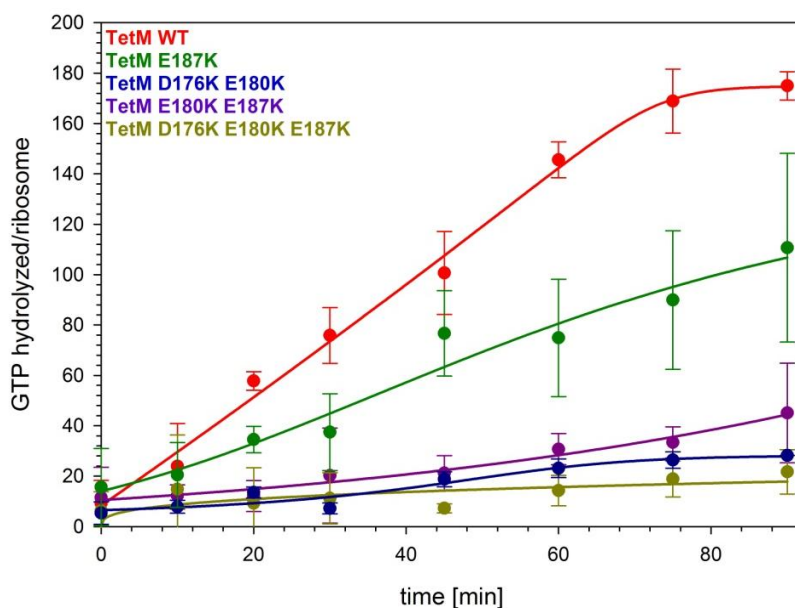


Figure 16: Effect of TetM G' domain mutations on the GTPase activity of the protein. GTP molecules per ribosome hydrolyzed over 90 min by TetM wild-type (red), TetM E187K (green), TetM D176K E180K (blue), TetM E180K E187K (dark pink) and TetM D176K E180K E187K (dark yellow). GTPase activity was quantified by the absorption at 620 nm of the complex formed between free phosphate and the dye Malachite Green. The error bars represent the standard deviation of the mean for three independent experiments.

The assay shows a strong decrease of GTPase activity from wild-type over single mutant to double- and triple mutants of TetM which were almost inactive. The rate of GTP hydrolysis appears rather slow with about 2 GTP molecules hydrolyzed per ribosome and minute. This is significantly slower than published in an earlier study that also investigated TetM's GTPase activity and reported a hydrolysis rate of about 5 GTP molecules per ribosome and minute⁴²³. A possible explanation for this finding is the fact that the TetM mutants were first purified one after another and stored at -80°C before they were analyzed simultaneously. The freezing and thawing resulted in visible aggregation of the protein. The precipitates were pelleted and the concentrations of the remaining TetM were determined before they were used in the assay. Still, the hydrolysis rates were lower than in a control experiment performed with freshly purified TetM wild-type which had similar rates than in the cited publication.

3.7 Tigecycline resistance selection

Ribosomal protection proteins like TetM do not confer resistance to third generation tetracycline antibiotics such as tigecycline⁴²⁴. To find out whether changes in the TetM amino acid sequence could create a mutant that does confer resistance to third generation tetracyclines, two serial dilutions were performed. Wild-type TetM on the plasmid pET-46 LIC was transformed into *E. coli* BL21 DE3, the strain was grown overnight in the presence of 0.1 µg/mL of tigecycline, which is below

the MIC of 0.25 µg/mL. On the second day the tigecycline concentration was raised by 0.1 µg/mL and the strain was grown overnight in the presence of 0.2 µg/mL tigecycline in fresh medium. This process was repeated until the MIC of the strain for tigecycline reached 7.0 µg/mL (see Figure 17). 60 days were necessary to reach 7.0 µg/mL and the resulting strain was termed WT60. An intermediate strain after 30 days, termed WT30, was also kept for analysis.

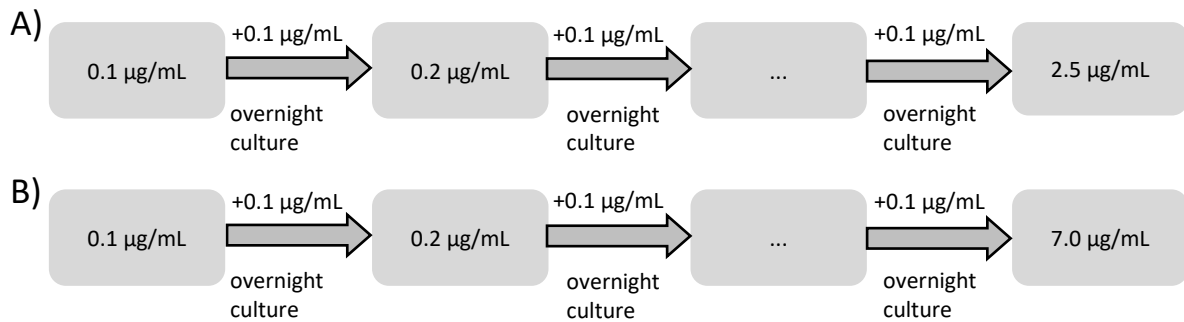


Figure 17: Serial dilution scheme of tigecycline resistance selection. Starting point were sub-MIC 0.1 µg/mL, tigecycline concentrations were raised in 0.1 µg/mL steps. A) *E. coli* BL21 DE3 transformed with TetM-RM could be selected to a final concentration of 2.5 µg/mL tigecycline. B) *E. coli* BL21 DE3 transformed with TetM-WT could be selected to a final concentration of 7.0 µg/mL tigecycline.

A second serial dilution was performed with *E. coli* BL21 DE3 that contained TetM with random mutations within loop III on the plasmid pET-46 LIC. To create the mutations, random primer (see list of primers No. 10) were created. These primers contain overlaps with the sequence before (forward primer) or after (reverse primer) loop III with a random sequence within the loop. The primers were used to perform MEGAWHOP (see Materials and Methods 5.5) with TetM wild-type on the plasmid pET-46 LIC as template. The resulting plasmids were transformed into *E. coli* BL21 DE3 and the serial dilution was performed identical to the WT-strain. The final strain after 60 days, termed RM60 reached a MIC of 2.5 µg/mL of tigecycline. As for the WT-strain, an intermediate strain after 30 days was kept for analysis.

After 60 days, both the WT60 and the RM60 strains showed significant resistance to tigecycline (see Figure 18).

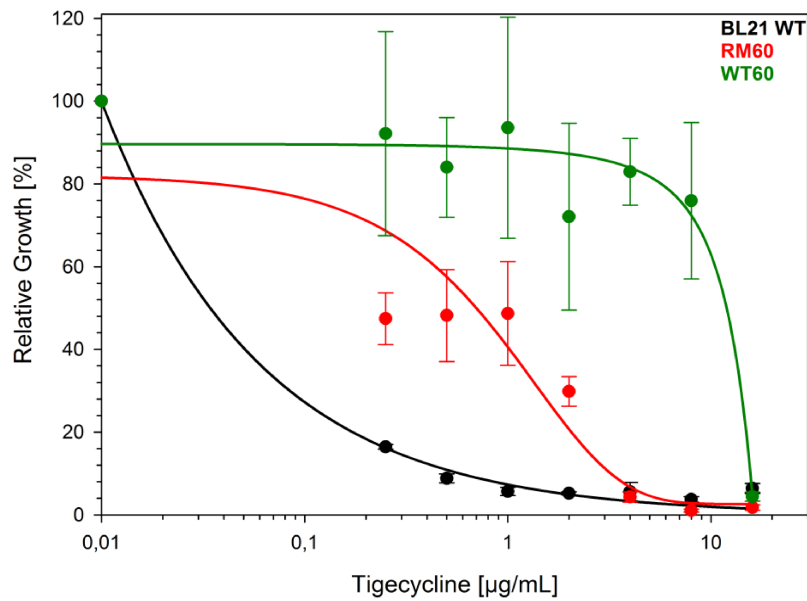


Figure 18: Quantification of tigecycline resistance of the RM60 and WT60 strains. Relative growth of *E. coli* BL21 DE3 wild-type (black), RM60 (red) and WT60 (green) in the presence of increasing concentrations of tigecycline. The growth of the cultures was determined by OD₆₀₀ measurement after 20 h of incubation. The growth of the strains in the absence of tigecycline was defined as 100%. The error bars of the RM60 and WT60 curves represent the standard deviation of the mean for three independent experiments, the control experiment with *E. coli* BL21 DE3 wild-type was only performed once.

Plasmids containing TetM were isolated from both serial dilution strains after 60 days. The plasmids of the TetM wild-type-strain were sequenced but no mutations in the ribosomal protection protein were detected. Consistently, the plasmids of the TetM-RM strain were transformed into wild-type *E. coli* BL21 DE3 cells and they were re-analyzed for tigecycline resistance but no increase in MIC could be detected. Therefore, mutations in TetM cannot explain the resistance phenotype of the WT60 and RM60 strains, suggesting that other genomic mutations may have arisen. Therefore, the whole genomes of the final WT60 and RM60 strains as well as the intermediate WT30 and RM30 strains were sequenced (see Materials and Methods 5.20). Numerous mutations compared to the parental *E. coli* BL21 DE3 strain were observed (see Table 2).

Table 2: Mutations found in tigecycline serial dilution strains WT60 and RM60.

Wild-type TetM strain day 30 (WT30)		
Genomic mutation	Gene	Changes on amino acid level
T455131G	Transcriptional repressor <i>acrR</i>	L109V
Duplication of 10bp 1568697-1568706	Transcriptional repressor <i>marR</i>	Disrupts coding sequence
G1665930A	Global transcription regulator <i>slyA</i>	Q31STOP
C3314272G	Ribosomal protein S10	V57L
C4097383A	RNA polymerase subunit beta	T1328N
G4239373T	Sensory histidine kinase	R237S
Wild-type TetM strain day 60 (WT60): one additional mutation		
Genomic mutation	Gene	Changes on amino acid level
Deletion of 7bp 3809872-3809878	F ₀ F ₁ ATP synthase subunit C	Disrupts coding sequence
Random-mutation TetM strain day 30 (RM30)		
Genomic mutation	Gene	Changes on amino acid level
G452464C	Multidrug efflux protein <i>acrB</i>	T329S
G455077T	Transcriptional repressor <i>acrR</i>	E91STOP
Deletion of 4bp 1568517-1568520	Transcriptional repressor <i>marR</i>	Disrupts coding sequence
Deletion of 1371bp 1664544-1665914	Anhydro-N-acetylmuramic acid kinase; Outer membrane lipoprotein <i>slyB</i> ; Global transcriptional regulator <i>slyA</i>	Disrupts coding sequence of three genes
Integration of an IS-element 2447410-2447418	GDP-mannose pyrophosphatase <i>nudK</i>	Disrupts coding sequence
C4097383T	RNA polymerase beta subunit	T1328I
Deletion of 28 bp 4240622-4240649	Component of the <i>basR-basS</i> system	Disrupts coding sequence
Random-mutation TetM strain day 60 (RM60): no additional mutations		

Mutations were found in the regulation of the expression of the efflux pump AcrAB, which belongs to the class of resistance-nodulation-cell division efflux systems. The complex is composed of the secondary transporter AcrB that integrates into the inner membrane as a trimer and the periplasmic AcrA-hexamer that links AcrB to the outer membrane pore TolC⁴²⁵. The AcrAB-TolC complex confers resistance to a wide variety of antibiotics, dyes and detergents, such as tetracyclines, chloramphenicol, fluoroquinolones, β -lactams, macrolides, fusidic acid, ethidium bromide, crystal violet, sodium dodecyl sulfate and bile acids⁴²⁶. The expression level of AcrAB is negatively regulated

by the repressor protein AcrR⁴²⁷. The gene of *acrR* lies upstream of the *acrA* and *acrB* genes, the AcrR repressor directly interacts with the *acr* promoter located between *acrR* and *acrAB* (see Figure 18). Besides its repressor, the AcrAB pump also possesses activator proteins. In *E. coli*, the general transcriptional activators SoxS, Rob and MarA enhance the expression of AcrAB. MarA itself is regulated by the *mar* regulon⁴²⁸. In other bacteria like *Klebsiella pneumoniae*, the RamA global transcriptional activator increases the expression of AcrAB^{429,430}. The expression of RamA is repressed by RamR in a similar way that AcrR represses AcrAB production (see Figure 19).

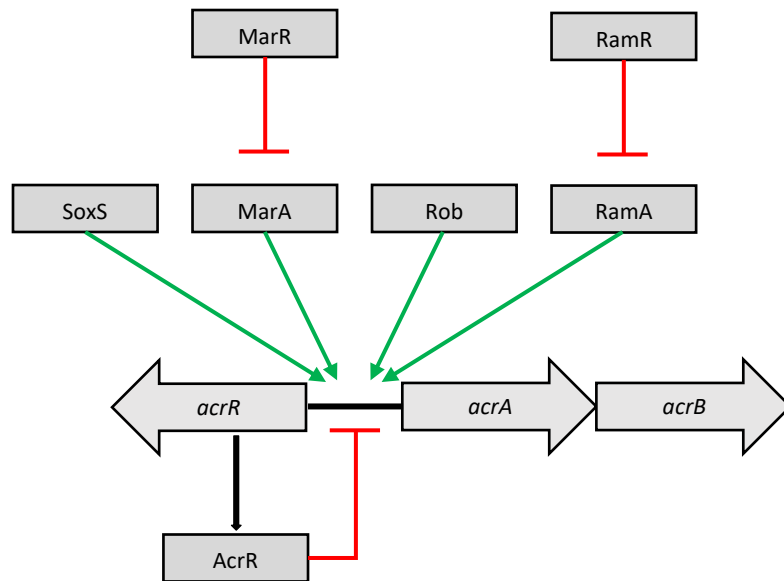


Figure 19: Overview of expression regulation of the AcrAB efflux pump^{429,431}. AcrR is the product of the *acrR* gene (black arrow) and represses the expression of AcrAB (red inhibition line). SoxS, MarA and Rob activate AcrAB expression in *E. coli* (green arrow); RamA activates AcrAB expression in *Klebsiella pneumoniae*. MarA and RamA production is repressed by MarR and RamR in a similar way than AcrAB by AcrR.

Over-expression of AcrAB has been reported previously to confer tigecycline resistance and was therefore not further analyzed⁴³². On the other hand, mutations within AcrB itself have not been reported before. The point mutation G452464C causes an amino acid exchange in AcrB: T329S. To test the effect of the mutation found in strains WT30 and WT60; AcrB was cloned into pQE-70 using MEGAWHOP (see Materials and Methods 5.5). The AcrB T329S mutation was introduced by site directed mutagenesis (see Materials and Methods 5.6). The AcrB knock-out strain BW25113 Δ *acrB* was transformed with *acrB* wild-type or *acrB* T329S and the effect on tigecycline resistance was analyzed in a growth assay (see Materials and Methods 5.7 and Figure 20). No difference between BW25113 Δ *acrB* transformed with AcrB wild-type or AcrB T329S is visible.

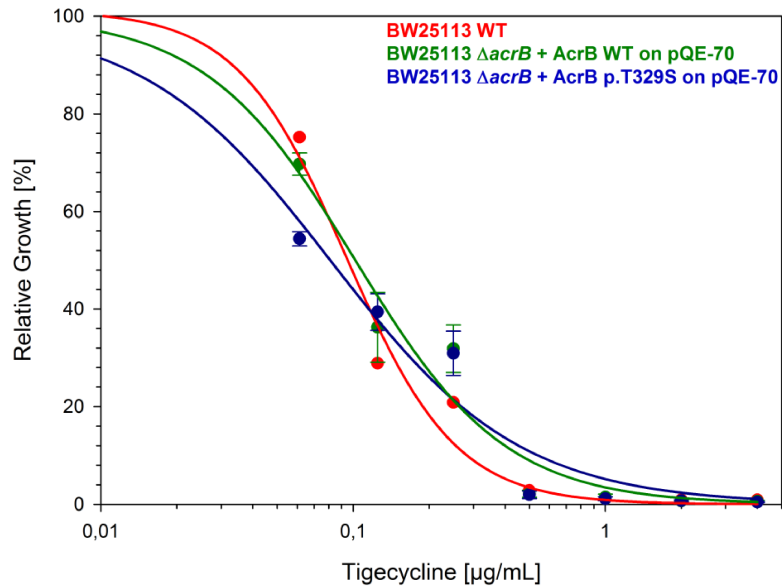


Figure 20: Effect of the AcrB T329S mutation on TetM's ability to confer resistance to tigecycline. Relative growth of *E. coli* BW25113 wild-type (red), BW25113 Δ acrB + AcrB wild-type on the plasmid pQE-70 (green) and BW25113 Δ acrB + AcrBT329S on pQE-70 (blue). The growth of the cultures was determined by OD₆₀₀ measurement after 20 h of incubation. The growth of the strains in the absence of tigecycline was defined as 100%. The error bars represent the standard deviation of the mean for three independent experiments.

In both the WT and RM serial dilution strains the transcriptional regulator SlyA is deactivated. In WT30 the mutation C1665928T converts glutamine 31 to an internal stop codon. In RM30 a deletion of 1371 nucleotides disrupts the coding sequence of three genes including the sequence coding for the N-terminal 29 amino acids of SlyA and the complete sequence of *slyB*. SlyA belongs to the MarR family of transcription regulation proteins⁴³³, which negatively regulate the expression of various resistance genes⁴²⁸. To validate the effect that the deactivations of *slyA* and *slyB* have on tigecycline, *E. coli* single-gene knock-out strains⁴³⁴ BW25113 Δ slyA and BW25113 Δ slyB were tested for tigecycline resistance (see Figure 21).

The deletion of *slyA* and *slyB* only had a small effect on tigecycline susceptibility. In the presence of 0.5 µg/mL of tigecycline, BW25113 Δ slyA and BW25113 Δ slyB still showed moderate growth, while the parental BW25113 strain could not grow anymore.

A further point mutation in the *rpsJ* gene coding for ribosomal protein S10 has been identified in the genome of WT30. The mutation results in the amino acid exchange valine 57 to leucine. This mutation in ribosomal protein S10 has already been described in the literature to confer resistance to tetracycline in *Neisseria gonorrhoeae*⁴³⁵ and to tigecycline in *Klebsiella pneumoniae*⁴³⁶ and was not further analyzed.

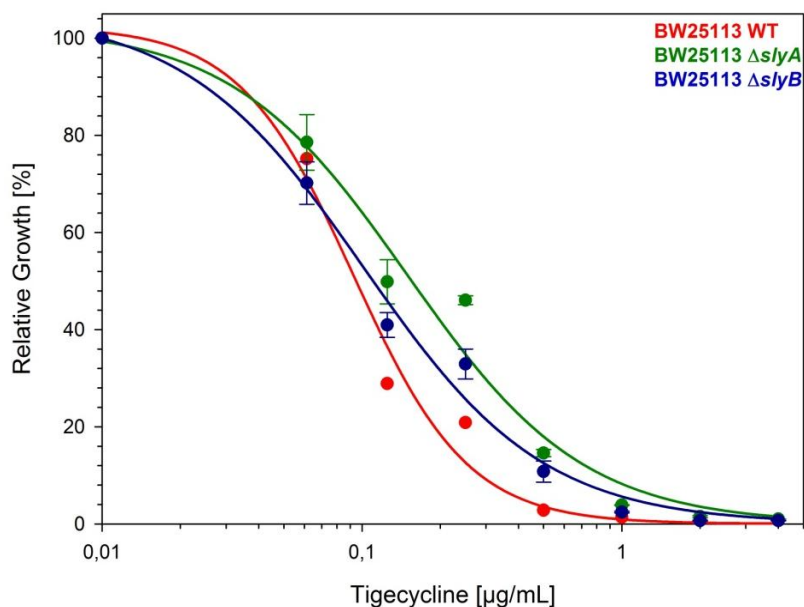


Figure 21: Effect of *slyA* or *slyB* knockout on tigecycline susceptibility. Relative growth of *E. coli* BW25113 wild-type (red), BW25113 $\Delta slyA$ (green) and BW25113 $\Delta slyB$ (blue). The growth of the cultures was determined by OD₆₀₀ measurement after 20 h of incubation. The growth of the strains in the absence of tigecycline was defined as 100%. The error bars represent the standard deviation of the mean for three independent experiments.

The selection strain WT60 was also tested for multi-resistance against other antibiotics. WT60 showed higher resistance against first- and second-generation tetracycline antibiotics compared with the parental BL21 DE3 strain expressing wild-type TetM (see Table 3).

Table 3: MIC₉₀ values of *E. coli* BL21 DE3; *E. coli* BL21 DE3+TetM WT and selection strain WT60 against tetracycline antibiotics.

	BL21 DE3 WT	BL21 + TetM WT	WT60
Tetracycline	0.5 µg/mL	8 µg/mL	>128 µg/mL
Oxytetracycline	0.5 µg/mL	5 µg/mL	>128 µg/mL
Chlorotetracycline	0.5 µg/mL	7 µg/mL	>128 µg/mL
Tigecycline	0.2 µg/mL	0.2 µg/mL	15 µg/mL

MIC₉₀ values of WT60 were further determined against non-tetracycline antibiotics (see Table 4) to see whether the strain developed a multi-resistant phenotype.

Table 4: MIC₉₀ values of WT60 strain against antibiotics unrelated to tetracycline compared with *E. coli* BL21 DE3 wild type strain.

	BL21 DE3 WT	WT60
Chloramphenicol	4 µg/mL	32 µg/mL
Kanamycin	2 µg/mL	2µg/mL
Norfloxacin	0,5 µg/mL	2 µg/mL
Rifampicin	6.25 µg/mL	25 µg/mL

Chloramphenicol and norfloxacin and rifampicin have already been reported to be substrates of the AcrAB efflux pump complex^{255,437,438}, confirming the over-expression of AcrAB in the WT60 strain. On the other hand no difference in kanamycin susceptibility is visible in the serial dilution strain which has not been reported to be a substrate for the efflux pump complex.

3.8 Effect of thermorubin on bacterial and eukaryotic translation

Thermorubin has been reported to be non-toxic for eukaryotic cells³²⁴. This could either be due to low affinity of the antibiotic to eukaryotic ribosomes or due to inefficient uptake into the eukaryotic cell or due to a combination of both. To get further information about the reason for its good toxicity profile, *in vitro* translation reactions were performed using *E. coli* and Rabbit reticulocytes lysates (see Materials and Methods 5.17 and 5.18) in the presence of increasing concentrations of thermorubin (see Figure 22).

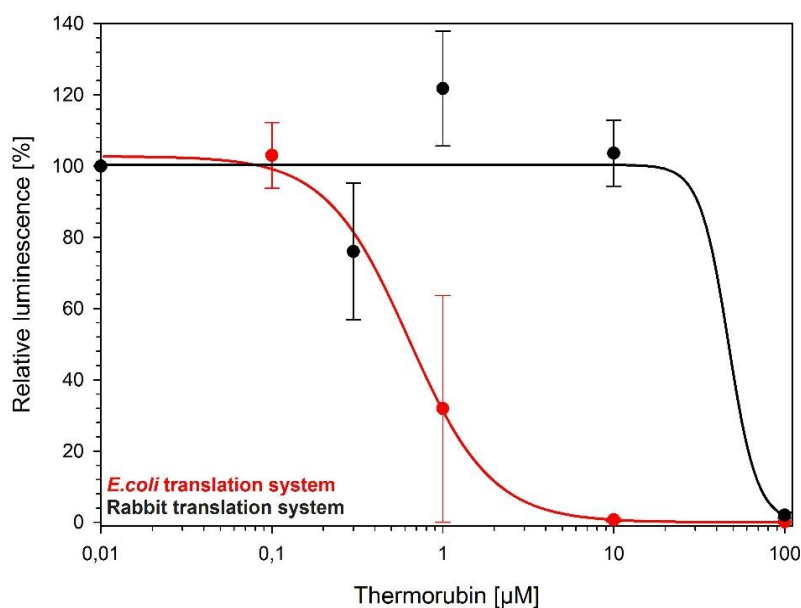


Figure 22: Inhibition of translation of the reporter protein Firefly Luciferase (Fluc) by thermorubin. A coupled *in vitro* transcription/translation system on the basis of an *E. coli* cell extract (red) or in an *in vitro* translation system on the basis of a rabbit reticulocyte lysate (black) expressed Fluc in the presence of different concentrations of thermorubin. The expression of the Fluc was quantified by luminescence measurement after 1h of incubation at 30°C. The luminescence in the absence of thermorubin was defined as 100%, error bars represent the standard deviation of the mean of three independent experiments.

The inhibitory effect of thermorubin on eukaryotic translation was 100-fold lower than when using a bacterial translation system i.e. IC_{50} of 0.7 µM for *E. coli* compared with 70 µM for the rabbit system.

No resistance mechanisms against thermorubin have been reported so far. In 1991 a patent was submitted showing that a fragment of about 4 kb of the genome of the thermorubin producer *Thermoactinomyces antibioticus* ATCC14570 can confer resistance when cloned and transformed into *E. coli* but no mechanism of action was published⁴³⁹. Therefore, a thermorubin resistant strain was generated to gain insights into the ability of bacteria to become resistant against thermorubin.

3.9 Construction of a thermorubin resistant strain

A serial dilution was performed to create a thermorubin resistant strain (see Materials and Methods 5.21 and Figure 22). *E. coli* BW25113 $\Delta sbmA$, with an MIC of 20 $\mu\text{g}/\text{mL}$, was used as starting point.

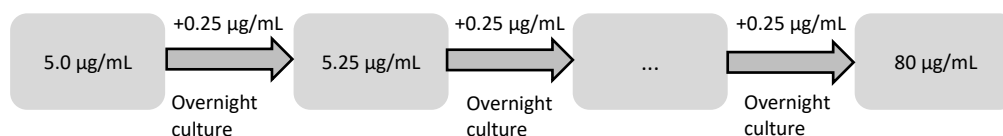


Figure 23: Serial dilution scheme of thermorubin resistance selection using *E. coli* BW25113 $\Delta sbmA$. Starting point were sub-MIC 2.0 $\mu\text{g}/\text{mL}$, thermorubin concentration was raised in 0.25 $\mu\text{g}/\text{mL}$ steps to a final concentration of 80 $\mu\text{g}/\text{mL}$.

A culture of *E. coli* BW25113 $\Delta sbmA$ was grown in the presence of 5.0 $\mu\text{g}/\text{mL}$ of thermorubin over night. On the second day the overnight culture was used to inoculate fresh medium with 5.25 $\mu\text{g}/\text{mL}$ of thermorubin. This process was repeated until the bacteria were able to grow in the presence of 80 $\mu\text{g}/\text{mL}$ of thermorubin. The final strain was named T80. The MIC for thermorubin was determined (see Material and Methods 5.7 and Figure 25). Mutations in the 16S rRNA were suspected to be the reason for the resistance, however, sequencing of the DNA encoding the 16S rRNA of the T80 strain did not reveal any mutations. Therefore, the whole genome was sequenced (see Materials and Methods 5.22). Two single point mutations and a region with four mutations compared to the parental BW25113 $\Delta sbmA$ strain were found (see Table 5).

Table 5: List of mutations identified by whole genome sequencing of the strain T80 compared to the parental *E. coli* BW25113 $\Delta sbmA$ strain.

Genomic mutation	Gene	Changes on amino acid level
T3774480C G3774486C C3774493G A3774500G	Not within an open reading frame	None
A2811218C	transcriptional repressor <i>emrR</i>	Q150P
T3905227C	Glutamine-fructose-6-phosphate aminotransferase	None

Mutation A2811218C results in an amino acid exchange of Q150P in the transcriptional repressor EmrR. EmrR regulates the expression of the efflux pump complex EmrAB-TolC, which confers resistance to the antibiotics nalidixic acid and thiolactomycin. EmrAB further reduces the

susceptibility to the protonophores carbonyl cyanide *m*-chlorophenylhydrazone and tetrachlorosalicylanilide⁴⁴⁰. The complex contains a dimer of the inner membrane protein EmrB, a dimer of the periplasmic protein EmrA and a single copy of the outer membrane pore TolC⁴⁴¹. The *emrR* gene is part of the *emrRAB* operon. The EmrR protein regulates the transcription of the whole operon by binding on the promoter site of the operon down-regulating the expression of the EmrAB-efflux pump complex⁴⁴² (see Figure 24).

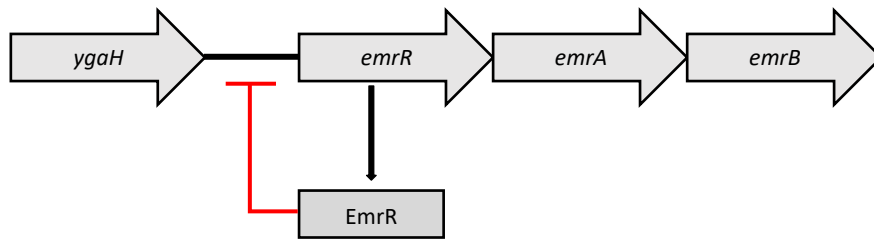


Figure 24: Organization of the *emrRAB* operon. EmrR is the product of the *emrR* gene (black arrow), it inhibits the transcription of the *emrRAB* operon (red inhibition line) by direct binding into the promoter site of the operon⁴⁴².

The BW25113 $\Delta emrR$ strain showed a high level of thermorubin resistance, although the MIC of the T80 selection strain was not attained (see Figure 26). Therefore, the A2811218C mutation was introduced into the genome of BW25113 (see Figure 25).

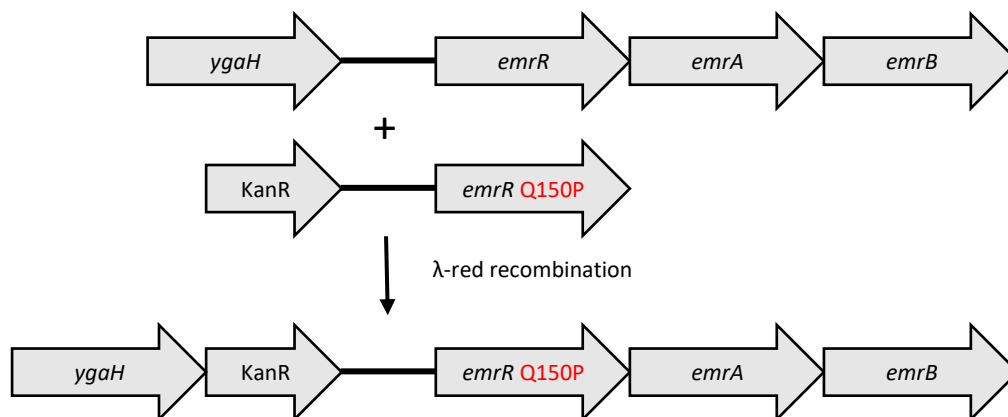


Figure 25: Construction of genomic mutation Q150P in the gene coding EmrR. The kanamycin cassette of the Keio collection⁴³⁴ was introduced between the native promoter region of the *emrRAB* operon and the upstream gene *ygaH*. The resulting strain was termed P80.

The kanamycin resistance cassette from the Keio collection⁴³⁴ was cloned in front of the native promoter region of the gene coding for EmrR containing the Q150P mutation on the plasmid pQE-70. PCR product of this plasmid containing an overlap with the gene *ygaH* was produced and used as a template for λ red recombination (see Materials and Methods 5.23 and Figure 25). The resulting strain carrying the genomic mutation inside the *emrR* gene was termed P80. The ability of the genomically mutated BW25113 to grow in the presence of thermorubin was comparable to the

BW25113 $\Delta emrR$ knockout strain, showing that a single point mutation can inactivate the protein (see Figure 26).

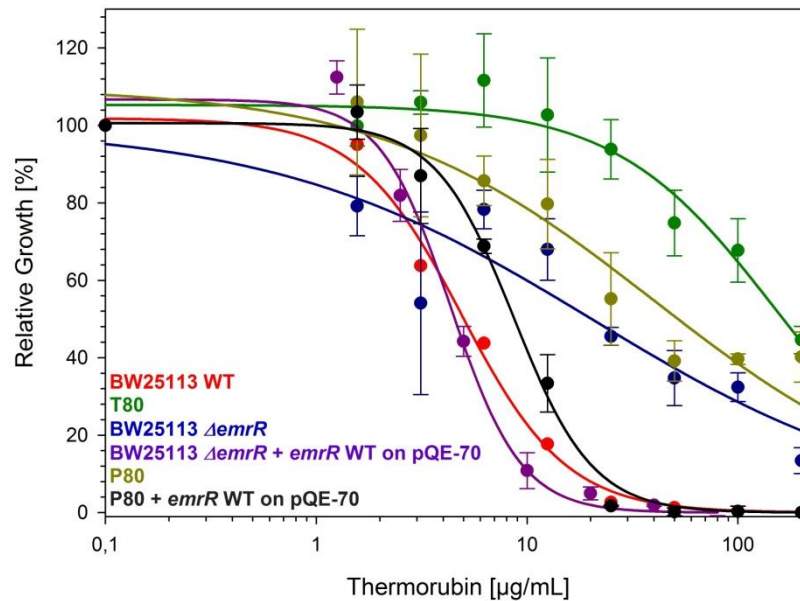


Figure 26: Effect of the EmrR mutation Q150P on thermorubin resistance. Relative growth of *E. coli* BW25113 wild-type (red), T80 (green), BW25113 $\Delta emrR$ (blue), BW25113 $\Delta emrR$ + *emrR* wild-type on pQE-70 (dark pink), P80 (BW25113 containing the mutation Q150P in the gene for EmrR) (dark yellow), P80 transformed with *emrR* wild-type on the plasmid pQE-70 (black) in the presence of growing concentrations of thermorubin. The growth of the cultures was determined by OD₆₀₀ measurement after 20 h of incubation. The growth of the strains in the absence of thermorubin was defined as 100%. The error bars represent the standard deviation of the mean for three independent experiments.

The effect of the *emrR* knockout or of the EmrR-Q150P mutation was verified by the creation of competent cells of BW25113 $\Delta emrR$ and of P80, which were then transformed wild-type *emrR* on the plasmid pQE-70. The effect of the deletion and mutation could both be reversed by the expression of the wild-type EmrR (see Figure 26).

The EmrAB efflux pump is associated with resistance against the first generation quinolone antibiotic nalidixic acid⁴⁴⁰. To verify the effect of the EmrR Q150P mutation on EmrAB expression, the nalidixic acid susceptibility of the T80 and of the P80 strain was tested. Both strains showed reduced susceptibility to nalidixic acid compared to parental BW25113 i.e. both strains could still grow in the presence of 60 µg/mL whereas the wild-type strain had an MIC of 30 µg/mL. The effect was reversed by expression of the wild-type EmrR from the plasmid pQE-70 in the P80 strain carrying the genomic mutation (see Figure 27).

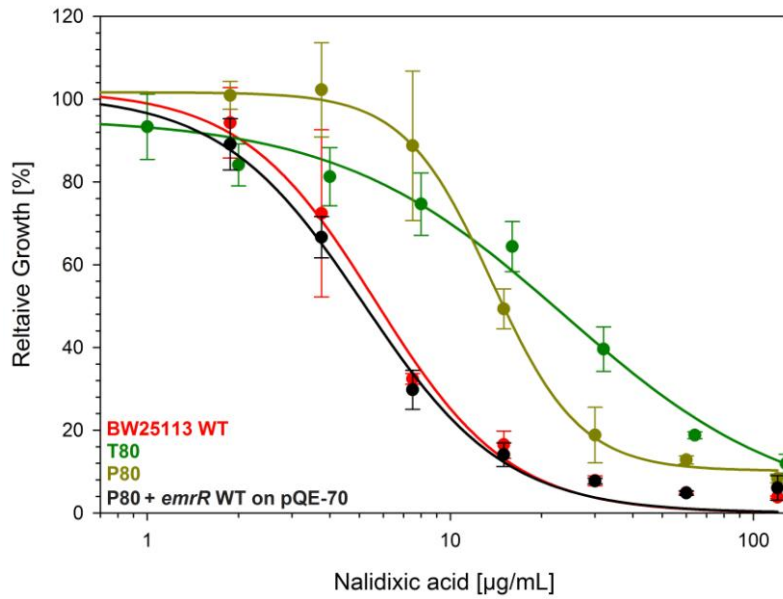


Figure 27: Effect of the EmrR mutation Q150P on nalidixic acid resistance. Relative growth of *E. coli* BW25113 wild-type (red), T80 (green), BW25113 $\Delta emrR$ (blue), P80 (BW25113 containing the mutation Q150P in the gene coding for EmrR) (dark yellow), P80 transformed with *emrR* wild-type on the plasmid pQE-70 (black) in the presence of increasing concentrations of nalidixic acid. The growth of the cultures was determined by OD₆₀₀ measurement after 20 h of incubation. The growth of the strains in the absence of nalidixic acid was defined as 100%. The error bars represent the standard deviation of the mean for three independent experiments.

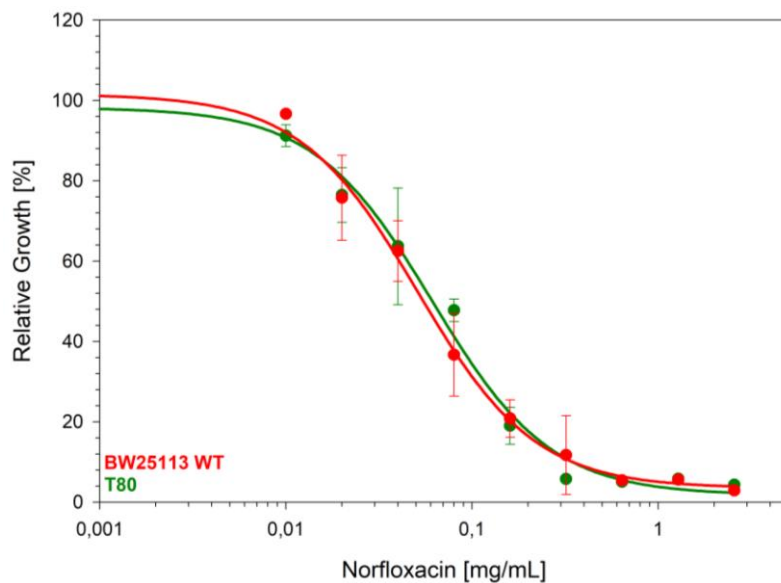


Figure 28: Comparison of norfloxacin susceptibilities of T80 and BW25113 wild-type. Relative growth of *E. coli* BW25113 wild-type (red) and T80 (green) in the presence of increasing concentrations of norfloxacin. The growth of the cultures was determined by OD₆₀₀ measurement after 20 h of incubation. The growth of the strains in the absence of norfloxacin was defined as 100%. The error bars represent the standard deviation of the mean for three independent experiments.

On the other hand, EmrAB has been reported to confer no resistance to second generation fluoroquinolones⁴⁴³. To confirm the mechanism of T80 resistance the strain and BW25113 wild-type were tested against fluoroquinolone norfloxacin (see Figure 28). As expected, no differences in

growth were observed between wild-type *E. coli* BW25113 and the selection strain T80 in the presence of norfloxacin, with both strains having MICs of 0.3 µg/mL.

A further group of four mutations was found in the genome of T80. These mutations are not located within an open reading frame, but are instead positioned between the ORFs encoding LidR, a transcriptional regulator involved in L-lactate metabolism⁴⁴⁴, and the tRNA 2'-O-methyltransferase, TrmL⁴⁴⁵. No connection between these mutations and the thermorubin resistant phenotype were obvious, therefore these mutations were not analyzed further. The only other mutation found in the T80 genome T3905227C results in a silent mutation in glutamine-fructose-6-phosphate aminotransferase and was therefore also not analyzed further.

3.10 Inhibition of *E. coli* in vitro translation by peptide antibiotics

Proline-rich antimicrobial peptides (PrAMPs) have been shown to inhibit translation⁴⁴⁶, but only few have been characterized in detail^{359,447,448}. PrAMPs from mammals and arthropods as well as amphibian antimicrobial peptides of *Xenopus spp.* were tested for their possible inhibitory effect on coupled *in vitro* transcription/translation based on an *E. coli* cell extracts using Firefly luciferase as a reporter protein (see Materials and Methods 5.17).

3.10.1 Characterization of mammalian PrAMPs

Bac7 from *Bos taurus* has already been shown to be a potent translation inhibitor⁴⁴⁶. Other PrAMPs of mammalian origin like Bac11 from *Ovis aries* or PR39 from *Sus scrofa* show high sequence similarity to Bac7 and were therefore tested for their translation inhibition potential.

Table 6: Amino acid sequences of mammalian PrAMPs tested for their translation inhibition potential.

Peptide name	Amino acid sequence	Species
PR-39	RRRPRPPYLPRPRPPFFPPRLPPRIPPGFPPRFPPR FP	<i>Sus scrofa</i>
Bac11 (1-25)	RRLRPRRPRLPRPRPRPRPRSLPLPRPKPRPIPRP LPLPRPRPKPIPRPLPLPRPRRRIIPRPLPLPRPRP PIPRPLPLPQPQPSPIPRPL	<i>Ovis aries</i>
Bac7	RRIRPRPPRLPRPRRPLPFPRPGRRPIPRPLPFPRP GRRPIPRPLPFPRPGRRPIPRPL	<i>Bos taurus</i>

The mammalian PrAMPs Bac11(1-25) and PR-39 were tested for their ability to inhibit an *in vitro* translation reaction (see Materials and Methods 5.17). Both PrAMPs showed excellent inhibitory activity (see Figure 29).

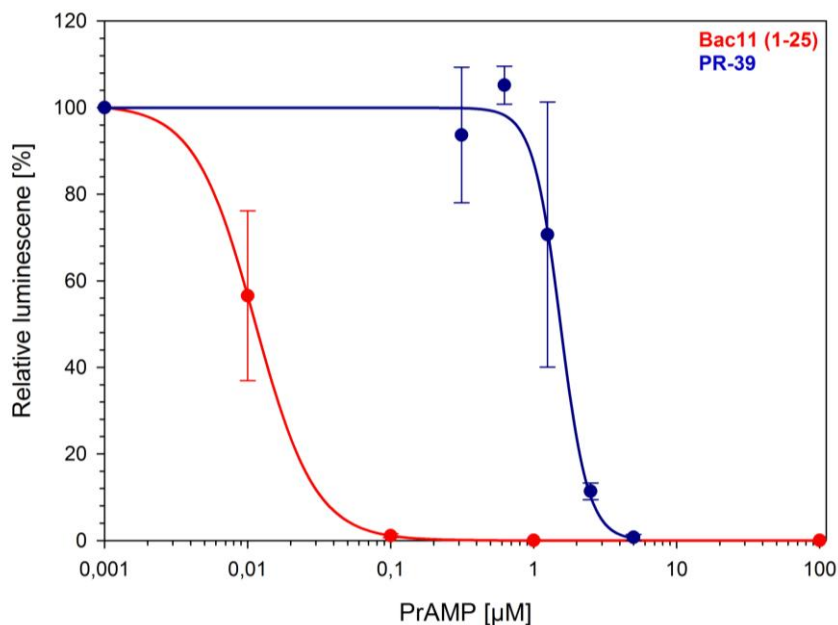


Figure 29: Inhibition of translation of the reporter protein Firefly luciferase (Fluc) by mammalian PrAMPs. A coupled *in vitro* transcription/translation system on the basis of an *E. coli* cell extract expressed Fluc in the presence of different concentrations of Bac11(1-25) (red) and PR-39 (blue). The expression of the Fluc was quantified by luminescence measurement after 1h of incubation at 30°C. The luminescence in the absence of an antibiotic was defined as 100%, error bars represent the standard deviation of the mean of three independent experiments.

PR-39, with an IC_{50} of about 1.5 μ M, was slightly less efficient in inhibiting the reaction than bovine Bac7, which was previously reported to have an IC_{50} of 0.8 μ M⁴¹⁴. In contrast, Bac11 (1-25) from *Ovis aries* was >10-fold more efficient displaying an IC_{50} of 0.02 μ M. Thus, mammalian PrAMPs are potent translation inhibitors that should be considered interesting lead compounds for clinical usage. However, one major drawback associated with the use of PrAMPs as therapeutics is their susceptibility to proteases.

3.9.2 Construction and testing of retro-D-Bac7

In order to improve the protease stability of antimicrobial peptides, replacements of the natural occurring L-amino acids with D-amino acids has been performed. However, the drawback was a significant loss of antimicrobial activity³⁵⁷. One reason might be that the different orientation of the side chains does not allow the correct interactions with the target of the peptide. To assess this

hypothesis, a retro-D-derivative of Bac7 was generated in which the amino acid sequence was reversed and the L-amino acids were replaced with D-amino acids (see Figure 30).

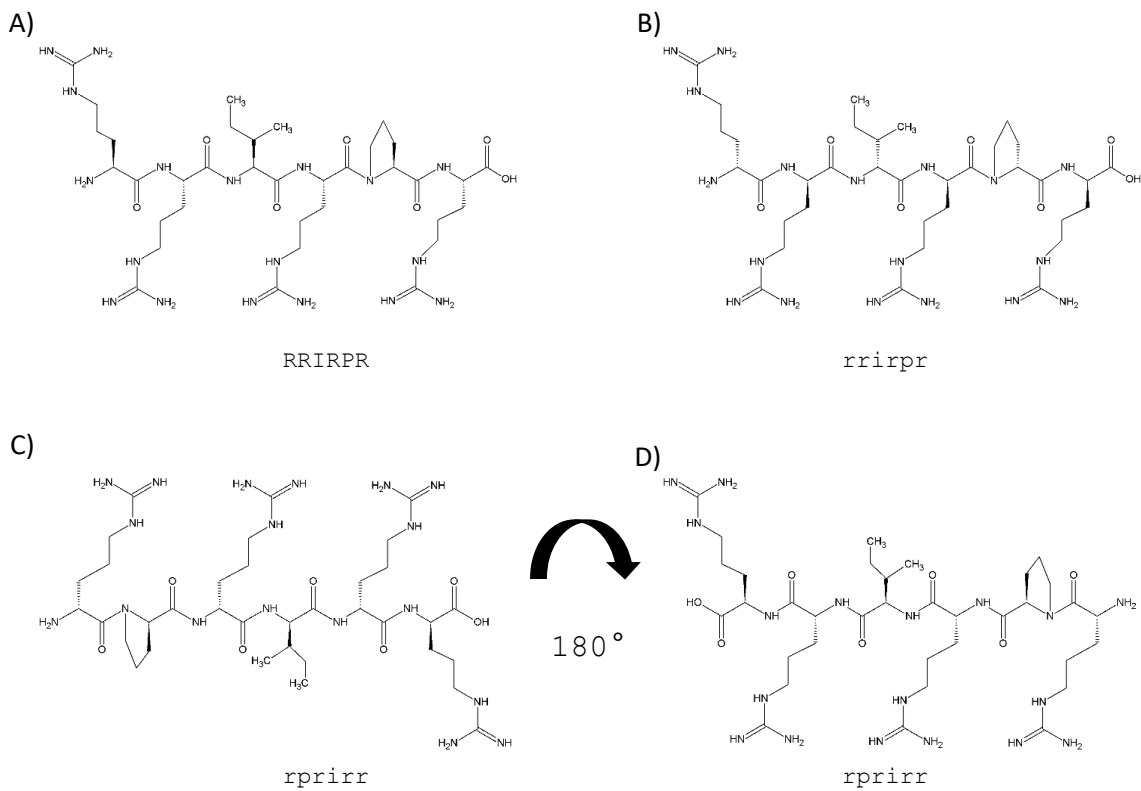


Figure 30: Chemical structures of the first six residues of the PrAMP Bac7. A) L-peptide hexamer RRIRPR B) D-peptide hexamer rrirpr C) retro-D-peptide rprirr D) retro-D-peptide rprirr flipped by 180°.

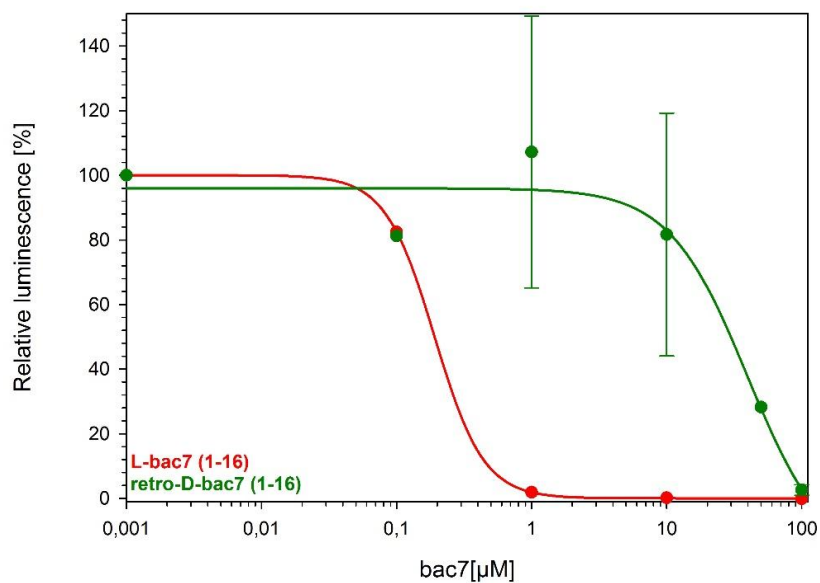


Figure 31: Inhibition of translation of the reporter protein Firefly luciferase (Fluc) by L-Bac7 and retro-D-Bac7. A coupled *in vitro* transcription/translation system on the basis of an *E. coli* cell extract expressed Fluc in the presence of different concentrations of L-Bac7 (1-16) (red) and retro-D-Bac7 (1-16). The expression of the Fluc was quantified by luminescence measurement after 1h of incubation at 30°C. The luminescence in the absence of an antibiotic was defined as 100%, error bars represent the standard deviation of the mean of three independent experiments.

The orientations of the amino acid side chains of natural L-peptide and the flipped retro-D-peptide are identical. The inverse sequence derivative of Bac7(1-16) was synthesized with D-amino acids and was named retro-D-Bac7 (1-16). The activity of retro-D-Bac7(1-16) was tested for its ability to inhibit a coupled *in vitro* transcription/translation reaction based on an *E. coli* cell extract(see Figure 31).

The replacement of the natural L-amino acids with the retro-D-amino acid sequence did not yield a compound with significant inhibitory activity. The concentration required to inhibit translation was 100-times higher than that of naturally occurring Bac7(1-16) derivative.

3.10.3 Characterization of arthropod PrAMPs

PrAMPs have also been found in arthropods, some of them show sequence similarity to mammalian PrAMPs, whereas others are totally different^{402,447}. Some arthropod PrAMPs, like Onc112, pyrrococin and metalnikowin I, have already been shown to be potent translation inhibitors^{414,415}. They share high sequence homology to each other (see Figure 10) and have been shown to bind to the ribosome in a similar way. However numerous PrAMPs containing no or only little sequence homology have been found in insects as well^{359,447}. To determine whether they also inhibit translation, PrAMPs without sequence similarity to Onc112 were selected and analyzed. Apidaecins were the first class of arthropod PrAMPs that were identified³⁶³. First in the European honeybee *Apis mellifera* and later also in related species like *Apis cerana*³⁶². Several isoforms of apidaecins are known, further, semi-synthetic derivatives with improved antibacterial properties and increased serum stability were developed^{449,450}. To determine their potential as translation inhibitors, the two natural occurring apidaecins Api1A and Api1AL and the two semi-synthetic derivatives Api88 and Api137 were selected (see table 7).

Table 7. Amino acid sequences of apidaecin PrAMPs used in this thesis. gu: N, N, N', N'-tetramethylguanidino;

O: L-ornithine.

Peptide name	Amino acid sequence
Api1A	GNNRPVYIPQRPPHPRI
Api1AL	GNNRPVYIPQRPPHPRL
Api88	gu-ONNRPVYIPRPPHPRL-NH ₂
Api137	gu-ONNRPVYIPRPPHPRL-OH

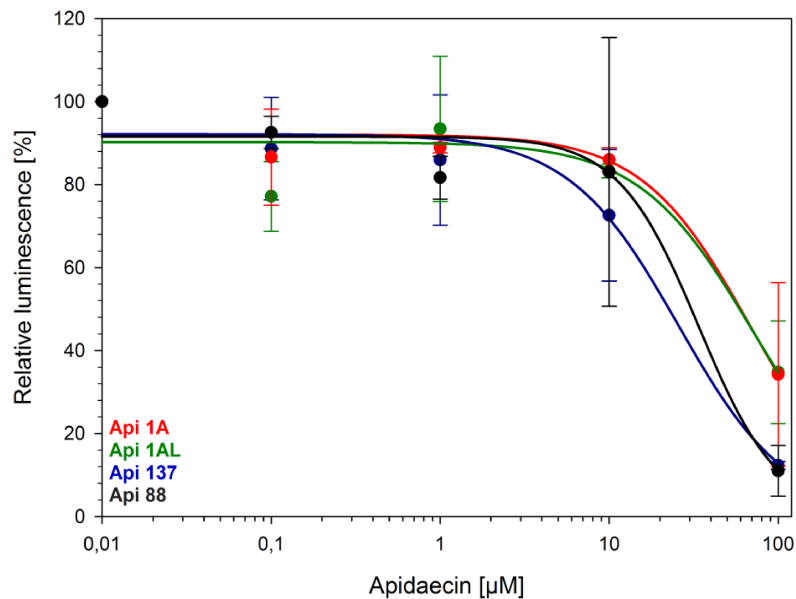


Figure 32: Inhibition of translation of the reporter protein Firefly luciferase (Fluc) by apidaecins. A coupled *in vitro* transcription/translation system on the basis of an *E. coli* cell extract expressed Fluc in the presence of increasing concentrations of Api1A (red), Api1AL (green), Api137 (blue) and Api88 (black). The expression of the Fluc was quantified by luminescence measurement after 1h of incubation at 30°C. The luminescence in the absence of an antibiotic was defined as 100%, error bars represent the standard deviation of the mean of two independent experiments.

The apidaecins were titrated into a coupled *in vitro* transcription/translation system based on an *E. coli* cell extract (see Materials and Methods 5.17 and Figure 32). The assay showed moderate translation inhibition activity of the apidaecins compared with mammalian PrAMPs (see Figure 32). The semi-synthetic Api88 and Api137 performed a bit better than natural occurring Api1A and Api1AL.

Abaecin is another PrAMP from *Apis mellifera* and contains numerous proline and arginine residues^{447,451}. Abaecin has been shown to inhibit the growth of different bacteria *in vivo*⁴⁰⁵. Its secondary structure was predicted to be α -helical which would suggest that it targets the bacterial membrane rather than the ribosome⁴⁵¹, nevertheless, it was still tested because of possible secondary effects on translation due to the proline/arginine content. Metchnikowin is a PrAMP of *Drosophila melanogaster*, it has been shown to be active against bacteria and especially against fungi⁴⁵². Its gene codes for a 52 transcript which contains a precursor sequence of 26 amino acids and the mature PrAMP which is also 26 amino acids long⁴⁵³. Two isoforms have been found but they only differ in one amino acid in the precursor-region and one amino acid in the mature PrAMP. β (1,3)-glucanosyltransferase Gel1 (FgBGT), an enzyme that is involved in the biosynthesis of fungal cell wall has been identified as the target for metchnikowin in fungi⁴⁵⁴. However not all fungi are affected by the peptide, in contrast it has been shown to be very specific⁴⁵⁵. As bacteria do not contain this enzyme, it was tested whether metchnikowin also acts on the synthesis of proteins. Drosocin has

been shown to be a potent inhibitor of bacterial growth *in vivo* only if it carries an O-glycosylation on threonine 11³⁶⁶. However, it remains unclear whether the glycosylation is required for cellular uptake and/or for target inhibition. The drosocin used in this thesis did not possess the O-glycosylation.

Table 8: Amino acid sequence of arthropod PrAMPs tested for their translation inhibition potential. The N-terminal 31 amino acids that were used in this thesis are printed in bold.

Peptide name	Amino acid sequence	Species
Abaecin	YVPLPNVPQPGRRPFPTFPGQGPFNPKIKWPQGY	<i>Apis mellifera</i>
Drosocin	GKPRPYSPRPTSHPRPIRV	<i>Drosophila melanogaster</i>
Metchnikowin	HRHQGPIFDTRPSPFNPNQPRPGPIY	<i>Drosophila melanogaster</i>
Penaeidin-1 (1-31)	YRGGYTGP IPRPPPIGRPPLRLVVCACYRLS VSDAR NCCIKFGSCCHLVK	<i>Penaeus vannamei</i>

The arthropod PrAMPs abaecin, metchnikowin, drosocin and penaeidin-1 (1-31) were all tested for inhibitory activity in an *E. coli in vitro* transcription/translation system (see Figure 33). Penaeidin-1 isolated from the white-leg shrimp *Penaeus vannamei* is a peptide with a total length of 50 amino acids containing an N-terminal proline-rich region and a C-terminal cysteine-rich region⁴⁵⁶. The proline-rich 31 N-terminal amino acids were chosen for analysis (see Table 9). The PrAMPs abaecin, metchnikowin, drosocin and penaeidin-1 (1-31) did inhibit the translation system but only at very high concentrations above 100 μ M (see Figure 33).

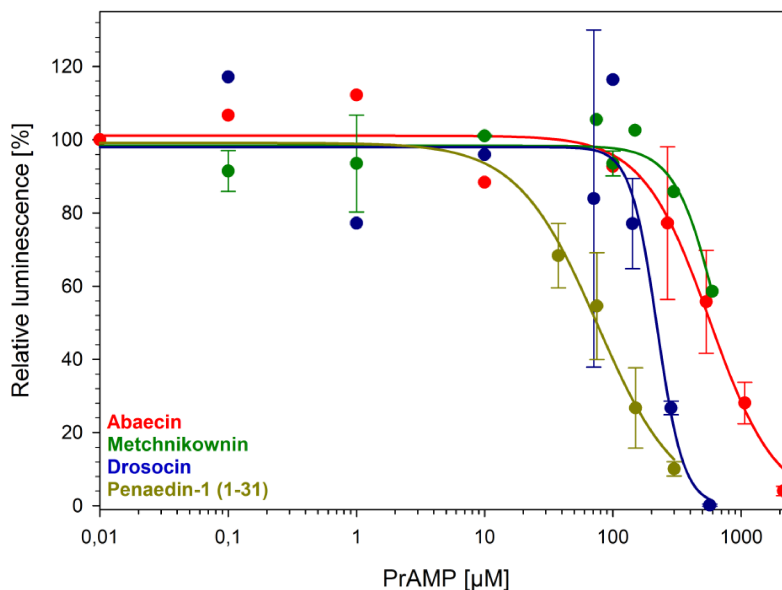


Figure 33: Inhibition of translation of the reporter protein Firefly luciferase (Fluc) by insect PrAMPs. A coupled *in vitro* transcription/translation system on the basis of an *E. coli* cell extract expressed Fluc in the presence of increasing concentrations of abaecin (red), metchnikowin (green), drosocin (blue) and penaedin-1 (1-31) (dark yellow). The expression of the Fluc was quantified by luminescence measurement after 1h of incubation at 30°C. The luminescence in the absence of an antibiotic was defined as 100%, error bars represent the standard deviation of the mean of three independent experiments.

3.10.4 Characterization of antimicrobial peptides of amphibian origin

Numerous peptides were found in the skin secretion of different frog species. Magainins belong to the best-characterized classes of amphibian AMPs, they have been shown to be bactericidal but not hemolytic at antibacterial concentrations. Other amphibian AMPs can be classified as fragments of the caerulein-⁴⁵⁷ and PGLa⁴⁵⁸-precursors proteins. Pxt-2 was isolate from the skin of *Xenopus tropicalis* among 12 other AMPs⁴⁵⁹. It has been shown to be highly active *in vivo* against *E. coli* and *S. aureus* with little hemolytic activity against rat blood, unlike other peptides of its class that either showed weak activity against bacterial growth *in vivo* and/or strong hemolytic activity against blood cells. The last amphibian AMP, XT-1 was found in another study in the skin secretion of *Xenopus tropicalis* among six other peptides⁴⁶⁰. It showed good activity against *E. coli* and *S. aureus* with moderate activity against *Candida albicans* and moderate hemolytic activity. One representative of magainins, caerulein- and PGLa-precursors and the peptides Pxt-2 and XT-1 (see table 10) were chosen for analysis to determine whether (secondary-)effects on translation exist.

Table 9: Amino acid sequences of antimicrobial peptides of different *Xenopus* species.

Peptide name	Amino acid sequence	Species
Magainin-1	GIGKFLHSAGKFGKAFVGEIMKS	<i>Xenopus laevis</i>
CPF-MW1	GLGSLLGKAFKFGKTVGKMMGGAPREQ	<i>Xenopus muelleri</i>
PGLa-AM1	GMASKAGSVLGKVAKVALKAAL	<i>Xenopus amieti</i>
Pxt-2	FIGALLRPALKLLA	<i>Xenopus tropicalis</i>
XT-1	GFLGPLLKLAAGVAKVIPHLIPSRQQ	<i>Xenopus tropicalis</i>

Xenopus peptides were tested for their ability to inhibit an *in vitro* translation system on the basis of an *E. coli* cell extract (see Figure 34 and Materials and Methods 5.17).

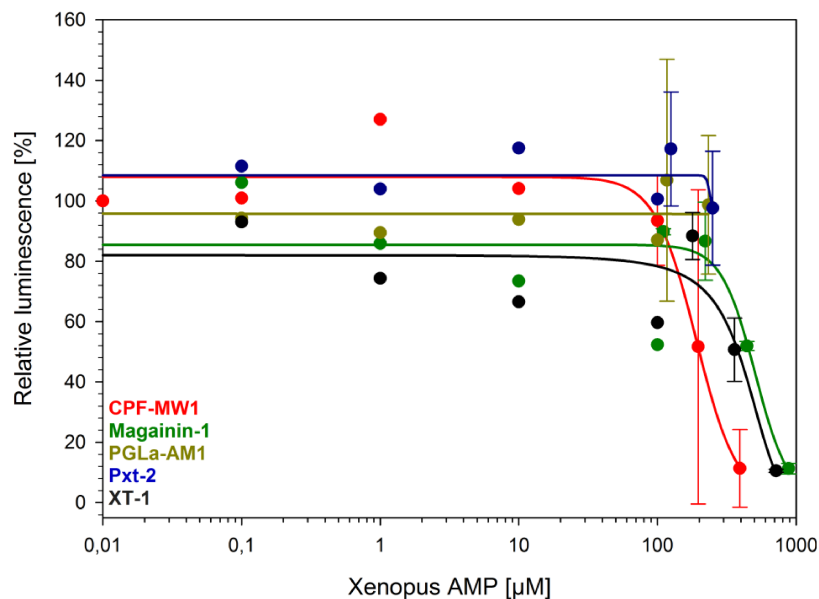


Figure 34: Inhibition of translation of the reporter protein Firefly luciferase (Fluc) by amphibian AMPs. A coupled *in vitro* transcription/translation system on the basis of an *E. coli* cell extract expressed Fluc in the presence of increasing concentrations of CPF-MW-1 (red), Magainin-1 (green), PGLa-AM-1 (dark yellow), Pxt-2 (blue) and XT-1 (black). The expression of the Fluc was quantified by luminescence measurement after 1h of incubation at 30°C. The luminescence in the absence of an antibiotic was defined as 100%, error bars represent the standard deviation of the mean of three independent experiments.

The *Xenopus* AMPs showed no inhibitory effect on translation at concentrations comparable with PrAMPs like Bac7 or Onc112. 400µM of CPF-MW1 and 1000 µM of Magainin-1 and XT-1 were necessary to inhibit the reaction. Whereas the highest tested concentrations of Pxt-2 and PGLa-AM1 could not stop the expression of the reporter protein.

4. Discussion and Outlook

4.1.1 Proline 509 of TetM interacts with the tetracycline binding site

The new cryo-EM structure of TetM with a resolution of 3.9 Å allows a more detailed look into the mechanism of action of this ribosome protection protein than was possible before. Like already published before, loop III of domain IV represents the key feature of ribosome protection proteins pushing the drug from the ribosome^{256,257}. However, an earlier publication claimed that the amino acids Y506 and Y507 of TetM are the residues removing tetracycline from its binding site by changing the conformation of C1054 of the 16S rRNA that forms a stacking interaction with ring D of tetracycline²⁵⁶. The double mutant TetM Y506A/Y507A has been shown to be unable to confer resistance against tetracycline whereas the triple mutant TetM S508A/P509A/V510A was almost as active as wild-type TetM. The corresponding tyrosines in TetM analogs Tet(O) and Tet(S) were also mutated to alanine resulting in the same decrease of resistance⁴⁰². The new structure still sees an important role for the tyrosines but shows that the tyrosines do not directly interact with the drug binding site. Instead P509 overlaps with the tetracycline binding site via stacking interactions with C1054 of the 16S rRNA. The tyrosines are required to stabilize the correct conformation of loop III. Y506 interacts with G467 of Loop II and C1051 of helix 34 of the 16S rRNA and Y507 interact with E435 of loop I positioning P509 into the right position. In addition, W442 of loop I of domain IV interacts with V510 of loop III to further stabilize its conformation. The finding that TetM still works if P509 is mutated to alanine indicates that residue 509 overlaps with the tetracycline binding site via backbone interactions rather than with its side chain as long as the conformation of loop III is stabilized by loops I and II. The mutation W442A did not have an impact on tetracycline resistance by itself but it destabilized loop III's conformation in a way that the double mutants W442A/S508A and W442A/P509A were almost inactive. The fact that serine and proline are conserved at positions 3 and 4 within loop III over all 12 known RPPs whereas there are some variations at positions 1 and 2 of the loop further supports the importance of these residues⁴⁰². Instead of YY, FF and FA were found in loop III of the RPPs Tet and TetB(P). TetM mutants Y506F/Y507F and Y506F/Y507A were less active but could still confer resistance when transformed into *E. coli* BL21 DE3. The activity of the TetM Y506F/Y507A in *E. coli* is surprising as this amino acid sequence was found in the RPP Tet isolated from *Streptomyces lividans*. An earlier study found that this RPP does not confer resistance when transformed into *E. coli*⁴⁶¹, however only these two amino acids were mutated whereas the overall sequences of Tet and TetM differs at many more positions. Furthermore, the RPP OtrA of the

oxytetracycline producer *Streptomyces rimosus* was reported to contain the amino acids VR at the corresponding positions within loop III⁴¹⁷. TetM mutants carrying the Y506V or the Y506V/Y507R mutations were unable to confer tetracycline resistance (see Figure 11). One explanation for these findings is that the stabilization of loop III's conformation within TetM, performed by aromatic tyrosines 506 and 507, can also be created by aromatic phenylalanine's even though with lower efficiency, whereas a replacement of the aromatic tyrosine 506 with hydrophobic valine is not sufficient to bring loop III in the right position to remove tetracycline from its binding site. The OtrA of this thesis was cloned from cDNA of *Streptomyces rimosus subsp. rimosus* ATCC 10970 containing some differences to the published sequence (see Appendix A), its loop III possesses the amino acid composition FASPV instead of VRSPV and has been shown to be unable to confer tetracycline resistance (see Figure 11). On the other hand, TetM mutated to FASPV in loop III was able to confer resistance, therefore it cannot only be loop III of OtrA which is incompatible with the *E. coli* ribosome. The overall amino acid sequences of OtrA and TetM differ drastically, they show an identity of only 37% compared to 77% between TetM and TetO (see Appendix B and Appendix C). It would therefore be very interesting to see a structure of OtrA bound to the ribosome of *S. rimosus* to understand how the conformation of OtrA's loop III is stabilized in its native context and why it cannot work in *E. coli*.

A cryo-EM study of TetO bound to the *E. coli* ribosome came to a similar conclusion than the TetM structures showing loop III to overlap with the tetracycline binding site²⁵⁷. The authors further described a different role for loop I claiming that it rearranges the 30S subunit to form a corridor from the tetracycline binding site to the outside of the ribosome explaining how the drug leaves the ribosome. However the claimed conformation of loop I of the TetO publication would overlap with the mRNA binding site making this conformation unlikely^{402,462}.

4.1.2 The G' domain of TetM is vital for its GTPase activity

Mutations on the G' domain diminished TetM's ability to confer tetracycline resistance, in case of the triple mutation D176K E180K E187K, it was reduced to zero. It could be shown that deficits in the GTPase activity of TetM are the result of the mutations. Ribosome protection proteins bind to the ribosome in their GTP-form, hydrolysis of GTP is not required for removal of tetracycline from the ribosome as it was reported that TetM analog TetO still decreases the affinity of tetracycline to the ribosome when bound to non-hydrolysable GTP analogs GMPPNP or GTPγS³⁹⁷, however hydrolysis of GTP is necessary for multiple turnover of RPPs^{421,462}. Therefore the reduced GTPase activity explains why G' domain mutants lost the ability to confer tetracycline resistance *in vivo*. However it was not

clarified whether the mutants cannot hydrolyze GTP anymore or whether the subsequent release of inorganic phosphate (Pi) is affected by the mutation. Elongation factor G is highly homologous to TetM²⁵⁶ and in EF-G the consequences of mutations in EF-G's G' domain and mutations on G' domain's binding partner, the C-terminal domain of ribosomal proteins L7/L12 have been further analyzed and have been reported to cause a problem with phosphate release^{418,419}. The release of Pi is not required for EF-G's activity in translocation but for the dissociation of EF-G from the ribosome afterwards^{418,463}. Similar experiments could be performed with TetM to clarify the exact reason for the loss of GTPase activity of the TetM G' domain mutants. Further, it has been shown that L7/L12 are required for stable binding of the elongation GTPases EF-G, RF3 and IF2 by the finding that L7/L12 depleted ribosomes cannot bind these factors in their GTP form stably⁴⁶⁴. The GTPase activity of EF-G was reduced to zero in the absence of L7/L12. However in the same study an EF-G mutant lacking the G' domain was created. It hydrolyzed GTP with lower efficiency than wild-type EF-G but was immune against the depletion of L7/L12. It would be very interesting to repeat these experiments with TetM/TetM Δ G' to see whether similar findings will result.

4.1.3 Over-expression of the AcrAB efflux pump complex is the major source of tigecycline resistance in the RM60 and WT60 serial dilution strains

No TetM mutation that confers resistance to third generation tigecycline could be gained by serial dilution of the drug with a culture of BL21 DE3 containing wild-type TetM or TetM with random mutations in loop III. However, another study reported that the deletion of leucine 505 and mutations of serine 508, serine 310 and glutamine 620 resulted in TetM variants which reduced the susceptibility to tigecycline⁴⁶⁵. The L505 deletion resulted in a phenotype that was able to grow in the presence of 0.5 μ g/mL of tigecycline compared to 0.1 μ g/mL for bacteria expressing wild-type TetM. However TetM Δ L505 lost its ability to confer resistance against tetracycline, doxycycline and minocycline completely. A possible explanation for this paradoxical finding is that the deletion of L505 reduces the overlap of loop III with the tetracycline binding site but on the other hand enables the RPP to disturb the interactions of tigecycline's 9-t-butylglycylamido group with the ribosome which is not present in all other tested tetracyclines. The impacts of the S508R and S508G mutations alone were too small to be significant however double mutations S508R/Q620R and S310P/S508R resulted in MICs of 0.4 μ g/mL and 0.25 μ g/mL respectively. The first representing a 4-fold effect compared to wild-type TetM whereas the second only gained a 2.5-fold higher MIC which is at the border of significance. The double mutants were also less efficient in conferring resistance to tetracycline and minocycline however the effect was smaller than for TetM Δ L505, whereas on the

other hand the double mutations had almost no effect on doxycycline resistance. Q620R and S310P alone had no significant effect on tigecycline or doxycycline resistance but resulted in a slightly higher resistance to tetracycline and minocycline. S310 is too far away to directly influence the interaction of loop III with the drug binding site, however an indirect mechanism remains possible. As TetM competes with tetracyclines for ribosome binding, a higher affinity of the factor to the ribosome through S310P mutation would explain the superior activity of the mutants to remove tigecycline from the ribosome. Q620 on the other hand is part of a linker that connects domain V of TetM with a C-terminal α -helix that has been shown to interact with h44. As the deletion of the helix has been reported to inactivate TetM²⁵⁶ this interaction is important for the binding of TetM to the ribosome, the Q620R mutation might enhance this process. However the effects of S310, S508 and Q620 mutations are only minor and will probably not lead to a TetM variant with a clinically relevant level of tigecycline resistance.

Still, the existence of TetM mutants conferring reduced susceptibility to tigecycline raises the question why no TetM mutations were found in the RM60 or WT60 strain after the serial dilution. The random mutagenesis of loop III of TetM should have contained all possible amino acid combinations for the residues 506-511 including S508R and S508G, however these mutations by themselves were without a significant effect. On the other hand no deletions were introduced into the random mutagenesis of loop III. A possible explanation for the absence of TetM mutations in RM60 and WT60 lies in the low efficiency of these mutants compared with the high concentrations of tigecycline (up to 7 $\mu\text{g}/\text{mL}$, compared with an MIC of only 0.5 $\mu\text{g}/\text{mL}$ in case of the ΔL505 mutant) that were added during the serial dilutions. Even if the bacteria did develop TetM mutants conferring low level resistance to tigecycline these did not survive the higher concentrations that were added in the further course of the experiment. Therefore the bacteria had to find another way how to deal with the presence of high tigecycline concentrations.

Whole genome sequencing of the serial dilution strains WT30, WT60, RM30 and RM60 identified numerous mutations at other loci than TetM. Mutations in the regulation system of the AcrAB efflux pump system and ribosomal protein S10 have already been reported to confer tigecycline resistance and were therefore not further analyzed^{432,435,436}. The mutation T329S within AcrB itself however was not reported before. It was reproduced by transformation of the mutated version of AcrB into the AcrB knockout strain BW25113 ΔacrB with AcrB wild-type transformed in the BW25113 ΔacrB as a control. No difference between the strains expressing AcrB T329S or wild-type were visible (see Figure 19). This finding is rather surprising as the efflux pump component AcrB plays a key role in the tigecycline resistance of these strains. A mutation in the sequence of AcrB has already been reported to increase the resistance of *Salmonella typhimurium* against ciprofloxacin⁴⁶⁶, however the T329S

mutation of the RM30 strain did not fulfil this task. Additionally, the gene for the protein SlyA was inactivated in both serial dilution strains. In the case of WT30, Glu31 was mutated to a stop codon whereas RM30 had a 1371 bp deletion in the genome removing the N-terminal 29 amino acids of the sequence of *slyA* and the whole sequence for *slyB*. SlyA belongs to the MarR family of transcription regulation proteins⁴³³, which negatively regulate the expression of various resistance genes⁴²⁸. Comparison of BW25113 Δ *slyA* to wild-type BW25113 only showed a very small effect of the knock-out on the susceptibility to tigecycline which is at the border of significance. However the fact that the gene was inactivated in two independent serial dilutions using two different ways of inactivation indicates that this knock-out plays a role for the phenotype of the strains. A possible explanation for the lack of BW25113 Δ *slyA*'s tigecycline resistance would be that the knock-out of SlyA exclusively works in the context of other mutations that developed during the serial dilution. In the RM30 strain, the sequence of the gene for SlyB has been deleted. SlyB has been reported to be an outer membrane protein in *Burkholderia multivorans*⁴⁶⁷. The knock-out strain BW25113 Δ *slyB* showed again only a minor decrease in tigecycline susceptibility compared with the parental BW25113 strain. All other mutations of the tigecycline serial dilution strains were not further analyzed. Mutations in ATP synthase subunit C; DNA dependent RNA polymerase, histidine kinase BasR and NUDIX hydrolase have no direct connection with antibiotic susceptibility and were not further analyzed, although secondary effects cannot be excluded.

All in all, the over-expression of the AcrAB efflux pump system caused by the inactivation of *marR* and the mutation of *acrR* in both serial dilutions are the major reason for the tigecycline resistance of the RM60 and WT60 strains, the mutation within *acrB* had no effect whereas the knock-out of *slyA* in both serial dilution strains and the knock-out of *slyB* in the RM30 strain only gained a minor reduction in susceptibility when tested by themselves but might enhance the resistance in combination with other mutations found in the strains.

Over-expression of AcrAB has already been detected in clinical isolates of various bacteria⁴⁶⁸⁻⁴⁷⁰. Given the large amounts of tigecycline and other tetracycline antibiotics used in human and animal medicine at the moment⁵⁸, it is predictable that this mechanism of tigecycline resistance will spread in the near future. One possible solution would be the parallel application of tigecycline with an efflux pump inhibitor. This strategy has been reported to limit the efficiency of numerous efflux pumps against a variety of antibiotics^{288,471,472}. Piperazine arylideneimidazolones were reported to inhibit the AcrAB-TolC efflux pump complex decreasing the MICs of oxacillin, linezolid and clarithromycin for *E. coli* cells⁴⁷³. It would be very interesting to test whether the MICs for tigecycline would decrease again if the RM60 and WT60 strains of this thesis were grown in the presence of tigecycline and a piperazine arylideneimidazolone or another suitable efflux pump inhibitor.

4.2 Thermorubin is an antibiotic with specificity to bacterial ribosomes and a substrate of the EmrAB efflux pump complex

Thermorubin proved to be an efficient translation inhibitor under laboratory conditions. The *in vitro* translation assays showed that it inhibits bacterial protein synthesis at concentrations of 10 μ M. On the other hand, it was less efficient in the eukaryotic system where 100 μ M were needed to stop the expression of the reporter protein. The results are in line with an earlier study reporting that low concentrations of thermorubin are enough to inhibit the growth of both Gram-positive and Gram-negative bacteria *in vivo* while the antibiotic was not able to prevent the growth of yeast and filamentous fungi³²⁴. With the *in vitro* assay, it could be shown that this difference is not (only) caused by inefficient uptake of the drug into eukaryotic cells, instead a clear difference was found between the inhibition of bacterial and cytoplasmic eukaryotic ribosomes. On the other hand mitochondrial ribosomes have not been tested. Due to the high similarity of bacterial and mitochondrial ribosomes¹⁵² it would be very interesting to see how much thermorubin will be necessary to inhibit them.

The whole genome sequencing of the thermorubin serial dilution strain T80 showed a mutation in the gene for the transcription regulator protein EmrR which suppresses the expression of the efflux pump system EmrAB-TolC^{440,442}. It has already been reported that the insertion of a nucleotide into the sequence of *emrR*, which creates a frame-shift, results in a phenotype resistant to the antibiotic thiolactomycin and to the protonophore carbonyl cyanide *m*-chlorophenylhydrazone⁴⁴⁰. The data presented here show that a single point mutation, leading to the amino acid exchange Q150P, is enough to reach the same effect. The thermorubin resistant phenotype of the T80 selection strain was partly reproduced by introduction of the mutation into the genome of *E. coli* BW25113 using the λ -red recombinase system⁴⁷⁴, the resulting strain was termed P80. P80 and the *emrR* knock-out strain BW25113 Δ *emrR* showed significant thermorubin resistance although the level of resistance of the T80 strain was not reached. Further, the T80 and the P80 strain were resistant against the quinolone antibiotic nalidixic acid but not against the second generation fluoroquinolone norfloxacin. This finding is in line with an earlier study showing nalidixic acid but not norfloxacin to be a substrate of the EmrAB-TolC efflux pump complex⁴⁴⁰. Two more loci of mutation were found in the genome of T80 compared to the parental strain. The cluster of the four mutations T3774480C, G3774486C, C3774493G, A3774500G is not located within an open reading frame and was therefore not further analyzed. The last nucleotide exchange T3905227C creates a silent mutation in the gene for glutamine-fructose-6-phosphate aminotransferase which has no obvious connection to antibiotic susceptibility and was also not further analyzed. The over-expression of the multidrug efflux pump EmrAB is the first documented thermorubin resistance mechanism, however more are thinkable. As

thermorubin exclusively interacts with ribosomal RNA^{332,416}, it is imaginable that mutations within or near the drug binding site might change its conformation in a way that the drug cannot bind anymore. Numerous antibiotic resistant pathogens are exploiting mutations or modification of their rRNA to decrease the affinity of drugs to their ribosomes^{266,267}. No rRNA mutations were identified within the T80 genome but rRNA mutations in *E. coli* generally develop slowly because *E. coli* possesses seven ORFs for rRNA⁴⁷⁵ making *E. coli* an unfavourable model organism for these kinds of mutations. Therefore a special *E. coli* knockout strain, SQ110 $\Delta tolC$, was created by the Mankin group that has only one ORF for rRNA⁴⁷⁶. One could use this special strain to repeat the selection experiment in order to identify rRNA mutations that confer resistance to thermorubin. As this strain does not contain the outer membrane pore TolC it is impossible to recreate resistance based on EmrAB over-expression as this efflux pump requires TolC⁴⁷⁷. Site directed mutagenesis of nucleotides involved in thermorubin binding, namely C1409G; A1401U; G1491U; G1491A, were introduced into the plasmid pAM552 which was transformed into *E. coli* SQ171 $\Delta tolC$ to substitute the plasmid pCSacB that carries the sequence for wild-type rRNA whereas all genomic ORFs coding for rRNA have been deleted (see Materials and Methods 5.13)⁴⁷⁸. The mutation was intentioned to break the hydrogen bond C1409-G1491 which have been reported to be part of the thermorubin binding site³³². But no resistance was observed (data not shown). This either means that a single point mutation is not enough to lower the affinity of the drug to the ribosome or that the plasmid exchange was not successful. The control experiment showing no paromomycin resistance for G1491U even though this mutation was reported to confer resistance⁴⁷⁹ questions the success of the plasmid exchange. Because thermorubin interacts with both the 16S and the 23S rRNA and that all tested mutations were exclusively on the 16S rRNA, one could imagine that the binding affinity of the drug to the unaltered part of its binding site on the 23S rRNA was enough for thermorubin to bind. It would be interesting to further mutate the 23S rRNA part of the thermorubin binding site, alone and in combination with mutations on its 16S rRNA part, to see whether this could create a thermorubin resistant ribosome.

In spite of its high antimicrobial activity and low toxicity, neither naturally occurring thermorubin, nor semi-synthetic derivatives of this drug are in clinical use. The main reason is the lack of water solubility of the drug that makes oral application impossible. It has been shown to efficiently protect mice when infected with *Streptococcus pyogenes* as long as the drug was administered intraperitoneally whereas the antibiotic was not able to protect the mice when administered orally or subcutaneously³²⁵. Lack of water solubility and/or inactivation by serum proteins were discussed to be the most likely reasons for the poor bioavailability by the authors. In all experiments of this thesis, the drug was dissolved in dimethylsulfoxide (DMSO), the final concentration of the solvent

was 4.8% in the *in vivo* MIC assays and <4% in the *in vitro* translation assays. DMSO is used in human medicine but its application is linked with side effects^{480,481}, it would also be difficult to reach the necessary DMSO concentration during treatment, therefore it should not be used to solve thermorubin for antimicrobial therapy. Instead, chemical modification of the drug adding polar groups/removing non-polar groups could enhance water solubility. Another possibility would be a change in pH value to increase solubility, which is used to enhance the bioavailability of other drugs⁴⁸². Some lipophilic drugs are encapsulated into polymeric micelles or cyclic oligosaccharides for administration⁴⁸³. Similar approaches could create bio-available thermorubin derivatives or bring thermorubin to its target site.

4.3 Amythiamicin D derivative 3a possesses superior translation inhibiting properties compared to the parental compound inhibiting elongation factor Tu

De novo synthesis enabled the production and analysis of amythiamicin D and the three chemically derivatives 3a, 3b and 3c underlining the high value of this technique for the production of highly branched natural molecules and for the creation of semi-synthetic derivatives. Derivative 3b was totally inactive *in vivo* and *in vitro* at all tested concentrations. The 1H-NMR and molecular dynamics simulations indicate that the steric conformation of derivative 3b destabilizes the overall macrocycle conformation that was found in parental amythiamicin D and derivatives 3a and 3c. This conformation was also seen in the crystal structure of GE2270 A bound to EF-Tu-GDPNP^{188,344} suggesting that it is required for the binding of this kind of drugs to the elongation factor. Derivative 3c was also completely inactive, molecular dynamics simulations indicate that polar groups next to the hydrophobic benzyloxymethyl group destabilize the conformation of the macrocycle of the derivative. Derivative 3a showed lower antibacterial potential *in vivo* compared to natural occurring amythiamicin D. On the other hand, it inhibited the *in vitro* translation assay at a lower concentration than the parental compound. A higher affinity of derivative 3a to the drug target coupled with a decrease of membrane permeability caused by the replacement of the isopropyl group of the natural thiopeptide with the hydroxymethyl group of derivative 3a would be an explanation for this paradox results. Due to the high similarities in the chemical structures of amythiamicins and GE2270 A, it was assumed that the first inhibit the formation of the ternary complex of EF-Tu, GTP and an aminoacyl tRNA the same way that was found for GE2270 A. The addition of external EF-Tu could restore translation in the presence of inhibitory concentrations of derivative 3a indicating that derivative 3a indeed targets the elongation factor. The finding that the EF-Tu mutation G257S, that has been

shown to confer resistance against GE2270 A³⁸¹, also confers resistance against amythiamicins suggests that both antibiotics share the same binding site on EF-Tu.

Cross-resistance between amythiamicins and GE2270 A with clinically established EF-Tu inhibitors is unlikely to appear as their binding site is different from the other EF-Tu targeting drugs, such as enacyloxin II and kirromycin. However, a partial overlap with the binding site of GE2270 A and clinically established pulvomycin has been found^{186,484} and it should be examined whether mutations on EF-Tu conferring pulvomycin resistance are also able to create a thiopeptide resistant EF-Tu mutant. One major problem limiting the clinical application of thiopeptides in general is the lack of water solubility of this kind of antimicrobial. Like thermorubin, amythiamicin D and its derivatives were dissolved in DMSO for all experiments of paper 1. The same strategies discussed for thermorubin could be used to overcome this problem. A further way to create thiopeptide derivatives that is not available for small molecule antibiotics lies in the nature of thiopeptide production. As these antimicrobials are processed precursor peptides, derivatives could be gained by changes in the amino acid sequence of the precursor peptide and/or in changes of the processing enzymes⁴⁸⁵.

A way to bypass the solubility problem is the topical use of thiopeptides. Thiostrepton, another thiopeptide antibiotic with a different mode of action but with the same solubility issue⁴⁸⁶, for example is already in use as a component of Animax[®] ointment (Dechra Veterinary Products) in animal medicine. The GE2270 A derivative NAI003 is in clinical trials to cure infection of *Propionibacterium acnes*, a typical skin pathogen⁴⁸⁷. These two examples represent first steps for thiopeptides into clinical practice but the bio-availability problem has to be solved for applications beyond topical use.

4.4.1 Proline-rich antimicrobial peptides inhibit translation by binding to the bacterial ribosome

The crystal structures of Onc112, Bac7, metalnikowin I or pyrrocoricin bound to the ribosome of *Thermus thermophilus* showed that all these peptides bind in a reverse orientation in the ribosomal exit tunnel, with the N-terminal residues reaching into the PTC. In the Onc112 structure, residues 1-12 could be well resolved while the C-terminus remained flexible. A second crystal structure of Onc112 bound to the *Thermus thermophilus* ribosome published by another group could see the N-terminal residues 1-13 but not the C-terminal ones, confirming the flexibility of the C-terminus⁴¹⁶. The N-terminus of Bac7 (1-16) further contains a substructure with Arg6 pushed between Arg2 and Arg4 forming a positively charged block, that is not present in the insect peptides. Onc112 and

Bac7(1-16) allow subunit joining during initiation but the overlap of the drug binding site with the binding site of A-site tRNA indicates that they prevent the accommodation of amino acyl-tRNAs into the A-site. The finding that Bac7(1-35) also inhibits eukaryotic translation explains why it is stored as an inactive pro-peptide that is only matured when pathogens are recognized⁴¹⁰⁻⁴¹². Onc112 exploits the inner membrane transporter SbmA for its uptake into the bacterial cell, the same pathway that was already described for Bac7, as the knock-out strain BW25113 $\Delta sbmA$ was able to grow in significantly higher concentrations of Onc112 than the parental strain containing the transporter²⁴⁹. However for Bac7, the proton antiporter MdtM has been identified as an alternative way for the PrAMP to enter the bacteria cell²⁵². It would be interesting to test whether that is also the case for insect derived PrAMPs like Onc112 or pyrrolicin. The other tested mammalian proline-rich antimicrobial peptides Bac11 and PR-39 turned out to inhibit translation at similar or even lower concentrations than Bac7. The high sequence homology between Bac11 and PR-39 with Bac7 suggests that they bind to the ribosome in a similar way. Especially regarding the first 16 residues which have been shown to be sufficient for ribosome inhibition by Bac7. Bac11(1-16) and Bac7(1-16) only differ by two amino acids, at position three there is leucine in case of Bac11 and isoleucine in the case of Bac7; at position seven Bac11 has an arginine instead of the proline of Bac7. PR-39 shows some differences to Bac7 but can still be aligned (see Figure 10). The tested apidaecins inhibited the translation reaction at much higher concentrations of about 100 μM for the semi-synthetic derivatives Api88 and Api137. In contrast, low MIC values for apidaecin against *E. coli* have been published. One study presents MICs of 4 $\mu\text{g}/\text{mL}$ for *E. coli* ATCC 25922 and 0.5 $\mu\text{g}/\text{mL}$ for *E. coli* BL21 AI⁴⁴⁹. Still, Api137 was shown to interact with a single binding site on the ribosome⁴⁴⁸. However, its mechanism of action differs from other PrAMPs like Onc112 or Bac7. Instead of blocking the A-site preventing tRNA accommodation, it traps class I release factors (RF1 or RF2) on the ribosome after the release of the nascent peptide chain^{448,488}. The low MICs mean that the apidaecin concentration that is necessary to inhibit the growth of *E. coli* is remarkably lower than the concentration that is required to inhibit the intracellular target of the drug. A possible explanation for this discrepancy would be an intracellular accumulation of the peptide. It has been shown that SbmA actively transports the peptide through the inner membrane which could create a higher intracellular concentration than at the outside of the cell²⁴⁹. However the accumulation would be rather high and no such effects were observed in case of other SbmA substrates like Onc112 or Bac7.

Drosocin and peaeidin 1 (1-31) inhibited the translation reaction only at high concentrations but they were not tested in their natural form. The tested drosocin lacked the O-glycosylation at Thr11. This has been reported to be required for antibacterial activity *in vivo*, in its O-glycosylated form it showed bacteriicidal activity at concentrations of 0.075 μM against *E. coli* and of 0.5 μM against *M.*

*luteus*³⁶⁶. The finding that 500 μM of non-O-glycosylated drosocin were necessary to inhibit the *in vitro* reaction either means that the modification is necessary for target binding and not (only) for uptake into the bacterial cell or that drosocin targets another cellular process than translation. A repetition of the experiment with O-glycosylated drosocin has to be performed to finally answer whether drosocin acts as a translation inhibitor or not. 300 μM of penaeidin-1 almost inhibited the translation reaction. However only the N-terminal 31 (out of 50) amino acids of penaeidin-1 were tested as the proline-rich N-terminal domain shows some similarities to translation inhibiting PrAMPs (see Figure 10). It would be interesting to see whether full-length penaeidin-1 is able to inhibit a translation reaction at lower concentrations than the N-terminus alone.

The other arthropod peptides and all *Xenopus* AMPs were tested in their native forms. 2000 μM of abaecin were necessary to inhibit the reaction, which is significantly higher than the *in vivo* MICs of 25-50 $\mu\text{g/mL}$ (6.4-12.8 μM) published for different *E. coli* strains⁴⁰⁵. Another study however found that abaecin alone was unable to inhibit the growth of *E. coli* D31 at concentrations up to 200 μM ⁴⁸⁹. Instead a cooperative mode of action was published showing abaecin to work together with hymenoptaecin to inhibit bacterial growth when 1.3 μM of hymenoptaecin (which are inactive by themselves) are administered in parallel to 20 μM of abaecin. The authors claimed that the pore forming hymenoptaecin enables abaecin to enter the bacterial cell to target which they identified as the chaperone DnaK. However DnaK has already been proposed to be the target for other PrAMPs and it turned out not to be the primary target for these peptides^{370,490}. To validate the effect of abaecin on DnaK it would be interesting to see whether a DnaK knockout strain remains susceptible to the hymenoptaecin/abaecin combination, like a DnaK knockout has been reported to have no influence on the susceptibility to Onc112 or Api137⁴¹³.

In case of metchnikowin, the highest tested concentration of 600 μM did not inhibit the translation reaction, a repetition of the experiment using higher concentrations than 600 μM is necessary to determine the final IC_{90} . Metchnikowin has been shown to inhibit the growth of Gram-positive bacterium *Micrococcus luteus* and of the filamentous fungus *Neurospora crassa* at concentrations as little as 0.5-1 μM , however in the same study the growth of (Gram-negative) *E. coli* was not inhibited at 5 μM of metchnikowin, the highest concentration tested⁴⁵². The authors of this study reported a bactericidal/fungicidal mechanism of action for the peptide. A further study, describing $\beta(1,3)$ -glucanoyltransferase Gel1 (FgBGT) as the intracellular target for metchnikowin in fungi, supports the proposed fungicidal mechanism as this is an enzyme involved in the biosynthesis of fungal cell wall⁴⁵⁴. Metchnikowin can be seen as a potent antifungal peptide, in this role, it has already been shown to perform well when introduced into the genome of plants as an alternative to chemical fungicides⁴⁹¹. On the other hand the mechanism of action against bacteria remains unclear,

however, the finding that it is more active against a Gram-positive than against Gram-negative bacteria indicates that the cell envelope is the most probable target of this peptide.

The *Xenopus* peptides were reported to target the bacterial membrane^{492,493}. It was analyzed whether secondary effects on translation occur. High concentrations of magainin-1 (883 μM), CPF-MW1 (393 μM) and XT-1 (717 μM) inhibited the translation reaction almost completely whereas the highest tested concentrations of PGLa-AM1 (233 μM) and Pxt-2 (250 μM) were not able to stop the synthesis of the reporter protein. In an earlier publication magainin 2 has been shown to inhibit the growth of *E. coli* at 5 $\mu\text{g}/\text{mL}$ and to perform bacteriolysis at 10 $\mu\text{g}/\text{mL}$ (4.15 μM), the authors of this study claimed a similar activity for magainin-1 without publishing the data³⁷². This is significantly lower than the IC_{90} of 883 μM found for translation inhibition. Another study found an MIC of 12.5 μM for magainin-1 against *E. coli* and an MIC of 3 μM for CPF-MW1 against *E. coli*⁴⁹³. Again far lower than the concentration of CPF-MW1 that was necessary to inhibit the translation reaction. In a study characterizing XT-1, only 6 μM of the peptide were required to inhibit the growth of *E. coli in vivo*⁴⁶⁰. It appears unlikely that magainin-1, CPF-MW1 and XT-1 target protein synthesis *in vivo*. The inhibition at very high concentrations probably results from unspecific binding of the positively charged peptides to the negatively charged rRNA of the ribosome rather than from specific interaction with a defined binding site. Even if there is a discrete binding site on the ribosome for these peptides it would not have a biological significance as the bacterial membranes would be lysed long before the concentration would be reached that is necessary to inhibit translation. For PGLa-AM1 and Pxt-2 on the other hand no final conclusions can be drawn, a repetition of the experiments with higher concentrations are necessary to determine the IC_{90} s; however the finding that more than 200 μM did not inhibit the translation reaction suggests a similar behaviour of the peptides compared to the other *Xenopus* peptides.

4.4.2 Clinical use of antimicrobial peptides is limited by stability of the compounds and possible development of cross-resistance

Some antimicrobial peptides are already in clinical trials⁴⁹⁴, some of which are derivatives of human cathelicidin LL-37. The administration of AMPs similar to contents of the human innate immune system includes the danger that bacteria develop resistance mechanisms that would also decrease the efficiency of the innate immune system. In a recent study, *Staphylococcus aureus* was serially diluted with LL-37 and the proline-rich antimicrobial peptide PR-39. Both strains became less susceptible to human LL-37 and human β -defensins hBD1 and hBD4 although the amino acid sequences of PR-39 and LL-37/ β -defensins show no similarities⁴⁹⁵. Thickening of the bacterial cell wall

and/or reduced uptake of the AMPs during resistance selection were discussed to be reasons for the unexpected cross-resistance by the authors. Another possible mechanism of cross-resistance between antimicrobial peptides without sequence similarities and different modes of action is the secretion of proteases by bacteria. This mechanism of resistance has already been found in some pathogens with resistance against LL-37^{496,497}.

Bacteria might react with changes in their cell membrane and an increase of protease secretion as a reaction of a future use of antimicrobial peptides in clinical practice. Therefore, It should be carefully examined whether these effects are controllable or whether the clinical use of AMPs in human or animal medicine could create pathogens which are even more dangerous than the multi-resistant bacteria that should be cured by using AMPs.

4.4.3 Incorporation of peptidomimetics into the amino acid sequence of PrAMPs could generate protease stable derivatives

A major drawback of using peptides as antibiotics (or drugs in general) is their susceptibility to proteases which would target orally administered drugs in the digestion system as well as in the blood stream. One way of dealing with this problem is the confinement of AMPs as topical agents to cure skin infections avoiding contact with many proteases. Some AMPs, like the magainin II derivative pexiganan, are in development for this purpose⁴⁹⁸. A more general approach is the creation of protease resistant AMP derivatives. Developments like the semi-synthetic derivatives Onc112 and Onc72 have already been reported to exhibit superior protease stability through the substitution of two residues with the unnatural amino acids D-arginine or L-ornithine respectively⁴⁰³.

A recent study, describing the antibacterial effect of the N-terminal arginine-rich domain of the hepatitis B core protein points into the same direction. It could be shown that the substitution of all natural L-arginines with unnatural D-arginines creates a protease stable derivative while maintaining antimicrobial activity against almost all tested strains⁴⁹⁹. Retro-D-bac7(1-16) did not fulfil this expectation, the concentration needed to inhibit the *in vitro* translation system is 100 times higher than for the L-fragment. One possible reason is the conformation of the D-prolines which is not compensated by the inversion of the sequence. Further, the N-terminal amino group and the C-terminal carboxyl group were not inversed. A new derivative inverting the amino acid sequence, changing all amino acids into D-conformation but keeping all prolines in natural L-configuration and at their position and also changing the terminal groups would be an interesting next step to create a protease stable PrAMP derivative.

An alternative to D-amino acids could be the incorporation of other peptidomimetics (see Figure 35)⁵⁰⁰. In depsipeptides/thiodepsipeptides, half of the peptide bonds are replaced by ester bonds or thioester bonds respectively. The side chains are still attached to the α -carbon atom of the peptide chain. Depsipeptides and thiodepsipeptides are common modification in various natural products including antibiotics. Valinomycin for example is a cyclic depsipeptide antibiotic produced by *Streptomyces spp.* inhibiting bacterial growth by transporting potassium across the bacterial membrane destroying its potential^{236,237}. The translation inhibitor nosiheptide contains one thioester bond and was in use in animal medicine but did not make it into human medicine^{501,502}. In peptoids on the other hand, the side-chain is not attached to the α -carbon but to the nitrogen atom of the peptide bond whereas another CH_2 group is added between the α -carbon and the carbon atom forming the peptide bond in β -peptides⁵⁰³. Peptoids and β -peptides are not part of natural occurring peptides, although β -alanine is an intermediate product of pantothenic acid synthesis which is further used for the production of coenzyme A^{504,505}. But, some synthetic peptides containing β -amino acids have been published. A promising example is the design of a magainin-derivative using β -peptides which has been shown to exhibit similar antimicrobial activity than the parental magainin with low hemolytic toxicity⁵⁰⁶.

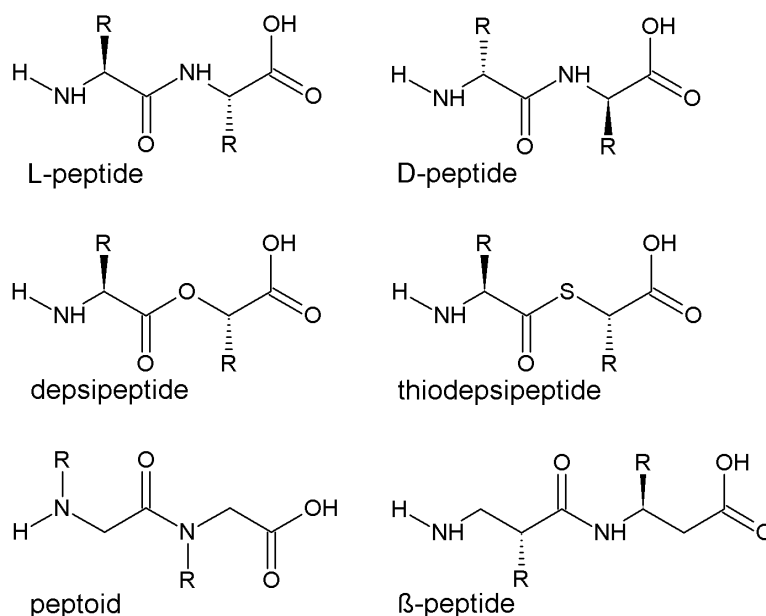


Figure 35: Chemical structures of peptidomimetics. L-peptides are the building block of natural proteins. The inversion of the stereochemistry leads to D-peptides. In depsipeptide every second peptide bond is replaced by an ester bond, in thiodepsipeptides by a thioester bond. The side chain is connected to the nitrogen atoms in peptoids⁵⁰⁷ whereas β -peptides⁵⁰⁸ contain an additional CH_2 group between the carboxyl group and the CH_2 group carrying the side chain.

Proteases cannot target chains of peptidomimetics making them completely immune. Therefore, resistance against peptidomimetic derivatives of AMPs through an increase of protease secretion would also be impossible protecting the efficiency of the innate immune system from possible multi-resistant pathogens that could develop through the application of protease susceptible peptide drugs.

Taken together, complete or partial replacement of natural L-amino acids to peptidomimetics could result in new derivatives of antimicrobial peptides with increased stability and without loss of antimicrobial activity paving the way for this kind of antibiotics into clinical use.

5. Materials and Methods

5.1 Production of chemically competent cells

100 mL of LB medium were inoculated with 1 mL of overnight culture. Bacteria were grown at 37°C/150 rpm to an OD₆₀₀ of 0.6-0.8. Cells were harvested at 3000g/15min/4°C and washed once with ice-cold 100 mL MgCl₂ solution (100 mM). Cells were centrifuged again and resuspended in 2 mL of ice-cold 100 mM CaCl₂/15% glycerol solution. The suspension was aliquoted into 100 µL portions and zip frozen in liquid nitrogen to be stored at -80°C.

5.2 Production of electro-competent cells

100 mL of LB medium were inoculated with 1 mL of overnight culture. Cells were grown to an OD₆₀₀ of 0.4-0.5 and harvested at 3000g/15 min/4°C. The pellet was washed twice with 100 mL of ice-cold water and once with 50 mL of 10% glycerol. The pellet was resuspended in 200 µL 10 % glycerol, aliquoted into 40 µL fraction and snap-frozen in liquid nitrogen to be stored at -80°C.

5.3 Heat shock transformation

Chemically competent cells were thawed on ice. 1 µL of plasmid DNA (20-100 ng) was added. Bacteria were incubated for 30 min on ice, heat-shocked for 30 s at 42 °C in a Thermomixer (Eppendorf) and incubated for another 2 min on ice. 800 µL of LB medium (see Buffers and Media) were added before another incubation step of 60 min at 37 °C followed. Cells were either plated on LB-Agar Plates or directly used to inoculate an overnight culture in liquid medium.

5.4 Transformation with the electroporation method

Electro-competent cells were thawed and added into a 0.1 cm Gene Pulser® (BIO RAD Cat. No. 1652083) cuvette. One µL of plasmid DNA or PCR product were added. The cuvette was incubated on ice for 2 min, dried and adjusted into an *E. coli* pulser (BIO RAD Cat. No. 165-2104). One electroshock at 1.8 kV was performed. Cells were resuspended in 750 µL of pre-warmed (37°C) LB medium and incubated at 37°C/700 rpm.

5.5 Megaprimer PCR of whole plasmid (MEGAWHOP) cloning

Primers containing overlaps with the desired gene and the target plasmid were designed. Genomic DNA or lysed bacteria were taken as template for PCR to create megaprimer. Genomic DNA of *Streptomyces rimosus subsp. rimosus* ATCC 10970 (DSM No. 40260) was used as template for OtrA cloning. In a second PCR, the megaprimer were incorporated into the target plasmid. PCR was performed using peqSTAR Thermocycler (peqlabs), Xtreme KOD HOT-polymerase (Merck Cat. No. 71975-3) was used for both PCRs. The PCR product was incubated for 3h with 35 units of DpnI (NEB Cat. No. R0176L) at 37°C/750rpm. PCR purification was performed using QIAquick® PCR Purification Kit 250 (QIAGEN Cat. No. 28106) following the instructions of the manufacturer. 50-80ng of purified PCR product were transformed into *E. coli* XL-1 blue (NEB Cat. No. C3019I) to inoculate 5 mL of LB medium. The culture was grown over night at 37°C/150rpm. Plasmids were isolated and the success of the insertion was observed by sequencing.

5.6 Site directed mutagenesis

The PCR primers containing the desired mutation were designed following the suggestions of the manufacturer of the Polymerase. PCR was performed using peqSTAR Thermocycler (peqlabs), Xtreme KOD HOT-polymerase (Merck Cat. No. 71975-3) was used. PCR product was incubated for 3h with 35 units of DpnI (NEB Cat. No. R0176L) at 37°C/750rpm. PCR purification was performed using QIAquick® PCR Purification Kit 250 (QIAGEN Cat. No. 28106) following the instructions of the manufacturer. 50-80ng of purified PCR were transformed into *E. coli* XL-1 blue (NEB Cat. No. C3019I) to inoculate 5 mL of LB medium. The culture was grown over night at 37°C/150rpm. Plasmids were isolated and the success of the mutagenesis was observed by sequencing.

5.7 MIC determination

Overnight cultures were diluted 1:100 in fresh LB medium, 1 mM of IPTG and/or antibiotics were added when needed. 200 µL of test cultures were transferred into a well of a 96 well Microtest plate (SARSTEDT REF 82.1581). 10 µL of antibiotic solution were added. Plates were incubated at 37°C/400rpm in a thermomixer (Eppendorf) for 17-20h. OD₆₀₀ was measured in a TECAN infinite 1000 plate reader.

5.8 Test purification of proteins

100 mL of LB medium were inoculated with 1 mL of overnight culture. Cells were grown at 37°C/150 rpm to an OD₆₀₀ of 0.5-0.6. Expression of the desired protein was started by adding 1mM of IPTG. Cells were harvested after 2h of further incubation by centrifugation at 3000g/4°C. 630 µL of lysis buffer (see Buffers and Media), 70µL of lysozyme (10 mg/mL; Sigma Aldrich Cat. No. L6876-25G) and 2 µL of DNase I (10 mg/mL) were added. Mixture was incubated on ice for 30 min and frozen overnight at -80°C. After thawing, purification was performed using QIAprep Spin® Miniprep Kit (250) (QIAGEN Cat. No. 27106) kit following the instructions of the manufacturer. Samples were analyzed via SDS Page.

5.9 Large scale protein purification

1.6 L of LB medium were inoculated with 20 mL of overnight culture. 1% of ethanol was added. Cells were grown to an OD₆₀₀ of 0.3-0.4 at 37°C/120rpm. Temperature was reduced to 30°C. At an OD₆₀₀ of 0.5-0.6 over-expression was started by addition of 1 mM of IPTG and stopped after 2h. Cells were harvested by centrifugation at 3000g/20min/4°C. Cells were resuspended in 25 mL of lysis buffer and lysed using a MICROFLUIDICS microfluidizer at 18000 psi in two passages. Lysate was centrifuged in an SS34 rotor at 17000g/15min/4°C. Supernatant was mixed with 1 mL of Protino® Ni-NTA beads (Machery-Nagel Cat. No. 45400.25) and incubated for 1 hour at 4°C under permanent mixing. The suspension was transferred to a chromatography column (BioRad Cat. No. 7321010). The beads were washed twice with 5 mL of washing buffer and eluted twice with 1 mL of elution buffer. Elutions were pooled for size exclusion chromatography using a High load 16/60 Superdex 75 column (GE Healthcare Product code 28989333). Samples of all steps of the Ni²⁺ purification and all relevant gel filtration fractions were analyzed via SDS Page. Fractions containing clean protein were pooled and centrifuged through a centrifuge filter (Merck-Millipore Cat. No. UFC803008) to raise the concentration. The final concentration of the protein was determined by absorbance measurement at 280 nm⁵⁰⁹.

5.10 SDS Page

SDS PAGES⁵¹⁰ were performed with 15% acrylamide gels at 180V for one hour. The gels were stained for 15 minutes in EtOH-Comassie staining solution; destained with destain solution containing 50% of EtOH and 10 % of acetic acid until clean bands appeared.

5.11 Isolation of ribosomes

The isolation of ribosomes was based on earlier protocols^{166,511}. 1.6 L of LB medium were inoculated with 20 mL of overnight culture. Cells were grown at 37°C/120rpm to an OD₆₀₀ of 1.8 and harvested through centrifugation at 3000g/20min/4°C. Cell pellet was resuspended in 30 mL of cell buffer and lysed in a MICROFLUIDICS microfluidizer at 18000 psi in two passages. DNase I was added to a final concentration of 0.2 µg/mL and incubated on ice for 30 min. Lysate was centrifuged at 14000g/30 min/4°C. Supernatant was mixed with 30% sucrose cushion solution and centrifuged at 20000rpm/30min in a Ti-70 rotor. Supernatant was overlaid in Ti45 tubes over a 7mL 30% sucrose solution and centrifuged at 44000rpm/25h/4°C in a Ti45 rotor. Pellets were resuspended in 1mL sucrose gradient buffer and loaded on a 10-40% sucrose gradient to be centrifuged at 19000rpm/14h/4°C in a SW40 rotor. The gradient was fractionated on a Piston gradient Fractionator (Biocomp) and pelleted at 41600rpm/19.7h/4°C in a Ti45 rotor. Pellets were resuspended in 1 mL of sucrose gradient buffer. The concentration was determined measuring the OD₂₆₀.

5.12 Phosphatase assays

Phosphatase assays to quantify GTPase activity were performed using Malachite Green Phosphate Assay Kit⁴²³ (BioAssaySystems Cat. No. POMG-25H). Standard curve was created following the instructions of the manufacturer. Each reaction contained 30 nM of purified ribosomes and 60 nM of purified; nuclease free water was added to a final volume of 70 µL. The reaction was started by the addition of 10 µL of 160 mM GTP. Reactions were incubated for 10, 20, 30, 45, 60, 75 and 90 min at room temperature. 20 µL of working solution were added. After 30 min of further incubation at room temperature, OD₆₂₀ was measured in a Tecan INFINITE M1000 plate reader.

5.13 Mutation of the ribosomal RNA

Mutations were introduced into the plasmid pAM552^{476,478,512} via site directed mutagenesis. The plasmid was transformed into chemically competent *E. coli* SQ171 $\Delta toIC^{512}$ and plated on LB-Agar containing 100 µg/mL ampicillin. Single colonies were picked and transferred on a LB-Agar plate with 5% sucrose+100µg/mL ampicillin and on a LB-Agar plate containing 50 µg/mL kanamycin. Colonies that grew on the sucrose/ampicillin plate but not on the kanamycin plate were selected to inoculate 5 mL of LB medium containing the same sucrose/ampicillin concentration and grown overnight. The presence of the mutation was verified by sequencing.

5.14 S12 extract preparation

The preparation of S12 extracts was based on an earlier protocol³⁸⁰. 100 mL of medium were inoculated with one mL of overnight culture. If the extract was prepared from *E. coli* containing rRNA mutations the culture was grown in LB medium with additional 5% sucrose. Cells were incubated at 37°C/150rpm to an OD₆₀₀ of 0.7-0.9. The culture was harvested via centrifugation at 3000g/4°C/20min. Washed twice with Buffer A and resuspended in 2 mL of Buffer B. *E. coli* cells were lysed using Branson Sonifier 250 with Output control set to 5 and Duty Cycle set to 30%. Lysate was centrifuged for 10 min at 12000g. Supernatant was aliquoted into 100µL fraction and zip-frozen in liquid nitrogen. S12 extracts were stored at -80°C.

5.15 In vitro transcription

Firefly luciferase (Fluc) on the plasmid pIVEX 2.3 was used as a template to create Fluc PCR product using primers containing overlaps with the luciferase and a 5' T7 promoter sequence (see list of primers 64). Transcription reaction mixture containing 40 mM Tris (pH 7.9); 2.5 mM Spermidine; 26 mM MgCl₂; 0.01% Triton X-100; 5 mM DTT; 6,25 mM of each XTP; 4 µL T7-Polymerase were assembled on ice. Fluc PCR Product was added to a final volume of 100 µL. The mixture was incubated for 4 hours at 30°C with 750 of shaking in a Thermomixer (Eppendorf). 150 µL of nuclease free water and 125 µL of LiCl solution (7.5 mM LiCl + 50 mM EDTA) were added. The mixture was frozen over night at -80°C. After thawing it was centrifuged for 20 min at 14000 rpm/4°C in an Eppendorf centrifuge 5415R. The pellet was washed with 1 mL of 70% ethanol and centrifuged again for 10 min at 14000 rpm/4°C for 10 min. The dried pellet was dissolved in nuclease free water to gain a final concentration of 200 ng/µL of mRNA.

5.16 In vitro Translation on the basis of an S12 extract

Reaction mix was generated on ice containing 0.24 M hepes (pH=8.2); 65 mM Glucose; 2.5 mM PEG 8000; 4.4 µg tRNA; 1.2 mM ATP; 0.85 mM; 0.85 µg folinic acid; 0.05 M DTT; 90 mM potassium glutamate; 80 mM ammonium acetate; 20 mM K₂HPO₄; 2.1 mM Cysteine; 1.8 mM of each amino acid; 7.5 mM MgOAc; 6.75 µL cell extract; 175 pmol Fluc mRNA. All reactions were aliquoted into PCR tubes to a final volume of 24 µL. 1 µL Antibiotic and/or protein solutions were added. Reaction time was 60 min at 30°C/750°C. 5 µL of each reaction were taken as sample and pipetted into a well of a 96 well plate (Greiner-bio-one REF 655095) containing 5 µL of Kanamycin (50 mg/mL). 40 µL of Fluc Substrate (Promega Cat. No. E1501) were added to each well, measurement of the activity of the

produced luciferase was done by measuring emitted light of luciferin oxidation catalyzed by the luciferase in a TECAN infinite M1000 plate reader.

5.17 *In vitro* transcription/translation using Rapid Translation Kit

The coupled *in vitro* transcription/translation method was based on earlier protocols^{513,514}. The RTS 100 *E. coli* HY kit was delivered by biotechRabbit (Cat. No. BR1400201). 130 pmol of PCR product (ds DNA) of Firefly luciferase was produced using primers 64 (see list of primers). A promoter for T7-bacteriophage DNA dependent RNA polymerase was cloned before the sequence for the luciferase (see plasmid map of Fluc in pIVEX 2.3). Reaction mixes were assembled following the instructions of the manufacturer and aliquoted to 5 μ L reactions. 1 μ L of antibiotic solution was added to each reaction. The mixtures were incubated in an Eppendorf Thermomixer R for 1 h at 30°C/750 rpm. 0.5 μ L of each reaction was taken as sample and added into a well of a 96 well plate (Greiner Bio-One ref. 655207) containing 7.5 μ L of Kanamycin (50mg/mL) solution. 40 μ L of Fluc Substrate (Promega Cat. No. E1501) were added to each well, measurement of the activity of the produced luciferase was done by measuring emitted light of luciferin oxidation catalyzed by the luciferase in a TECAN infinite M1000 plate reader.

5.18 *In vitro* translation using Rabbit Reticulocyte Lysate system

The Rabbit Reticulocyte Lysate kit was delivered by Promega (Cat. No. L4960). Reaction mixture was assembled following the instructions of the manufacturer, and aliquoted to single 5 μ L reactions. 1 μ L of antibiotic solution was added to every reaction. The mixtures were incubated in an Eppendorf Thermomixer R for 1H at 30°C/400 rpm. One μ L of each reaction was taken as sample and transferred into wells of a 96 well plate (Greiner Bio-One ref. 655207) containing 7 μ L of Kanamycin solution (50mg/mL). 40 μ L of Fluc Substrate (Promega Cat. No. E1501) were added to each well, measurement of the activity of the produced luciferase was done by measuring emitted light of luciferin oxidation catalyzed by the luciferase in a TECAN infinite M1000 plate reader.

5.19 Random mutagenesis of TetM

Primers containing 15 random nucleotides instead of the sequence of loop III of domain IV and an overlap with the sequences 5' and 3' of loop 3 (see list of primers No 1 and No 10) were used for MEGAWHOP. TetM on the plasmid pet-46 LIC was used as template to create a library of loop 3 mutants.

5.20 Tigecycline serial dilution

TetM wild-type on pET-46 LIC and TetM containing the random mutagenesis of loop III of domain IV were transformed into one aliquot of BL21 DE3 (NEB Cat. No. C25271) each. The resulting cultures were used to inoculate 20 mL of LB medium containing 0.1 µg/mL of tigecycline. Culture was grown overnight. 1 mL of this culture was used to inoculate another 20 mL of fresh LB medium, tigecycline concentration was increased by 0.1 µg/mL. Procedure was repeated until the addition of further tigecycline inhibited the growth of the bacteria. To identify the mutations responsible for the resistance, the whole genomes of the serial dilution strains were sequenced at Helmholtz Zentrum für Infektionsforschung Saarbrücken by the laboratory of Prof. Dr. Rolf Müller⁵¹⁵.

5.21 Thermorubin serial dilution

20 mL of LB medium were inoculated with one mL of *E. coli* BW25113 $\Delta sbmA$ overnight culture. Thermorubin was added to a final concentration of 5 µg/mL (25% of MIC). Culture was grown overnight. 1 mL of this culture was used to inoculate another 20 mL of fresh LB medium, Thermorubin concentration was increased by 0.25 µg/mL. Procedure was repeated until the bacteria were able to grow in 80 µg/mL of Thermorubin (=4xMIC). The final strain was therefore named T80.

5.22 Whole genome sequencing of thermorubin resistant strain T80

Genomic DNA of T80 was isolated using Wizard® Genomic DNA Purification Kit (Promega Cat. No. A1120) following the instructions of the manufacturer. DNA was indexed using Accel-NGS 1S Plus DNA Library Kit (Swift Biosciences Cat. No. 10024) for bar code primer D710 (TCCGCGAA). The DNA was sequenced on an Illumina HighSeq 1500 sequencer. Resulting data were analyzed on the Galaxy platform of the Blum work group to identify genomic mutations.

5.23 Genomic Mutation

Genomic mutation was performed using λ -red system⁴⁷⁴. First, electro competent cells of *E. coli* BW25113 containing *pdk46* were produced. The *emrR* gene was cloned into pQE-70 with the Q150P mutation observed in T80's genome sequencing with a Kanamycin-resistance cassette in front of the gene. PCR primers with overlaps for the construct on pQE-70 and the target locus inside of the *E. coli* genome were designed (see list of primers No 71). PCR product was transformed into *E. coli* BW25113 containing *pdk46*. Cells were incubated at 30°C for one hour before temperature was raised to 37°C. Cells were plated on LB-Agar containing Kanamycin. Success of mutation was confirmed by sequencing, the final strain was termed P80.

6. Buffers and Media

6.1 Media

LB Medium (1L)

NaCl	10g
Yeast extract	5g
Tryptone	10g

Tryptone	16g
NaH ₂ PO ₄ ·xH ₂ O	3.04 g
Na ₂ HPO ₄	7.12 g
Glucose	19.8 g

YPTG Medium (1L)

NaCl	5g
Yeast extract	10g

YP Medium (1L)

Yeast extract	10 g
Tryptone	20 g

6.2 Protein purification buffers

Lysis buffer

NaCl	300 mM
NaH ₂ PO ₄	50 mM pH=7,4
Imidazole	5mM

Elution buffer

NaCl	300 mM
NaH ₂ PO ₄	50 mM pH=7.4
Imidazole	500mM

Wash buffer

NaCl	300 mM
NaH ₂ PO ₄	50 mM pH=7.4
Imidazole	10mM

Gelfiltration buffer

Hepes	50 mM pH= 7.8
KCl	100 mM
NaCl	200 mM
MgCl ₂	10 mM
Glycerol	2%

6.3 Ribosome purification buffers

Cell buffer

Hepes	10 mM pH=7.8
MgCl ₂	30 mM
NH ₄ Cl	150 mM
β-Mercaptoethanol	6 mM

Sucrose cushion buffer

Hepes	50 mM pH=7.8
Mg(CH ₃ COO) ₂	30 mM
NH ₄ Cl	500 mM
Sucrose	1.1 M

Sucrose gradient buffer A

Hepes	10 mM pH=7.8
MgCl ₂	30 mM
NH ₄ Cl	75 mM
β-Mercaptoethanol	6 mM
Sucrose	10%/40%

Sucrose gradient buffer B: Sucrose gradient buffer A without sucrose.

7. Plasmid maps

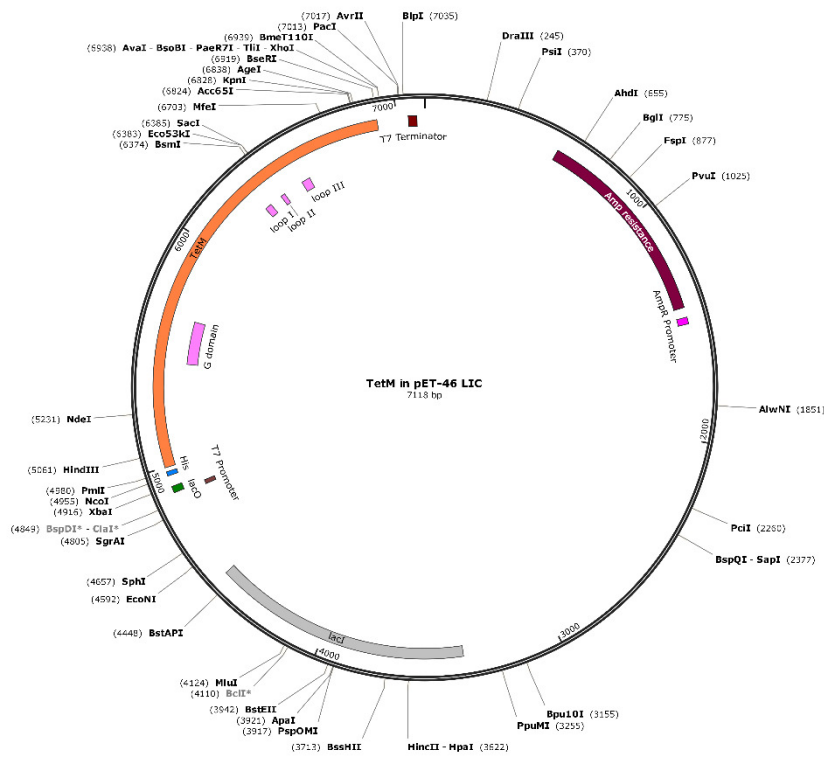


Figure 36: Plasmid map of TetM in the plasmid pET-46 Ek/LIC. The loci of mutations: the G' domain and loops I, II and III are highlighted.

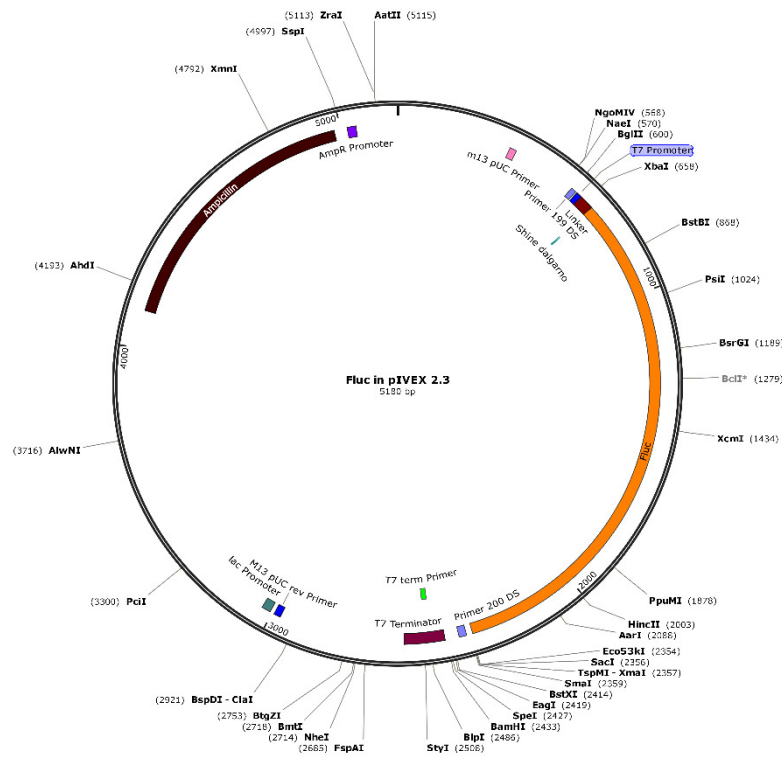


Figure 37: Plasmid map of Firefly luciferase (Fluc) in the plasmid pIVEX 2.3.

8. List of Primers

1	Loop Random Mutation for.	tttaagtatggcttaNNNNNNNNNNNNNNNNNagtagtaccacagcagat
	Loop Random Mutation rev.	atctgctgggggtactNNNNNNNNNNNNNNNNtaagccataacttaaa
2	TetM E173K for.	aactttaccgaatctaaacaatgggatacggta
	TetM E173K rev.	taccgtatcccattgttttagattcggtaaagtt
3	TetM D176K for.	gaatctgaacaatggaaacggtaatagagggga
	TetM D176K rev.	tccctctattaccgtttccattgttcagattc
4	TetM E180K for.	tgggatacggtaataaaaggaaacgatgacctt
	TetM E180K rev.	aaggatcatcgtttccctttattaccgtatccca
5	TetM E187K for.	aacgatgaccttttaagaaatataatgtccgggt
	TetM E187K rev.	accggacataatattcttttaaaggatcatcggt
6	TetM D173K for 2	GTGTGTGTGACGaaactttaccgaatctaaacaatgg
	TetM D173K rev 2	ccattgttttagattcggtaaagttCGTCACACACAC
7	TetM D176K for 2	gaatctgaacaatggaaacggtaatagagggg
	TetM D176K rev 2	ccctctattaccgtttccattgttcagattc
8	TetM E180K for 2	caatgggatacggtaataaaggaaacgatgaccttttagag
	TetM E180K rev 2	ctctaaaaggatcatcgtttccctttattaccgtatcccattg
9	TetM E187K for 2	cgatgaccttttaagaaatataatgtccggtaaattcattag
	TetM E187K rev 2	ctaattgatttaccggacataatattcttttaaaggatcatcg
10	TetM Random Mutation for 2	ctgttttaagtatggcttaNNNNNNNagccctgttagtaccacagc
	TetM Random Mutation rev 2	gctgggggtactaacagggctNNNNNNNtaagccataacttaaaacag
11	TetM D176K for 3	ccgaatctgaacaatggaaacggtaatagaggggaaacg
	TetM D176K rev 3	cgtttccctctattaccgtttccattgttcagattcgg
12	TetM E187K for 3	gagggaaacgatgaccttttaagaaatataatgtccggtaaattcattag
	TetM E187K rev 3	ctaattgatttaccggacataatattcttttaaaggatcatcgtttcctc
13	TetM Random Mutation phosphorylated primers for	P-NNNtatagccctgttagtaccacagcag
	TetM Random Mutation phosphorylated primers rev	P-taagccataacttaaaacagattttacagtcctcagc
14	TetO Y507A for	ctgttttgaaTatggattgtatgagagtcctgtaagtacccccgag
	TetO Y507A rev	ctgcgggggtacttacaggactcgcatacaatccatAttcaaaacag
15	TetO Y506A Y507A for	ctgttttgaaTatggattggcggcagtcctgtaagtacccccgag
	TetO Y506A Y507A rev	ctgcgggggtacttacaggactcgccgccaatccatAttcaaaacag
16	TetS Y512A for	ctgttttaagtatggcttatatgagagccctgtcagtagccagcag
	TetS Y512A rev	ctgctggcgtactgacagggctcgcatatagaccataacttaaaacag
17	TetS Y511A Y512A for	gatctgttttaagtatggcttagcggcagagccctgtcagtagccagcag
	TetS Y511A Y512A rev	ctgctggcgtactgacagggctcgccgctagaccataacttaaaacag

		agatc
18	TetM D183K for	gagggaaac aagg accttttagagaaatataatgtccg
	TetM D183K rev	ctaaaaggtc ctt gtttccctctattaccgatatccattg
19	TetM D176K E180K for	caatgg aag acggtaata aagg gaaacgatgaccttttagagaa tatatg
	TetM D176K E180K rev	gtttcc ctt tattaccgt ctt ccattgttcagattcggtaaagtt cgtc
20	TetM E180K E187K for	ggaaacgatgacctttta aag aaatataatgtccggtaaatacatta g
	TetM E180K E187K rev	catatattt ctt taaaaggtcatcgtttcc ctt tattaccg
21	TetO Y507A for 2	gaaTatggattgtat gcg agtcctgtaagtacccccgcagacttt c
	TetO Y507A rev 2	ggtacttacaggact cg atacaatccatAttcaaaacagatttt aCagtctgtcac
22	TetS Y512A for 2	gttttaagtatggctatat gcg agccctgtcagtagccagcag atttccgaatg
	TetS Y512A rev 2	gctggcgtagctgacagggct cg catatagaccataacttaaaacag atcttacagtc
23	TetM D183K for 2	gatacggtaatagagggaaac AAG gaccttttagagaaatataatg tccggtaaatac
	TetM D183K rev 2	catatatttctctaaaaggtc CTT gtttccctctattaccgatatc ccattgttcag
24	TetM E180K E187K for 2	gtaata AAG gaaacgatgacctttta AAG aaatataatgtccgggt aatcattag
	TetM E180K E187K rev 2	gattaccggacatatattt CTT taaaaggtcatcgtttcc CTTt attaccg
25	TetS Y511A Y512A for 2	gttttaagtatggctta GCGGCG agccctgtcagtagccagcag atttccgaatg
	TetS Y511A Y512A rev 2	gctggcgtagctgacagggct cgccgc tagaccataacttaaaacag atcttacagtc
26	TetS Y511A Y512A for 3	gttttaagtatggctta GCGGCG agccctgtcagtagccagcag atttc
	TetS Y511A Y512A rev 3	gctggcgtagctgacagggct cgccgc tagaccataacttaaaacag atc
27	TetM Y506V for	gttttaagtatggctta GTA tatagccctgtagtagccccagcag
	TetM Y506V rev	gtactaacagggctata TAC taagccataacttaaaacagatttta c
28	TetM Y507R for	gttttaagtatggcttatac AGA agccctgtagtagccccagcag attttc
	TetM Y507R rev	gctggggtagctaacagggct TCT gtataagccataacttaaaacag attttac
29	TetM Y506V Y507R for	gttttaagtatggctta GTAAGA agccctgtagtagccccagcag attttc
	TetM Y506V Y507R rev	gctggggtagctaacagggct TCTTAC taagccataacttaaaacag attttac
30	TetM Y506F Y507S V510L for	gatggcttaTTTTCTagccct TTG agtagccccagcagattttcg gatgcttg
	TetM Y506F Y507S V510L rev	catccgaaaatctgctggggtagct CAA agggctAGAAAAtaagcc ataacttaaaac
31	TetM Y506F Y507F V510A for	gatggcttaTTTTTTagccct GCT agtagccccagcagattttcg gatgcttg
	TetM Y506F Y507F V510A rev	catccgaaaatctgctggggtagct AGC agggctAAAAAaagcc ataacttaaaac
32	TetM Y506F Y507S for	gttttaagtatggcttaTTT TCT agccctgtagtagccccagcag attttc
	TetM Y506F Y507S rev	gctggggtagctaacagggct AGAAAA aagccataacttaaaacag attttac
33	TetM S465Y for	cagtatgagagctcggtt TAT cttgataacttaaatcaatcattt

		c
	TetM S465Y rev	gatttaagtatccaagATAaaccgagctctcatactgcattccac
34	TetM L466Y for	gagagctcggtttctTATggatacttaaataatcaatcatttcaaaatg
	TetM L466Y rev	gattgatttaagtatccATAAgaaccgagctctcatactgcattc
35	TetM G467Y for	gagctcggtttctctTATtacttaaataatcaatcatttcaaaatgag
	TetM G467Y rev	gaaatgattgatttaagtaATAaagagaaaccgagctctcatactgcattc
36	TetM Y468F for	ctcggtttctcttgggTTTttaaataatcaatcatttcaaaatgcag
	TetM Y468F rev	gaaatgattgatttaaAAAtccaagagaaaccgagctctcatac
37	TetM L466G for	gagagctcggtttctGGCggatacttaaataatcaatcatttcaaaatg
	TetM L466G rev	gattgatttaagtatccGCCagaaaccgagctctcatactgcattc
38	TetM Y468G for	ctcggtttctcttgggGGCttaaataatcaatcatttcaaaatgcag
	TetM Y468G rev	gaaatgattgatttaaGCCtccaagagaaaccgagctctcatac
39	TetM S465Y L466Y for	cagtatgagagctcgggtTATTATggatacttaaataatcaatcattc
	TetM S465Y L466Y rev	gatttaagtatccATAATAaaccgagctctcatactgcattccac
40	TetM L466G Y468G for	ctcggtttctGGCggaGGCttaaataatcaatcatttcaaaatgcag
	TetM L466G Y468G rev	ctgcattttgaaatgattgatttaaGCCTccGCCagaaaccgag
41	TetM Y506C for	gttttaagtatggcttaTGCtatagccctgtagtaccagcag
	TetM Y506C rev	gtactaacagggctataGCAtaagccatacttaaacaagattttac
42	TetM Y507C ro	gttttaagtatggcttatacTGCagccctgtagtaccagcagattttc
	TetM Y507C rev	ctgggtactaacagggctGCAgtataagccatacttaaacaagattttac
43	TetM S508C for	gtatggcttatactatTGCcctgtagtaccagcagattttc
	TetM S508C rev	ctgggtactaacagggCAatagtagataagccatacttaaacaag
44	TetM P509C for	gcttatactatagcTGCgtagtaccagcagattttcggatg
	TetM P509C rev	ctgctgggtactaacGCAgctatagtagataagccatacttaaacaag
45	TetM V510C for	cttatactatagccctTGCagtagtaccagcagattttcggatgcttg
	TetM V510C rev	gaaaatctgctgggtactGCAagggtatagtagataagccatacttaaacaag
46	TetM S511C for	cttatactatagccctggtTGCacccagcagattttcggatgcttgctc
	TetM S511C rev	gaaaatctgctgggtGCAaacagggctatagtagataagccatac
47	TetM F635A for	gataaagtagatataatGCGaataaaataacttagaccgggcttc
	TetM F635A rev	gtctaagttattttattCGCcatatatacgtactttatctatccgac
48	TetM F635D for	gataaagtagatataatGATAaataaaataacttagaccgggcttc
	TetM F635D rev	gtctaagttattttattATCcatatatacgtactttatctatccgac
49	TetM N636A for	gataaagtagatataatttcGCGaaaataacttagaccgggcttcctcctc
	TetM N636A rev	gaagccgggtctaagttattttCGCgaacatatacgtactttatctatccgac
50	TetM N636D for	gataaagtagatataatttcGATaaaataacttagaccgggcttcctcctc

	TetM N636D rev	gaagcccggctctaagttatTTTATCgaacatatatcgactttatctatccgac
51	TetM W442A for	gtgccgccaatcctttcGCGgcttccattggtttatctgtatcacgcttc
	TetM W442A rev	gataaaccaatggaagcCGCgaaaggatttggcggcacttcgatgtgaatg
52	TetM W442C for	gtgccgccaatcctttcTGCgcttccattggtttatctgtatcacgcttc
	TetM W442C rev	gataaaccaatggaagcGCAgaaaggatttggcggcacttcgatgtgaatg
53	TetM W442H for	gtgccgccaatcctttcCATgcttccattggtttatctgtatcacgcttc
	TetM W442H rev	gataaaccaatggaagcATGgaaaggatttggcggcacttcgatgtgaatg
54	TetM V510R for	cttatactatagccctCGTagtacccagcagatTTTcggatgcttg
	TetM V510R rev	gaaaatctgctgggtactACGagggtatagtataagccatacttaaac
55	TetM F516A for	gttagtaccagcagatGCGcggatgcttgctcctattgtattggaac
	TetM F516A rev	caataggagcaagcatccgCGCatctgctgggtactaacagggctatag
56	TetM F516D for	gttagtaccagcagatGATcggatgcttgctcctattgtattggaac
	TetM F516D rev	caataggagcaagcatccgATCcatctgctgggtactaacagggctatag
57	TetM K637A for	gtacgatatatgttcaatGCGataacttagaccgggttctcctcctc
	TetM K637A rev	gaagcccggctctaagttatCGCattgaacatatatcgactttatctatc
58	TetM K637D for	gtacgatatatgttcaatGATataacttagaccgggttctcctcctc
	TetM K637D rev	gaagcccggctctaagttatATCattgaacatatatcgactttatctatc
59	TetM P440A for	catcgaagtgccgccaatGCGttctgggcttccattggtttatctg
	Tetm P440A rev	gataaaccaatggaagcccagaaCGCatttggcggcacttcgatgtgaatg
60	TetM G467A for	gagctcggtttctcttGCGtacttaaatcaatcatttcaaaatgcag
	TetM G467A rev	gaaatgattgatttaagtaCGCaagagaaaccgagctctcactgcattc
61	TetM F516A II for	gttagtaccagcagatGCGcggatgcttgctcctattgtattggaac
	TetM F516A II rev	caataggagcaagcatccgCGCatctgctgggtactaacagggctatag
62	TetM F516D II for	gttagtaccagcagatGATcggatgcttgctcctattgtattggaac
	TetM F516D II rev	caataggagcaagcatccgATCcatctgctgggtactaacagggctatag
63	TetM L466G G467A Y468G for	gagctcggtttcttGGCGGGGttaaatcaatcatttcaaaatgcag
	TetM L466G G467A Y468G rev	gaaatgattgatttaaGCCCCGCCagaaaccgagctctcactgcattc
64	Fluc PCR product for IVT	cgagatctcgatcccgc
	Fluc PCR product for IVT	ttattaatgatgatgatgatg
65	TetM S465G for	cagatgagagctcgggtGGCcttgatacttaaatcaatcattt

9. List of software

The thesis was written using Microsoft Office versions 2007 and 2013.

Figures 1, 3, 4 and 5 were created using Adobe Illustrator Version CS6.

Figures 2,6,7,8,30 and 35 were created using ACD/ChemSketch.

ACD/ChemSketch (Freeware), File Version C10E41, Build 76694, Advanced Chemistry Development, Inc., Toronto, ON, Canada, www.acdlabs.com, 2015.

Figures 11, 13, 16, 18, 20, 21, 22, 26, 27, 28, 29, 31, 32, 33 and 34 were created using SigmaPlot Version 13.0.

Amino acid alignments of Figures 9, 10 and 12 were created using Clustal omega:

<https://www.ebi.ac.uk/Tools/msa/clustalo/>

and were edited in Boxshade:

https://embnet.vital-it.ch/software/BOX_form.html

The genome of strain T80 was analyzed using Integrated Genome Viewer version 2.3.94.

All plasmid maps were created using SnapGene® Viewer version 2.7.1

The References-chapter of this thesis was created using Citavi version 5.7

10. References

1. Tacconelli, E. WHO-PPL-Short_Summary_25Feb-ET_NM_WHO. http://www.who.int/medicines/publications/WHO-PPL-Short_Summary_25Feb-ET_NM_WHO.pdf. (accessed, 19 March 2018).
2. Shallcross, L. J. & Davies, D. S. C. Antibiotic overuse. A key driver of antimicrobial resistance. *Br. J. Gen. Pract.* **64**, 604–605 (2014).
3. Martin, M. J., Thottathil, S. E. & Newman, T. B. Antibiotics Overuse in Animal Agriculture. A Call to Action for Health Care Providers. *Am. J. Public Health.* **105**, 2409–2410 (2015).
4. Bundesamt für Verbraucherschutz und Lebensmittelsicherheit, Paul-Ehrlich-Gesellschaft für Chemotherapie e.V. *GERMAP 2015-Bericht über den Antibiotikaverbrauch und die Verbreitung von Antibiotikaresistenzen in der Human und Veterinärmedizin in Deutschland. Antiinfectives Intelligence* (Rheinbach, 2016).
5. Wallmann Jürgen, Reimer Inke, Heberer Thomas. Abgabemengenerfassung antimikrobiell wirksamer Stoffe in Deutschland 2015. Auswertung der nach DIMDI-AMV eingereichten Daten 2015 und Vergleich mit den Daten aus den Vorjahren. *Deutsches Tierärzteblatt*, 1650–1657 (2016).
6. Lübbert, C. *et al.* Environmental pollution with antimicrobial agents from bulk drug manufacturing industries in Hyderabad, South India, is associated with dissemination of extended-spectrum beta-lactamase and carbapenemase-producing pathogens. *Infection.* **45**, 479–491 (2017).
7. Domagk, G. Chemotherapie der bakteriellen Infektionen. *Angew. Chem.* **48**, 657–667 (1935).
8. Domagk, G. Ein Beitrag zur Chemotherapie der bakteriellen Infektionen. *Dtsch. Med. Wochenschr.* **61**, 250–253 (1935).
9. Kirby, W. M. & Rantz, L. A. Sulfonamide Resistance. *Cal. West. Med.* **57**, 174–175 (1942).
10. ABRAHAM, E. P. & CHAIN, E. An Enzyme from Bacteria able to Destroy Penicillin. *Nature.* **146**, 837 (1940).
11. CHAIN, E. *et al.* PENICILLIN AS A CHEMOTHERAPEUTIC AGENT. *Lancet.* **236**, 226–228 (1940).
12. Lobanovska, M. & Pilla, G. Penicillin's Discovery and Antibiotic Resistance. Lessons for the Future? *Yale J. Biol. Med.* **90**, 135–145 (2017).
13. Fraser, I. Penicillin. Early trials in war casualties. *Br. Med. J.* **289**, 1723–1725 (1984).
14. Gould, K. Antibiotics. From prehistory to the present day. *J. Antimicrob. Chemother.* **71**, 572–575 (2016).
15. van Leeuwenhoek, A. Part of a Letter from Mr Antony van Leeuwenhoek, F. R. S. concerning Green Weeds Growing in Water, and Some Animalcula Found about Them. *Phil. Trans.* **23**, 1304–1311 (1702).
16. Gest, H. The discovery of microorganisms by Robert Hooke and Antoni Van Leeuwenhoek, fellows of the Royal Society. *Notes Rec. R. Soc. Lond.* **58**, 187–201 (2004).
17. Burdon-Sanderson J. Memoirs: The Origin and Distribution of Microzymes (Bacteria) in Water and the Circumstances which determine their Existence in the Tissues and Liquids of the Living Body. *J. Cell Sci.*, 323–352 (1871).
18. Roberts, W. Studies on Biogenesis. *Phil. Trans.* **164**, 457–477 (1874).

19. Duckett, S. Ernest Duchesne and the concept of fungal antibiotic therapy. *Lancet*. **354**, 2068–2071 (1999).
20. Bentley, R. Bartolomeo Gosio, 1863-1944. An appreciation. *Adv. Appl. Microbiol.* **48**, 229–250 (2001).
21. Gosio Bartolomeo. Ricerche batteriologiche e chimiche sulle alterazioni del mais. Contributo all'eziologia della pellagra. *Rivista d'Igiene e Sanità Pubblica* **Volume 7**, n.21 484-487 e n.22 869-888 (1896).
22. Gosio Barolomeo. Contributo all'eziologia della pellagra; ricerche chimiche e batteriologiche sulle alterazioni del mais. *Giornale della Reale Accademia di Medicina di Torino* **61**, 484–487 (1893).
23. Okamoto, M. *et al.* Therapeutic drug monitoring of mycophenolic acid in renal transplant recipients. *Transplant. Proc.* **37**, 859–860 (2005).
24. Moore, R. A. & Derry, S. Systematic review and meta-analysis of randomised trials and cohort studies of mycophenolate mofetil in lupus nephritis. *Arthritis. Res. Ther.* **8**, R182 (2006).
25. Parascandola, J. *History of Salvarsan (Arsphenamine)*. (John Wiley & Sons, Ltd eLS., 2001).
26. Ehrlich Paul. Die Behandlung der Syphilis mit dem Ehrlichschen Präparat 606. *Dtsch. Med. Wochenschr.*, 1893–1896 (1901).
27. Browning CH, M. I. The treatment of syphilis by salvarsan. *Br. Med. J.* **2**, 654–655 (1911).
28. Ehrlich Paul. Address in Pathology, ON CHEMIOTHERAPY. Delivered before the Seventeenth International Congress of Medicine. *Br. Med. J.* **2**, 353–359 (1913).
29. Williams, K. J. The introduction of 'chemotherapy' using arsphenamine - the first magic bullet. *J. R. Soc. Med.* **102**, 343–348 (2009).
30. Fleming Alexander. On the antibacterial action of cultures of a penicillium, with special reference to their use in the isolation of B. Influenzae. *Br. J. Exp. Pathol.* **10**, 226–236 (1929).
31. Lesch, J. E. *The first miracle drugs. How the sulfa drugs transformed medicine* (Oxford University Press, Oxford, New York, 2007).
32. Tréfouël, J., Tréfouël, T., Nitti, F., Bovet, D. Activité du p-aminophénylsulfamide sur l'infection streptococcique expérimentale de la souris et du lapin. *C. R. Seances Soc. Biol. Fil.* **120**, 756–758 (1935).
33. Schatz, A., Bugle, E. & Waksman, S. A. Streptomycin, a Substance Exhibiting Antibiotic Activity Against Gram-Positive and Gram-Negative Bacteria. *Exp. Biol. Med.* **55**, 66–69 (1944).
34. Waksman, S. A. & Flynn, J. E. History of the word 'antibiotic'. *J. Hist. Med. Allied Sci.* **28**, 284–286 (1973).
35. Clatworthy, A. E., Pierson, E. & Hung, D. T. Targeting virulence. A new paradigm for antimicrobial therapy. *Nat. Chem. Biol.* **3**, 541–548 (2007).
36. Deak, D., Outtersson, K., Powers, J. H. & Kesselheim, A. S. Progress in the Fight Against Multidrug-Resistant Bacteria? A Review of U.S. Food and Drug Administration-Approved Antibiotics, 2010-2015. *Ann. Intern. Med.* **165**, 363–372 (2016).
37. Koul, A. *et al.* Diarylquinolines target subunit c of mycobacterial ATP synthase. *Nat. Chem. Biol.* **3**, 323–324 (2007).
38. Wright, D. E. The orthosomycins, a new family of antibiotics. *Tetrahedron.* **35**, 1207–1237 (1979).

39. Mason, D. J., Dietz, A. & DeBoer, C. *Lincomycin, a new antibiotic. 1. Discovery and biological properties. Antimicrobial Agents and Chemotherapy* 1962. 554-559 (J. C. Sylvester, Ed. Ann Arbor, Mich., Braun-Brumfield, Inc., 1963).
40. Bhuyana, B. K., Dietz, A. & Smith, C. G. Pactamycin, a new antitumor antibiotic. I. Discovery and biological properties. *Antimicrob. Agents Chemother.* **184**, 1050–1056 (1961).
41. Novak, R. & Shlaes, D. M. The pleuromutilin antibiotics. A new class for human use. *Curr. Opin. Investig. Drugs.* **11**, 182–191 (2010).
42. EHRLICH, J., SMITH, R. M., PENNER, M. A., ANDERSON, L. E. & BRATTON, A. C. Antimicrobial activity of *Streptomyces floridae* and of Viomycin. *Am. Rev. Tuberc.* **63**, 7–16 (1951).
43. GODTFREDSSEN, W. O., JAHNSEN, S., LORCK, H., ROHOLT, K. & TYBRING, L. Fusidic acid. A new antibiotic. *Nature.* **193**, 987 (1962).
44. Wolf, H., Chinali, G. & Parmeggiani, A. Kirromycin, an inhibitor of protein biosynthesis that acts on elongation factor Tu. *Proc. Natl. Acad. Sci. U S A.* **71**, 4910–4914 (1974).
45. SU, T. L. Micrococcin, an antibacterial substance formed by a strain of *Micrococcus*. *Br. J. Exp. Pathol.* **29**, 473–481 (1948).
46. Fuller, A. T. *et al.* Pseudomonic acid. An antibiotic produced by *Pseudomonas fluorescens*. *Nature.* **234**, 416–417 (1971).
47. SHULL, G. M. & SARDINAS, J. L. PA-94, an antibiotic identical with D-4-amino-3-isoxazolidinone (cycloserine, oxamycin). *Antibiot. Chemother. (Northfield).* **5**, 398–399 (1955).
48. Hendlin, D., Stapley, E. O. & Jackson, M. Phosphomycin, a new antibiotic produced by strains of streptomyces. *Science.* **166**, 122–123 (1969).
49. Hoeksema, H., Johnson, J. L. & Hinman, J. W. Structural studies on streptonivicin, a new antibiotic. *J. Am. Chem. Soc.*, 6710–6711 (1955).
50. MATTICK, A. T. R. & HIRSCH, A. Further observations on an inhibitory substance (nisin) from lactic streptococci. *Lancet.* **2**, 5–8 (1947).
51. AINSWORTH, G. C., BROWN, A. M. & BROWNLIE, G. Aerosporin, an antibiotic produced by *Bacillus aerosporus* Greer. *Nature.* **159**, 263 (1947).
52. Johnson, B. A., Anker, H. & Meleney, F. L. BACITRACIN. A NEW ANTIBIOTIC PRODUCED BY A MEMBER OF THE B. SUBTILIS GROUP. *Science.* **102**, 376–377 (1945).
53. Katagiri, K. *et al.* A new antibiotic. Furanomycin, an isoleucine antagonist. *J. Med. Chem.* **10**, 1149–1154 (1967).
54. Watanabe, T., Izaki, K. & Takahashi, H. New polyenic antibiotics active against gram-positive and -negative bacteria. I. Isolation and purification of antibiotics produced by *Gluconobacter* sp. W-315. *J. Antibiot.* **35**, 1141–1147 (1982).
55. ZIEF, M., WOODSIDE, R. & SCHMITZ, H. Pulvomycin. *Antibiot. Chemother. (Northfield).* **7**, 384–386 (1957).
56. ROTH, B., FALCO, E. A., HITCHINGS, G. H. & BUSHBY, S. R. 5-BENZYL-2,4-DIAMINOPYRIMIDINES AS ANTIBACTERIAL AGENTS. I. SYNTHESIS AND ANTIBACTERIAL ACTIVITY IN VITRO. *J. Med. Pharm. Chem.* **91**, 1103–1123 (1962).
57. Hotchkiss, R. D. & Dubos, R. J. Bactericidal fractions from an aerobic sporulating bacillus. *J. Biol. Chem.* **136**, 803–804 (1949).
58. Hamad, B. The antibiotics market. *Nat. Rev. Drug Discov.* **9**, 675–676 (2010).

59. BARNUM, C. P. & HUSEBY, R. A. Some quantitative analyses of the particulate fractions from mouse liver cell cytoplasm. *Arch. Biochem.* **19**, 17–23 (1948).
60. PETERMANN, M. L. & HAMILTON, M. G. An ultracentrifugal analysis of the macromolecular particles of normal and leukemic mouse spleen. *Cancer. Res.* **12**, 373–378 (1952).
61. PALADE, G. E. A small particulate component of the cytoplasm. *J. Biophys. Biochem. Cytol.* **1**, 59–68 (1955).
62. Steitz, T. A. & Moore, P. B. RNA, the first macromolecular catalyst. The ribosome is a ribozyme. *Trends Biochem. Sci.* **28**, 411–418 (2003).
63. Nissen, P., Hansen, J., Ban, N., Moore, P. B. & Steitz, T. A. The structural basis of ribosome activity in peptide bond synthesis. *Science.* **289**, 920–930 (2000).
64. Blattner, F. R. *et al.* The complete genome sequence of Escherichia coli K-12. *Science.* **277**, 1453–1462 (1997).
65. Deutscher, M. P. Maturation and degradation of ribosomal RNA in bacteria. *Prog. Mol. Biol. Transl. Sci.* **85**, 369–391 (2009).
66. Held, W. A., Ballou, B., Mizushima, S. & Nomura, M. Assembly mapping of 30 S ribosomal proteins from Escherichia coli. Further studies. *J. Biol. Chem.* **249**, 3103–3111 (1974).
67. Herold, M. & Nierhaus, K. H. Incorporation of six additional proteins to complete the assembly map of the 50 S subunit from Escherichia coli ribosomes. *J. Biol. Chem.* **262**, 8826–8833 (1987).
68. Laursen, B. S., Sørensen, H. P., Mortensen, K. K. & Sperling-Petersen, H. U. Initiation of protein synthesis in bacteria. *Microbiol. Mol. Biol. Rev.* **69**, 101–123 (2005).
69. Moazed, D., Samaha, R. R., Gualerzi, C. & Noller, H. F. Specific protection of 16 S rRNA by translational initiation factors. *J. Mol. Biol.* **248**, 207–210 (1995).
70. Petrelli, D. *et al.* Translation initiation factor IF3. Two domains, five functions, one mechanism? *EMBO J.* **20**, 4560–4569 (2001).
71. Milon, P. *et al.* The ribosome-bound initiation factor 2 recruits initiator tRNA to the 30S initiation complex. *EMBO Rep.* **11**, 312–316 (2010).
72. Shine, J. & Dalgarno, L. The 3'-terminal sequence of Escherichia coli 16S ribosomal RNA. Complementarity to nonsense triplets and ribosome binding sites. *Proc. Natl. Acad. Sci. U S A.* **71**, 1342–1346 (1974).
73. Steitz, J. A. Polypeptide chain initiation. Nucleotide sequences of the three ribosomal binding sites in bacteriophage R17 RNA. *Nature.* **224**, 957–964 (1969).
74. Chen, H., Bjerknes, M., Kumar, R. & Jay, E. Determination of the optimal aligned spacing between the Shine-Dalgarno sequence and the translation initiation codon of Escherichia coli mRNAs. *Nucleic Acids Res.* **22**, 4953–4957 (1994).
75. Ma, J., Campbell, A. & Karlin, S. Correlations between Shine-Dalgarno sequences and gene features such as predicted expression levels and operon structures. *J. Bacteriol.* **184**, 5733–5745 (2002).
76. Ringquist, S. *et al.* Translation initiation in Escherichia coli. Sequences within the ribosome-binding site. *Mol. Microbiol.* **6**, 1219–1229 (1992).
77. Milón, P., Maracci, C., Filonava, L., Gualerzi, C. O. & Rodnina, M. V. Real-time assembly landscape of bacterial 30S translation initiation complex. *Nat. Struct. Mol. Biol.* **19**, 609–615 (2012).

78. Lam, S. S. & Schimmel, P. R. Equilibrium measurements of cognate and noncognate interactions between aminoacyl transfer RNA synthetases and transfer RNA. *Biochemistry*. **14**, 2775–2780 (1975).
79. Francklyn, C. S. DNA polymerases and aminoacyl-tRNA synthetases. Shared mechanisms for ensuring the fidelity of gene expression. *Biochemistry*. **47**, 11695–11703 (2008).
80. WATSON, J. D. & CRICK, F. H. Molecular structure of nucleic acids; a structure for deoxyribose nucleic acid. *Nature*. **171**, 737–738 (1953).
81. Nirenberg, M. *et al.* RNA codewords and protein synthesis, VII. On the general nature of the RNA code. *Proc. Natl. Acad. Sci. U S A*. **53**, 1161–1168 (1965).
82. Rodnina, M. V., Pape, T., Fricke, R., Kuhn, L. & Wintermeyer, W. Initial binding of the elongation factor Tu.GTP.aminoacyl-tRNA complex preceding codon recognition on the ribosome. *J. Biol. Chem.* **271**, 646–652 (1996).
83. Ogle, J. M. *et al.* Recognition of cognate transfer RNA by the 30S ribosomal subunit. *Science*. **292**, 897–902 (2001).
84. Carter, A. P. *et al.* Functional insights from the structure of the 30S ribosomal subunit and its interactions with antibiotics. *Nature*. **407**, 340–348 (2000).
85. Ogle, J. M., Murphy, F. V., Tarry, M. J. & Ramakrishnan, V. Selection of tRNA by the ribosome requires a transition from an open to a closed form. *Cell*. **111**, 721–732 (2002).
86. Demeshkina, N., Jenner, L., Westhof, E., Yusupov, M. & Yusupova, G. A new understanding of the decoding principle on the ribosome. *Nature*. **484**, 256–259 (2012).
87. Voorhees, R. M. & Ramakrishnan, V. Structural basis of the translational elongation cycle. *Annu. Rev. Biochem.* **82**, 203–236 (2013).
88. Loveland, A. B., Demo, G., Grigorieff, N. & Korostelev, A. A. Ensemble cryo-EM elucidates the mechanism of translation fidelity. *Nature*. **546**, 113–117 (2017).
89. CRICK, F. H. Codon--anticodon pairing. The wobble hypothesis. *J. Mol. Biol.* **19**, 548–555 (1966).
90. Valle, M. *et al.* Cryo-EM reveals an active role for aminoacyl-tRNA in the accommodation process. *EMBO J.* **21**, 3557–3567 (2002).
91. Daviter, T., Wieden, H.-J. & Rodnina, M. V. Essential role of histidine 84 in elongation factor Tu for the chemical step of GTP hydrolysis on the ribosome. *J. Mol. Biol.* **332**, 689–699 (2003).
92. Berchtold, H. *et al.* Crystal structure of active elongation factor Tu reveals major domain rearrangements. *Nature*. **365**, 126–132 (1993).
93. Voorhees, R. M., Schmeing, T. M., Kelley, A. C. & Ramakrishnan, V. The mechanism for activation of GTP hydrolysis on the ribosome. *Science*. **330**, 835–838 (2010).
94. Voorhees, R. M., Weixlbaumer, A., Loakes, D., Kelley, A. C. & Ramakrishnan, V. Insights into substrate stabilization from snapshots of the peptidyl transferase center of the intact 70S ribosome. *Nat. Struct. Mol. Biol.* **16**, 528–533 (2009).
95. Nissen, P. The Structural Basis of Ribosome Activity in Peptide Bond Synthesis. *Science*. **289**, 920–930 (2000).
96. Berg, J. M., Tymoczko, J. L., Stryer, L. & Gatto, G. J. *Biochemie*. 7th ed. (Springer Spektrum, Berlin, Heidelberg, 2014).
97. Polikanov, Y. S., Steitz, T. A. & Innis, C. A. A proton wire to couple aminoacyl-tRNA accommodation and peptide-bond formation on the ribosome. *Nat. Struct. Mol. Biol.* **21**, 787–793 (2014).

98. Rodnina, M. V., Savelsbergh, A., Katunin, V. I. & Wintermeyer, W. Hydrolysis of GTP by elongation factor G drives tRNA movement on the ribosome. *Nature*. **385**, 37–41 (1997).
99. Katunin, V. I., Savelsbergh, A., Rodnina, M. V. & Wintermeyer, W. Coupling of GTP hydrolysis by elongation factor G to translocation and factor recycling on the ribosome. *Biochemistry*. **41**, 12806–12812 (2002).
100. Moazed, D. & Noller, H. F. Intermediate states in the movement of transfer RNA in the ribosome. *Nature*. **342**, 142–148 (1989).
101. Adio, S. *et al.* Fluctuations between multiple EF-G-induced chimeric tRNA states during translocation on the ribosome. *Nat. Commun.* **6**, 7442 (2015).
102. Joseph, S. & Noller, H. F. EF-G-catalyzed translocation of anticodon stem-loop analogs of transfer RNA in the ribosome. *EMBO J.* **17**, 3478–3483 (1998).
103. Moazed, D., Robertson, J. M. & Noller, H. F. Interaction of elongation factors EF-G and EF-Tu with a conserved loop in 23S RNA. *Nature*. **334**, 362–364 (1988).
104. Shoji, S., Walker, S. E. & Fredrick, K. Ribosomal translocation. One step closer to the molecular mechanism. *ACS Chem. Biol.* **4**, 93–107 (2009).
105. Frank, J. & Agrawal, R. K. A ratchet-like inter-subunit reorganization of the ribosome during translocation. *Nature*. **406**, 318–322 (2000).
106. Stark, H., Rodnina, M. V., Wieden, H. J., van Heel, M. & Wintermeyer, W. Large-scale movement of elongation factor G and extensive conformational change of the ribosome during translocation. *Cell*. **100**, 301–309 (2000).
107. Schmeing, T. M., Moore, P. B. & Steitz, T. A. Structures of deacylated tRNA mimics bound to the E site of the large ribosomal subunit. *RNA*. **9**, 1345–1352 (2003).
108. Kennell, D. & Riezman, H. Transcription and translation initiation frequencies of the Escherichia coli lac operon. *J. Mol. Biol.* **114**, 1–21 (1977).
109. Sievers, A., Beringer, M., Rodnina, M. V. & Wolfenden, R. The ribosome as an entropy trap. *Proc. Natl. Acad. Sci. U S A.* **101**, 7897–7901 (2004).
110. Vogel, U. & Jensen, K. F. The RNA chain elongation rate in Escherichia coli depends on the growth rate. *J. Bacteriol.* **176**, 2807–2813 (1994).
111. Miller, O. L., Hamkalo, B. A. & Thomas, C. A. Visualization of bacterial genes in action. *Science*. **169**, 392–395 (1970).
112. Loftfield, R. B. & Vanderjagt, D. The frequency of errors in protein biosynthesis. *Biochem. J.* **128**, 1353–1356 (1972).
113. Kramer, E. B. & Farabaugh, P. J. The frequency of translational misreading errors in E. coli is largely determined by tRNA competition. *RNA*. **13**, 87–96 (2007).
114. Parker, J. Errors and alternatives in reading the universal genetic code. *Microbiol. Rev.* **53**, 273–298 (1989).
115. Bouadloun, F., Donner, D. & Kurland, C. G. Codon-specific missense errors in vivo. *EMBO J.* **2**, 1351–1356 (1983).
116. Ninio, J. Connections between translation, transcription and replication error-rates. *Biochimie*. **73**, 1517–1523 (1991).
117. Capecchi, M. R. Polypeptide chain termination in vitro. Isolation of a release factor. *Proc. Natl. Acad. Sci. U S A.* **58**, 1144–1151 (1967).

118. Scolnick, E., Tompkins, R., Caskey, T. & Nirenberg, M. Release factors differing in specificity for terminator codons. *Proc. Natl. Acad. Sci. U S A.* **61**, 768–774 (1968).
119. Ito, K., Uno, M. & Nakamura, Y. A tripeptide 'anticodon' deciphers stop codons in messenger RNA. *Nature.* **403**, 680–684 (2000).
120. Frolova, L. Y. *et al.* Mutations in the highly conserved GGQ motif of class 1 polypeptide release factors abolish ability of human eRF1 to trigger peptidyl-tRNA hydrolysis. *RNA.* **5**, 1014–1020 (1999).
121. Mora, L., Heurgué-Hamard, V., Zamaroczy, M. de, Kervestin, S. & Buckingham, R. H. Methylation of bacterial release factors RF1 and RF2 is required for normal translation termination in vivo. *J. Biol. Chem.* **282**, 35638–35645 (2007).
122. Dinçbas-Renqvist, V. *et al.* A post-translational modification in the GGQ motif of RF2 from *Escherichia coli* stimulates termination of translation. *EMBO J.* **19**, 6900–6907 (2000).
123. Heurgué-Hamard, V., Champ, S., Engström, A., Ehrenberg, M. & Buckingham, R. H. The hemK gene in *Escherichia coli* encodes the N(5)-glutamine methyltransferase that modifies peptide release factors. *EMBO J.* **21**, 769–778 (2002).
124. Pierson, W. E. *et al.* Uniformity of Peptide Release Is Maintained by Methylation of Release Factors. *Cell Rep.* **17**, 11–18 (2016).
125. Korostelev, A. A. Structural aspects of translation termination on the ribosome. *RNA.* **17**, 1409–1421 (2011).
126. Song, H. *et al.* The crystal structure of human eukaryotic release factor eRF1--mechanism of stop codon recognition and peptidyl-tRNA hydrolysis. *Cell.* **100**, 311–321 (2000).
127. Korostelev, A. *et al.* Crystal structure of a translation termination complex formed with release factor RF2. *Proc. Natl. Acad. Sci. U S A.* **105**, 19684–19689 (2008).
128. Zavialov, A. V., Buckingham, R. H. & Ehrenberg, M. A posttermination ribosomal complex is the guanine nucleotide exchange factor for peptide release factor RF3. *Cell.* **107**, 115–124 (2001).
129. Freistroffer, D. V., Pavlov, M. Y., MacDougall, J., Buckingham, R. H. & Ehrenberg, M. Release factor RF3 in *E. coli* accelerates the dissociation of release factors RF1 and RF2 from the ribosome in a GTP-dependent manner. *EMBO J.* **16**, 4126–4133 (1997).
130. Peske, F., Kuhlenkoetter, S., Rodnina, M. V. & Wintermeyer, W. Timing of GTP binding and hydrolysis by translation termination factor RF3. *Nucleic Acids Res.* **42**, 1812–1820 (2014).
131. Janosi, L., Shimizu, I. & Kaji, A. Ribosome recycling factor (ribosome releasing factor) is essential for bacterial growth. *Proc. Natl. Acad. Sci. U S A.* **91**, 4249–4253 (1994).
132. Pai, R. D. *et al.* Structural Insights into ribosome recycling factor interactions with the 70S ribosome. *J. Mol. Biol.* **376**, 1334–1347 (2008).
133. Agrawal, R. K. *et al.* Visualization of ribosome-recycling factor on the *Escherichia coli* 70S ribosome. Functional implications. *Proc. Natl. Acad. Sci. U S A.* **101**, 8900–8905 (2004).
134. Wilson, D. N. *et al.* X-ray crystallography study on ribosome recycling. The mechanism of binding and action of RRF on the 50S ribosomal subunit. *EMBO J.* **24**, 251–260 (2005).
135. Gao, N. *et al.* Mechanism for the disassembly of the posttermination complex inferred from cryo-EM studies. *Mol. Cell.* **18**, 663–674 (2005).
136. Gao, N., Zavialov, A. V., Ehrenberg, M. & Frank, J. Specific interaction between EF-G and RRF and its implication for GTP-dependent ribosome splitting into subunits. *J. Mol. Biol.* **374**, 1345–1358 (2007).

137. Fu, Z. *et al.* Key Intermediates in Ribosome Recycling Visualized by Time-Resolved Cryoelectron Microscopy. *Structure*. **24**, 2092–2101 (2016).
138. Zavialov, A. V., Haurlyiuk, V. V. & Ehrenberg, M. Splitting of the posttermination ribosome into subunits by the concerted action of RRF and EF-G. *Mol. Cell*. **18**, 675–686 (2005).
139. Hirokawa, G. *et al.* The role of ribosome recycling factor in dissociation of 70S ribosomes into subunits. *RNA*. **11**, 1317–1328 (2005).
140. Karimi, R., Pavlov, M. Y., Buckingham, R. H. & Ehrenberg, M. Novel roles for classical factors at the interface between translation termination and initiation. *Mol. Cell*. **3**, 601–609 (1999).
141. Kohanski, M. A., Dwyer, D. J., Hayete, B., Lawrence, C. A. & Collins, J. J. A common mechanism of cellular death induced by bactericidal antibiotics. *Cell*. **130**, 797–810 (2007).
142. Nguyen, Y. & Sperandio, V. Enterohemorrhagic E. coli (EHEC) pathogenesis. *Front. Cell. Infect. Microbiol.* **2**, 90 (2012).
143. Smith, K. E. *et al.* Antibiotic treatment of Escherichia coli O157 infection and the risk of hemolytic uremic syndrome, Minnesota. *Pediatr. Infect. Dis. J.* **31**, 37–41 (2012).
144. Ocampo, P. S. *et al.* Antagonism between bacteriostatic and bactericidal antibiotics is prevalent. *Antimicrob. Agents Chemother.* **58**, 4573–4582 (2014).
145. Bakker-Woudenberg, I. A. J. M., van Vianen, W., van Soolingen, D., Verbrugh, H. A. & van Agtmael, M. A. Antimycobacterial agents differ with respect to their bacteriostatic versus bactericidal activities in relation to time of exposure, mycobacterial growth phase, and their use in combination. *Antimicrob. Agents Chemother.* **49**, 2387–2398 (2005).
146. Davis, B. D. Mechanism of bactericidal action of aminoglycosides. *Microbiol. Rev.* **51**, 341–350 (1987).
147. DRAGO, L., VECCHI, E. de, NICOLA, L., LEGNANI, D. & GISMONDO, M. R. Kinetic bactericidal activity of telithromycin, azithromycin and clarithromycin against respiratory pathogens. *APMIS* **113**, 655–663 (2005).
148. Brender, J. R., McHenry, A. J. & Ramamoorthy, A. Does cholesterol play a role in the bacterial selectivity of antimicrobial peptides? *Front. Immunol.* **3**, 195 (2012).
149. van Bambeke, F., Michot, J.-M. & Tulkens, P. M. Antibiotic efflux pumps in eukaryotic cells. Occurrence and impact on antibiotic cellular pharmacokinetics, pharmacodynamics and toxicodynamics. *J. Antimicrob. Chemother.* **51**, 1067–1077 (2003).
150. Böttger, E. C., Springer, B., Prammananan, T., Kidan, Y. & Sander, P. Structural basis for selectivity and toxicity of ribosomal antibiotics. *EMBO Rep.* **2**, 318–323 (2001).
151. Budkevich, T. V., El'skaya, A. V. & Nierhaus, K. H. Features of 80S mammalian ribosome and its subunits. *Nucleic Acids Res.* **36**, 4736–4744 (2008).
152. Wang, X., Ryu, D., Houtkooper, R. H. & Auwerx, J. Antibiotic use and abuse. A threat to mitochondria and chloroplasts with impact on research, health, and environment. *Bioessays*. **37**, 1045–1053 (2015).
153. Schluenzen, F. *et al.* The antibiotic kasugamycin mimics mRNA nucleotides to destabilize tRNA binding and inhibit canonical translation initiation. *Nat. Struct. Mol. Biol.* **13**, 871–878 (2006).
154. Schuwirth, B. S. *et al.* Structural analysis of kasugamycin inhibition of translation. *Nat. Struct. Mol. Biol.* **13**, 879–886 (2006).

155. Moazed, D. & Noller, H. F. Interaction of antibiotics with functional sites in 16S ribosomal RNA. *Nature*. **327**, 389–394 (1987).
156. Pioletti, M. *et al.* Crystal structures of complexes of the small ribosomal subunit with tetracycline, edeine and IF3. *EMBO J.* **20**, 1829–1839 (2001).
157. Dinos, G. *et al.* Dissecting the ribosomal inhibition mechanisms of edeine and pactamycin. The universally conserved residues G693 and C795 regulate P-site RNA binding. *Mol. Cell*. **13**, 113–124 (2004).
158. Brandi, L. *et al.* Novel tetrapeptide inhibitors of bacterial protein synthesis produced by a *Streptomyces* sp. *Biochemistry*. **45**, 3692–3702 (2006).
159. Fabbretti, A. *et al.* Inhibition of translation initiation complex formation by GE81112 unravels a 16S rRNA structural switch involved in P-site decoding. *Proc. Natl. Acad. Sci. U S A.* **113**, E2286–95 (2016).
160. Belova, L., Tenson, T., Xiong, L., McNicholas, P. M. & Mankin, A. S. A novel site of antibiotic action in the ribosome. Interaction of evernimicin with the large ribosomal subunit. *Proc. Natl. Acad. Sci. U S A.* **98**, 3726–3731 (2001).
161. Arenz, S. *et al.* Structures of the orthosomycin antibiotics avilamycin and evernimicin in complex with the bacterial 70S ribosome. *Proc. Natl. Acad. Sci. U S A.* **113**, 7527–7532 (2016).
162. Fabbretti, A. *et al.* The antibiotic Furvina® targets the P-site of 30S ribosomal subunits and inhibits translation initiation displaying start codon bias. *Nucleic Acids Res.* **40**, 10366–10374 (2012).
163. Moazed, D. & Noller, H. F. Chloramphenicol, erythromycin, carbomycin and vernamycin B protect overlapping sites in the peptidyl transferase region of 23S ribosomal RNA. *Biochimie*. **69**, 879–884 (1987).
164. WISSEMAN, C. L., SMADEL, J. E., HAHN, F. E. & HOPPS, H. E. Mode of action of chloramphenicol. I. Action of chloramphenicol on assimilation of ammonia and on synthesis of proteins and nucleic acids in *Escherichia coli*. *J. Bacteriol.* **67**, 662–673 (1954).
165. Long, K. S. & Porse, B. T. A conserved chloramphenicol binding site at the entrance to the ribosomal peptide exit tunnel. *Nucleic Acids Res.* **31**, 7208–7215 (2003).
166. Schlünzen, F. *et al.* Structural basis for the interaction of antibiotics with the peptidyl transferase centre in eubacteria. *Nature*. **413**, 814–821 (2001).
167. Tenson, T., Lovmar, M. & Ehrenberg, M. The mechanism of action of macrolides, lincosamides and streptogramin B reveals the nascent peptide exit path in the ribosome. *J. Mol. Biol.* **330**, 1005–1014 (2003).
168. Davis, A. R., Gohara, D. W. & Yap, M.-N. F. Sequence selectivity of macrolide-induced translational attenuation. *Proc. Natl. Acad. Sci. U S A.* **111**, 15379–15384 (2014).
169. Brodersen, D. E. *et al.* The structural basis for the action of the antibiotics tetracycline, pactamycin, and hygromycin B on the 30S ribosomal subunit. *Cell*. **103**, 1143–1154 (2000).
170. Kotra, L. P., Haddad, J. & Mobashery, S. Aminoglycosides. Perspectives on mechanisms of action and resistance and strategies to counter resistance. *Antimicrob. Agents Chemother.* **44**, 3249–3256 (2000).
171. Fourmy, D., Recht, M. I., Blanchard, S. C. & Puglisi, J. D. Structure of the A site of *Escherichia coli* 16S ribosomal RNA complexed with an aminoglycoside antibiotic. *Science*. **274**, 1367–1371 (1996).

172. Wilson, D. N. *et al.* The oxazolidinone antibiotics perturb the ribosomal peptidyl-transferase center and effect tRNA positioning. *Proc. Natl. Acad. Sci. U S A.* **105**, 13339–13344 (2008).
173. Polikanov, Y. S. *et al.* Distinct tRNA Accommodation Intermediates Observed on the Ribosome with the Antibiotics Hygromycin A and A201A. *Mol. Cell.* **58**, 832–844 (2015).
174. Poulsen, S. M., Karlsson, M., Johansson, L. B. & Vester, B. The pleuromutilin drugs tiamulin and valnemulin bind to the RNA at the peptidyl transferase centre on the ribosome. *Mol. Microbiol.* **41**, 1091–1099 (2001).
175. Eyal, Z. *et al.* A novel pleuromutilin antibacterial compound, its binding mode and selectivity mechanism. *Sci. Rep.* **6**, 39004 (2016).
176. Vannuffel, P. & Cocito, C. Mechanism of action of streptogramins and macrolides. *Drugs.* **51 Suppl 1**, 20–30 (1996).
177. Johnston, N. J., Mukhtar, T. A. & Wright, G. D. Streptogramin antibiotics. Mode of action and resistance. *Curr. Drug Targets.* **3**, 335–344 (2002).
178. Beyer, D. & Pepper, K. The streptogramin antibiotics. Update on their mechanism of action. *Expert Opin. Investig. Drugs.* **7**, 591–599 (1998).
179. Stanley, R. E., Blaha, G., Grodzicki, R. L., Strickler, M. D. & Steitz, T. A. The structures of the anti-tuberculosis antibiotics viomycin and capreomycin bound to the 70S ribosome. *Nat. Struct. Mol. Biol.* **17**, 289–293 (2010).
180. Holm, M., Borg, A., Ehrenberg, M. & Sanyal, S. Molecular mechanism of viomycin inhibition of peptide elongation in bacteria. *Proc. Natl. Acad. Sci. U S A.* **113**, 978–983 (2016).
181. Svidritskiy, E., Ling, C., Ermolenko, D. N. & Korostelev, A. A. Blasticidin S inhibits translation by trapping deformed tRNA on the ribosome. *Proc. Natl. Acad. Sci. U S A.* **110**, 12283–12288 (2013).
182. Tanaka, N., Kinoshita, T. & Masukawa, H. Mechanism of protein synthesis inhibition by fusidic acid and related antibiotics. *Biochem. Biophys. Res. Commun.* **30**, 278–283 (1968).
183. Gao, Y.-G. *et al.* The structure of the ribosome with elongation factor G trapped in the posttranslocational state. *Science.* **326**, 694–699 (2009).
184. Hogg, T., Mesters, J. R. & Hilgenfeld, R. Inhibitory mechanisms of antibiotics targeting elongation factor Tu. *Curr. Protein Pept. Sci.* **3**, 121–131 (2002).
185. WOLF, H., CHINALI, G. & PARMEGGIANI, A. Mechanism of the Inhibition of Protein Synthesis by Kirromycin. Role of Elongation Factor Tu and Ribosomes. *Eur. J. Biochem.* **75**, 67–75 (1977).
186. PARMEGGIANI, A. *et al.* Enacyloxin IIa pinpoints a binding pocket of elongation factor Tu for development of novel antibiotics. *J. Biol. Chem.* **281**, 2893–2900 (2006).
187. Zuurmond, A. M., Olsthoorn-Tieleman, L. N., Martien de Graaf, J., Parmeggiani, A. & Kraal, B. Mutant EF-Tu species reveal novel features of the enacyloxin IIa inhibition mechanism on the ribosome. *J. Mol. Biol.* **294**, 627–637 (1999).
188. PARMEGGIANI, A. *et al.* Structural basis of the action of pulvomycin and GE2270 A on elongation factor Tu. *Biochemistry.* **45**, 6846–6857 (2006).
189. Kirillov, S. *et al.* Purpuromycin. An antibiotic inhibiting tRNA aminoacylation. *RNA.* **3**, 905–913 (1997).
190. Parenti, M. A., Hatfield, S. M. & Leyden, J. J. Mupirocin. A topical antibiotic with a unique structure and mechanism of action. *Clin. Pharm.* **6**, 761–770 (1987).
191. Hughes, J. & Mellows, G. Inhibition of isoleucyl-transfer ribonucleic acid synthetase in *Escherichia coli* by pseudomonic acid. *Biochem. J.* **176**, 305–318 (1978).

192. Kohno, T., Kohda, D., Haruki, M., Yokoyama, S. & Miyazawa, T. Nonprotein amino acid furanomycin, unlike isoleucine in chemical structure, is charged to isoleucine tRNA by isoleucyl-tRNA synthetase and incorporated into protein. *J. Biol. Chem.* **265**, 6931–6935 (1990).
193. Yanagisawa, T., Lee, J. T., Wu, H. C. & Kawakami, M. Relationship of protein structure of isoleucyl-tRNA synthetase with pseudomonic acid resistance of *Escherichia coli*. A proposed mode of action of pseudomonic acid as an inhibitor of isoleucyl-tRNA synthetase. *J. Biol. Chem.* **269**, 24304–24309 (1994).
194. Green, J. M. & Matthews, R. G. Folate Biosynthesis, Reduction, and Polyglutamylation and the Interconversion of Folate Derivatives. *EcoSal. Plus.* **2** (2007).
195. Illarionova, V. *et al.* Biosynthesis of tetrahydrofolate. Stereochemistry of dihydroneopterin aldolase. *J. Biol. Chem.* **277**, 28841–28847 (2002).
196. Bock, L., Miller, G. H., Schaper, K. J. & Seydel, J. K. Sulfonamide structure-activity relationships in a cell-free system. 2. Proof for the formation of a sulfonamide-containing folate analog. *J. Med. Chem.* **17**, 23–28 (1974).
197. Achari, A. *et al.* Crystal structure of the anti-bacterial sulfonamide drug target dihydropteroate synthase. *Nat. Struct. Biol.* **4**, 490–497 (1997).
198. Gleckman, R., Blagg, N. & Joubert, D. W. Trimethoprim. Mechanisms of action, antimicrobial activity, bacterial resistance, pharmacokinetics, adverse reactions, and therapeutic indications. *Pharmacotherapy.* **1**, 14–20 (1981).
199. Ma, C., Yang, X. & Lewis, P. J. Bacterial Transcription as a Target for Antibacterial Drug Development. *Microbiol. Mol. Biol. Rev.* **80**, 139–160 (2016).
200. Wehrli, W. Rifampin. Mechanisms of action and resistance. *Rev. Infect. Dis.* **5 Suppl 3**, S407-11 (1983).
201. Campbell, E. A. *et al.* Structural mechanism for rifampicin inhibition of bacterial rna polymerase. *Cell.* **104**, 901–912 (2001).
202. Sergio, S., Pirali, G., White, R. & Parenti, F. Lipiarmycin, a new antibiotic from *Actinoplanes* III. Mechanism of action. *J. Antibiot.* **28**, 543–549 (1975).
203. Tupin, A., Gualtieri, M., Leonetti, J.-P. & Brodolin, K. The transcription inhibitor lipiarmycin blocks DNA fitting into the RNA polymerase catalytic site. *EMBO J.* **29**, 2527–2537 (2010).
204. Wang, J. C. DNA topoisomerases. *Annu. Rev. Biochem.* **54**, 665–697 (1985).
205. Smith, D. H. & Davis, B. D. Mode of action of novobiocin in *Escherichia coli*. *J. Bacteriol.* **93**, 71–79 (1967).
206. Maxwell, A. The interaction between coumarin drugs and DNA gyrase. *Mol. Microbiol.* **9**, 681–686 (1993).
207. Anderson, V. E. & Osheroff, N. Type II topoisomerases as targets for quinolone antibacterials. Turning Dr. Jekyll into Mr. Hyde. *Curr. Pharm. Des.* **7**, 337–353 (2001).
208. Aldred, K. J., Kerns, R. J. & Osheroff, N. Mechanism of quinolone action and resistance. *Biochemistry.* **53**, 1565–1574 (2014).
209. Silhavy, T. J., Kahne, D. & Walker, S. The bacterial cell envelope. *Cold Spring Harb. Perspect. Biol.* **2**, a000414 (2010).
210. Senior, A. E., Nadanaciva, S. & Weber, J. The molecular mechanism of ATP synthesis by F1F0-ATP synthase. *Biochim. Biophys. Acta.* **1553**, 188–211 (2002).

211. Islam, S. T. & Lam, J. S. Topological mapping methods for α -helical bacterial membrane proteins--an update and a guide. *Microbiologyopen*. **2**, 350–364 (2013).
212. Glauner, B., Höltje, J. V. & Schwarz, U. The composition of the murein of Escherichia coli. *J. Biol. Chem.* **263**, 10088–10095 (1988).
213. Vollmer, W., Blanot, D. & Pedro, M. A. de. Peptidoglycan structure and architecture. *FEMS Microbiol. Rev.* **32**, 149–167 (2008).
214. Vollmer, W. & Bertsche, U. Murein (peptidoglycan) structure, architecture and biosynthesis in Escherichia coli. *Biochim. Biophys. Acta.* **1778**, 1714–1734 (2008).
215. Lambert, M. P. & Neuhaus, F. C. Mechanism of D-cycloserine action. Alanine racemase from Escherichia coli W. *J. Bacteriol.* **110**, 978–987 (1972).
216. Prosser, G. A. & Carvalho, L. P. S. de. Kinetic mechanism and inhibition of Mycobacterium tuberculosis D-alanine:D-alanine ligase by the antibiotic D-cycloserine. *FEBS. J.* **280**, 1150–1166 (2013).
217. Kim, D. H. *et al.* Characterization of a Cys115 to Asp substitution in the Escherichia coli cell wall biosynthetic enzyme UDP-GlcNAc enolpyruvyl transferase (MurA) that confers resistance to inactivation by the antibiotic fosfomicin. *Biochemistry.* **35**, 4923–4928 (1996).
218. Tipper, D. J. & Strominger, J. L. Mechanism of action of penicillins. A proposal based on their structural similarity to acyl-D-alanyl-D-alanine. *Proc. Natl. Acad. Sci. U S A.* **54**, 1133–1141 (1965).
219. Waxman, D. J., Yocum, R. R. & Strominger, J. L. Penicillins and cephalosporins are active site-directed acylating agents. Evidence in support of the substrate analogue hypothesis. *Philos. Trans. R. Soc. Lond., B, Biol. Sci.* **289**, 257–271 (1980).
220. Nicola, G., Tomberg, J., Pratt, R. F., Nicholas, R. A. & Davies, C. Crystal structures of covalent complexes of β -lactam antibiotics with Escherichia coli penicillin-binding protein 5. Toward an understanding of antibiotic specificity. *Biochemistry.* **49**, 8094–8104 (2010).
221. Reynolds, P. E. Control of peptidoglycan synthesis in vancomycin-resistant enterococci. D,D-peptidases and D,D-carboxypeptidases. *Cell. Mol. Life. Sci.* **54**, 325–331 (1998).
222. Perkins, H. R. Specificity of combination between mucopeptide precursors and vancomycin or ristocetin. *Biochem. J.* **111**, 195–205 (1969).
223. Stone, K. J. & Strominger, J. L. Mechanism of action of bacitracin. Complexation with metal ion and C 55 -isoprenyl pyrophosphate. *Proc. Natl. Acad. Sci. U S A.* **68**, 3223–3227 (1971).
224. Pollock, T. J., Thorne, L., Yamazaki, M., Mikolajczak, M. J. & Armentrout, R. W. Mechanism of bacitracin resistance in gram-negative bacteria that synthesize exopolysaccharides. *J. Bacteriol.* **176**, 6229–6237 (1994).
225. Bouhss, A., Trunkfield, A. E., Bugg, T. D. H. & Mengin-Lecreux, D. The biosynthesis of peptidoglycan lipid-linked intermediates. *FEMS Microbiol. Rev.* **32**, 208–233 (2008).
226. Berglund, N. A. *et al.* Interaction of the antimicrobial peptide polymyxin B1 with both membranes of E. coli. A molecular dynamics study. *PLoS Comput. Biol.* **11**, e1004180 (2015).
227. Velkov, T., Roberts, K. D., Nation, R. L., Thompson, P. E. & Li, J. Pharmacology of polymyxins. New insights into an 'old' class of antibiotics. *Future. Microbiol.* **8**, 711–724 (2013).
228. Velkov, T., Thompson, P. E., Nation, R. L. & Li, J. Structure--activity relationships of polymyxin antibiotics. *J. Med. Chem.* **53**, 1898–1916 (2010).
229. Daugelavicius, R., Bakiene, E. & Bamford, D. H. Stages of polymyxin B interaction with the Escherichia coli cell envelope. *Antimicrob. Agents Chemother.* **44**, 2969–2978 (2000).

230. Bierbaum, G. & Sahl, H.-G. Lantibiotics. Mode of action, biosynthesis and bioengineering. *Curr. Pharm. Biotechnol.* **10**, 2–18 (2009).
231. Hsu, S.-T. D. *et al.* The nisin-lipid II complex reveals a pyrophosphate cage that provides a blueprint for novel antibiotics. *Nat. Struct. Mol. Biol.* **11**, 963–967 (2004).
232. Scott, W. R. P., Baek, S.-B., Jung, D., Hancock, R. E. W. & Straus, S. K. NMR structural studies of the antibiotic lipopeptide daptomycin in DHPC micelles. *Biochim. Biophys. Acta.* **1768**, 3116–3126 (2007).
233. Silverman, J. A., Perlmutter, N. G. & Shapiro, H. M. Correlation of daptomycin bactericidal activity and membrane depolarization in *Staphylococcus aureus*. *Antimicrob. Agents Chemother.* **47**, 2538–2544 (2003).
234. Müller, A. *et al.* Daptomycin inhibits cell envelope synthesis by interfering with fluid membrane microdomains. *Proc. Natl. Acad. Sci. U S A.* **113**, E7077-E7086 (2016).
235. Burkhart, B. M. *et al.* Gramicidin D conformation, dynamics and membrane ion transport. *Biopolymers.* **51**, 129–144 (1999).
236. Ryabova, I. D., Gorneva, G. A. & Ovchinnikov, Y. A. Effect of valinomycin on ion transport in bacterial cells and on bacterial growth. *Biochim. Biophys. Acta.* **401**, 109–118 (1975).
237. Hladky, S. B., Leung, J. C. & Fitzgerald, W. J. The mechanism of ion conduction by valinomycin. Analysis of charge pulse responses. *Biophys. J.* **69**, 1758–1772 (1995).
238. Das, A., Hugenholtz, J., van Halbeek, H. & Ljungdahl, L. G. Structure and function of a menaquinone involved in electron transport in membranes of *Clostridium thermoautotrophicum* and *Clostridium thermoaceticum*. *J. Bacteriol.* **171**, 5823–5829 (1989).
239. Kurosu, M. & Begari, E. Vitamin K2 in electron transport system. Are enzymes involved in vitamin K2 biosynthesis promising drug targets? *Molecules.* **15**, 1531–1553 (2010).
240. Hamamoto, H. *et al.* Lysocin E is a new antibiotic that targets menaquinone in the bacterial membrane. *Nat. Chem. Biol.* **11**, 127–133 (2015).
241. Lakshmanan, M. & Xavier, A. S. Bedaquiline - The first ATP synthase inhibitor against multi drug resistant tuberculosis. *J. Young. Pharm.* **5**, 112–115 (2013).
242. Sir Alexander Fleming - Nobel Lecture: Penicillin.
https://www.nobelprize.org/nobel_prizes/medicine/laureates/1945/fleming-lecture.html.
(accessed, 19 March 2018).
243. Rosenblatt-Farrell, N. The landscape of antibiotic resistance. *Environ. Health Perspect.* **117**, A244-50 (2009).
244. Proctor, R. A. *et al.* Small colony variants. A pathogenic form of bacteria that facilitates persistent and recurrent infections. *Nat. Rev. Microbiol.* **4**, 295–305 (2006).
245. Høiby, N. *et al.* ESCMID guideline for the diagnosis and treatment of biofilm infections 2014. *Clin. Microbiol. Infect.* **21 Suppl 1**, S1-25 (2015).
246. Ciofu, O., Rojo-Molinero, E., Macià, M. D. & Oliver, A. Antibiotic treatment of biofilm infections. *APMIS.* **125**, 304–319 (2017).
247. Delcour, A. H. Outer membrane permeability and antibiotic resistance. *Biochim. Biophys. Acta.* **1794**, 808–816 (2009).
248. Livermore, D. M. Antibiotic uptake and transport by bacteria. *Scand. J. Infect. Dis. Suppl.* **74**, 15–22 (1990).

249. Runti, G. *et al.* Functional characterization of SbmA, a bacterial inner membrane transporter required for importing the antimicrobial peptide Bac7(1-35). *J. Bacteriol.* **195**, 5343–5351 (2013).
250. Quale, J., Bratu, S., Landman, D. & Heddurshetti, R. Molecular epidemiology and mechanisms of carbapenem resistance in *Acinetobacter baumannii* endemic in New York City. *Clin. Infect. Dis.* **37**, 214–220 (2003).
251. Poole, K. Resistance to beta-lactam antibiotics. *Cell. Mol. Life. Sci.* **61**, 2200–2223 (2004).
252. Krizsan, A., Knappe, D. & Hoffmann, R. Influence of the yjiL-mdtM Gene Cluster on the Antibacterial Activity of Proline-Rich Antimicrobial Peptides Overcoming *Escherichia coli* Resistance Induced by the Missing SbmA Transporter System. *Antimicrob. Agents Chemother.* **59**, 5992–5998 (2015).
253. Marger, M. D. & Saier, M. H. A major superfamily of transmembrane facilitators that catalyse uniport, symport and antiport. *Trends Biochem. Sci.* **18**, 13–20 (1993).
254. Zgurskaya, H. I. & Nikaido, H. Bypassing the periplasm. Reconstitution of the AcrAB multidrug efflux pump of *Escherichia coli*. *Proc. Natl. Acad. Sci. U S A.* **96**, 7190–7195 (1999).
255. Okusu, H., Ma, D. & Nikaido, H. AcrAB efflux pump plays a major role in the antibiotic resistance phenotype of *Escherichia coli* multiple-antibiotic-resistance (Mar) mutants. *J. Bacteriol.* **178**, 306–308 (1996).
256. Dönhöfer, A. *et al.* Structural basis for TetM-mediated tetracycline resistance. *Proc. Natl. Acad. Sci. U S A.* **109**, 16900–16905 (2012).
257. Li, W. *et al.* Mechanism of tetracycline resistance by ribosomal protection protein Tet(O). *Nat. Commun.* **4**, 1477 (2013).
258. Tomlinson, J. H., Thompson, G. S., Kalverda, A. P., Zhuravleva, A. & O'Neill, A. J. A target-protection mechanism of antibiotic resistance at atomic resolution. Insights into FusB-type fusidic acid resistance. *Sci. Rep.* **6**, 19524 (2016).
259. Flensburg, J. & Sköld, O. Massive overproduction of dihydrofolate reductase in bacteria as a response to the use of trimethoprim. *Eur. J. Biochem.* **162**, 473–476 (1987).
260. Palmer, A. C. & Kishony, R. Opposing effects of target overexpression reveal drug mechanisms. *Nat. Commun.* **5**, 4296 (2014).
261. Berger-Bächi, B. Expression of resistance to methicillin. *Trends. Microbiol.* **2**, 389–393 (1994).
262. Berger-Bächi, B. & Rohrer, S. Factors influencing methicillin resistance in staphylococci. *Arch. Microbiol.* **178**, 165–171 (2002).
263. Lambert, P. A. Bacterial resistance to antibiotics. Modified target sites. *Adv. Drug Deliv. Rev.* **57**, 1471–1485 (2005).
264. Besier, S., Ludwig, A., Brade, V. & Wichelhaus, T. A. Molecular analysis of fusidic acid resistance in *Staphylococcus aureus*. *Mol. Microbiol.* **47**, 463–469 (2003).
265. Antonio, M., McFerran, N. & Pallen, M. J. Mutations affecting the Rossman fold of isoleucyl-tRNA synthetase are correlated with low-level mupirocin resistance in *Staphylococcus aureus*. *Antimicrob. Agents Chemother.* **46**, 438–442 (2002).
266. Jalava, J., Vaara, M. & Huovinen, P. Mutation at the position 2058 of the 23S rRNA as a cause of macrolide resistance in *Streptococcus pyogenes*. *Ann. Clin. Microbiol. Antimicrob.* **3**, 5 (2004).
267. Haanperä, M., Huovinen, P. & Jalava, J. Detection and quantification of macrolide resistance mutations at positions 2058 and 2059 of the 23S rRNA gene by pyrosequencing. *Antimicrob. Agents Chemother.* **49**, 457–460 (2005).

268. Long, K. S., Poehlsgaard, J., Kehrenberg, C., Schwarz, S. & Vester, B. The Cfr rRNA methyltransferase confers resistance to Phenicol, Lincosamides, Oxazolidinones, Pleuromutilins, and Streptogramin A antibiotics. *Antimicrob. Agents Chemother.* **50**, 2500–2505 (2006).
269. Weisblum, B. Erythromycin resistance by ribosome modification. *Antimicrob. Agents Chemother.* **39**, 577–585 (1995).
270. Toh, S.-M. & Mankin, A. S. An indigenous posttranscriptional modification in the ribosomal peptidyl transferase center confers resistance to an array of protein synthesis inhibitors. *J. Mol. Biol.* **380**, 593–597 (2008).
271. Decatur, W. A. & Fournier, M. J. rRNA modifications and ribosome function. *Trends Biochem. Sci.* **27**, 344–351 (2002).
272. Lázaro, E. *et al.* A sparsomycin-resistant mutant of *Halobacterium salinarium* lacks a modification at nucleotide U2603 in the peptidyl transferase centre of 23 S rRNA. *J. Mol. Biol.* **261**, 231–238 (1996).
273. Lee, H., Hsu, F.-F., Turk, J. & Groisman, E. A. The PmrA-regulated pmrC gene mediates phosphoethanolamine modification of lipid A and polymyxin resistance in *Salmonella enterica*. *J. Bacteriol.* **186**, 4124–4133 (2004).
274. Bugg, T. D. *et al.* Molecular basis for vancomycin resistance in *Enterococcus faecium* BM4147. Biosynthesis of a depsipeptide peptidoglycan precursor by vancomycin resistance proteins VanH and VanA. *Biochemistry.* **30**, 10408–10415 (1991).
275. Konno, K., Feldmann, F. M. & McDermott, W. Pyrazinamide susceptibility and amidase activity of tubercle bacilli. *Am. Rev. Respir. Dis.* **95**, 461–469 (1967).
276. Zhang, Y., Scorpio, A., Nikaido, H. & Sun, Z. Role of acid pH and deficient efflux of pyrazinoic acid in unique susceptibility of *Mycobacterium tuberculosis* to pyrazinamide. *J. Bacteriol.* **181**, 2044–2049 (1999).
277. Ramirez, M. S. & Tolmasky, M. E. Aminoglycoside modifying enzymes. *Drug Resist. Updat.* **13**, 151–171 (2010).
278. Schwarz, S., Kehrenberg, C., Doublet, B. & Cloeckaert, A. Molecular basis of bacterial resistance to chloramphenicol and florfenicol. *FEMS Microbiol. Rev.* **28**, 519–542 (2004).
279. Paterson, D. L. & Bonomo, R. A. Extended-spectrum beta-lactamases. A clinical update. *Clin. Microbiol. Rev.* **18**, 657–686 (2005).
280. Volkens, G., Palm, G. J., Weiss, M. S., Wright, G. D. & Hinrichs, W. Structural basis for a new tetracycline resistance mechanism relying on the TetX monooxygenase. *FEBS Lett.* **585**, 1061–1066 (2011).
281. Nelson, M. L. & Levy, S. B. The history of the tetracyclines. *Ann. N. Y. Acad. Sci.* **1241**, 17–32 (2011).
282. Blondeau, J. M. The evolution and role of macrolides in infectious diseases. *Expert Opin. Pharmacother.* **3**, 1131–1151 (2002).
283. Andersson, M. I. & MacGowan, A. P. Development of the quinolones. *J. Antimicrob. Chemother.* **51 Suppl 1**, 1–11 (2003).
284. Abed, N. *et al.* An efficient system for intracellular delivery of beta-lactam antibiotics to overcome bacterial resistance. *Sci. Rep.* **5**, 13500 (2015).
285. Olivero-Verbel, J., Barreto-Maya, A., Bertel-Sevilla, A. & Stashenko, E. E. Composition, anti-quorum sensing and antimicrobial activity of essential oils from *Lippia alba*. *Braz. J. Microbiol.* **45**, 759–767 (2014).

286. Choo, J. H., Rukayadi, Y. & Hwang, J.-K. Inhibition of bacterial quorum sensing by vanilla extract. *Let. Appl. Microbiol.* **42**, 637–641 (2006).
287. Kaplan, J. B. Biofilm dispersal. Mechanisms, clinical implications, and potential therapeutic uses. *J. Dent. Res.* **89**, 205–218 (2010).
288. Tegos, G. P. *et al.* Microbial efflux pump inhibition. Tactics and strategies. *Curr. Pharm. Des.* **17**, 1291–1302 (2011).
289. Drawz, S. M. & Bonomo, R. A. Three decades of beta-lactamase inhibitors. *Clin. Microbiol. Rev.* **23**, 160–201 (2010).
290. Blondiaux, N. *et al.* Reversion of antibiotic resistance in *Mycobacterium tuberculosis* by spiroisoxazoline SMART-420. *Science.* **355**, 1206–1211 (2017).
291. Duggar, B. M. Aureomycin. A product of the continuing search for new antibiotics. *Ann. N. Y. Acad. Sci.* **1241**, 163–169 (2011).
292. Xiao, X.-Y. *et al.* Fluorocyclines. 1. 7-fluoro-9-pyrrolidinoacetamido-6-demethyl-6-deoxytetracycline. A potent, broad spectrum antibacterial agent. *J. Med. Chem.* **55**, 597–605 (2012).
293. Martell, M. J. & Boothe, J. H. The 6-Deoxytetracyclines. VII. Alkylated Aminotetracyclines Possessing Unique Antibacterial Activity. *J. Med. Chem.* **10**, 44–46 (1967).
294. Petersen, P. J., Jacobus, N. V., Weiss, W. J., Sum, P. E. & Testa, R. T. In vitro and in vivo antibacterial activities of a novel glycylicycline, the 9-t-butylglycylamido derivative of minocycline (GAR-936). *Antimicrob. Agents Chemother.* **43**, 738–744 (1999).
295. Noskin, G. A. Tigecycline. A new glycylicycline for treatment of serious infections. *Clin. Infect. Dis.* **41 Suppl 5**, S303-14 (2005).
296. Omadacycline vs Moxifloxacin for the Treatment of CABP (EudraCT #2013-004071-13) - Full Text View - ClinicalTrials.gov. <https://clinicaltrials.gov/ct2/show/NCT02531438>. (accessed, 19 March 2018).
297. Efficacy and Safety Study of Eravacycline Compared With Ertapenem in Complicated Intra-abdominal Infections - Study Results - ClinicalTrials.gov. <https://clinicaltrials.gov/ct2/show/results/NCT01844856>. (accessed, 19 March 2018).
298. Solomkin, J. *et al.* Assessing the Efficacy and Safety of Eravacycline vs Ertapenem in Complicated Intra-abdominal Infections in the Investigating Gram-Negative Infections Treated With Eravacycline (IGNITE 1) Trial. A Randomized Clinical Trial. *JAMA Surg.* **152**, 224–232 (2017).
299. Gotfried, M. H. *et al.* Comparison of Omadacycline and Tigecycline Pharmacokinetics in the Plasma, Epithelial Lining Fluid, and Alveolar Cells of Healthy Adult Subjects. *Antimicrob. Agents Chemother.* **61** (2017).
300. Roberts, M. C. Tetracycline therapy. Update. *Clin. Infect. Dis.* **36**, 462–467 (2003).
301. Varanda, F. *et al.* Solubility of Antibiotics in Different Solvents. 1. Hydrochloride Forms of Tetracycline, Moxifloxacin, and Ciprofloxacin. *Ind. Eng. Chem. Res.* **45**, 6368–6374 (2006).
302. Hughes, L. J., Stezowski, J. J. & Hughes, R. E. Chemical-structural properties of tetracycline derivatives. 7. Evidence for the coexistence of the zwitterionic and nonionized forms of the free base in solution. *J. Am. Chem. Soc.* **101**, 7655–7657 (1979).
303. Chukwudi, C. U. rRNA Binding Sites and the Molecular Mechanism of Action of the Tetracyclines. *Antimicrob. Agents Chemother.* **60**, 4433–4441 (2016).

304. Maxwell, I. H. Partial removal of bound transfer RNA from polysomes engaged in protein synthesis in vitro after addition of tetracycline. *Biochim. Biophys. Acta.* **138**, 337–346 (1967).
305. Geigenmüller, U. & Nierhaus, K. H. Tetracycline can inhibit tRNA binding to the ribosomal P site as well as to the A site. *Eur. J. Biochem.* **161**, 723–726 (1986).
306. Thanassi, D. G., Suh, G. S. & Nikaido, H. Role of outer membrane barrier in efflux-mediated tetracycline resistance of *Escherichia coli*. *J. Bacteriol.* **177**, 998–1007 (1995).
307. Yin, C. C. *et al.* The quarternary molecular architecture of TetA, a secondary tetracycline transporter from *Escherichia coli*. *Mol. Microbiol.* **38**, 482–492 (2000).
308. Zhang, T., Wang, C. G., Lv, J. C., Wang, R. S. & Zhong, X. H. Survey on tetracycline resistance and antibiotic-resistant genotype of avian *Escherichia coli* in North China. *Poult. Sci.* **91**, 2774–2777 (2012).
309. Connell, S. R., Tracz, D. M., Nierhaus, K. H. & Taylor, D. E. Ribosomal protection proteins and their mechanism of tetracycline resistance. *Antimicrob. Agents Chemother.* **47**, 3675–3681 (2003).
310. Yang, W. *et al.* TetX is a flavin-dependent monooxygenase conferring resistance to tetracycline antibiotics. *J. Biol. Chem.* **279**, 52346–52352 (2004).
311. Ross, J. I., Eady, E. A., Cove, J. H. & Cunliffe, W. J. 16S rRNA mutation associated with tetracycline resistance in a gram-positive bacterium. *Antimicrob. Agents Chemother.* **42**, 1702–1705 (1998).
312. Gerrits, M. M., Zoete, M. R. de, Arents, N. L. A., Kuipers, E. J. & Kusters, J. G. 16S rRNA Mutation-Mediated Tetracycline Resistance in *Helicobacter pylori*. *Antimicrob. Agents Chemother.* **46**, 2996–3000 (2002).
313. Dadashzadeh, K., Milani, M., Rahmati, M. & Akbarzadeh, A. Real-time PCR detection of 16S rRNA novel mutations associated with *Helicobacter pylori* tetracycline resistance in Iran. *Asian. Pac. J. Cancer Prev.* **15**, 8883–8886 (2014).
314. Clyde, D. F., Miller, R. M., DuPont, H. L. & Hornick, R. B. Antimalarial effects of tetracyclines in man. *J. Trop. Med. Hyg.* **74**, 238–242 (1971).
315. Tan, K. R., Magill, A. J., Parise, M. E. & Arguin, P. M. Doxycycline for malaria chemoprophylaxis and treatment. Report from the CDC expert meeting on malaria chemoprophylaxis. *Am. J. Trop. Med. Hyg.* **84**, 517–531 (2011).
316. Kiatfuengfoo, R., Suthiphongchai, T., Prapunwattana, P. & Yuthavong, Y. Mitochondria as the site of action of tetracycline on *Plasmodium falciparum*. *Mol. Biochem. Parasitol.* **34**, 109–115 (1989).
317. Prapunwattana, P., O'Sullivan, W. J. & Yuthavong, Y. Depression of *Plasmodium falciparum* dihydroorotate dehydrogenase activity in in vitro culture by tetracycline. *Mol. Biochem. Parasitol.* **27**, 119–124 (1988).
318. Mitscher, L. A. *et al.* Structure of chelocardin, a novel tetracycline antibiotic. *J. Am. Chem. Soc.* **92**, 6070–6071 (1970).
319. Rasmussen, B. *et al.* Molecular basis of tetracycline action. Identification of analogs whose primary target is not the bacterial ribosome. *Antimicrob. Agents Chemother.* **35**, 2306–2311 (1991).
320. Stepanek, J. J., Lukežič, T., Teichert, I., Petković, H. & Bandow, J. E. Dual mechanism of action of the atypical tetracycline chelocardin. *Biochim. Biophys. Acta.* **1864**, 645–654 (2016).

321. Chopra, I. Tetracycline analogs whose primary target is not the bacterial ribosome. *Antimicrob. Agents Chemother.* **38**, 637–640 (1994).
322. Hasan, T. & Khan, A. U. Phototoxicity of the tetracyclines. Photosensitized emission of singlet delta dioxygen. *Proc. Natl. Acad. Sci. U S A.* **83**, 4604–4606 (1986).
323. Hasan, T., Kochevar, I. E., McAuliffe, D. J., Cooperman, B. S. & Abdulah, D. Mechanism of tetracycline phototoxicity. *J. Invest. Dermatol.* **83**, 179–183 (1984).
324. CRAVERI, R., CORONELLI, C., PAGANI, H. & SENSI, P. THERMORUBIN, A NEW ANTIBIOTIC FROM A THERMOACTINOMYCETE. *Clin. Med. (Northfield).* **71**, 511–521 (1964).
325. Cavalleri, B., Turconi, M. & Pallanza, R. Synthesis and antibacterial activity of some derivatives of the antibiotic thermorubin. *J. Antibiot.* **38**, 1752–1760 (1985).
326. Johnson, F. *et al.* Thermorubin 1. Structure studies. *J. Am. Chem. Soc.* **102**, 5580–5585 (1980).
327. Pirali, G., Somma, S., Lancini, G. C. & Sala, F. Inhibition of peptide chain initiation in *Escherichia coli* by thermorubin. *Biochim. Biophys. Acta.* **366**, 310–318 (1974).
328. Lin, F. & Wishnia, A. The protein synthesis inhibitor thermorubin. 2. Mechanism of inhibition of initiation on *Escherichia coli* ribosomes. *Biochemistry.* **21**, 484–491 (1982).
329. Lin, F. L. & Wishnia, A. The protein synthesis inhibitor thermorubin. 1. Nature of the thermorubin-ribosome complex. *Biochemistry.* **21**, 477–483 (1982).
330. Hayashi, K. *et al.* Thermorubin and 2-hydroxyphenyl acetic acid, aldose reductase inhibitors. *J. Antibiot.* **48**, 1345–1346 (1995).
331. Tang, W. H., Martin, K. A. & Hwa, J. Aldose reductase, oxidative stress, and diabetic mellitus. *Front. Pharmacol.* **3**, 87 (2012).
332. Bulkeley, D., Johnson, F. & Steitz, T. A. The antibiotic thermorubin inhibits protein synthesis by binding to inter-subunit bridge B2a of the ribosome. *J. Mol. Biol.* **416**, 571–578 (2012).
333. DUTCHER, J. D. & VANDEPUTTE, J. Thiostrepton, a new antibiotic. II. Isolation and chemical characterization. *Antibiot. Annu.* **3**, 560–561 (1955).
334. ANDERSON, B., HODGKIN, D. C. & VISWAMITRA, M. A. The Structure of Thiostrepton. *Nature.* **225**, 233–235 (1970).
335. DONOVICK, R., PAGANO, J. F., STOUT, H. A. & WEINSTEIN, M. J. Thiostrepton, a new antibiotic. I. In vitro studies. *Antibiot. Annu.* **3**, 554–559 (1955).
336. Just-Baringo, X., Albericio, F. & Álvarez, M. Thiopeptide antibiotics. Retrospective and recent advances. *Mar. Drugs.* **12**, 317–351 (2014).
337. Bleich, R., Watrous, J. D., Dorrestein, P. C., Bowers, A. A. & Shank, E. A. Thiopeptide antibiotics stimulate biofilm formation in *Bacillus subtilis*. *Proc. Natl. Acad. Sci. U S A.* **112**, 3086–3091 (2015).
338. Bagley, M. C., Dale, J. W., Merritt, E. A. & Xiong, X. Thiopeptide antibiotics. *Chem. Rev.* **105**, 685–714 (2005).
339. Wieland Brown, L. C., Acker, M. G., Clardy, J., Walsh, C. T. & Fischbach, M. A. Thirteen posttranslational modifications convert a 14-residue peptide into the antibiotic thiocillin. *Proc. Natl. Acad. Sci. U S A.* **106**, 2549–2553 (2009).
340. Liao, R. *et al.* Thiopeptide biosynthesis featuring ribosomally synthesized precursor peptides and conserved posttranslational modifications. *Chem. Biol.* **16**, 141–147 (2009).

341. Shimanaka, K., Takahashi, Y., Iinuma, H., Naganawa, H. & Takeuchi, T. Novel antibiotics, amythiamicins. II. Structure elucidation of amythiamicin D. *J. Antibiot.* **47**, 1145–1152 (1994).
342. Anborgh, P. H. & Parmeggiani, A. New antibiotic that acts specifically on the GTP-bound form of elongation factor Tu. *EMBO J.* **10**, 779–784 (1991).
343. Shimanaka, K. *et al.* Novel antibiotics, amythiamicins. IV. A mutation in the elongation factor Tu gene in a resistant mutant of *B. subtilis*. *J. Antibiot.* **48**, 182–184 (1995).
344. Heffron, S. E. & Jurnak, F. Structure of an EF-Tu complex with a thiazolyl peptide antibiotic determined at 2.35 Å resolution. Atomic basis for GE2270A inhibition of EF-Tu. *Biochemistry.* **39**, 37–45 (2000).
345. Harms, J. M. *et al.* Translational regulation via L11. Molecular switches on the ribosome turned on and off by thiostrepton and micrococcin. *Mol. Cell.* **30**, 26–38 (2008).
346. Cameron, D. M., Thompson, J., March, P. E. & Dahlberg, A. E. Initiation factor IF2, thiostrepton and micrococcin prevent the binding of elongation factor G to the *Escherichia coli* ribosome. *J. Mol. Biol.* **319**, 27–35 (2002).
347. Zasloff, M. Antimicrobial peptides of multicellular organisms. *Nature.* **415**, 389–395 (2002).
348. Brogden, K. A. Antimicrobial peptides. Pore formers or metabolic inhibitors in bacteria? *Nat. Rev. Microbiol.* **3**, 238–250 (2005).
349. Kościuczuk, E. M. *et al.* Cathelicidins. Family of antimicrobial peptides. A review. *Mol. Biol. Rep.* **39**, 10957–10970 (2012).
350. Zanetti, M. Cathelicidins, multifunctional peptides of the innate immunity. *J. Leukoc. Biol.* **75**, 39–48 (2004).
351. Bals, R. & Wilson, J. M. Cathelicidins--a family of multifunctional antimicrobial peptides. *Cell. Mol. Life. Sci.* **60**, 711–720 (2003).
352. Cowland, J. B., Johnsen, A. H. & Borregaard, N. hCAP-18, a cathelin/pro-bactenecin-like protein of human neutrophil specific granules. *FEBS Lett.* **368**, 173–176 (1995).
353. Gudmundsson, G. H. *et al.* The human gene FALL39 and processing of the cathelin precursor to the antibacterial peptide LL-37 in granulocytes. *Eur. J. Biochem.* **238**, 325–332 (1996).
354. Wang, G. Human antimicrobial peptides and proteins. *Pharmaceuticals.* **7**, 545–594 (2014).
355. Turner, J., Cho, Y., Dinh, N. N., Waring, A. J. & Lehrer, R. I. Activities of LL-37, a cathelin-associated antimicrobial peptide of human neutrophils. *Antimicrob. Agents Chemother.* **42**, 2206–2214 (1998).
356. Casteels, P. & Tempst, P. Apidaecin-type peptide antibiotics function through a non-poreforming mechanism involving stereospecificity. *Biochem. Biophys. Res. Commun.* **199**, 339–345 (1994).
357. Podda, E. *et al.* Dual mode of action of Bac7, a proline-rich antibacterial peptide. *Biochim. Biophys. Acta.* **1760**, 1732–1740 (2006).
358. Boman, H. G., Agerberth, B. & Boman, A. Mechanisms of action on *Escherichia coli* of cecropin P1 and PR-39, two antibacterial peptides from pig intestine. *Infect. Immun.* **61**, 2978–2984 (1993).
359. Scocchi, M., Tossi, A. & Gennaro, R. Proline-rich antimicrobial peptides. Converging to a non-lytic mechanism of action. *Cell. Mol. Life. Sci.* **68**, 2317–2330 (2011).

360. Chernysh, S., Cociancich, S., Briand, J.-P., Hetru, C. & Bulet, P. The inducible antibacterial peptides of the Hemipteran insect *Palomena prasina*. Identification of a unique family of prolinerich peptides and of a novel insect defensin. *J. Insect Physiol.* **42**, 81–89 (1996).
361. Casteels-Josson, K., Capaci, T., Casteels, P. & Tempst, P. Apidaecin multi-peptide precursor structure. A putative mechanism for amplification of the insect antibacterial response. *EMBO J.* **12**, 1569–1578 (1993).
362. Xu, P., Shi, M. & Chen, X.-X. Antimicrobial peptide evolution in the Asiatic honey bee *Apis cerana*. *PLoS ONE.* **4**, e4239 (2009).
363. Casteels, P., Ampe, C., Jacobs, F., Vaeck, M. & Tempst, P. Apidaecins. Antibacterial peptides from honeybees. *EMBO J.* **8**, 2387–2391 (1989).
364. Cociancich, S. *et al.* Novel inducible antibacterial peptides from a hemipteran insect, the sap-sucking bug *Pyrrhocoris apterus*. *Biochem. J.* **300 (Pt 2)**, 567–575 (1994).
365. Schneider, M. & Dorn, A. Differential infectivity of two *Pseudomonas* species and the immune response in the milkweed bug, *Oncopeltus fasciatus* (Insecta. Hemiptera). *J. Invertebr. Pathol.* **78**, 135–140 (2001).
366. Bulet, P. *et al.* A novel inducible antibacterial peptide of *Drosophila* carries an O-glycosylated substitution. *J. Biol. Chem.* **268**, 14893–14897 (1993).
367. Destoumieux, D., Munoz, M., Bulet, P. & Bachère, E. Penaeidins, a family of antimicrobial peptides from penaeid shrimp (Crustacea, Decapoda). *Cell. Mol. Life. Sci.* **57**, 1260–1271 (2000).
368. Mattiuzzo, M. *et al.* Role of the *Escherichia coli* SbmA in the antimicrobial activity of proline-rich peptides. *Mol. Microbiol.* **66**, 151–163 (2007).
369. Narayanan, S. *et al.* Mechanism of *Escherichia coli* resistance to Pyrrhocoricin. *Antimicrob. Agents Chemother.* **58**, 2754–2762 (2014).
370. Scocchi, M. *et al.* The Proline-rich Antibacterial Peptide Bac7 Binds to and Inhibits in vitro the Molecular Chaperone DnaK. *Int. J. Pept. Res. Ther.* **15**, 147–155 (2009).
371. KUTSCHER, A. H., ZEGARELLI, E. V., RANKOW, R. M., MERCADANTE, J. & PIRO, J. D. Clinical laboratory studies on a new topical antibiotic. Thiostrepton. *Oral Surg. Oral Med. Oral Pathol.* **12**, 967–974 (1959).
372. Zasloff, M. Magainins, a class of antimicrobial peptides from *Xenopus* skin. Isolation, characterization of two active forms, and partial cDNA sequence of a precursor. *Proc. Natl. Acad. Sci. U S A.* **84**, 5449–5453 (1987).
373. Matsuzaki, K. Magainins as paradigm for the mode of action of pore forming polypeptides. *Biochim. Biophys. Acta.* **1376**, 391–400 (1998).
374. Huang, H. W. Molecular mechanism of antimicrobial peptides. The origin of cooperativity. *Biochim. Biophys. Acta.* **1758**, 1292–1302 (2006).
375. Matsuzaki, K., Sugishita, K., Fujii, N. & Miyajima, K. Molecular Basis for Membrane Selectivity of an Antimicrobial Peptide, Magainin 2. *Biochemistry.* **34**, 3423–3429 (2002).
376. Fuchs, P. C., Barry, A. L. & Brown, S. D. In vitro antimicrobial activity of MSI-78, a magainin analog. *Antimicrob. Agents Chemother.* **42**, 1213–1216 (1998).
377. Ge, Y. *et al.* In vitro antibacterial properties of pexiganan, an analog of magainin. *Antimicrob. Agents Chemother.* **43**, 782–788 (1999).

378. Shimanaka, K., Kinoshita, N., Iinuma, H., Hamada, M. & Takeuchi, T. Novel antibiotics, amythiamicins. I. Taxonomy, fermentation, isolation, physico-chemical properties, and antimicrobial activity. *J. Antibiot.* **47**, 668–674 (1994).
379. Nicolaou, K. C., Zou, B., Dethlefsen, D. H., Li, D. B. & Chen, D. Y.-K. Total synthesis of antibiotics GE2270A and GE2270T. *Angew. Chem. Int. Ed. Engl.* **45**, 7786–7792 (2006).
380. Kim, D. M., Kigawa, T., Choi, C. Y. & Yokoyama, S. A highly efficient cell-free protein synthesis system from *Escherichia coli*. *Eur. J. Biochem.* **239**, 881–886 (1996).
381. Zuurmond, A. M. *et al.* GE2270A-resistant mutations in elongation factor Tu allow productive aminoacyl-tRNA binding to EF-Tu.GTP.GE2270A complexes. *J. Mol. Biol.* **304**, 995–1005 (2000).
382. Stephens, C. R. *et al.* TERRAMYCIN. VIII. STRUCTURE OF AUREOMYCIN AND TERRAMYCIN. *J. Am. Chem. Soc.* **74**, 4976–4977 (1952).
383. Stephens, C. R. *et al.* The Structure of Aureomycin 1. *J. Am. Chem. Soc.* **76**, 3568–3575 (1954).
384. Hochstein, F. A. *et al.* The structure of Terramycin. *J. Am. Chem. Soc.* **75**, 5455–5475 (1953).
385. Stephens, C. R. *et al.* 6-Deoxytetracyclines. IV.1,2Preparation, C-6 Stereochemistry, and Reactions. *J. Am. Chem. Soc.* **85**, 2643–2652 (1963).
386. Connell, S. R. *et al.* The tetracycline resistance protein Tet(o) perturbs the conformation of the ribosomal decoding centre. *Mol. Microbiol.* **45**, 1463–1472 (2002).
387. Nelson, M., Hillen, W. & Greenwald, R. A. *Tetracyclines in Biology, Chemistry and Medicine* (Birkhäuser, Basel, 2001).
388. Jenner, L. *et al.* Structural basis for potent inhibitory activity of the antibiotic tigecycline during protein synthesis. *Proc. Natl. Acad. Sci. U S A.* **110**, 3812–3816 (2013).
389. Gale, E. G., Cundliffe, E., Reynolds, P. E., Richmond, M. H. & Waring, M. J. *Antibiotic inhibitors of ribosome function. In: The molecular basis of antibiotic action.* 278–379 (John Wiley and sons, Bristol, UK, 1981).
390. Blanchard, S. C., Gonzalez, R. L., Kim, H. D., Chu, S. & Puglisi, J. D. tRNA selection and kinetic proofreading in translation. *Nat. Struct. Mol. Biol.* **11**, 1008–1014 (2004).
391. Baucheron, S. *et al.* AcrAB-TolC directs efflux-mediated multidrug resistance in *Salmonella enterica* serovar typhimurium DT104. *Antimicrob. Agents Chemother.* **48**, 3729–3735 (2004).
392. Guillaume, G., Ledent, V., Moens, W. & Collard, J.-M. Phylogeny of efflux-mediated tetracycline resistance genes and related proteins revisited. *Microbial drug resistance (Larchmont, N.Y.)* **10**, 11–26 (2004).
393. Piddock, L. J. V. Multidrug-resistance efflux pumps - not just for resistance. *Nat. Rev. Microbiol.* **4**, 629–636 (2006).
394. Chopra, I. & Roberts, M. Tetracycline antibiotics. Mode of action, applications, molecular biology, and epidemiology of bacterial resistance. *Microbiol. Mol. Biol. Rev.* **65**, 232-60 ; second page, table of contents (2001).
395. Grossman, T. H. *et al.* Target- and resistance-based mechanistic studies with TP-434, a novel fluorocycline antibiotic. *Antimicrob. Agents Chemother.* **56**, 2559–2564 (2012).
396. Burdett, V. Purification and characterization of Tet(M), a protein that renders ribosomes resistant to tetracycline. *J. Biol. Chem.* **266**, 2872–2877 (1991).
397. Connell, S. R. *et al.* Mechanism of Tet(O)-mediated tetracycline resistance. *EMBO J.* **22**, 945–953 (2003).

398. Dailidienė, D. *et al.* Emergence of tetracycline resistance in *Helicobacter pylori*. Multiple mutational changes in 16S ribosomal DNA and other genetic loci. *Antimicrob. Agents Chemother.* **46**, 3940–3946 (2002).
399. Trieber, C. A. & Taylor, D. E. Mutations in the 16S rRNA genes of *Helicobacter pylori* mediate resistance to tetracycline. *J. Bacteriol.* **184**, 2131–2140 (2002).
400. Speer, B. S., Bedzyk, L. & Salyers, A. A. Evidence that a novel tetracycline resistance gene found on two *Bacteroides* transposons encodes an NADP-requiring oxidoreductase. *J. Bacteriol.* **173**, 176–183 (1991).
401. Volkens, G. *et al.* Putative dioxygen-binding sites and recognition of tigecycline and minocycline in the tetracycline-degrading monooxygenase TetX. *Acta Crystallogr. D Biol. Crystallogr.* **69**, 1758–1767 (2013).
402. Nguyen, F. *et al.* Tetracycline antibiotics and resistance mechanisms. *Biol. Chem.* **395**, 559–575 (2014).
403. Knappe, D., Kabankov, N. & Hoffmann, R. Bactericidal oncocin derivatives with superior serum stabilities. *Int. J. Antimicrob. Agents.* **37**, 166–170 (2011).
404. Gennaro, R., Skerlavaj, B. & Romeo, D. Purification, composition, and activity of two bactenecins, antibacterial peptides of bovine neutrophils. *Infect. Immun.* **57**, 3142–3146 (1989).
405. Casteels, P. *et al.* Isolation and characterization of abaecin, a major antibacterial response peptide in the honeybee (*Apis mellifera*). *Eur. J. Biochem.* **187**, 381–386 (1990).
406. Charlet, M. *et al.* Cloning of the gene encoding the antibacterial peptide drosocin involved in *Drosophila* immunity. Expression studies during the immune response. *Eur. J. Biochem.* **241**, 699–706 (1996).
407. Skerlavaj, B., Romeo, D. & Gennaro, R. Rapid membrane permeabilization and inhibition of vital functions of Gram-negative bacteria by bactenecins. *Infect. Immun.* **58**, 3724–3730 (1990).
408. Huttner, K. M., Lambeth, M. R., Burkin, H. R., Burkin, D. J. & Broad, T. E. Localization and genomic organization of sheep antimicrobial peptide genes. *Gene* **206**, 85–91 (1998).
409. Shamova, O. *et al.* Purification and properties of proline-rich antimicrobial peptides from sheep and goat leukocytes. *Infect. Immun.* **67**, 4106–4111 (1999).
410. Zanetti, M., Litteri, L., Gennaro, R., Horstmann, H. & Romeo, D. Bactenecins, defense polypeptides of bovine neutrophils, are generated from precursor molecules stored in the large granules. *J. Cell Biol.* **111**, 1363–1371 (1990).
411. Zanetti, M., Litteri, L., Griffiths, G., Gennaro, R. & Romeo, D. Stimulus-induced maturation of probactenecins, precursors of neutrophil antimicrobial polypeptides. *J. Immunol.* **146**, 4295–4300 (1991).
412. Scocchi, M., Skerlavaj, B., Romeo, D. & Gennaro, R. Proteolytic cleavage by neutrophil elastase converts inactive storage proforms to antibacterial bactenecins. *Eur. J. Biochem.* **209**, 589–595 (1992).
413. Krizsan, A. *et al.* Insect-derived proline-rich antimicrobial peptides kill bacteria by inhibiting bacterial protein translation at the 70S ribosome. *Angew. Chem. Int. Ed. Engl.* **53**, 12236–12239 (2014).
414. Seefeldt, A. C. *et al.* The proline-rich antimicrobial peptide Onc112 inhibits translation by blocking and destabilizing the initiation complex. *Nat. Struct. Mol. Biol.* **22**, 470–475 (2015).
415. Seefeldt, A. C. *et al.* Structure of the mammalian antimicrobial peptide Bac7(1-16) bound within the exit tunnel of a bacterial ribosome. *Nucleic Acids Res.* **44**, 2429–2438 (2016).

416. Roy, R. N., Lomakin, I. B., Gagnon, M. G. & Steitz, T. A. The mechanism of inhibition of protein synthesis by the proline-rich peptide oncocin. *Nat. Struct. Mol. Biol.* **22**, 466–469 (2015).
417. Doyle, D., McDowall, K. J., Butler, M. J. & Hunter, I. S. Characterization of an oxytetracycline-resistance gene, *otrA*, of *Streptomyces rimosus*. *Mol. Microbiol.* **5**, 2923–2933 (1991).
418. Savelsbergh, A., Mohr, D., Kothe, U., Wintermeyer, W. & Rodnina, M. V. Control of phosphate release from elongation factor G by ribosomal protein L7/12. *EMBO J.* **24**, 4316–4323 (2005).
419. Nechifor, R., Murataliev, M. & Wilson, K. S. Functional interactions between the G' subdomain of bacterial translation factor EF-G and ribosomal protein L7/L12. *J. Biol. Chem.* **282**, 36998–37005 (2007).
420. Diaconu, M. *et al.* Structural basis for the function of the ribosomal L7/12 stalk in factor binding and GTPase activation. *Cell.* **121**, 991–1004 (2005).
421. Burdett, V. Tet(M)-promoted release of tetracycline from ribosomes is GTP dependent. *J. Bacteriol.* **178**, 3246–3251 (1996).
422. Blaha, G. *et al.* Preparation of functional ribosomal complexes and effect of buffer conditions on tRNA positions observed by cryoelectron microscopy. *Meth. Enzymol.* **317**, 292–309 (2000).
423. Mikolajka, A. *et al.* Differential effects of thiopeptide and orthosomycin antibiotics on translational GTPases. *Chem. Biol.* **18**, 589–600 (2011).
424. Bergeron, J. *et al.* Glycylcyclines bind to the high-affinity tetracycline ribosomal binding site and evade Tet(M)- and Tet(O)-mediated ribosomal protection. *Antimicrob. Agents Chemother.* **40**, 2226–2228 (1996).
425. Du, D. *et al.* Structure of the AcrAB-TolC multidrug efflux pump. *Nature.* **509**, 512–515 (2014).
426. Elkins, C. A. & Nikaido, H. Substrate specificity of the RND-type multidrug efflux pumps AcrB and AcrD of *Escherichia coli* is determined predominantly by two large periplasmic loops. *J. Bacteriol.* **184**, 6490–6498 (2002).
427. Ma, D., Alberti, M., Lynch, C., Nikaido, H. & Hearst, J. E. The local repressor AcrR plays a modulating role in the regulation of *acrAB* genes of *Escherichia coli* by global stress signals. *Mol. Microbiol.* **19**, 101–112 (1996).
428. Alekshun, M. N. & Levy, S. B. The *mar* regulon. Multiple resistance to antibiotics and other toxic chemicals. *Trends. Microbiol.* **7**, 410–413 (1999).
429. Yamasaki, S. *et al.* The crystal structure of multidrug-resistance regulator RamR with multiple drugs. *Nat. Commun.* **4**, 2078 (2013).
430. George, A. M., Hall, R. M. & Stokes, H. W. Multidrug resistance in *Klebsiella pneumoniae*. A novel gene, *ramA*, confers a multidrug resistance phenotype in *Escherichia coli*. *Microbiology* **141** (Pt 8), 1909–1920 (1995).
431. Pourahmad Jaktaji, R. & Jazayeri, N. Expression of *acrA* and *acrB* Genes in *Escherichia coli* Mutants with or without *marR* or *acrR* Mutations. *Iran. J. Basic Med. Sci.* **16**, 1254–1258 (2013).
432. Visalli, M. A., Murphy, E., Projan, S. J. & Bradford, P. A. AcrAB multidrug efflux pump is associated with reduced levels of susceptibility to tigecycline (GAR-936) in *Proteus mirabilis*. *Antimicrob. Agents Chemother.* **47**, 665–669 (2003).
433. Haque, M. M., Kabir, M. S., Aini, L. Q., Hirata, H. & Tsuyumu, S. SlyA, a MarR family transcriptional regulator, is essential for virulence in *Dickeya dadantii* 3937. *J. Bacteriol.* **191**, 5409–5418 (2009).

434. Baba, T. *et al.* Construction of *Escherichia coli* K-12 in-frame, single-gene knockout mutants. The Keio collection. *Mol. Syst. Biol.* **2**, 2006.0008 (2006).
435. Hu, M., Nandi, S., Davies, C. & Nicholas, R. A. High-level chromosomally mediated tetracycline resistance in *Neisseria gonorrhoeae* results from a point mutation in the *rpsJ* gene encoding ribosomal protein S10 in combination with the *mtrR* and *penB* resistance determinants. *Antimicrob. Agents Chemother.* **49**, 4327–4334 (2005).
436. Villa, L., Feudi, C., Fortini, D., García-Fernández, A. & Carattoli, A. Genomics of KPC-producing *Klebsiella pneumoniae* sequence type 512 clone highlights the role of RamR and ribosomal S10 protein mutations in conferring tigecycline resistance. *Antimicrob. Agents Chemother.* **58**, 1707–1712 (2014).
437. Nikaido, H. Multiple antibiotic resistance and efflux. *Curr. Opin. Microbiol.* **1**, 516–523 (1998).
438. Pérez, A. *et al.* Involvement of the AcrAB-TolC efflux pump in the resistance, fitness, and virulence of *Enterobacter cloacae*. *Antimicrob. Agents Chemother.* **56**, 2084–2090 (2012).
439. Denaro, M. & Lorenzetti, R. (*GRUPPO LEPETIT Milano [IT]*). DNA-sequence conferring resistance to the antibiotic thermorubin. EP0430066A1 (1994).
440. Lomovskaya, O., Lewis, K. & Matin, A. EmrR is a negative regulator of the *Escherichia coli* multidrug resistance pump EmrAB. *J. Bacteriol.* **177**, 2328–2334 (1995).
441. Tanabe, M. *et al.* The multidrug resistance efflux complex, EmrAB from *Escherichia coli* forms a dimer in vitro. *Biochem. Biophys. Res. Commun.* **380**, 338–342 (2009).
442. Xiong, A. *et al.* The EmrR protein represses the *Escherichia coli* emrRAB multidrug resistance operon by directly binding to its promoter region. *Antimicrob. Agents Chemother.* **44**, 2905–2907 (2000).
443. Chen, S. *et al.* Contribution of target gene mutations and efflux to decreased susceptibility of *Salmonella enterica* serovar typhimurium to fluoroquinolones and other antimicrobials. *Antimicrob. Agents Chemother.* **51**, 535–542 (2007).
444. Aguilera, L. *et al.* Dual role of LldR in regulation of the LldPRD operon, involved in L-lactate metabolism in *Escherichia coli*. *J. Bacteriol.* **190**, 2997–3005 (2008).
445. Benítez-Páez, A., Villarroya, M., Douthwaite, S., Gabaldón, T. & Armengod, M.-E. YibK is the 2¹-O-methyltransferase TrmL that modifies the wobble nucleotide in *Escherichia coli* tRNA(Leu) isoacceptors. *RNA*. **16**, 2131–2143 (2010).
446. Mardirossian, M. *et al.* The host antimicrobial peptide Bac71-35 binds to bacterial ribosomal proteins and inhibits protein synthesis. *Chem. Biol.* **21**, 1639–1647 (2014).
447. Graf, M. *et al.* Proline-rich antimicrobial peptides targeting protein synthesis. *Nat. Prod. Rep.* **34**, 702–711 (2017).
448. Florin, T. *et al.* An antimicrobial peptide that inhibits translation by trapping release factors on the ribosome. *Nat. Struct. Mol. Biol.* **24**, 752–757 (2017).
449. Berthold, N. *et al.* Novel apidaecin 1b analogs with superior serum stabilities for treatment of infections by gram-negative pathogens. *Antimicrob. Agents Chemother.* **57**, 402–409 (2013).
450. Cziala, P. *et al.* Api88 is a novel antibacterial designer peptide to treat systemic infections with multidrug-resistant Gram-negative pathogens. *ACS Chem. Biol.* **7**, 1281–1291 (2012).
451. Luiz, D. P., Almeida, J. F., Goulart, L. R., Nicolau-Junior, N. & Ueira-Vieira, C. Heterologous expression of abaecin peptide from *Apis mellifera* in *Pichia pastoris*. *Microb. Cell. Fact.* **16**, 76 (2017).

452. Levashina, E. A. *et al.* Metchnikowin, a novel immune-inducible proline-rich peptide from *Drosophila* with antibacterial and antifungal properties. *Eur. J. Biochem.* **233**, 694–700 (1995).
453. Imler, J.-L. & Bulet, P. Antimicrobial peptides in *Drosophila*. Structures, activities and gene regulation. *Chem. Immunol. Allergy* **86**, 1–21 (2005).
454. Bolouri Moghaddam, M.-R., Vilcinskas, A. & Rahnamaeian, M. The insect-derived antimicrobial peptide metchnikowin targets *Fusarium graminearum* β (1,3)glucanoyltransferase Gel1, which is required for the maintenance of cell wall integrity. *Biol. Chem.* **398**, 491–498 (2017).
455. Moghaddam, M.-R. B., Gross, T., Becker, A., Vilcinskas, A. & Rahnamaeian, M. The selective antifungal activity of *Drosophila melanogaster* metchnikowin reflects the species-dependent inhibition of succinate-coenzyme Q reductase. *Sci. Rep.* **7**, 8192 (2017).
456. Destoumieux, D. *et al.* Penaeidins, a new family of antimicrobial peptides isolated from the shrimp *Penaeus vannamei* (Decapoda). *J. Biol. Chem.* **272**, 28398–28406 (1997).
457. Wakabayashi, T., Kato, H. & Tachibana, S. Complete nucleotide sequence of mRNA for caerulein precursor from *Xenopus* skin. The mRNA contains an unusual repetitive structure. *Nucleic Acids Res.* **13**, 1817–1828 (1985).
458. Gibson, B. W., Poulter, L., Williams, D. H. & Maggio, J. E. Novel peptide fragments originating from PGLa and the caerulein and xenopsin precursors from *Xenopus laevis*. *J. Biol. Chem.* **261**, 5341–5349 (1986).
459. Shigeri, Y. *et al.* Identification of novel peptides from amphibian (*Xenopus tropicalis*) skin by direct tissue MALDI-MS analysis. *FEBS. J.* **282**, 102–113 (2015).
460. Ali, M. F., Soto, A., Knoop, F. C. & Conlon, J.M. Antimicrobial peptides isolated from skin secretions of the diploid frog, *Xenopus tropicalis* (Pipidae). *Biochim. Biophys. Acta.* **1550**, 81–89 (2001).
461. Kessler, A., Dittrich, W., Betzler, M. & Schremppf, H. Cloning and analysis of a deletable tetracycline-resistance determinant of *Streptomyces lividans* 1326. *Mol. Microbiol.* **3**, 1103–1109 (1989).
462. Arenz, S., Nguyen, F., Beckmann, R. & Wilson, D. N. Cryo-EM structure of the tetracycline resistance protein TetM in complex with a translating ribosome at 3.9-Å resolution. *Proc. Natl. Acad. Sci. U S A.* **112**, 5401–5406 (2015).
463. Savelsbergh, A. *et al.* An elongation factor G-induced ribosome rearrangement precedes tRNA-mRNA translocation. *Mol. Cell.* **11**, 1517–1523 (2003).
464. Carlson, M. A. *et al.* Ribosomal protein L7/L12 is required for GTPase translation factors EF-G, RF3, and IF2 to bind in their GTP state to 70S ribosomes. *FEBS. J.* **284**, 1631–1643 (2017).
465. Linkevicius, M., Sandegren, L. & Andersson, D. I. Potential of Tetracycline Resistance Proteins To Evolve Tigecycline Resistance. *Antimicrob. Agents Chemother.* **60**, 789–796 (2016).
466. Blair, J. M. A. *et al.* AcrB drug-binding pocket substitution confers clinically relevant resistance and altered substrate specificity. *Proc. Natl. Acad. Sci. U S A.* **112**, 3511–3516 (2015).
467. Plesa, M., Hernalsteens, J.-P., Vandebussche, G., Ruyschaert, J.-M. & Cornelis, P. The SlyB outer membrane lipoprotein of *Burkholderia multivorans* contributes to membrane integrity. *Res. Microbiol.* **157**, 582–592 (2006).
468. Yuhan, Y., Ziyun, Y., Yongbo, Z., Fuqiang, L. & Qinghua, Z. Over expression of AdeABC and AcrAB-TolC efflux systems confers tigecycline resistance in clinical isolates of *Acinetobacter baumannii* and *Klebsiella pneumoniae*. *Rev. Soc. Bras. Med. Trop.* **49**, 165–171 (2016).

469. Juan, C.-H., Huang, Y.-W., Lin, Y.-T., Yang, T.-C. & Wang, F.-D. Risk Factors, Outcomes, and Mechanisms of Tigecycline-Nonsusceptible *Klebsiella pneumoniae* Bacteremia. *Antimicrob. Agents Chemother.* **60**, 7357–7363 (2016).
470. Sato, T. *et al.* Tigecycline Nonsusceptibility Occurs Exclusively in Fluoroquinolone-Resistant *Escherichia coli* Clinical Isolates, Including the Major Multidrug-Resistant Lineages O25b:H4-ST131-H30R and O1-ST648. *Antimicrob. Agents Chemother.* **61** (2017).
471. Tintino, S. R. *et al.* Tannic acid affects the phenotype of *Staphylococcus aureus* resistant to tetracycline and erythromycin by inhibition of efflux pumps. *Bioorg. Chem.* **74**, 197–200 (2017).
472. Siriyong, T. *et al.* Conessine as a novel inhibitor of multidrug efflux pump systems in *Pseudomonas aeruginosa*. *BMC Complement Altern. Med.* **17**, 405 (2017).
473. Bohnert, J. A. *et al.* Novel Piperazine Arylideneimidazolones Inhibit the AcrAB-TolC Pump in *Escherichia coli* and Simultaneously Act as Fluorescent Membrane Probes in a Combined Real-Time Influx and Efflux Assay. *Antimicrob. Agents Chemother.* **60**, 1974–1983 (2016).
474. Datsenko, K. A. & Wanner, B. L. One-step inactivation of chromosomal genes in *Escherichia coli* K-12 using PCR products. *Proc. Natl. Acad. Sci. U S A.* **97**, 6640–6645 (2000).
475. Lindahl, L. & Zengel, J. M. Ribosomal genes in *Escherichia coli*. *Annu. Rev. Genet.* **20**, 297–326 (1986).
476. Orelle, C. *et al.* Tools for characterizing bacterial protein synthesis inhibitors. *Antimicrob. Agents Chemother.* **57**, 5994–6004 (2013).
477. Horiyama, T., Yamaguchi, A. & Nishino, K. TolC dependency of multidrug efflux systems in *Salmonella enterica* serovar Typhimurium. *J. Antimicrob. Chemother.* **65**, 1372–1376 (2010).
478. Zaporjets, D., French, S. & Squires, C. L. Products transcribed from rearranged *rrn* genes of *Escherichia coli* can assemble to form functional ribosomes. *J. Bacteriol.* **185**, 6921–6927 (2003).
479. Stasio, E. A. de, Moazed, D., Noller, H. F. & Dahlberg, A. E. Mutations in 16S ribosomal RNA disrupt antibiotic–RNA interactions. *EMBO J.* **8**, 1213–1216 (1989).
480. Hanslick, J. L. *et al.* Dimethyl sulfoxide (DMSO) produces widespread apoptosis in the developing central nervous system. *Neurobiol. Dis.* **34**, 1–10 (2009).
481. Galvao, J. *et al.* Unexpected low-dose toxicity of the universal solvent DMSO. *FASEB J.* **28**, 1317–1330 (2014).
482. Yu, X., Zipp, G. L. & Davidson, G. W. The effect of temperature and pH on the solubility of quinolone compounds. Estimation of heat of fusion. *Pharm. Res.* **11**, 522–527 (1994).
483. Kalepu, S. & Nekkanti, V. Insoluble drug delivery strategies. Review of recent advances and business prospects. *Acta Pharm. Sin. B.* **5**, 442–453 (2015).
484. PARMEGGIANI, A. & Nissen, P. Elongation factor Tu-targeted antibiotics. Four different structures, two mechanisms of action. *FEBS Lett.* **580**, 4576–4581 (2006).
485. Zhang, F. & Kelly, W. L. In vivo production of thiopeptide variants. *Meth. Enzymol.* **516**, 3–24 (2012).
486. Weisblum, B. & Demohn, V. Thiostrepton, an inhibitor of 50S ribosome subunit function. *J. Bacteriol.* **101**, 1073–1075 (1970).
487. Fabbretti, A. *et al.* A Derivative of the Thiopeptide GE2270A Highly Selective against *Propionibacterium acnes*. *Antimicrob. Agents Chemother.* **59**, 4560–4568 (2015).
488. Matsumoto, K. *et al.* In vivo target exploration of apidaecin based on Acquired Resistance induced by Gene Overexpression (ARGO assay). *Sci. Rep.* **7**, 12136 (2017).

489. Rahnamaeian, M. *et al.* Insect antimicrobial peptides show potentiating functional interactions against Gram-negative bacteria. *Proc. Biol. Sci.* **282**, 20150293 (2015).
490. Knappe, D. *et al.* Proline-rich Antimicrobial Peptides Optimized for Binding to Escherichia coli Chaperone DnaK. *Protein Pept. Lett.* **23**, 1061–1071 (2016).
491. Rahnamaeian, M. *et al.* Insect peptide metchnikowin confers on barley a selective capacity for resistance to fungal ascomycetes pathogens. *J. Exp. Bot.* **60**, 4105–4114 (2009).
492. Bechinger, B., Zasloff, M. & Opella, S. J. Structure and orientation of the antibiotic peptide magainin in membranes by solid-state nuclear magnetic resonance spectroscopy. *Protein Sci.* **2**, 2077–2084 (1993).
493. Mechkarska, M. *et al.* Peptidomic analysis of skin secretions demonstrates that the allopatric populations of *Xenopus muelleri* (Pipidae) are not conspecific. *Peptides* **32**, 1502–1508 (2011).
494. Fox, J. L. Antimicrobial peptides stage a comeback. *Nat. Biotechnol.* **31**, 379–382 (2013).
495. Kubicek-Sutherland, J. Z. *et al.* Antimicrobial peptide exposure selects for *Staphylococcus aureus* resistance to human defence peptides. *J. Antimicrob. Chemother.* **72**, 115–127 (2017).
496. Schmidtchen, A., Frick, I.-M., Andersson, E., Tapper, H. & Björck, L. Proteinases of common pathogenic bacteria degrade and inactivate the antibacterial peptide LL-37. *Mol. Microbiol.* **46**, 157–168 (2002).
497. Sieprawska-Lupa, M. *et al.* Degradation of human antimicrobial peptide LL-37 by *Staphylococcus aureus*-derived proteinases. *Antimicrob. Agents Chemother.* **48**, 4673–4679 (2004).
498. Goldstein, E. J. C., Citron, D. M., Tyrrell, K. L. & Leoncio, E. S. In Vitro Activities of Pexiganan and 10 Comparator Antimicrobials against 502 Anaerobic Isolates Recovered from Skin and Skin Structure Infections. *Antimicrob. Agents Chemother.* **61** (2017).
499. Chen, H.-L., Su, P.-Y. & Shih, C. Improvement of in vivo antimicrobial activity of HBcARD peptides by D-arginine replacement. *Appl. Microbiol. Biotechnol.* **100**, 9125–9132 (2016).
500. Avan, I., Hall, C. D. & Katritzky, A. R. Peptidomimetics via modifications of amino acids and peptide bonds. *Chem. Soc. Rev.* **43**, 3575–3594 (2014).
501. Cundliffe, E. & Thompson, J. The mode of action of nosiheptide (multhiomycin) and the mechanism of resistance in the producing organism. *J. Gen. Microbiol.* **126**, 185–192 (1981).
502. Benazet, F. & Cartier, J. R. Effect of nosiheptide as a feed additive in chicks on the quantity, duration, prevalence of excretion, and resistance to antibacterial agents of *Salmonella typhimurium*; on the proportion of *Escherichia coli* and other coliforms resistant to antibacterial agents; and on their degree and spectrum of resistance. *Poult. Sci.* **59**, 1405–1415 (1980).
503. Miller, S. M. *et al.* Comparison of the proteolytic susceptibilities of homologous L-amino acid, D-amino acid, and N-substituted glycine peptide and peptoid oligomers. *Drug Dev. Res.* **35**, 20–32 (1995).
504. MAAS, W. K. Pantothenate studies. III. Description of the extracted pantothenate-synthesizing enzyme of *Escherichia coli*. *J. Biol. Chem.* **198**, 23–32 (1952).
505. Begley, T. P., Kinsland, C. & Strauss, E. The biosynthesis of coenzyme A in bacteria. *Vitam. Horm.* **61**, 157–171 (2001).
506. Porter, E. A., Weisblum, B. & Gellman, S. H. Mimicry of Host-Defense Peptides by Unnatural Oligomers. Antimicrobial β -Peptides. *J. Am. Chem. Soc.* **124**, 7324–7330 (2002).

507. Simon, R. J. *et al.* Peptoids. A modular approach to drug discovery. *Proc. Natl. Acad. Sci. U S A.* **89**, 9367–9371 (1992).
508. Beke, T., Somlai, C. & Perczel, A. Toward a rational design of beta-peptide structures. *J. Comput. Chem.* **27**, 20–38 (2006).
509. Grimsley, G. R. & Pace, C. N. Spectrophotometric determination of protein concentration. *Curr. Protoc. Protein Sci.* **Chapter 3**, Unit 3.1 (2004).
510. Gallagher, S. R. One-dimensional SDS gel electrophoresis of proteins. *Current protocols in immunology* **Chapter 8**, Unit 8.4 (2006).
511. Graham, J. M. *Subcellular fractionation. A practical approach* (IRL Press, Oxford, 1997).
512. Asai, T., Zaporjets, D., Squires, C. & Squires, C. L. An Escherichia coli strain with all chromosomal rRNA operons inactivated. Complete exchange of rRNA genes between bacteria. *Proc. Natl. Acad. Sci. U S A.* **96**, 1971–1976 (1999).
513. Starosta, A. L. *et al.* Identification of distinct thiopeptide-antibiotic precursor lead compounds using translation machinery assays. *Chem. Biol.* **16**, 1087–1096 (2009).
514. Starosta, A. L. *et al.* Interplay between the ribosomal tunnel, nascent chain, and macrolides influences drug inhibition. *Chem. Biol.* **17**, 504–514 (2010).
515. Kling, A. *et al.* Antibiotics. Targeting DnaN for tuberculosis therapy using novel griselimycins. *Science.* **348**, 1106–1112 (2015).

Appendix A: Amino acid alignment of OtrA isoforms

CAA37477.1	1	MNKLNLGILAHVDAGKTSLTERLLHRTGVIDEVGSVDAGTTTTDSMELERQGITIRSAV
OtrA3-4	1	MNKLNLGILAHVDAGKTSLTERLLHRTGVIDEVGSVDAGTTTTDSMELERQGITIRSAV
CAA37477.1	61	ATFVLDLKVNLIDTPGHSDFISEVERALGVLDGAVLVVSAVEGVQPQTRILMRTLRLG
OtrA3-4	61	ATFVLDLKVNLIDTPGHSDFISEVERALGVLDGAVLVVSAVEGVQPQTRILMRTLRLG
CAA37477.1	121	IPTLVFVNKIDRGGARPDGVLREIRDRLTPAAVALSAVADAGTPRARAIALGPDTPDFA
OtrA3-4	121	IPTLVFVNKIDRGGARPDGVLREIRDRLTPAAVALSAVADAGTPRARAIALGPDTPDFA
CAA37477.1	181	VRVGEELLADHDDAFLTAYLDEEHVLTEKEYAEELAAQTARGLVHPVYFGSALTGEGLDHL
OtrA3-4	181	VRVGEELLADHDDAFLTAYLDEEHVLTEKEYAEELAAQTARGLVHPVYFGSALTGEGLDHL
CAA37477.1	241	-----VHGIRELLPSVHASQDAPLRATVFKVDR
OtrA3-4	241	VHGIRELLPSVHASQHPVYFGSALTGEGLDHLVHGIRELLPSVHASQDAPLRATVFKVDR
CAA37477.1	269	GARGEAVAYLRLLVSGTLGTRDSVTLHRVDHTGRVTEHAGRITLRFVFEHGSATSETRATA
OtrA3-4	301	GARGEAVAYLRLLVSGTLGTRDSVTLHRVDHTGRVTEHAGRITLRFVFEHGSATSETRATA
CAA37477.1	329	GDIAQAWGLKDVVRGDRAGHLDGPPPRNFFAPPSLETVIRPERPEEAGRLHAALRMLDEQ
OtrA3-4	361	GDIAQAWGLKDVVRGDRAGHLDGPPPRNFFAPPSLETVIRPERPEEAGRLHAALRMLDEQ
CAA37477.1	389	DPSIDLRLQDEENAAGAVVRLYGEVQKEILGSTLAESFGVRRVDFPTRTVCIKPVGTGEA
OtrA3-4	421	DPSIDLRLQDEENAAGAVVRLYGEVQKEILGSTLAESFGVRRVDFPTRTVCIKPVGTGEA
CAA37477.1	449	LIELDTRTHNYFWGAPWVCASDRPSPARAITFRLAVELGSLPLAFHKATEETVHTTLRHG
OtrA3-4	481	LIELDTRTHNYFWATVGLRVG-PAEPCAGITFRLAVELGSLPLAFHKATEETVHTTLRHG
CAA37477.1	509	LYGWQVTDCAVTLTRTGVRSPVSAADDFRKANARLVLMDALGRAGTEVHEPVSSFELEVPE
OtrA3-4	540	LYGWQVTDCAVTLTRTGFAFSPVSAADDFRKAATP-LVLMDALRQAGTEVHEPVSSFELEVPE
CAA37477.1	569	AARLSPVLAKLAEELGATPGVPTAEGDVFRLEGTMPTSLVHDFNQRPVGLTQEGGVFLAEH
OtrA3-4	599	AARLSPVLAKLAEELGATPGVPTAEGDVFRLEGTMPTSLVHDFNQRPVGLTQEGGVFLAEH
CAA37477.1	629	RGYRPAVGQPPVRRPRPEGPNPLNRDEYILHVLKRV
OtrA3-4	659	RGYRPAVGQPPVRRPRPEGPNPLNRDEYILHVLKRV

CAA37477.1: originally published sequence for OtrA⁴¹⁷.

OtrA3-4: cloned in this thesis out of genomic DNA of *Streptomyces rimosus subsp. rimosus* ATCC 10970 (DSM No.40260)

Appendix B: Amino acid alignment of OtrA and TetM

```

OtrA 1 MNKLNIGILAHVDAGKTSLTERLLHRTGVIDEVGSVDACTTTTDSMELERQRGITIRSAV
TetM 1 MKLINIGVLAHVDAGKTLTESLLYNSGATTEIGSVDKGTRTDNTLLERQRGITIQTGI

OtrA 61 AIFVLDLKVNLIDTPGHSDFI SEVERALGVLDGAVLVVSAVEGVQPQTRILMRLRRIG
TetM 61 TSEQWENTKVNLIIDTPGHMDFLAEVYRSLSVLDGAILLISAKDGVQAQTRILFHALRKMG

OtrA 121 IPTLVFNKIDRGGARPDGVLRITRDRLTPAAVALSAADAGTFRARAIALGPDTPDFA
TetM 121 IPTLFFINKIDQNGIDLSTVYQDIKEKLSAEIIVIKQKVELY--PNVCVTNFTES--E---

OtrA 181 VVVGELADHDAAFLTAYLDEEHVLTKEFYAEVLAQTARGLVHPVYFGSALTEGGLDEL
TetM 174 --QWDTVIFGNDDLLEKYMVGKSL-EALVLEQVESIRFQNCSEFLYHGSAKSNIGIDNL

OtrA 241 VHCIRELLSVVHASQDAFLRATVFKVDRGARGEAVAYLRIVSGTLGTRDSVTLHRVDHTG
TetM 231 IETVTKNFYSSTHRGPSELCGNVFKIEYTKRQRILAYIRLYSGVHLHLDSSVRVSEKEKIK

OtrA 301 RVTETHAGRITAVRFEHGSATSETRATAGDIAQAWGLKDVVVGDRACHLDGPPENF--F
TetM 291 V-TE-----MYTSINGELCKIDRAYSCEIVILQN-EFLKLNVLGDTKLLPQRKKLEN

OtrA 359 APESLETVIRPERPEEAGRLHAALRMLDEQDPSLDLRQDEENAAGAVVRLYGEVQKEIIG
TetM 342 PHELLQTVPEPSKPEQREMLLDALLEISLSDPLIRYYVDS-TTHEIILSFLGKVMQMEVIS

OtrA 419 STLAESLGVRRVRFDPTRTVCIKPKVGTGEALTELDTRTHNYFWCAPWVCASDRPSPARAI
TetM 401 ALIQEKHVEIELKEPTVHYMERPLKNABYTHIEVPP-NPFWASIGL SVSPLP-LGSGM

OtrA 479 TIRLAVELGSLPLAFHKATEETVHTTLRHGLYGWQVTDCAVTLTRTGVRSPVSAADDFRK
TetM 459 QVSSVSLGYLNQSEFQNAVMEGIRYGCQGLYGWVTDCKLCFKYGLYSPVSTPADFRM

OtrA 539 ANARIVLMDALGRAGTEVHEPVSSFELEVPAARLSPVLAKLAEALGATPGVPTAEGDVFRL
TetM 519 L-APIVLEQVLKKGAGTELEPYLSFKIYAPQEYLSRAYNDAPKYCANIVDTQLKNNEVIL

OtrA 599 EGTMPSTLVHDEINQRVPGLTQEGVFLAEHRGYLPAVGOEPVPRPRPEGPNLNDEYILH
TetM 578 SGEIPARCTQEVRSDLTFFTINGRSVCLTEELKGYHVTTEGEVVCQPRRPNRSR-IDKVRVYMFN

OtrA 659 VIKRV
TetM 637 KLT--

```

OtrA: GenBank: CAA37477.1

TetM: GenBank: CAA63530.2

Appendix C: Amino acid alignment of TetO and TetM

```

TetO   1  MKIINLGI LAHV DAGKTTLTESL LYTSGAIAELGSVDEGTRTRD TMNLERQRGITIQTAV
TetM   1  MKLIINIGV LAHV DAGKTTLTESL LLYNSGAI TELGSVDKGTTRTDNTLLERQRGITIQTGI

TetO   61  TSFQWEDV KVNII DTPGHMDFLAEVYRSLSVLDGAVLLVSAKDGIQAQTRILFHALQIMK
TetM   61  TSFQWENTK VNIIDTPGHMDFLAEVYRSLSVLDGAILL VSAKDGVAQTRILFHALRKMKG

TetO   121 IPTIFFINKIDQEGIDLPMVYREMKAKLSSEIIVKQKVGQHPHINVTDNDDMEQWDAVIM
TetM   121 IPTIFFINKIDQNGIDLSTVYQDIKEKLSAEIIVKQKVELYPNVCVTNFTSEQWDTVIE

TetO   181 GNDELLLEKYMSGKPFKMSLELQEENRRFQNGILFPVYHGSAKNNIGIROLIEVIASKFYS
TetM   181 GNDELLLEKYMSGKSLLELQEESIRFQNCSLFPLYHGSAKSNIGIDNLIIEVITNKFYS

TetO   241 STPEGQSEL CGVFKIEYSEKRRRFVYVRIYSGTLHLRDVIRISEKEKIKITEMCVPTNG
TetM   241 STHRGPSEL CGNVFKIEYTKKRRLAYIRIYSGV LHLRDSVRVSEKEKIKVTEMVTSING

TetO   301 ELYSSDIAACSGDIVILPNDVLOLNSILGNEILLPQRKTIENPPLMLQTTAVKKESEOREI
TetM   301 ELCKIDRAYSGEIVILQNEFLKLSVLDGDTKLLPQRKTIENPPLMLQTTVEPSKPEOREM

TetO   361 LLGALTEISDGDPLLRKYVDITTHEIILSFLGNVQMEVISCALLEEKYHVEAEIKEPTVIY
TetM   361 LLDALLEISDSDPLLRKYVDSTTHEIILSFLGNVQMEVISCALLEEKYHVEAEIKEPTVIY

TetO   421 MERPLRKA EYTIHIEVPPNPFWASVGLSTEPLPIGSGQYESSVSLGYLNQSFQNAVMEG
TetM   421 MERPLRKA EYTIHIEVPPNPFWASVGLSTEPLPIGSGQYESSVSLGYLNQSFQNAVMEG

TetO   481 VLYGCEQGLYGMVTDCKICFELYGLYSPVSTPADFRLLSPIVLEQALKKAGTELLEPYL
TetM   481 IRYGCEQGLYGMVTDCKICFELYGLYSPVSTPADFRMLASPIVLEQV LKKAGTELLEPYL

TetO   541 HETIYAPQEYLSRAYHDAPRYCADIVSTQIKNDEVILKGEIPARCIQEYRNDLTCFTNGQ
TetM   541 SETIYAPQEYLSRAYNDAPRYCANIVDTQIKNDEVILS GEIPARCIQEYRSDLTFCFTNGR

TetO   601 GVCLTELKGYQPAIGKFTCPRRPNSRIDKVRHMFHKL A
TetM   601 SVCLTELKGYHVTTCPEVCPRRPNSRIDKVRHMFHKNIT

```

TetM: GenBank: EFQ13124.1

TetO: NCBI Reference Sequence: WP_010790859.1

DOI: 10.1002/cmdc.201300323

Amythiamicin D and Related Thiopeptides as Inhibitors of the Bacterial Elongation Factor EF-Tu: Modification of the Amino Acid at Carbon Atom C2 of Ring C Dramatically Influences Activity

Stefan Gross,^[a] Fabian Nguyen,^[b] Matthias Bierschenk,^[c] Daniel Sohmen,^[b] Thomas Menzel,^[d] Iris Antes,^{*[c]} Daniel N. Wilson,^{*[b]} and Thorsten Bach^{*[a]}

Three analogues of amythiamicin D, which differ in the substitution pattern at the methine group adjacent to C2 of the thiazole ring C, were prepared by de novo total synthesis. In amythiamicin D, this carbon atom is (*S*)-isopropyl substituted. Two of the new analogues carry a hydroxymethyl in place of the isopropyl group, one at an *S*- (compound **3a**) and the other at an *R*-configured stereogenic center (**3b**). The third analogue, **3c**, contains a benzyloxymethyl group at an *S*-configured stereogenic center. Compounds **3b** and **3c** showed no inhibitory effect toward various bacterial strains, nor did they influence the translation of firefly luciferase. In stark contrast, compound **3a** inhibited the growth of Gram-positive bacteria *Staphylococ-*

cus aureus (strains NCTC and Mu50) and *Listeria monocytogenes* EGD. In the firefly luciferase assay it proved more potent than amythiamicin D, and rescue experiments provided evidence that translation inhibition is due to binding to the bacterial elongation factor Tu (EF-Tu). The results were rationalized by structural investigations and by molecular dynamics simulations of the free compounds in solution and bound to the EF-Tu binding site. The low affinity of compound **3b** was attributed to the absence of a critical hydrogen bond, which stabilizes the conformation required for binding to EF-Tu. Compound **3c** was shown not to comply with the binding properties of the binding site.

Introduction

The bacterial elongation factor Tu (EF-Tu) was first described in 1966^[1] and plays a crucial role in bacterial protein biosynthesis.^[2] EF-Tu is a guanosine triphosphatase (GTPase) and displays high binding affinity for aminoacyl transfer RNA (aa-tRNA) in the GTP-bound form.^[3] During translation, EF-Tu is responsible for the delivery of aa-tRNA to the ribosome in the form of a ternary complex with GTP. Upon delivering the correct aa-tRNA to the ribosome—that is, specific for the mRNA codon—GTP hy-

drolisis occurs, allowing dissociation of EF-Tu from the ribosome and accommodation of the aa-tRNA. Peptide bond formation then occurs, incorporating the newly delivered amino acid into the growing peptide chain.^[4]

EF-Tu has been established as a validated drug target; it is a ubiquitous enzyme essential for bacterial protein biosynthesis.^[5] EF-Tu differs significantly from the human elongation factor eEF-1, guaranteeing desirable target specificity. Currently, four structurally distinct compound classes are known to inhibit EF-Tu efficiently, for which prototypical examples are kirromycin, enacycloxin Ila, pulvomycin, and GE2270 A (**1**). It has been shown that the binding sites of pulvomycin and GE2270 A are similar,^[6] whereas kirromycin^[7] and enacycloxin Ila^[8] possess a different mode of action. GE2270 A and pulvomycin hinder the formation of the ternary complex between EF-Tu, GTP, and aa-tRNA by binding to domain D2 of the enzyme. Binding of GE2270 A and related thiopeptides does not influence the GTPase activity of EF-Tu,^[9] in accordance with the fact that binding of GE2270 A to EF-Tu does not significantly affect the catalytically active domain D1 of the protein.^[6] Structural information about the interaction between GE2270 A and EF-Tu is based on crystallographic data obtained for EF-Tu-GDPNP-GE2270 A (GDPNP = guanosine-5'-(β , γ -imino)-triphosphate)^[6b] and EF-Tu-GDP-GE2270 A (GDP = guanosine diphosphate).^[6a] Binding occurs essentially along the cyclic thiopeptide, whereas peripheral substituents are less important for binding. All known naturally occurring GE2270 analogues,^[10]

[a] Dr. S. Gross, Prof. Dr. T. Bach

Lehrstuhl für Organische Chemie I, Technische Universität München
Lichtenbergstr. 4, 85747 Garching (Germany)
E-mail: thorsten.bach@ch.tum.de

[b] F. Nguyen, D. Sohmen, Dr. D. N. Wilson

Gene Center, Department for Biochemistry, and
Center for integrated Protein Science Munich (CiPSM)
Ludwig Maximilian University of Munich
Feodor-Lynen-Str. 25, 81377 Munich (Germany)
E-mail: wilson@genzentrum.lmu.de

[c] M. Bierschenk, Prof. Dr. I. Antes

Protein Modelling, Department for Life Sciences, and
Center for integrated Protein Science Munich (CiPSM)
Technische Universität München
Emil-Erlenmeyer-Forum 8, 85354 Freising (Germany)
E-mail: antes@wzw.tum.de

[d] Dr. T. Menzel

Lehrstuhl für Organische Chemie II, Technische Universität München
Lichtenbergstr. 4, 85747 Garching (Germany)

Supporting information for this article is available on the WWW under
<http://dx.doi.org/10.1002/cmdc.201300323>.

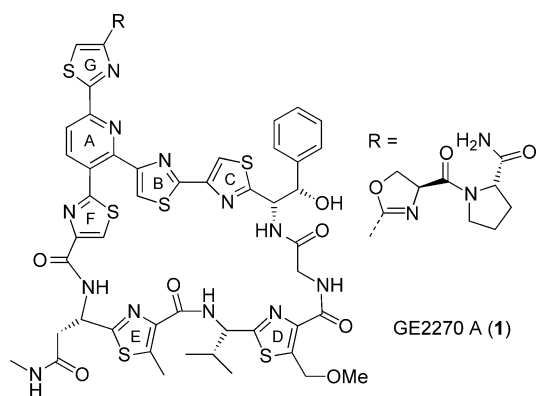


Figure 1. Ring numbering in the thiazolyl peptide GE2270 A (1).

which vary in the substituents at rings D and G or at the asparagine-derived amide in the southwestern part of the molecule (Figure 1), show an inhibitory effect on EF-Tu.^[9–11] Because hydrolysis of the oxazoline (R at ring G) to a carboxylic acid is facile, several modification studies were devoted to derivatization at this site. In an early study the acid and reduced derivatives of it were converted by conventional nucleophilic displacement reactions into a plethora of compounds.^[12] It was shown that these modifications can lead to a higher aqueous solubility while retaining biological activity. More recently, the same thiazole carboxylic acid was degraded by a Curtius rearrangement to deliver the respective 4-aminothiazole.^[13] Derivatives of this compound showed promising activity toward several multi-resistant bacterial strains.^[14] Optimization studies led to the discovery of two compounds with excellent physicochemical properties, including high water solubility.^[15] Further development resulted in an investigational drug (LFF571), which shows superior activity against *Clostridium difficile*, a bacterium responsible for severe infections of the large intestine.^[16]

Chemical modifications were also performed at the phenylglycine-derived northeastern part of GE2270 A located at position C2 of thiazole ring C.^[17] Removal of the α -hydroxybenzyl group led to a complete loss of activity, whereas some activity was retained in other derivatives in which the phenyl group was still present. It was thus concluded that this part is inserted into a lipophilic cavity of EF-Tu. Crystallographic data confirmed this view regarding the position of the phenyl group,^[6] but also indicated a hydrogen bond between the hydroxy group of the phenylglycine to amino acid Glu226 of EF-Tu. The proximity of this binding site to domain D1 of EF-Tu and in particular to an α helix (His85–Ala97), the C-terminal end of which is located in direct proximity to the catalytically active site, makes this position attractive for further studies.

The research presented herein addresses the latter issue by studying non-natural thiopeptides^[18] for the first time, which were synthesized *de novo* and modified at this critical site. Compounds **3** (Figure 2) are analogues of amythiamicin D (**2**). In the amythiamicins,^[19] which are closely related to the GE factors, the residue at C2 of thiazole ring C is derived from (*S*)-valine. Hydrogen bond formation with Glu226 of EF-Tu is

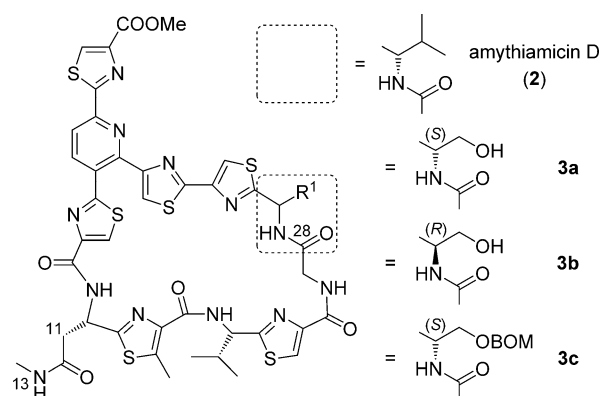


Figure 2. Molecules **2** and **3 a–c**, of which the antibiotic activity and mode of action on EF-Tu was investigated in this study.

therefore unfeasible. However, there is evidence that the amythiamicins also inhibit EF-Tu,^[11,20] although they have been studied less thoroughly than GE2270 A. Compound **3 a** bears a hydroxymethyl group at an *S*-configured stereogenic center, mimicking the α -hydroxybenzyl group present in GE2270 A. Compound **3 b** is an epimer of compound **3 a**, exhibiting the non-natural *R* configuration at the stereogenic center. Compound **3 c** has a lipophilic benzyloxymethyl (BOM) group instead of the polar hydroxy group.

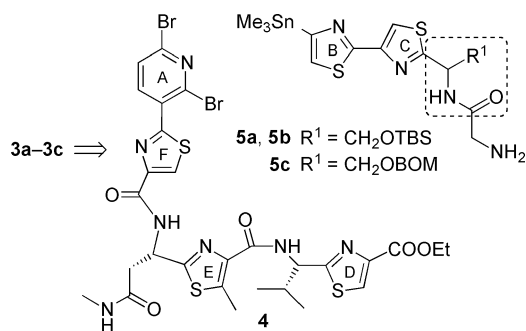
Results and Discussion

De novo synthesis of thiopeptides **3 a–3 c**

The synthetic strategy^[21] toward compounds **3** was based on earlier work that had culminated in the total synthesis of GE2270 A^[22] and amythiamicins C and D.^[23] Key to this strategy was the use of 2,6-dibromo-3-iodopyridine as pivotal building block, to which the various thiazolyl fragments were coupled in successive order.

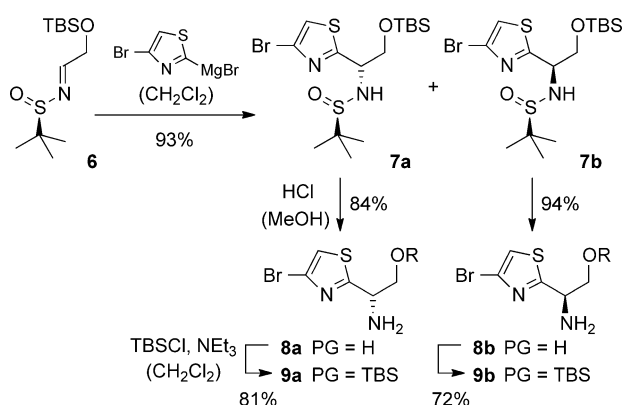
In this context, the synthesis of the southern fragment **4** of compounds **3** was reported earlier,^[23] and its synthesis is not discussed further. It is available from (*S*)-valine in seven steps and with an overall yield of 22%. While the southern trithiazolyl part (rings D–F) and the northern thiazolyl fragment (ring G) of compounds **2** and **3** are identical, synthetic access to the eastern part (rings B and C) had to be individually secured by preparation of compounds **5** (Scheme 1, TBS = *tert*-butyldimethylsilyl).

The Grignard addition to chiral sulfinyl imines has been established by Ellman et al. as a useful method to generate chiral amines,^[24] and it was previously shown that 4-bromthiazolyl-2-magnesium bromide adds efficiently to various imines derived from enantiomerically pure *tert*-butylsulfonamide.^[23] The auxiliary can be cleaved after addition by acidic methanolysis. A putative starting material for the desired target compound was consequently an appropriately protected glycolaldehyde. Upon monosilylation of glycol, the resulting primary alcohol was oxidized to the respective aldehyde by Swern oxidation, which in turn was immediately converted into the known^[25] imine **6** by



Scheme 1. Retrosynthetic disconnection of compounds **3 a–3 c** leading to different eastern fragments **5 a–5 c**, which were to be individually synthesized. See Figure 2 for the configuration in the dashed (----) box.

treatment with commercially available (*R*)-*tert*-butylsulfonamide (see Supporting Information for details). Grignard addition of the above-mentioned thiazolyl magnesium bromide (prepared by bromine magnesium exchange of 2,4-dibromothiazole with isopropyl magnesium bromide in THF/Et₂O^[26]) proceeded smoothly and delivered the desired products **7** as a mixture of diastereomers (Scheme 2). Gratifyingly, their separation by

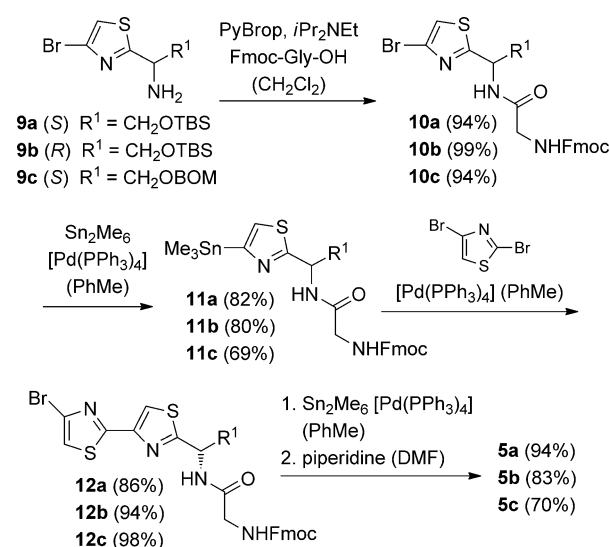


Scheme 2. Preparation of enantiomeric amino alcohols **8 a** and **8 b** via the respective diastereomeric sulfonil amines **7 a** and **7 b** and their conversion into the O-protected amino alcohols **9 a** and **9 b**.

chromatography was facile, and products **7 a** and **7 b** were employed as individual diastereomers in the next step. Given that both enantiomeric amino alcohols **8 a** and **8 b** were required for our further investigations, the Grignard addition was not thoroughly optimized. When performed at -78°C in a 6:1 solvent mixture of CH₂Cl₂ and ethers (THF/Et₂O), there was no notable diastereoselectivity. As previously observed,^[23] a larger fraction of CH₂Cl₂ was required to achieve diastereoselectivity. In the present case, the diastereomeric ratio (**7 a**/**7 b**) improved to 73:27 in a 14:1 mixture of CH₂Cl₂/ether. The configuration at the newly formed stereogenic center was determined by the Mosher method^[27] upon removal of the chiral auxiliary (Supporting Information). The major enantiomer of the diastereoselective addition was shown to be *S*-configured. Based on the conventional model for the Grignard addition to chiral sulfonil imines,^[24] the result appears surprising, but the unusual behav-

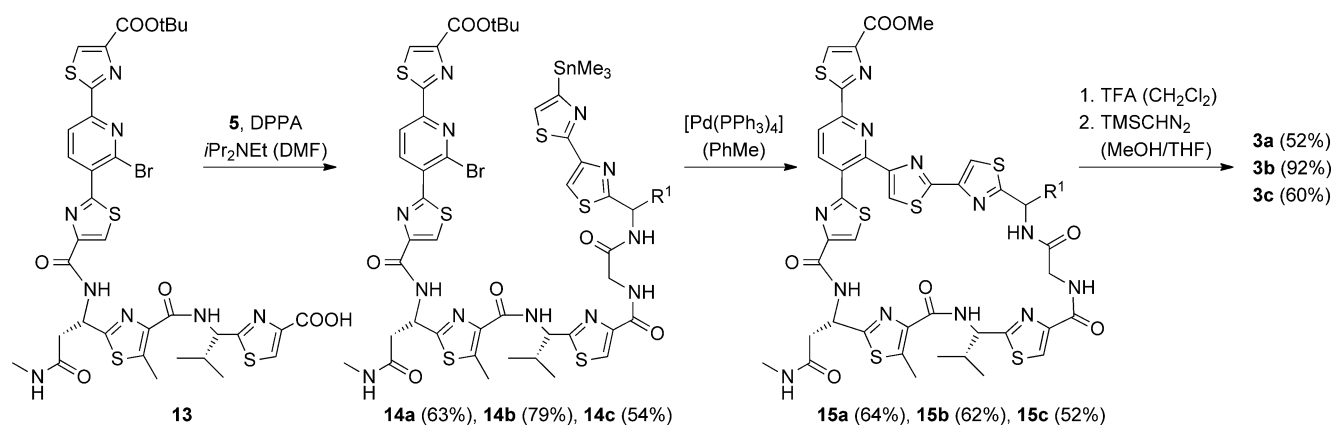
ior of imine **6** had been previously discussed by Barrow et al.^[25]

Because removal of the auxiliary also led to silyl deprotection, the silyl group was installed again by treatment of alcohols **8** with TBSCl/NEt₃. Introduction of the BOM group was facile at this stage and delivered the required amine **9 c** from amino alcohol **8 a** (Supporting Information). Peptide coupling of amines **9** to 9-fluorenylmethoxycarbonyl (Fmoc)-protected glycine (Fmoc-Gly-OH) was achieved by treatment of the coupling partners with bromotri(pyrrolidino)phosphonium hexafluorophosphate (PyBrop).^[28] To convert bromides **10** into suitable nucleophiles for a regioselective cross-coupling reaction with the second thiazole fragment,^[29] a stannylation was performed with hexamethylditin at 100 °C in toluene using tetrakis(triphenylphosphine)palladium as the catalyst.^[30] Stannanes **11** underwent a smooth Stille cross-coupling^[31] with 2,4-dibromothiazole,^[32] which was used in slight excess (1.4 equiv), yielding the desired dithiazoles **12** in high yields (Scheme 3).



Scheme 3. Synthesis of stannylated compounds **5 a–5 c** from the respective bromothiazoles **9 a–9 c**, employing regioselective Stille cross-coupling reactions on 2,4-dibromothiazole as the key step.

4-Bromodithiazoles **12** were converted into the corresponding stannanes by another palladium-catalyzed stannyl debromination. Removal of the Fmoc protecting group with piperidine delivered the free amines **5** in high yields. The order of events for the incorporation of building blocks **5** into a pyridine fragment and the choice of this fragment was based on previous experience (Scheme 4). In the synthesis of GE2270 A,^[22] it had been found that a macrocyclization by Stille cross-coupling after preceding amide bond formation provides significantly higher yields than an initial Stille cross-coupling followed by macrolactamization. In the synthesis of amythiamicin C,^[23] it was found that amide bond formation with the acid derived from ester **4** is feasible, but the subsequent ring closure, which requires a regioselective Stille cross-coupling at C2 of the pyridine core, is not sufficiently selective. Therefore,



Scheme 4. Peptide bond formation between pyridine core fragment **13** and the individual building blocks **5a–5c** (cf. Schemes 1–3) followed by a macrocyclization via Stille cross-coupling and two functional group transformation steps toward products **3a–3c**. The hydrolysis of the *tert*-butyl ester **15b** with TFA was followed by addition of HF-py to complete the desilylation.

ester **4** was converted according to known methodology^[23] into the previously described pyridine fragment **13**. Coupling of the two fragments to amides **14** was achieved with diphenylphosphoryl azide (DPPA)^[33] in the presence of Hünig's base. We were pleased to note that the Stille cross-coupling protocol was also successful for substrates **14** and delivered macrolactams **15** in moderate to good yields. Cleavage of the *tert*-butyl ester in ring G was possible with trifluoroacetic acid (TFA), which also led to cleavage of the TBS ether. Because TBS deprotection was relatively slow for substrate **15a** leading to side reactions and a diminished yield, deprotection of substrate **15b** was performed by an initial treatment with TFA and subsequent addition of HF-pyridine. Yields were significantly higher with this modification than the TFA deprotection used for **15a**. Conversion of the free acids into the desired methyl esters **3** was performed with trimethylsilyl diazomethane.

Biological activity and translation assays

To assess the biological activities of amythiamicin D (**2**) and the synthetic derivatives **3a–3c**, the minimal inhibitory concentration (MIC) was determined for the Gram-positive bacteria *Staphylococcus aureus* (strains NCTC and Mu50), *Listeria monocytogenes* EGD and *Streptococcus pyogenes* ATCC 10231, as well as the Gram-negative bacterium *Pseudomonas aeruginosa* PA01 and compared with control antibiotics kirromycin and the aminoglycoside kanamycin (Table 1).^[34] Amythiamicin D was previously shown to inhibit the growth of many Gram-positive bacteria, but not Gram-negative bacteria such as *E. coli*.^[19] We consistently found that compound **2** displays excellent biological activity against *S. aureus* and *L. monocytogenes* with an MIC₅₀ value of 0.32 μM, yet displays no activity against *S. pyogenes* or *P. aeruginosa*. A similar activity profile was observed for the synthetic derivative **3a**, although the MIC values were somewhat higher for the *S. aureus* and *L. monocytogenes* strains, when compared with **2**. In contrast, compounds **3b** and **3c**

Table 1. Minimal inhibitory concentrations of synthetic derivatives **3a–3c** relative to amythiamicin D (**2**), kirromycin, and kanamycin.

Strain	MIC [μM]					
	kanamycin	kirromycin	2	3a	3b	3c
<i>S. aureus</i> NCTC 8325	2.56	> 100	0.32	0.64	> 100	> 100
<i>S. aureus</i> Mu50	> 100	> 100	0.32	1.28	> 100	> 100
<i>L. monocytogenes</i> EGD-e	12.8	2.56	0.32	5.12	> 100	> 100
<i>S. pyogenes</i> ATCC 10231	100	0.32	> 100	> 100	> 100	> 100
<i>P. aeruginosa</i> PA01	> 100	> 100	> 100	> 100	> 100	> 100

displayed no activity against any of the strains tested, even at concentrations up to 100 μM (Table 1).

Although amythiamicins display poor activity against Gram-negative organisms such as *P. aeruginosa* (Table 1) and *E. coli*,^[19] inhibitory effects of amythiamicins on translation of poly(U)-directed poly(Phe) synthesis using an *E. coli* in vitro translation system has been demonstrated.^[20] This indicates that the inactivity of amythiamicins in blocking bacterial growth can be related to other factors such as membrane penetration rather than a lack of effect on translation. Therefore, to directly assess the effect of amythiamicin derivatives **3a–3c** on protein synthesis, we monitored the translation of firefly luciferase (Fluc) in an *E. coli* cell-free in vitro translation system in the presence of increasing concentrations of amythiamicin D (**2**) or one of the synthetic derivatives **3a–3c** (Figure 3A). As expected,^[20] **2** is a potent inhibitor of protein synthesis with a half-inhibitory concentration (IC₅₀ value) of ~10 μM. Surprisingly, however, the synthetic derivative **3a** displayed improved inhibitory activity, with IC₅₀ ~4 μM, at least twofold better than amythiamicin D. In contrast, derivatives **3b** and **3c** were completely inactive, even at high drug concentrations up to 40 μM. This suggests that the lack of effect of thiopeptides **3b** and **3c** on the growth of *S. aureus* and *L. monocytogenes* strains (Table 1) may indeed be due to an inability to inhibit protein synthesis, rather than an inability to penetrate the cell wall.

The structural similarity between amythiamicins and GE2270 A (**1**) suggests that amythiamicins also inhibit transla-

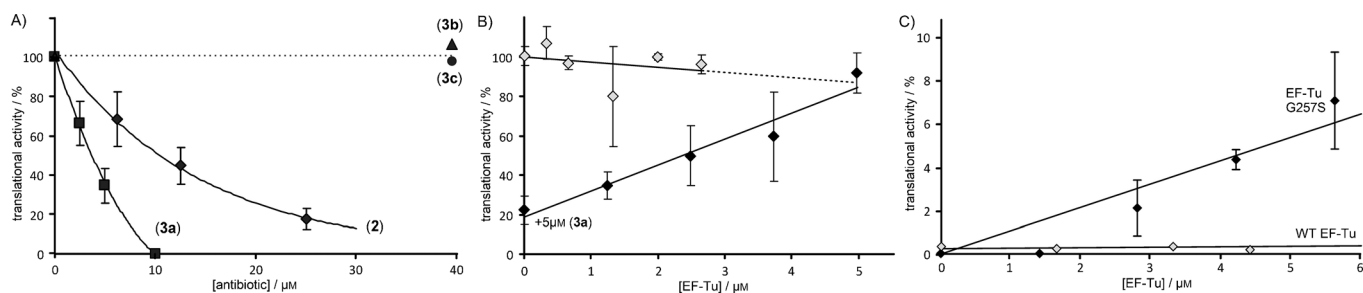


Figure 3. Translation inhibition by amythiamicin D and synthetic derivatives. A) Effect of increasing concentrations of amythiamicin D (**2**, \blacklozenge) and the amythiamicin D derivative **3a** (\blacksquare), **3b** (\blacktriangle), and **3c** (\bullet) on the translation of firefly luciferase. B) Effect of increasing concentrations of EF-Tu in the presence of 5 μM amythiamicin D derivatives **3a** (\blacklozenge) and absence of drug (\diamond). C) Effect of increasing concentrations of wild-type EF-Tu (\diamond) or EF-Tu-G257S (\blacklozenge) in the presence of 30 μM amythiamicin D derivatives **3a** (\blacklozenge). The firefly luminescence in the absence of drug was assigned as 100%, and error bars display the standard deviation from the mean for three individual experiments.

tion by interaction with EF-Tu, consistent with the observation that resistance to amythiamicins results from mutation with *tufA*, the gene for EF-Tu.^[20] We reasoned that if EF-Tu is the target of amythiamicin derivative **3a**, then increasing the concentration of EF-Tu within the in vitro translation assays should relieve the inhibition of translation resulting from amythiamicins. As is apparent in Figure 3B, the presence of **3a** at 5 μM decreases translation to 20%, which can be restored to 100% by the addition of an extra 5 μM recombinantly purified EF-Tu protein. As a control, the presence of additional EF-Tu was shown to have no significant effect on translation of Fluc in the absence of the drug.

The rescue of translation by the presence of additional EF-Tu is analogous to the target overexpression mechanisms that are used by some bacteria to obtain resistance to various antibiotics.^[35] Consistently, when the same experiment was performed in the presence of higher saturating concentrations of **3a** (30 μM), no rescue was observed (Figure 3C).

Next, we rationalized that if amythiamicins do indeed target EF-Tu, then titrating in an EF-Tu mutant protein that is resistant to thiopeptides should rescue translation to some extent, even in the presence of saturating drug concentrations. It has been reported that mutation of glycine at position 257 to serine in *E. coli* EF-Tu confers resistance to the thiopeptide GE2270 A by allowing simultaneous binding of the antibiotic and aa-tRNA to EF-Tu.^[36] We found that EF-Tu-G257S protein alone inhibits translation by $\sim 60\%$ at 1 μM (Supporting Information). Nevertheless, in the presence of 30 μM **3a**, it was indeed possible to rescue translation with the EF-Tu-G257S mutant, but not with wild-type EF-Tu. These findings not only support that the amythiamicin D derivative **3a** binds to EF-Tu, but also suggests that it interacts with EF-Tu in a manner analogous to GE2270 A, as expected based on the similarity in their chemical structures.

Structural investigations

The experimental structure of GE2270 A bound to EF-Tu-GDPNP^[6b] was used to investigate the structural basis of the binding behavior of the synthesized compounds; GE2270 A binds competitively to the aa-tRNA binding site of

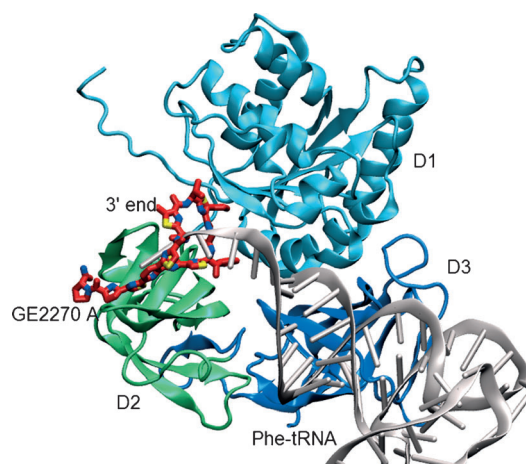


Figure 4. Structure of EF-Tu-GDPNP (blue/green ribbons) with bound GE2270 A (red sticks) (PDB ID: 2C77).^[6b] The additionally shown Phe-tRNA strand (grey) was extracted from the corresponding superimposed EF-Tu-GDPNP:Phe-tRNA structure (PDB ID: 1TTT),^[37] and superimposition was performed based on the EF-Tu backbone.

EF-Tu (Figure 4). The binding site of GE2270 A is located at the interface between domains D1 and D2, where the aa-tRNA binds with its 3' end. GE2270 A predominantly binds to D2 with the upper part of its thiazolyl ring contacting D1 in EF-Tu-GDPNP. Through binding of the antibiotic the interface geometry is widened, leading to a gap between the two domains in which the antibiotic compound is bound. Consequently, the binding site is blocked and thus binding of the 3' end of the aa-tRNA is inhibited by steric hindrance (Figure 4).

To elucidate the structural basis for the different binding behaviors of compounds **2** and **3a–3c** we first investigated their structures in aqueous solution by preliminary NMR experiments (Supporting Information) and by more extensive molecular dynamics (MD) and docking simulations. In previous work,^[38] it was established by a detailed NMR study of amythiamicin D that a single hydrogen bond is present between the carbonyl group at C28 and the proton at N13 (Figure 2), significantly stabilizing the ring conformation. The same hydrogen bond is present in the crystal structure of the EF-Tu-GDPNP-GE2270 A complex (Figure 4),^[6b] indicating that the stabilized

ring conformation in solution is retained upon binding to EF-Tu. As a result of the fixed conformation, the diastereotopic protons at the methylene group C11 of the side chain between rings E and F result in distinct peaks, which are clearly separated in the ^1H NMR spectrum (see ^1H NMR data in the Supporting Information). In stark contrast, a significant peak broadening was detected for the same protons in the ^1H NMR spectrum of compound **3b**. Only one peak was recorded at room temperature, which was significantly broadened upon cooling (Supporting Information). Although this observation could be explained by other biophysical effects, it is most likely to indicate that the unusual *R*-stereogenic center at R^1 in compound **3b** leads to significant changes in the ring conformation and to a higher degree of ring flexibility, averaging out the environment of the two protons. The higher flexibility, in turn, appears to be due to the lack of a hydrogen bond between the carbonyl group at C28 and the proton at N13 in **3b**.

To further investigate this topic we performed MD simulations of the free compounds in solution and bound to the EF-Tu binding site. The solution results are shown in Figure 5. For compounds **2**, **3a**, and **3c** the same predominant ring conformation was observed (Figure 5A–C,E and Supporting Information (SI) figure SI4) for all three compounds. This conformation is very similar to the bound conformation of GE2270 A in EF-Tu (Figure 4) and is in agreement with the NMR results, as the

ring is stabilized in all three cases by the same hydrogen bond between the C28 carbonyl group and the proton at N13 as also observed by Lewis et al.^[38] In compound **3b** the *R*-stereogenic center at C2 of the thiazole ring C leads to a geometrical inversion of its bonds to its neighboring ring atoms and its side chain. This causes a 180° rotation of the neighboring peptide group containing C28, and thus the ring stabilizing the hydrogen bond between N13 and the C28 carbonyl group is broken (Figure 5D, SI figure SI4d). Therefore, significant alterations in the overall ring conformation can be observed, together with a higher flexibility in its side chains. This leads to a different and less planar overall conformation than the ring conformation of compounds **2**, **3a**, and **3c** (see Figure 5E,F). Therefore compound **3b** has different steric and interaction requirements for successful protein binding. As the bound conformation of GE2270 A is close to the solution structures of compounds **2**, **3a**, and **3c** and also features the conserved hydrogen bond, it can be assumed that adopting this conformation in solution is a prerequisite for stable binding of the compounds to EF-Tu, which may explain the nonbinding behavior of compound **3b** (Figure 3).

To further substantiate this hypothesis, docking-based MD simulations were performed for all four compounds using the docking software DynaDock.^[39] As the algorithm is MD based, it allows full flexibility of the whole system and a proper treatment of the changes in the protein binding site upon ligand binding. This is important in the case of EF-Tu, as the binding site is very flexible, and large movements can be observed upon ligand binding. For the docking simulations the compounds were placed within the binding site based on their solution conformation of the ring system. Conformational sampling of all side chains and rotation and translation of the whole compound was then performed. In a second step, MD simulations were performed for the best-docked conformations to investigate the stability of the predicted complexes.

The final equilibrated structures after MD refinement are provided in Figure 6 and in the Supporting Information (figures SI1 and SI2). In the case of compounds **2** and **3a**, stable complexes with a bound ring conformation close to GE2270 A could be obtained, indicating stable, strong binding to EF-Tu (see SI figure SI1c,d). In both cases a strong hydrogen bond network was formed between the ring system and the neighboring residues Asn285 and Gln98, which is further stabilized by an additional hydrogen bond between His67 and Gln98. The ring-stabilizing intramolecular C28O–N13 hydrogen bond as observed for GE2270 A was retained (SI figure SI6). In addition, for the hydroxy group at R^1 in compound **3a**, fluctuating hydrogen bonds were observed with Glu226, Thr239, and Gln98 (SI figure SI2a).

This hydrogen bond pattern is consistent with the pattern observed for the experimental structure of the EF-Tu-GDPNP-GE2270 A complex.^[6b] In both cases the hydroxy groups of R^1 (Figure 1) form additional hydrogen bonds, but the hydrogen bond pattern of the hydroxy group is more restricted in GE2270 A due to the steric lock position by the additional phenyl ring. The hydroxy group in compound **3a** is very flexible and is thus able to form alternative hydrogen bonds

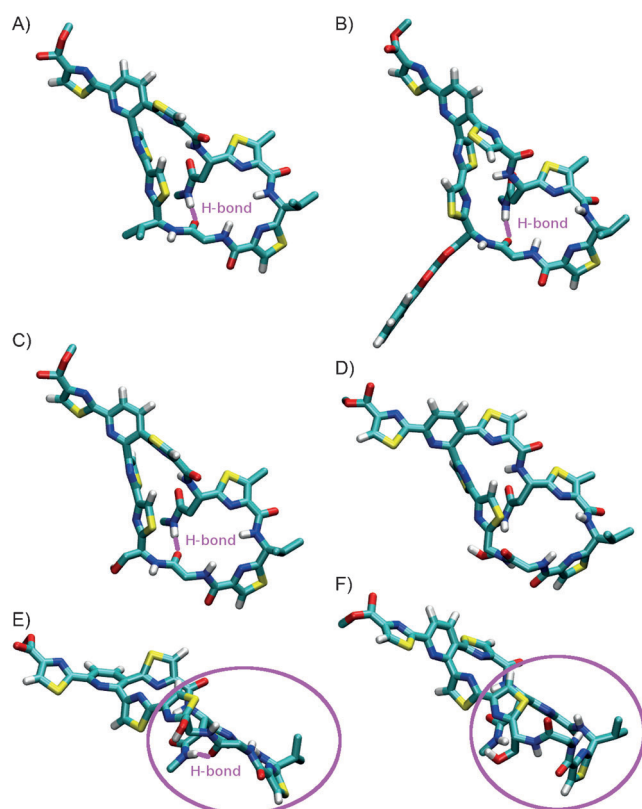


Figure 5. Solution structures of compounds A) **2**, B) **3c**, C,E) **3a**, and D,F) **3b** after 1 ns MD simulation. In E) and F) compounds **3a** and **3b** are shown with the ring plane being rotated by 90° with respect to the perspective shown in parts C) and D).

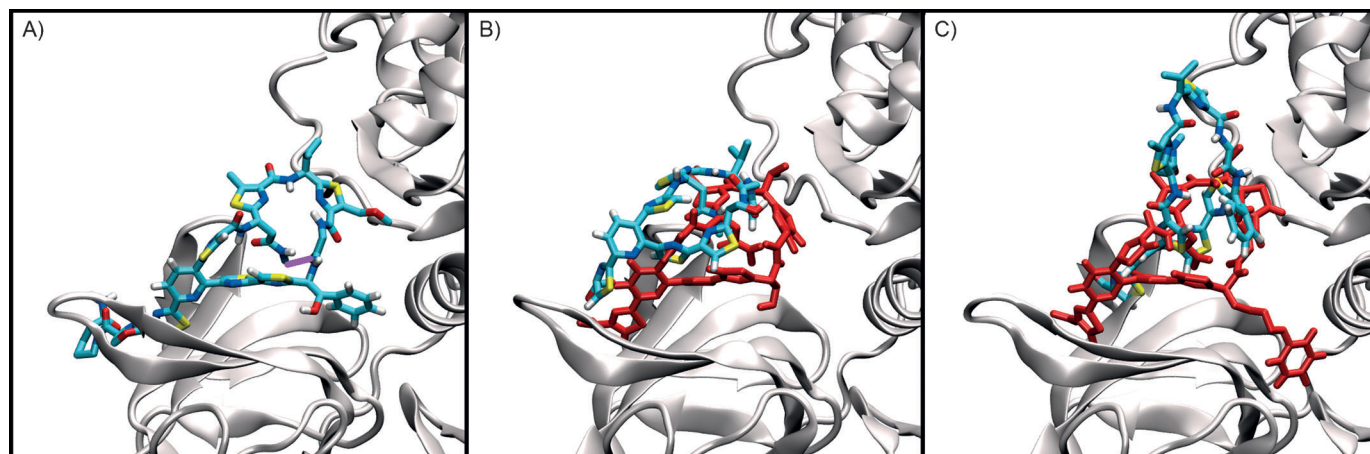


Figure 6. Stable binding of A) GE2270 A (1) and unstable binding of compounds B) **3b** and C) **3c** after 1 ns MD simulations. The final ligand conformations of the simulations are shown in stick representation colored by atom type. The starting conformations of compounds **3b** and **3c** are provided in red for comparison. The ring-stabilizing hydrogen bond is shown in magenta.

throughout the surrounding lipophilic sub-pocket. Consequently, its position fluctuates between the corresponding hydrogen bond forming residues.

The nonbinding behavior of compound **3c** is more difficult to explain: During the initial placement of compound **3c** only one favorable binding mode was found in which the BOM side chain is located in a stretched conformation inside a side cavity of the binding site (Figure 6c, red ligand conformation). However, due to the large amount of charged and polar side chains alongside this cavity, the bound conformation is not stable during the following MD simulation, leading to an altered ring conformation and movement of the BOM side chain out of its cavity (Figure 6C, SI figure S15). Therefore, it is unlikely that BOM moves into this cavity during the real binding process, explaining its nonbinding behavior.

In the case of compounds **3b** and **3c**, the MD simulations showed that the complexes are not stable, as the compounds slowly move out of the binding site (Figure 6B,C, SI figure S15). In the case of compound **3b** this is due to inversion of the binding geometry at the *R*-stereogenic center and thus formation of a bulky ring conformation, which is not compatible with the rather flat β -sheet-based surface of the binding site and its hydrogen bonding pattern, thus leading to a movement of the ligand out of the binding site (Figure 6B, SI figures S11b and S15), consistent with the lack of EF-Tu binding observed experimentally (Figure 3).

Conclusions

Based on an expedient synthetic access, three analogues (**3a–3c**) of amythiamicin D (**2**) have become available, which cannot be obtained by degradation studies or any other means. Translation studies revealed that compound **3a** shows enhanced potency in EF-Tu inhibition relative to the natural product. The activity of both amythiamicin D and compound **3a** could be nicely corroborated based on MD simulations: Compounds **3b** and **3c** were inactive in both antibacterial and in vitro translation assays. The nonbinding behavior of **3b** can

be explained by a ring conformation that is—due to the absence of a crucial hydrogen bond—different from those of the other thiopeptides. The conformational change is induced by the stereogenic center at the crucial methine carbon atom adjacent to C2 of thiazole ring C, which is distinct from the **2** and **3a** *R* configuration. The inactivity of **3c** is remarkable because it was envisioned that the lipophilic BOM group would be complementary to the hydrophobic pocket between domains D2 and D3. However, due to the size, electrostatic properties, and flexibility of the BOM group, it appears that it does not comply with the binding properties of the binding site.

The present study is the first to have used de novo synthesized non-natural thiopeptides. It provides unambiguous evidence that readily available synthetic analogues of the amythiamicins and the GE factors bind efficiently to the previously described binding site of EF-Tu. In this regard, compound **3a** can serve as a versatile scaffold to study the effect of various substitution patterns on the activity of EF-Tu and on conformational changes induced by non-natural ligands.

Experimental Section

Synthetic studies: Experimental procedures and characterization data (including NMR spectra) for all new compounds are provided in the Supporting Information. Analytical data for the three amythiamicin derivatives **3a–3c** are given below.

Thiopeptide 3a. $R_f=0.35$ ($\text{CH}_2\text{Cl}_2/\text{MeOH}=10:1$, UV); $[\alpha]_D^{20}=+33.0 \text{ cm}^3 \text{ g}^{-1} \text{ dm}^{-1}$ ($c=0.10$ in CHCl_3); $^1\text{H NMR}$ (CDCl_3 , 500 MHz): $\delta=0.93$ (d, $^3J=6.5$ Hz, 3H), 1.00 (d, $^3J=6.7$ Hz, 3H), 2.19 (m, 1H), 2.40 (brs, 2H), 2.62 (brs, 3H), 2.68 (s, 3H), 4.01 (s, 3H), 4.12 (brs, 2H), 4.28 (d, $^2J=17.1$ Hz, 1H), 4.63 (d, $^2J=17.1$ Hz, 1H), 5.28–5.34 (m, 2H), 5.47 (s, 1H), 6.76 (brs, 1H), 7.34 (s, 1H), 7.92 (s, 1H), 7.99–8.10 (m, 2H), 8.06 (d, $^3J=7.5$ Hz, 1H), 8.11 (s, 1H), 8.24–8.35 (m, 4H), 8.37 ppm (d, $^3J=7.5$ Hz, 1H); $^{13}\text{C NMR}$ (CDCl_3 , 126 MHz): $\delta=12.6$, 18.5, 19.0, 26.3, 35.0, 38.3, 42.8, 49.1, 52.7, 54.7, 55.0, 64.2, 115.8, 118.9, 121.7, 123.8, 125.4, 128.2, 130.6, 139.7, 141.3, 142.2, 148.2, 148.6, 148.8, 150.0, 150.7, 154.0, 160.3, 160.7, 161.4, 161.7, 161.8, 165.1, 166.0, 168.7, 169.2, 169.8, 170.3, 170.4 ppm; IR (ATR): $\tilde{\nu}=2956$ (w), 2924 (m), 2850 (w), 1654 (m), 1542 (m), 766 (w), 667 cm^{-1}

(w); MS (ESI): m/z (%) = 1041 (45), 1019 (100); HRMS (ESI): m/z = $C_{41}H_{39}N_{12}O_8S_6$ [$M+H$]⁺, calcd: 1019.1333, found: 1019.1332.

Thiopeptide 3b. R_f = 0.35 ($CH_2Cl_2/MeOH$ = 10:1, UV); $[\alpha]_D^{20}$ = +33.0 $cm^3 g^{-1} dm^{-1}$ (c = 0.10 in $CHCl_3$); 1H NMR ($CDCl_3$, 500 MHz): δ = 0.93 (d, 3J = 6.5 Hz, 3H), 1.00 (d, 3J = 6.7 Hz, 3H), 2.19 (m, 1H), 2.40 (brs, 2H), 2.62 (brs, 3H), 2.68 (s, 3H), 4.01 (s, 3H), 4.12 (brs, 2H), 4.28 (d, 2J = 17.1 Hz, 1H), 4.63 (d, 2J = 17.1 Hz, 1H), 5.28–5.34 (m, 2H), 5.47 (s, 1H), 6.76 (brs, 1H), 7.34 (s, 1H), 7.92 (s, 1H), 7.99–8.10 (m, 2H), 8.06 (d, 3J = 7.5 Hz, 1H), 8.11 (s, 1H), 8.24–8.35 (m, 4H), 8.37 ppm (d, 3J = 7.5 Hz, 1H); ^{13}C NMR ($CDCl_3$, 126 MHz): δ = 12.6, 18.5, 19.0, 26.3, 35.0, 38.3, 42.8, 49.1, 52.7, 54.7, 55.0, 64.2, 115.8, 118.9, 121.7, 123.8, 125.4, 128.2, 130.6, 139.7, 141.3, 142.2, 148.2, 148.6, 148.8, 150.0, 150.7, 154.0, 160.3, 160.7, 161.4, 161.7, 161.8, 165.1, 166.0, 168.7, 169.2, 169.8, 170.3, 170.4 ppm; IR (ATR): $\tilde{\nu}$ = 2956 (w), 2924 (m), 2850 (w), 1654 (m), 1542 (m), 766 (w), 667 cm^{-1} (w); MS (ESI): m/z (%) = 1041 (45), 1019 (100); HRMS (ESI): m/z = $C_{41}H_{39}N_{12}O_8S_6$ [$M+H$]⁺, calcd: 1019.1333, found: 1019.1332.

Thiopeptide 3c. R_f = 0.20 ($CH_2Cl_2/MeOH$ = 20:1, UV); $[\alpha]_D^{20}$ = +137 $cm^3 g^{-1} dm^{-1}$ (c = 0.09 in $CHCl_3$); 1H NMR ($CDCl_3$, 500 MHz): δ = 0.88 (d, 3J = 6.8 Hz, 3H), 0.96 (dd, 2J = 17.5 Hz, 3J = 5.9 Hz, 1H), 1.00 (d, 3J = 6.8 Hz, 3H), 2.28 (m, 1H), 2.63 (d, 3J = 4.8 Hz, 3H), 2.65 (s, 3H), 2.70 (dd, 2J = 17.5 Hz, 3J = 3.5 Hz, 1H), 3.59 (dd, 2J = 17.6 Hz, 3J = 3.3 Hz, 1H), 3.94 (dd, 2J = 10.7 Hz, 3J = 3.6 Hz, 1H), 4.01 (dd, 2J = 10.7 Hz, 3J = 4.0 Hz, 1H), 4.02 (s, 3H), 4.59 (d, 2J = 11.7 Hz, 1H), 4.67 (d, 2J = 11.7 Hz, 1H), 4.79 (dd, 2J = 17.6 Hz, 3J = 9.7 Hz, 1H), 4.84 (d, 2J = 6.8 Hz, 1H), 4.89 (d, 2J = 6.8 Hz, 1H), 5.23 (dd, 2J = 7.9 Hz, 4.7 Hz, 1H), 5.39 (m, 2H), 6.80 (d, 3J = 4.8 Hz, 1H), 6.91 (d, 3J = 6.0 Hz, 1H), 7.27 (s, 1H), 7.33–7.42 (m, 5H), 7.71 (dd, 3J = 9.7, 3.3 Hz, 1H), 8.11 (s, 1H), 8.13 (d, 3J = 8.1 Hz, 1H), 8.26 (s, 1H), 8.36 (s, 1H), 8.38 (s, 1H), 8.38 (d, 3J = 8.1 Hz, 1H), 8.76 (d, 3J = 7.9 Hz, 1H), 8.99 ppm (d, 3J = 9.2 Hz, 1H); ^{13}C NMR ($CDCl_3$, 126 MHz): δ = 12.3, 18.0, 18.4, 26.2, 34.7, 38.3, 41.1, 48.2, 52.6, 53.3, 56.1, 69.9, 70.8, 95.9, 115.0, 118.7, 123.2, 123.8, 125.2, 127.7, 127.9, 128.3, 128.8, 130.5, 137.1, 140.4, 140.5, 142.1, 148.2, 148.4, 148.8, 150.2, 150.3, 150.5, 154.5, 159.8, 161.2, 161.3, 161.8, 162.0, 164.8, 167.6, 168.5, 169.0, 169.7, 170.7 ppm; IR (ATR): $\tilde{\nu}$ = 2928 (w), 1658 (s), 1543 (s), 1494 (m), 1210 (m), 1051 (m), 751 cm^{-1} (s); MS (ESI): m/z (%) = 1161 (50), 1139 (100), 1107 (4); HRMS (ESI): m/z = $C_{49}H_{47}N_{12}O_9S_6$ [$M+H$]⁺, calcd: 1139.1907, found: 1139.1887.

Determination of MIC values:^[40] Substances were added in different concentrations to 1 mL B-broth [yeast extract (5.0 g), tryptic peptone (10.0 g), NaCl (5.0 g), K_2HPO_4 (1.0 g), H_2O (1.0 L)] including a control with DMSO. The tubes were inoculated with 1×10^6 bacteria per mL (OD: 0.6–0.8) and incubated overnight with shaking at 37 °C. The OD₆₀₀ value of 1:10 diluted overnight cultures was measured to determine the minimal inhibitory concentration (MIC). All experiments were conducted at least in triplicate, and DMSO served as control.

Reagents, bacterial strains, and vectors: The *E. coli* EF-Tu gene (*tufA*) cloned into pPROEX-Ht-b was a kind gift from Prof. Knud Nierhaus (MPIMG, Berlin).

In vitro translation assays: In vitro translation assays were performed using a homemade *E. coli* strain BL21 (Invitrogen) S12 lysate-based system, as described previously.^[41] As before,^[42] translation of the firefly luciferase (Fluc) reporter was monitored by measuring the luciferase activity in the presence and absence of antibiotic and/or EF-Tu.

Protein expression and purification: The QuikChange Site-directed Mutagenesis kit (Stratagene) was used to generate *E. coli* EF-Tu mutant G257S in pPROEX-Ht-b. Wild-type EF-Tu and the G257S

mutant were overexpressed in *E. coli* strain BL21(DE3) and purified using the N-terminal histidine tags via Ni-NTA affinity columns (QIAGEN) and subsequent gel-filtration chromatography on HiLoad 16/60 Superdex 75 prep grade column (Amersham-Pharmacia) in a buffer containing 20 mM HEPES (pH 7.8) and 150 mM NaCl.

Computational studies: Details of the methods employed for in silico experiments as well as additional figures (SI1–SI6) and a brief discussion of the simulation details are provided in the Supporting Information.

Acknowledgements

This work was supported by the EMBO young investigator program and the Deutsche Forschungsgemeinschaft (WI3285/1-2 to D.N.W.). S.G. acknowledges support by the TUM Graduate School. I.A. and M.B. acknowledge support by the Deutsche Forschungsgemeinschaft (CiPSM cluster of excellence and SFB 1035).

Keywords: antibiotics • molecular modeling • natural products • protein biosynthesis • structure–activity relationships

- [1] J. Lucas-Lenard, F. Lipmann, *Proc. Natl. Acad. Sci. USA* **1966**, *55*, 1562–1566.
- [2] Reviews: a) R. Berisio, A. Ruggiero, L. Vitagliano, *Isr. J. Chem.* **2010**, *50*, 71–79; b) I. M. Krab, A. Parmeggiani, *Prog. Nucleic-Acid Res. Mol. Biol.* **2002**, *71*, 513–551.
- [3] H. Berchtold, L. Reshetnikova, C. O. A. Reiser, N. K. Schirmer, M. Sprinzl, R. Hilgenfeld, *Nature* **1993**, *365*, 126–132.
- [4] For an overview on protein biosynthesis see: D. Voet, C. W. Pratt, J. G. Voet, *Fundamentals in Biochemistry: Life at the Molecular Level*, 4th ed., Wiley, Hoboken, **2012**, pp. 962–1012.
- [5] A. Parmeggiani, P. Nissen, *FEBS Lett.* **2006**, *580*, 4576–4581.
- [6] a) S. E. Heffron, F. Journak, *Biochemistry* **2000**, *39*, 37–45; b) A. Parmeggiani, I. M. Krab, S. Okamura, R. C. Nielsen, J. Nyborg, P. Nissen, *Biochemistry* **2006**, *45*, 6846–6857. Protein numbering for EF-Tu was taken from the latter publication.
- [7] A. Parmeggiani, I. M. Krab, T. Watanabe, R. C. Nielsen, C. Dahlberg, J. Nyborg, P. Nissen, *J. Biol. Chem.* **2006**, *281*, 2893–2900.
- [8] L. Vogeley, G. J. Palm, J. R. Mesters, R. Hilgenfeld, *J. Biol. Chem.* **2001**, *276*, 17149–17155.
- [9] P. H. Anborgh, A. Parmeggiani, *J. Biol. Chem.* **1993**, *268*, 24622–24628.
- [10] a) E. Selva, G. Beretta, N. Montanini, G. S. Saddler, L. Gastaldo, P. Ferrari, R. Lorenzetti, P. Landini, F. Ripamonti, B. P. Goldstein, M. Berti, L. Montanaro, M. Denaro, *J. Antibiot.* **1991**, *44*, 693–701; b) J. Kettenring, L. Colombo, P. Ferrari, P. Tavecchia, M. Nebuloni, K. Vékey, G. G. Gallo, E. Selva, *J. Antibiot.* **1991**, *44*, 702–715; c) E. Selva, P. Ferrari, M. Kurz, P. Tavecchia, L. Colombo, S. Stella, E. Restelli, B. P. Goldstein, F. Ripamonti, M. Denaro, *J. Antibiot.* **1995**, *48*, 1039–1042; d) P. Tavecchia, P. Gentili, M. Kurz, C. Sottani, R. Bonfichi, E. Selva, S. Lociuoro, E. Restelli, R. Ciabatti, *Tetrahedron* **1995**, *51*, 4867–4890.
- [11] E. Selva, N. Montanini, S. Stella, A. Soffientini, L. Gastaldo, M. Denaro, *J. Antibiot.* **1997**, *50*, 22–26.
- [12] J. Clough, S. Chen, E. M. Gordon, C. Hackbarth, S. Lam, J. Trias, R. J. White, G. Candiani, S. Donadio, G. Romanò, R. Ciabatti, J. W. Jacobs, *Bioorg. Med. Chem. Lett.* **2003**, *13*, 3409–3414.
- [13] M. J. LaMarche, J. A. Leeds, J. Dzink-Fox, K. Gunderson, P. Krastel, K. Memmert, M. A. Patane, E. M. Rann, E. Schmitt, S. Tiamfook, B. Wang, *J. Med. Chem.* **2011**, *54*, 2517–2521.
- [14] J. A. Leeds, M. J. LaMarche, J. T. Brewer, S. M. Bushell, G. Deng, J. M. Dewhurst, J. Dzink-Fox, E. Gangl, A. Jain, L. Lee, M. Lilly, K. Manni, S. Mullin, G. Neckermann, C. Osborne, D. Palestrant, M. A. Patane, A. Raimondi, S. Ranjitkar, E. M. Rann, M. Sachdeva, J. Shao, S. Tiamfook, L. Whitehead, D. Yu, *Antimicrob. Agents Chemother.* **2011**, *55*, 5277–5283.
- [15] M. J. LaMarche, J. A. Leeds, K. Amaral, J. T. Brewer, S. M. Bushell, J. M. Dewhurst, J. Dzink-Fox, E. Gangl, J. Goldovitz, A. Jain, S. Mullin, G. Neck-

- ermann, C. Osborne, D. Palestrant, M. A. Patane, E. M. Rann, M. Sachdeva, J. Shao, S. Tiamfook, L. Whitehead, D. Yu, *J. Med. Chem.* **2011**, *54*, 8099–8109.
- [16] J. A. Leeds, M. Sachdeva, S. Mullin, J. Dzink-Fox, M. J. LaMarche, *J. Med. Chem.* **2012**, *55*, 2376–2387.
- [17] S. Lociuero, P. Tavecchia, E. Marzorati, P. Landini, B. P. Goldstein, M. Denaro, R. Ciabatti, *J. Antibiot.* **1997**, *50*, 344–349.
- [18] Reviews: a) M. C. Bagley, J. W. Dale, E. A. Merritt, X. Xiong, *Chem. Rev.* **2005**, *105*, 685–714; b) R. A. Hughes, C. J. Moody, *Angew. Chem.* **2007**, *119*, 8076–8101; *Angew. Chem. Int. Ed.* **2007**, *46*, 7930–7954.
- [19] a) K. Shimanaka, N. Kinoshita, H. Iinuma, M. Hamada, T. Takeuchi, *J. Antibiot.* **1994**, *47*, 668–674; b) K. Shimanaka, Y. Takahashi, H. Iinuma, H. Naganawa, T. Takeuchi, *J. Antibiot.* **1994**, *47*, 1145–1152; c) K. Shimanaka, Y. Takahashi, H. Iinuma, H. Naganawa, T. Takeuchi, *J. Antibiot.* **1994**, *47*, 1153–1159.
- [20] K. Shimanaka, H. Iinuma, M. Hamada, *J. Antibiot.* **1995**, *48*, 182–184.
- [21] Selected references to completed total syntheses of thiopeptides: a) K. C. Nicolaou, B. S. Safina, M. Zak, S. H. Lee, M. Nevalainen, M. Bella, A. A. Estrada, C. Funke, F. J. Zécri, S. Bulat, *J. Am. Chem. Soc.* **2005**, *127*, 11159–11175; b) K. C. Nicolaou, M. Zak, B. S. Safina, A. A. Estrada, S. H. Lee, M. Nevalainen, *J. Am. Chem. Soc.* **2005**, *127*, 11176–11183; c) R. A. Hughes, S. P. Thompson, L. Alcaraz, C. J. Moody, *J. Am. Chem. Soc.* **2005**, *127*, 15644–15651; d) K. C. Nicolaou, B. Zou, D. H. Dethé, D. B. Li, D. Y.-K. Chen, *Angew. Chem.* **2006**, *118*, 7950–7956; *Angew. Chem. Int. Ed.* **2006**, *45*, 7786–7792; e) K. C. Nicolaou, D. H. Dethé, G. Y. C. Leung, B. Zou, D. Y.-K. Chen, *Chem. Asian J.* **2008**, *3*, 413–429; f) T. i. Mori, S. Higashibayashi, T. Goto, M. Kohno, Y. Satouchi, K. Shinko, K. Suzuki, S. Suzuki, H. Tohmiya, K. Hashimoto, M. Nakata, *Chem. Asian J.* **2008**, *3*, 984–1012; g) D. Lefranc, M. A. Ciufolini, *Angew. Chem.* **2009**, *121*, 4262–4265; D. Lefranc, M. A. Ciufolini, *Angew. Chem. Int. Ed.* **2009**, *48*, 4198–4201; h) D. Lefranc, M. A. Ciufolini, *Nat. Prod. Rep.* **2010**, *27*, 330–342; i) V. S. Aulakh, M. A. Ciufolini, *J. Am. Chem. Soc.* **2011**, *133*, 5900–5904; j) K. C. Nicolaou, *Angew. Chem.* **2012**, *124*, 12582–12604; *Angew. Chem. Int. Ed.* **2012**, *51*, 12414–12436.
- [22] a) H. M. Müller, O. Delgado, T. Bach, *Angew. Chem.* **2007**, *119*, 4855–4858; *Angew. Chem. Int. Ed.* **2007**, *46*, 4771–4774; b) O. Delgado, H. M. Müller, T. Bach, *Chem. Eur. J.* **2008**, *14*, 2322–2339.
- [23] C. Ammer, T. Bach, *Chem. Eur. J.* **2010**, *16*, 14083–14093.
- [24] a) G. Liu, D. A. Cogan, J. A. Ellman, *J. Am. Chem. Soc.* **1997**, *119*, 9913–9914; b) G. Liu, D. A. Cogan, T. D. Owens, T. P. Tang, J. A. Ellman, *J. Org. Chem.* **1999**, *64*, 1278–1284; c) D. A. Cogan, G. Liu, J. Ellman, *Tetrahedron* **1999**, *55*, 8883–8904; d) J. A. Ellman, T. D. Owens, T. P. Tang, *Acc. Chem. Res.* **2002**, *35*, 984–995.
- [25] J. C. Barrow, P. L. Ngo, J. M. Pellicore, H. G. Selnick, P. G. Nanterment, *Tetrahedron Lett.* **2001**, *42*, 2051–2054.
- [26] A. Spieß, G. Heckmann, T. Bach, *Synlett* **2004**, 131–133.
- [27] a) J. A. Dale, H. S. Mosher, *J. Am. Chem. Soc.* **1973**, *95*, 512–519; b) T. R. Hoye, C. S. Jeffrey, F. Shao, *Nat. Protoc.* **2007**, *2*, 2451–2458.
- [28] E. Frérot, J. Coste, A. Pantaloni, M.-N. Dufour, P. Jouin, *Tetrahedron* **1991**, *47*, 259–270.
- [29] S. Gross, S. Heuser, C. Ammer, G. Heckmann, T. Bach, *Synthesis* **2011**, 199–206.
- [30] H. Azizian, C. Eaborn, A. Pidcock, *J. Organomet. Chem.* **1981**, *215*, 49–58.
- [31] a) D. Milstein, J. K. Stille, *J. Am. Chem. Soc.* **1979**, *101*, 4992–4998; b) J. K. Stille, *Angew. Chem.* **1986**, *98*, 504–519; *Angew. Chem. Int. Ed. Engl.* **1986**, *25*, 508–524; c) V. Farina, V. Krishnamurthy, W. J. Scott, *Org. React.* **1997**, *50*, 1–652.
- [32] a) T. Bach, S. Heuser, *J. Org. Chem.* **2002**, *67*, 5789–5795; b) G. Heckmann, T. Bach, *Angew. Chem.* **2005**, *117*, 1223–1226; *Angew. Chem. Int. Ed.* **2005**, *44*, 1199–1201.
- [33] a) Y. Hamada, S. Shioiri, *Tetrahedron Lett.* **1982**, *23*, 235–236; b) L. Qian, Z. Sun, T. Deffo, K. Bowman Mertes, *Tetrahedron Lett.* **1990**, *31*, 6469–6472; c) S. Jayaprakash, G. Pattenden, M. S. Viljoen, C. Wilson, *Tetrahedron* **2003**, *59*, 6637–6646.
- [34] M. Misumi, N. Tanaka, *Biochem. Biophys. Res. Commun.* **1980**, *92*, 647–654.
- [35] I. Chopra, *J. Antimicrob. Chemother.* **1998**, *41*, 584–588.
- [36] A. M. Zuurmond, J. Martien de Graaf, L. N. Olsthoorn-Tielemans, B. Y. van Duyl, V. G. Möhrle, F. Jurnak, J. R. Mesters, R. Hilgenfeld, B. Kraal, *J. Mol. Biol.* **2000**, *304*, 995–1005.
- [37] P. Nissen, M. Kjeldgaard, S. Thirup, G. Polekhina, L. Reshetnikova, B. F. Clark, J. Nyborg, *Science* **1995**, *270*, 1464–1472.
- [38] R. J. Lewis, R. A. Hughes, L. Alcaraz, S. P. Thompson, C. J. Moody, *Chem. Commun.* **2006**, 4215–4217.
- [39] I. Antes, *Proteins* **2010**, *78*, 1084–1104.
- [40] M. B. Nodwell, H. Menz, S. F. Kirsch, S. A. Sieber, *ChemBioChem* **2012**, *13*, 1439–1446.
- [41] T. W. Kim, H. C. Kim, I. S. Oh, D. M. A. Kim, *Biotechnol. Bioprocess Eng.* **2008**, *13*, 464–469.
- [42] a) A. L. Starosta, H. Qin, A. Mikolajka, G. Y. Leung, K. Schwinghammer, K. C. Nicolaou, D. Y. Chen, B. S. Cooperman, D. N. Wilson, *Chem. Biol.* **2009**, *16*, 1087–1096; b) A. L. Starosta, V. V. Karpenko, A. V. Shishkina, A. Mikolajka, N. V. Sumbatyan, F. Schluenzen, G. A. Korshunova, A. A. Bogdanov, D. N. Wilson, *Chem. Biol.* **2010**, *17*, 504–514.

Received: July 26, 2013

Published online on September 17, 2013

Review

Fabian Nguyen, Agata L. Starosta, Stefan Arenz, Daniel Sohmen, Alexandra Dönhöfer and Daniel N. Wilson*

Tetracycline antibiotics and resistance mechanisms

Abstract: The ribosome and protein synthesis are major targets within the cell for inhibition by antibiotics, such as the tetracyclines. The tetracycline family of antibiotics represent a large and diverse group of compounds, ranging from the naturally produced chlortetracycline, introduced into medical usage in the 1940s, to second and third generation semi-synthetic derivatives of tetracycline, such as doxycycline, minocycline and more recently the glycylcycline tigecycline. Here we describe the mode of interaction of tetracyclines with the ribosome and mechanism of action of this class of antibiotics to inhibit translation. Additionally, we provide an overview of the diverse mechanisms by which bacteria obtain resistance to tetracyclines, ranging from efflux, drug modification, target mutation and the employment of specialized ribosome protection proteins.

Keywords: glycylcycline; resistance; ribosome; tetracycline; tigecycline; translation.

*Corresponding author: Daniel N. Wilson, Gene Center and Department of Biochemistry, University of Munich, Feodor-Lynenstr. 25, D-81377 Munich, Germany; and Center for Integrated Protein Science Munich (CiPSM), University of Munich, Feodor-Lynenstr. 25, D-81377 Munich, Germany, e-mail: wilson@lmb.uni-muenchen.de
Fabian Nguyen, Agata L. Starosta, Stefan Arenz, Daniel Sohmen and Alexandra Dönhöfer: Gene Center and Department of Biochemistry, University of Munich, Feodor-Lynenstr. 25, D-81377 Munich, Germany

Introduction: the ribosome as a target for antibiotics

The ribosome is one of the major targets within the bacterial cell for antibiotics, with a diverse range of antibiotics that have been discovered and shown to inhibit a variety of distinct steps during protein synthesis (Sohmen et al., 2009a,b; Wilson, 2009, 2013). This wealth of biochemical and structural data has demonstrated that the majority of

antibiotics interact with the functional centers of the ribosome: Many clinically important antibiotics bind at or near to the peptidyltransferase center (PTC) on the large ribosomal subunit where peptide bond formation occurs; these include the chloramphenicols, pleuromutilins (retapamulin), oxazolidinones (linezolid), lincosamides (lincomycin), macrolides (erythromycin), ketolides (telithromycin) and streptogramins (quinupristin and dalfopristin). On the small ribosomal subunit, antibiotic binding sites are clustered along the path of the mRNA and tRNAs, for example, spectinomycin, streptomycin, aminoglycosides (kanamycin), tuberactinomycins (viomycin) and tetracyclines (doxycycline) (Sohmen et al., 2009a,b; Wilson, 2009, 2013). This review focuses on the latter class of antibiotics, the tetracyclines, which bind at the decoding center of the small subunit, i.e., where the codon of the mRNA is recognized by the anticodon of the tRNA. There have been many excellent reviews on different aspects of tetracycline inhibition and tetracycline resistance mechanisms (Roberts, 1996; Chopra and Roberts, 2001; Connell et al., 2003b; Thaker et al., 2010; Nelson and Levy, 2011), so here we focus on the most recent biochemical and structural insights with an emphasis on aspects related directly to the translation machinery.

The tetracycline class of antibiotics

Discovery and chemical structure of tetracyclines

The first compound belonging to the tetracycline family, chlortetracycline, was discovered in 1948 by Dr. Benjamin Duggar working at Lederle Laboratories (American Cyanamid) (Duggar, 1948). Chlortetracycline (Figure 1A) was isolated from *Streptomyces aureofaciens*, and called aureomycin because of the gold coloring of the bacteria (Duggar, 1948). Shortly afterwards, in the early 1950s Alexander Finlay from Pfizer discovered oxytetracycline

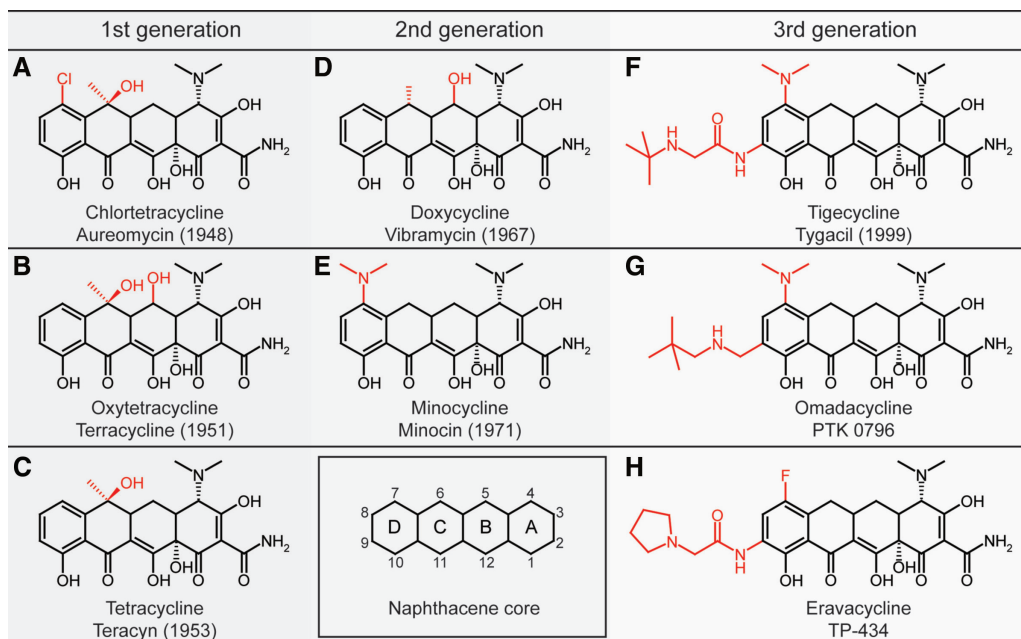


Figure 1 Chemical structures of tetracyclines.

Chemical structures of (A–C) first generation tetracyclines. (A) chlortetracycline (aureomycin), (B) oxytetracycline (terracycline) and (C) tetracycline (teracycline), (D–E) second generation tetracyclines; (D) doxycycline (vibramycin) and (E) minocycline (minocin), and (F–G) third generation tetracyclines; (F) the glycylicycline tigecycline (tygacil), (G) the aminomethylcycline omadacycline (PTK 0796) and (H) the fluorocycline eravacycline (TP-434). The numbers in parentheses indicates the year the antibiotic was discovered/reported. The inset of the DCBA naphthacene core provides the carbon atom assignments for rings A–D.

(Figure 1B), a secondary metabolite of soil bacteria *Streptomyces rimosus* from the Terra Haute, Indiana, and therefore called ‘terramycin’ (Finlay et al., 1950). Although both antibiotics were already on the market, their chemical structure remained elusive until 1953. The chemical structures of chlortetracycline and oxytetracycline (Figure 1A and B) were the results of joint efforts of a Pfizer team, together with the Nobel Prize laureate, Robert B. Woodward (Stephens et al., 1952, 1954; Hochstein et al., 1953).

The basis of these structures is the DCBA naphthacene core comprising four aromatic rings (inset to Figure 1), therefore this family of antibiotics was named ‘tetracyclines’ (Stephens et al., 1952). It was noted that compared with oxytetracycline, chlortetracycline lacks a hydroxyl group at the C5 position of ring B and has a chlorine atom substituent present at the C7 position of ring D (Figure 1A and B). Moreover, as a result of chemical modifications, Pfizer-Woodward described C7-deschloro derivative of chlortetracycline, with a higher potency against bacterial pathogens, which was called ‘tetracycline’ (Figure 1C, teracycline) (Conover et al., 1953), because it is the simplest member of the ‘tetracycline’ family of antibiotics. Subsequently, tetracycline was also detected in the broth of *S. aureofaciens* (Backus et al., 1954) and

S. rimosus (Perlman et al., 1960), consistent with the discovery that tetracycline is a precursor of chlortetracycline (McCormick et al., 1960).

Soon after the discovery of first generation tetracyclines, Pfizer and Lederle began developing the second generation tetracycline compounds with improved pharmacokinetic properties, increased antimicrobial potency and decreased toxicity. A series of chemical modifications of ring C led Pfizer to the semi-synthesis of methacycline (Boothe et al., 1959; Blackwood et al., 1961), which was further used as a precursor for the synthesis of doxycycline (Figure 1D; Vibramycin) (C6-deoxy-tetracycline) (Stephens et al., 1963), one of the most commonly used tetracyclines to date. Additionally, Lederle analyzed biogenesis mutants of chlortetracycline in *S. aureofaciens*, and discovered the precursor demeclocycline (C6-demethyl-C7-chlorotetracycline) (McCormick et al., 1957), which was further reduced to sancycline (C6-demethyl-C6-deoxytetracycline), a tetracycline with the minimal chemical features necessary to retain antimicrobial activity (McCormick et al., 1960). Subsequently, sancycline was converted to C7-aminosancycline or minocycline (Figure 1E; Minocin) (Martell and Boothe, 1967), the most powerful tetracycline of that period, and the last tetracycline to be introduced into the market in the 20th century.

Emerging antibiotic resistance renewed interest in the development of a third generation of tetracyclines. In the late 1980s, Lederle (later Wyeth) reopened the tetracycline program. Already known tetracycline derivatives were re-evaluated and their action revisited according to the recent knowledge about tetracycline action (Tally et al., 1995), leading to a focus on modifications of the C7 and C9 positions of ring D of the tetracycline core. The breakthrough came with the synthesis of a series of C9-aminotetracyclines bearing a glycyloxy moiety (Sum et al., 1994), leading to the development of a new class of third generation tetracyclines, referred to as glycyloxytetracyclines. A glycyloxy derivative of minocycline, tigecycline (Figure F; Tygacyl) (Petersen et al., 1999), with a *t*-butyl amine group was one of the most potent antimicrobials and is the first tetracycline introduced into the market in over 40 years. Currently, two additional third generation tetracyclines are in phase III clinical trials: Omadacycline (PTK 0796; Figure 1G) is a 9-alkylaminomethyl derivative of minocycline (aminomethylcycline) (Draper et al., 2013) and was developed by Paratek Pharmaceuticals, which applies transition metal-based chemistry to produce tetracycline derivatives (Nelson et al., 2003). Conversely, Tetrphase Pharmaceuticals utilized Meyers' chemistry (Sun et al., 2008) to obtain the fluorocycline eravacycline (TP-434; Figure 1H), which bears C7-fluoro and C9-pyrrolidinoacetamido modifications of ring D (Grossman et al., 2012).

The binding site of tetracycline on the 30S subunit and 70S ribosome

X-ray structures of tetracycline in complex with the *Thermus thermophilus* 30S subunit provided the first direct visualization of the drug binding sites (Figure 2A) (Brodersen et al., 2000; Pioletti et al., 2001). In the first study, the crystals were soaked in 80 μM tetracycline and the structure determined to 3.4 Å revealed two tetracycline binding sites on the 30S subunit (Brodersen et al., 2000). By contrast, in the second study crystals were soaked in 4 μM tetracycline and the resulting structure at 4.5 Å reported six distinct tetracycline binding sites (Pioletti et al., 2001). However, only one tetracycline binding site was common between the two studies, termed the 'primary binding site' (Tet1), which is located at the base of the head of the 30S subunit (Figure 2A), and was subsequently verified biochemically (Connell et al., 2002). The identification of multiple lower occupancy secondary binding sites (Tet2) was not unexpected, as earlier biochemical evidence indicated that tetracyclines have multiple binding sites on the small and large subunit (Gale et al., 1981). For example,

tetracycline binding enhances the reactivity of U1052 and C1054 of the 16S rRNA present in the primary binding site, but also protects the nucleotide A892, located in one of the secondary binding sites, from chemical modification (Moazed and Noller, 1987). Recently, an X-ray structure of tetracycline bound to an initiation complex comprising the *T. thermophilus* 70S ribosome bound with P-site tRNA^{Met} and mRNA was determined at 3.5 Å (Jenner et al., 2013). Interestingly, only one molecule of tetracycline was bound to the 70S ribosome, namely at the primary binding site (Figure 2B) and no secondary binding sites were observed (Jenner et al., 2013), re-emphasizing the higher affinity and occupancy of the primary binding site relative to the secondary binding sites.

In the primary binding site, tetracycline utilizes the hydrophilic surface of the molecule to interact with the irregular minor groove of helix 34 (h34) and the loop of h31 of the 16S rRNA (Figure 2C). This is consistent with the observations that alterations of the hydrophilic surface (C1–C4, C10–C12) of tetracycline abolish the antimicrobial activity of the drug, whereas the hydrophobic surface (C5–C9) is more amenable to modification without loss of inhibitory activity (Nelson, 2001), as seen in many natural product tetracyclines (Figure 1). The hydrophilic side of tetracycline establishes hydrogen-bond interactions with the phosphate-oxygen atoms of nucleotides C1054, G1197 and G1198 in h34 of the 16S rRNA, directly and/or via coordination of a magnesium ion (Mg1) (Figure 2C) (Brodersen et al., 2000; Pioletti et al., 2001; Jenner et al., 2013). The possibility of an additional magnesium ion (Mg2) mediating the interaction between the phosphate backbone of G966 in h31 and ring A of tetracycline was proposed based on the recent 70S structure (Jenner et al., 2013). These findings are consistent with the earlier studies indicating the importance of divalent magnesium for binding of tetracycline to the ribosome (White and Cantor, 1971).

The interaction of tetracycline with the backbone of the rRNA, rather than by establishing sequence-specific nucleobase interactions (Figure 2C), is consistent with the broad-spectrum activity of tetracycline antibiotics (Bradford and Jones, 2012). The single interaction between ring D of tetracycline and the nucleobase of C1054 of the 16S rRNA involves stacking interactions (Figure 2C) and is therefore unlikely to be sequence-specific. The high structural conservation of the tetracycline binding site in eukaryotic ribosomes (Ben-Shem et al., 2011) is consistent with the documented inhibitory activity of tetracycline against eukaryotic translation *in vitro* (Budkevich et al., 2008). Thus, antibiotic uptake probably makes a larger contribution to the natural resistance of eukaryotic cells to tetracyclines.

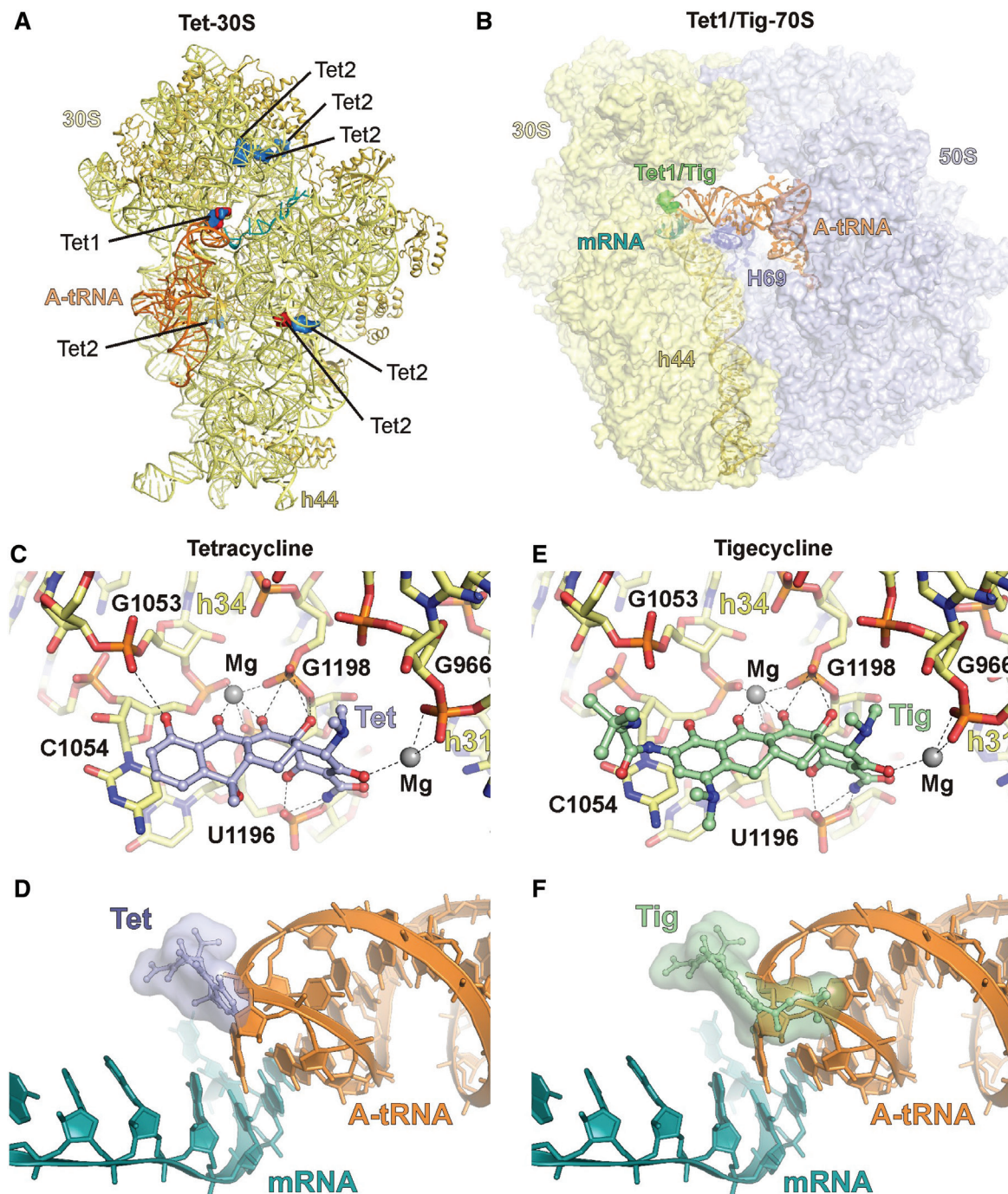


Figure 2 Binding site of tetracyclines on the ribosome.

(A) Primary (Tet1) and secondary (Tet2) binding sites of tetracycline on the 30S subunit (Brodersen et al., 2000; Pioletti et al., 2001). (B) Binding site of tetracycline/tigecycline (Tet1/Tig) on the 70S ribosome (30S, yellow; 50S, blue) (Jenner et al., 2013) relative to mRNA (teal), A-tRNA (orange) (Voorhees et al., 2009). h44 of the 16S rRNA and H69 of the 23S rRNA are indicated for reference. (C) Interaction of tetracycline within the primary binding site (Jenner et al., 2013). The charged side of tetracyclines coordinates magnesium ions to interact with the backbone of residues h34 and h31. (D) Binding position of tetracycline (Jenner et al., 2013) relative to mRNA (teal) and A-tRNA (orange) (Voorhees et al., 2009). (E) Interaction of tigecycline within the primary binding site, illustrating the additional interaction between the C9-substitution of tigecycline and C1054 of the 16S rRNA (Jenner et al., 2013). (F) Binding position of tigecycline (Jenner et al., 2013) relative to mRNA (teal) and A-tRNA (orange) (Voorhees et al., 2009).

The mechanism of action of tetracyclines during translation

During translation, aminoacyl-tRNAs are delivered to the ribosome by the elongation factor EF-Tu. A proof-reading process ensues that monitors correctness of the interaction between the anticodon of the aminoacyl-tRNA and the A-site codon of the mRNA. Selection of the correct or cognate tRNA stimulates the GTP hydrolysis activity of EF-Tu, resulting in conformational changes in EF-Tu that lead to dissociation of EF-Tu·GDP from the ribosome, and the concomitant accommodation of the aminoacyl-tRNA into the A-site. The primary binding site of tetracycline is located within the decoding center of the small subunit and overlaps in position with the anticodon loop of an A-site bound tRNA (Figure 2B and D). Specifically, rings C and D of tetracycline sterically clash with the first nucleotide of the anticodon of the tRNA that interacts with the third (or wobble) base of the A-site codon of the mRNA (Figure 2D). The competition for ribosome binding between tetracycline and A-tRNA was observed during the crystallization of the tetracycline-70S complex, where initial co-crystallization studies using 60 μM tetracycline and five-fold excess of tRNA^{Met} (over ribosomes) led to non-specific binding of tRNA^{Met} to the A-site, rather than tetracycline (Jenner et al., 2013). To obtain electron density for tetracycline, co-crystallization experiments were performed with higher concentrations of tetracycline (300 μM) coupled with lower excess (1.5-fold) of tRNA^{Met}. These findings are consistent with biochemical experiments demonstrating that tetracycline inhibits binding of tRNAs to the ribosomal A-site, but not the ribosome-stimulated EF-Tu GTPase activity (Gale et al., 1981; Blanchard et al., 2004). Specifically, single molecule FRET experiments indicate that in the presence of tetracycline (40 μM ; $10\times K_d$), aminoacyl-tRNA accommodation is efficiently blocked, resulting in repetitive ternary complex binding and release events (Blanchard et al., 2004; Geggier et al., 2010; Jenner et al., 2013). Indeed, the overlap between tetracycline and A-tRNA is similar regardless of whether the A-tRNA is still bound to EF-Tu in an initial selection state or whether the A-tRNA has fully accommodated into the A-site on the 70S ribosome.

Second generation tetracycline derivatives: doxycycline and minocycline

Second generation tetracyclines, such as doxycycline and, in particular, minocycline, exhibit superior antimicrobial

activities compared to tetracycline against a range of Gram-negative (e.g., *Escherichia coli* and *Pseudomonas aeruginosa*) and especially Gram-positive (*Staphylococcus aureus* and *Enterococcus faecalis*) bacteria (Bradford and Jones, 2012), including some strains of tetracycline-resistant bacteria (Testa et al., 1993; Sum et al., 1994). Consistently, minocycline has a ~20-fold higher affinity to the ribosome than tetracycline (but 5-fold lower than tigecycline) and inhibits *in vitro* translation 2–7-fold more efficiently than tetracycline (Bergeron et al., 1996; Olson et al., 2006). The similarity in chemical structure between minocycline and tetracycline (Figure 1) and the ability of minocycline to compete with tetracycline for ribosome binding (Olson et al., 2006), suggests that minocycline binds analogously to the ribosome as tetracycline. Presumably the improved binding properties of minocycline result from presence of the C7-dimethylamido group on ring D that may facilitate stacking interactions with C1054 (Figure 2C). Additionally, second generation tetracyclines, such as minocycline, are more lipophilic than their parent compounds and as a result display better absorption and pharmacokinetic parameters (Agwuh and MacGowan, 2006).

Third generation tetracycline derivatives: glycylicyclines and tigecycline

The third generation of tetracycline derivatives includes the glycylicyclines, which bear an N,N-dimethylglycylamido (DMG) moiety on the C9 position of ring D (Figure 1F) (Barden et al., 1994; Sum et al., 1994). Compared to first (e.g., tetracycline) and second generation tetracyclines (e.g., minocycline), the 9-DMG derivatives of minocycline (termed tigecycline or DMG-MINO) (Figure 1F) and sancycline (DMG-DMDOT) display improved inhibitory activities against a wide range of Gram-positive and negative bacteria and in particular have similar minimal inhibitory concentrations against susceptible and resistant bacterial strains (Testa et al., 1993; Barden et al., 1994; Sum et al., 1994). Consistently, glycylicyclines, such as tigecycline, exhibit ~10–30 fold lower half inhibitory concentrations (IC_{50}) during *in vitro* translation compared with tetracycline (Bergeron et al., 1996; Olson et al., 2006; Grossman et al., 2012; Jenner et al., 2013) as well as having improved ribosome binding properties. Specifically, DMG-DMDOT and DMG-DOX bind to the ribosome with a ~5-fold higher affinity than tetracycline (Bergeron et al., 1996), whereas tigecycline has been reported to have a ~10–100-fold higher binding affinity for the ribosome compared to tetracycline (Olson et al., 2006; Grossman et al., 2012; Jenner et al., 2013).

A 3.3 Å resolution X-ray structure of tigecycline bound to the *T. thermophilus* 70S ribosome reveals that tigecycline binds to the decoding center on the 30S subunit analogously to tetracycline (Figure 2B) (Jenner et al., 2013). No secondary binding sites were observed (Jenner et al., 2013). Moreover, unlike tetracycline, crystallization in the presence of 60 µM tigecycline and 5-fold excess of tRNA^{Met} (over ribosomes) was sufficient to yield clear electron density for the drug and prevent non-specific binding of tRNA^{Met} to the A-site, thus re-emphasizing the higher binding affinity of tigecycline for the ribosome compared to tetracycline. As expected, based on the common features of the chemical structures of tetracycline and tigecycline (Figure 1C and F), tigecycline uses the polar face of the drug to establish an analogous network of hydrogen-bond interactions with two Mg²⁺ ions and the phosphate-oxygen backbone of h34 and h31 of the 16S rRNA (Figure 2E). The similarity in binding site of tigecycline with tetracycline is also supported by the competition between tigecycline and tetracycline for ribosome binding (Olson et al., 2006; Grossman et al., 2012; Jenner et al., 2013), as well as the similarity in chemical footprinting and hydroxyl-radical cleavage patterns generated in the presence of either drug (Moazed and Noller, 1987; Bauer et al., 2004). However, in the case of tigecycline, ~10-fold lower concentrations of the drug were required compared to tetracycline in order to generate the same modification patterns (Bauer et al., 2004).

The major differences between tigecycline and tetracycline are the 7-dimethylamido and 9-t-butylglycylamido substitutions attached to ring D of tigecycline (Figure 1F). While the 7-dimethylamido moiety does not appear to establish interactions with the ribosome, the glycylic nitrogen atom of the 9-t-butylglycylamido moiety of tigecycline stacks with the π -orbital of nucleobase C1054 (Figure 2E). The remainder of the 9-t-butylglycylamido moiety of tigecycline adopts a very rigid conformation (although it does not make any apparent contact with the ribosome), which may contribute to the stacking interaction with C1054. Indeed, the interaction of tigecycline with C1054 appears to further enhance the stacking interaction between C1054 and U1196 (Figure 2E), similar to what is seen when tRNA is bound to the A-site (Schmeing et al., 2009). Thus, the stacking interaction between the 9-t-butylglycylamido moiety of tigecycline and C1054 and U1196, which is lacking or less optimal in tetracycline (Figure 2E), provides a structural basis for the improved ribosome binding properties of tigecycline. Additionally, the 9-t-butylglycylamido moiety of tigecycline significantly increases the steric overlap of tigecycline and the anticodon loop of the A-tRNA (Figure 2F), compared to the modest overlap observed between tetracycline and the A-tRNA (Figure 2D). Collectively, the enhanced binding affinity of tigecycline,

together with the increased steric overlap with the A-tRNA, provides a likely explanation for the increased effectiveness of tigecycline (2 µM) to prevent stable binding of the ternary complex EF-Tu-GTP-aa-tRNA to the A-site, compared to 40 µM tetracycline (Jenner et al., 2013).

Third generation tetracycline derivatives: omadacycline and eravacycline

Two additional third generation tetracycline derivatives with C9 substitutions on ring D, which display broad-spectrum activity against tetracycline-susceptible and -resistant bacterial strains, are in phase III clinical trials. Omadacycline is an aminomethylcycline (Figure 1G) developed by Paratek Pharmaceuticals (Boston, MA, USA; Draper et al., 2013). Competition studies with radiolabeled tetracycline indicate that omadacycline has a 2-fold higher affinity for the ribosome than tetracycline and, consistently, omadacycline inhibits *in vitro* translation at 2-fold lower drug concentrations than tetracycline (Draper et al., 2013; Jenner et al., 2013). Eravacycline (Tetraphase Pharmaceuticals, Watertown, MA) is a glycylicycline bearing a fluorine atom at position C7 and a pyrrolidinoacetamido group at the C9 of ring D (Figure 1H). Competition studies with radiolabelled tetracycline indicate that eravacycline has 10-fold higher affinity for the ribosome than tetracycline and inhibits *in vitro* translation at 4-fold lower drug concentrations than tetracycline (Grossman et al., 2012). The similar ribosome binding affinity of eravacycline (0.2 µM) and tigecycline (0.2 µM) (Grossman et al., 2012; Jenner et al., 2013) and the reduced affinity of compounds with amide bond replacements in the 9-position, such as omadacycline (2 µM) (Draper et al., 2013; Jenner et al., 2013) and 9-propylpyrrolidyl-7-fluorocycline (4 µM) (Jenner et al., 2013) is consistent with an important role of the amide to strengthen the stacking interactions of the C9 substitution with C1054. Introduction of an additional aromatic ring E to generate pentacyclines (Sun et al., 2010) also improves the binding and inhibitory properties of the drug relative to tetracycline (Jenner et al., 2013), further supporting the hypothesis that stacking interactions with C1054 enhance the binding and inhibitory properties of tetracycline derivatives.

Tetracycline resistance mechanisms

There are four main mechanisms by which bacteria can acquire resistance to tetracyclines (Table 1). In addition, innate mechanisms exist because some bacteria

Table 1 Tetracycline resistance determinants.

Efflux		Ribosomal protection	Degradation	rRNA mutations
<i>tetA</i>	<i>tet31</i>	<i>tetM</i>	<i>tetX</i>	G1058C
<i>tetB</i>	<i>tet33</i>	<i>tetO</i>	<i>tet37</i>	A926T
<i>tetC</i>	<i>tet35</i>	<i>tetQ</i>		G927T
<i>tetD</i>	<i>tet38</i>	<i>tetS</i>		A928C
<i>tetE</i>	<i>tet39</i>	<i>tetT</i>		ΔG942
<i>tetG</i>	<i>tet40</i>	<i>tetW</i>		
<i>tetH</i>	<i>tet41</i>	<i>tetB(P)</i>		
<i>tetJ</i>	<i>tet42</i>	<i>tet32</i>		
<i>tetK</i>	<i>tet45</i>	<i>tet36</i>		
<i>tetL</i>	<i>tetAB(46)</i>	<i>tet44</i>		
<i>tetA(P)</i>	<i>tc3</i>	<i>otrA</i>		
<i>tetV</i>	<i>otrC</i>	<i>tet</i>		
<i>tetY</i>	<i>otrB</i>			
<i>tetZ</i>				
<i>tet30</i>				

are naturally more resistant to tetracyclines due to differences in the permeability of the cell membrane. For example, Gram-negative bacteria are naturally resistant to several antibiotics because of the presence of a lipopolysaccharide containing outer membrane layer. In addition, the presence of small molecule transporters can also act on drugs to differing extents in different bacteria, conferring resistance by pumping the drugs out of the cell. Of the acquired resistance mechanisms, the most prevalent tetracycline resistance mechanism is efflux, with 28 distinct classes of efflux pumps identified so far (Table 1). Following closely are the so-called ribosome protection proteins, which bind to the ribosome and remove the drug from its binding site, with 12 distinct classes reported (Table 1). Less prevalent resistance mechanisms include two distinct genes that encode monooxygenases, which modify tetracyclines and promote their degradation, and mutations within the 16S rRNA that reduce the binding affinity of the drug for the ribosome (Table 1). In addition, a novel tetracycline resistance determinant, *tetU*, encoded on the plasmid pKq10 in *E. faecium* has been reported to confer some tetracycline resistance (Ridenhour et al., 1996), however, a recent study questions the validity of this conclusion (Caryl et al., 2012).

Efflux pumps to expel tetracycline from the cell

The 28 different classes of efflux pumps (Table 1) present in Gram-negative and Gram-positive bacteria fall into seven

defined groups based primarily on sequence homology (Guillaume et al., 2004). By far the largest group are the group 1 drug-H⁺ antiporters containing 12 transmembrane helices, and comprise the well characterized tetracycline efflux pumps, such as TetA, the most frequently occurring tetracycline-resistance determinant in Gram-negative bacteria. Although no structures exist for tetracycline efflux pumps, the high homology of the group 1 efflux pumps like TetA with the major facilitator superfamily (MFS) of secondary active transporters, implies a similar membrane topology and structural ‘inward-outward’ mechanism of action within the cell membrane (Figure 3A). Such efflux proteins exchange a proton (H⁺) for the tetracycline molecule against a concentration gradient (Piddock, 2006). Most tetracycline efflux pumps confer resistance to tetracycline, but are less effective against second generation doxycycline and minocycline, and confer little or no resistance to third generation glycylicyclines, such as tigecycline (Chopra and Roberts, 2001). For example, the MIC of *E. coli* strain DH10B expressing the TetA efflux pump is >128 μg/ml for tetracycline, 32 μg/ml for doxycycline, 8 μg/ml for minocycline and 1 μg/ml for tigecycline (Grossman et al., 2012). Nevertheless, laboratory-derived mutations in *tetA* and *tetB* have been generated that can confer some glycylicycline resistance, but at the expense of tetracycline resistance (Guay et al., 1994).

In many cases, there is a fitness cost associated with the expression of antibiotic resistance genes, therefore many bacteria regulate the expression of the resistance gene(s) using translational attenuation, transcriptional attenuation and translational coupling (Chopra and Roberts, 2001). Another mechanism that is used for regulation of *tet* resistance genes is negative control by a Tet repressor protein (TetR) (Hillen and Berens, 1994; Saenger et al., 2000). In the absence of tetracycline, TetR binds as a homodimer to two tandemly orientated *tet* operators to block transcription of the efflux pump (Figure 3B), such as observed in the structure of the TetR-DNA complex (Figure 3C) (Orth et al., 2000). However, in the presence of tetracycline, the drug binds to TetR, which dissociates from the *tet* operator, thus inducing transcription and induction of expression of the TetA efflux pump (Figure 3B) (Saenger et al., 2000). In some cases, the *tetR* gene is also encoded directly in front of the efflux pump, and therefore TetR will rebind the *tet* operator only when insufficient amounts of tetracycline are in the cell and re-block transcription of its own gene and that of the downstream efflux pump (Hillen and Berens, 1994). Crystal structures of tetracycline in complex with the TetR homodimer reveal that tetracycline binds to the C-terminal effector-binding domain and induces conformational changes in

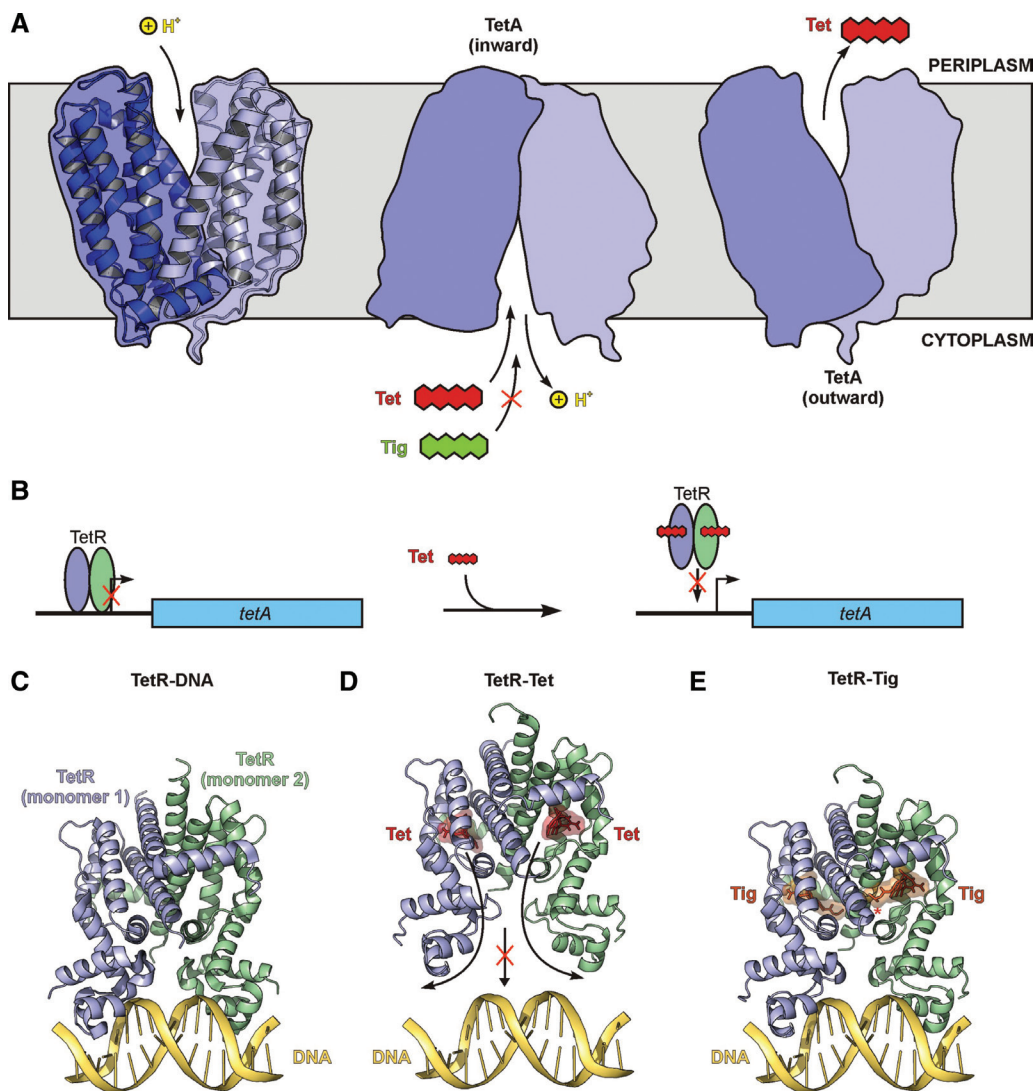


Figure 3 TetR-mediated regulation of the tetracycline resistance TetA efflux pump.

(A) Schematic for mechanism of action of efflux pump TetA, illustrating that efflux of tetracycline (but not tigecycline) is coupled to proton transport. The homology model for the TetA efflux pump was generated by HHPred (Söding et al., 2005) based on similarity with the proton-driven MFS transporter YajR from *Escherichia coli* (PDB ID 2WDO) (Jiang et al., 2013). (B) Schematic for TetR-mediated regulation of TetA, illustrating that tetracycline binding to the TetR homodimer leads to activation of transcription of the *tetA* gene. (C–E) Structures of TetR homodimer in complex with (C) DNA (Orth et al., 2000), (D) tetracycline (Hinrichs et al., 1994; Kisker et al., 1995) and (E) tigecycline (Orth et al., 1999). In (D), the binding of tetracycline to the C-terminal effector domain induces conformational changes in the DNA-binding domain (arrowed) that leads to loss of interaction with the DNA.

the N-terminal helix-turn-helix DNA-binding domain of TetR (Hinrichs et al., 1994; Kisker et al., 1995). The conformational changes lead to an increase in the separation of the DNA-binding domains such that interaction with the *tet* operator sequence of the DNA is precluded (Figure 3D) (Orth et al., 2000; Saenger et al., 2000). Although glycyliclones, such as tigecycline, can bind to the C-terminal effector-binding domain of TetR, this interaction induces only a limited conformational change in the DNA-binding domain (Figure 3E) (Orth et al., 1999), consistent with the reduced (5-fold) induction of TetR-regulated TetA

expression observed in the presence of tigecycline compared to tetracycline (Orth et al., 1999).

Modification of tetracyclines leads to drug degradation

The *tetX* and *tet37* tetracycline resistance determinants encode FAD-requiring monooxygenases (Figure 4A) that confer resistance to tetracyclines through modification of the drug (Speer et al., 1991; Yang et al., 2004). The

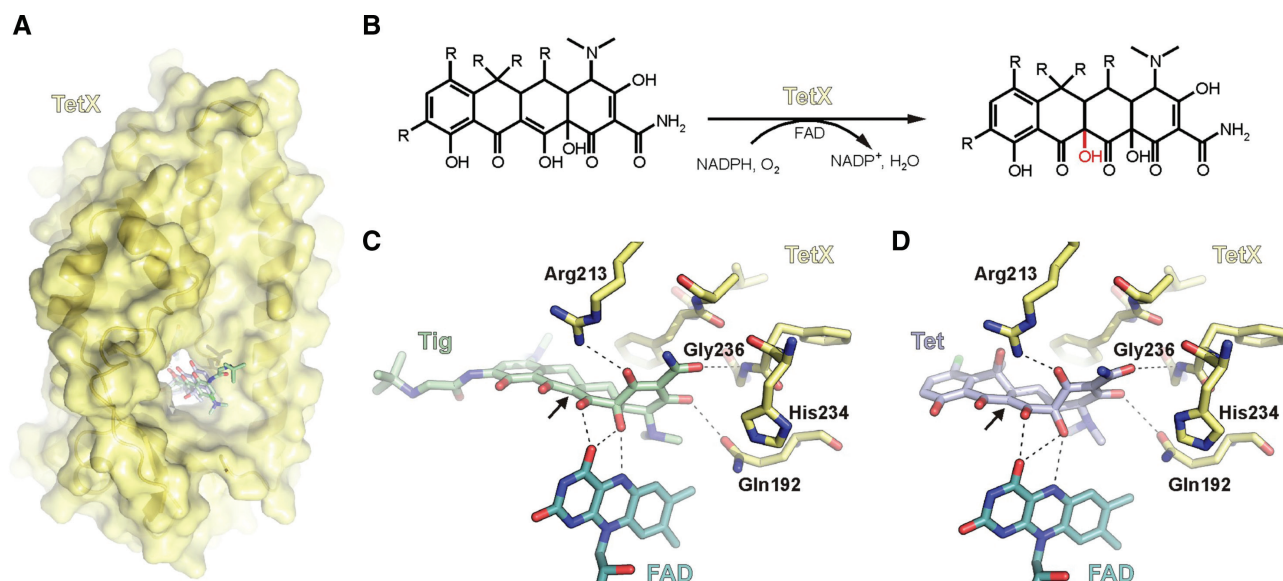


Figure 4 Tetracycline resistance via drug modification and degradation.

(A) Overlay of structures of the TetX monooxygenase (yellow) in complex with tigecycline (green) (Volkers et al., 2013) or tetracycline (blue) (Volkers et al., 2011). (B) Reaction pathway for TetX-mediated hydroxylation of tetracycline, which requires cofactors FAD, NADPH₂ and O₂. (C–D) FAD and residues of TetX recognize moieties of ring A and B of (C) tigecycline (Volkers et al., 2013) and (D) tetracycline (Volkers et al., 2011) to mediate hydroxylation of position C11a (arrowed), which leads to degradation of the drugs.

monooxygenases utilize NADPH and O₂ to hydroxylate position C11a located between ring B and C of tetracyclines (Figure 4B). The hydroxylated form of the drug has significantly altered chemical properties that perturb the magnesium coordination properties of the drug and presumably therefore reduce the drugs affinity for the ribosome. Moreover, the hydroxylated tetracycline undergoes a non-enzymatic decomposition. The requirement of O₂ for the monooxygenase activity means that the resistance mechanism only operates in bacteria growing in aerobic conditions.

Crystal structures indicate that monooxygenases, such as TetX, recognize the common core of the tetracyclines, specifically moieties present on rings A and B of the drug (Volkers et al., 2011, 2013), thus explaining why these enzymes also modify tetracycline derivatives, such as the glycycline tigecycline (Moore et al., 2005), which has an identical ring A and B arrangement as tetracycline (Figure 1C and F). Moreover, the ring D substitutions present in glycyclines protrude from the active site (Figure 4A) and therefore do not prevent binding and modification of these derivatives by the TetX enzyme (Volkers et al., 2013). While C11a-hydroxytigecycline has an MIC of 64 µg/ml against *E. coli* compared to 0.5 µg/ml for tigecycline, the presence of the *tetX* gene in *E. coli* results in an MIC of only 2 µg/ml for tigecycline but 128 µg/ml for tetracycline (Moore et al., 2005; Grossman et al., 2012). This suggests that even if tigecycline is a substrate

for TetX, the enzymatic reaction is severely impaired with tigecycline compared to tetracycline. Furthermore, there have not been any reports to date of TetX in clinical isolates conferring tetracycline resistance therefore, at present, TetX is unlikely to influence the effectiveness of new glycyclines, such as tigecycline.

Ribosome mutations conferring resistance to tetracyclines

Mutations conferring resistance to tetracycline antibiotics have been reported within the 16S rRNA. The first reported mutation was a G1058C substitution in h34 of the 16S rRNA of clinical isolates of the Gram-positive bacteria *Propionibacterium acnes* (Ross et al., 1998). These bacterial isolates encode three homozygous copies of the rRNA bearing the G1058C substitution, resulting in an increased MIC for tetracycline as well as for doxycycline and minocycline (Ross et al., 1998). Some resistance (4-fold increase in MIC) to tetracycline was also observed when the 16S rRNA operon bearing the G1058C substitution was overexpressed from a plasmid in a wildtype *E. coli* strain bearing seven copies of the susceptible 16S rRNA operon (Ross et al., 1998). Overexpression of the G1058C rRNA operon in an *E. coli* strain lacking the seven rRNA operons produced an 8-fold increase in MIC for tetracycline and tigecycline (Bauer et al., 2004). Consistently, tetracycline has a lower affinity for ribosomes

bearing the G1058C mutations than wildtype ribosomes (Nonaka et al., 2005). In wildtype bacterial ribosomes, G1058 forms a base-pair interaction with U1199 in h34, which would be disrupted by a G1058C mutation. Therefore, the decreased affinity of tetracycline for G1058C containing ribosomes most likely results from local conformational perturbations of the neighboring nucleotides G1197 and G1198 that are involved in direct interactions with tetracycline as well as in the coordination of a Mg^{2+} ion (Figure 2C).

Tetracycline resistance mutations have also been identified within the stem loop of helix 31 of the 16S rRNA in *Helicobacter pylori* strains, with the triple mutation A965U/G966U/A967C conferring high-level resistance against tetracycline (Dailidienė et al., 2002; Trieber and Taylor, 2002) as well as an increased MIC for doxycycline and minocycline (Gerrits et al., 2002). Overexpression of the ${}_{965}\text{AGA-UUC}_{967}$ triple mutation containing rRNA operon in an *E. coli* strain lacking the seven rRNA operons produced a 4-fold increased MIC for tetracycline and tigecycline (Bauer et al., 2004). Studies performing systematic site-directed mutagenesis of positions 965–967 indicate that the strength of the tetracycline resistance was generally proportional to the severity of the changes relative to the wildtype sequence, i.e., with single and double mutations tending to confer lower level resistance than triple mutations (Gerrits et al., 2003; Nonaka et al., 2005). Consistently, binding of tetracycline was the least efficient to ribosomes bearing the triple mutation (AGA-UUC), although still reduced for ribosomes bearing single mutations (e.g., AGC or GGA) when compared with wildtype (AGA) ribosomes (Nonaka et al., 2005). The decreased affinity of tetracycline for ribosomes bearing mutations in positions 965–967 most likely arises from perturbations in the conformation of the loop of helix 31, thus disrupting the interaction between the phosphate-oxygen of G966 of the 16S rRNA and the Mg^{2+} ion that is coordinated by ring A of tetracycline (Figure 2C). It is noteworthy that although the AGA-UUC triple mutation and G1058C cause a similar fold increase in the MIC for tigecycline and tetracycline, the absolute MIC₉₀ of tigecycline for G1058C (1 $\mu\text{g}/\text{ml}$) and AGA-UUC (0.5 $\mu\text{g}/\text{ml}$) is still 16-fold lower when compared with the respective MIC₉₀s for tetracycline (Bauer et al., 2004), consistent with the increased affinity and effectiveness of tigecycline over tetracycline.

Factor-assisted protection: ribosome protection proteins

To date, there are 12 distinct classes of ribosome protection proteins (RPPs) that confer resistance to tetracycline

(Table 1), with the best-characterized being TetO and TetM (reviewed by Connell et al., 2003a). TetO is usually found on plasmids present in *Campylobacter* species, but has also been discovered chromosomally in several Gram-positive organisms, e.g., *Streptococcus* and *Staphylococcus* (Roberts, 1994). In contrast, TetM, which is usually present on conjugative transposons (such as Tn916 and Tn1545), was first identified in *Streptococcus* sp., but has subsequently been found in a wide variety of Gram-positive and Gram-negative species (Roberts, 1994). The different classes of RPPs have high homology with one another; for example, TetO from *Campylobacter jejuni* displays >75% identity (>85% similarity) with TetM from *E. faecalis*. The presence of mosaic RPPs comprising regions from distinct RPP classes have also been reported, for example the novel mosaic *tetS/M* gene identified in foodborne strains of *Streptococcus bovis* (Barile et al., 2012). In general, RPPs are thought to have derived from *otrA*, which confers tetracycline resistance in the natural producer of oxytetracycline, *Streptomyces rimosus* (Doyle et al., 1991).

Sequence alignments indicate that RPPs are GTPases with the most significant homology (~25% identity and ~35% similarity) to translation factor EF-G (Burdett, 1991), which has allowed homology models for RPPs such as TetM to be generated (Dönhöfer et al., 2012) (Figure 5A–D). However, RPPs, such as TetM, cannot complement temperature sensitive *E. coli* EF-G (or *B. subtilis* EF-Tu) mutants (Burdett, 1991) and thus RPPs are considered paralogs of EF-G that have attained the specialized function to improve translation in the presence of tetracycline (Connell et al., 2003a) (Figure 5E). Analogous to EF-G, biochemical studies indicate that TetM and TetO bind to both GTP and GDP (Burdett, 1991; Taylor et al., 1995), and that mutation of the conserved Asn128 of the nucleotide binding G4 motif within the G domain of TetO results in reduced tetracycline resistance (Grewal et al., 1993), consistent with the importance of GTP binding for RPP action. Moreover, binding of TetO and TetM to the ribosome requires GTP or GDPNP, and does not occur with GDP (Dantley et al., 1998; Trieber et al., 1998). The GTPase activities of both TetM and TetO are stimulated (10–20-fold) by the presence of ribosomes (Burdett, 1991; Taylor et al., 1995; Connell et al., 2003b), however the release of tetracycline from the ribosome by TetM or TetO can occur in the presence of non-hydrolyzable GTP analogs, such as GDPNP (Burdett, 1996; Trieber et al., 1998; Connell et al., 2002). This indicates that GTP hydrolysis is not strictly necessary for tetracycline release, but rather for dissociation of the RPP from the ribosome. Curiously, the ribosome-dependent GTPase of TetM, but not of EF-G, is slightly stimulated by the presence (up to 1 mM) of tetracycline (Burdett, 1996). In contrast, the

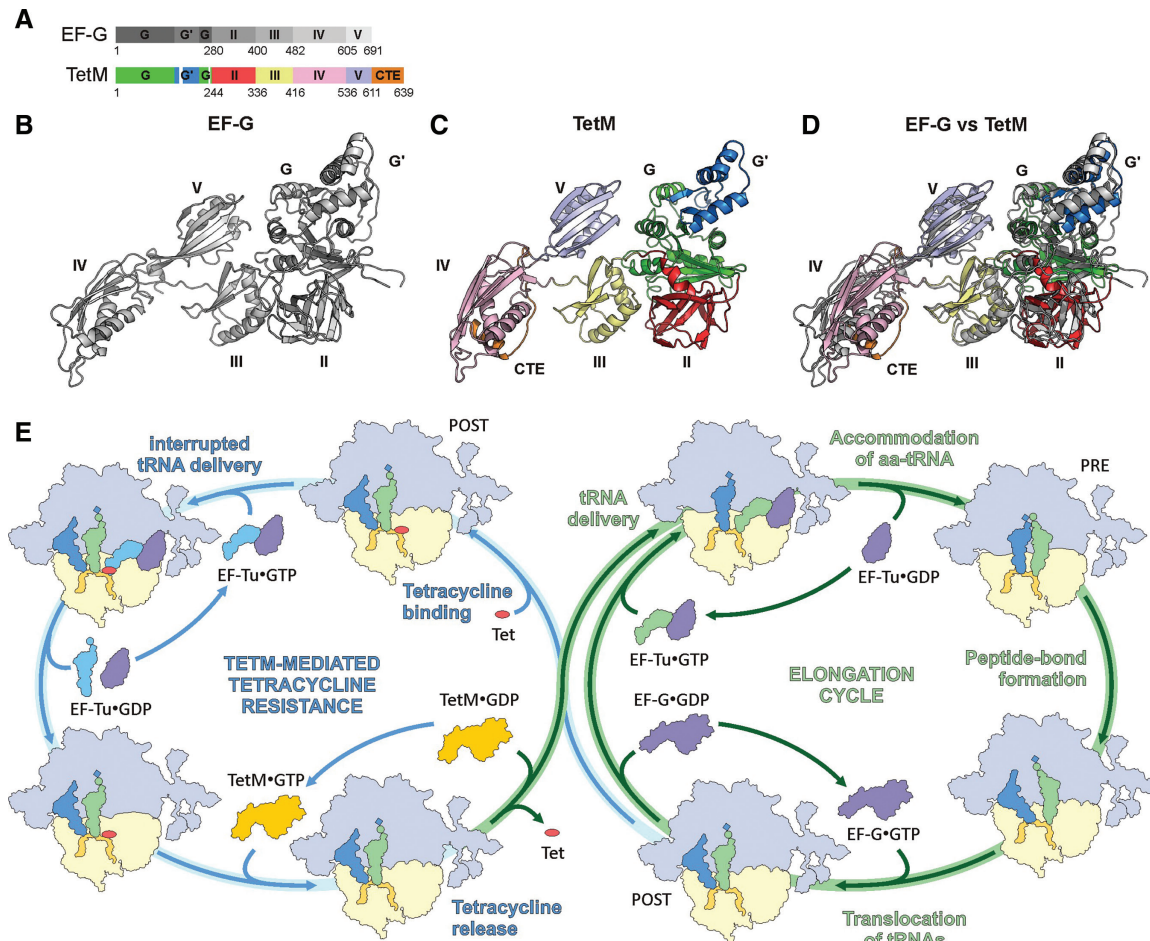


Figure 5 Tetracycline resistance mediated by ribosome protection proteins.

(A) Schematic comparing the domain arrangement of EF-G and the RPP TetM. (B–D) Comparison of (B) the crystal structure of *Thermus thermophilus* EF-G (PDB ID 2WRI) (Gao et al., 2009) with a homology model for TetM [colored as in (A); PDB ID 3J25 (Dönhöfer et al., 2012)] and (D) superimposition of (B) and (E). (E) Schematic illustrating the translation elongation cycle (green) and cycle of tetracycline inhibition and TetM-mediated tetracycline resistance (blue).

ribosome-dependent GTPase activity of TetM and TetO is inhibited by thiostrepton (Connell et al., 2003b; Starosta et al., 2009; Mikolajka et al., 2011) and the toxin α -sarcin (Connell et al., 2003b), as observed previously for other translation factors, such as EF-G (Wilson, 2009).

TetO binds preferentially to the POST translational state ribosome (Connell et al., 2003b), which is expected as during translation elongation, it is the POST state ribosome that is stabilized by the action of tetracycline to prevent delivery of aa-tRNA to the ribosomal A-site (Figure 5E). Cryo-electron microscopy (EM) structures of TetM (Figure 6A) and TetO (Figure 6B) in complex with ribosome reveal that RPPs occupy a similar binding site as EF-G (Figure 6C) (Spahn et al., 2001; Dönhöfer et al., 2012; Li et al., 2013), consistent with the competition observed between TetM and EF-G for ribosome binding (Dantley et al., 1998). As EF-G binds to the PRE translational state and specifically stabilizes

a rotated ribosome with hybrid site tRNAs before converting it into a POST state (Figure 5E), RPPs are unlikely to compete with EF-G during translation in the cell. Competition between RPPs and EF-G/EF-Tu might however explain the inhibition observed when high concentrations of RPPs are used in *in vitro* translation systems (Trieber et al., 1998).

Although no crystal structures of RPPs exist to date, the cryo-EM structure of the TetM-70S complex (Figure 6A) was sufficiently resolved (~ 7 Å resolution) as to allow docking of a molecular model for the TetM protein, generated based on homology with EF-G (Figure 5A–D) (Dönhöfer et al., 2012). This exercise led to the discovery of a conserved C-terminal extension (CTE) in RPPs that adopts a short α -helix, which is absent in EF-G (Figure 5A–D). Truncation of the CTE abolished the ability of TetM to confer resistance to tetracycline in *E. coli*, indicating the critical importance of the

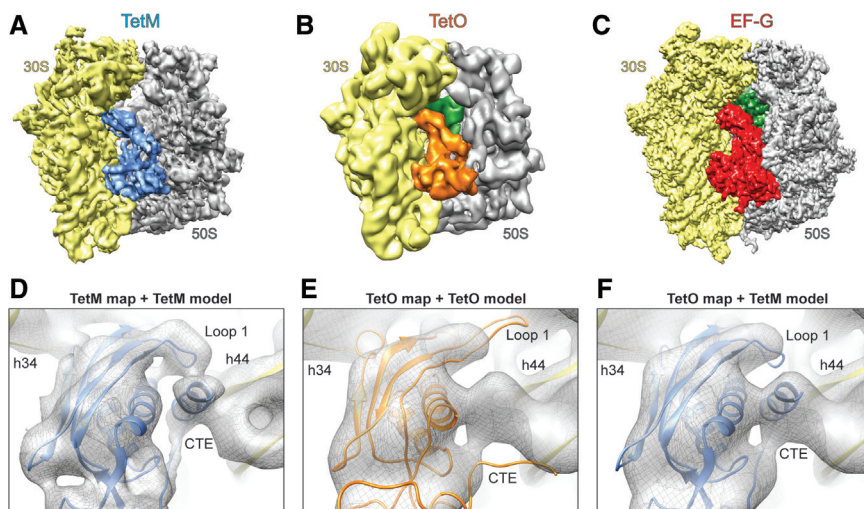


Figure 6 Structures of TetM, TetO and EF-G in complex with the 70S ribosome.

(A–C) Cryo-EM structures of (A) TetM (blue) (Dönhöfer et al., 2012) and (B) TetO (orange) (Li et al., 2013) on the ribosome, compared with (C) the binding position of EF-G (red) (Gao et al., 2009). (D–F) Cryo-EM map (grey) of the (D) TetM-70S (Dönhöfer et al., 2012) complex or (E, F) TetO-70S (Li et al., 2013) complex, with molecular model for domain IV of (D, F) TetM (blue) (Dönhöfer et al., 2012) and (E) TetO (orange) (Li et al., 2013).

short α -helix for TetM function (Dönhöfer et al., 2012). On the ribosome, the CTE of TetM is observed to be sandwiched between domain IV of TetM and helix 44 (h44) of the 16S rRNA (Figure 6D), consistent with chemical patterns in h44 observed upon TetO binding (Connell et al., 2002; Dönhöfer et al., 2012). Although the CTE of TetO was modeled differently in the 10 Å resolution cryo-EM structure of the TetO-70S complex (Figure 6E) (Li et al., 2013), the electron density of the TetO-70S map suggests that the CTE of TetO does in fact adopt a short α -helix and interact with h44 as observed in the TetM-70S structure (Figure 6D and E), and consistent with the high identity (>75%) between TetM and TetO. A similar discrepancy was also observed for loop 1 of domain IV, which was modeled in an extended conformation in the TetO-70S complex (Figure 6D) and proposed to form, together with surrounding rRNA nucleotides, a corridor which the tetracycline molecule navigates during its release from the ribosome (Li et al., 2013). However, careful inspection of the cryo-EM maps of both the TetO and TetM complexes does not support an extended conformation, but rather suggests that loop 1 adopts a kinked conformation for both TetO and TetM in order to establish interactions with the CTE (Figure 6D and E). In contrast, both the TetO-70S and TetM-70S structures are in agreement with respect to an interaction between loop 2 of domain IV and nucleotides in h34 (Dönhöfer et al., 2012; Li et al., 2013), consistent with the chemical protections of h34 observed upon TetO binding to the ribosome (Connell et al., 2002; Connell et al., 2003b).

In the first cryo-EM structure of a TetO-70S complex at 16 Å, density for TetO was not observed to overlap with tetracycline in the primary binding site, leading to the proposal that the RPPs remove tetracycline from the ribosome, not directly, but by inducing a local disturbance in h34 (Spahn et al., 2001). However, the subsequent higher resolution RPP-70S structures reveal that loop 3 of domain IV interacts with the vicinity of C1054 of the 16S rRNA (Dönhöfer et al., 2012; Li et al., 2013), and thus directly encroaches upon the binding site of tetracycline (Figure 7A and B), and more extensively tigecycline (Figure 7C) (Jenner et al., 2013). This suggests that residues within loop 3 of RPPs are involved in directly dislodging tetracycline from its binding site. Alanine scanning mutagenesis of loop 3 of domain IV of TetM however did not reveal any single critical amino acid, but rather the double Y506A/Y507A mutation was required to abolish TetM-mediated tetracycline resistance (Dönhöfer et al., 2012). Surprisingly, despite the high sequence conservation of loop 3 across different RPPs (Figure 7D), a single mutation Y507A was reported to inactivate *C. jejuni* TetO (Li et al., 2013). The system used to assess the tetracycline resistance however yielded only ~2-fold changes in MIC for the wildtype TetO protein (Li et al., 2013), whereas >10-fold differences were observed with wildtype TetM (Dönhöfer et al., 2012). Therefore, a reanalysis of *C. jejuni* TetO and *Listeria monocytogenes* TetS was performed, revealing that like TetM, these RPPs confer a >10-fold increase in MIC compared to the parental strain, and that while the

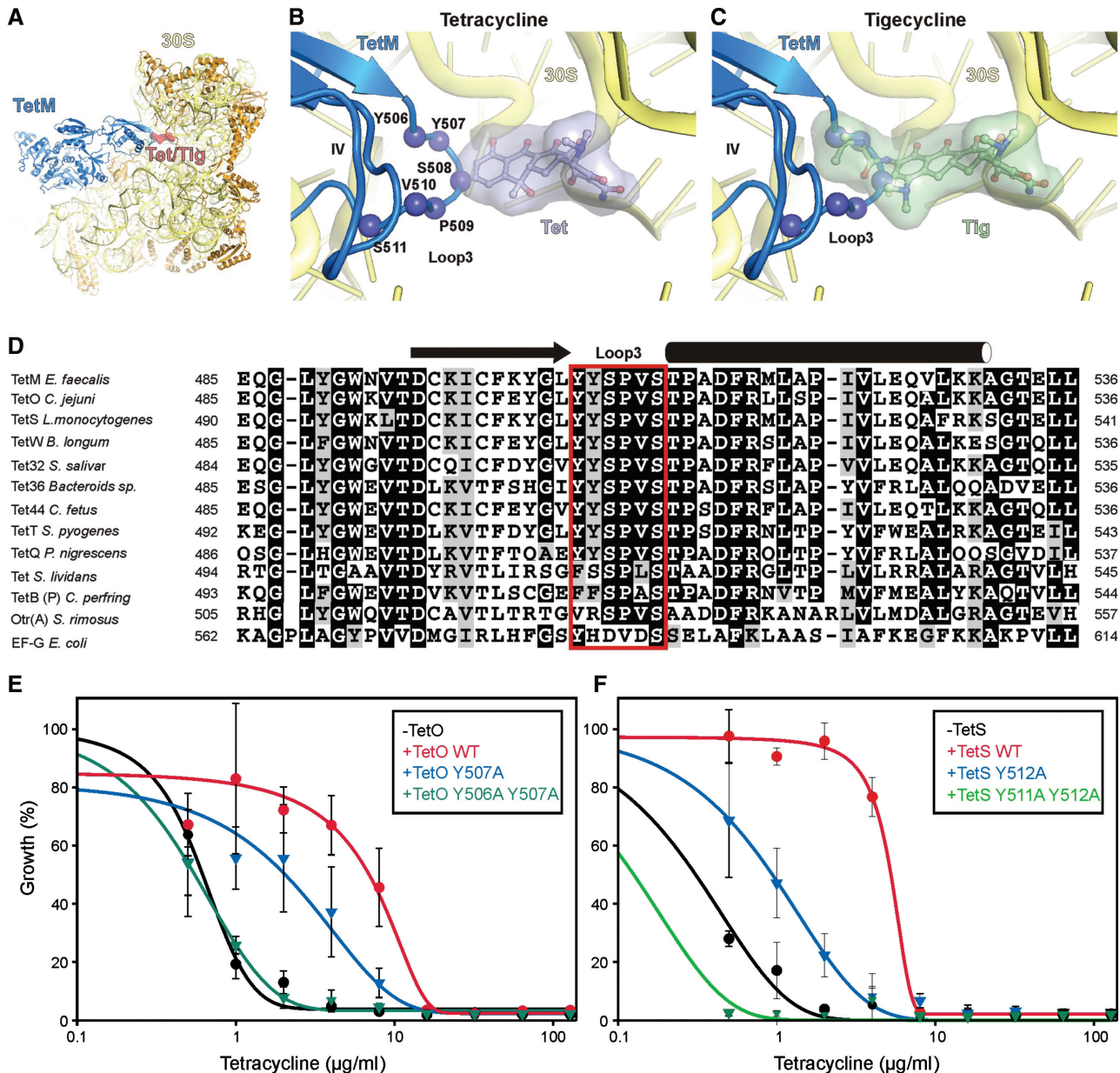


Figure 7 The role of Loop 3 of domain IV of RPPs for tetracycline resistance.

(A) Overview of relative position of TetM (blue) (Dönhöfer et al., 2012), tetracycline/tigecycline (red) (Jenner et al., 2013) and 30S subunit (yellow). (B–C) Relative binding positions of loop 3 of domain IV of TetM (Dönhöfer et al., 2012) compared to (B) tetracycline (blue) and (C) tigecycline (green) (Jenner et al., 2013). (D) Sequence alignment of RPPs showing conservation of loop 3 (red box) of domain IV (black boxes indicate identical residues, grey boxes indicate similar residues). (E–F) Growth curves of wildtype *E. coli* strain BL21 (-TetO or -TetS, black) in the presence of increasing concentrations of tetracycline (0–128 µg/ml) compared with the WT strain harboring a plasmid encoding wildtype (E) *C. jejuni* TetO (+TetO WT, red) or (F) *L. monocytogenes* TetS (+TetS WT, red), or single (blue) or double (green) mutants. Experiments were performed as described in (Dönhöfer et al., 2012).

single mutation Y507A reduces the MIC, the Y506A/Y507A double mutation was necessary to completely inactivate TetO and TetS (Figure 7E and F), as reported previously for TetM (Dönhöfer et al., 2012). Based on these findings, it is tempting to speculate that these aromatic tyrosine residues in loop 3 establish stacking interactions with

C1054 to dislodge tetracycline from its binding, however, higher resolution structures of RPP-70S complexes will be required to validate this hypothesis.

The enhancement of C1054 to chemical modification that is observed upon TetO binding remains subsequent to dissociation of TetO from the ribosome, suggesting that

RPPs may imprint a defined conformation of C1054 in the ribosome, which on one the hand prevents rebinding of tetracycline and on the other hand favors delivery of the aa-tRNA by EF-Tu (Connell et al., 2002, 2003a,b). In this context, it is interesting to note that mutations in the *miaA* gene of *E. coli* interfere with the ability of TetM and TetO to confer tetracycline resistance (Burdett, 1993; Taylor et al., 1998). The *miaA* gene encodes an enzyme involved in the modification of tRNA position A37, which is located 3' adjacent to the anticodon of tRNAs that decode codons starting with U (Esberg and Bjork, 1995). The modification [2-methylthio-N₆-(D₂-isopentenyl)adenosine] has been shown to stabilize the anticodon-codon interaction by improving stacking interactions (Vacher et al., 1984), and the lack of this modification significantly reduces the affinity of these tRNAs for the ribosome as well as reducing the efficiency and fidelity of translation (Vacher et al., 1984; Esberg and Bjork, 1995). Thus, the lower level of tetracycline resistance in *E. coli* *miaA* mutants suggests that RPP induced alterations within the decoding site that promote binding of modified tRNAs are unfavourable for binding of the unmodified aminoacyl-tRNAs.

Although RPPs increase the MIC for tetracycline, doxycycline and minocycline, these proteins have little or no effect on the potency of third generation tetracyclines,

such tigecycline, eravacycline and omadacycline (Grossman et al., 2012; Draper et al., 2013; Jenner et al., 2013). The ability of third generation tetracyclines to overcome TetM action does not appear to be related only to an increase in binding affinity compared to tetracycline, since omadacycline displays a similar affinity to azacycline, which does not overcome TetM action (Jenner et al., 2013). The C9-moiety of the third generation tetracyclines might therefore contribute not only to the binding affinity of the drug, but also enhance the on-rate of the drug as well as sterically hinder residues within loop 3 of the TetM from accessing nucleotide C1054 to dislodge the drug from its binding site on the ribosome (Figure 7C). It will be interesting to see whether alterations within loop 3 of domain IV can give rise to RPPs that confer resistance against third generation tetracyclines, such as tigecycline.

Acknowledgments: This work was supported by Deutsche Forschungsgemeinschaft FOR1805 (Grant WI3285/2-1 to D.N.W.) and the European Molecular Biology Organisation (EMBO) Young Investigator Programme (D.N.W.); A.L.S. is funded by an AXA Research Fund Postdoctoral Fellowship.

Received December 6, 2013; accepted January 30, 2014; previously published online February 5, 2014

References

- Agwuh, K.N. and MacGowan, A. (2006). Pharmacokinetics and pharmacodynamics of the tetracyclines including glycylicyclines. *J. Antimicrob. Chemother.* *58*, 256–265.
- Backus, E.J., Duggar, B.M., and Campbell, T.H. (1954). Variation in *Streptomyces aureofaciens*. *Ann. NY Acad. Sci.* *60*, 86–101.
- Barden, T.C., Buckwalter, B.L., Testa, R.T., Petersen, P.J., and Lee, V.J. (1994). "Glycylcyclines". 3. 9-Aminodoxycyclinecarboxamides. *J. Med. Chem.* *37*, 3205–3211.
- Barile, S., Devirgiliis, C., and Perozzi, G. (2012). Molecular characterization of a novel mosaic tet(S/M) gene encoding tetracycline resistance in foodborne strains of *Streptococcus bovis*. *Microbiology* *158*, 2353–2362.
- Bauer, G., Berens, C., Projan, S., and Hillen, W. (2004). Comparison of tetracycline and tigecycline binding to ribosomes mapped by dimethylsulphate and drug-directed Fe²⁺ cleavage of 16S rRNA. *J. Antimicrob. Chemother.* *53*, 592–599.
- Ben-Shem, A., Garreau de Loubresse, N., Melnikov, S., Jenner, L., Yusupova, G., and Yusupov, M. (2011). The structure of the eukaryotic ribosome at 3.0 Å resolution. *Science* *334*, 1524–1529.
- Bergeron, J., Ammirati, M., Danley, D., James, L., Norcia, M., Retsema, J., Strick, C.A., Su, W.G., Sutcliffe, J., and Wondrack, L. (1996). Glycylcyclines bind to the high-affinity tetracycline ribosomal binding site and evade Tet(M)- and Tet(O)-mediated ribosomal protection. *Antimicrob. Agents Chemother.* *40*, 2226–2228.
- Blackwood, R.K., Beereboom, J.J., Rennhard, H.H., von Wittenau, M.S., and Stephens, C.R. (1961). 6-methylenetetracyclines. I. a new class of tetracycline antibiotics. *J. Am. Chem. Soc.* *83*, 2773–2775.
- Blanchard, S.C., Gonzalez, R.L., Kim, H.D., Chu, S., and Puglisi, J.D. (2004). tRNA selection and kinetic proofreading in translation. *Nat. Struct. Mol. Biol.* *11*, 1008–1014.
- Boothe, J.H., Kende, A.S., Fields, T.L., and Wilkinson, R.G. (1959). Total synthesis of tetracyclines. I. (±)-dedimethylamino-12a-deoxy-6-demethylanhydrochlortetracycline. *J. Am. Chem. Soc.* *81*, 1006–1007.
- Bradford, P.A., and Jones, C.H. (2012). Tetracyclines. In: *Antibiotic Discovery and Development*, Dougherty, T.J. and Puccim, M.J., eds. (New York: Springer), pp. 147–179.
- Brodersen, D.E., Clemons, W.M., Carter, A.P., Morgan-Warren, R.J., Wimberly, B.T., and Ramakrishnan, V. (2000). The structural basis for the action of the antibiotics tetracycline, pactamycin, and hygromycin B on the 30S ribosomal subunit. *Cell* *103*, 1143–1154.
- Budkevich, T.V., El'skaya, A.V., and Nierhaus, K.H. (2008). Features of 80S mammalian ribosome and its subunits. *Nucleic Acids Res.* *36*, 4736–4744.
- Burdett, V. (1991). Purification and characterization of Tet(M), a protein that renders ribosomes resistant to tetracycline. *J. Biol. Chem.* *266*, 2872–2877.

- Burdett, V. (1993). transfer-RNA modification activity is necessary for Tet(M)-mediated tetracycline resistance. *J. Bacteriol.* *175*, 7209–7215.
- Burdett, V. (1996). Tet(M)-promoted release of tetracycline from ribosomes is GTP dependent. *J. Bacteriol.* *178*, 3246–3251.
- Caryl, J.A., Cox, G., Trimble, S., and O'Neill, A.J. (2012). “tet(U)” is not a tetracycline resistance determinant. *Antimicrob. Agents Chemother.* *56*, 3378–3379.
- Chopra, I. and Roberts, M. (2001). Tetracycline antibiotics: mode of action, applications, molecular biology, and epidemiology of bacterial resistance. *Microbiol. Mol. Biol. Rev.* *65*, 232–260.
- Connell, S.R., Trieber, C.A., Stelzl, U., Einfeldt, E., Taylor, D.E., and Nierhaus, K.H. (2002). The tetracycline resistance protein Tet(O) perturbs the conformation of the ribosomal decoding centre. *Mol. Microbiol.* *45*, 1463–1472.
- Connell, S.R., Tracz, D.M., Nierhaus, K.H., and Taylor, D.E. (2003a). Ribosomal protection proteins and their mechanism of tetracycline resistance. *Antimicrob. Agents Chemother.* *47*, 3675–3681.
- Connell, S.R., Trieber, C.A., Dinos, G.P., Einfeldt, E., Taylor, D.E., and Nierhaus, K.H. (2003b). Mechanism of Tet(O)-mediated tetracycline resistance. *EMBO J.* *22*, 945–953.
- Conover, L.H., Moreland, W.T., English, A.R., Stephens, C.R., and Pilgrim, F.J. (1953). Terramycin. Xi. Tetracycline. *J. Am. Chem. Soc.* *75*, 4622–4623.
- Dailidienė, D., Bertoli, M.T., Miciulevičienė, J., Mukhopadhyay, A.K., Dailide, G., Pascasio, M.A., Kupcinskis, L., and Berg, D.E. (2002). Emergence of tetracycline resistance in *Helicobacter pylori*: multiple mutational changes in 16S ribosomal DNA and other genetic loci. *Antimicrob. Agents Chemother.* *46*, 3940–3946.
- Dantley, K., Dannelly, H., and Burdett, V. (1998). Binding interaction between Tet(M) and the ribosome: requirements for binding. *J. Bacteriol.* *180*, 4089–4092.
- Dönhöfer, A., Franckenberg, S., Wickles, S., Berninghausen, O., Beckmann, R., and Wilson, D.N. (2012). Structural basis for TetM-mediated tetracycline resistance. *Proc. Natl. Acad. Sci. USA* *109*, 16900–16905.
- Doyle, D., McDowall, K.J., Butler, M.J., and Hunter, I.S. (1991). Characterization of an oxytetracycline-resistance gene, *otrA*, of *Streptomyces rimosus*. *Mol. Microbiol.* *5*, 2923–2933.
- Draper, M.P., Weir, S., Macone, A., Donatelli, J., Trieber, C.A., Tanaka, S.K., and Levy, S.B. (2013). The mechanism of action of the novel aminomethylcycline antibiotic omadacycline. *Antimicrob. Agents Chemother.* Sep 16. [Epub ahead of print] doi: 10.1128/AAC.01066-13.
- Duggar, B.M. (1948). Aureomycin; a product of the continuing search for new antibiotics. *Ann. NY Acad. Sci.* *51*, 177–181.
- Esberg, B. and Bjork, G.R. (1995). The methylthio group (ms(2)) of N-6-(4-hydroxyisopentenyl)-2-methylthioadenosine (ms(2)io(6)A) present next to the anticodon contributes to the decoding efficiency of the tRNA. *J. Bacteriol.* *177*, 1967–1975.
- Finlay, A.C., Hobby, G.L., P'an, S.Y., Regna, P.P., Routien, J.B., Seeley, D.B., Shull, G.M., Sobin, B.A., Solomons, I.A., Vinson, J.W., et al. (1950). Terramycin, a new antibiotic. *Science* *111*, 85.
- Gale, E.F., Cundliffe, E., Reynolds, P.E., Richmond, M.H., and Waring, M.J. (1981). Antibiotic inhibitors of ribosome function. In: *The Molecular Basis of Antibiotic Action* (Bristol, UK: John Wiley and Sons), pp. 278–379.
- Gao, Y.G., Selmer, M., Dunham, C.M., Weixlbaumer, A., Kelley, A.C., and Ramakrishnan, V. (2009). The structure of the ribosome with elongation factor G trapped in the posttranslocational state. *Science* *326*, 694–699.
- Geggie, P., Dave, R., Feldman, M.B., Terry, D.S., Altman, R.B., Munro, J.B., and Blanchard, S.C. (2010). Conformational sampling of aminoacyl-tRNA during selection on the bacterial ribosome. *J. Mol. Biol.* *399*, 576–595.
- Gerrits, M.M., de Zoete, M.R., Arents, N.L., Kuipers, E.J., and Kusters, J.G. (2002). 16S rRNA mutation-mediated tetracycline resistance in *Helicobacter pylori*. *Antimicrob. Agents Chemother.* *46*, 2996–3000.
- Gerrits, M.M., Berning, M., Van Vliet, A.H., Kuipers, E.J., and Kusters, J.G. (2003). Effects of 16S rRNA gene mutations on tetracycline resistance in *Helicobacter pylori*. *Antimicrob. Agents Chemother.* *47*, 2984–2986.
- Grewal, J., Manavathu, E.K., and Taylor, D.E. (1993). Effect of mutational alteration of Asn-128 in the putative GTP-binding domain of tetracycline resistance determinant Tet(O) from *Campylobacter jejuni*. *Antimicrob. Agents Chemother.* *37*, 2645–2649.
- Grossman, T.H., Starosta, A.L., Fyfe, C., O'Brien, W., Rothstein, D.M., Mikolajka, A., Wilson, D.N., and Sutcliffe, J.A. (2012). Target- and resistance-based mechanistic studies with TP-434, a novel fluorocycline antibiotic. *Antimicrob. Agents Chemother.* *56*, 2559–2564.
- Guay, G.G., Tuckman, M., and Rothstein, D.M. (1994). Mutations in the tetA(B) gene that cause a change in substrate specificity of the tetracycline efflux pump. *Antimicrob. Agents Chemother.* *38*, 857–860.
- Guillaume, G., Ledent, V., Moens, W., and Collard, J.M. (2004). Phylogeny of efflux-mediated tetracycline resistance genes and related proteins revisited. *Microb. Drug Resist.* *10*, 11–26.
- Hillen, W. and Berens, C. (1994). Mechanisms underlying expression of Tn10 encoded tetracycline resistance. *Annu. Rev. Microbiol.* *48*, 345–369.
- Hinrichs, W., Kisker, C., Duvel, M., Muller, A., Tovar, K., Hillen, W., and Saenger, W. (1994). Structure of the Tet repressor-tetracycline complex and regulation of antibiotic resistance. *Science* *264*, 418–420.
- Hochstein, F.A., Stephens, C.R., Conover, L.H., Regna, P.P., Pasternack, R., Gordon, P.N., Pilgrim, F.J., Brunings, K.J., and Woodward, R.B. (1953). The structure of terramycin_{1,2}. *J. Am. Chem. Soc.* *75*, 5455–5475.
- Jenner, L., Starosta, A.L., Terry, D.S., Mikolajka, A., Filonava, L., Yusupov, M., Blanchard, S.C., Wilson, D.N., and Yusupova, G. (2013). Structural basis for potent inhibitory activity of the antibiotic tigecycline during protein synthesis. *Proc. Natl. Acad. Sci. USA* *110*, 3812–3816.
- Jiang, D., Zhao, Y., Wang, X., Fan, J., Heng, J., Liu, X., Feng, W., Kang, X., Huang, B., Liu, J., et al. (2013). Structure of the YajR transporter suggests a transport mechanism based on the conserved motif A. *Proc. Natl. Acad. Sci. USA* *110*, 14664–14669.
- Kisker, C., Hinrichs, W., Tovar, K., Hillen, W., and Saenger, W. (1995). The complex formed between Tet repressor and tetracycline-Mg²⁺ reveals mechanism of antibiotic resistance. *J. Mol. Biol.* *247*, 260–280.
- Li, W., Atkinson, G.C., Thakor, N.S., Allas, U., Lu, C.C., Chan, K.Y., Tenson, T., Schulten, K., Wilson, K.S., Hauryliuk, V., et al. (2013). Mechanism of tetracycline resistance by ribosomal protection protein Tet(O). *Nat. Commun.* *4*, 1477.

- Martell, M.J., Jr. and Boothe, J.H. (1967). The 6-deoxytetracyclines. VII. Alkylated aminotetracyclines possessing unique antibacterial activity. *J. Med. Chem.* **10**, 44–46.
- McCormick, J.R.D., Sjolander, N.O., Hirsch, U., Jensen, E.R., and Doerschuk, A.P. (1957). A new family of antibiotics: the demethyltetracyclines. *J. Am. Chem. Soc.* **79**, 4561–4563.
- McCormick, J.R.D., Hirsch, U., Sjolander, N.O., and Doerschuk, A.P. (1960). Cosynthesis of tetracyclines by pairs of *Streptomyces aureofaciens* mutants. *J. Am. Chem. Soc.* **82**, 5006–5007.
- Mikolajka, A., Liu, H., Chen, Y., Starosta, A.L., Marquez, V., Ivanova, M., Cooperman, B.S., and Wilson, D.N. (2011). Differential effects of thiopeptide and orthosomycin antibiotics on translational GTPases. *Chem. Biol.* **18**, 589–600.
- Moazed, D. and Noller, H.F. (1987). Interaction of antibiotics with functional sites in 16S ribosomal RNA. *Nature* **327**, 389–394.
- Moore, I.F., Hughes, D.W., and Wright, G.D. (2005). Tigecycline is modified by the flavin-dependent monooxygenase TetX. *Biochemistry* **44**, 11829–11835.
- Nelson, M.L. (2001). The chemistry and cellular biology of the tetracyclines. In: *Tetracyclines in Biology, Chemistry and Medicine*, M.L. Nelson, W. Hillen, and R.A. Greenwald, eds. (Switzerland: Birkhäuser Verlag), pp. 3–63.
- Nelson, M.L. and Levy, S.B. (2011). The history of the tetracyclines. *Ann. N.Y. Acad. Sci.* **1241**, 17–32.
- Nelson, M.L., Ismail, M.Y., McIntyre, L., Bhatia, B., Viski, P., Hawkins, P., Rennie, G., Andorsky, D., Messersmith, D., Stapleton, K., et al. (2003). Versatile and facile synthesis of diverse semisynthetic tetracycline derivatives via Pd-catalyzed reactions. *J. Org. Chem.* **68**, 5838–5851.
- Nonaka, L., Connell, S.R., and Taylor, D.E. (2005). 16S rRNA mutations that confer tetracycline resistance in *Helicobacter pylori* decrease drug binding in *Escherichia coli* ribosomes. *J. Bacteriol.* **187**, 3708–3712.
- Olson, M.W., Ruzin, A., Feyfant, E., Rush, T.S., 3rd, O'Connell, J., and Bradford, P.A. (2006). Functional, biophysical, and structural bases for antibacterial activity of tigecycline. *Antimicrob. Agents Chemother.* **50**, 2156–2166.
- Orth, P., Schnappinger, D., Sum, P.E., Ellestad, G.A., Hillen, W., Saenger, W., and Hinrichs, W. (1999). Crystal structure of the tet repressor in complex with a novel tetracycline, 9-(N,N-dimethylglycylamido)-6-demethyl-6-deoxy-tetracycline. *J. Mol. Biol.* **285**, 455–461.
- Orth, P., Schnappinger, D., Hillen, W., Saenger, W., and Hinrichs, W. (2000). Structural basis of gene regulation by the tetracycline inducible Tet repressor-operator system. *Nat. Struct. Biol.* **7**, 215–219.
- Perlman, D., Heuser, L.J., Dutcher, J.D., Barrett, J.M., and Boska, J.A. (1960). Biosynthesis of tetracycline by 5-hydroxy-tetracycline-producing cultures of *Streptomyces rimosus*. *J. Bacteriol.* **80**, 419–420.
- Petersen, P.J., Jacobus, N.V., Weiss, W.J., Sum, P.E., and Testa, R.T. (1999). In vitro and in vivo antibacterial activities of a novel glycylicycline, the 9-t-butylglycylamido derivative of minocycline (GAR-936). *Antimicrob. Agents Chemother.* **43**, 738–744.
- Piddock, L.J. (2006). Multidrug-resistance efflux pumps-not just for resistance. *Nat. Rev. Microbiol.* **4**, 629–636.
- Pioletti, M., Schlunzen, F., Harms, J., Zarivach, R., Gluhmann, M., Avila, H., Bashan, A., Bartels, H., Auerbach, T., Jacobi, C., et al. (2001). Crystal structures of complexes of the small ribosomal subunit with tetracycline, edeine and IF3. *EMBO J.* **20**, 1829–1839.
- Ridenhour, M.B., Fletcher, H.M., Mortensen, J.E., and Daneo-Moore, L. (1996). A novel tetracycline-resistant determinant, tet(U), is encoded on the plasmid pKq10 in *Enterococcus faecium*. *Plasmid* **35**, 71–80.
- Roberts, M.C. (1994). Epidemiology of tetracycline-resistance determinants. *Trends Microbiol.* **2**, 353–357.
- Roberts, M.C. (1996). Tetracycline resistance determinants: Mechanisms of action, regulation of expression, genetic mobility, and distribution. *FEMS Microbiol. Rev.* **19**, 1–24.
- Ross, J.I., Eady, E.A., Cove, J.H., and Cunliffe, W.J. (1998). 16S rRNA mutation associated with tetracycline resistance in a Gram-positive bacterium. *Antimicrob. Agents Chemother.* **42**, 1702–1705.
- Saenger, W., Orth, P., Kisker, C., Hillen, W., and Hinrichs, W. (2000). The tetracycline repressor—a paradigm for a biological switch. *Angew Chem. Int. Ed. Engl.* **39**, 2042–2052.
- Schmeing, T.M., Voorhees, R.M., Kelley, A.C., Gao, Y.G., Murphy, F.V.T., Weir, J.R., and Ramakrishnan, V. (2009). The crystal structure of the ribosome bound to EF-Tu and aminoacyl-tRNA. *Science* **326**, 688–694.
- Söding, J., Biegert, A., and Lupas, A.N. (2005). The HHpred interactive server for protein homology detection and structure prediction. *Nucleic Acids Res.* **33**, W244–W248.
- Sohmen, D., Harms, J.M., Schlunzen, F., and Wilson, D.N. (2009a). Enhanced SnapShot: Antibiotic inhibition of protein synthesis II. *Cell* **139**, 212–212 e211.
- Sohmen, D., Harms, J.M., Schlunzen, F., and Wilson, D.N. (2009b). SnapShot: antibiotic inhibition of protein synthesis I. *Cell* **138**, 1248 e1241.
- Spahn, C.M., Blaha, G., Agrawal, R.K., Penczek, P., Grassucci, R.A., Trieber, C.A., Connell, S.R., Taylor, D.E., Nierhaus, K.H., and Frank, J. (2001). Localization of the ribosomal protection protein Tet(O) on the ribosome and the mechanism of tetracycline resistance. *Mol. Cell* **7**, 1037–1045.
- Speer, B.S., Bedzyk, L., and Salyers, A.A. (1991). Evidence that a novel tetracycline resistance gene found on two *Bacteroides* transposons encodes an NADP-requiring oxidoreductase. *J. Bacteriol.* **173**, 176–183.
- Starosta, A.L., Qin, H., Mikolajka, A., Leung, G.Y., Schwinghammer, K., Nicolaou, K.C., Chen, D.Y., Cooperman, B.S., and Wilson, D.N. (2009). Identification of distinct thiopeptide-antibiotic precursor lead compounds using translation machinery assays. *Chem Biol* **16**, 1087–1096.
- Stephens, C.R., Conover, L.H., Hochstein, F.A., Regna, P.P., Pilgrim, F.J., Brunings, K.J., and Woodward, R.B. (1952). Terramycin. VIII. Structure of aureomycin and terramycin. *J. Am. Chem. Soc.* **74**, 4976–4977.
- Stephens, C.R., Conover, L.H., Pasternack, R., Hochstein, F.A., Moreland, W.T., Regna, P.P., Pilgrim, F.J., Brunings, K.J., and Woodward, R.B. (1954). The structure of Aureomycin1. *J. Am. Chem. Soc.* **76**, 3568–3575.
- Stephens, C.R., Beereboom, J.J., Rennhard, H.H., Gordon, P.N., Murai, K., Blackwood, R.K., and von Wittenau, M.S. (1963). 6-Deoxytetracyclines. IV.1,2 Preparation, C-6 Stereochemistry, and Reactions. *J. Am. Chem. Soc.* **85**, 2643–2652.
- Sum, P.E., Lee, V.J., Testa, R.T., Hlavka, J.J., Ellestad, G.A., Bloom, J.D., Gluzman, Y., and Tally, F.P. (1994). Glycylicyclines. 1. A new generation of potent antibacterial agents through modification of 9-aminotetracyclines. *J. Med. Chem.* **37**, 184–188.

- Sun, C., Wang, Q., Brubaker, J.D., Wright, P.M., Lerner, C.D., Noson, K., Charest, M., Siegel, D.R., Wang, Y.M., and Myers, A.G. (2008). A robust platform for the synthesis of new tetracycline antibiotics. *J. Am. Chem. Soc.* *130*, 17913–17927.
- Sun, C., Hunt, D.K., Clark, R.B., Lofland, D., O'Brien, W.J., Plamondon, L., and Xiao, X.Y. (2010). Synthesis and antibacterial activity of pentacyclines: a novel class of tetracycline analogs. *J. Med. Chem.* *54*, 3704–3731.
- Tally, F.T., Ellestad, G.A., and Testa, R.T. (1995). Glycylcyclines: a new generation of tetracyclines. *J. Antimicrob. Chemother.* *35*, 449–452.
- Taylor, D.E., Jerome, L.J., Grewal, J., and Chang, N. (1995). Tet(O), a protein that mediates ribosomal protection to tetracycline, binds, and hydrolyses GTP. *Can. J. Microbiol.* *41*, 965–970.
- Taylor, D.E., Trieber, C.A., Trescher, G., and Bekkering, M. (1998). Host mutations (*miaA* and *rpsL*) reduce tetracycline resistance mediated by Tet(O) and Tet(M). *Antimicrob. Agents Chemother.* *42*, 59–64.
- Testa, R.T., Petersen, P.J., Jacobus, N.V., Sum, P.E., Lee, V.J., and Tally, F.P. (1993). *In vitro* and *in vivo* antibacterial activities of the glycylcyclines, a new class of semisynthetic tetracyclines. *Antimicrob. Agents Chemother.* *37*, 2270–2277.
- Thaker, M., Spanogiannopoulos, P., and Wright, G.D. (2010). The tetracycline resistome. *Cell. Mol. Life Sci.* *67*, 419–431.
- Trieber, C.A. and Taylor, D.E. (2002). Mutations in the 16S rRNA genes of *Helicobacter pylori* mediate resistance to tetracycline. *J. Bacteriol.* *184*, 2131–2140.
- Trieber, C.A., Burkhardt, N., Nierhaus, K.H., and Taylor, D.E. (1998). Ribosomal protection from tetracycline mediated by Tet(O) interaction with ribosomes is GTP-dependent. *Biol. Chem.* *379*, 847–855.
- Vacher, J., Grosjean, H., Houssier, C., and Buckingham, R.H. (1984). The effect of point mutations affecting *Escherichia coli* tryptophan tRNA on anticodon-anticodon interactions and on UGA suppression. *J. Mol. Biol.* *177*, 329–342.
- Volkers, G., Palm, G.J., Weiss, M.S., Wright, G.D., and Hinrichs, W. (2011). Structural basis for a new tetracycline resistance mechanism relying on the TetX monooxygenase. *FEBS Lett.* *585*, 1061–1066.
- Volkers, G., Damas, J.M., Palm, G.J., Panjikar, S., Soares, C.M., and Hinrichs, W. (2013). Putative dioxygen-binding sites and recognition of tigecycline and minocycline in the tetracycline-degrading monooxygenase TetX. *Acta Crystallogr. D Biol. Crystallogr.* *69*, 1758–1767.
- Voorhees, R.M., Weixlbaumer, A., Loakes, D., Kelley, A.C., and Ramakrishnan, V. (2009). Insights into substrate stabilization from snapshots of the peptidyl transferase center of the intact 70S ribosome. *Nat. Struct. Mol. Biol.* *16*, 528–533.
- White, J.P. and Cantor, C.R. (1971). Role of magnesium in the binding of tetracycline to *Escherichia coli* ribosomes. *J. Mol. Biol.* *58*, 397–400.
- Wilson, D.N. (2009). The A-Z of bacterial translation inhibitors. *Crit. Rev. Biochem. Mol. Biol.* *44*, 393–433.
- Wilson, D.N. (2013). Ribosome-targeting antibiotics and bacterial resistance mechanisms. *Nat. Rev. Microbiol.*, *12*, 35–48.
- Yang, W., Moore, I.F., Koteva, K.P., Bareich, D.C., Hughes, D.W., and Wright, G.D. (2004). TetX is a flavin-dependent monooxygenase conferring resistance to tetracycline antibiotics. *J. Biol. Chem.* *279*, 52346–52352.

Cryo-EM structure of the tetracycline resistance protein TetM in complex with a translating ribosome at 3.9-Å resolution

Stefan Arenz^a, Fabian Nguyen^a, Roland Beckmann^{a,b}, and Daniel N. Wilson^{a,b,1}

^aGene Center and Department for Biochemistry, University of Munich, 81377 Munich, Germany; and ^bCenter for integrated Protein Science Munich (CIPSM), University of Munich, 81377 Munich, Germany

Edited by Peter B. Moore, Yale University, New Haven, CT, and approved March 20, 2015 (received for review January 28, 2015)

Ribosome protection proteins (RPPs) confer resistance to tetracycline by binding to the ribosome and chasing the drug from its binding site. Current models for RPP action are derived from 7.2- to 16-Å resolution structures of RPPs bound to vacant or nontranslating ribosomes. Here we present a cryo-electron microscopy reconstruction of the RPP TetM in complex with a translating ribosome at 3.9-Å resolution. The structure reveals the contacts of TetM with the ribosome, including interaction between the conserved and functionally critical C-terminal extension of TetM with a unique splayed conformation of nucleotides A1492 and A1493 at the decoding center of the small subunit. The resolution enables us to unambiguously model the side chains of the amino acid residues comprising loop III in domain IV of TetM, revealing that the tyrosine residues Y506 and Y507 are not responsible for drug-release as suggested previously but rather for intrafactor contacts that appear to stabilize the conformation of loop III. Instead, Pro509 at the tip of loop III is located directly within the tetracycline binding site where it interacts with nucleotide C1054 of the 16S rRNA, such that RPP action uses Pro509, rather than Y506/Y507, to directly dislodge and release tetracycline from the ribosome.

ribosome | antibiotic | tetracycline | resistance | TetM

The ribosome is one of the major targets for antibiotics within the bacterial cell (1, 2). A well-characterized class of broad-spectrum antibiotics in clinical use are the tetracyclines, which bind to elongating ribosomes and inhibit delivery of the EF-Tu•GTP•aa-tRNA ternary complex to the A-site (1, 3). X-ray crystal structures of ribosomal particles in complex with tetracycline have revealed that the primary drug binding site is located in helix 34 (h34) of the 16S rRNA, overlapping the binding position of the anticodon-stem loop of an A-site tRNA (4–6). The widespread use of tetracyclines has led to an increase in tetracycline resistance among clinically relevant pathogenic bacteria, thus limiting the medical utility of many members of this class (7). Drug efflux and ribosome protection are the most common tetracycline resistance mechanisms acquired by bacteria (8) and have led to the development of the third generation of tetracycline derivatives, such as tigecycline, which display enhanced antimicrobial activity and overcome both the efflux and ribosome protection resistance mechanisms (6, 9–11).

To date, there are 12 distinct classes of ribosome protection proteins (RPPs) that confer resistance to tetracycline, with the most prevalent and best characterized being TetO and TetM (3, 8, 12). The different classes of RPPs have high homology with one another; for example, *Campylobacter jejuni* TetO displays >75% identity (>85% similarity) with *Enterococcus faecalis* TetM. Based on the presence of conserved nucleotide binding motifs, RPPs are grouped together within the translation factor superfamily of GTPases (13). Accordingly, TetO and TetM catalyze the release of tetracycline from the ribosome in a GTP-dependent manner (14, 15). Biochemical studies indicate that, although GTPase activity is necessary for multiturnover of RPPs, GTP hydrolysis is not strictly required to dislodge tetracycline

because the drug is also released when nonhydrolysable GTP analogs are used (14, 15).

Nonhydrolysable GTP analogs have been used to trap RPPs on the ribosome for structural analysis by cryo-EM. The first structure of an RPP-ribosome complex was a cryo-EM reconstruction of a TetO•70S complex at 16-Å resolution. This structure revealed that TetO binds analogously to the ribosome as translation elongation factor EF-G (16), consistent with the significant homology (~25/35% identity/similarity) between RPPs and EF-G (17). Because the electron density for TetO did not come within 6 Å of the tetracycline-binding site (16), TetO was suggested to chase the drug from the ribosome by inducing conformational changes within h34 (12, 16, 18). In contrast, two subsequent structures at higher resolution, a TetM•70S complex at 7.2 Å (19) and a TetO•70S complex at 9.6 Å (20), revealed electron density for the RPPs directly overlapping with the tetracycline binding site. Based on the homology with EF-G, molecular models for the RPPs were generated and docked into the cryo-EM maps, suggesting that residues within loop III of domain IV of TetM/TetO come into direct contact with the tetracycline molecule (19, 20). Consistently, mutagenesis studies identified specific residues within loop III that are critical for RPP activity (19–21), in particular the conserved tyrosine residues Y506 and Y507 (19, 20). However, the exact role of these tyrosine residues and a detailed molecular understanding of the mechanism by which RPPs dislodge tetracycline from its binding site was not possible at the reported resolutions.

Here we present a cryo-EM structure of TetM in complex with a translating ribosome at an average resolution of 3.9 Å. Local

Significance

The ribosome, the protein-synthesizing machine in the cell, is a major target for antibiotics, such as tetracyclines. The widespread usage of tetracyclines has led to an increase in tetracycline resistance amongst medically relevant pathogenic bacteria, limiting their utility. Many bacteria obtain tetracycline resistance via ribosome protection proteins, such as TetM and TetO, that bind to the ribosome and chase tetracycline from its binding site. We have determined a structure of TetM bound to a translating ribosome at 3.9 Å, providing molecular insight into how TetM interacts with the ribosome to dislodge the drug from its binding site.

Author contributions: S.A., F.N., and D.N.W. designed research; S.A. and F.N. performed research; S.A., F.N., R.B., and D.N.W. analyzed data; and S.A. and D.N.W. wrote the paper.

The authors declare no conflict of interest.

This article is a PNAS Direct Submission.

Freely available online through the PNAS open access option.

Data deposition: The atomic coordinates have been deposited in the Protein Data Bank (PDB), www.pdb.org (PDB ID code 3J9Y), and the cryo-EM map has been deposited in the Electron Microscopy Data Bank (EMDB), www.emdatabank.org (EMDB ID code EMD-6311).

¹To whom correspondence should be addressed. Email: wilson@genzentrum.lmu.de.

This article contains supporting information online at www.pnas.org/lookup/suppl/doi:10.1073/pnas.1501775112/-DCSupplemental.

resolution calculations indicate that the majority of the core of the ribosome and domain IV of TetM extends toward 3.5 Å, enabling bulky side chains to be modeled. We provide a detailed account of the interactions between TetM and the ribosome, in particular revealing a complex network of interactions of the C-terminal helix and domain IV of TetM with the ribosomal decoding site and intersubunit bridge B2a. The structure reveals that Pro509 at the tip of loop III, rather than the previously identified tyrosine Y506 and Y507, overlaps the binding site of tetracycline and is therefore directly involved in releasing tetracycline from the ribosome.

Results and Discussion

Cryo-EM Structure and Molecular Model of a TetM•RNC. In our previous study (19), the TetM•70S complex was formed using vacant 70S ribosomes, which led to high heterogeneity because the vacant ribosomes adopted both rotated and nonrotated states. Moreover, because TetM only interacts with the nonrotated ribosomes, the heterogeneity reduced the overall occupancy of TetM on the ribosome. A further reduction in occupancy resulted from the presence of tigecycline, the binding of which (contrary to initial expectations; refs. 16 and 19) was mutually exclusive with TetM binding (19). As a result, the final reconstruction of the TetM•70S complex was derived from only 52,701 (12%) of the initial 406,687 particles and yielded a resolution of 7.2 Å (19). To reduce sample heterogeneity and increase the TetM occupancy, we omitted tigecycline and formed a complex between TetM and a translating, rather than vacant, 70S ribosome. We have previously prepared and determined cryo-EM structures of 70S ribosomes stalled during translation of Erm leader peptides by the presence of the macrolide antibiotic erythromycin (22–24). These studies revealed that the ErmCL-stalled ribosome is an ideal substrate for TetM binding because the ribosome adopts a nonrotated conformation with a peptidyl-tRNA in the P-site and a vacant A-site (22, 24). Therefore, the ErmCL-stalled ribosomes

were bound with TetM in presence of the nonhydrolysable GTP analog, GTPCP, and the resulting sample was subjected to multi-particle cryo-EM (*Materials and Methods*).

Data were collected on a Titan Krios transmission electron microscope, fitted with a Falcon II direct electron detector, and processed with the SPIDER software package (25). After removal of nonaligning and edge particles, in silico sorting revealed the presence of two subpopulations of ribosomes bearing peptidyl-tRNA in the P-site, and either a vacant A-site (25%) or an A-site occupied by TetM (75%) (*SI Appendix, Fig. S1A*). The latter volume, which we term the TetM•ribosome nascent chain complex (TetM•RNC), contained 78,186 particles and was refined further to produce a final cryo-EM map of the TetM•RNC (Fig. 1A) with an average resolution of 3.9 Å (based on the Fourier shell correlation cutoff at 0.143, *SI Appendix, Fig. S1B*). Similar to our recent cryo-EM structure of the ErmCL-RNC (22), local resolution calculations indicate that the ribosomal core of the TetM•RNC extends to 3.5 Å (*SI Appendix, Fig. S1C and D*). The resolution of domains I–V of TetM was predominantly between 3.5–4.5 Å (Fig. 1B), but with some regions extending to >5 Å, indicating flexibility as observed recently for other ribosome-bound ligands (26–29). Strand separation in β -sheets and the pitch of helices is observed, allowing a more accurate and complete backbone model to be presented for all 639 residues in domains I–V of TetM (Fig. 1C).

Moreover, the high resolution of the ribosome enabled us to more precisely map the sites of interaction with TetM (Fig. 1D and *SI Appendix, Table S1*) compared with previous reports (16, 19, 20). Overall, the interactions of TetM are similar to those for translation GTPases, such as EF-G (30), such that on the 50S subunit, the G domain of TetM contacts the sarcin-ricin loop (SRL, H95 of the 23S rRNA) and ribosomal protein L6, whereas the G' subdomain interacts with one of the C-terminal domains of L7 (Fig. 1D and E and *SI Appendix, Fig. S2A–F*). Domain V of TetM inserts into the cleft formed by H43/H44 of the

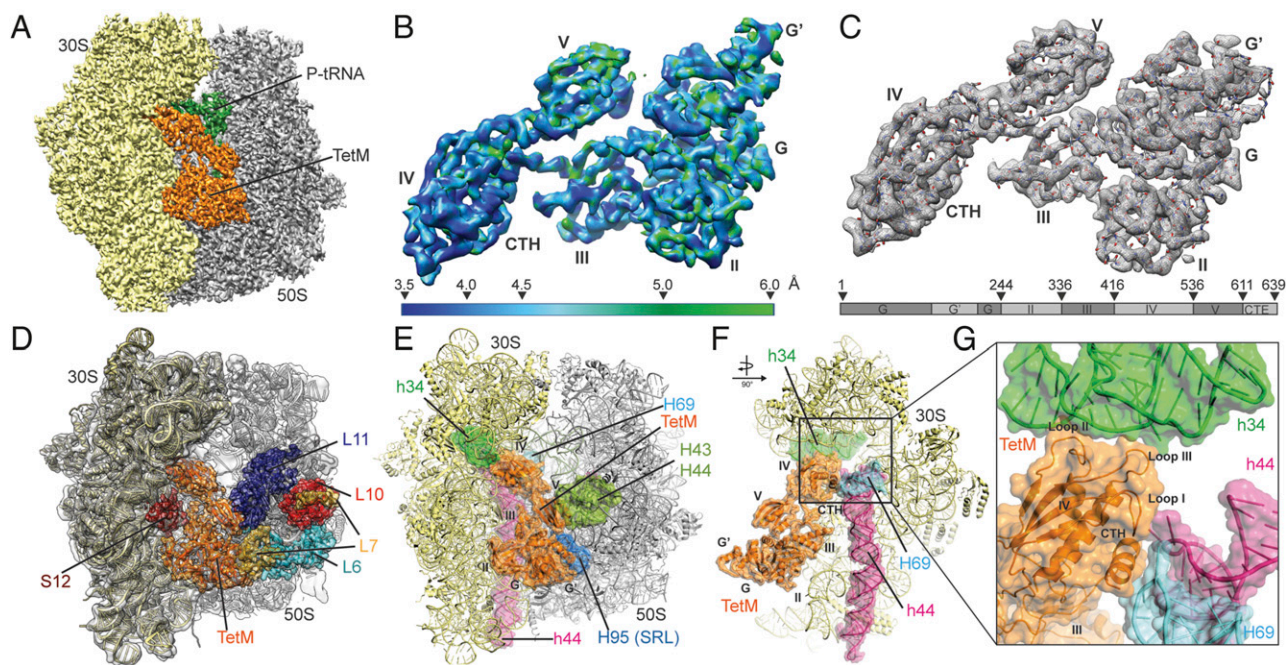


Fig. 1. Cryo-EM reconstruction of TetM•RNC. (A) Cryo-EM density map of the TetM•RNC, with TetM (orange), 30S (yellow), 50S (gray), and P-tRNA (green). (B and C) Extracted cryo-EM density for TetM colored according to local resolution (B) and with fitted polyaniline model into the density (gray mesh) for domains I (G domain), G' subdomain, II, III, IV, V, and C-terminal extension (CTE) (C). (D) Overview of the TetM•RNC showing cryo-EM density with fitted models for 30S (yellow) and 50S (gray) subunits, and TetM (orange). Ribosomal proteins contacting TetM are colored (S12, brown; L6, cyan; L7, yellow; L10, red; L11, violet). (E) Model for the TetM•RNC with rRNA helices that interact with TetM colored (h34, green; h44, pink; H43/H44, dark green; H69, light blue; H95, dark blue). (F) Side-view of E. (G) Side view of E with zoom onto 16S rRNA helices h34 (green) and h44 (pink) and 23S rRNA helix H69 (blue) that directly interact with domain IV and the CTH of TetM (orange).

23S rRNA and L11, overlapping the binding site of thiostrepton (31) (*SI Appendix, Fig. S2 A–F*) and explaining the inhibition of TetM by this antibiotic (32–34). On the small subunit, domain III of TetM contacts ribosomal protein S12 (Fig. 1 *D* and *E*), whereas domain IV of TetM wedges between the head and body of the 30S, reaching into the decoding center where contacts with h34 (head) and h44 (body) of the 16S rRNA are observed, as well as between the C-terminal extension of TetM and H69 of the 23S rRNA (Fig. 1 *F* and *G*).

Interaction of Domain IV of TetM with the 30S Subunit. Domain IV of TetM comprises a four-stranded β -sheet and two α -helices, with an overall $\beta\beta\beta\alpha$ topology. Three loops (termed Loop I, II, and III) protrude from the distal end of domain IV of TetM (Fig. 2*A*). The proline-rich loop I, located between β_4 and β_3 , was modeled differently in the recent TetM- and TetO-bound ribosome structures (3, 19, 20). In our structure, loop I adopts a bent conformation to establish interactions with the C-terminal helix α_{CTE} of TetM (Fig. 2*A*), similar to that predicted previously for TetM (19), but quite unlike the extended conformation suggested for TetO (20) (*SI Appendix, Fig. S3 A–D*). We believe that a bent conformation of loop I of TetO would be more consistent with the electron density for the TetO•70S complex as well as with the high sequence conservation between TetO and TetM (*SI Appendix, Fig. S3 A–F*). Moreover, the extended conformation modeled for the TetO•70S structure is incompatible with the presence of mRNA (*SI Appendix, Fig. S3A*), suggesting that loop I is unlikely to form part of a corridor that tetracycline navigates during its release from the ribosome (20).

The density for Loop II between β_4 and α_4 is poorly ordered, however interaction with helix 34 of the 16S rRNA is apparent, with residues Ser465 and Leu466 of TetM coming into close proximity with the backbone of C1209 and the nucleobase of C1214 (Fig. 2*B*). This finding is in agreement with the protection of C1214 from DMS modification upon TetO binding to the ribosome (18, 32). With the exception of Gly467, the residues of loop II are not highly conserved and mutagenesis of these residues exhibited only moderate effects on TetM activity (*SI Appendix, Fig. S3 G and H*). We note, however, that shortening of the loop by removal of two amino acids was previously shown to completely inactivate TetO (20).

Interaction of TetM at the Ribosomal Decoding Site. The C-terminal extension (CTE) of TetM comprises a short 11-aa α -helix (residues 627–637) connected to domain V by a flexible linker (Fig. 2*C*), consistent with previous reports (19). Sequence alignments, secondary structure predictions, as well as the electron density for the TetO•70S complex (*SI Appendix, Fig. S4 A–F*) lead us to suggest that the topology of the CTE observed here for TetM is a conserved feature of all RPPs. The C-terminal helix (CTH) is likely to stabilize domain IV of TetM on the ribosome, as we observe contact between the CTH and A1913 located at the tip of H69 of the 23S rRNA (Fig. 2*C*). A1913 adopts a very defined position, similar to that observed when A-tRNA or A/T-tRNA (in complex with EF-Tu) is bound to the ribosome (35, 36) (Fig. 2*D* and *SI Appendix, Fig. S4 G and H*), but distinct from the conformation observed in the absence of A-tRNA where A1913 inserts into h44 of the 16S rRNA (6) (Fig. 2*D*). Although nucleotides A1492 and A1493 of h44 exhibit some flexibility

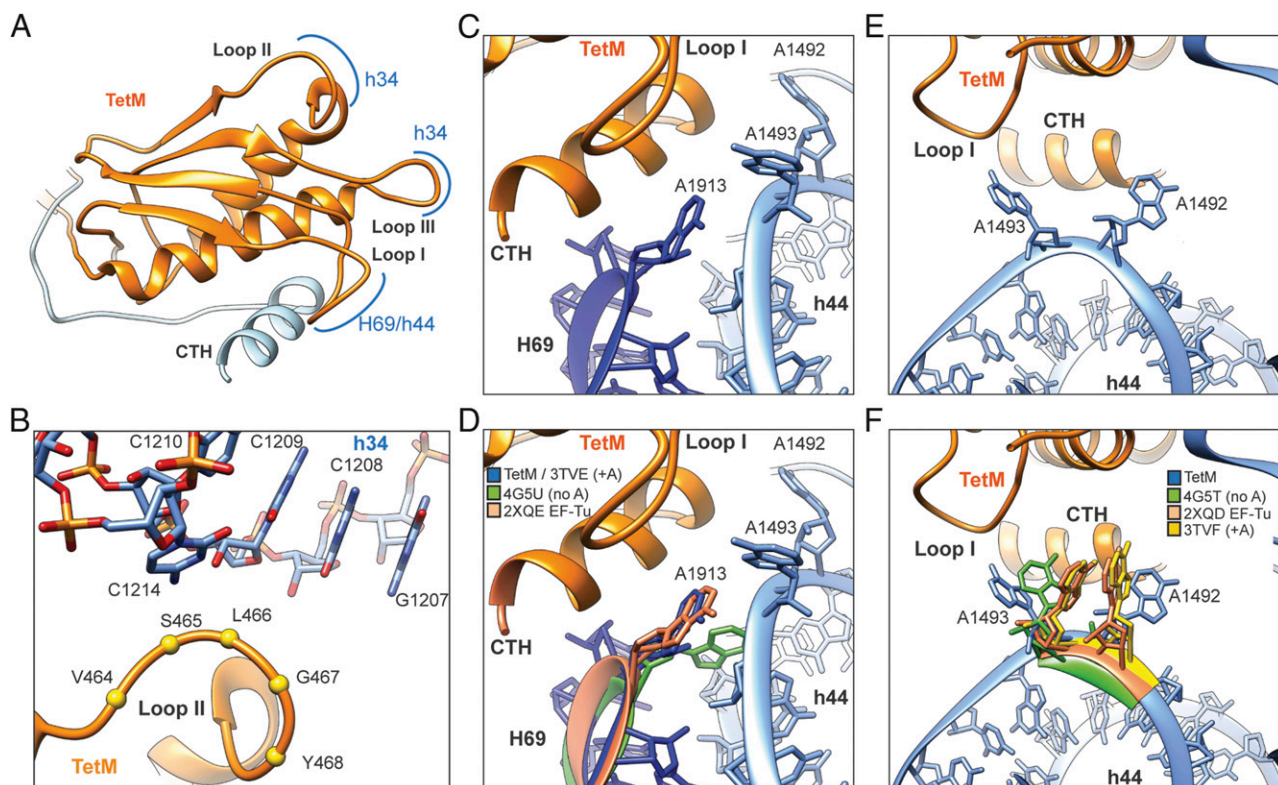


Fig. 2. Interactions of domain IV and the CTH of TetM. (*A*) Overview of domain IV (orange) and the C-terminal extension (cyan) of TetM, indicating interaction of loops I–III with rRNA helices h34, h44 and H69 as well as loop I with the C-terminal helix (CTH) of TetM. (*B*) Proximity of loop II residues ($C\alpha$ atoms shown as yellow spheres) to the nucleotides C1209, C1051 and C1214 of h34 of the 16S rRNA. (*C* and *D*) Interaction of the CTH of TetM (orange) with nucleotide A1913 of H69 of 23S rRNA (deep blue). In *D*, the positions of A1913 with ribosome lacking A-tRNA (green, PDB 4G5U; ref. 6) or containing A-tRNA (blue, PDB 3TVE; ref. 36) or A/T-tRNA (pink, PDB 2XQE; ref. 35) are shown. (*E* and *F*) Flipped-out conformations of nucleotides A1492 and A1493 of h44 of the 16S rRNA (blue) upon TetM (orange) binding to the ribosome. In *F*, the positions of A1492 and A1493 with ribosome lacking A-tRNA (green, PDB 4G5T; ref. 6) or containing A-tRNA (blue, PDB 3TVF; ref. 36) or A/T-tRNA (pink, PDB 2XQD; ref. 35) are shown.

(SI Appendix, Fig. S4 I and J), both nucleotides clearly adopt preferred conformations when TetM is bound, such that both nucleotides are flipped-out of h44 and extend toward Loop I and the CTH, respectively, of TetM (Fig. 2E). The flipping of A1492 and A1493 by TetM binding was suggested previously at 7.2 Å (19) to resemble the conformation observed during decoding of the mRNA-tRNA duplex (35–37) (Fig. 2F). At higher resolution, however, it is evident that the exact conformations of A1492 and A1493 are distinct and the nucleotides adopt an unusual splayed conformation (Fig. 2E and F), which to our knowledge has not been observed before. The most similar conformation for A1493 was observed in the P-tRNA bound ribosome with a vacant A-site (Fig. 2F); however, in this structure, A1492 remains buried within h44. Although the resolution of the previous TetO•70S structures (16, 20) was insufficient to unambiguously assign the conformational state of A1492 and A1493, biochemical studies suggest that binding of TetO to the ribosome also flips A1493 from h44, as indicated by exposure of A1408 of the 16S rRNA to DMS modification (18, 19). Because removal of the CTH by truncation of 17 amino acids inactivates TetM (19), it is likely that the interaction of TetM, and presumably TetO, with A1492 and A1493 is critical for stabilization of the RPP on the ribosome.

Pro509 of Loop III of TetM Directly Encroaches Upon the Tetracycline-Binding Site. Loop III of TetM linking β_5 to helix α_4 is the best resolved part of the TetM structure with a local resolution predominantly around 3.5 Å, which enabled the bulky aromatic sidechains, such as tyrosines and phenylalanines, to be modeled (Fig. 3A and B). In contrast to the previous TetM/O•70S reconstructions at lower resolution (19, 20), where the density for Loop III was ambiguous (SI Appendix, Fig. S5A and B), we are confident of the register of the amino acids within Loop III of TetM as well as the orientation of the side chains in most cases (Fig. 3A and B and SI Appendix, Fig. S5C). Based on this model, Pro509 at the tip of loop III stacks against C1054 within h34 of the 16S rRNA (Fig. 3C), explaining the protection of C1054 from DMS modification observed upon TetO binding to the ribosome (18). C1054 comprises part of the primary tetracycline-

binding site and establishes stacking interactions with ring D of tetracycline (4–6) (Fig. 3D). Our structure indicates that Pro509 of Loop III of TetM clashes with tetracycline and is therefore directly responsible for dislodging the drug from the ribosome (Fig. 3D). This contrasts with previous suggestions that the two conserved tyrosines, Y506 and Y507, within loop III of TetM are directly involved in tetracycline release (19, 20). It is worth noting that although Pro509 is identical in all available RPP sequences, Y506 and Y507 are substituted with Phe/Val and Ser/Phe/Arg, respectively, in some RPPs (SI Appendix, Fig. S5D). Our structure would also suggest that shortening loop III would remove the overlap with tetracycline, consistent with the lack of activity of TetO mutants where two residues were deleted from loop III (20). Although tigecycline exhibits an even greater overlap with TetM (Fig. 3E), we believe that, in addition to the increased affinity of tigecycline compared with tetracycline (10, 11, 38), the C9-glycyl substituent of tigecycline hinders access of the loop III residues to C1054 and thus contributes to tigecyclines ability to overcome TetM-mediated resistance (6, 11).

Stabilization of Loop III Is Critical for TetM Activity. Given that Ser508 and Pro509 located at the tip of Loop III are invariant in all available RPP sequences (SI Appendix, Fig. S5D), it is somewhat surprising that these and neighboring residues can be mutated to alanine with little or no effect on RPP activity (3, 19). Similarly, the double SP508-509/AA and triple SPV508-510/AAA mutants of TetM were also shown to retain tetracycline resistance activity (19). In silico mutagenesis based on our refined model indicated that if loop III of the triple SPV508-510/AAA mutant adopts the same conformation as the wildtype TetM then the backbone of Ala509 would maintain a steric clash with tetracycline (Fig. 4A), providing a possible explanation for the retention in activity of the mutant. In contrast, mutation of Y506/Y507 completely inactivates TetM/TetO (3, 19, 20), indicating an important role for these tyrosine residues. Indeed, in our structure, both tyrosines are involved in intradomain interactions linking loop III with loops I and II (Fig. 4B). Specifically, Y507 comes within 3.5 Å of E435 within loop I and the side chain OH of Y506 is within hydrogen bonding distance to

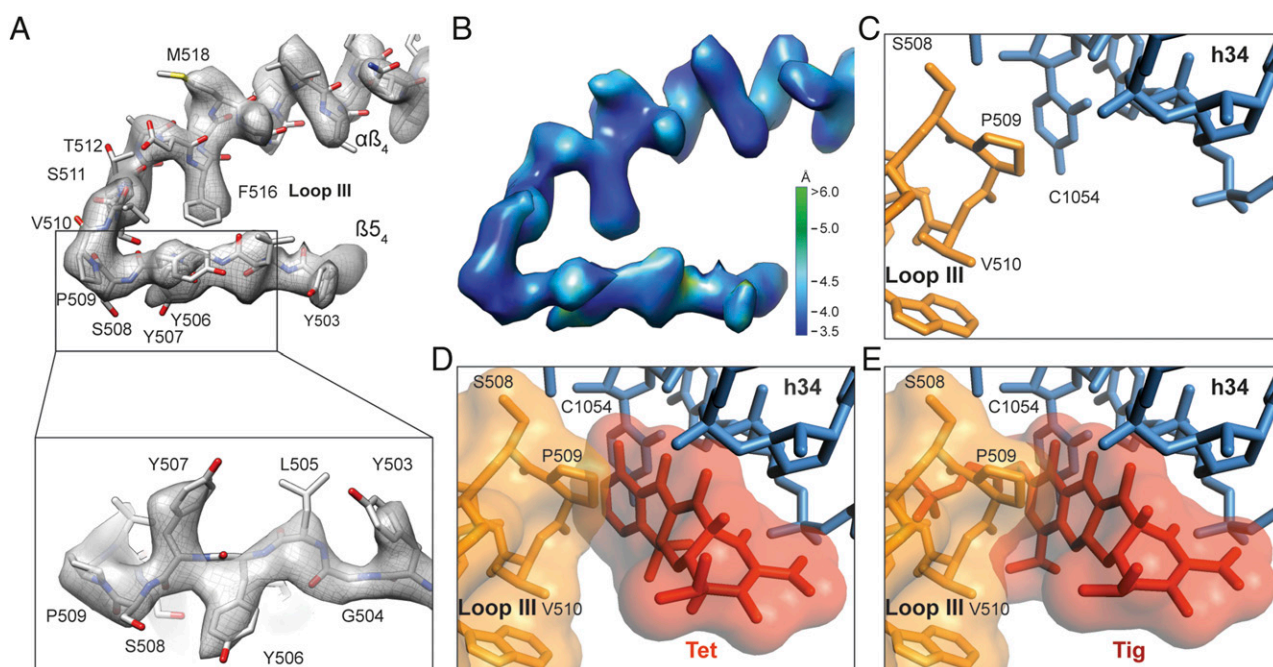


Fig. 3. The role of loop III in TetM in tetracycline resistance. (A and B) Extracted Cryo-EM density of loop III of domain IV in TetM (gray mesh) with molecular model for loop III (A) and colored according to local resolution (B). (C) Stacking interaction of P509 at the tip of loop III (orange) with nucleotide C1054 of h34 of the 16S rRNA (blue). (D and E) Comparison of the binding positions of loop III of TetM domain IV (orange) with (D) tetracycline (Tet) and (E) tigecycline (Tig; ref. 6).

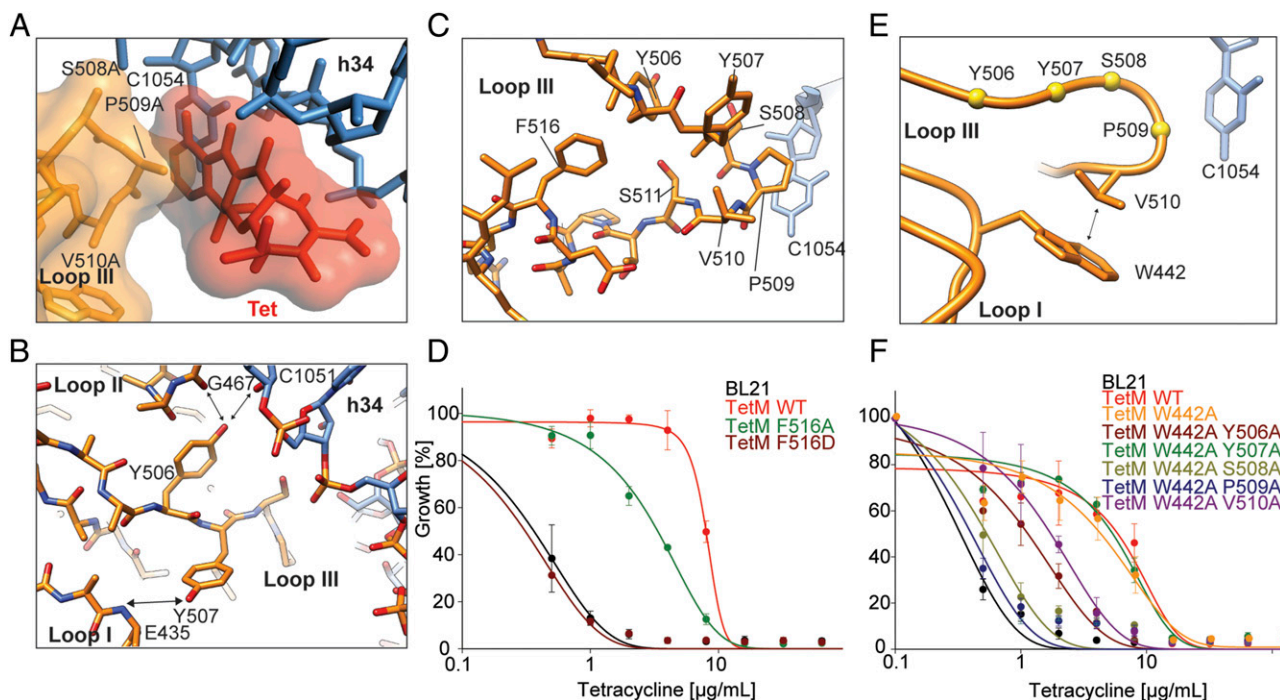


Fig. 4. Stabilization of loop III in TetM via intra-TetM interactions ensures TetM activity. (A) Relative binding position of TetM triple mutant SPV508-510AAA (orange) and tetracycline (Tet, red; ref. 6). (B) Tyrosine residues Y506 and Y507 of loop III of TetM domain IV (orange) stabilize the conformation of loop III via interactions with G467 of loop II, 16S rRNA residue C1051 and residue E435 of loop I, respectively. (C) Localization of TetM residue F516 within the hydrophobic pocket formed by loop III. (D) Growth curves of wildtype *E. coli* strain BL21 (black) in the presence of increasing concentrations of tetracycline (0–128 $\mu\text{g}/\text{mL}$) compared with the wildtype strain harboring a plasmid encoding wildtype TetM (red) and TetM single mutants F516A (green) and F516D (brown). (E) Interaction between the sidechain V510 of loop III of TetM with the invariant tryptophan (W442) located in loop I. (F) as in D but with TetM mutant W442A (orange) and the double mutants W442A/Y506A (brown), W442A/Y507A (green), W442A/S508A (olive), W442A/P509A (blue) and W442A/V510A (violet). In D and F, the error bars represent the SD from the mean for three independent experiments.

the carbonyl of G467 in loop II, as well as to the ribose 2' OH of C1051 in h34 of the 16S rRNA (Fig. 4B). Collectively, these results suggest that the role of Y506 and Y507 within loop III is to stabilize the conformation of loop III.

To further investigate the importance of the stabilization of loop III for TetM activity, we analyzed the activity of two additional TetM mutants: The first mutations were introduced at position F516. F516 is invariant in all RPP sequences (*SI Appendix, Fig. S5D*), and the phenylalanine side chain is well resolved within the hydrophobic core of loop III, where it clamps the proximal end of helix αB_4 to the distal end of strand β_5 (Figs. 3A and 4C). To monitor activity of TetM, the growth of wild-type *Escherichia coli* strain BL21 (–TetM) in the presence of increasing concentrations of tetracycline (0–128 $\mu\text{g}/\text{mL}$) was

compared with the same strain bearing a plasmid overexpressing either *Enterococcus faecalis* TetM (+TetM) or one of the TetM variants (Fig. 4D). In the absence of TetM, the wild-type *Escherichia coli* strain (black circles) is sensitive to tetracycline with a minimal inhibitory concentration (MIC_{50}) of $\sim 0.6 \mu\text{g}/\text{mL}$, whereas as before (19), overexpression of *Enterococcus faecalis* TetM (red circles) raises the MIC_{50} by 14-fold to $\sim 10 \mu\text{g}/\text{mL}$ (Fig. 4D). Although mutation of F516 to alanine (F516A) had a modest affect on TetM activity ($\text{MIC}_{50} \sim 3 \mu\text{g}/\text{mL}$), mutation of F516 to the negatively charged Asp (F516D) led to a complete loss of activity (Fig. 4D), consistent with the importance of F516 for providing a hydrophobic environment to maintain the defined conformation of loop III necessary for tetracycline release. Another possible source of stabilization of Loop III is the

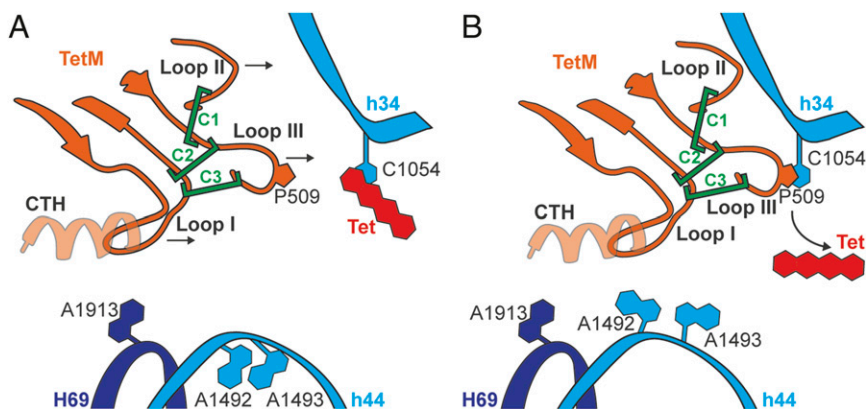


Fig. 5. Schematic model for TetM-mediated tetracycline resistance. (A and B) Upon TetM binding to tetracycline bound ribosomes, the proline residue P509 located at the tip of loop III of domain IV is directly responsible for chasing the drug off the ribosome by interacting with its binding site nucleotide C1054 of the 16S rRNA. (B) TetM binding to the ribosome leads to interaction of the C-terminal helix (CTH) with 23S rRNA nucleotide A1913 (dark blue) and induces 16S rRNA decoding nucleotides A1492 and A1493 (blue) to flip out of helix 44 (h44) of the 16S rRNA. Intramolecular interactions that stabilize the conformation of loop III are represented as green clamps with C1 illustrating the interaction Y506/G467, C2 for Y507/E435 and C3 for V510/W442.

interaction between the side chain of V510 and an invariant tryptophan (W442) located within loop I (Fig. 4E). Although mutation of W442 to alanine (W442A) alone did not affect the activity of TetM, the presence of the W442A mutation made loop III sensitive to secondary mutations. In particular, mutations of S508 or P509 to alanine in the context of W442A abolished TetM activity (Fig. 4F), whereas wild-type activity was observed for TetM with single S508A or P509A mutations (19). Collectively, these results illustrate the importance of the structural integrity of loop III in the positioning residues S508 and P509 located at the tip of loop III, which is necessary for efficient tetracycline resistance.

Conclusion

In conclusion, our structure enables a molecular model to be presented for how TetM confers resistance to tetracycline by dislodging the drug from its binding site on the ribosome (Fig. 5 A and B): Specifically, Pro509 within loop III of domain IV of TetM directly overlaps in position with ring D of tetracycline and thus dislodges the drug from the ribosome. TetM is proposed to prevent rebinding of tetracycline by altering the conformation of nucleotides such as C1054 within the drug binding site that persist following TetM dissociation (12, 18, 19, 32). Within the constraints of the current resolution, TetM does not appear to alter the conformation of C1054 to prevent drug rebinding (*SI Appendix, Fig. SSE*), however, we cannot rule out that such an alteration occurs during GTP hydrolysis and dissociation of TetM from the ribosome. Previous studies identified two conserved tyrosines within loop III of TetM as being important for tetracycline resistance (3, 19, 20). Here we show that these tyrosine residues are not directly involved in displacing the drug

from its binding site, but rather act like clamps (termed C1 and C2) that stabilize the loop III of domain IV of TetM by establishing intradomain interactions with loop I and II of TetM (Fig. 5A). We also identify an additional clamp C3 between loop I and III that is important for stabilization of loop III. Additionally, domain IV of TetM is positioned on the ribosome for tetracycline displacement via interaction of loop I and the CTH with residues located within intersubunit bridge B2a, namely, A1913 of H69 of the 23S rRNA and a splayed conformation of decoding site nucleotides A1492 and A1493 (Fig. 5B). We believe that the molecular details and mechanism of action reported here for TetM will be conserved for other ribosome protection proteins, such as TetO, that also confer resistance to tetracycline.

Materials and Methods

Enterococcus faecalis TetM was purified as described (34) and bound to ErmCL-RNC (22). Cryo-EM data were collected using the EPU software on a Titan Krios TEM (FEI) and processed using the SPIDER software package (25). The backbone model of *Enterococcus faecalis* TetM was initially generated using HHpred (39), then manually fitted using Chimera (40) and refined using Coot (41) and PHENIX (42). A structure of the *Escherichia coli* 70S ribosome (43) was fitted the cryo-EM density using Chimera (40), manually adjusted and then refined with Coot (41). Site-specific mutations were introduced into the *tetM* gene using KOD Xtreme Hot Start Polymerase according to the manufacturers instructions and minimal inhibitory concentrations were determined as described (11, 19). Detailed materials and methods can be found in the *SI Appendix, SI Materials and Methods*.

ACKNOWLEDGMENTS. We thank Rishi Matadeen and Sacha DeCarlo for data collection at the NeCEN facility (Leiden, Netherlands) and Dr. A. L. Starosta for helpful comments. This work was supported by the Deutsche Forschungsgemeinschaft GRK1721 and FOR1805 (WI3285/3-1, to D.N.W.).

- Wilson DN (2009) The A-Z of bacterial translation inhibitors. *Crit Rev Biochem Mol Biol* 44(6):393–433.
- Wilson DN (2014) Ribosome-targeting antibiotics and mechanisms of bacterial resistance. *Nat Rev Microbiol* 12(1):35–48.
- Nguyen F, et al. (2014) Tetracycline antibiotics and resistance mechanisms. *Biol Chem* 395(5):559–575.
- Brodersen DE, et al. (2000) The structural basis for the action of the antibiotics tetracycline, pactamycin, and hygromycin B on the 30S ribosomal subunit. *Cell* 103(7):1143–1154.
- Pioletti M, et al. (2001) Crystal structures of complexes of the small ribosomal subunit with tetracycline, edeine and IF3. *EMBO J* 20(8):1829–1839.
- Jenner L, et al. (2013) Structural basis for potent inhibitory activity of the antibiotic tigecycline during protein synthesis. *Proc Natl Acad Sci USA* 110(10):3812–3816.
- Roberts MC (2005) Update on acquired tetracycline resistance genes. *FEMS Microbiol Lett* 245(2):195–203.
- Chopra I, Roberts M (2001) Tetracycline antibiotics: Mode of action, applications, molecular biology, and epidemiology of bacterial resistance. *Microbiol Mol Biol Rev* 65(2):232–260.
- Chopra I (2002) New developments in tetracycline antibiotics: Glycylcyclines and tetracycline efflux pump inhibitors. *Drug Resist Updat* 5(3–4):119–125.
- Bergeron J, et al. (1996) Glycylcyclines bind to the high-affinity tetracycline ribosomal binding site and evade Tet(M)- and Tet(O)-mediated ribosomal protection. *Antimicrob Agents Chemother* 40(9):2226–2228.
- Grossman TH, et al. (2012) Target- and resistance-based mechanistic studies with TP-434, a novel fluorocycline antibiotic. *Antimicrob Agents Chemother* 56(5):2559–2564.
- Connell SR, Tracz DM, Nierhaus KH, Taylor DE (2003) Ribosomal protection proteins and their mechanism of tetracycline resistance. *Antimicrob Agents Chemother* 47(12):3675–3681.
- Leipe DD, Wolf YI, Koonin EV, Aravind L (2002) Classification and evolution of P-loop GTPases and related ATPases. *J Mol Biol* 317(1):41–72.
- Burdett V (1996) Tet(M)-promoted release of tetracycline from ribosomes is GTP dependent. *J Bacteriol* 178(11):3246–3251.
- Trieber CA, Burkhardt N, Nierhaus KH, Taylor DE (1998) Ribosomal protection from tetracycline mediated by Tet(O): Tet(O) interaction with ribosomes is GTP-dependent. *Biol Chem* 379(7):847–855.
- Spahn CM, et al. (2001) Localization of the ribosomal protection protein Tet(O) on the ribosome and the mechanism of tetracycline resistance. *Mol Cell* 7(5):1037–1045.
- Burdett V (1991) Purification and characterization of Tet(M), a protein that renders ribosomes resistant to tetracycline. *J Biol Chem* 266(5):2872–2877.
- Connell SR, et al. (2002) The tetracycline resistance protein Tet(o) perturbs the conformation of the ribosomal decoding centre. *Mol Microbiol* 45(6):1463–1472.
- Dönhöfer A, et al. (2012) Structural basis for TetM-mediated tetracycline resistance. *Proc Natl Acad Sci USA* 109(42):16900–16905.
- Li W, et al. (2013) Mechanism of tetracycline resistance by ribosomal protection protein Tet(O). *Nat Commun* 4:1477.
- Thakor NS, et al. (2008) Chimeras of bacterial translation factors Tet(O) and EF-G. *FEBS Lett* 582(9):1386–1390.
- Arenz S, et al. (2014) Drug sensing by the ribosome induces translational arrest via active site perturbation. *Mol Cell* 56(3):446–452.
- Arenz S, et al. (2014) Molecular basis for erythromycin-dependent ribosome stalling during translation of the ErmBL leader peptide. *Nat Commun* 5:3501.
- Byrgazov K, et al. (2015) Structural basis for the interaction of protein S1 with the *Escherichia coli* ribosome. *Nucleic Acids Res* 43(1):661–673.
- Frank J, et al. (1996) SPIDER and WEB: Processing and visualization of images in 3D electron microscopy and related fields. *J Struct Biol* 116(1):190–199.
- Fernández IS, Bai XC, Murshudov G, Scheres SH, Ramakrishnan V (2014) Initiation of translation by cricket paralysis virus IRES requires its translocation in the ribosome. *Cell* 157(4):823–831.
- Hussain T, et al. (2014) Structural changes enable start codon recognition by the eukaryotic translation initiation complex. *Cell* 159(3):597–607.
- Voorhees RM, Fernández IS, Scheres SH, Hegde RS (2014) Structure of the mammalian ribosome-Sec61 complex to 3.4 Å resolution. *Cell* 157(7):1632–1643.
- Shao S, Brown A, Santhanam B, Hegde RS (2015) Structure and assembly pathway of the ribosome quality control complex. *Mol Cell* 57(3):433–444.
- Gao YG, et al. (2009) The structure of the ribosome with elongation factor G trapped in the posttranslational state. *Science* 326(5953):694–699.
- Harms JM, et al. (2008) Translational regulation via L11: Molecular switches on the ribosome turned on and off by thiostrepton and micrococin. *Mol Cell* 30(1):26–38.
- Connell SR, et al. (2003) Mechanism of Tet(O)-mediated tetracycline resistance. *EMBO J* 22(4):945–953.
- Starosta AL, et al. (2009) Identification of distinct thiopeptide-antibiotic precursor lead compounds using translation machinery assays. *Chem Biol* 16(10):1087–1096.
- Mikolajka A, et al. (2011) Differential effects of thiopeptide and orthosomycin antibiotics on translational GTPases. *Chem Biol* 18(5):589–600.
- Voorhees RM, Schmeing TM, Kelley AC, Ramakrishnan V (2010) The mechanism for activation of GTP hydrolysis on the ribosome. *Science* 330(6005):835–838.
- Demeshkina N, Jenner L, Westhof E, Yusupov M, Yusupova G (2012) A new understanding of the decoding principle on the ribosome. *Nature* 484(7393):256–259.
- Ogle JM, Carter AP, Ramakrishnan V (2003) Insights into the decoding mechanism from recent ribosome structures. *Trends Biochem Sci* 28(5):259–266.
- Olson MW, et al. (2006) Functional, biophysical, and structural bases for antibacterial activity of tigecycline. *Antimicrob Agents Chemother* 50(6):2156–2166.
- Soding J, Biegert A, Lupas AN (2005) The HHpred interactive server for protein homology detection and structure prediction. *Nucleic Acids Res* 33(Web server issue):W244–W248.
- Pettersen EF, et al. (2004) UCSF Chimera—a visualization system for exploratory research and analysis. *J Comput Chem* 25(13):1605–1612.
- Emsley P, Cowtan K (2004) Coot: Model-building tools for molecular graphics. *Acta Crystallogr D Biol Crystallogr* 60(Pt 12 Pt 1):2126–2132.
- Adams PD, et al. (2010) PHENIX: A comprehensive Python-based system for macromolecular structure solution. *Acta Crystallogr D Biol Crystallogr* 66(Pt 2):213–221.
- Fischer N, et al. (2015) Structure of the *E. coli* ribosome-EF-Tu complex at <3 Å resolution by C-corrected cryo-EM. *Nature*, 10.1038/nature14275.

Supporting Information

Arenz et al

SI Materials and Methods

Purification of TetM protein

Enterococcus faecalis TetM from TnFO1 (Q47810) was cloned into pET-46 Ek/LIC (Novagene) with an N-terminal 6x histidine tag. The plasmid was transformed into *E. coli* BL21(DE3) (Novagene) and incubated at 37°C/120 rpm overnight in 20 mL LB medium containing 100 µg/mL ampicillin. A volume of 20 mL overnight culture was used to inoculate 1.6 L of LB medium containing 100 µg/mL ampicillin. The culture was grown at 37°C/120 rpm to an OD₆₀₀ of 0.3. The temperature was then reduced to 30°C and 16 mL of ethanol was added until the OD₆₀₀ value reached 0.6. Expression of TetM was induced by adding 1.6 ml of 1mM IPTG. After 2hrs, cells were harvested by centrifugation at 3000 x g for 15 min at 4°C and subsequently resuspended in 25 mL Lysis buffer (50 mM NaH₂PO₄, 300 mM NaCl, 5 mM Imidazole, pH 8.0). Cells were lysed using the M-110L Microfluidizer (Microfluidics) and the lysate cleared by centrifugation at 17000 x g for 15 min at 4°C. The cleared lysate was then incubated at 4°C for 1h with 1 mL Ni-NTA agarose beads (Machery-Nagel) and loaded onto a 20 mL Econopac Chromatography column (Biorad). Beads were washed twice with 5 mL Wash buffer (50 mM NaH₂PO₄, 300 mM NaCl, 10 mM Imidazole, pH 8.0) and eluted in 2 mL Elution buffer (50 mM NaH₂PO₄, 300 mM NaCl, 250 mM Imidazole, pH 8.0). The eluate was further purified by gel filtration using a Superdex™ 75 pg column (Amersham) and GF buffer (50 mM Hepes, 100 mM KCl, 200 mM NaCl, 10 mM MgCl₂, 5 mM β-Mercaptoethanol, 10% Glycerol).

Site directed mutagenesis

Site directed mutagenesis was performed using the whole plasmid PCR method. Primers are attached in **Supplementary Table 2**. *E. faecalis tetM* on pET-46 Ek/LIC (Novagene) was used as a template. Double mutants W442A + loop III were produced using loop III mutants as templates (1). KOD Xtreme™ Hot Start Polymerase (Novagene) was used in the following PCR program: 94°C 2 min; 20x (98°C 10sec, 63°C 30sec, 68°C 7min); 68°C 7min.

Generation and purification of ErmCL-SRC

ErmCL-SRC was generated following the same procedure as previously described (2). The 2*XermCL* construct contained a T7 promoter followed by a strong ribosome binding site (RBS) spaced by 7 nucleotides (nts) to the ATG start codon of the first *ermCL* cistron. A linker of 22

nts separated the stop codon of the first *ermCL* cistron and the start codon of the second *ermCL* cistron. The linker also comprised the strong RBS 7 nts upstream of the ATG start codon of the second *ermCL* cistron, enabling initiation of translation independent from the first *ermCL* cistron. Each *ermCL* cistron encoded amino acids 1-19 corresponding to ErmCL leader peptide (Genbank accession number V01278) present on macrolide resistance plasmid pE194 (3, 4). *In vitro* translation of the *2xermCL* construct was performed using the Rapid Translation System RTS 100 *E. coli* HY Kit (Roche) and was carried-out in the presence of 10 μ M erythromycin (ERY) for 1h at 30 °C. The ErmCL-SRC was purified from the disome fractions on sucrose gradients and concentrated using Amicon Ultra-0.5 mL Centrifugal Filters (Millipore). Monosomes of the ErmCL-SRC were obtained by annealing a short DNA oligonucleotide (5'-ttctcttataaaact-3', Metabion) to the linker between the *ermCL* cistrons of the disomes, generating a DNA-RNA hybrid that was cleaved by RNase H (NEB) treatment in buffer A at 25°C for 1h. The ErmCL-SRC monosomes were then purified and concentrated using the Amicon Ultra-0.5 mL Centrifugal Filters (Millipore).

Generation of TetM•RNCs

The ErmCL-SRC (0.5 μ M) was incubated with a 4-fold excess (2 μ M) of purified recombinant TetM protein in the presence of 500 μ M GDPCP in buffer A (50 mM HEPES-KOH, pH7.4, 100 mM KOAc, 25 mM Mg(OAc)₂, 6 mM β -mercaptoethanol, 100 μ M evernimicin and 10 μ M erythromycin) for 30 min at 30°C. Thereafter, the binding reaction was diluted using buffer A to yield a final ribosome concentration of 4 A₂₆₀/ml for cryo-grid preparation.

Cryo-electron microscopy and single particle reconstruction

The TetM•RNC (4 A₂₆₀/ml) was applied to 2 nm pre-coated Quantifoil R3/3 holey carbon supported grids and vitrified using a Vitrobot Mark IV (FEI Company). Data collection was performed using the EPU software at NeCEN (Leiden, Netherlands) on a Titan Krios transmission electron microscope (TEM) (FEI, Holland) equipped with a Falcon II direct electron detector at 300 kV with a magnification of 125,085x, a pixelsize of 1.108 Å and a defocus range of 0.9-2.2 μ m. The data were provided as a series of seven frames (dose per frame is 4 e⁻/Å²) from which we summed frames 1-6 (accumulated dose of 24 e⁻/Å²) after alignment using Motion Correction software (5). Images were processed using a frequency-limited refinement protocol that helps prevent over-fitting (6), specifically by truncation of high frequencies (in this case at 7-8 Å using a Butterworth filter). Power spectra and defocus values were determined using the SPIDER TF ED command and recorded images were manually inspected for good areas and power-spectra quality. Data were processed further using the

SPIDER software package (7), in combination with an automated workflow as described previously (8). After initial, automated particle selection based on the program SIGNATURE (9), initial alignment was performed with 127,205 particles, using *E. coli* 70S ribosome as a reference structure (2). After removal of noisy particles (22,207 particles), the dataset could be sorted into two main subpopulations using an incremental K-means-like method of unsupervised 3D sorting (10): The first subpopulation (26,814 particles; 25%) was defined by the presence of stoichiometric density for P-site tRNA. The second, major subpopulation (78,186 particles; 75%) was defined by the presence of stoichiometric densities for P-tRNA and TetM (*SI Appendix, Figure S1A*), and could be refined further to produce a map with an average resolution of 3.9 Å (0.143 FSC, *SI Appendix, Figure S1B*). The final refined map was subjected to the program EMBFACTOR (11) in order to apply an automatically determined negative B-factor for sharpening of the map. Local resolution calculations were performed using Resmap (12) revealing that the resolution of the majority of the core of the 30S and 50S subunits extended to 3.5 Å (*SI Appendix, Figure S1C*).

Molecular modelling and map-docking procedures

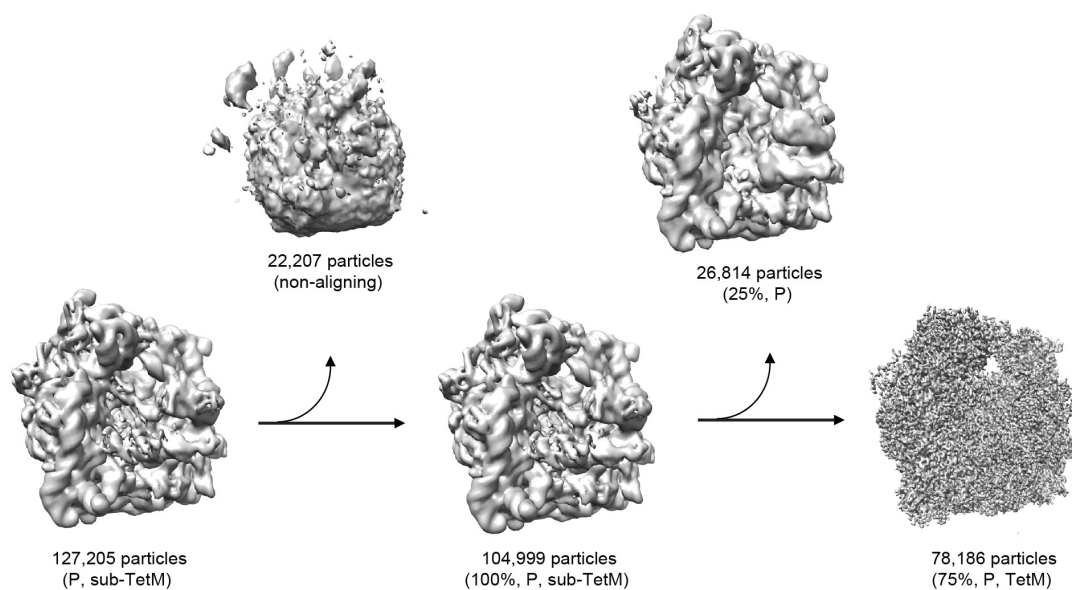
The initial molecular model for the 70S ribosome of the TetM•RNC was based on the cryo-EM structure of an *E. coli* 70S ribosome (PDB ID 5AFI, (13)). The 30S and 50S subunits were fitted as rigid bodies and were manually adjusted and refined in Coot (14). The model for the C-terminal domain of L7 was based on a rigid body fit of the NMR structure of L7/L12 (1RQU, (15)). The molecular model for TetM was initially based on a homology model using EF-G as a template (generated by HHPred (16) and Modeller (17)). The model was split into five domains, which were individually fitted into the EM density as rigid bodies and then manually adjusted and refined using Coot (14) and PHENIX (18). Since the resolution of domains I-III and V of TetM was insufficient to model the amino acid side chains, only a backbone trace was generated. Domain IV of TetM was resolved up to 3.5 Å allowing the bulky amino acid side-chains in loop III to be modelled.

Figure preparation

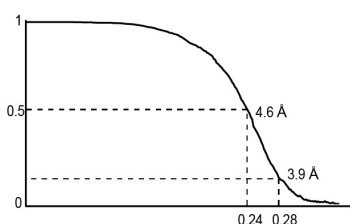
Figures showing electron densities and atomic models were generated using UCSF Chimera (19) and PyMOL Molecular Graphics System (Version 1.5.0.4 Schrödinger, LLC).

Supplementary Figures

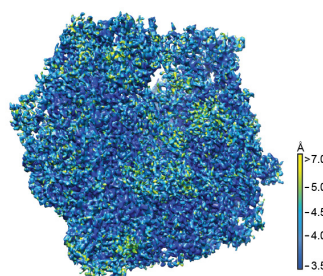
A



B



C



D

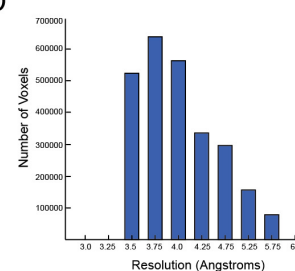


Figure S1 Cryo-EM reconstruction of the TetM•RNC. (A) *In silico* sorting of the TetM•RNC dataset. After removal of non-aligning and edge particles, sorting of the dataset yielded two homogenous sub-datasets. The vast majority of the particles (75%; 78,186 particles in total) contained stoichiometric density for P-tRNA as well as for TetM and this subpopulation was chosen for refinement. (B) Fourier-shell correlation curve of the refined final map, indicating the average resolution of the TetM•RNC is 3.9 Å. (C) Overview of the TetM•RNC colored according to the local resolution as calculated using ResMap (12). (D) Histogram generated by ResMap showing the number of voxels of the cryo-EM map of the TetM•RNC distributed across the resolution bins ranging from 3.5 Å to 6.0 Å.

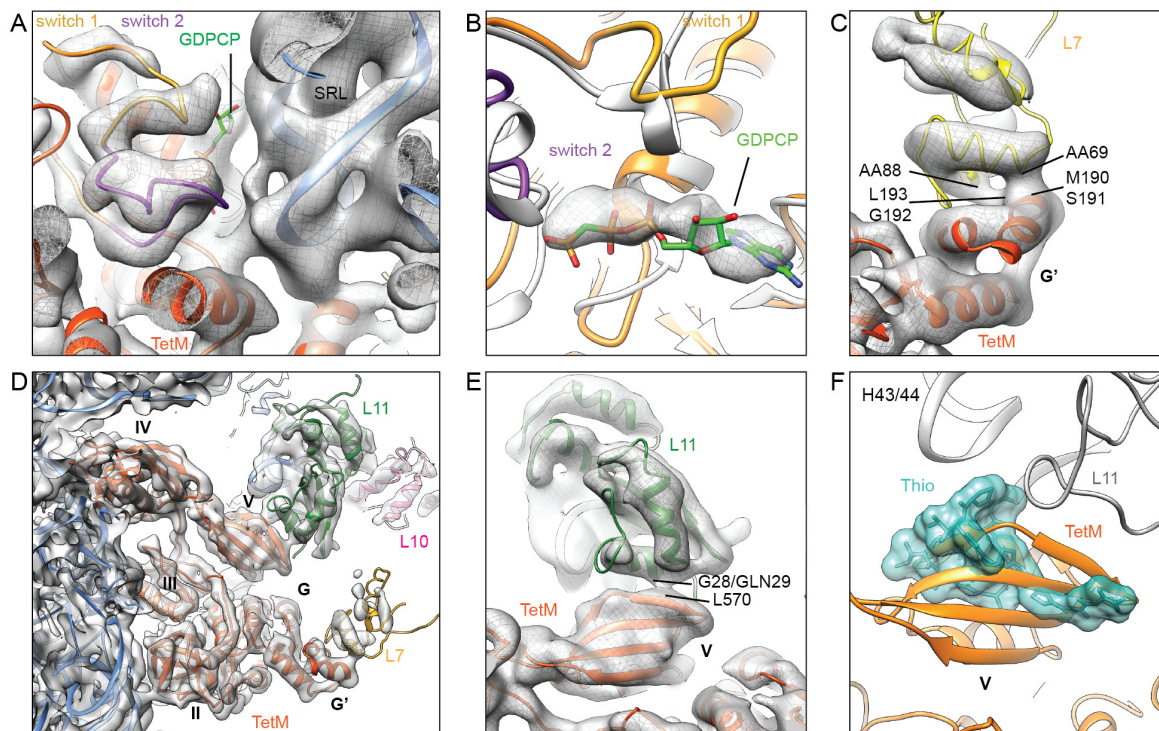


Figure S2 Interaction of TetM with the large ribosomal subunit. (A) Interaction of the G domain of TetM with the sarcin-ricin loop (SRL) of the 23S rRNA (blue). The switch 1 (yellow) and switch 2 (purple) loops are indicated, as is the putative position for the GDPCP molecule (green). (B) Comparison of the conformation of switch 1 and 2 loops of TetM with equivalent region of EF-G (PDB ID 4CR1). Putative density for GDPCP molecule (grey mesh) corresponds with the position of the GDPNP molecule (green) from the EF-G structure (PDB ID 4CR1) aligned to the TetM based on the G domain. (C) Interaction between the C-terminal domain of L7/L12 (yellow) and the G' domain of TetM (orange). (D) Overview of TetM (orange) showing interaction with L7 (yellow) and L11 (green). (E) Interaction between L11 (green) and domain V of TetM (orange). (F) Overlap in the binding site of domain V of TetM (orange) with the antibiotic thioStrepton (cyan). In panels (A) and (C-E), the cryo-EM density for the TetM-RNC is shown as a grey mesh.

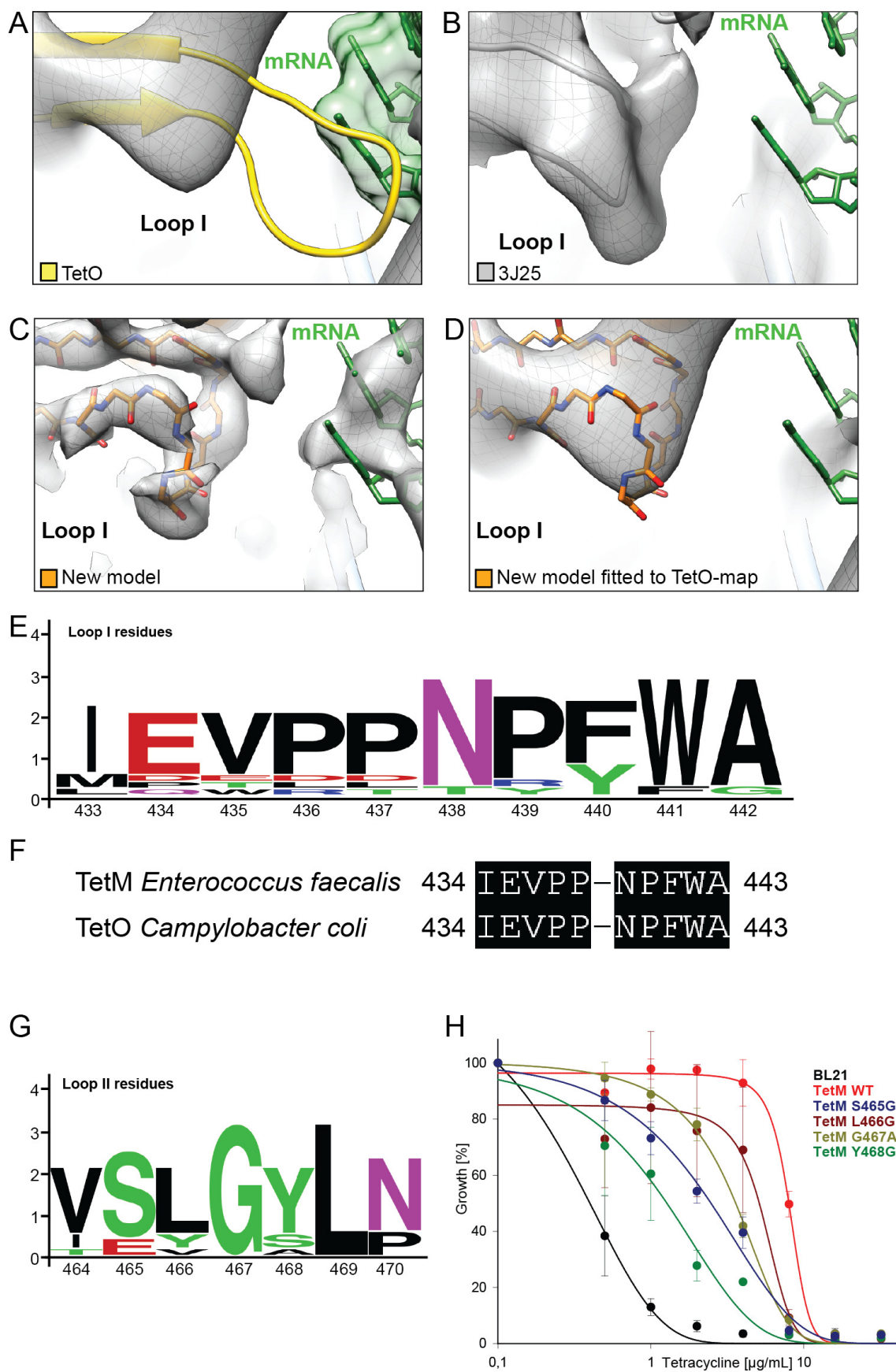


Figure S3 Analysis of loops I and II of domain IV of TetM. (A-D) Cryo-EM map (grey mesh) of (A, D) TetO•70S complex (20), (B) TetM•70S complex (1) and (C) TetM•RNC, with molecular model for loop I of domain IV of (A) TetO (yellow, (20)), (B) TetM (grey, PDB

3J25, (1)) and (C, D) the revised molecular model for loop I of domain IV of TetM based on the cryo-EM map of the TetM•RNC at 3.9 Å resolution (orange). (E) Logo-Plot of residues 433-443 of loop I of domain IV of TetM, numbered according to *Enterococcus faecalis* TetM. (F) Sequence alignment of residues 433-443 of loop I of *Enterococcus faecalis* TetM and *Campylobacter coli* TetO. (G) Logo-plot of residues 464-470 forming loop II of TetM domain IV. (H) Growth curves of wildtype *E. coli* strain BL21 (black) in the presence of increasing concentrations of tetracycline (0-128 µg/ml) compared with the wildtype strain harboring a plasmid encoding wildtype TetM (red) or TetM single mutants S465G (blue), L466G (brown), G467A (olive) and Y468G (green).

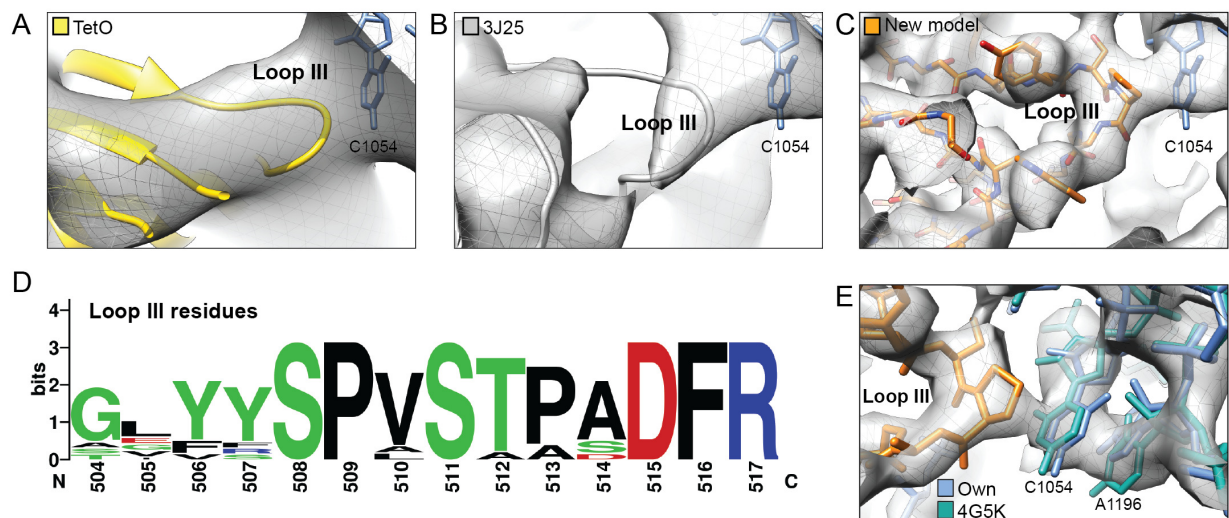


Figure S5 Structures of loop III of domain IV in TetO and TetM. (A-C) Cryo-EM map (grey mesh) of (A) TetO•70S complex (20), (B) TetM•70S complex (1) and (C) TetM•RNC, with molecular model for loop III of domain IV of (A) TetO (yellow, (20)), (B) TetM (grey, PDB 3J25, (1)) and (C) the revised molecular model for loop I of domain IV of TetM based on the cryo-EM map of the TetM•RNC at 3.9 Å resolution (orange). (D) Logo-Plot of residues 504-517 of loop III of domain IV of TetM, numbered according to *Enterococcus faecalis* TetM. (E) Cryo-EM density (grey mesh) the TetM•RNC with molecular models for TetM (orange), and a comparison of the conformation of C1054 of the 16S rRNA from the TetM•RNC (blue) with the tetracycline-bound conformation (cyan, (21)).

Supplementary Table 1

TetM			Ribosome	
Domain	Region	Residue	Region	Residue
G				
	loop between 1 ₁ and A ₁	V12	23S rRNA, H95 (SRL)	G2661
	loop between A ₁ and 2 ₁	G53	23S rRNA, H95 (SRL)	G2663
	loop between 3 ₁ and B ₁	H78	23S rRNA, H95 (SRL)	A2662
	loop between 4 ₁ and C ₁	K102	23S rRNA, H95 (SRL)	A2657
	C1	A107	23S rRNA, H95 (SRL)	G2661
	loop between 5 ₁ and D ₁	Q132	23S rRNA, H95 (SRL)	A2657
	loop between 5 ₁ and D ₁	G134	L6	V91, G92
G'	B _G	M190,S191	L7-CTD, helix α 4	V69
	B _G	G192,L193	L7-CTD, helix α 4	V88
II	3 ₂	R278	16S rRNA, h5 (body)	U368
	5 ₂	T292	16S rRNA, h5 (body)	U358
	6 ₂	L304	16S rRNA, h5 (body)	A55
III	A ₃	D363	S12	H77
IV	loop II between 4 ₄ and A ₄	S465, L466, G467	16S rRNA, h34 (head)	backbone C1214, C1209, C1051
	loop III between 5 ₄ and B ₄	Y506, S508, P509	16S rRNA, h34 (head)	backbone C1051 U1052, C1054
	loop III between 5 ₄ and B ₄	P513	16S rRNA, h18 (body)	C518
	loop III between 5 ₄ and B ₄	R517	16S rRNA, h18 (body)	C519
V	A5	Y555	23S rRNA, H43/H44	A1095
	A5	K560	23S rRNA, H89	U2473
	2 ₅	L570	L11 3 ₁₀ -helix	G28, Q29
	B5	T594, F595	L6	K175, K176
	B5	T594, F595	23S rRNA, H95 (SRL)	A2660
	B5	N598, G599	23S rRNA, H95 (SRL)	A2660
CTE	loop between 4 ₅ and C ₅	R627	S12	L49
	C ₅	R632	23S rRNA, H69	C1913
	C ₅	F635, N636	23S rRNA, H69	C1914

Supplementary Table 2

Construct	Primer sense/ antisense (5' – 3')
TetM W442A	5'-GTGCCGCAAATCCTTTCGCGGCTTCCATTGGTTTATCTGTATCACCGCTTC-3' 5'-GATAAACCAATGGAAGCCGCGAAAGGATTTGGCGGCACTTCGATGTGAATG-3'
TetM S465G	5'-CAGTATGAGAGCTCGGTTGGCCTTGGATACTTAAATCAATCATTTC-3' 5'-GATTTAAGTATCCAAGGCCAACCGAGCTCTCATACTGCATTCCAC-3'
TetM L466G	5'-GAGAGCTCGGTTTCTGGCGGATACTTAAATCAATCATTTCAAAATG-3' 5'-GATTGATTTAAGTATCCGCCAGAAACCGAGCTCTCATACTGCATTTC-3'
TetM G467A	5'-GAGCTCGGTTTCTCTTGGCTACTTAAATCAATCATTTCAAAATGCAG-3' 5'-GAAATGATTGATTTAAGTACGCCAAGAGAAACCGAGCTCTCATACTGCATTTC-3'
TetM Y468G	5'-CTCGGTTTCTCTTGGAGGCTTAAATCAATCATTTCAAAATGCAG-3' 5'-GAAATGATTGATTTAAGCCTCCAAGAGAAACCGAGCTCTCATACTGCATTTC-3'
TetM F516A	5'-GTTAGTACCCAGCAGATGCGCGGATGCTTGCTCCTATTGTATTGGAAC-3' 5'-CAATAGGAGCAAGCATCCGCGCATCTGCTGGGGTACTAACAGGGCTATAG-3'
TetM F516D	5'-GTTAGTACCCAGCAGATGATCGGATGCTTGCTCCTATTGTATTGGAAC-3' 5'-CAATAGGAGCAAGCATCCGATCATCTGCTGGGGTACTAACAGGGCTATAG-3'

References

1. Dönhöfer A, *et al.* (2012) Structural basis for TetM-mediated tetracycline resistance. *Proc. Natl. Acad. Sci. USA* 109(42):16900-16905.
2. Arenz S, *et al.* (2014) Drug Sensing by the Ribosome Induces Translational Arrest via Active Site Perturbation. *Mol Cell* 56(3):446-452.
3. Iordanescu S (1976) Three distinct plasmids originating in the same *Staphylococcus aureus* strain. *Archives roumaines de pathologie experimentales et de microbiologie* 35(1-2):111-118.
4. Narayanan CS & Dubnau D (1985) Evidence for the translational attenuation model: ribosome-binding studies and structural analysis with an in vitro run-off transcript of *ermC*. *Nucleic Acids Res* 13(20):7307-7326.
5. Li X, *et al.* (2013) Electron counting and beam-induced motion correction enable near-atomic-resolution single-particle cryo-EM. *Nat Methods* 10(6):584-590.
6. Scheres SH & Chen S (2012) Prevention of overfitting in cryo-EM structure determination. *Nat Methods* 9(9):853-854.
7. Frank J, *et al.* (1996) SPIDER and WEB: processing and visualization of images in 3D electron microscopy and related fields. *J Struct Biol* 116(1):190-199.
8. Becker T, *et al.* (2012) Structural basis of highly conserved ribosome recycling in eukaryotes and archaea. *Nature* 482(7386):501-506.
9. Chen JZ & Grigorieff N (2007) SIGNATURE: a single-particle selection system for molecular electron microscopy. *J. Struct. Biol.* 157(1):168-173.
10. Loerke J, Giesebrecht J, & Spahn CM (2010) Multiparticle cryo-EM of ribosomes. *Methods Enzymol* 483:161-177.
11. Fernandez JJ, Luque D, Caston JR, & Carrascosa JL (2008) Sharpening high resolution information in single particle electron cryomicroscopy. *J Struct Biol* 164(1):170-175.
12. Kucukelbir A, Sigworth FJ, & Tagare HD (2014) Quantifying the local resolution of cryo-EM density maps. *Nat Methods* 11(1):63-65.
13. Fischer N, *et al.* (2015) Structure of the *E. coli* ribosome-EF-Tu complex at <3 Å resolution by C-corrected cryo-EM. *Nature*.
14. Emsley P & Cowtan K (2004) Coot: Model-Building Tools for Molecular Graphics. *Acta Crystallographica Section D - Biological Crystallography* 60:2126-2132.
15. Bocharov EV, *et al.* (2004) From structure and dynamics of protein L7/L12 to molecular switching in ribosome. *J. Biol. Chem.* 279(17):17697-17706.
16. Soding J, Biegert A, & Lupas AN (2005) The HHpred interactive server for protein homology detection and structure prediction. *Nucleic Acids Res* 33(Web Server issue):W244-248.
17. Eswar N, Eramian D, Webb B, Shen MY, & Sali A (2008) Protein structure modeling with MODELLER. *Methods Mol Biol* 426:145-159.
18. Adams PD, *et al.* (2010) PHENIX: a comprehensive Python-based system for macromolecular structure solution. *Acta Crystallogr D Biol Crystallogr* 66(Pt 2):213-221.
19. Pettersen EF, *et al.* (2004) UCSF Chimera - A Visualization System for Exploratory Research and Analysis. *J. Comput. Chem.* 25(13):1605-1612.
20. Li W, *et al.* (2013) Mechanism of tetracycline resistance by ribosomal protection protein Tet(O). *Nat. Commun.* 4:1477.
21. Jenner L, *et al.* (2013) Structural basis for potent inhibitory activity of the antibiotic tigecycline during protein synthesis. *Proc Natl Acad Sci U S A* 110(10):3812-3816.

The proline-rich antimicrobial peptide Onc112 inhibits translation by blocking and destabilizing the initiation complex

A Carolin Seefeldt^{1,2,6}, Fabian Nguyen^{3,6}, Stéphanie Antunes^{1,4,6}, Natacha Pérébasquine^{1,2}, Michael Graf³, Stefan Arenz³, K Kishore Inampudi^{1,2}, Céline Douat^{1,4}, Gilles Guichard^{1,4}, Daniel N Wilson^{3,5} & C Axel Innis^{1,2}

The increasing prevalence of multidrug-resistant pathogenic bacteria is making current antibiotics obsolete. Proline-rich antimicrobial peptides (PrAMPs) display potent activity against Gram-negative bacteria and thus represent an avenue for antibiotic development. PrAMPs from the oncocin family interact with the ribosome to inhibit translation, but their mode of action has remained unclear. Here we have determined a structure of the Onc112 peptide in complex with the *Thermus thermophilus* 70S ribosome at a resolution of 3.1 Å by X-ray crystallography. The Onc112 peptide binds within the ribosomal exit tunnel and extends toward the peptidyl transferase center, where it overlaps with the binding site for an aminoacyl-tRNA. We show biochemically that the binding of Onc112 blocks and destabilizes the initiation complex, thus preventing entry into the elongation phase. Our findings provide a basis for the future development of this class of potent antimicrobial agents.

Antimicrobial peptides form a diverse group of molecules that are produced as part of the innate immune response of all multicellular organisms¹. Among these, PrAMPs have garnered considerable attention as a possible means of countering the rapid increase in bacterial resistance to classical antibiotics^{2,3}. Unlike many peptides that kill bacteria by disrupting their cell membrane, PrAMPs are transported into the cytoplasm by specialized transporters, such as SbmA in Gram-negative bacteria^{4,5}, where they inhibit specific intracellular targets. Given that such transport mechanisms are absent in mammalian cells, and only limited interactions with intracellular eukaryotic proteins have been detected, PrAMPs are generally considered to be nontoxic⁶ and therefore an attractive alternative to existing antimicrobials. Interestingly, some PrAMPs can cross the blood-brain barrier to selectively target brain cells, thus further highlighting their potential for the treatment of cerebral infections or for brain-specific drug delivery⁷.

Initial efforts to locate bacterial targets for PrAMPs led to the identification of the heat-shock protein DnaK as the prime candidate for inhibition⁸. Short proline-rich peptides (of 18–20 amino acids (aa)) such as oncocin, drosocin, pyrrolicorin or apidaecin were previously shown to bind to this bacterial chaperone in a stereospecific manner, thus leading to the development of improved PrAMP derivatives with increased affinity for DnaK^{9–12}. However, subsequent studies into the antimicrobial properties of PrAMPs¹³ have suggested that these peptides are likely to use additional modes of action to inhibit growth. For example, a C-terminally truncated version of the apidaecin 1b peptide results in a loss of antimicrobial activity but no observable decrease

in DnaK binding or cellular uptake¹³. Similarly, oncocin (Onc72 and Onc112) and apidaecin (Api88 and Api137) derivatives were found to inhibit the growth of a *dnaK*-deletion strain as efficiently as that of the *dnaK*-containing parental strain¹⁴. Further investigation revealed that these PrAMPs have an additional target within the bacterial cell, namely the ribosome¹⁴. Although such PrAMPs have been shown to bind to the ribosome and inhibit translation¹⁴, the mechanism by which they inhibit translation has so far not been determined.

Here, we set out to address this issue by obtaining a 3.1-Å-resolution X-ray crystallography structure of the *Thermus thermophilus* 70S ribosome (*Th70S*) in complex with a peptidyl (P)-site-bound deacylated tRNA_i^{Met} and Onc112, a representative of the oncocin family of PrAMPs produced by the milkweed bug (*Oncopeltus fasciatus*)¹⁵. The structure reveals that the N-terminal residues 1–12 of Onc112 bind to the upper region of the ribosomal exit tunnel, overlapping the binding site for the CCA end of an aminoacyl (A)-site tRNA at the peptidyl transferase center. Consistently with this, we showed biochemically that Onc112 allows translation to initiate but destabilizes the initiation complex and thus prevents subsequent entry of affected ribosomes into the translation-elongation phase. Moreover, we demonstrated that although truncation of the C-terminal portion of Onc112 is dispensable for ribosome binding, it is essential for antimicrobial activity. We believe that these findings will provide an excellent basis for the design of improved antibacterial compounds, either peptidic or peptidomimetic, that inhibit translation by targeting the ribosomal exit tunnel.

¹Institut Européen de Chimie et Biologie, Université de Bordeaux, Pessac, France. ²INSERM U869, Bordeaux, France. ³Gene Center, Department of Biochemistry, University of Munich, Munich, Germany. ⁴Université de Bordeaux, CNRS, Institut Polytechnique de Bordeaux, UMR 5248, Institut de Chimie et Biologie des Membranes et des Nano-objets (CBMN), Pessac, France. ⁵Center for Integrated Protein Science Munich (CiPSM), University of Munich, Munich, Germany.

⁶These authors contributed equally to this work. Correspondence should be addressed to C.A.I. (axel.innis@inserm.fr) or D.N.W. (wilson@imb.uni-muenchen.de).

Received 26 February; accepted 22 April; published online 18 May 2015; doi:10.1038/nsmb.3034

RESULTS

Onc112 binds in a reverse orientation within the exit tunnel

We obtained the structure herein referred to as *Tth70S*–Onc112 by soaking the 19-aa Onc112 peptide (VDKPPYLPRPRPPPrIYNr-NH₂, in which r denotes D-arginine) into crystals of *Tth70S* ribosomes in complex with a P-site-bound deacylated tRNA_i^{Met} and a short mRNA (Table 1). Using a minimally biased $F_o - F_c$ map calculated after refinement of a model comprising *Tth70S* ribosomes, tRNA_i^{Met} and mRNA but lacking Onc112, we could see clear density that could be attributed to the N-terminal two-thirds of the Onc112 peptide (Fig. 1). Interestingly, the peptide is bound inside the tunnel with a reversed orientation relative to the growing polypeptide chain during protein synthesis, i.e., with its N terminus located near the peptidyl transferase center and its C terminus extending into the exit tunnel toward the constriction formed by ribosomal proteins L4 and L22. Despite the reversed orientation, the location of the Onc112 peptide overlaps to varying extents with the path of nascent polypeptide chains that have been visualized within the ribosomal tunnel^{16–18} (Supplementary Fig. 1). The conformation of Onc112 bound to the ribosome is extended, in a manner similar to but distinct from that observed previously for oncocin in complex with DnaK¹⁰ (Supplementary Fig. 2). Our CD studies suggest that, in solution, the Onc112 peptide adopts an essentially random conformation, with short stretches of poly(Pro)II helix, specifically, 6% α -helix, 54% random coil, 30% PPII and 6% β -sheet (Supplementary Fig. 3).

Interaction between Onc112 and 23S rRNA of the exit tunnel

Comparison of the *Tth70S*–Onc112 structure with that of a *Tth70S* ribosome featuring tRNA_i^{Met} bound to the P site¹⁹ reveals that several nucleotides of the 23S rRNA undergo a conformational change upon binding of Onc112 to the ribosome (Fig. 2a). U2506 shifts to occupy a position similar to that observed upon binding of aminoacyl-tRNA to the A site of the ribosome^{20,21}. In the presence of Onc112, U2585, which is very flexible in many crystal structures, adopts a defined position similar to that modeled in the structure of a vacant *Escherichia coli* 70S ribosome²². In addition, A2062 shifts to provide space for Onc112, adopting a similar conformation to that observed previously in the presence of the ErmBL nascent chain²³. Thus, binding of Onc112 to the ribosome is accompanied by an induced fit involving several 23S rRNA nucleotides that are generally known for their dynamic behavior within the peptidyl transferase center and ribosomal tunnel.

Electron density for the Onc112 peptide was strongest for residues Val1–Pro8 and became weaker after Pro10, thus making it difficult to model the peptide beyond Pro12 (Fig. 1). We observed three sets of interactions between the N-terminal 10 aa of Onc112 and nucleotides of the 23S rRNA (Fig. 2b). The first set involves aa 1–3 of Onc112 and encompasses eight potential hydrogen-bond interactions (Fig. 2b,c). Val1 of Onc112 can form three hydrogen bonds with nucleotides of the 23S rRNA; two via its α -amine to the N3 atom of C2573 and the O3' atom of C2507; and one via its carbonyl oxygen to the N4 atom of C2573. Three additional hydrogen bonds are possible between the side chain carboxylic acid of Asp2 and the N1 and N2 atoms of G2553 or the 2'-OH of C2507. The positively charged side chain of Lys3 extends into a negatively charged cavity, displacing a hydrated magnesium ion that is present at this site in other *Tth70S* ribosome structures²⁰, and it interacts with the backbone phosphates of A2453 (Fig. 2c) and U2493 (not shown). Substitution of Val1, Asp2 and especially Lys3 by alanine in Onc72 leads to a loss of antimicrobial activity¹⁰, whereas, as expected, a D2E mutant of Onc112 retained both *in vitro* and *in vivo* activity (Supplementary Fig. 4). The K3A

Table 1 Data collection and refinement statistics

	<i>Tth70S</i> –Onc112 ^a
Data collection	
Space group	$P2_12_12_1$
Cell dimensions	
<i>a</i> , <i>b</i> , <i>c</i> (Å)	209.30, 452.29, 624.12
α , β , γ (°)	90.0, 90.0, 90.0
Resolution (Å)	50 (3.1)
R_{merge}	25.5% (166.4%)
$I / \sigma I$	5.47 (0.95)
Completeness (%)	99.1 (98.8)
Redundancy	3.8 (3.6)
Refinement	
Resolution (Å)	3.1
No. reflections	3,999,403
$R_{\text{work}} / R_{\text{free}}$	23.08 / 27.13
No. atoms	
Protein / RNA	91,758 / 195,737
Ligand/ion	2,333
B factors	
Protein / RNA	64.81 / 63.15
Ligand/ion	51.31
r.m.s. deviations	
Bond lengths (Å)	0.015
Bond angles (°)	0.809

^aStructure determined from a single crystal.

substitution in Onc72 reduced its ribosome binding affinity by a factor of 4.3 and lowered the half-maximal inhibitory concentration (IC₅₀) for *in vitro* translation more than 18-fold¹⁴.

The second set of interactions involves the side chains of Tyr6 and Leu7 of Onc112 (Fig. 2b,d). The aromatic side chain of Tyr6 establishes a π -stacking interaction with C2452 of the 23S rRNA (Fig. 2d). In addition, the side chain hydroxyl of Tyr6 hydrogen-bonds with an undetermined ion that is coordinated by the backbone phosphate of U2506 and the O2 atoms of C2452 and U2504. The hydrophobic cavity occupied by the Tyr6 side chain also accommodates the side chain of Leu7 of Onc112, which packs against the phenol moiety of Tyr6, whereas the backbone of Leu7 forms two hydrogen bonds with U2506 (Fig. 2b,d). The compact hydrophobic core formed by Tyr6 and Leu7 is likely to be key in anchoring the Onc112 peptide to the tunnel because mutagenesis experiments have shown that alanine substitution of either residue in Onc72 reduces the ribosome binding affinity by a factor of 7 and results in a complete loss of inhibitory activity on translation *in vitro*¹⁴. In contrast, mutation of Leu7 in Onc112 to cyclohexylalanine, which would preserve the hydrophobic environment, resulted in retention of inhibitory activity on translation *in vitro* but unexpectedly led to a loss of antimicrobial activity (Supplementary Fig. 4).

Additional interactions with the ribosome encompass the PRPRP motif of Onc112 (Fig. 2b) and include a π -stacking interaction between the guanidino group of Arg9 of Onc112 and the base of C2610 (Fig. 2e). Although substitution of Arg11 with alanine in Onc72 also reduces the ribosome binding affinity and inhibitory properties of the peptide¹⁴, we observed very little density for the side chain of this residue, thus suggesting that it could be important for the overall electrostatic properties of the peptide rather than for a defined interaction with the ribosome (Fig. 1). The high conservation of the 23S rRNA nucleotides that comprise the ribosome-binding site of Onc112 is consistent with the broad spectrum of antimicrobial

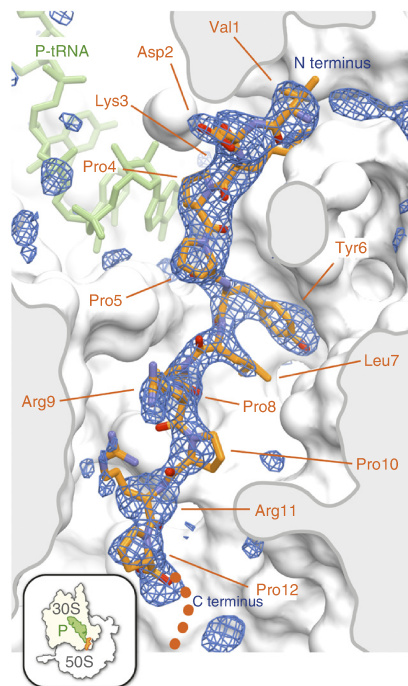
Figure 1 Onc112-binding site within the exit tunnel of the ribosome. Transverse section of the exit tunnel of the *Tth70S* ribosome showing the binding site for the Onc112 peptide (orange). Minimally biased $F_o - F_c$ difference map contoured at $+3.0\sigma$ (blue) is observable for the first 12 amino acids of Onc112 (**VDKPPYLPRPRP**PrRiYNR-NH₂; residues 1–12 are bold and underlined). Initiator tRNA_{i^{Met}} bound at the P site is shown in green. Inset shows the view chosen to display the Onc112 peptide relative to the complete 70S ribosome.

activity displayed by this and related PrAMPs against a range of Gram-negative bacteria^{10,24}.

Onc112 allows translation to initiate but blocks elongation

Comparison of the *Tth70S*–Onc112 structure with that of the *Tth70S* ribosome in the preattack state of peptide-bond formation²⁰ indicated that the binding of Onc112 to the ribosome would prevent accommodation of the CCA end of an incoming aminoacyl-tRNA via steric occlusion of the ribosomal A site at the peptidyl transferase center (Fig. 3a). Indeed, Asp2 of Onc112 directly interacts with G2553, a residue located within helix H92 of the 23S rRNA, termed the A loop, that normally stabilizes the A site tRNA at the peptidyl transferase center via Watson–Crick base-pairing with nucleotide C75 of its CCA end.

In order to determine the step of translation that Onc112 inhibits, we performed cell-free protein synthesis and monitored the location of the ribosomes on the mRNA (Fig. 3b and Supplementary Data Set 1), by using toe-printing assays^{25,26}. In the absence of Onc112 or antibiotic, ribosomes were able to initiate at the AUG start codon and translate through the open reading frame, but they became trapped on the downstream isoleucine codon because isoleucine was omitted from the translation mix. In the presence of the antibiotics clindamycin or thiostrepton, ribosomes accumulated at the start codon and could not translate down to the isoleucine codon because these antibiotics prevent delivery and/or accommodation of the first aminoacyl-tRNA directly following the initiation codon²⁷. We observed similar results when performing the toe-printing assay with increasing concentrations of the Onc112 peptide, namely a loss



of the band corresponding to ribosomes stalled at the isoleucine codon and an increase in the band corresponding to the ribosomes accumulating at the start codon. These findings indicate that Onc112 allows subunit joining and formation of the 70S initiation complex but prevents accommodation of the first aminoacyl-tRNA at the A site, as suggested by steric overlap between Onc112 and an A-site tRNA (Fig. 3a). This contrasts with a bona fide translation-initiation inhibitor, such as edeine, which interferes with the stable binding of fMet-tRNA_{i^{Met}} to the 30S subunit and thus prevents 70S initiation-complex formation²⁸, in agreement with the lack of a toe-print band at the start codon in the presence of edeine (Fig. 3b).

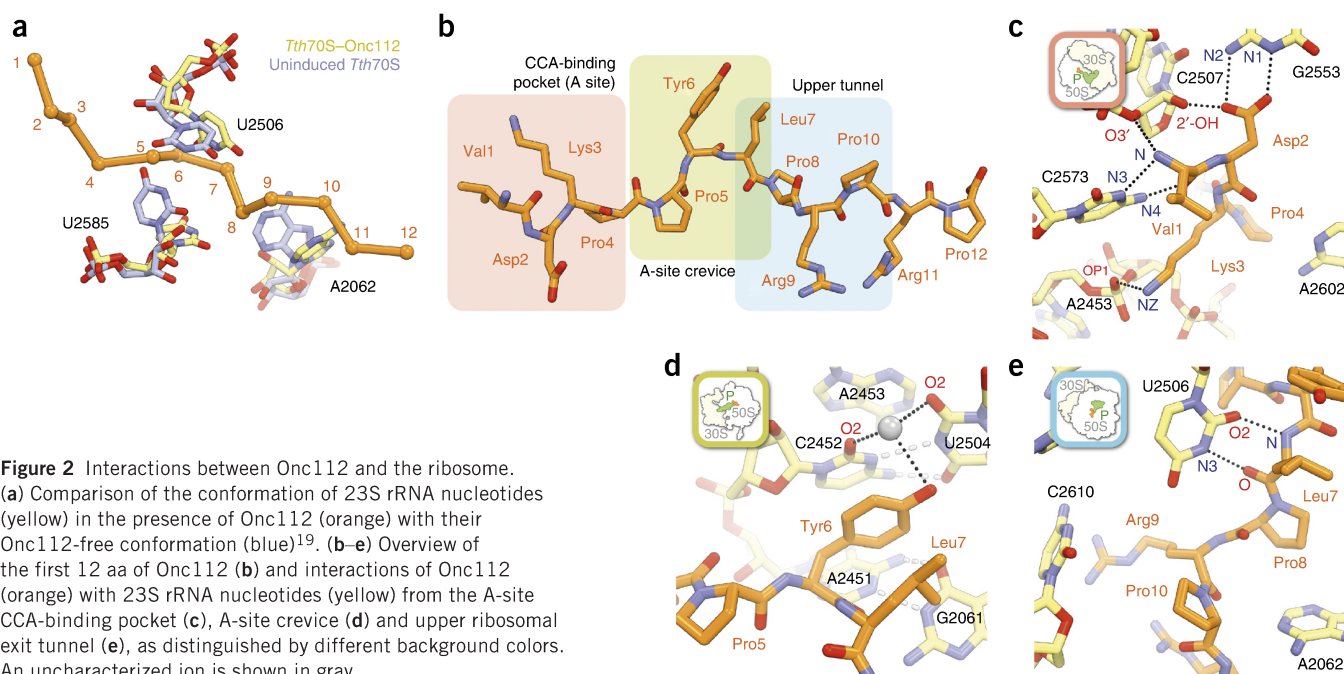
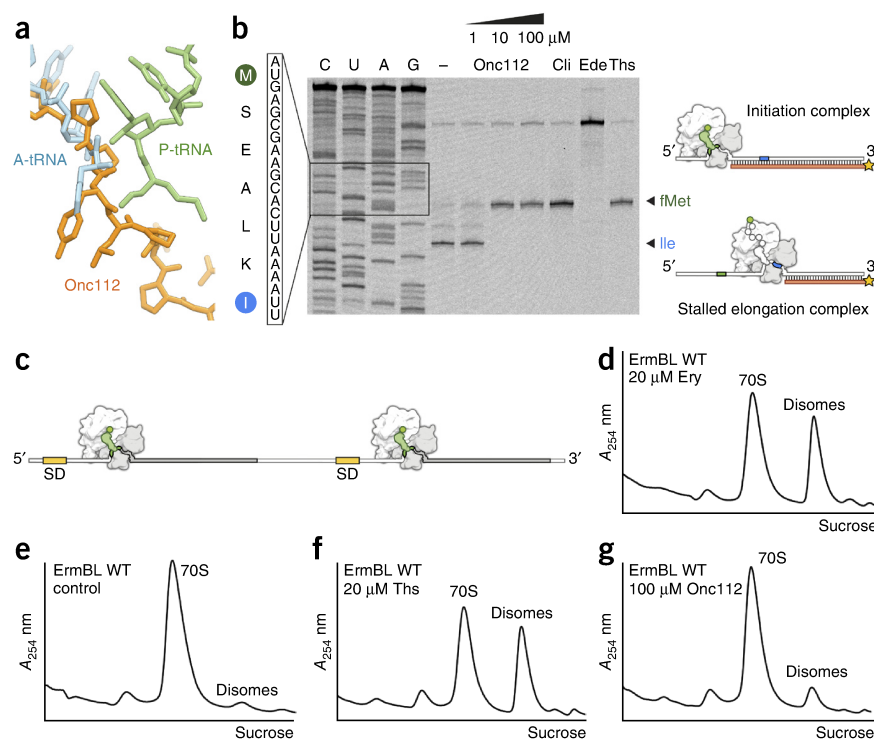


Figure 2 Interactions between Onc112 and the ribosome. (a) Comparison of the conformation of 23S rRNA nucleotides (yellow) in the presence of Onc112 (orange) with their Onc112-free conformation (blue)¹⁹. (b–e) Overview of the first 12 aa of Onc112 (b) and interactions of Onc112 (orange) with 23S rRNA nucleotides (yellow) from the A-site CCA-binding pocket (c), A-site crevice (d) and upper ribosomal exit tunnel (e), as distinguished by different background colors. An uncharacterized ion is shown in gray.

Figure 3 Onc112 blocks and destabilizes the initiation complex. **(a)** Structural comparison of Phe-tRNA^{Phe} (blue) in the A site and fMet-tRNA^{Met} in the P site (green)²⁰ with the binding site of Onc112 (orange). **(b)** Toe-printing assay performed in the absence (–) or presence of increasing concentrations (1 μ M, 10 μ M and 100 μ M) of Onc112, 50 μ M clindamycin (Cli), 50 μ M edeine (Ede) or 100 μ M thiostrepton (Ths). Sequencing lanes for C, U, A and G and the sequence surrounding the toe-print bands (arrows) when ribosomes accumulate at the AUG start codon (green, initiation complex) or the isoleucine codon (blue, stalled elongation complex) are included for reference, as illustrated graphically. The uncropped gel image for the toe-printing assay is in **Supplementary Data Set 1**. **(c–g)** Schematic **(c)** showing the dicistronic ErmBL mRNA that was used to monitor disome formation with sucrose gradients in the presence **(d)** or absence **(e)** of 20 μ M erythromycin (Ery) or the presence of 20 μ M thiostrepton **(f)** or 100 μ M Onc112 **(g)**. In **c**, SD denotes the Shine-Dalgarno sequence. *A*, absorbance.



Onc112 destabilizes the translation-initiation complex

We noticed that the toe-print bands at the start codon in the presence of Onc112 were consistently weaker than those observed in the presence of clindamycin or thiostrepton (**Fig. 3b** and data not shown), thus suggesting that Onc112 may also perturb the placement of fMet-tRNA^{Met} at the P site. In the *Tth70S*–Onc112 structure, the P-site tRNA is uncharged, and its terminal A76 residue undergoes a conformational change that positions it ~3.4 Å away from the Onc112 peptide. *In vivo*, however, we would expect fMet-tRNA^{Met} to bind to the peptidyl transferase center in the same manner as in the *Tth70S* ribosome preattack complexes²⁰, such that the formyl group of the fMet moiety would sterically clash with residues Tyr6 and Leu7 of the Onc112 peptide (**Fig. 3a**). Consequently, we used sucrose gradients to monitor disome formation upon translating a dicistronic ErmBL mRNA *in vitro*, in order to investigate the stability of the translation-initiation complex formed in the presence of Onc112 (**Fig. 3c–g**). As a positive control, we performed translation in the presence of the macrolide erythromycin, which acts synergistically with the ErmBL polypeptide

chain within the ribosomal tunnel to stall translation at a specific site on the mRNA²⁹. Because the mRNA was dicistronic, two stalled ribosomes on a single mRNA led to the formation of disomes that could be visualized on a sucrose gradient (**Fig. 3d**), as shown previously^{16,23}. We observed negligible disome formation in the absence of erythromycin because the ribosomes rapidly translated the short ORF and were released from the mRNA (**Fig. 3e**). As expected, thiostrepton, which allows 70S initiation-complex formation but prevents elongation (**Fig. 3b**), also led to efficient disome formation (**Fig. 3f**). In contrast, the presence of Onc112, even at concentrations as high as 100 μ M, resulted in only a small increase in disomes (**Fig. 3g**). This leads us to suggest that the 70S initiation complexes formed in the presence of Onc112 are unstable, presumably because the Onc112 peptide encroaches onto fMet-tRNA^{Met}, thus causing it to dissociate from the ribosome under the nonequilibrium conditions (centrifugation and sucrose density) used in the disome assay.

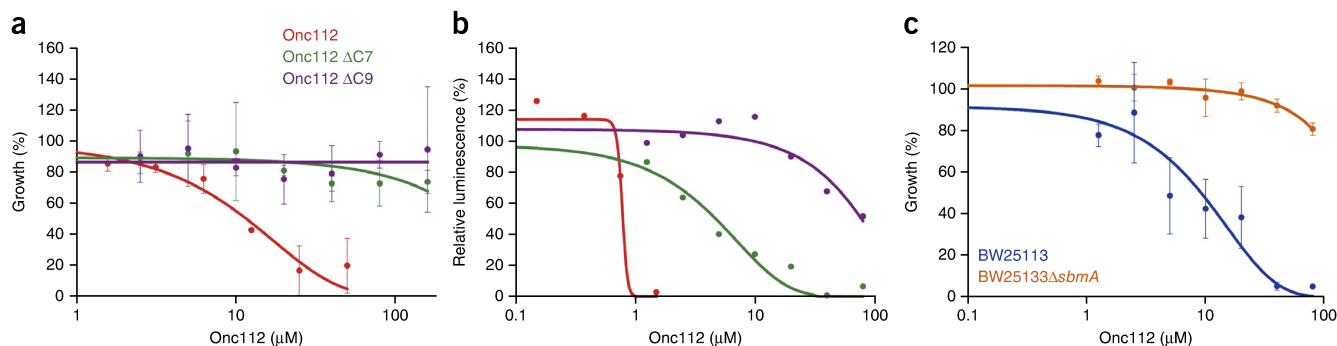
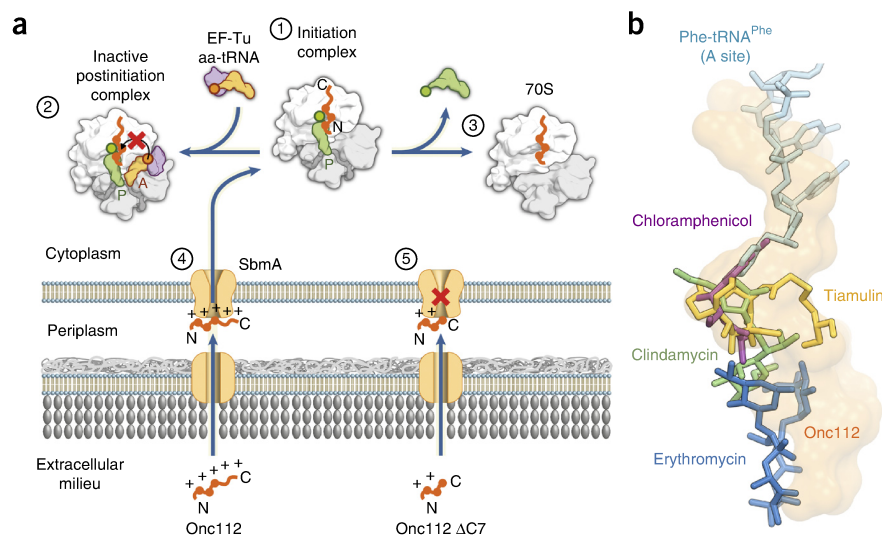


Figure 4 Characterization of Onc112, its C-terminally truncated derivatives and its membrane transporter in Gram-negative bacteria. **(a,b)** Effect of Onc112 (red) and C-terminally truncated Onc112 derivatives Onc112 Δ C7 (green) and Onc112 Δ C9 (purple) on overnight growth of *E. coli* strain BL21(DE3) **(a)** and the luminescence resulting from the *in vitro* translation of Fluc **(b)**. **(c)** Effect of Onc112 on overnight growth of *E. coli* strain BW25113 (blue) or BW25113 Δ *sbmA* (orange). In **a** and **c**, error bars represent mean \pm s.d. for triplicate experiments, whereas the experiment in **b** was performed in duplicate, with the plotted points representing the mean value. The growth or luminescence measured in the absence of peptide was assigned as 100% in all cases.

Figure 5 Mechanism of action and overlap of Onc112 with antibiotics that target the large subunit of the ribosome. (a) Model for the mechanism of action of Onc112.

(1) Onc112 binds within the exit tunnel of the ribosome with a reverse orientation relative to a nascent polypeptide chain. (2) Onc112 allows formation of a translation-initiation complex but prevents accommodation of the aminoacyl-tRNA (aa-tRNA) at the A site of the peptidyl transferase center. (3) The initiation complex is destabilized, thus leading to dissociation of the fMet-tRNA^{Met} from the P site. Although full-length Onc112 can efficiently penetrate the bacterial cell membrane by using the SbmA transporter (4), C-terminal truncation of Onc112 reduces its antimicrobial activity (5), presumably owing to impaired uptake. (b) Relative

binding position of Onc112 (orange) on the ribosome, compared with those of well-characterized translation inhibitors chloramphenicol (purple)^{32,33}, clindamycin (green)³³, tiamulin (yellow)³⁴ and erythromycin (blue)^{32,33} as well as an A site-bound Phe-tRNA^{Phe} (ref. 20).



Onc112 C terminus is needed for uptake, not ribosome binding

The lack of density for the C terminus of Onc112 (residues 13–19) hinted that this region is dispensable for ribosome binding, yet its high degree of conservation suggested that it may nevertheless be necessary for antimicrobial activity. In order to assess the role of the C-terminal region of Onc112, we prepared truncated versions of this peptide, Onc112 ΔC7 and Onc112 ΔC9, which lacked the last 7 and 9 aa, respectively. We then determined the half-minimal inhibitory concentration (MIC₅₀) for the growth of *E. coli* strain BL21(DE3) in the presence of full-length Onc112 and compared it with those of the truncated Onc112 ΔC7 and Onc112 ΔC9 derivatives (Fig. 4a). As expected, the full-length Onc112 displayed good activity, inhibiting growth with an MIC₅₀ of 10 μM, a value similar to that reported previously¹⁴. In contrast, truncation of 7 or 9 aa from the C terminus of Onc112 led to a complete loss of inhibitory activity, even at concentrations above 100 μM (Fig. 4a). To ascertain whether the truncated Onc112 peptides could still bind to the ribosome and inhibit translation, we monitored *in vitro* translation of firefly luciferase (Fluc) by measuring luminescence after 60 min of translation in the presence of increasing concentrations of either full-length Onc112 or the truncated Onc112 ΔC7 and Onc112 ΔC9 derivatives (Fig. 4b). As expected, the full-length peptide displayed excellent activity, inhibiting translation of Fluc with an IC₅₀ of 0.8 μM (Fig. 4b), a value similar to that reported when the same system was used for well-characterized translation inhibitors such as chloramphenicol³⁰. In contrast to their lack of antimicrobial activity (Fig. 4a), both truncated Onc112 peptides displayed some inhibitory activity with the *in vitro*-translation system (Fig. 4b), albeit with a reduced efficiency relative to that of full-length Onc112. Specifically, the Onc112 ΔC7 peptide consisting of residues 1–12 of Onc112 had an IC₅₀ of 5 μM, which was only six times greater than that of full-length Onc112, a result consistent with our structure-based prediction that these residues comprise the major ribosome binding determinants. In contrast, the Onc112 ΔC9 peptide consisting of aa 1–10 of Onc112 had an IC₅₀ of 80 μM, which was 16 times greater than that of Onc112 ΔC7 and two orders of magnitude greater than that of full-length Onc112. These results illustrate the contribution of Arg11 to efficient ribosome binding and translation inhibition, as reported previously¹⁴.

Although the inner-membrane protein SbmA has been shown to be responsible for the uptake of the eukaryotic PrAMPs Bac7 and PR39 (refs. 4,5), the only insect PrAMP tested so far was apidaecin Ib⁴. In order to assess the role of SbmA in the uptake of Onc112, we compared the growth of an *E. coli* strain lacking the *sbmA* gene (Δ*sbmA*) with the parental strain BW25113 in the presence of increasing concentrations of Onc112 (Fig. 4c). As expected, the full-length Onc112 displayed excellent activity against the susceptible SbmA-containing parental strain, inhibiting growth with an MIC₅₀ of 8 μM (Fig. 4c), a value similar to that observed with the BL21(DE3) strain (Fig. 4a). In contrast, the Δ*sbmA* strain displayed increased resistance to Onc112, such that even with 100 μM Onc112, growth was reduced by only 20% (Fig. 4c). These findings indicate that SbmA is indeed necessary for the uptake of Onc112 into Gram-negative bacteria, such as *E. coli*, and provide further support for the proposition that the SbmA transporter is involved in the mechanism of action of the entire group of the PrAMPs⁴.

DISCUSSION

From our structural and biochemical data, we propose a model to explain the mechanism by which PrAMPs such as oncocin inhibit translation (Fig. 5a). We have shown that the binding of Onc112 to the ribosomal exit tunnel allows formation of the 70S initiation complex but prevents accommodation of the aminoacyl-tRNA into the A site (Fig. 5a, steps 1 and 2). Additionally, we propose that Onc112 destabilizes the postinitiation complex by inducing dissociation of fMet-tRNA^{Met} from the P site (Fig. 5a, step 3). Finally, our data also suggest that positively charged residues distributed along the entire length of the Onc112 sequence are necessary for ensuring the efficient SbmA-mediated uptake of Onc112 into the cell, whereas residues from the N-terminal moiety of Onc112 are responsible for targeting this peptide to the ribosome (Fig. 5a, steps 4 and 5). We believe that this mechanism of action is likely to be the same for other PrAMPs, such as drosocin, pyrrothocoricin and apidaecin, which share many of the residues of Onc112 that are important for its ribosome binding and antimicrobial function.

The binding site for Onc112 within the ribosomal exit tunnel overlaps with the binding sites for a majority of the antibiotics that target the large subunit of the ribosome (Fig. 5b), such as the

chloramphenicols, pleuromutilins (for example, tiamulin) and lincosamides (for example, clindamycin), which inhibit peptide-bond formation by preventing the correct positioning of the tRNA substrates, as well as the macrolides (for example, erythromycin), which abort translation by interfering with the movement of the nascent polypeptide chain through the ribosomal exit tunnel²⁷. Given the substantial spatial overlap that exists between the binding sites for these antibiotics and the regions of the tunnel that interact with Onc112 (Fig. 5b) and presumably with several other PrAMPs, it appears likely that such antimicrobial peptides represent a vast, untapped resource for the development of new therapeutics. Several strategies have been pursued to design improved or entirely new antimicrobials that target the exit tunnel of the ribosome³¹. One approach consists of modifying existing antibiotics to create semisynthetic compounds that possess enhanced antimicrobial properties, including better affinity for mutated or modified ribosomes, the ability to evade drug modification or degradation pathways, increased solubility, improved uptake and reduced efflux. Other strategies involve designing chimeric antibiotics from drugs with adjacent binding sites (for example, macrolide-chloramphenicol or linezolid-sparsomycin) or developing entirely new scaffolds, as exemplified by the oxazolidinone linezolid. The ability to produce new scaffolds based on peptides, such as Onc112, that display potent activity against a diverse range of Gram-negative bacteria represents an exciting avenue for the development of future antimicrobials.

METHODS

Methods and any associated references are available in the [online version of the paper](#).

Accession codes. Coordinates and structure factors have been deposited in the Protein Data Bank under accession code [4ZER](#).

Note: Any Supplementary Information and Source Data files are available in the [online version of the paper](#).

ACKNOWLEDGMENTS

We thank the staff at the European Synchrotron Radiation Facility (beamline ID-29) for help during data collection and B. Kauffmann and S. Massip at the Institut Européen de Chimie et Biologie for help with crystal freezing and screening. We also thank C. Mackereth for discussions and advice. This research was supported by grants from the Agence Nationale pour la Recherche (ANR-14-CE09-0001 to C.A.I., G.G. and D.N.W.), Région Aquitaine (2012-13-01-009 to C.A.I.), the Fondation pour la Recherche Médicale (AJE201133 to C.A.I.), the European Union (PCIG14-GA-2013-631479 to C.A.I.), the CNRS (C.D.) and the Deutsche Forschungsgemeinschaft (FOR1805, W13285/4-1 and GRK1721 to D.N.W.). Predoctoral fellowships from the Direction Générale de l'Armement and Région Aquitaine (S. Antunes) and INSERM and Région Aquitaine (A.C.S.) are gratefully acknowledged.

AUTHOR CONTRIBUTIONS

A.C.S. performed structure solution, model building and analysis. N.P. prepared and crystallized ribosomes. N.P. and C.A.I. collected X-ray crystallography data. F.N. performed growth and *in vitro*-translation inhibition assays. S. Antunes and C.D. synthesized the peptides and performed NMR, CD and electrospray ionization high-resolution MS experiments. M.G. performed toe-printing assays. S. Arenz performed disome assays. K.K.I. prepared tRNA^{Met}. G.G., D.N.W. and C.A.I. designed experiments, interpreted data and wrote the manuscript.

COMPETING FINANCIAL INTERESTS

The authors declare no competing financial interests.

Reprints and permissions information is available online at <http://www.nature.com/reprints/index.html>.

1. Wang, G. *et al.* Antimicrobial peptides in 2014. *Pharmaceuticals (Basel)* **8**, 123–150 (2015).

2. Casteels, P., Ampe, C., Jacobs, F., Vaecq, M. & Tempst, P. Apidaecins: antibacterial peptides from honeybees. *EMBO J.* **8**, 2387–2391 (1989).
3. Li, W. *et al.* Proline-rich antimicrobial peptides: potential therapeutics against antibiotic-resistant bacteria. *Amino Acids* **46**, 2287–2294 (2014).
4. Mattiuzzo, M. *et al.* Role of the *Escherichia coli* SbmA in the antimicrobial activity of proline-rich peptides. *Mol. Microbiol.* **66**, 151–163 (2007).
5. Runti, G. *et al.* Functional characterization of SbmA, a bacterial inner membrane transporter required for importing the antimicrobial peptide Bac7 (1–35). *J. Bacteriol.* **195**, 5343–5351 (2013).
6. Hansen, A., Schäfer, I., Knappe, D., Seibel, P. & Hoffmann, R. Intracellular toxicity of proline-rich antimicrobial peptides shuttled into mammalian cells by the cell-penetrating peptide penetratin. *Antimicrob. Agents Chemother.* **56**, 5194–5201 (2012).
7. Stalmans, S. *et al.* Blood-brain barrier transport of short proline-rich antimicrobial peptides. *Protein Pept. Lett.* **21**, 399–406 (2014).
8. Otvos, L. *et al.* Interaction between heat shock proteins and antimicrobial peptides. *Biochemistry* **39**, 14150–14159 (2000).
9. Czihal, P. *et al.* Api88 is a novel antibacterial designer peptide to treat systemic infections with multidrug-resistant Gram-negative pathogens. *ACS Chem. Biol.* **7**, 1281–1291 (2012).
10. Knappe, D. *et al.* Rational design of oncocin derivatives with superior protease stabilities and antibacterial activities based on the high-resolution structure of the oncocin–DnaK complex. *ChemBioChem* **12**, 874–876 (2011).
11. Zahn, M. *et al.* Structural studies on the forward and reverse binding modes of peptides to the chaperone DnaK. *J. Mol. Biol.* **425**, 2463–2479 (2013).
12. Zahn, M. *et al.* Structural identification of DnaK binding sites within bovine and sheep bacteriocin Bac7. *Protein Pept. Lett.* **21**, 407–412 (2014).
13. Berthold, N. & Hoffmann, R. Cellular uptake of apidaecin 1b and related analogs in Gram-negative bacteria reveals novel antibacterial mechanism for proline-rich antimicrobial peptides. *Protein Pept. Lett.* **21**, 391–398 (2014).
14. Krizsan, A. *et al.* Insect-derived proline-rich antimicrobial peptides kill bacteria by inhibiting bacterial protein translation at the 70 S ribosome. *Angew. Chem. Int. Ed. Engl.* **53**, 12236–12239 (2014).
15. Schneider, M. & Dorn, A. Differential infectivity of two *Pseudomonas* species and the immune response in the milkweed bug, *Oncopeltus fasciatus* (Insecta: Hemiptera). *J. Invertebr. Pathol.* **78**, 135–140 (2001).
16. Arenz, S. *et al.* Drug sensing by the ribosome induces translational arrest via active site perturbation. *Mol. Cell* **56**, 446–452 (2014).
17. Bischoff, L., Berninghausen, O. & Beckmann, R. Molecular basis for the ribosome functioning as an L-tryptophan sensor. *Cell Reports* **9**, 469–475 (2014).
18. Shao, S. & Hegde, R.S. Reconstitution of a minimal ribosome-associated ubiquitination pathway with purified factors. *Mol. Cell* **55**, 880–890 (2014).
19. Jenner, L. *et al.* Structural basis for potent inhibitory activity of the antibiotic tigecycline during protein synthesis. *Proc. Natl. Acad. Sci. USA* **110**, 3812–3816 (2013).
20. Polikanov, Y.S., Steitz, T.A. & Innis, C.A. A proton wire to couple aminoacyl-tRNA accommodation and peptide-bond formation on the ribosome. *Nat. Struct. Mol. Biol.* **21**, 787–793 (2014).
21. Schmeing, T.M., Huang, K.S., Strobel, S.A. & Steitz, T.A. An induced-fit mechanism to promote peptide bond formation and exclude hydrolysis of peptidyl-tRNA. *Nature* **438**, 520–524 (2005).
22. Schuwirth, B.S. *et al.* Structures of the bacterial ribosome at 3.5 Å resolution. *Science* **310**, 827–834 (2005).
23. Arenz, S. *et al.* Molecular basis for erythromycin-dependent ribosome stalling during translation of the ErmBL leader peptide. *Nat. Commun.* **5**, 3501 (2014).
24. Knappe, D. *et al.* Oncocin (VDKPPYLPRPRRIYNR-NH₂): a novel antibacterial peptide optimized against Gram-negative human pathogens. *J. Med. Chem.* **53**, 5240–5247 (2010).
25. Hartz, D., McPheeters, D.S., Traut, R. & Gold, L. Extension inhibition analysis of translation initiation complexes. *Methods Enzymol.* **164**, 419–425 (1988).
26. Starosta, A.L. *et al.* Translational stalling at polyproline stretches is modulated by the sequence context upstream of the stall site. *Nucleic Acids Res.* **42**, 10711–10719 (2014).
27. Wilson, D.N. The A–Z of bacterial translation inhibitors. *Crit. Rev. Biochem. Mol. Biol.* **44**, 393–433 (2009).
28. Dinos, G. *et al.* Dissecting the ribosomal inhibition mechanisms of edeine and pactamycin: the universally conserved residues G693 and C795 regulate P-site RNA binding. *Mol. Cell* **13**, 113–124 (2004).
29. Vázquez-Laslop, N., Ramu, H., Klepacki, D., Kannan, K. & Mankin, A.S. The key function of a conserved and modified rRNA residue in the ribosomal response to the nascent peptide. *EMBO J.* **29**, 3108–3117 (2010).
30. Starosta, A.L. *et al.* Interplay between the ribosomal tunnel, nascent chain, and macrolides influences drug inhibition. *Chem. Biol.* **17**, 504–514 (2010).
31. Wilson, D.N. Ribosome-targeting antibiotics and mechanisms of bacterial resistance. *Nat. Rev. Microbiol.* **12**, 35–48 (2014).
32. Bulkley, D., Innis, C.A., Blaha, G. & Steitz, T.A. Revisiting the structures of several antibiotics bound to the bacterial ribosome. *Proc. Natl. Acad. Sci. USA* **107**, 17158–17163 (2010).
33. Dunkle, J.A., Xiong, L., Mankin, A.S. & Cate, J.H. Structures of the *Escherichia coli* ribosome with antibiotics bound near the peptidyl transferase center explain spectra of drug action. *Proc. Natl. Acad. Sci. USA* **107**, 17152–17157 (2010).
34. Schlünzen, F., Pyetan, E., Fucini, P., Yonath, A. & Harms, J.M. Inhibition of peptide bond formation by pleuromutilins: the structure of the 50S ribosomal subunit from *Deinococcus radiodurans* in complex with tiamulin. *Mol. Microbiol.* **54**, 1287–1294 (2004).

ONLINE METHODS

Peptide synthesis. Commercially available reagents were used throughout without purification. *N,N*-dimethylformamide (DMF, peptide synthesis-quality grade) was purchased from Carlo Erba, and piperidine and trifluoroacetic acid (TFA) were purchased from Alfa Aesar. Rink amide PS resin was purchased from PolyPeptide Laboratories. *N,N'*-diisopropylcarbodiimide (DIC), Oxyma and all standard *N*-Fmoc-protected L and D amino acids were purchased from Iris Biotech. *N*-Fmoc-cyclohexylalanine-OH (Fmoc-Cha-OH) was purchased from PolyPeptide laboratories. RP-HPLC-quality acetonitrile (CH₃CN, Sigma-Aldrich) and MilliQ water were used for RP-HPLC analyses and purification. Analytical RP-HPLC analyses were performed on a Dionex U3000SD with a Macherey-Nagel Nucleodur column (4.6 × 100 mm, 3 μm) at a flow rate of 1 ml min⁻¹ at 50 °C. The mobile phase was composed of 0.1% (v/v) TFA-H₂O (solvent A) and 0.1% TFA-CH₃CN (solvent B). Purification was performed on a Gilson GX-281 with a Macherey-Nagel Nucleodur VP250/21 100–5 C18ec column (21 × 250 mm, 5 μm) at a flow rate of 20 mL min⁻¹. The solid-phase syntheses of peptides were conducted on an automated Liberty Blue System synthesizer (CEM μWaves S.A.S.). ¹H NMR spectra were recorded on a DPX-400 NMR spectrometer (Bruker Biospin) with a vertical 9.4T narrow-bore/ultrashield magnet operating at 400 MHz for ¹H observation by means of a 5-mm direct QNP ¹H/¹³C/³¹P/¹⁹F probe with gradient capabilities (Supplementary Fig. 5). ESI-MS analyses were carried out on a Thermo Exactive from the Mass Spectrometry Laboratory at the European Institute of Chemistry and Biology (UMS 3033-IECB), Pessac, France (Supplementary Fig. 5).

All peptides were synthesized on Rink Amide PS resin (0.79 mmol/g) with a five-fold excess of reagents for the coupling step (0.2 M *N*-Fmoc-amino acid solution (in DMF) with 0.5 M DIC (in DMF) and 1.0 M Oxyma (in DMF)). Coupling of *N*-Fmoc-protected L- and D-arginine-OH was performed twice at 25 °C without microwaves for 1,500 s. Other amino acid couplings were performed first at 90 °C, 170 W, 115 s then at 90 °C, 30 W, 110 s. Fmoc removal was performed with a solution of 20% piperidine in DMF at 75 °C with 155 W for 15 s then 90 °C, 35 W, 50 s. After completion of the synthesis, the peptide resin was washed three times with DCM. Cleavage was performed by treatment with 5 mL of a freshly prepared TFA/TIS/H₂O solution for 240 min at room temperature. The resin was then filtered off, and the TFA solution was concentrated under reduced pressure. The crude products were precipitated as TFA salts in the presence of Et₂O and purified with the appropriate gradient (10–30% of B in 20 min) by semipreparative RP-HPLC. The compounds were freeze dried, and TFA was exchanged with HCl by two repetitive freeze-drying cycles in 0.1 N HCl solution³⁵.

The list of peptides prepared for this study and details concerning their synthesis is as follows:

Onc112. H-Val-Asp-Lys-Pro-Pro-Tyr-Leu-Pro-Arg-Pro-Arg-Pro-Arg-(D-Arg)-Ile-Tyr-Asn-(D-Arg)-NH₂ (2,389.85 g mol⁻¹). Synthesis of Onc112 (0.1-mmol scale): 24 mg (10% yield); RP HPLC *t*_R 4.11 min (gradient 10–50% of B in 10 min); ESI HRMS (*m/z*): found 1,195.70 [M + 2H]²⁺, 797.47 [M + 3H]³⁺, 598.35 [M + 4H]⁴⁺, and 478.88 [M + 5H]⁵⁺.

Onc112 ΔC7. H-Val-Asp-Lys-Pro-Pro-Tyr-Leu-Pro-Arg-Pro-Arg-Pro-NH₂ (1,433.73 g mol⁻¹). Synthesis of Onc112 ΔC7 (0.15-mmol scale): 79.4 mg (37% yield); RP HPLC *t*_R 3.54 min (gradient 10–50% of B in 10 min); ESI HRMS (*m/z*): [M + H]⁺ calcd for C₆₇H₁₀₈H₂₀O₁₅, 1,433.83758 found 1,433.84017, with 717.42 [M + 2H]²⁺ and 478.61 [M + 3H]³⁺.

Onc112 ΔC9. H-Val-Asp-Lys-Pro-Pro-Tyr-Leu-Pro-Arg-Pro-NH₂ (1,180.42 g mol⁻¹). Synthesis of Onc112 ΔC9. (0.1-mmol scale): 22.6 mg (19% yield); RP HPLC *t*_R 4.78 min (gradient 10–50% of B in 10 min); ESI HRMS (*m/z*): [M + H]⁺ calcd for C₅₆H₈₉H₁₅O₁₃, 1,180.63370 found 1,180.68368, with [M + 2H]²⁺ 590.84 and [M + 3H]³⁺ 394.23.

Onc112 D2E. H-Val-Glu-Lys-Pro-Pro-Tyr-Leu-Pro-Arg-Pro-Arg-Pro-Arg-(D-Arg)-Ile-Tyr-Asn-(D-Arg)-NH₂ (2,403.88 g mol⁻¹). Synthesis of Onc112 D2E (0.05-mmol scale): 11.6 mg (10% yield); RP HPLC *t*_R 5.75 min (gradient 10–50% of B in 10 min); ESI HRMS (*m/z*): found 1316.70 [M + 2H]²⁺, 840.14 [M + 3H]³⁺ and 601.86 [M + 4H]⁴⁺.

Onc112 L7Cha. H-Val-Asp-Lys-Pro-Pro-Tyr-Cha-Pro-Arg-Pro-Arg-Pro-Arg-(D-Arg)-Ile-Tyr-Asn-(D-Arg)-NH₂ (2,429.92 g mol⁻¹). Synthesis of Onc112 L7Cha (0.05-mmol scale): 6.9 mg (6% yield); RP HPLC *t*_R 5.28 min (gradient 10–50% of B in 10 min); ESI HRMS (*m/z*): found 1,252.18 [M + 2H]²⁺, 822.80 [M + 3H]³⁺ and 608.36 [M + 4H]⁴⁺.

CD spectroscopy. CD spectra of peptides were recorded on a J-815 Jasco spectropolarimeter (Jasco France). Data are expressed in terms of total molar ellipticity in deg cm² dmol⁻¹. CD spectra for the Onc112 peptide were acquired at four different concentrations in phosphate buffer (pH 7.6, 10 mM) between 180 and 280 nm with a rectangular quartz cell with a path length of 1 mm (Hellma 110-QS 1 mm) averaging over two runs. Secondary-structure proportion was estimated from the CD spectra with the deconvolution program CDFriend (S. Buchoux (Unité de Génie Enzymatique et Cellulaire, UMR 6022 CNRS-Université de Picardie Jules Verne) and E. Dufourc (Université de Bordeaux, CNRS, Institut Polytechnique de Bordeaux, UMR 5248 Institut de Chimie et Biologie des Membranes et des Nano-objets (CBMN); available upon request), unpublished). This program uses standard curves obtained for each canonical structure (α-helix, β-sheet, helix-polyproline type II and random coil) with L₁K₂ (alternated hydrophobic leucine and hydrophilic/charged lysine residues) peptides of known length, secondary structure and CD spectra. The program implements a simulated annealing algorithm to get the best combination of α-helix, β-sheet, helix-II and random coil that exhibits the lowest normalized r.m.s. deviation with respect to the experimental spectrum^{36–38}. The algorithm yielded the following assessment for the Onc112 peptide: 54% random coil, 30% helix-PPII, 6% α-helix and 6% β-sheet content.

Purification of *T. thermophilus* 70S ribosomes. *Tth*70S ribosomes were purified as described previously³⁹ and resuspended in buffer containing 5 mM HEPES-KOH, pH 7.5, 50 mM KCl, 10 mM NH₄Cl, and 10 mM Mg(CH₃COO)₂ to yield a final concentration of 26–32 mg/mL. For storage, *Tth*70S ribosomes were flash frozen in liquid nitrogen and kept at –80 °C.

Preparation of mRNA and tRNA^{Met}. Synthetic mRNA with the sequence 5'-GGC AAG GAG GUA AAA AUG CGU UUU CGU-3' was obtained from Eurogentec. This mRNA contains a Shine-Dalgarno sequence and an AUG start codon followed by several additional codons. *E. coli* tRNA^{Met} was overexpressed in *E. coli* HB101 cells and purified as described previously⁴⁰.

Complex formation. A ternary complex containing *Tth*70S ribosomes, mRNA and deacylated tRNA^{Met} was formed by mixing of 5 μM *Tth*70S ribosomes with 10 μM mRNA and incubating at 55 °C for 10 min. For the next step, 20 μM tRNA^{Met} was added, and the mixture was incubated at 37 °C for 10 min. Before the complexes for crystallization were used, the sample was incubated at room temperature for at least 15 min. All complexes were centrifuged briefly before use for crystallization. The final buffer conditions were 5 mM HEPES-KOH, pH 7.6, 50 mM KCl, 10 mM NH₄Cl and 10 mM Mg(CH₃COO)₂.

Crystallization. Published conditions were used as a starting point for screening crystallization conditions by vapor diffusion in sitting-drop trays at 20 °C (refs. 20,39). Crystallization drops consisted of 3 μl of ternary complex and 3–4 μl of reservoir solution containing 100 mM Tris-HCl, pH 7.6, 2.9% (v/v) PEG 20000, 7–10% (v/v) MPD and 175 mM arginine. Crystals appeared within 2–3 d and grew to ~1,000 × 100 × 100 μm within 7–8 d. For cryoprotection, the concentration of MPD was increased in a stepwise manner to yield a final concentration of 40% (v/v). The ionic composition during cryoprotection was 100 mM Tris-HCl, pH 7.6, 2.9% (v/v) PEG 20000, 50 mM KCl, 10 mM NH₄Cl and 10 mM Mg(CH₃COO)₂. *Tth*70S–Onc112 complexes were obtained by soaking 10–20 μM of Onc112 dissolved in the final cryoprotection solution overnight at 20 °C. Crystals were then flash frozen in a nitrogen cryostream at 80 K for subsequent data collection.

Data collection and processing. Diffraction data were collected at beamline ID29 of the European Synchrotron Radiation Facility (ESRF) in Grenoble, France. A complete data set was obtained by merging 0.1° oscillation data collected at 100 K with a wavelength of 0.97625 Å from multiple regions of the same crystal. Initial data processing, including integration and scaling, were performed with XDS⁴¹. All of the data collected could be indexed in the P2₁2₁2₁ space group, with unit-cell dimensions around 210 Å × 450 Å × 625 Å and an asymmetric unit containing two copies of the *Tth*70S ribosome.

Model building and refinement. Initial phases were obtained by molecular replacement performed with Phaser⁴². The search model was obtained from

a high-resolution structure of the *Thh70S* ribosome (PDB 4Y4O). Restrained crystallographic refinement was carried out with Phenix⁴³ and consisted of a single cycle of rigid-body refinement followed by multiple cycles of positional and individual *B*-factor refinement. Rigid bodies comprised four domains from the small 30S subunit (head, body, spur and helix h44) and three domains from the large 50S subunit (body, L1 stalk and the C terminus of ribosomal protein L9). Noncrystallographic symmetry restraints between the two copies of the *Thh70S* ribosome in the asymmetric unit were also applied during refinement. After confirming that a single tRNA was bound to the P site and that additional density corresponding to the Onc112 peptide was visible inside the exit tunnel in a minimally biased $F_o - F_c$ map, a model for Onc112 was built with Rappert⁴⁴ and Coot⁴⁵. The models for the tRNA and mRNA were obtained from a high-resolution structure of the *Thh70S* ribosome preattack complex (PDB 1VY4). Further refinement and model validation were carried out in Phenix and on the MolProbity server⁴⁶, respectively. In the final model, 0.65% of protein residues were classified as Ramachandran outliers, and 94.38% had favorable backbone conformations.

In vitro-translation assay. The inhibition of firefly luciferase (Fluc) synthesis by Onc112 was assessed with an *E. coli* lysate-based transcription-translation coupled assay (RTS100, 5Prime) as described previously for other translational inhibitors³⁰. Briefly, 6- μ L reactions, with or without Onc112/antibiotic were mixed according to the manufacturer's description and incubated for 1 h at 30 °C with shaking (1,000 r.p.m.). 1 μ L of each reaction was stopped with 7 μ L kanamycin (50 μ g/ μ L) and then diluted with 40 μ L of luciferase assay substrate (Promega) into a white 96-well chimney flat-bottom microtiter plate (Greiner). The luminescence was then measured with a Tecan Infinite M1000 plate reader. Relative values were determined by defining the luminescence value of the sample without inhibitor as 100%.

Growth inhibition assays. Determination of the minimal inhibitory concentration (MIC) of Onc112 was performed as described previously for other antibiotics³⁰. Specifically, an overnight culture of *E. coli* strain BL21(DE3) (Invitrogen), BW25113 or Keio deletion strain BW25113 Δ *sbmA* (plate 61, well 10E)⁴⁷ was diluted 1:100 to an OD₆₀₀ of ~0.02, and 200 μ L of the diluted cells was then transferred into individual wells of a 96-well plate (Sarstedt). Either 10 μ L of Onc112, Onc112 derivative peptide or water was added to each well. Plates were then incubated overnight in a thermomixer (Eppendorf) at 37 °C/350 r.p.m. The OD₆₀₀ was measured in a Tecan Infinite M1000 plate reader, and the relative growth was calculated by defining the growth of samples without antibiotic as 100%.

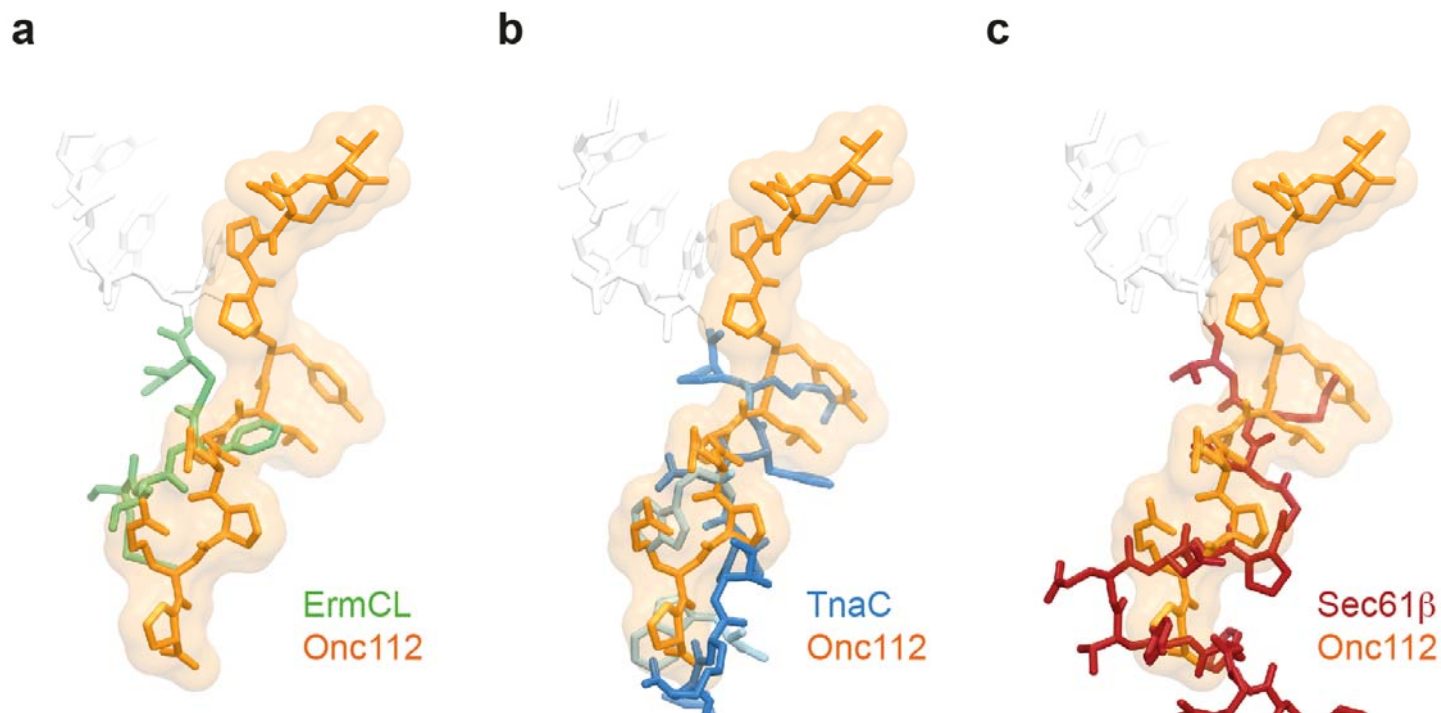
Toe-printing assay. The position of the ribosome on the mRNA was monitored with a toe-printing assay based on an *in vitro*-coupled transcription-translation system with the PURExpress *in vitro* protein synthesis kit (NEB)²⁶. Briefly, each translation reaction consisted of 1 μ L solution A, 0.5 μ L Δ isoleucine + tryptophan amino acid mixture, 0.5 μ L tRNA mixture, 1.5 μ L solution B, 1 μ L (0.5 pmol) hns40aa template: (5'-*ATTAATACGACTCACTATAGGGATATAAGGAGGA AAACATATGAGCGAAGCACTTAAATTTCTGAACAACATCCGCTACTC TTCTGTCGCAGGCAAGAGAATGTACACTTGAACGCTGGGAAGAAAT GCTGGAAAAATTAGAAGTTGTGTTAACGAAACGTTGGATTTTGTAAGTGATAGAATTCTATCGTTAATAAGCAAAATTCATTATAACC*-3', with start codon ATG, catch isoleucine codon ATT and stop codon TAA in bold, the hns40aa ORF underlined and primer-binding sites in italics) and 0.5 μ L additional agents (nuclease-free water, Onc112 or antibiotics). Translation was performed in the absence of isoleucine at 37 °C for 15 min at 500 r.p.m. in 1.5-mL reaction tubes. Ile-tRNA aminoacylation was further prevented by the use of the

Ile-tRNA synthetase inhibitor mupirocin. After translation, 2 pmol Alexa647-labeled NV-1 toe-print primer (5'-GGTTATAATGAATTTTGCTTATTAAC-3') was added to each reaction and incubated at 37 °C without shaking for 5 min. Reverse transcription was performed with 0.5 μ L of AMV RT (NEB), 0.1 μ L dNTP mix (10 mM) and 0.4 μ L Pure System Buffer and incubated at 37 °C for 20 min. Reverse transcription was quenched and RNA degraded by addition of 1 μ L 10 M NaOH and incubation for at least 15 min at 37 °C and then was neutralized with 0.82 μ L of 12 M HCl. 20 μ L toe-print resuspension buffer and 200 μ L PN1 buffer were added to each reaction before treatment with a QIAquick Nucleotide Removal Kit (Qiagen). The Alexa647-labeled DNA was then eluted from the QIAquick columns with 80 μ L of nuclease-free water. A vacuum concentrator was used to vaporize the solvent, and the Alexa647-labeled DNA was then dissolved into 3.5 μ L of formamide dye. The samples were heated to 95 °C for 5 min before being applied onto a 6% polyacrylamide (19:1) sequencing gel containing 7 M urea. Gel electrophoresis was performed at 40 W and 2,000 V for 2 h. The GE Typhoon FLA9500 imaging system was subsequently used to scan the polyacrylamide gel.

Disome formation assay. The disome formation assay was performed as described previously^{16,23}. Briefly, *in vitro* translation of the 2xermBL construct was performed with the Rapid Translation System RTS 100 *E. coli* HY Kit (Roche). Translations were carried out for 1 h at 30 °C and then analyzed on 10–55% sucrose-density gradients (in a buffer containing 50 mM HEPES-KOH, pH 7.4, 100 mM KOAc, 25 mM Mg(OAc)₂ and 6 mM β -mercaptoethanol) by centrifugation at 154,693g (SW-40 Ti, Beckman Coulter) for 2.5 h at 4 °C.

Figure preparation. Figures showing electron density and atomic models were generated with PyMOL (<http://www.pymol.org/>).

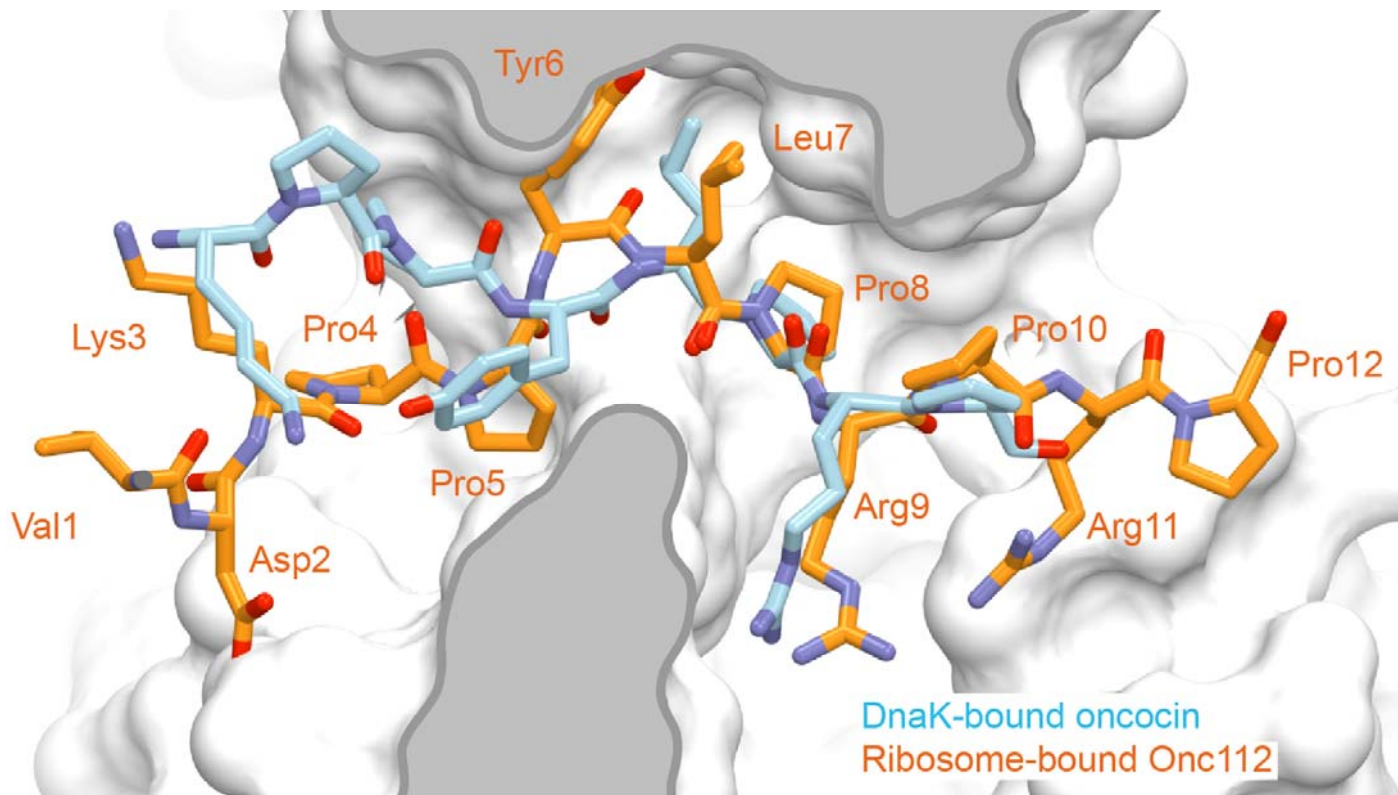
35. Brazier, S.P., Ramesh, B., Haris, P.I., Lee, D.C. & Srai, S.K. Secondary structure analysis of the putative membrane-associated domains of the inward rectifier K⁺ channel ROMK1. *Biochem. J.* **335**, 375–380 (1998).
36. Jean-François, F. *et al.* Variability in secondary structure of the antimicrobial peptide Cateslytin in powder, solution, DPC micelles and at the air-water interface. *Eur. Biophys. J.* **36**, 1019–1027 (2007).
37. Jobin, M.L. *et al.* The enhanced membrane interaction and perturbation of a cell penetrating peptide in the presence of anionic lipids: toward an understanding of its selectivity for cancer cells. *Biochim. Biophys. Acta* **1828**, 1457–1470 (2013).
38. Khemtémourian, L., Buchoux, S., Aussenac, F. & Dufourc, E.J. Dimerization of Neu/Erb2 transmembrane domain is controlled by membrane curvature. *Eur. Biophys. J.* **36**, 107–112 (2007).
39. Selmer, M. *et al.* Structure of the 70S ribosome complexed with mRNA and tRNA. *Science* **313**, 1935–1942 (2006).
40. Schmitt, E., Blanquet, S. & Mechulam, Y. Crystallization and preliminary X-ray analysis of *Escherichia coli* methionyl-tRNA^{Met} formyltransferase complexed with formyl-methionyl-tRNA^{Met}. *Acta Crystallogr. D Biol. Crystallogr.* **55**, 332–334 (1999).
41. Kabsch, W. Xds. *Acta Crystallogr. D Biol. Crystallogr.* **66**, 125–132 (2010).
42. McCoy, A.J. *et al.* Phaser crystallographic software. *J. Appl. Crystallogr.* **40**, 658–674 (2007).
43. Adams, P.D. *et al.* PHENIX: a comprehensive Python-based system for macromolecular structure solution. *Acta Crystallogr. D Biol. Crystallogr.* **66**, 213–221 (2010).
44. de Bakker, P.I., DePristo, M.A., Burke, D.F. & Blundell, T.L. *Ab initio* construction of polypeptide fragments: accuracy of loop decoy discrimination by an all-atom statistical potential and the AMBER force field with the Generalized Born solvation model. *Proteins* **51**, 21–40 (2003).
45. Emsley, P. & Cowtan, K. Coot: model-building tools for molecular graphics. *Acta Crystallogr. D Biol. Crystallogr.* **60**, 2126–2132 (2004).
46. Chen, V.B. *et al.* MolProbity: all-atom structure validation for macromolecular crystallography. *Acta Crystallogr. D Biol. Crystallogr.* **66**, 12–21 (2010).
47. Baba, T. *et al.* Construction of *Escherichia coli* K-12 in-frame, single-gene knockout mutants: the Keio collection. *Mol. Syst. Biol.* **2**, 2006.0008 (2006).



Supplementary Figure 1

Overlap of Onc112 with nascent polypeptide chains in the ribosome exit tunnel.

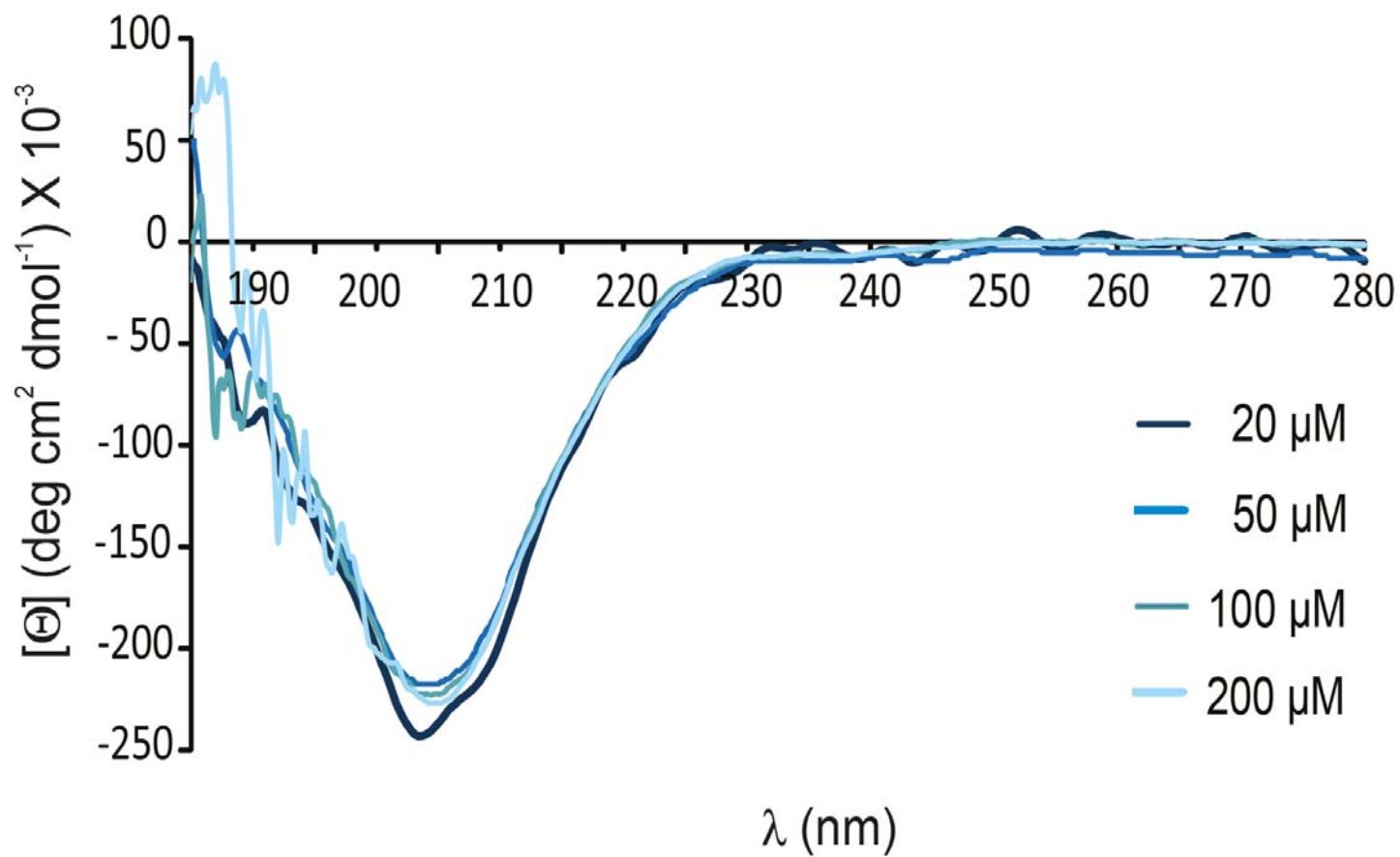
Comparison of the binding position of Onc112 (orange) with (a) ErmCL (green), (b) TnaC (blue) and Sec61 β (red) nascent chains. In (a)-(c), the CCA-end of the P-tRNA is shown in white and in (b) the two tryptophan molecules are in cyan.



Supplementary Figure 2

Comparison of *Tth70S*–Onc112 with the DnaK–oncocin complex.

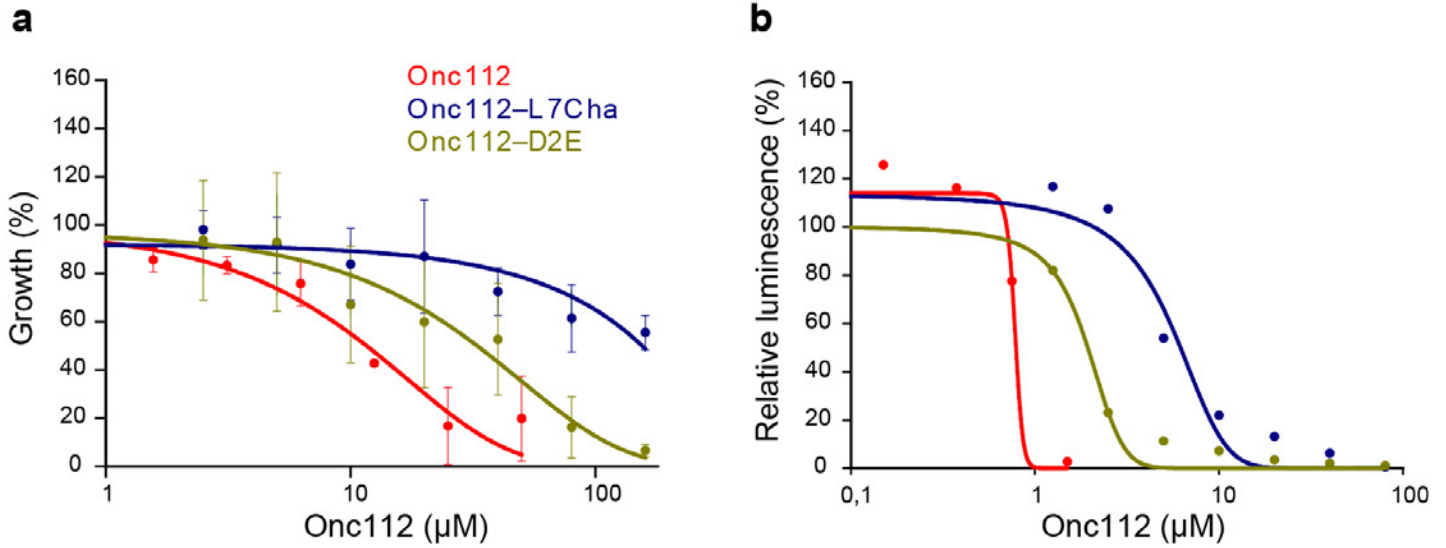
The conformation of residues Lys3–Pro10 of the Oncocin peptide O2 (cyan, $\text{VDKPPYLPRPRPPROIYNO-NH}_2$, where O represents ornithine) in complex with DnaK (white surface representation) was compared with residues Val1–Pro12 of Onc112 (orange) from the ribosome-bound Onc112 structure.



Supplementary Figure 3

Conformation of the Onc112 peptide in solution.

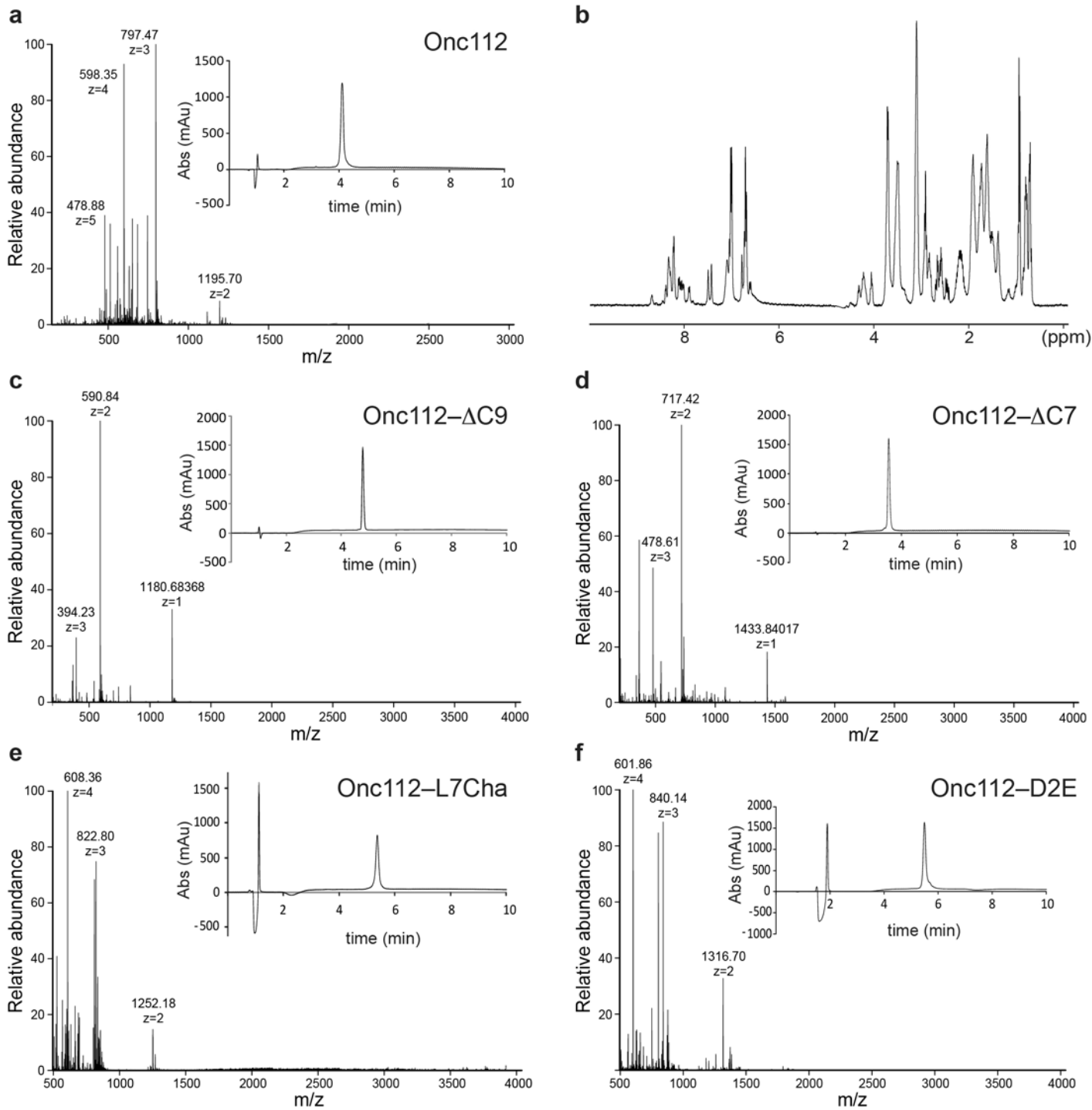
Far-UV circular dichroism (CD) spectra of the Onc112 peptide at concentrations ranging from 20 to 200 μM .



Supplementary Figure 4

Inhibitory activity of Onc112 peptide derivatives.

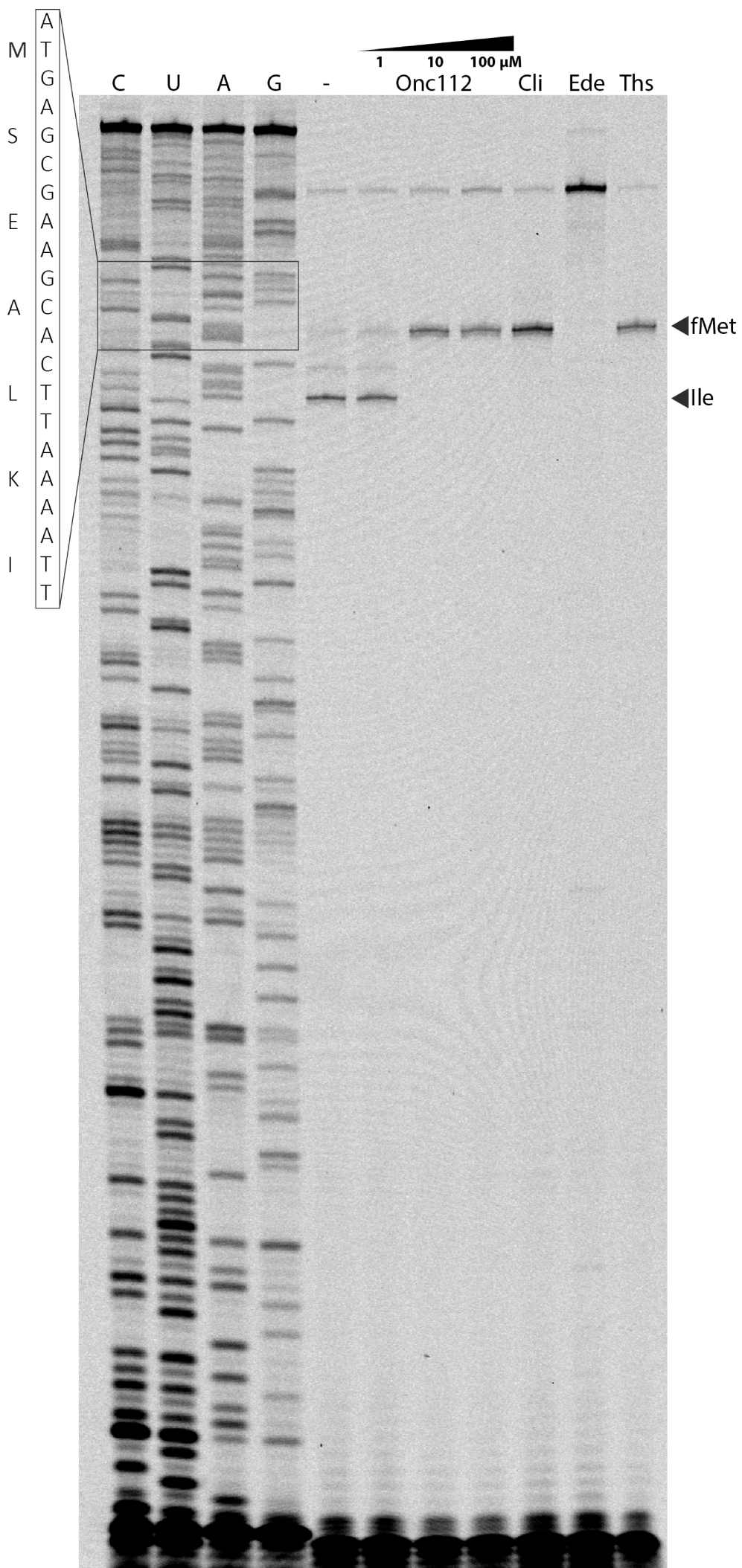
(a-b) Effect of Onc112 (red) and Onc112 derivatives Onc112-L7Cha (blue) and Onc112-D2E (olive) on (a) the overnight growth of *E. coli* strain BL21(DE3) and (b) the luminescence resulting from the *in vitro* translation of firefly luciferase (Fluc). In (a), the error bars represent the standard deviation (s.d.) from the mean for a triplicate experiment ($n=3$). In (b), the experiment was performed in duplicate ($n=2$). The growth or luminescence measured in the absence of peptide was assigned as 100%.



Supplementary Figure 5

Validation of Onc112 and derivatives.

(a) Electrospray ionization high resolution mass spectrometry (ESI-HRMS) and reverse phase (RP) high performance liquid chromatography (HPLC), and (b) ^1H nuclear magnetic resonance (NMR) spectra of the Onc112 peptide. (c-f) ESI-HRMS and RP HPLC of the (c) Onc112- ΔC9 , (d) Onc112- ΔC7 , (e) Onc112-L7Cha and (f) Onc112-D2E peptides.



Structure of the mammalian antimicrobial peptide Bac7(1–16) bound within the exit tunnel of a bacterial ribosome

A. Carolin Seefeldt^{1,2,3,†}, Michael Graf^{4,†}, Natacha Pérébasquine^{1,2,3}, Fabian Nguyen⁴, Stefan Arenz⁴, Mario Mardirossian⁵, Marco Scocchi⁵, Daniel N. Wilson^{4,6,*} and C. Axel Innis^{1,2,3,*}

¹Institut Européen de Chimie et Biologie, University of Bordeaux, Pessac 33607, France, ²U1212, Inserm, Bordeaux 33076, France, ³UMR 5320, CNRS, Bordeaux 33076, France, ⁴Gene Center and Department for Biochemistry, University of Munich, Munich 81377, Germany, ⁵Department of Life Sciences, University of Trieste, Trieste 34127, Italy and ⁶Center for integrated Protein Science Munich (CiPSM), University of Munich, Munich 81377, Germany

Received October 13, 2015; Revised December 22, 2015; Accepted December 28, 2015

ABSTRACT

Proline-rich antimicrobial peptides (PrAMPs) produced as part of the innate immune response of animals, insects and plants represent a vast, untapped resource for the treatment of multidrug-resistant bacterial infections. PrAMPs such as oncocin or batenecin-7 (Bac7) interact with the bacterial ribosome to inhibit translation, but their supposed specificity as inhibitors of bacterial rather than mammalian protein synthesis remains unclear, despite being key to developing drugs with low toxicity. Here, we present crystal structures of the *Thermus thermophilus* 70S ribosome in complex with the first 16 residues of mammalian Bac7, as well as the insect-derived PrAMPs metalnikowin I and pyrrocoricin. The structures reveal that the mammalian Bac7 interacts with a similar region of the ribosome as insect-derived PrAMPs. Consistently, Bac7 and the oncocin derivative Onc112 compete effectively with antibiotics, such as erythromycin, which target the ribosomal exit tunnel. Moreover, we demonstrate that Bac7 allows initiation complex formation but prevents entry into the elongation phase of translation, and show that it inhibits translation on both mammalian and bacterial ribosomes, explaining why this peptide needs to be stored as an inactive propeptide. These findings highlight the need to consider the specificity of PrAMP derivatives for the bacterial ribosome in future drug development efforts.

INTRODUCTION

Antimicrobial peptides (AMPs) represent a large and diverse group of molecules that form part of the innate immune response of a variety of invertebrate, plant and animal species (1). While many AMPs kill bacteria by disrupting the bacterial cell membrane, there is growing evidence that some AMPs have intracellular targets (1). Members of one such class of non-membranolytic peptides are referred to as proline-rich AMPs (PrAMPs) and are present in the hemolymph of several species of insects and crustaceans, as well as in the neutrophils of many mammals (2). PrAMPs exhibit potent antimicrobial activity against a broad range of bacteria, especially Gram-negative, and are therefore considered as potential lead candidates for the development of therapeutic antimicrobial agents (3). Well-characterized insect PrAMPs include the apidaecins produced by bees (*Apis mellifera*) and wasps (*Apis Vespididae*), pyrrocoricin from firebugs (*Pyrrocoris apterus*), drosocins from fruit flies (*Drosophila*), metalnikowins from the green shield bug (*Palomena prasina*) and the milkweed bug (*Oncopeltus fasciatus*) oncocins (2,4,5). PrAMPs are synthesized as inactive precursors, which undergo proteolysis to release the active peptide. In contrast to the active insect peptides, which are generally <21 amino acids in length, the active mammalian mature forms tend to be much longer; for example, the porcine PR-39 is 39 residues long, whereas the bovine batenecin-7 (Bac7), which is also found in sheep and goats, is 60 residues long (2). Nevertheless, C-terminally truncated versions of the mammalian PrAMPs retain antimicrobial activity (6–9) and exhibit high sequence similarity with the insect PrAMPs. Indeed, the Bac7(1–16) and Bac7(1–35) derivatives corresponding to the first 16 and

*To whom correspondence should be addressed. Tel: +33 540 006 149; Fax: +33 540 002 215; Email: axel.innis@inserm.fr

Correspondence may also be addressed to Daniel N. Wilson. Tel: +49 89 2180 76903; Fax: +49 89 2180 76945; Email: wilson@lmb.uni-muenchen.de

†These authors contributed equally to the paper as first authors.

35 residues of Bac7, respectively, display similar, if not improved, antimicrobial activities compared to the full-length processed Bac7 peptide (6,10,11). For instance, Bac7(1–35) reduces mortality from *Salmonella typhimurium* in a mouse model of infection (12) as well as in a rat model for septic shock (13).

The insect-derived PrAMPs apidaecin and oncocin, as well as the mammalian Bac7, penetrate the bacterial cell membrane mainly via the SbmA transporter present in many Gram-negative bacteria (10,14). Early studies identified interactions between both insect and mammalian PrAMPs and DnaK, suggesting that this molecular chaperone was the common intracellular target (2,15). However, subsequent studies questioned the relevance of this interaction by demonstrating that these PrAMPs also display an equally potent antimicrobial activity against bacterial strains lacking the *dnaK* gene (16–18). Instead, apidaecin, oncocin and Bac7 were shown to bind to the ribosome and inhibit translation (17,19). Subsequent crystal structures of the oncocin derivative Onc112 in complex with the bacterial 70S ribosome revealed that this peptide binds with a reverse orientation in the ribosomal tunnel and blocks binding of the aminoacyl-tRNA to the A-site (20,21). However, there are no crystal structures to date of a mammalian PrAMP in complex with the ribosome.

Here we present 2.8–2.9 Å resolution X-ray structures of the *Thermus thermophilus* 70S (*Tth*70S) ribosome in complex with either the mammalian Bac7 derivative Bac7(1–16) or the insect-derived PrAMPs metalnikowin I or pyrrococin. The structures reveal that Bac7(1–16), metalnikowin I and pyrrococin bind within the ribosomal tunnel with a reverse orientation compared to a nascent polypeptide chain, as observed previously for oncocin (20,21). In contrast to the insect PrAMPs oncocin, metalnikowin I and pyrrococin, the mammalian Bac7(1–16) utilizes multiple arginine side chains to establish stacking interactions with exposed nucleotide bases of the rRNA, and we show that its unique N-terminal RIR motif is critical for inhibiting translation. Like oncocin, metalnikowin I and pyrrococin, the binding site of Bac7 overlaps with that of the A-tRNA, consistent with our biochemical studies indicating that Bac7(1–16) allows 70S initiation complex formation, but prevents subsequent rounds of translation elongation. Furthermore, we demonstrate that Bac7(1–35) displays activity in a mammalian *in vitro* translation system, providing a possible explanation for why Bac7 is produced as a pre-pro-peptide that is targeted to large granules and phagosomes, thus avoiding direct contact between the active peptide and the mammalian ribosome.

MATERIALS AND METHODS

Peptide synthesis and purification

The Bac7 N-terminal fragments Bac7(1–16; RRIR-PRPPRLPRPR), Bac7(1–35; RRIRPRPPRL-PRPRRPLPFPRPGPRPIPRPLPFP) and Bac7(5–35; PRPPRLPRPRRPLPFPRPGPRPIPRPLPFP) were synthesized on solid phase and purified by reversed-phase HPLC as described previously (22). Their concentrations were determined as reported previously (4). All peptides, with a purity of at least 95%, were stored in

milliQ water at -80°C until use. The Onc112 peptide was obtained from an earlier study (21). Metalnikowin I (VDKPDYRPRRPPNM) and pyrrococin (VDKG-SYLRPTPPRPIYNRN) were synthesized to 97.5 and 98.1% purity by NovoPro Bioscience (China).

Purification of *T. thermophilus* 70S ribosomes

*Tth*70S ribosomes were purified as described earlier (23) and resuspended in buffer containing 5 mM HEPES-KOH, pH 7.5, 50 mM KCl, 10 mM NH_4Cl and 10 mM $\text{Mg}(\text{CH}_3\text{COO})_2$ to yield a final concentration of ~ 30 mg/ml. *Tth*70S ribosomes were flash frozen in liquid nitrogen and kept at -80°C for storage.

Preparation of mRNA, tRNA_i^{Met} and YfiA

Synthetic mRNA containing a Shine-Dalgarno sequence and an AUG start codon followed by a phenylalanine codon (5'-GGC AAG GAG GUA AAA AUG UUC UAA -3') was purchased from Eurogentec. *Escherichia coli* tRNA_i^{Met} was overexpressed in *E. coli* HB101 cells and purified as described previously (24). YfiA was overexpressed in BL21 Star cells and purified as described previously (25).

Complex formation

A quaternary complex containing *Tth*70S ribosomes, mRNA, deacylated tRNA_i^{Met} and Bac7(1–16) peptide was prepared by mixing of 5 μM *Tth*70S ribosomes with 10 μM mRNA and 50 μM Bac7(1–16), and incubating at 55°C for 10 min. After addition of 20 μM tRNA_i^{Met}, the mixture was incubated at 37°C for 10 min. The sample was then incubated at room temperature for at least 15 min and centrifuged briefly prior to use. Ternary complexes containing 50 μM metalnikowin I or pyrrococin, 5 μM *Tth*70S ribosomes and 50 μM YfiA were formed by incubation for 30 min at room temperature. The final buffer conditions were 5 mM HEPES-KOH, pH 7.6, 50 mM KCl, 10 mM NH_4Cl and 10 mM $\text{Mg}(\text{CH}_3\text{COO})_2$.

Crystallization

Published conditions were used as a starting point for screening crystallization conditions by vapour diffusion in sitting-drop trays at 20°C (23,26). Crystallization drops consisted of 3 μl of quaternary or ternary complexes and 3–4 μl of reservoir solution containing 100 mM Tris-HCl, pH 7.6, 2.9% (v/v) PEG 20,000, 7–10% (v/v) 2-methyl-2,4-pentanediol (MPD) and 175 mM arginine. Crystals appeared within 2–3 days and grew to $\sim 1000 \times 100 \times 100$ μm within 7–8 days. For cryoprotection, the concentration of MPD was increased in a stepwise manner to yield a final concentration of 40% (v/v). The ionic composition during cryoprotection was 100 mM Tris-HCl, pH 7.6, 2.9% (v/v) PEG 20,000, 50 mM KCl, 10 mM NH_4Cl and 10 mM $\text{Mg}(\text{CH}_3\text{COO})_2$. Crystals were flash frozen in a nitrogen cryostream at 80 K for subsequent data collection.

Data collection and processing

Diffraction data for Bac7(1–16) were collected at PROXIMA-2A, a beamline at the SOLEIL synchrotron (Saclay, France) equipped with an ADSC Q315 detector. A complete dataset was obtained by merging 0.25° oscillation data collected at 100 K with a wavelength of 0.98011 Å from multiple regions of the same crystal. Diffraction data for metalnikowin I and pyrrocoricin were collected at PROXIMA-1, a beamline at the SOLEIL synchrotron equipped with a DECTRIS PILATUS 6M detector. Complete datasets were obtained by merging 0.1° oscillation data collected at 100 K with a wavelength of 0.97857 Å from multiple regions of the crystal. Initial data processing, including integration and scaling, was performed with X-ray Detector Software (XDS) (27). The data could be indexed in the $P2_12_12_1$ space group, with unit-cell dimensions approximating $210 \times 450 \times 625$ Å and an asymmetric unit containing two copies of the *Tth70S* ribosome.

Model building and refinement

Initial phases were obtained by molecular replacement performed with Phaser (28). The search model was obtained from a high-resolution structure of the *Tth70S* ribosome (PDB ID: 4Y4O) (29) where the RNA backbone had been further improved with the ERRASER-Phenix pipeline (30), using the deposited structure factors. Restrained crystallographic refinement was carried out with Phenix (31) and consisted of a single cycle of rigid-body refinement followed by multiple cycles of positional and individual *B*-factor refinement. Rigid bodies comprised four domains from the small 30S subunit (head, body, spur and helix h44) and three domains from the large 50S subunit (body, L1 stalk and the C terminus of ribosomal protein L9). Non-crystallographic symmetry restraints between the two copies of the *Tth70S* ribosome in the asymmetric unit were also applied during refinement. After confirming that a single tRNA was bound to the P site or that YfiA was present at the decoding center, and that additional density corresponding to the PrAMPs was visible within the exit tunnel in a minimally biased $F_o - F_c$ map, models of the corresponding PrAMPs were built in Coot (32). The models for the tRNA and mRNA were obtained from a high-resolution structure of the *Tth70S* ribosome pre-attack complex (PDB ID: 1VY4). The model for YfiA was obtained from a high resolution *Tth70S* ribosome structure (PDB ID: 4Y4O). Further refinement and model validation was carried out in Phenix (31) and on the MolProbity server (33), respectively. In the final models, 0.56–0.95% of protein residues were classified as Ramachandran outliers, and 92.4–94.3% had favourable backbone conformations (Supplementary Table S1). Coordinates and structure factors have been deposited in the Protein Data Bank under accession codes 5F8K (Bac7(1–16)), 5FDU (Metalnikowin I) and 5FDV (Pyrrocoricin).

In vitro translation assays

Escherichia coli lysate-based transcription-translation coupled assay (RTS100, 5Prime) were performed as described previously for other translational inhibitors (34). Briefly, 6

μl reactions, with or without PrAMP were mixed according to the manufacturer's description and incubated for 1 h at 30°C with shaking (750 rpm). A total of 0.5 μl of each reaction were stopped with 7.5 μl kanamycin (50 μg/μl). The effect of Bac7(1–35) on eukaryotic translation was determined using Rabbit Reticulocyte Lysate System (Promega). A total of 6 μl reactions, with or without Bac7(1–35) were mixed according to the manufacturer's description and incubated for 1 h at 30°C with shaking (300 rpm). A total of 5 μl of each reaction were stopped in 5 μl kanamycin (50 μg/μl). All samples were diluted with 40 μl of Luciferase assays substrate (Promega) into a white 96-well chimney flat bottom microtiter plate (Greiner). The luminescence was then measured using a Tecan Infinite M1000 plate reader. Relative values were determined by defining the luminescence value of the sample without inhibitor as 100%.

Toe-printing assay

The position of the ribosome on the mRNA was monitored with a toe-printing assay (35) based on an *in vitro*-coupled transcription-translation system with the PURExpress *in vitro* protein synthesis kit (NEB), as described previously (21,36). Briefly, each translation reaction consisted of 1 μl solution A, 0.5 μl Δisoleucine amino acid mixture, 0.5 μl tRNA mixture, 1.5 μl solution B, 0.5 μl (0.5 pmol) hns37aa template: (5'-ATTAATACGACTCACTATAGGGATATAAGGAGGAAAACATatgAGCGAAGCACTTAAAattCTGAACAACCTGCGTACTCTTCGTGCGCAGGCAAGACCGCCGCCGCTTGAACGCTGGAAGAAATGCTGGAAAAATTA GAAGTTGTTGTTtaaGTGATAGAATTCTATCGTTAATAAGCAAATTCATTATAAC-3', with start codon ATG, catch isoleucine codon ATT and stop codon TAA in bold, the hns37aa ORF underlined and toe-print primer binding site in italics) and 0.5 μl additional agents (nuclease-free water, water dissolved Bac7(1–35) Bac7(1–16), Bac7(5–35) (1, 10 or 100 μM final concentration) or antibiotics (100 μM thiostrepton, 50 μM edeine, 50 μM clindamycin final concentration)). Translation was performed in the absence of isoleucine at 37°C for 15 min at 500 rpm in 1.5 ml reaction tubes. After translation, 2 pmol Alexa647-labelled NV-1 toe-print primer (5'-GGTTATAATGAATTTTGCTTATTAAC-3') was added to each reaction. Reverse transcription was performed with 0.5 μl of AMV RT (NEB), 0.1 μl dNTP mix (10 mM) and 0.4 μl Pure System Buffer and incubated at 37°C for 20 min. Reverse transcription was quenched and RNA degraded by addition of 1 μl 10 M NaOH and incubation for at least 15 min at 37°C and then was neutralized with 0.82 μl of 12 M HCl. 20 μl toe-print resuspension buffer and 200 μl PN1 buffer were added to each reaction before treatment with a QIAquick Nucleotide Removal Kit (Qiagen). The Alexa647-labelled DNA was then eluted from the QIAquick columns with 80 μl of nuclease-free water. A vacuum concentrator was used to vaporize the solvent and the Alexa647-labelled DNA was then dissolved into 3.5 μl of formamide dye. The samples were heated to 95°C for 5 min before being applied onto a 6% polyacrylamide (19:1) sequencing gel containing 7 M urea. Gel electrophoresis was performed at 40 W and 2000 V for 2 h. The GE

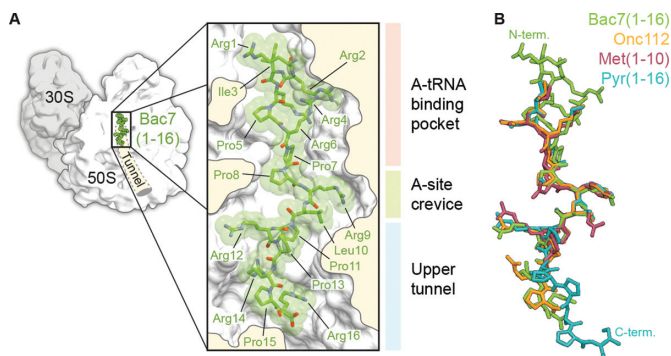


Figure 1. Binding site of Bac7(1–16) on the ribosome and comparison with Onc112. **(A)** Overview and closeup view of a cross-section of the *Tth70S* ribosomal exit tunnel showing the Bac7(1–16) peptide (RRIR-PRPPRLPRPRPR) in green and highlighting the three regions of interaction with the ribosome: the A-tRNA binding pocket (light pink), the A-site crevice (light green) and the upper section of the exit tunnel (light blue). **(B)** Structural comparison of Bac7(1–16) (green) with Onc112 (orange)(20,21), MetI(1–10) (burgundy) and Pyr(1–16) (cyan), highlighting the distinct structure of the Bac7 N-terminus (N-term) and the Pyr C-terminus (C-term).

Typhoon FLA9500 imaging system was subsequently used to scan the polyacrylamide gel.

Filter binding assay

Filter binding assays were performed as described previously (34,37). Briefly, 3 pmol of 70S ribosomes purified from BL21 *E. coli* strain were exposed to 30 pmol of radiolabelled [¹⁴C]-Erythromycin (Perkin Elmer; 110 dpm/pmol) in presence of 1x filter binding buffer (10 mM HEPES/KOH [pH 7.4], 30 mM MgCl₂, 150 mM NH₄Cl and 6 mM β-mercaptoethanol) for 15 min at 37°C. Our controls indicated that approximately 65% of the 70S ribosomes (2 pmol) contained [¹⁴C]-Erythromycin previous to the addition of the different PrAMPs. The PrAMPs were diluted in nuclease-free water to a concentration of 1 mM, 100 μM and 10 μM. 2 μl of each PrAMP stock dilution (Onc112, Bac7(1–35), Bac7(1–16) and Bac7(5–35)) were transferred to the respective tube resulting in final concentrations of 100, 10 and 1 μM. Reactions were incubated for an additional 25 min at 37°C. Afterwards the 20 μl samples were passed through a HA-type nitrocellulose filter from Millipore (0.45 μm pore size) and the filter subsequently washed three times with 1 ml 1x filter binding buffer. Scintillation counting was performed in the presence of Rotiszint[®] eco plus Scintillant. All reactions were performed in duplicate and results were analysed using GraphPad Prism 5. Error bars represent the standard deviation from the mean.

Disome formation assay

The disome formation assay was performed as described previously (38,39). Briefly, *in vitro* translation of the 2xermBL construct was performed using the Rapid Translation System RTS 100 *E. coli* HY Kit (Roche). Translations were carried-out for 1 h at 30°C and then analysed on 10–55% sucrose density gradients (in a buffer containing 50 mM HEPES-KOH, pH 7.4, 100 mM KOAc, 25 mM

Mg(OAc)₂, 6 mM β-mercaptoethanol) by centrifugation at 154 693 × *g* (SW-40 Ti, Beckman Coulter) for 2.5 h at 4°C.

RESULTS

The N-terminus of Bac7 adopts a compact conformation

We obtained a structure referred to here as *Tth70S*-Bac7 from co-crystals of *Tth70S* ribosomes in complex with deacylated tRNA^{Met}, a short mRNA and Bac7(1–16) (Supplementary Table S1). In addition, we obtained two additional structures, *Tth70S*-MetI and *Tth70S*-Pyr, from co-crystals of *Tth70S* ribosomes in complex with YfiA and either metalnikowin I or pyrrocoricin, respectively (Supplementary Table S1). The quality of the electron density in the minimally biased F_O-F_C difference maps calculated after refinement of a model comprising *Tth70S* ribosomes and tRNA^{Met}/mRNA or YfiA, made it possible to build a model for the entire Bac7(1–16; RRIRPRPPRLPRPRPR), the first 10 (of 15; VDKPDYRPRPRPPNM) residues of metalnikowin I (MetI) and the first 16 (of 20; VDKGSYLPRPTPPRPIYNRN) residues of pyrrocoricin (Pyr), as well as to position several neighbouring solvent molecules (Supplementary Figure S1). Like the insect-derived Onc112 peptide (20,21), MetI, Pyr and Bac7(1–16) all bind to the ribosomal exit tunnel in a reverse orientation relative to the nascent polypeptide chain and make extensive interactions with three distinct regions of the large 50S ribosomal subunit: the A-tRNA binding pocket, the A-site crevice and the upper section of the nascent polypeptide exit tunnel (Figure 1A, B and Supplementary Figure S1). A nearly identical, extended backbone conformation is seen for residues 7–13 of Bac7(1–16) and residues 4–10 of Onc112, MetI and Pyr, with Arg9 of Bac7(1–16) substituting for Tyr6 of Onc112, MetI and Pyr (Figure 1B). The structural similarity however does not extend to the N-terminus of Bac7(1–16), where the first six residues adopt a structure that deviates substantially from that of the shorter N-terminus of the insert-derived PrAMPs. Indeed, arginine residues within this region are arranged such that the side chain of Arg6 is sandwiched between the side chains of Arg2 and Arg4 to form a compact, positively charged structure (Figure 1A and B). The binding site of Bac7(1–16) suggests that the additional C-terminal residues of Bac7(1–35) and of the full-length Bac7 (60 residues) would occupy the entire length of the ribosomal tunnel. Consistently, a photocrosslinkable derivative of Bac7(1–35) has been cross-linked to two ribosomal proteins of ~16 and 25 kDa (19), which we suggest to be L22 and L4, respectively, based on their size and close proximity to the Bac7(1–16) binding site (Supplementary Figure S2). Compared to Onc112 and MetI, additional density for the C-terminal PRPR motif (residues 13–16) of Pyr is observed extending deeper into the tunnel (Figure 1 and Supplementary Figure S1). With the exception of Arg14 for which no density is observed, the PRPR motif is quite well ordered despite not forming any obvious direct interactions with the ribosome.

Bac7 makes extensive interactions with the 50S ribosomal subunit

As with Onc112 (20,21), binding of Bac7(1–16) to the ribosome is accompanied by an induced fit involving 23S rRNA residues A2062, U2506 and U2585 (Supplementary Figure S3A; *E. coli* numbering is used throughout this work for the 23S rRNA), such that the base of this last nucleotide occupies a position that would normally clash with the formyl-methionyl moiety of fMet-tRNA_i^{Met} bound to the P-site of an initiation complex (Supplementary Figure S3B). Three modes of interaction are observed between Bac7(1–16) and the large 50S ribosomal subunit (Figure 2A–E).

First, the N-terminal region of Bac7(1–16) forms multiple hydrogen bonds and salt bridges with the A-tRNA binding pocket of the ribosome (Figure 2A and B). In particular, the compact structure formed by Arg2, Arg4 and Arg6 provides a positively charged N-terminal anchor that displaces two magnesium ions from a deep groove lined by 23S rRNA residues C2452, A2453 and G2454 on one side, and residues U2493 and G2494 on the other (Figure 2B). This groove differs from the standard A-form RNA major groove in that it occurs between two unpaired, antiparallel strands of the 23S rRNA. Consequently, the compact arginine structure at the N-terminus of Bac7(1–16) is ideally sized and shaped to fit into this groove and the resulting interaction is likely to be specific in spite of its simple electrostatic nature. Further contacts in this region are likely to increase the specificity of Bac7(1–16) for the ribosome, such as the two hydrogen bonds between the side chain of Arg1 and 23S rRNA residues U2555 and C2556, and four hydrogen bonds between the backbone of Bac7(1–16) residues Arg2-Arg4 and 23S rRNA residues U2492, U2493 and C2573 (Figure 2A).

Second, the unusually high arginine (50%) and proline (37.5%) content of Bac7(1–16) restricts the types of contacts that this peptide can establish with the ribosome. This results in π -stacking interactions between the side chains of Arg2, Arg9, Arg12, Arg14 and Arg16 and exposed bases of 23S rRNA residues C2573, C2452/U2504, C2610, C2586 and A2062, respectively. Additional rigidity within the peptide is provided through the packing of Arg1 against Ile3 and Arg9 against Leu10, and through the compact arginine stack described above (Figure 2C).

Third, numerous possible hydrogen bonds can be established between the backbone of Bac7(1–16) and the ribosome (Figure 2A, D and E), including many indirect interactions via ordered solvent molecules (Figure 2D and E). Many of the water-mediated contacts suggested for *Tth*70S-Bac7 are likely to occur with oncocin, even though the lower resolution of the earlier *Tth*70S-Onc112 structures precluded the modelling of any water molecules (20,21). In addition, interactions such as those between 23S rRNA residue U2506 and the backbone of Bac7(1–16) residues Arg9 and Leu10 were also proposed to occur between the Onc112 peptide and the ribosome (20,21).

Bac7 and Onc112 compete with erythromycin for ribosome binding

The C-terminal residues 12–16 of Bac7(1–16) overlap with the binding site of the macrolide antibiotic erythromycin

on the bacterial ribosome (40,41), in particular with the region occupied by the cladinose sugar and part of the lactone ring (Figure 3A). Consistently, we could demonstrate that Bac7(1–16) and Bac7(1–35) efficiently compete with the binding of radiolabelled erythromycin to the 70S ribosome (Figure 3B). Similarly, Onc112 also efficiently competed with erythromycin (Figure 3B), as expected based on the similarity in binding mode with the ribosome for these regions of Onc112 and Bac7 (Figure 1B). In contrast, Bac7(5–35) was a poor competitor of erythromycin (Figure 3B), indicating that the highly cationic N-terminus of Bac7 and its interaction with the A-tRNA binding pocket (Figure 2B) are important for high affinity binding of Bac7 to the ribosome. Indeed, Bac7 derivatives lacking the first four N-terminal residues (RRIR), Bac7(5–35) and Bac7(5–23), exhibit dramatically reduced minimal inhibitory concentrations (MIC) against Gram-negative strains, such as *E. coli*, as well as *Salmonella typhimurium* (6). We note, however, that the internalization of Bac7(5–35) into bacteria is reduced, indicating that the N-terminal RRIR motif also plays an important role for cell penetration (11).

Bac7 allows initiation, but prevents translation elongation

Consistent with the erythromycin binding assays and in agreement with previous results (Figure 4A) (19), we observed that Bac7(1–35) inhibits the production of luciferase with an IC₅₀ of 1 μ M in an *E. coli* *in vitro* translation system, similar to MetI and Pyr (Supplementary Figure S1), as well as that observed previously for Onc112 (20,21). Bac7(1–16) was an equally potent inhibitor as Bac7(1–35), consistent with the similar MICs observed for these two derivatives (6,10,11). In contrast, Bac7(5–35) inhibited *in vitro* translation with an IC₅₀ of 10 μ M, i.e. 10-fold higher than observed for Bac7(1–16) or Bac7(1–35), indicating that the reduced affinity for the ribosome, together with reduced cellular uptake (11), results in the higher MIC of the Bac7(5–35) derivative (6,42).

Next we investigated the mechanism of inhibition by Bac7 using two *in vitro* translation assays. First, we compared the effect of Bac7(1–35) and Bac7(5–35) on the stabilization of disomes formed upon the stalling of ribosomes on a dicistronic mRNA (in this case 2XErmBL mRNA), as measured by sucrose gradient centrifugation (21,38,39). In the absence of inhibitor, the majority of ribosomes are present as 70S monosomes (control in Figure 4B), whereas the presence of erythromycin leads to translational arrest of the ribosomes on both cistrons of the 2XErmBL mRNA, thereby generating the expected disome peaks (Ery in Figure 4B). Consistent with the *in vitro* translation assays (Figure 4A), translation inhibition and thus disome formation was observed in the presence of 10 μ M Bac7(1–35), whereas even 100 μ M of Bac7(5–35) did not produce significant disomes (Figure 4B). These findings suggest that Bac7(1–35) but not Bac7(5–35) stabilizes an arrested ribosome complex, as observed previously for Onc112 (21).

Second, to monitor the exact site of translation inhibition of the Bac7 derivatives, we employed a toeprinting assay, which uses reverse transcription from the 3' end of an mRNA to determine the exact location of the ribosomes that are translating it (35). In the absence of in-

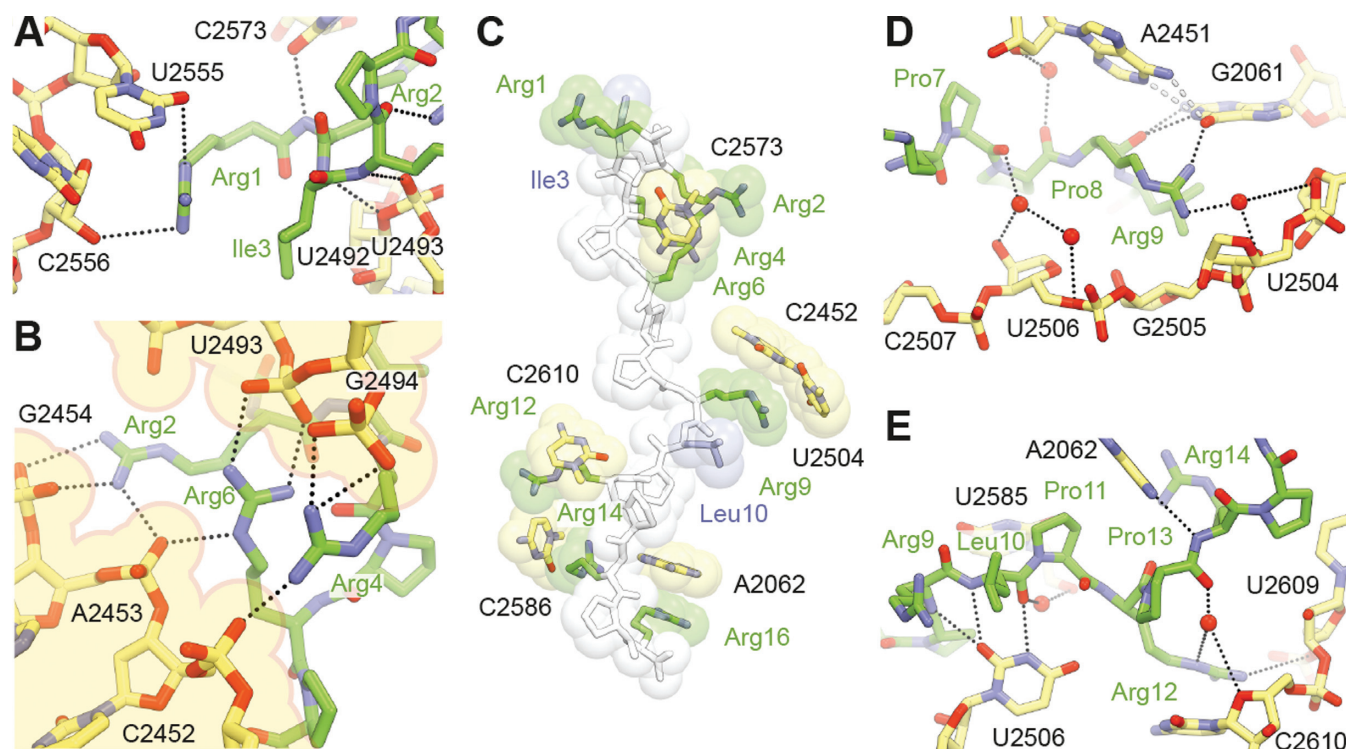


Figure 2. Interactions between Bac7(1–16) and the ribosome. (A) Bac7(1–16) (green) makes extensive contacts with the A-site tRNA binding region of the ribosome, in particular (B) electrostatic interactions between its N-terminal arginine stack and a deep groove lined by phosphate groups from the 23S rRNA (B). (C) π -stacking interactions between arginine side chains (green) of Bac7(1–16) and 23S rRNA bases contribute to much of the binding and are reinforced through further packing against aliphatic side chains (blue). (D and E) Water-mediated contacts between the peptide and the ribosome are also proposed to occur further down the exit tunnel, in addition to direct hydrogen bonding interactions between the two.

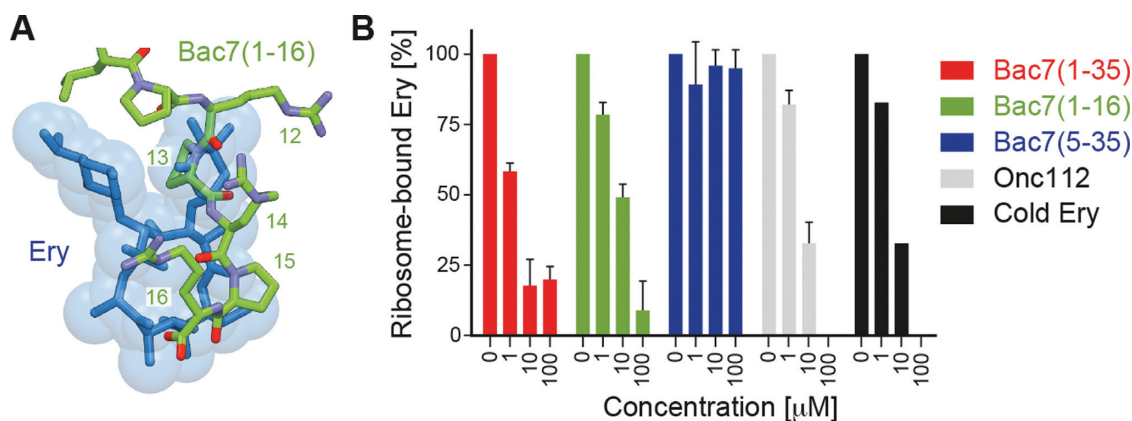


Figure 3. Competition between Bac7 derivatives and erythromycin. (A) Superimposition of the binding site of erythromycin (blue) (40,41) with residues 11–16 of Bac7(1–16) (green). (B) A filter binding assay was used to monitor competition between radiolabelled [14 C]-erythromycin and increasing concentrations (1–100 μ M) of Bac7(1–35) (red), Bac7(1–16) (green), Bac7(5–35) (blue), Onc112 (grey) and cold (non-radioactive) erythromycin (ery, black).

hibitor, ribosomes initiated at the AUG start codon of the mRNA, translated through the open reading frame and ultimately became stalled on an isoleucine codon (Figure 4C) due to the omission of isoleucine from the translation mix. In the presence of thiostrepton or clindamycin, ribosomes accumulated at the AUG codon (Figure 4C), since these antibiotics prevent delivery and/or accommodation of aminoacyl-tRNA at the A-site directly following initiation (43). Similar results were observed when using the Bac7(1–35) and Bac7(1–16) derivatives, such that complete

inhibition of translation elongation was observed at a peptide concentration of 10 μ M (Figure 4C). These findings suggest that like Onc112 (21), Bac7 allows subunit joining and fMet-tRNA_i^{Met} binding, but prevents accommodation of the first aminoacyl-tRNA at the A-site, as suggested by the overlap in the binding site of Bac7 and the CCA-end of an A-tRNA (Figure 4D). Curiously, the toeprint for ribosomes stalled during initiation became weaker at 100 μ M of Bac7(1–16) and Bac7(1–35) and the signal for the full-length mRNA became stronger, similar to the effect ob-

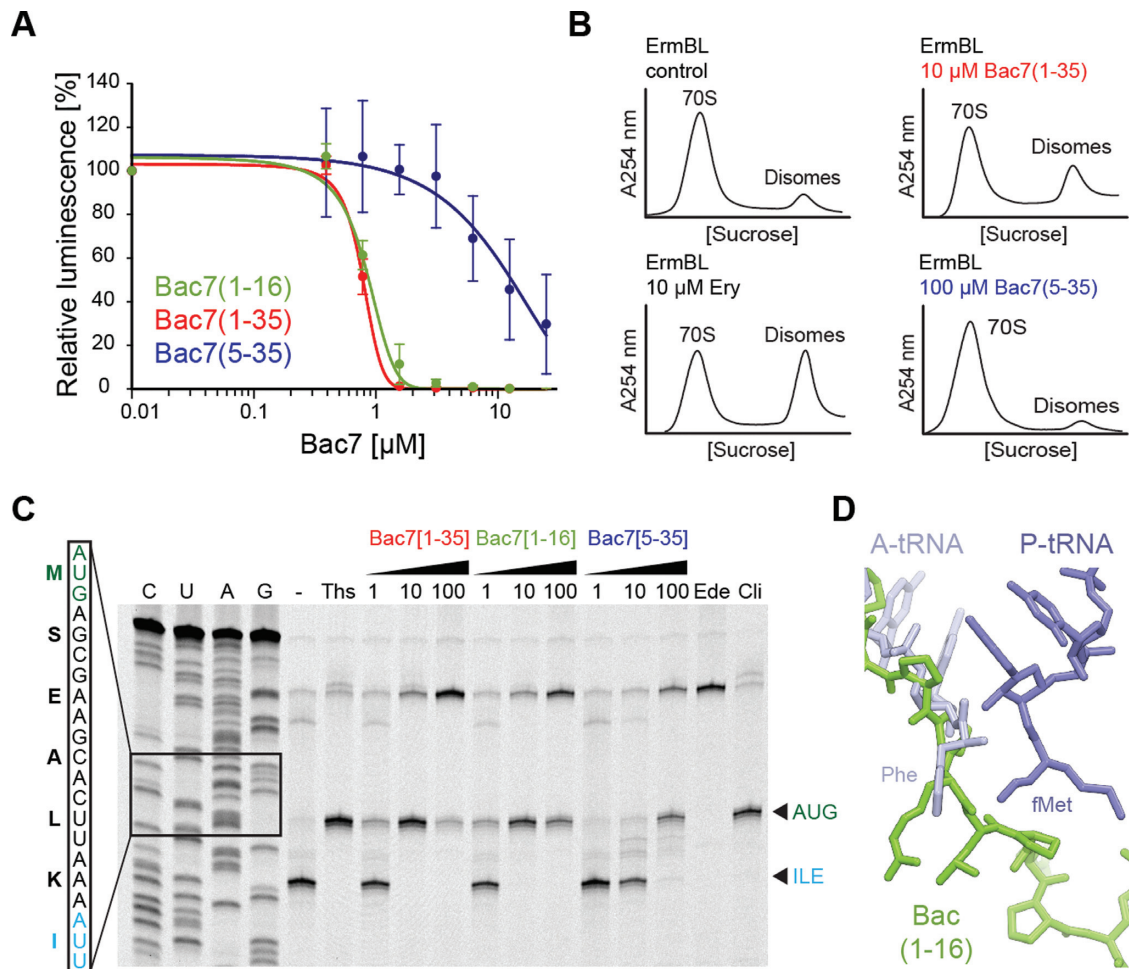


Figure 4. Mechanism of action of Bac7 on the ribosome. **(A)** Effects of increasing concentrations of Bac7 derivatives Bac7(1–16) (green), Bac7(1–35) (red) and Bac7(5–35) (blue) on the luminescence resulting from the *in vitro* translation of firefly luciferase (Fluc) using an *Escherichia coli* lysate-based system. The error bars represent the standard deviation from the mean for triplicate experiments and the luminescence is normalized relative to that measured in the absence of peptide, which was assigned as 100%. **(B)** Sucrose gradient profiles to monitor disome formation from *in vitro* translation of the 2X_{ErmBL} mRNA in the absence (control) or presence of 20 μ M erythromycin (Ery), 10 μ M Bac7(1–35) (red) or 100 μ M Bac7(5–35) (blue). **(C)** Toe-printing assay performed in the absence (–) or presence of increasing concentrations (1, 10, 100 μ M) of Bac7(1–35), Bac7(1–16) or Bac7(5–35), or 100 μ M thiostrepton (Ths), 50 μ M edeine (Ede) or 50 μ M clindamycin (Cli). Sequencing lanes for C, U, A and G and the sequence surrounding the toe-print bands (arrowed) when ribosomes accumulate at the AUG start codon (green, initiation complex) or the isoleucine codon (blue, stalled elongation complex) are included for reference. **(D)** Structural comparison of Phe-tRNA^{Phe} (slate) in the A-site and fMet-tRNA_i^{Met} in the P-site (blue) (26) with the binding site of Bac7(1–16) (green).

served when the antibiotic edeine was used (Figure 4C). Edeine prevents 70S initiation complex formation by destabilizing fMet-tRNA_i^{Met} binding to the 30S subunit (43). Thus, Bac7 may have a similar effect when high cytosolic concentrations are achieved through active uptake into the cell, possibly due to the presence of non-specific interactions with the ribosome. In contrast to Bac7(1–16) and Bac7(1–35), Bac7(5–35) only stabilized the initiation complex at a much higher concentration (100 μ M) (Figure 4C). This is consistent with a reduced affinity of Bac7(5–35) for the ribosome and reinforces the critical role played by the first four residues of Bac7 in its inhibitory activity (Figure 1A) (6,42).

Bac7 inhibits eukaryotic translation *in vitro*

Bac7(1–35) is internalized by mammalian cells (42,44), yet no toxicity has been observed, even at concentrations well above those effective against microbes (12,13,42), raising the question as to whether Bac7 binds to eukaryotic cytosolic ribosomes. A comparison of the binding site of Bac7(1–16) on the bacterial 70S ribosome with the equivalent region of a mammalian 80S ribosome reveals that the rRNA nucleotide sequence is highly conserved. Structurally, the conformation of three 25S rRNA nucleotides, C4519 (C2573), U4452 (U2506) and A3908 (A2602), would be expected to preclude Bac7(1–16) from binding to the mammalian ribosome (Figure 5A). Nevertheless, these nucleotides are highly mobile and adopt different conformations depending on the functional state of the ribosome (26,39,45,46), suggesting that conformational rearrangements of these nu-

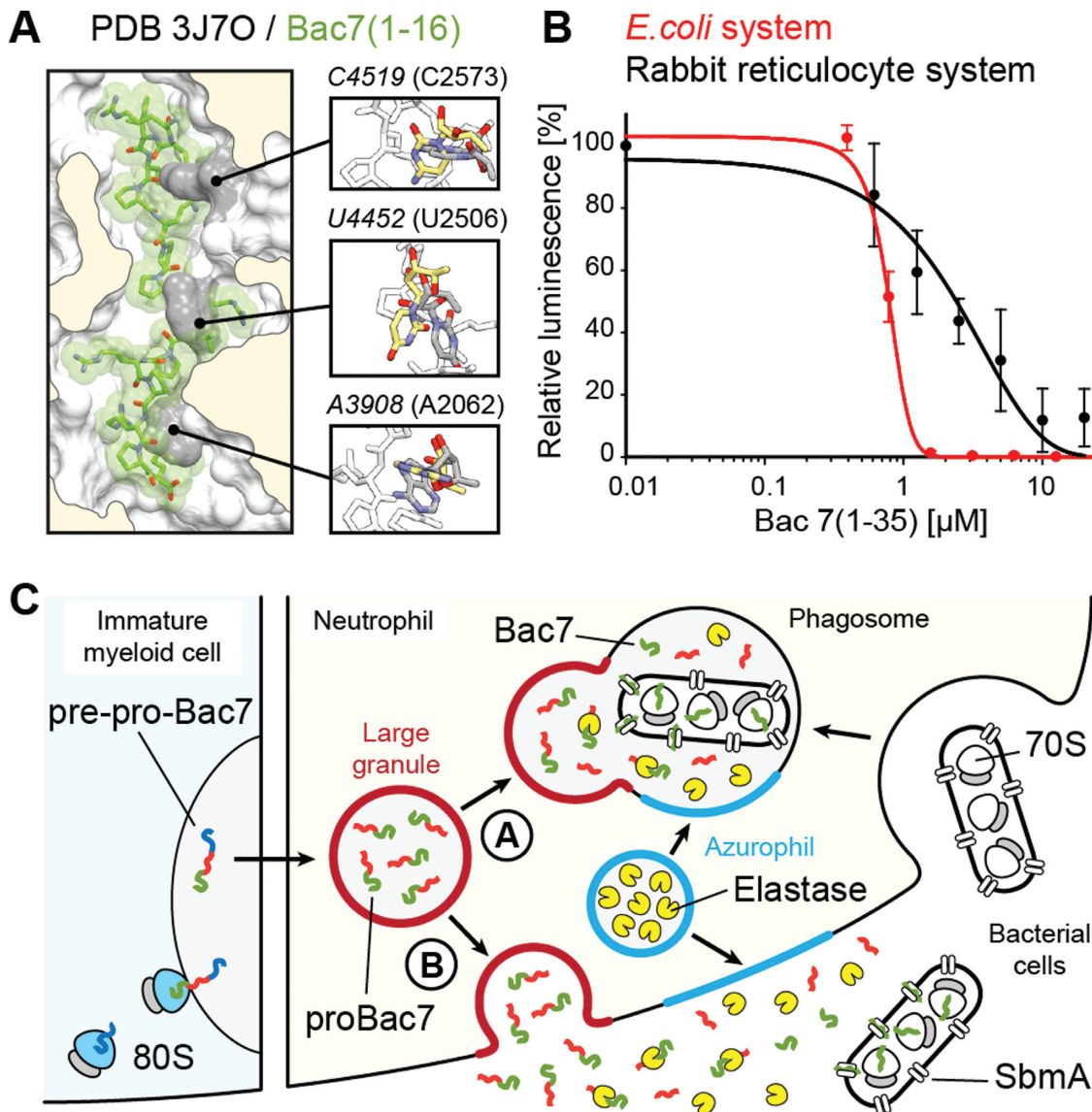


Figure 5. Specificity of Bac7 for bacterial and eukaryotic ribosomes. (A) Superimposition of Bac7(1–16) (green) onto a mammalian 80S ribosome (PDB ID: 3J7O) (47) on the basis of the 23S and 25S rRNA chains in the corresponding structures, with inset illustrating three rRNA nucleotides whose conformation differs in the 80S (grey) and *Tth*70S-Bac7 (yellow) structures. (B) Effect of increasing concentrations of Bac7(1–35) on the luminescence resulting from the *in vitro* translation of firefly luciferase (Fluc) using an *Escherichia coli* lysate-based system (red) or rabbit reticulocyte-based system (black). The error bars represent the standard deviation from the mean for triplicate experiments and the fluorescence is normalized relative to that measured in the absence of peptide, which was assigned as 100%. (C) Model for the targeting of proBac7 to large granules and its processing by elastase to yield active Bac7 peptide. The latter is transported through the bacterial inner membrane by the SbmA transporter and binds within the tunnel of bacterial ribosomes to inhibit translation.

cleotides could allow Bac7(1–16) binding. Indeed, we observed that increasing concentrations of Bac7(1–35) inhibited *in vitro* translation using a rabbit reticulocyte system (Figure 5B). Bac7(1–35) exhibited an IC_{50} of 2.5 μ M, only 2.5-fold higher than that observed in the *E. coli* *in vitro* translation system (Figure 5B). The excellent inhibitory activity of Bac7(1–35) on mammalian ribosomes, combined with its lack of toxicity on mammalian cells (42), would be consistent with a mechanism of internalization via an endocytotic process (42) to ensure that Bac7 minimizes contact with the mammalian cytosolic ribosomes.

DISCUSSION

Our finding that Bac7 is active against eukaryotic translation, together with the current literature, allows us to present a model that explains how and why the mammalian cell prevents the active Bac7 peptide from being present in the cytoplasm (Figure 5C). Bac7 is produced by immature myeloid cells as a pre-pro-Bac7 precursor that is targeted to large granules, where it is stored as pro-Bac7 in differentiated neutrophils (48). The inactive proBac7 is cleaved by elastase, a serine protease that is present in azurophil granules, either upon (A) fusion with the phagosome, or (B) exocytosis and release into the extracellular matrix (Figure

5C) (48,49). The resulting activated Bac7 peptide can then enter into the bacterial cell through the SbmA transporter (10), where it subsequently binds to the ribosome to inhibit translation (Figure 5C) (19). Our structure of the Tth70S–Bac7 complex reveals specifically how Bac7 interacts with the bacterial ribosome (Figures 1 and 2) and inhibits translation by allowing initiation but preventing translation elongation (Figure 3). Although the overall mechanism of action of Bac7 is similar to that of insect-derived AMPs like oncocin (20,21), the high arginine content of Bac7 leads to a distinct mode of binding to the ribosome, namely through electrostatic and stacking interactions with the backbone and bases of 23S rRNA nucleotides, respectively (Figure 2C). It will be interesting to see whether such interactions are the basis for the translational arrest that has been observed when the ribosome translates a nascent polypeptide chain bearing positively charged arginine residues (50,51).

ACCESSION NUMBERS

PDB IDs: 5F8K, 5FDU, 5FDV.

SUPPLEMENTARY DATA

Supplementary Data are available at NAR Online.

ACKNOWLEDGEMENT

We thank the staff at the SOLEIL synchrotron (beamlines PROXIMA-2A and PROXIMA-1) for help during data collection and B. Kauffmann and S. Massip at the Institut Européen de Chimie et Biologie for help with crystal freezing and screening.

FUNDING

Agence Nationale pour la Recherche [ANR-14-CE09-0001 to C.A.I., D.N.W.]; Conseil Régional d'Aquitaine [2012-13-01-009 to C.A.I.]; European Union [PCIG14-GA-2013-631479 to C.A.I.]; Deutsche Forschungsgemeinschaft [FOR1805, WI3285/4-1, GRK1721 to D.N.W.]; Fondo Ricerca di Ateneo [FRA2014 to M.S.]; Institut National de la Santé et de la Recherche Médicale Pre-doctoral Fellowship (to A.C.S.); Conseil Régional d'Aquitaine Pre-doctoral Fellowship (to A.C.S.). Funding for open access charge: Institut National de la Santé et de la Recherche Médicale [PCIG14-GA-2013-631479 to C.A.I.].

Conflict of interest statement. None declared.

REFERENCES

- Brogden, K.A. (2005) Antimicrobial peptides: pore formers or metabolic inhibitors in bacteria? *Nat. Rev. Microbiol.*, **3**, 238–250.
- Scocchi, M., Tossi, A. and Gennaro, R. (2011) Proline-rich antimicrobial peptides: converging to a non-lytic mechanism of action. *Cell. Mol. Life Sci.*, **68**, 2317–2330.
- Li, W., Tailhades, J., O'Brien-Simpson, N.M., Separovic, F., Otvos, L. Jr, Hossain, M.A. and Wade, J.D. (2014) Proline-rich antimicrobial peptides: potential therapeutics against antibiotic-resistant bacteria. *Amino Acids*, **46**, 2287–2294.
- Ebbensgaard, A., Mordhorst, H., Overgaard, M.T., Nielsen, C.G., Aarestrup, F.M. and Hansen, E.B. (2015) Comparative evaluation of the antimicrobial activity of different antimicrobial peptides against a range of pathogenic bacteria. *PLoS One*, **10**, e0144611.
- Chernysh, S., Cociancich, S., Briand, J.P., Hetru, C. and Bulet, P. (1996) The inducible antibacterial peptides of the Hemipteran insect *Palomena prasina*: identification of a unique family of proline rich peptides and of a novel insect defensin. *J. Insect. Physiol.*, **42**, 81–89.
- Benincasa, M., Scocchi, M., Podda, E., Skerlavaj, B., Dolzani, L. and Gennaro, R. (2004) Antimicrobial activity of Bac7 fragments against drug-resistant clinical isolates. *Peptides*, **25**, 2055–2061.
- Chan, Y.R., Zanetti, M., Gennaro, R. and Gallo, R.L. (2001) Anti-microbial activity and cell binding are controlled by sequence determinants in the anti-microbial peptide PR-39. *J. Invest. Dermatol.*, **116**, 230–235.
- Frank, R.W., Gennaro, R., Schneider, K., Przybylski, M. and Romeo, D. (1990) Amino acid sequences of two proline-rich bactericins. Antimicrobial peptides of bovine neutrophils. *J. Biol. Chem.*, **265**, 18871–18874.
- Tokunaga, Y., Niidome, T., Hatakeyama, T. and Aoyagi, H. (2001) Antibacterial activity of bactenecin 5 fragments and their interaction with phospholipid membranes. *J. Pept. Sci.*, **7**, 297–304.
- Mattiuzzo, M., Bandiera, A., Gennaro, R., Benincasa, M., Pacor, S., Antcheva, N. and Scocchi, M. (2007) Role of the Escherichia coli SbmA in the antimicrobial activity of proline-rich peptides. *Mol. Microbiol.*, **66**, 151–163.
- Podda, E., Benincasa, M., Pacor, S., Micali, F., Mattiuzzo, M., Gennaro, R. and Scocchi, M. (2006) Dual mode of action of Bac7, a proline-rich antibacterial peptide. *Biochim. Biophys. Acta*, **1760**, 1732–1740.
- Benincasa, M., Pelillo, C., Zorzet, S., Garrovo, C., Biffi, S., Gennaro, R. and Scocchi, M. (2010) The proline-rich peptide Bac7 (1–35) reduces mortality from Salmonella typhimurium in a mouse model of infection. *BMC Microbiol.*, **10**, 178.
- Ghiselli, R., Giacometti, A., Cirioni, O., Circo, R., Mocchegiani, F., Skerlavaj, B., D'Amato, G., Scalise, G., Zanetti, M. and Saba, V. (2003) Neutralization of endotoxin in vitro and in vivo by Bac7(1–35), a proline-rich antibacterial peptide. *Shock*, **19**, 577–581.
- Krizsan, A., Knappe, D. and Hoffmann, R. (2015) Influence of yjiL and upstream genes on the antibacterial activity of proline-rich antimicrobial peptides overcoming Escherichia coli resistance induced by the missing SbmA transporter system. *Antimicrob. Agents Chemother.*, **59**, 5992–5998.
- Otvos, L., O.I., Rogers, M.E., Consolvo, P.J., Condie, B.A., Lovas, S., Bulet, P. and Blaszczyk-Thurin, M. (2000) Interaction between heat shock proteins and antimicrobial peptides. *Biochemistry*, **39**, 14150–14159.
- Czihal, P., Knappe, D., Fritsche, S., Zahn, M., Berthold, N., Piantavigna, S., Müller, U., Van Dorpe, S., Herth, N., Binas, A. et al. (2012) Api88 is a novel antibacterial designer peptide to treat systemic infections with multidrug-resistant gram-negative pathogens. *ACS Chem. Biol.*, **7**, 1281–1291.
- Krizsan, A., Volke, D., Weinert, S., Sträter, N., Knappe, D. and Hoffmann, R. (2014) Insect-derived proline-rich antimicrobial peptides kill bacteria by inhibiting bacterial protein translation at the 70 S ribosome. *Angew. Chem. Int. Ed.*, **53**, 12236–12239.
- Scocchi, M., Lüthy, C., Decarli, P., Mignogna, G., Christen, P. and Gennaro, R. (2009) The proline-rich antibacterial peptide Bac7 binds to and inhibits in vitro the molecular chaperone DnaK. *Int. J. Pept. Res. Therapeut.*, **15**, 147–155.
- Mardirossian, M., Grzela, R., Giglione, C., Meinel, T., Gennaro, R., Mergaert, P. and Scocchi, M. (2014) The host antimicrobial peptide Bac71–35 binds to bacterial ribosomal proteins and inhibits protein synthesis. *Chem. Biol.*, **21**, 1639–1647.
- Roy, R.N., Lomakin, I.B., Gagnon, M.G. and Steitz, T.A. (2015) The mechanism of inhibition of protein synthesis by the proline-rich peptide oncocin. *Nat. Struct. Mol. Biol.*, **22**, 466–469.
- Seefeldt, A.C., Nguyen, F., Antunes, S., Perebaskin, N., Graf, M., Arenz, S., Inampudi, K.K., Douat, C., Guichard, G., Wilson, D.N. et al. (2015) The proline-rich antimicrobial peptide Oncl12 inhibits translation by blocking and destabilizing the initiation complex. *Nat. Struct. Mol. Biol.*, **22**, 470–475.
- Guida, F., Benincasa, M., Zahariev, S., Scocchi, M., Berti, F., Gennaro, R. and Tossi, A. (2015) Effect of size and N-terminal residue characteristics on bacterial cell penetration and antibacterial activity of the proline-rich peptide Bac7. *J. Med. Chem.*, **58**, 1195–1204.
- Selmer, M., Dunham, C.M., Murphy, F.V., Weixlbaumer, A., Petry, S., Kelley, A.C., Weir, J.R. and Ramakrishnan, V. (2006) Structure of the

- 70S ribosome complexed with mRNA and tRNA. *Science*, **313**, 1935–1942.
24. Schmitt, E., Blanquet, S. and Mechulam, Y. (1999) Crystallization and preliminary X-ray analysis of *Escherichia coli* methionyl-tRNA^{Met} formyltransferase complexed with formyl-methionyl-tRNA^{Met}. *Acta Crystallogr. D*, **55**, 332–334.
 25. Polikanov, Y.S., Blaha, G.M. and Steitz, T.A. (2012) How hibernation factors RMF, HPF, and YfiA turn off protein synthesis. *Science*, **336**, 915–918.
 26. Polikanov, Y.S., Steitz, T.A. and Innis, C.A. (2014) A proton wire to couple aminoacyl-tRNA accommodation and peptide-bond formation on the ribosome. *Nat. Struct. Mol. Biol.*, **21**, 787–793.
 27. Kabsch, W. (2010) Xds. *Acta Crystallogr. D Biol. Crystallogr.*, **66**, 125–132.
 28. McCoy, A.J., Grosse-Kunstleve, R.W., Adams, P.D., Winn, M.D., Storoni, L.C. and Read, R.J. (2007) Phaser crystallographic software. *J. Appl. Crystallogr.*, **40**, 658–674.
 29. Polikanov, Y.S., Melnikov, S.V., Soll, D. and Steitz, T.A. (2015) Structural insights into the role of rRNA modifications in protein synthesis and ribosome assembly. *Nat. Struct. Mol. Biol.*, **22**, 342–344.
 30. Chou, F.C., Echols, N., Terwilliger, T.C. and Das, R. (2016) RNA structure refinement using the ERRASER-phenix pipeline. *Methods Mol. Biol.*, **1320**, 269–282.
 31. Adams, P.D., Afonine, P.V., Bunkoczi, G., Chen, V.B., Davis, I.W., Echols, N., Headd, J.J., Hung, L.W., Kapral, G.J., Grosse-Kunstleve, R.W. *et al.* (2010) PHENIX: a comprehensive Python-based system for macromolecular structure solution. *Acta Crystallogr. D Biol. Crystallogr.*, **66**, 213–221.
 32. Emsley, P. and Cowtan, K. (2004) Coot: model-building tools for molecular graphics. *Acta Crystallogr. D Biol. Crystallogr.*, **60**, 2126–2132.
 33. Chen, V.B., Arendall, W.B. 3rd, Headd, J.J., Keedy, D.A., Immormino, R.M., Kapral, G.J., Murray, L.W., Richardson, J.S. and Richardson, D.C. (2010) MolProbity: all-atom structure validation for macromolecular crystallography. *Acta Crystallogr. D Biol. Crystallogr.*, **66**, 12–21.
 34. Starosta, A.L., Karpenko, V.V., Shishkina, A.V., Mikolajka, A., Sumbatyan, N.V., Schlutzen, F., Korshunova, G.A., Bogdanov, A.A. and Wilson, D.N. (2010) Interplay between the ribosomal tunnel, nascent chain, and macrolides influences drug inhibition. *Chem. Biol.*, **17**, 504–514.
 35. Hartz, D., McPheeters, D.S., Traut, R. and Gold, L. (1988) Extension inhibition analysis of translation initiation complexes. *Methods Enzymol.*, **164**, 419–425.
 36. Starosta, A.L., Lassak, J., Peil, L., Atkinson, G.C., Virumäe, K., Tenson, T., Remme, J., Jung, K. and Wilson, D.N. (2014) Translational stalling at polyproline stretches is modulated by the sequence context upstream of the stall site. *Nucleic Acids Res.*, **42**, 10711–10719.
 37. Polikanov, Y.S., Starosta, A.L., Juetter, M.F., Altman, R.B., Terry, D.S., Lu, W., Burnett, B.J., Dinos, G., Reynolds, K.A., Blanchard, S.C. *et al.* (2015) Distinct tRNA accommodation intermediates observed on the ribosome with the antibiotics hygromycin A and A201A. *Mol. Cell*, **58**, 832–844.
 38. Arenz, S., Meydan, S., Starosta, A.L., Berninghausen, O., Beckmann, R., Vazquez-Laslop, N. and Wilson, D.N. (2014) Drug sensing by the ribosome induces translational arrest via active site perturbation. *Mol. Cell*, **56**, 446–452.
 39. Arenz, S., Ramu, H., Gupta, P., Berninghausen, O., Beckmann, R., Vazquez-Laslop, N., Mankin, A.S. and Wilson, D.N. (2014) Molecular basis for erythromycin-dependent ribosome stalling during translation of the ErmBL leader peptide. *Nat. Commun.*, **5**, 3501.
 40. Bulkley, D., Innis, C.A., Blaha, G. and Steitz, T.A. (2010) Revisiting the structures of several antibiotics bound to the bacterial ribosome. *Proc. Natl. Acad. Sci.*, **107**, 17158–17163.
 41. Dunkle, J.A., Xiong, L., Mankin, A.S. and Cate, J.H. (2010) Structures of the *Escherichia coli* ribosome with antibiotics bound near the peptidyl transferase center explain spectra of drug action. *Proc. Natl. Acad. Sci. U.S.A.*, **107**, 17152–17157.
 42. Tomasinsig, L., Skerlavaj, B., Papo, N., Giabbai, B., Shai, Y. and Zanetti, M. (2006) Mechanistic and functional studies of the interaction of a proline-rich antimicrobial peptide with mammalian cells. *J. Biol. Chem.*, **281**, 383–391.
 43. Wilson, D.N. (2009) The A-Z of bacterial translation inhibitors. *Crit. Rev. Biochem. Mol. Biol.*, **44**, 393–433.
 44. Sadler, K., Eom, K.D., Yang, J.L., Dimitrova, Y. and Tam, J.P. (2002) Translocating proline-rich peptides from the antimicrobial peptide bactenecin 7. *Biochemistry*, **41**, 14150–14157.
 45. Schmeing, T.M., Huang, K.S., Strobel, S.A. and Steitz, T.A. (2005) An induced-fit mechanism to promote peptide bond formation and exclude hydrolysis of peptidyl-tRNA. *Nature*, **438**, 520–524.
 46. Schuwirth, B.S., Borovinskaya, M.A., Hau, C.W., Zhang, W., Vila-Sanjurjo, A., Holton, J.M. and Cate, J.H. (2005) Structures of the bacterial ribosome at 3.5 Å resolution. *Science*, **310**, 827–834.
 47. Voorhees, R.M., Fernandez, I.S., Scheres, S.H. and Hegde, R.S. (2014) Structure of the mammalian ribosome-Sec61 complex to 3.4 Å resolution. *Cell*, **157**, 1632–1643.
 48. Zanetti, M., Litteri, L., Gennaro, R., Horstmann, H. and Romeo, D. (1990) Bactenecins, defense polypeptides of bovine neutrophils, are generated from precursor molecules stored in the large granules. *J. Cell Biol.*, **111**, 1363–1371.
 49. Scocchi, M., Skerlavaj, B., Romeo, D. and Gennaro, R. (1992) Proteolytic cleavage by neutrophil elastase converts inactive storage proforms to antibacterial bactenecins. *Eur. J. Biochem.*, **209**, 589–595.
 50. Dimitrova, L.N., Kuroha, K., Tatematsu, T. and Inada, T. (2009) Nascent peptide-dependent translation arrest leads to Not4p-mediated protein degradation by the proteasome. *J. Biol. Chem.*, **284**, 10343–10352.
 51. Lu, J. and Deutsch, C. (2008) Electrostatics in the ribosomal tunnel modulate chain elongation rates. *J. Mol. Biol.*, **384**, 73–86.

SUPPLEMENTARY ONLINE MATERIALS

for

Structure of the mammalian antimicrobial peptide Bac7(1-16) bound within the exit tunnel of a bacterial ribosome

A. Carolin Seefeldt^{1,2,3}, Michael Graf⁴, Natacha Pérébaskine^{1,2,3}, Fabian Nguyen⁴, Stefan Arenz⁴, Mario Mardirossian⁵, Marco Scocchi⁵, Daniel N. Wilson^{4,6,*} and C. Axel Innis^{1,2,3,*}

¹ Institut Européen de Chimie et Biologie, University of Bordeaux, Pessac, 33607, France

² U1212, Inserm, Bordeaux, 33076, France

³ UMR[---], CNRS, Bordeaux, 33076, France

⁴ Gene Center and Department for Biochemistry, University of Munich, Munich, 81377, Germany

⁵ Department of Life Sciences, University of Trieste, Trieste, 34127, Italy

⁶ Center for integrated Protein Science Munich (CiPSM), University of Munich, Munich, 81377, Germany

* To whom correspondence should be addressed. Tel: +33 540006149; Fax: +33 540002215; Email: axel.innis@inserm.fr. Correspondence may also be addressed to: wilson@lmb.uni-muenchen.de.

The authors wish it to be known that, in their opinion, the first two authors should be regarded as joint First Authors.

Table S1. X-ray data processing and crystallographic refinement statistics

	Bac7(1-16)	MetI	Pyr
PDB code	5F8K	5FDU	5FDV
Space group	P2 ₁ 2 ₁ 2 ₁	P2 ₁ 2 ₁ 2 ₁	P2 ₁ 2 ₁ 2 ₁
Unit cell dimensions			
a	209.8 Å	209.7 Å	209.9 Å
b	450.3 Å	448.1 Å	450.1 Å
c	622.2 Å	623.4 Å	622.9 Å
α	90.0°	90.0°	90.0°
β	90.0°	90.0°	90.0°
γ	90.0°	90.0°	90.0°
Data processing			
Resolution	50 Å – 2.8 Å	50 Å – 2.9 Å	50 Å – 2.8 Å
R _{Merge}	51.3% (233.9%)	17.0% (181.0%)	17.8% (229.7%)
I/ σ I	5.71 (0.95)	11.61 (1.10)	15.99 (1.29)
CC 1/2	95.7 (16.1)	99.7 (34.9)	99.9 (41.1)
Completeness	99.6% (97.6%)	99.6% (99.5%)	100% (100%)
Redundancy	8.3 (8.1)	6.9 (6.7)	13.8 (13.4)
Refinement			
R _{work} /R _{free}	24.8% / 29.2%	18.3% / 23.4%	18.9% / 24.0%
Bond deviations	0.018 Å	0.030 Å	0.029 Å
Angle deviations	1.083°	1.976°	1.942°
Figure of merit	0.80	0.84	0.83
Ramachandran outliers	0.56%	0.95%	0.87%
Favorable backbone	94.3%	92.4%	93.3%

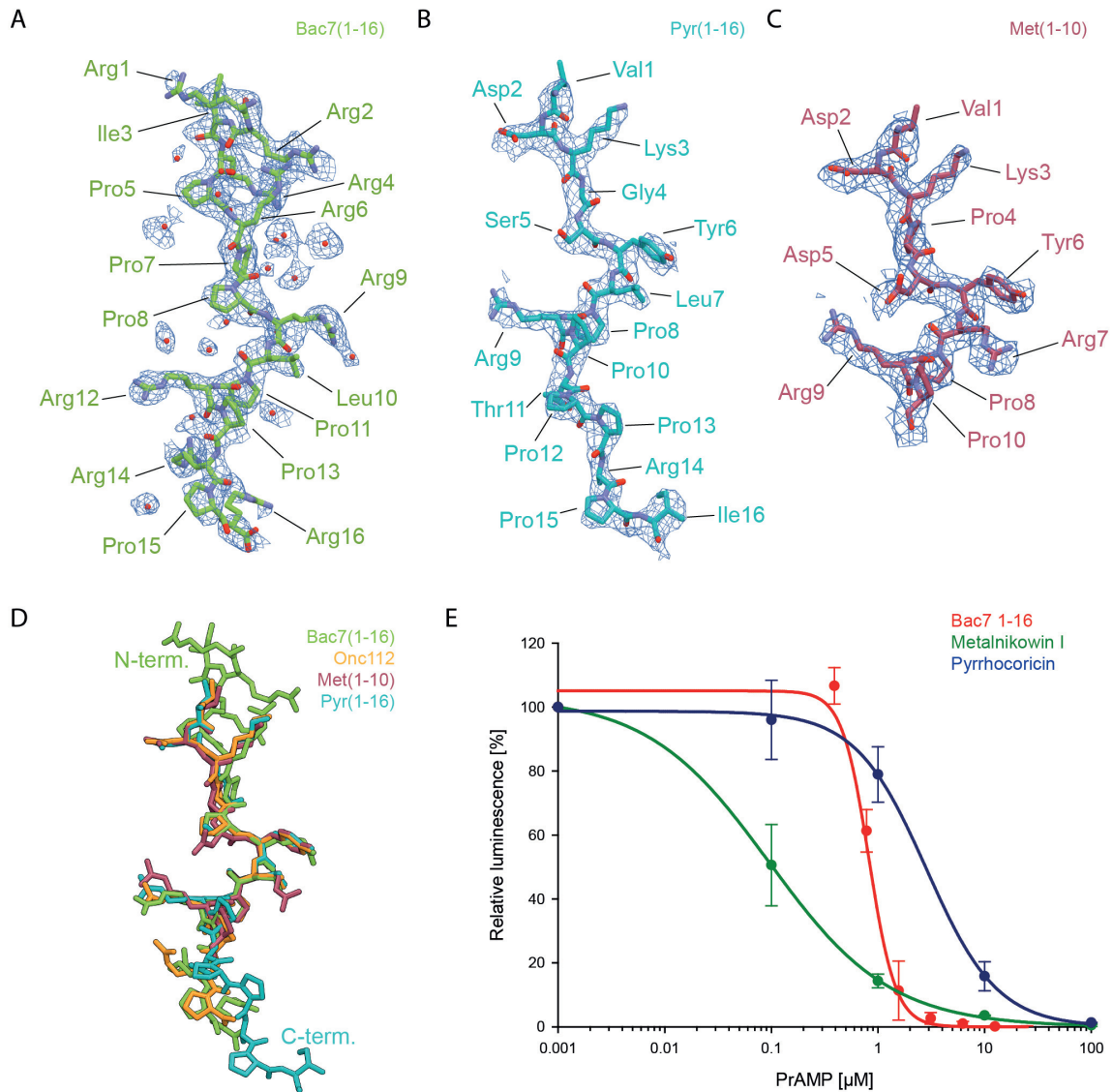


Figure S1. Minimally biased electron density for (A) the Bac7(1-16) peptide (green) and surrounding solvent molecules, as well as the (B) Pyr(1-16) (cyan) and (C) MetI(1-10) (burgundy) peptides. The peptides are shown in the same orientation as in Figure 1A and solvent molecules are displayed as spheres (red). Continuous density for the entire peptide and clear density for the solvent molecules are observed in a minimally biased $F_o - F_c$ difference map contoured at $+2.0\sigma$ (blue mesh). (D) Superimposition of the Bac7(1-16), Onc112(1-12) (orange), Pyr(1-16) and MetI(1-10) peptides. (E) Effects of increasing concentrations of Bac7(1-16) (red), Metalnikowin I (green) and Pyrrhocoricin (green) on the luminescence resulting from the *in vitro* translation of firefly luciferase (Fluc) using an *E. coli* lysate-based system. The error bars represent the standard deviation from the mean for triplicate experiments and the luminescence is normalized relative to that measured in the absence of peptide, which was assigned as 100%.

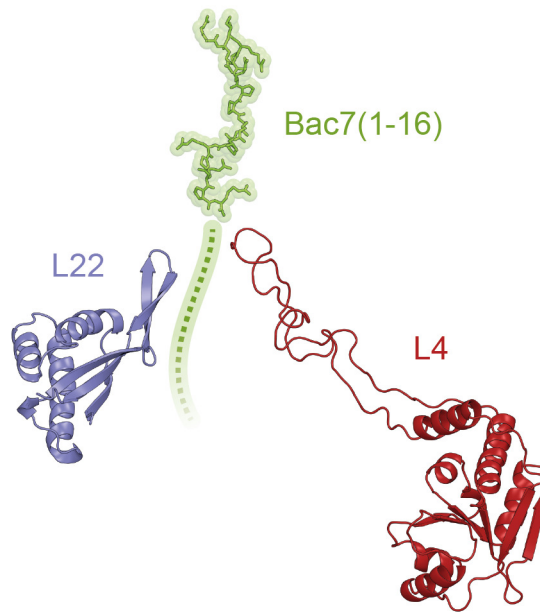


Figure S2. Relative position of the ribosome-bound Bac7(1-16) peptide (green) to the ribosomal proteins L4 (red) and L22 (blue) that reach into the lumen of the ribosomal tunnel. The proposed path for the full-length Bac7 peptide is shown as a dotted green line.

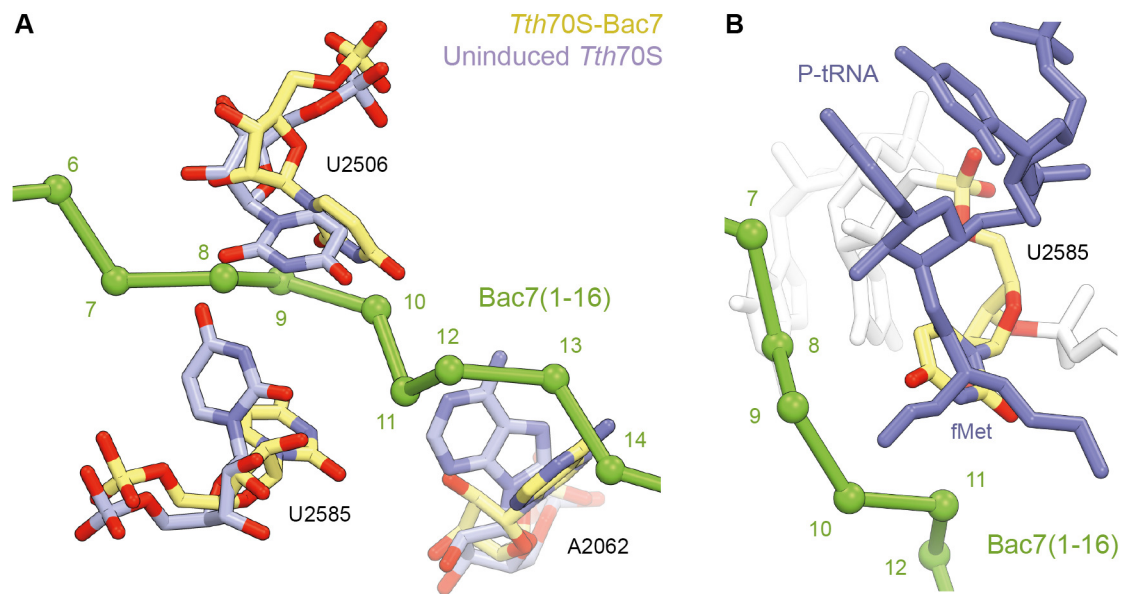
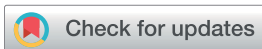


Figure S3. (A) Conformational changes in 23S rRNA nucleotides A2062, U2506 and U2585 that take place upon binding of Bac7(1-16) to the ribosome. Nucleotides from the *Tth70S*-Bac7 structure are shown in yellow, while nucleotides in the Bac7-free or “uninduced” conformation are in blue (1). (B) Clash between the formyl-methionyl moiety of a P-site bound fMet-tRNA^{Met} (blue) and 23S rRNA residue U2585 in its Bac7-bound conformation (yellow). Bac7(1-16) is shown as a green C α -trace in both panels.

SUPPLEMENTARY REFERENCES

1. Jenner, L., Starosta, A.L., Terry, D.S., Mikolajka, A., Filonava, L., Yusupov, M., Blanchard, S.C., Wilson, D.N. and Yusupova, G. (2013) Structural basis for potent inhibitory activity of the antibiotic tigecycline during protein synthesis. *Proceedings of the National Academy of Sciences of the United States of America*, **110**, 3812-3816.



Cite this: *Nat. Prod. Rep.*, 2017, **34**, 702

Proline-rich antimicrobial peptides targeting protein synthesis

Michael Graf,^a Mario Mardirossian,^a Fabian Nguyen,^a A. Carolin Seefeldt,^b Gilles Guichard,^c Marco Scocchi,^d C. Axel Innis^b and Daniel N. Wilson^{b*ae}

Covering: up to 2017

The innate immune system employs a broad array of antimicrobial peptides (AMPs) to attack invading microorganisms. While most AMPs act by permeabilizing the bacterial membrane, specific subclasses of AMPs have been identified that pass through membranes and inhibit bacterial growth by targeting fundamental intracellular processes. One such subclass is the proline-rich antimicrobial peptides (PrAMPs) that bind to the ribosome and interfere with the process of protein synthesis. A diverse range of PrAMPs have been identified in insects, such as bees, wasps and beetles, and crustaceans, such as crabs, as well as in mammals, such as cows, sheep, goats and pigs. Mechanistically, the best-characterized PrAMPs are the insect oncocins, such as Onc112, and bovine bactenecins, such as Bac7. Biochemical and structural studies have revealed that these PrAMPs bind within the ribosomal exit tunnel with a reverse orientation compared to a nascent polypeptide chain. The PrAMPs allow initiation but prevent the transition into the elongation phase of translation. Insight into the interactions of PrAMPs with their ribosomal target provides the opportunity to further develop these peptides as novel antimicrobial agents.

Received 24th March 2017

DOI: 10.1039/c7np00020k

rsc.li/npr

1 Discovery of PrAMPs

The innate immune system uses a broad range of antimicrobial peptides (AMP) as the first line of defense to kill invading microorganisms. AMPs inhibit the proliferation of bacteria and therefore can prevent the establishment of an infection. They can either be induced through pathogen sensing receptors or are continuously secreted into body fluids.¹ Based on their nature and composition they can be divided into amphiphilic peptides, with two to four β -strands, amphipathic α -helices, loop structures and extended structures.² Although most of these five classes inhibit bacterial cells by permeabilizing the membrane, the action of AMPs is not limited to the surface of pathogens.³ Some AMPs have intracellular targets which affect the metabolism of the invading organism,⁴ such as the subclass of Proline-rich Antimicrobial

Peptides (PrAMPs).^{5–7} PrAMPs belong to the group of cationic peptides that are enriched in proline residues and are often arranged in conserved patterns together with arginine residues (Fig. 1A and B). PrAMPs appear to be irregularly dispersed amongst animals, being so far only identified in some arthropods (insects and crustaceans) and mammals (Fig. 1A). The discovery of the first PrAMP started with apidaecin in the late 1980s.⁸ Casteels and coworkers injected a sub-lethal dose of *Escherichia coli* cells into the body cavity of adult bees and subsequently monitored the appearance of AMPs by HPLC.⁸ This led to the identification of three active forms of apidaecin which were further characterized with respect to their molecular mass and amino acid sequence.⁸ The discovery of apidaecins was quickly followed by the identification of other insect and mammalian PrAMPs. Insect PrAMPs include abaecin from the honey bee *Apis mellifera*,⁹ drosocin from the fruit fly *Drosophila melanogaster*,¹⁰ pyr-rhocoricin from the firebeetle *Pyrhcoris apterus*,¹¹ metalnikowin-1 from the green shield bug *Palomena prasina*¹² and oncocin from the milkweed bug *Oncopeltus fasciatus*^{13,14} (Fig. 1A). In crustaceans, the PrAMP Arasin 1 has been isolated from the spider crab *Hyas araneus*¹⁹ as well as a PrAMP with similarity to Bac7 from the shore crab *Carcinus maenas*.²⁰ Two distinct mammalian PrAMPs have been identified in ruminant species, such as cows (e.g. *Bos taurus*),¹⁵ sheep (e.g. *Ovis aries*)^{16,17} and goats (e.g. *Capra hircus*) (Fig. 1A).^{16,17} These PrAMPs were named bactenecin 5 and 7 (Bac5 and Bac7) due

^aGene Center, Department for Biochemistry and Center for Integrated Protein Sciences Munich (CiPS-M), University of Munich, 81377 Munich, Germany

^bUniv. Bordeaux, ARNA Laboratory, Inserm U1212, CNRS UMR 5320, IECB, 33607 Pessac, France

^cUniversité de Bordeaux, CNRS, Institut Polytechnique de Bordeaux, UMR 5248, Institut de Chimie et Biologie des Membranes et des Nano-objets (CBMN), IECB, 33607 Pessac, France

^dDepartment of Life Sciences, University of Trieste, Trieste, 34127, Italy

^eInstitute for Biochemistry and Molecular Biology, University of Hamburg, 20148 Hamburg, Germany. E-mail: Daniel.Wilson@chemie.uni-hamburg.de; Fax: +49 40 4283 82848; Tel: +49 40 4283 82841

† These authors contributed equally.

to the molecular weight of the mature peptides being 5 and 7 kDa, respectively.¹⁵ In pigs the corresponding PrAMP homolog to Bac7 has been called PR-39 due to its length of 39 amino acids.¹⁸ Additional bactenecin-like PrAMPs, such as Bac4, Bac6.5 and Bac11, were identified in the sheep genome,¹⁶ but remain to be characterized.

2 Synthesis of PrAMPs

The synthesis of AMPs, including PrAMPs, occurs mainly in response to invading bacteria.¹ While most of the PrAMPs characterized to date are synthesized by the ribosome as inactive precursors, interestingly, their paths of activation differ significantly between species.

Mammalian Bac5/Bac7 peptides are produced, as other non-proline-rich mammalian AMPs, by immature myeloid cells as pre-pro-peptide precursors (Fig. 2A). The Bac5 and Bac7 pre-pro-

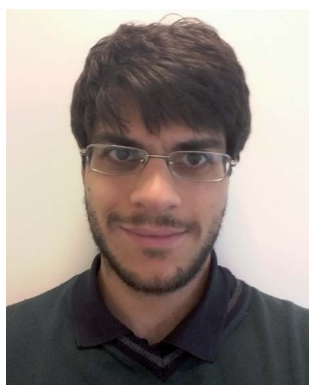
peptides comprise a 29 aa pre-signal followed by a 101 aa pro-region. Bac5/Bac7 are targeted to large granules, where the targeting signals are cleaved upon import to yield pro-peptides in differentiated neutrophils.²¹ When the immune system recognizes invading bacteria, the maturation of pro-Bacs is triggered by secretion and mixing of the contents of large and azurophil granules.²² The inactive pro-Bacs are then cleaved by elastase, a serine protease that is present in azurophil, either upon (i) fusion with the phagosome, or (ii) exocytosis and release into the extracellular matrix (Fig. 2A).^{22,23} The mature Bac5 (43 aa) and Bac7 (60 aa) peptides can then pass through the bacterial cell membrane *via* the SbmA transporter (see next section), where they can subsequently interact with their intracellular target (Fig. 2A).^{24,25} Similarly, cDNA analysis showed that the pig PR-39 is synthesized as a 172 aa pre-pro-PR-39 peptide, which is comprised of a 29 aa signal sequence, a 101 aa pro-region and a 42 aa N-terminal PR-39-containing region.



Michael Graf initially studied Biology at the Technical University Aachen, Germany from 2009 until 2011. Subsequently, Michael studied Biochemistry from 2012 until 2014 at the Ludwig Maximilian University (LMU) in Munich, Germany. His Master thesis was conducted at the University of Illinois at Chicago in the group of Prof. Alexander Mankin. Currently, Michael is a Ph.D. student in the Wilson group at the Gene Center, LMU.



Fabian Nguyen received his master degree in Biochemistry at the Ludwig Maximilian University, Munich in 2013. Currently, he is pursuing his Ph.D. in Biochemistry in the group of Daniel Wilson at the Gene Center, LMU. His main fields of interest are the characterization of novel antibiotics and resistance mechanisms.



Mario Mardirossian studied Biology obtaining a Master Degree in Functional Genomics at the University of Trieste, Italy, and a Master of Genetics at the University Diderot-Paris 7, Paris, France. He received a Ph.D. in Molecular Biomedicine in 2012 at the University of Trieste where he worked as a post-doc until 2015. In 2015, Mario obtained a Talent mobility grant to work in the

group of Prof. Wilson at the Ludwig Maximilian University, Munich, Germany. Mario is currently working at the University of Trieste with a research focus on antimicrobial peptides, particularly on the proline-rich peptides, their molecular mode of action and their optimization.



Daniel Wilson studied Biochemistry in Wellington, New Zealand from 1989–1992 and received his PhD from Otago University, Dunedin, New Zealand in 1999. Daniel was awarded an Alexander von Humboldt fellowship and was post-doc at the Max-Planck Institute for Molecular Genetics in Berlin from 2001–2006. In 2007, Daniel established an independent research group at the Gene

Center, Ludwig Maximilian University of Munich. Daniel was awarded an EMBO young investigator program (YIP) fellowship in 2010 and the GlaxoSmithKline (GSK) Medical Research Award in 2011. Since October 2016, Daniel holds a Chair as Professor for Biochemistry at the University of Hamburg. Daniel's research is focused on regulation of protein synthesis in general and with an emphasis on ribosome-targeting antibiotics and bacterial resistance mechanisms.

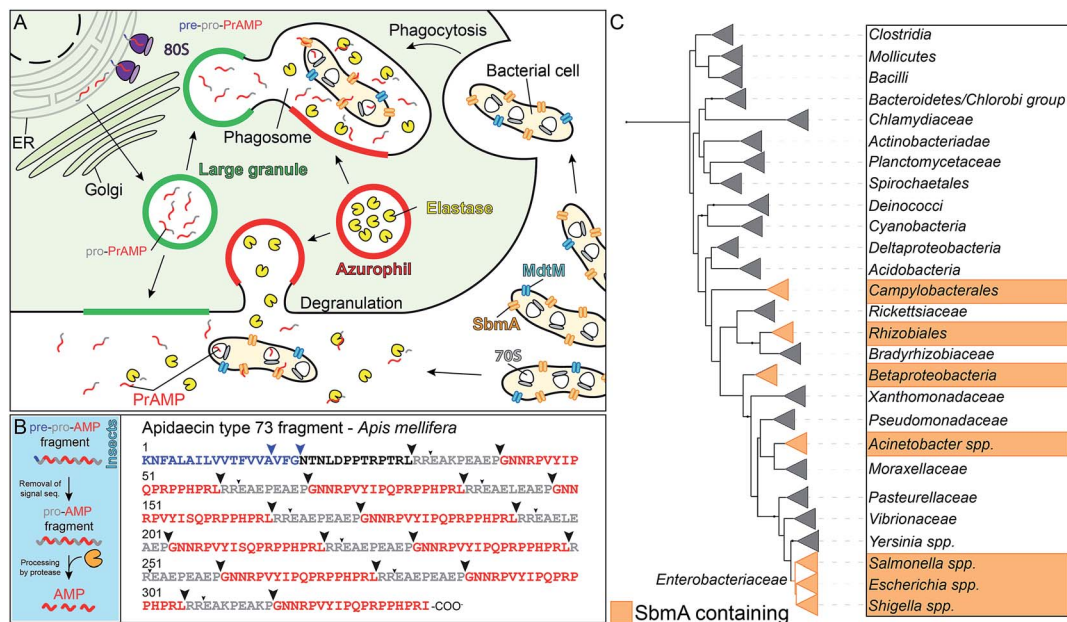


Fig. 2 Synthesis of PrAMPs. (A) Mammalian PrAMPs are synthesized as pre-pro-sequences and targeted to large granules. The PrAMPs are activated upon bacterial infection by fusion of pro-PrAMP containing large granules with the elastase-containing azurophil granules and either the plasmamembrane or the phagosome. Elastase activates the mature PrAMP by removal of the pro-sequence. The activated PrAMP is transported *via* SbmA (or to a lesser extent MdtM) into the bacterial cell. (B) Schematic (left) illustrating the activation of insect PrAMPs synthesized as multiple copies within one open reading frame. Liberation of the mature peptide involves the processing of a pre-pro-AMP by amino-, carboxy- and endoproteases. An example for a pre-pro form (right) of apidaecin type 73 fragment from *Apis mellifera*, which contains several isoforms of mature apidaecin. Putative cleavage sites are highlighted with arrows. (C) Phylogenetic tree showing distribution of SbmA (orange) across Eubacteria. Bacterial groups that have some members carrying SbmA have been highlighted in orange. The iTOL software was used to draw the tree.³⁷

under restrictive conditions, with a higher permeabilizing activity correlating with longer and more hydrophobic peptides.³¹ This contradiction was resolved when a dual mode of action was demonstrated for shorter fragments of Bac7, such as Bac7(1-35), against *Enterobacteriaceae*.³² The lytic mode of action was relegated to a secondary effect of this molecule, observable only in the presence of high peptide concentrations (starting from 16 μM), much above the bacteriostatic and bactericidal levels (0.5 μM and 1 μM respectively).³²

The non-lytic mode of action of PrAMPs implies the presence of one or more transporters for cellular uptake into bacteria. The principal “Trojan horse” exploited by insect and mammalian PrAMPs was shown to be the inner membrane protein SbmA.²⁴ The SbmA transporter is also involved in uptake of the microcins B17,³³ J25,³⁴ and of the non-ribosomal peptide antibiotic bleomycin.³⁵ SbmA transports PrAMPs inside the bacterial cytosol exploiting the electrochemical proton gradient across the inner membrane³⁶ and is the major transporter responsible for their uptake.²⁴ The physiological role of SbmA still remains unclear, but this protein can be found in phylogenetically distant species of Gram-negative bacteria (Fig. 2C).³⁷ Evidence for SbmA homologs can be found amongst *Gamma-proteobacteria*, in particular, the *Enterobacteriaceae* (e.g. *E. coli*, *S. dysenteriae*, *S. enterica*, and *Klebsiella pneumoniae*) and *Pseudomonadales* (*A. baumannii*), but also amongst *Alpha-proteobacteria* such as *Rhizobiales* (e.g. *S. meliloti*, *A. tumefaciens* and *B. abortus*), *Beta-proteobacteria* (e.g. *Neisseria meningitidis*), and *Epsilon-proteobacteria* (*Campylobacter spp.*) (Fig. 2C). The

deletion of the *sbmA* gene in bacteria did not fully confer resistance towards PrAMPs, but significantly reduced their sensitivity.²⁴ This is likely due to a decrease but not abolishment of peptide internalization in bacteria in the absence of SbmA (or presence of non-functional SbmA),²⁴ indicating that SbmA is not the only transporter for uptake of PrAMPs. Indeed, a second transport mechanism for PrAMP uptake was recently discovered, namely, the inner membrane protein MdtM.³⁸ MdtM is an efflux pump that extrudes antibiotics from the bacterial cytosol.^{39,40} Simultaneous deletions of MdtM and SbmA in *E. coli* further decreased the susceptibility of bacteria to some PrAMPs, but not to all of them.³⁸ For PrAMPs with a dual mode of action, such as Bac7 or the synthetic A3-APO, the lytic mode of action becomes dominant at high concentrations, thus obliterating the advantage that the deletion mutants have over wild-type bacteria.³⁸

Interestingly, there is a link between the presence of transporters for PrAMPs in the membrane of a bacterial species and the mode of action of the PrAMP towards a specific microorganism. For example, *Pseudomonas aeruginosa* does not have SbmA, therefore PrAMPs cannot easily reach the cytosol to inhibit bacterial growth by targeting specific intracellular pathways. The antimicrobial effect of Bac7 fragments is indeed lower on *Pseudomonas sp.* if compared with other bacterial species in which an *sbmA* gene is present.⁴¹ Similarly, insect PrAMPs are also less active toward *P. aeruginosa* strains, and studies optimizing apidaecins with improved antimicrobial activity toward this pathogen, ended up selecting for derivatives

with more membranolytic capabilities.⁴² However, if the exogenous *E. coli* SbmA is expressed in *P. aeruginosa* PA01, an increase in internalization and antimicrobial activity was observed.⁴³ On the other hand, the PrAMP becomes less permeabilizing toward the bacterial cell. SbmA seems therefore to drain Bac7 from the membrane, keeping the local concentration lower and thereby as a consequence reducing membrane damage by the PrAMP.⁴³

4 Intracellular targets of PrAMPs

Despite the identification of several PrAMPs, the exact target of these peptides remained elusive for a long time and in the beginning it was even unclear whether PrAMPs were lytic, like most other AMPs, or whether they utilize a completely different mode of action. Five years after the initial discovery of apidaecin, permeabilization assays suggested that the PrAMP apidaecin utilizes a non-lytic mechanism⁵ and inhibits bacteria by targeting intracellular components.⁶ *In vivo* metabolic labeling assays monitoring the incorporation of radioactive methionine indicated that protein synthesis may be the intracellular target of apidaecin,⁶ however, these findings were initially not investigated further. The second target suggested for PrAMP interaction were the chaperones of the Hsp70 family.⁴⁴ In co-immunoprecipitation assays the DnaK chaperone was shown to co-purify with PrAMPs, such as drosocin, pyrrothocin, apidaecin 1a⁴⁴ and Bac7(1-35).⁴⁵ Subsequent structural studies visualized the interactions of PrAMPs with DnaK and revealed that PrAMPs bind within the same pocket as natural DnaK substrates.^{46–48} The hypothesis that DnaK is the primary target for PrAMP action was challenged when studies reported that DnaK-deficient strains still remained susceptible to Bac7(1-35) treatment.⁴⁵ Subsequently, similar results were also obtained for the insect PrAMPs oncocin and apidaecin.⁴⁹ Thus, the interaction of PrAMPs with DnaK appeared to be a secondary effect, suggesting the existence of another intracellular target for PrAMP action.

To identify the physiological target of PrAMPs, synthetic derivatives of the insect PrAMP oncocin and apidaecin were biotin-labeled and used to “fish” for interactors within bacterial extracts.⁴⁹ This led to the identification of ribosomal proteins, suggesting that ribosomes may be the major target of PrAMPs.⁴⁹ Consistently, oncocins and apidaecins derivatives were shown to bind to *E. coli* 70S ribosomes and inhibit *E. coli* protein synthesis using *in vitro* transcription/translation assays.⁴⁹ A second independent study reached the same conclusion, demonstrating that the mammalian PrAMP Bac7 co-sedimented with bacterial ribosomes, inhibited *in vitro* transcription/translation reactions using bacterial lysates and blocked protein synthesis in living bacteria.²⁵ Recently, apidaecin was proposed to have a distinct mechanism of action compared to other insect PrAMPs, such as oncocin, namely, by interfering with the assembly of the large ribosomal subunit.⁵⁰ However, it remains to be determined whether this is a direct effect on assembly or an indirect effect resulting from inhibition of translation. Nevertheless, competition assays with other translation inhibitors indicate that the apidaecin binding site

on the ribosome may differ somewhat from that of oncocin.⁵⁰ A distinct mechanism of action for apidaecins compared to oncocins is also supported by differences in the importance of their C- and N-terminal residues, respectively,^{6,41,49,51} as discussed in the following section.

5 Structure activity relationships of PrAMPs

The antimicrobial potency of PrAMPs is most effective against Gram-negative bacteria, especially *Enterobacteriaceae* such as *E. coli*, whereas Gram-positive bacteria are generally less susceptible to PrAMPs, presumably due to the absence of specific transporters, such as SbmA.⁷ Given the potential of native PrAMPs for development as antibacterial compounds against Gram-negative bacteria, efforts have been made to identify which residues are crucial or dispensable for their inhibitory activity. The best-characterized PrAMP derivatives are those related to the insect oncocins and apidaecins, as well as the bovine Bac7.

The original sequencing analysis of oncocin did not reveal the nature of the residue at position 11 (see Fig. 1A),¹³ yet further mutagenesis studies indicated that the antimicrobial efficiency of oncocin derivatives strongly depends on this position.¹⁴ For example, oncocin derivatives containing Pro11 or Thr11 displayed significantly worse MICs (128 $\mu\text{g mL}^{-1}$) against *E. coli* compared to derivatives with Arg11 (8 $\mu\text{g mL}^{-1}$). Subsequent removal of Asn18 and addition of an amino group to the C-terminus, coupled with the additional replacement of both Arg15 and Arg19 with either D-arginine or L-ornithine, led to the development of Onc112 and Onc72 derivatives, respectively, both of which displayed increased serum stability without loss in antimicrobial activity against *E. coli* and *Micrococcus luteus* strains.^{14,52} Onc72 showed moderate activity against different *E. coli* strains with MICs ranging from 18–44 $\mu\text{g mL}^{-1}$, whereas Onc112 was more active against *E. coli* in diluted tryptic broth media with MICs of 2.5–6.8 $\mu\text{g mL}^{-1}$.⁵³ Alanine-scanning mutagenesis of oncocin revealed that replacement of Tyr6 or Leu7 with Ala led to a 32-fold increase of MIC against *E. coli*,⁴⁸ whereas these mutations had little effect on the MIC against *P. aeruginosa*.⁵⁴ Onc112 and Onc72 both display potent inhibitory activity in *E. coli in vitro* translation systems.⁴⁹ While Onc112 derivatives lacking the last seven C-terminal residues (Onc112 Δ 7) retained some translation inhibition activity, truncation of an additional two residues (Onc112 Δ 9) led to complete loss of activity.⁵⁵ Both derivatives were unable to inhibit the growth of *E. coli* BL21(DE3) in undiluted LB medium at concentrations up to 383 $\mu\text{g mL}^{-1}$, while full-length Onc112 inhibited the growth at 60 $\mu\text{g mL}^{-1}$ indicating that the very C-terminus of oncocin is more important for cellular uptake than for ribosome binding and inhibition.⁵⁵ An oncocin derivative lacking the first two N-terminal residues (Onc112 Δ VD) had reduced capacity to inhibit bacterial growth *in vivo* and protein synthesis *in vitro*,⁵¹ illustrating the significance of N-terminal residues for activity.

Given the increased length (60 aa) of Bac7 compared to insect PrAMPs (<20 aa), structure-activity studies on Bac7 have

so far focussed mainly on analyzing activity of truncated Bac7 derivatives, rather than specific amino acid substitutions.⁴¹ These studies demonstrated that the first 35 N-terminal residues of Bac7 are necessary and sufficient to inhibit bacterial growth with the same efficacy as the full-length native peptide. Bac7(1-35) was shown to display excellent activity ($\text{MIC} \leq 8.4 \mu\text{g mL}^{-1}$) against a range of clinically relevant Gram-negative pathogens, such as *E. coli*, *A. baumannii*, *K. pneumoniae* and *Salmonella enterica*.⁴¹ The Bac7 peptide can be further shortened to encompass only the first 16 N-terminal residues (Bac7(1-16)), sacrificing only partially its antimicrobial potency, whereas further truncation of even one amino acid (Bac7(1-15)) leads to a complete loss of antimicrobial activity.⁴¹ The loss of activity of Bac7(1-15) results from impaired transport into the cytosol, indicating that Bac7(1-16) is the shortest Bac7 PrAMP that is efficiently taken up by bacterial cells.⁵⁶ Unlike the C-terminal truncations, removal of the two N-terminal arginine residues of Bac7(1-23) increases the MIC by 8-fold⁵⁶ and truncation of the first four N-terminal residues basically inactivated Bac7(1-35).⁴¹ Thus, only the first 16 amino acids of the full 60 of the native Bac7 are crucial for its killing activity. Similarly, N-terminally truncated Bac7(5-35) was shown to have reduced inhibitory activity compared to both Bac7(1-16) and Bac7(1-35) when analyzed using *E. coli* *in vitro* translation assays.⁵⁷ This indicates that the first 16 amino acids of Bac7 are necessary to inhibit bacterial growth, and are also necessary to efficiently block protein synthesis.

The first insights into which apidaecin residues are critical for its inhibitory activity came from a comparative analysis of natural apidaecin-type peptides from a diverse range of insects.⁵⁸ Comparison of these peptides revealed a conserved core containing the sequence R/KPxxxPxxPRPPHPRI/L. Deviations from the C-terminal consensus severely reduced the antimicrobial activity of apidaecins, for example, an exchange of penultimate Arg by Ala in hornet apidaecin resulted in an 2500-fold increase in MIC (from $0.01 \mu\text{g mL}^{-1}$ for the wildtype to $25 \mu\text{g mL}^{-1}$).⁶ In contrast, substitutions within the middle or N-terminal part of hornet apidaecin produced milder effects.⁶ The promising MIC values made apidaecin a potential candidate for the development of new antimicrobial agents, however, apidaecin displayed low stability in mouse serum.⁵⁹ In order to improve serum stability, the honey bee apidaecin 1b was modified with an N-terminal tetramethylguanidino-L-ornithine group instead of a glycine, yielding the apidaecin derivative Api137.⁵⁹ In addition to increased serum stability, Api137 also exhibited a slightly improved MIC against *E. coli* strains.⁵⁹ In accordance with previous studies,⁶ the C-terminal of Api137 was shown to be crucial for activity *in vivo*.⁴⁹ In the absence of the last C-terminal Leu18 residue, the MIC of Api137 increased by 16-fold (from $4 \mu\text{g mL}^{-1}$ to $66 \mu\text{g mL}^{-1}$),⁴⁹ whereas removal of the last two residues (Arg17-Leu18), increased the MIC towards *E. coli* ~140-fold (to $578 \mu\text{g mL}^{-1}$). By contrast, mutations within the N-terminal region, for example the Arg4Ala mutation, did not significantly alter the MIC.⁴⁹ Thus, unlike oncocin and Bac7 where the N-terminal terminus is critical for antimicrobial activity and the C-terminus is to a large extent dispensable, it is

the C-terminus of apidaecins that is important for activity whereas the N-terminus appears to be less critical.

6 Interaction of PrAMPs with the 70S ribosome

The reports that PrAMPs bind to ribosomes and inhibit protein synthesis^{25,49} prompted two independent studies to determine structures of the oncocin derivative Onc112 in complex with the bacterial 70S ribosome.^{55,60} Subsequently, structures were also reported for the insect PrAMPs pyrrococin (Pyr) and metalnikowin-1 (Met) as well as mammalian Bac7 bound to the ribosome.^{51,57} These structures revealed that these PrAMPs all interact with the large (50S) subunit of the ribosome, specifically, binding within the ribosomal exit tunnel (Fig. 3A and B). The binding site of the PrAMPs was visualized within the upper region of the exit tunnel, adjacent to the binding site of a peptidyl-tRNA and overlaps with the path of the nascent polypeptide through the tunnel (Fig. 3C).

Within the tunnel, the PrAMPs adopt an elongated conformation, predominantly consisting of random coil interspersed with stretches of *trans*-polyproline helices (type II). The PrAMPs bind with an opposite orientation compared to a nascent polypeptide chain (for example MifM), namely, with the N-terminus located at the tunnel entry and the C-terminus extending deeper into the tunnel (Fig. 3C). For each of the insect PrAMPs, the C-terminal residues (4 aa, 5 aa and 6 aa of Pyr, Met and Onc112, respectively) were not visualized in the structure (Fig. 3B), suggesting that they are not crucial for stabilizing the interaction with the ribosome.^{51,55,57,60} Similarly, while all 16 residues of Bac7(1-16) were observed,⁵⁷ only 19 residues of Bac7(1-35) were visible with the C-terminal 16 residues being disordered. Consistently, the native Bac7 is 60 aa long however the C-terminus of Bac7 is less crucial for activity and C-terminal truncated derivatives of native Bac7, such as Bac7(1-16), have been shown to retain activity.⁴¹

PrAMP interaction with the 70S ribosome is facilitated by a multitude of hydrogen bonds and stacking interactions (Fig. 3D–F).^{51,55,57,60} The majority of hydrogen bonds are formed between the peptide backbone of PrAMP with the nucleobases of the 23S rRNA. The high content of *trans*-proline residues within PrAMPs seems to be important for maintaining the elongated structure that maximizes the interaction of the peptide backbone with the surrounding rRNA. For insect PrAMPs, such as Onc112, Pyr and Met, additional hydrogen bond interactions are established by amino acid sidechains within the N-terminus of the PrAMP, specifically, Asp2 (D2) interacts with the nucleobase of G2553 and Lys3 (K3) with the phosphate-oxygen rRNA of A2453 (Fig. 3D). Two conserved stacking interactions are observed for the insect PrAMPs Onc112, Pyr and Met, namely, Arg9 (R9) stacks upon 23S rRNA nucleotide C2610 whereas Tyr6 is stacked between C2452 and the neighboring Leu7/Asp7 sidechain of the PrAMP.^{51,55,57,60} These stacking interactions are likely to be important, since exchange of Arg9 by Ala leads to a loss of activity when tested in *P. aeruginosa*,⁵⁴ and substitutions of Tyr6 or Leu7 with Ala in

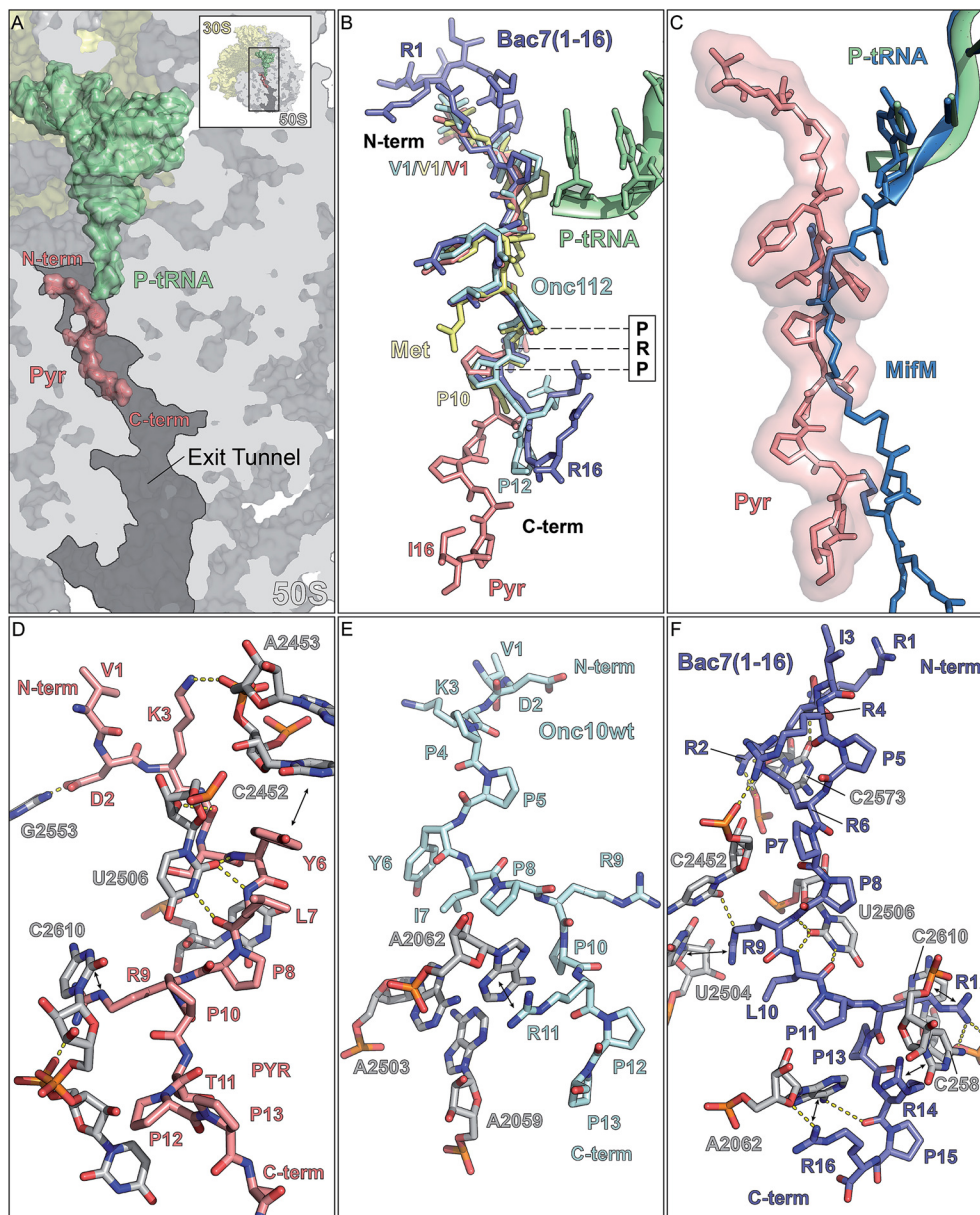


Fig. 3 Binding site of PrAMP within the ribosomal exit tunnel. (A) Overview showing the binding site of pyrrocorcin (Pyr, salmon) within the exit tunnel of the 50S subunit (grey) with P-site tRNA (green). (B) Superimposition of mammalian Bac7(1-16) (light blue) and insect derived PrAMPs Onc112 (cyan), metalnikowin-1 (Met, yellow) and Pyr (salmon), with the conserved PRP motif highlighted. (C) Binding position of Pyr (salmon) relative to the MifM polypeptide chain (dark blue). (D–F) Interactions of (D) insect Pyr (salmon), (E) Onc112 (cyan) and (F) mammalian Bac7(1-16) with nucleotides situated within the polypeptide exit tunnel. Hydrogen bonds are indicated as dashed yellow lines and stacking interactions with arrows.

oncocin reduce the inhibitory activity in *E. coli* by 32-fold.⁴⁸ Mutations within the ribosomal tunnel, namely, A2503C or A2059C, increased resistance against Onc112 by about 4-fold, and the double mutation by more than 15-fold.⁵¹ While neither of these rRNA nucleotides directly contacts Onc112, both residues interact with A2062, which in turn forms stacking interaction with the peptide (Fig. 3E).⁵¹ In addition to revealing the importance of A2062 for Onc112 activity, the mutagenesis data establishes the ribosome as the immediate cellular target of Onc112 and probably other PrAMPs.⁵¹

Compared to insect PrAMPs, the mammalian Bac7(1-16) contains many more arginine residues. In fact, half (8) of the 16 residues are arginines, which establish multiple hydrogen bonding and stacking interactions with the 23S rRNA (Fig. 3F). The two stacking interactions observed in the insect PrAMPs from Tyr6 and Arg9 have equivalents in Bac7(1-16), namely, Arg9 in Bac7(1-16), which occupies the position of Tyr6, and Arg12, which aligns with Arg9 of insect PrAMPs within the conserved core PRP motif (Fig. 1A and B). This centrally conserved core region is the most structurally conserved region

between PrAMPs, with diverse conformations being observed for the N- and C-terminally flanking regions of the various PrAMPs. Bac7(1-16) establishes another three stacking interactions involving the sidechains of Arg2, Arg14 and Arg16 with 23S rRNA nucleotides C2573, C2586 and A2062, respectively (Fig. 3F).^{51,57} The N-terminus of Bac7(1-16) is particularly arginine-rich, comprising Arg1, Arg2, Arg4 and Arg6, which generate a positively charged compacted structure that anchors the N-terminus of the PrAMP to the negatively charged cleft created by the surrounding rRNA. Truncations of four N-terminal residues of Bac7(1-35) inactivated the PrAMP indicating that these interactions are also likely to be critical for Bac7 activity.⁴¹

7 Mechanism of action of PrAMPs

The outcome of initiation of translation is the presence of the initiator fMet-tRNA interacting with the AUG start codon of the mRNA located within the P-site of the ribosome (Fig. 4A). Translation elongation ensues with the delivery of an aminoacylated tRNA (aa-tRNA) to the ribosomal A-site of the ribosome by the elongation factor EF-Tu (Fig. 4B). Correct recognition of the codon of the mRNA by the anticodon of the aa-tRNA leads to dissociation of EF-Tu from the ribosome and accommodation of the aa-tRNA on the large subunit (Fig. 4C). The binding position of PrAMPs, such as Onc112 and Bac7(1-35), on the ribosome indicates that they would allow delivery of the aa-tRNA by EF-Tu to the ribosome, but would prevent accommodation of the aa-tRNA on the large subunit (Fig. 4D). Specifically, overlapping the structure of an accommodated aa-tRNA shows a steric clash between the aminoacylated CCA-end of the A-tRNA and the N-terminal residues of these PrAMPs (Fig. 4E and F).^{51,55,57,60} Bac7 shows the largest extension into the A-site, surpassing Onc112, Pyr (Fig. 4E) and Met by four amino acids at the N-terminus (Fig. 4F).^{51,57} This is consistent with the loss of

activity of Onc112 derivatives lacking the first two N-terminal residues and the reduced activity and binding affinity of N-terminal truncated Bac7 derivatives.^{51,57} In contrast, the N-terminus of the PrAMPs does not significantly overlap with the binding position of the P-tRNA, which is in agreement with biochemical assays demonstrating that these PrAMPs allow binding of the initiator tRNA at the P-site during translation initiation but prevent the transition from initiation into the elongation cycle to occur.^{51,55,57} Presumably, once ribosomes are translating, they are immune to the effects of PrAMPs, such as oncocin, since the binding position of PrAMPs within the ribosomal exit tunnel is likely to be incompatible with the presence of a nascent polypeptide chain (Fig. 3C). Thus, PrAMPs are likely to bind to ribosomes following termination of translation when the polypeptide chain has been released from the ribosome. Additionally, PrAMPs could bind during the late stages of ribosome biogenesis when the binding pocket has formed on the large ribosomal particle.

8 Outlook

A structural understanding of how different PrAMPs interact with components of the ribosome provides further insight into which residues of the PrAMPs as well as which interactions are critical for their inhibitory activity. Importantly, the structures also reveal which regions of the PrAMPs are less important and can be further modified to increase stability and solubility as well as establish additional interactions with the ribosome to increase the binding affinity. This latter point may become important since the binding site of PrAMPs overlaps with many known translation inhibitors, such as chloramphenicol, clindamycin and erythromycin (Fig. 4G).^{55,60,61} Therefore, it will be important to assess cross-resistance between such antibiotics and PrAMPs, especially since initial reports reveal some ribosomal mutations that confer erythromycin resistance also

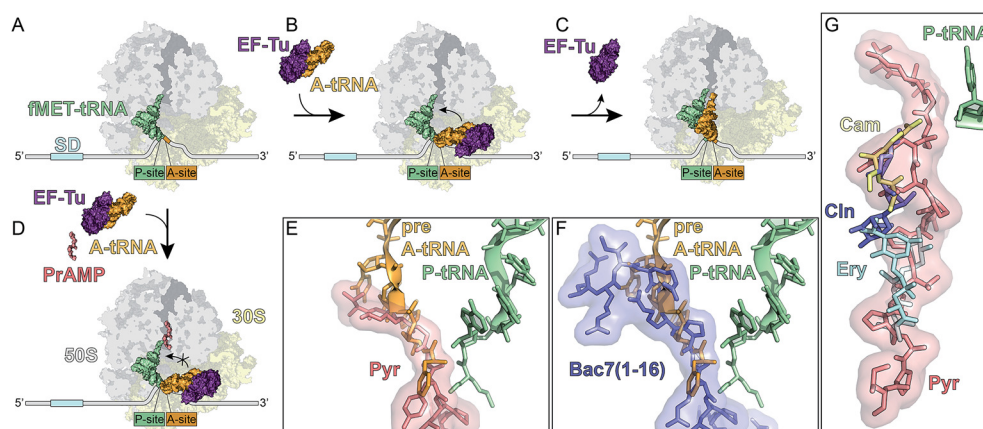


Fig. 4 Inhibition of protein synthesis by PrAMPs. (A–C) Canonical translation in absence of protein synthesis inhibitors, showing (A) translation initiation with initiator P-tRNA (green) bound to the ribosomal P-site. (B) Delivery of aa-tRNA to the A-site, followed by (C) tRNA accommodation into the A-site on the large subunit and subsequent departure of EF-Tu. (D) In the presence of PrAMPs, such as oncocin, aa-tRNA delivery can occur however the aa-tRNA accommodation is blocked. (E and F) Superimposition of (E) insect Pyr (salmon) and (F) mammalian Bac7(1-16) with accommodated aa-tRNA (bright orange). (G) Superimposition of antibiotics chloramphenicol (Cam; yellow), clindamycin (Cln; slate) and erythromycin (Ery; cyan) with the binding position of the insect PrAMP Pyr (salmon).

reduce PrAMP inhibition.⁵⁴ PrAMPs, such as Bac7, also bind to and inhibit translation on eukaryotic ribosomes, albeit less efficiently than on bacterial ribosomes,⁵⁷ thus raising issues of toxicity. Fortunately, it seems that most PrAMPs do not penetrate eukaryotic membranes, however, maintaining the non-lytic mechanism of the PrAMPs during optimization will be critical to avoid disrupting the eukaryotic cell membranes. One major concern for development of PrAMPs as an antimicrobial is the ease with which resistance arises in bacteria *via* mutation of the SbmA transporter. Whether these resistant strains can be overcome by the next generation PrAMPs remains to be seen. Lastly, it is unclear as to the full scope of PrAMPs across different species and, in particular, as to the conservation in terms of mechanism of action. Initial indications suggest that PrAMPs such as drosocin and apidaecin may differ from those of well-characterized PrAMPs such as oncocin and Bac7.

9 Acknowledgements

We would like to thank funding agencies for enabling work in our laboratories related to this topic: Agence Nationale pour la Recherche [ANR-14-CE09-0001 to C. A. I., G. G. and D. N. W.]; Deutsche Forschungsgemeinschaft [FOR1805, WI3285/4-1, GRK1721 to D. N. W.]; European Union [PCIG14-GA-2013-631479 to C. A. I.]; Fondo Ricerca di Ateneo [FRA2014 to M. S.]. Joint Inserm and Conseil Régional d'Aquitaine pre-doctoral fellowship awarded to A. C. S. and Talent³ fellowship awarded to M. M.

10 References

- 1 M. Zasloff, *N. Engl. J. Med.*, 2002, **347**, 1199–1200.
- 2 H. Jenssen, P. Hamill and R. E. Hancock, *Clin. Microbiol. Rev.*, 2006, **19**, 491–511.
- 3 K. A. Brogden, *Nat. Rev. Microbiol.*, 2005, **3**, 238–250.
- 4 P. Nicolas, *FEBS J.*, 2009, **276**, 6483–6496.
- 5 P. Casteels and P. Tempst, *Biochem. Biophys. Res. Commun.*, 1994, **199**, 339–345.
- 6 M. Castle, A. Nazarian, S. S. Yi and P. Tempst, *J. Biol. Chem.*, 1999, **274**, 32555–32564.
- 7 M. Scocchi, A. Tossi and R. Gennaro, *Cell. Mol. Life Sci.*, 2011, **68**, 2317–2330.
- 8 P. Casteels, C. Ampe, F. Jacobs, M. Vaeck and P. Tempst, *EMBO J.*, 1989, **8**, 2387–2391.
- 9 P. Casteels, C. Ampe, L. Riviere, J. Van Damme, C. Elicone, M. Fleming, F. Jacobs and P. Tempst, *Eur. J. Biochem.*, 1990, **187**, 381–386.
- 10 P. Bulet, J. L. Dimarcq, C. Hetru, M. Lagueux, M. Charlet, G. Hegy, A. Van Dorsselaer and J. A. Hoffmann, *J. Biol. Chem.*, 1993, **268**, 14893–14897.
- 11 S. Cociancich, A. Dupont, G. Hegy, R. Lanot, F. Holder, C. Hetru, J. A. Hoffmann and P. Bulet, *Biochem. J.*, 1994, **300**(Pt 2), 567–575.
- 12 S. Chernysh, S. Cociancich, J. P. Briand, C. Hetru and P. Bulet, *J. Insect Physiol.*, 1996, **42**, 81–89.
- 13 M. Schneider and A. Dorn, *J. Invertebr. Pathol.*, 2001, **78**, 135–140.
- 14 D. Knappe, S. Piantavigna, A. Hansen, A. Mechler, A. Binas, O. Nolte, L. L. Martin and R. Hoffmann, *J. Med. Chem.*, 2010, **53**, 5240–5247.
- 15 R. Gennaro, B. Skerlavaj and D. Romeo, *Infect. Immun.*, 1989, **57**, 3142–3146.
- 16 K. M. Huttner, M. R. Lambeth, H. R. Burkin, D. J. Burkin and T. E. Broad, *Gene*, 1998, **206**, 85–91.
- 17 O. Shamova, K. A. Brogden, C. Zhao, T. Nguyen, V. N. Kokryakov and R. I. Lehrer, *Infect. Immun.*, 1999, **67**, 4106–4111.
- 18 B. Agerberth, J. Y. Lee, T. Bergman, M. Carlquist, H. G. Boman, V. Mutt and H. Jornvall, *Eur. J. Biochem.*, 1991, **202**, 849–854.
- 19 K. Stensvag, T. Haug, S. V. Sperstad, O. Rekdal, B. Indrevoll and O. B. Styrvold, *Dev. Comp. Immunol.*, 2008, **32**, 275–285.
- 20 D. Schnapp, G. D. Kemp and V. J. Smith, *Eur. J. Biochem.*, 1996, **240**, 532–539.
- 21 M. Zanetti, L. Litteri, R. Gennaro, H. Horstmann and D. Romeo, *J. Cell Biol.*, 1990, **111**, 1363–1371.
- 22 M. Zanetti, L. Litteri, G. Griffiths, R. Gennaro and D. Romeo, *J. Immunol.*, 1991, **146**, 4295–4300.
- 23 M. Scocchi, B. Skerlavaj, D. Romeo and R. Gennaro, *Eur. J. Biochem.*, 1992, **209**, 589–595.
- 24 M. Mattiuzzo, A. Bandiera, R. Gennaro, M. Benincasa, S. Pacor, N. Antcheva and M. Scocchi, *Mol. Microbiol.*, 2007, **66**, 151–163.
- 25 M. Mardirossian, R. Grzela, C. Giglione, T. Meinel, R. Gennaro, P. Mergaert and M. Scocchi, *Chem. Biol.*, 2014, **21**, 1639–1647.
- 26 P. Storici and M. Zanetti, *Biochem. Biophys. Res. Commun.*, 1993, **196**, 1058–1065.
- 27 M. Charlet, M. Lagueux, J. M. Reichhart, D. Hoffmann, A. Braun and M. Meister, *Eur. J. Biochem.*, 1996, **241**, 699–706.
- 28 K. Casteels-Josson, T. Capaci, P. Casteels and P. Tempst, *EMBO J.*, 1993, **12**, 1569–1578.
- 29 P. Xu, M. Shi and X. X. Chen, *PLoS One*, 2009, **4**, e4239.
- 30 H. G. Boman, B. Agerberth and A. Boman, *Infect. Immun.*, 1993, **61**, 2978–2984.
- 31 B. Skerlavaj, D. Romeo and R. Gennaro, *Infect. Immun.*, 1990, **58**, 3724–3730.
- 32 E. Podda, M. Benincasa, S. Pacor, F. Micali, M. Mattiuzzo, R. Gennaro and M. Scocchi, *Biochim. Biophys. Acta*, 2006, **1760**, 1732–1740.
- 33 M. Lavina, A. P. Pugsley and F. Moreno, *J. Gen. Microbiol.*, 1986, **132**, 1685–1693.
- 34 R. E. de Cristobal, J. O. Solbiati, A. M. Zenoff, P. A. Vincent, R. A. Salomon, J. Yuzenkova, K. Severinov and R. N. Farias, *J. Bacteriol.*, 2006, **188**, 3324–3328.
- 35 P. Yorgey, J. Lee, J. Kordel, E. Vivas, P. Warner, D. Jebaratnam and R. Kolter, *Proc. Natl. Acad. Sci. U. S. A.*, 1994, **91**, 4519–4523.
- 36 G. Runti, C. Lopez Ruiz Mdel, T. Stoilova, R. Hussain, M. Jennions, H. G. Choudhury, M. Benincasa, R. Gennaro, K. Beis and M. Scocchi, *J. Bacteriol.*, 2013, **195**, 5343–5351.
- 37 I. Letunic and P. Bork, *Nucleic Acids Res.*, 2016, **44**, W242–W245.

- 38 A. Krizsan, D. Knappe and R. Hoffmann, *Antimicrob. Agents Chemother.*, 2015, **59**, 5992–5998.
- 39 I. T. Paulsen, L. Nguyen, M. K. Sliwinski, R. Rabus and M. H. Saier Jr, *J. Mol. Biol.*, 2000, **301**, 75–100.
- 40 S. R. Holdsworth and C. J. Law, *Biochimie*, 2012, **94**, 1334–1346.
- 41 M. Benincasa, M. Scocchi, E. Podda, B. Skerlavaj, L. Dolzani and R. Gennaro, *Peptides*, 2004, **25**, 2055–2061.
- 42 M. E. Bluhm, V. A. Schneider, I. Schafer, S. Piantavigna, T. Goldbach, D. Knappe, P. Seibel, L. L. Martin, E. J. Veldhuizen and R. Hoffmann, *Front Cell Dev. Biol.*, 2016, **4**, 39.
- 43 G. Runti, M. Benincasa, G. Giuffrida, G. Devescovi, V. Venturi, R. Gennaro and M. Scocchi, *Antimicrob. Agents Chemother.*, 2017, **61**, e01660.
- 44 L. Otvos Jr, I. O. M. E. Rogers, P. J. Consolvo, B. A. Condie, S. Lovas, P. Bulet and M. Blaszczyk-Thurin, *Biochemistry*, 2000, **39**, 14150–14159.
- 45 M. Scocchi, C. Lüthy, P. Decarli, G. Mignogna, P. Christen and R. Gennaro, *Int. J. Pept. Res. Ther.*, 2009, **15**, 147–155.
- 46 M. Zahn, B. Kieslich, N. Berthold, D. Knappe, R. Hoffmann and N. Strater, *Protein Pept. Lett.*, 2014, **21**, 407–412.
- 47 M. Zahn, N. Berthold, B. Kieslich, D. Knappe, R. Hoffmann and N. Strater, *J. Mol. Biol.*, 2013, **425**, 2463–2479.
- 48 D. Knappe, M. Zahn, U. Sauer, G. Schiffer, N. Strater and R. Hoffmann, *ChemBioChem*, 2011, **12**, 874–876.
- 49 A. Krizsan, D. Volke, S. Weinert, N. Strater, D. Knappe and R. Hoffmann, *Angew. Chem., Int. Ed. Engl.*, 2014, **53**, 12236–12239.
- 50 A. Krizsan, C. Prah, T. Goldbach, D. Knappe and R. Hoffmann, *ChemBioChem*, 2015, **16**, 2304–2308.
- 51 M. G. Gagnon, R. N. Roy, I. B. Lomakin, T. Florin, A. S. Mankin and T. A. Steitz, *Nucleic Acids Res.*, 2016, **44**, 2439–2450.
- 52 D. Knappe, N. Kabankov and R. Hoffmann, *Int. J. Antimicrob. Agents*, 2011, **37**, 166–170.
- 53 D. Knappe, N. Kabankov, N. Herth and R. Hoffmann, *Future Med. Chem.*, 2016, **8**, 1035–1045.
- 54 D. Knappe, S. Ruden, S. Langanke, T. Tikko, J. Ritzler, R. Mikut, L. L. Martin, R. Hoffmann and K. Hilpert, *Amino Acids*, 2016, **48**, 269–280.
- 55 A. C. Seefeldt, F. Nguyen, S. Antunes, N. Perebaskine, M. Graf, S. Arenz, K. K. Inampudi, C. Douat, G. Guichard, D. N. Wilson and C. A. Innis, *Nat. Struct. Mol. Biol.*, 2015, **22**, 470–475.
- 56 F. Guida, M. Benincasa, S. Zahariev, M. Scocchi, F. Berti, R. Gennaro and A. Tossi, *J. Med. Chem.*, 2015, **58**, 1195–1204.
- 57 A. C. Seefeldt, M. Graf, N. Perebaskine, F. Nguyen, S. Arenz, M. Mardirossian, M. Scocchi, D. N. Wilson and C. A. Innis, *Nucleic Acids Res.*, 2016, **44**, 2429–2438.
- 58 P. Casteels, J. Romagnolo, M. Castle, K. Casteels-Josson, H. Erdjument-Bromage and P. Tempst, *J. Biol. Chem.*, 1994, **269**, 26107–26115.
- 59 N. Berthold, P. Czihal, S. Fritsche, U. Sauer, G. Schiffer, D. Knappe, G. Alber and R. Hoffmann, *Antimicrob. Agents Chemother.*, 2013, **57**, 402–409.
- 60 R. N. Roy, I. B. Lomakin, M. G. Gagnon and T. A. Steitz, *Nat. Struct. Mol. Biol.*, 2015, **22**, 466–469.
- 61 J. A. Dunkle, L. Xiong, A. S. Mankin and J. H. Cate, *Proc. Natl. Acad. Sci. U. S. A.*, 2010, **107**, 17152–17157.
- 62 G. E. Crooks, G. Hon, J. M. Chandonia and S. E. Brenner, *Genome Res.*, 2004, **14**, 1188–1190.